E949 Technical Note K-074.v1

Analysis of the 2/3 E949 pnn2 data

Joss Ives, Benji Lewis, Zhe Wang, David E. Jaffe

August 20, 2008

Abstract

Contents

List of Tables

List of Figures

Data set	(units of 10^{-10}) Branching fraction	90% CL upper limit
pnn1 publication [20]	$1.47^{+1.30}_{-0.89}$	3.22
E949 pnn2 (this analysis)	$7.89^{+9.26}_{-5.10}$	20.3
All pnn analyses	$1.73^{+1.15}_{-1.05}$	3.35
SM prediction [20]	0.80 ± 0.11	–

Table 1: Summary of the branching fraction measurements. The central value and 68% CL interval are given in the central column. The rightmost column contains the 90% CL upper limit. The second and bottom rows are taken from the most recent pnn1 publication [20]. The third row is the branching fraction for this analysis alone. The fourth row is the combined result of all E787 and E949 pnn1 and pnn2 analyses. See Table 89 and Section 14.4.3 for more details.

1 Executive Summary

The branching fraction measured by this analysis is given in Table 1 and compared with the latest pnn1 result. The Table also gives the $K^+ \to \pi^+\nu\bar{\nu}$ branching fraction from all E787 and E949 pnn analyses since 1995. The 68% CL interval has changed from $(0.58, 2.77) \times 10^{-10}$ [20] to $(0.68, 2.88) \times 10^{-10}$ and remains consistent with the SM at less than one standard deviation. Section 14.4.3 contains more details and gives the branching fractions evaluated for different subsets of the data.

Expected backgrounds from the 1/3 and 2/3 analyses are given in Table 3. The single event sensitivity and total acceptance are compared with previous analyses in Table 1. Significant progress has been made in increasing the acceptance of the pnn2 analysis with respect to E787 although the E949 pnn2 acceptance still does not attain the level of the E949 pnn1 acceptance. For comparison, the total background of the E787 pnn2 analysis was 1.216 ± 0.249(Table 30 of [7]), so this analysis has succeeded in a 40% increase in the acceptance while maintaining the same total background level and retaining some discriminating power within the signal region as can be seen with the improved acceptance to background in the cleanest cell.

A number of small changes to the analysis have occurred since Technical Note K-073 [1] that described all the changes to the analysis with respect to the prior pnn2 analysis and the E949 pnn1 analysis. None of these changes had a profound effect on the conclusions from the 1/3 note. In addition, it was judged that none of these changes induced a bias in the background estimates made with the 2/3 sample.

This note is organized as follows. Section 2 summarizes the changes with respect to the 1/3 analysis note [1]. The $K_{\pi 2}$-scatter, $K_{\pi 2\gamma}$, beam, muon, charge exchange (CEX) and K_{e4} background estimates are given in Sections 3, 4, 5, 6, 7 and 8, respectively. Studies to ascertain the effect of contamination of the $K_{\pi 2}$ background samples by muons and beam events are presented in Section 9. In the cases considered, the effect of contamination was determined to alter the background estimate by a negligible amount ($< 1\%$). Section 11 describes the acceptance measuremnts and Section 12 contains the estimate of the kaon exposure. The investigation of flaws and loopholes with a single-cut-failure study is described in Section 13. The sensitivity of the analysis and the expected results for a branching fraction measurement are evaluated in Section 14.

Acceptance	Value	Reference
E949 pnn2 (entire)	$(1.366 \pm 0.016 \pm 0.052) \times 10^{-3}$	Table 84
E949 pnn2 (cleanest)	$(0.436 \pm 0.007^{+0.015}_{-0.019}) \times 10^{-3}$	Table 84
1996 pnn2	$(0.764 \pm 0.013 \pm 0.006) \times 10^{-3}$	Table 4.31 of [7]
1997 pnn2	$(0.971 \pm 0.014 \pm 0.021) \times 10^{-3}$	Table 4.31 of [7]
E949 pnn1 (entire)	$(2.22 \pm 0.07 \pm 0.15) \times 10^{-3}$	[16]
SES		
E949 pnn2 (entire)	$(4.28 \pm 0.43) \times 10^{-10}$	Table 84
E949 pnn2 (cleanest)	$(13.42 \pm 1.34) \times 10^{-10}$	Table 84
1996+1997 pnn2	$(6.87 \pm 0.04) \times 10^{-10}$	p.152 of [7]
E949 pnn1 (entire)	$(2.55 \pm 0.20) \times 10^{-10}$	[16]

Table 2: Comparison of the total acceptance, including the $T \bullet 2$ and stopping fraction f_s, for this analysis, the previous E787 pnn2 analyses and the E949 pnn1 analysis in the top part of the table. The lower part of the table contains the single-event-sensitivity for this analysis, the combined E787 pnn2 analysis and the E949 pnn1 analysis. The number of stopped kaons is 1.7096×10^{12}, 1.7275×10^{12} and 1.77×10^{12} for the E949 pnn2, E787 pnn2 and E949 pnn1 analyses, respectively.

Background	Entire signal region						Cleanest signal cell		
Component	1/3			2/3			2/3		
$K_{\pi 2}$TT scatter	0.537	± 0.188	$^{+0.069}_{-0.215}$	0.619	± 0.150	$^{+0.067}_{-0.100}$	0.1021	± 0.0244	$^{+0.0111}_{-0.0165}$
$K_{\pi 2}$RS scatter	0.0220	± 0.0056	± 0.0021	0.0303	± 0.0054	$^{+0.0038}_{-0.0039}$	0.0050	± 0.0009	± 0.0007
$K_{\pi 2\gamma}$	0.0514	± 0.0086	$^{+0.0042}_{-0.0038}$	0.0757	± 0.0073	$^{+0.0062}_{-0.0056}$	0.0170	± 0.0016	$^{+0.0014}_{-0.0013}$
K_{e4}	0.235	± 0.118	$^{+0.310}_{-0.166}$	0.176	± 0.072	$^{+0.233}_{-0.124}$	0.0252	± 0.0103	$^{+0.033}_{-0.018}$
CEX	0.076	± 0.044	$^{+0.058}_{-0.015}$	0.013	± 0.013	$^{+0.010}_{-0.003}$	0.0007	± 0.0007	$^{+0.0005}_{-0.0002}$
Muon	0.0246	± 0.0246		0.0114	± 0.0114		0.0014	± 0.0014	
Two-beam(KK)	0.00359	± 0.00359		0.000458	± 0.000458				
Two-beam($K\pi$)	0.00126	± 0.00126		0.000650	± 0.000650				
One-beam	0.00046	± 0.00046		0.00023	± 0.00023				
Beam total	0.0053	± 0.0038		0.00134	± 0.00083		0.0004	± 0.0003	
Total	0.9513	± 0.2279	$^{+0.4433}_{-0.4019}$	0.9267	± 0.1675	$^{+0.3200}_{-0.2365}$	0.152	± 0.027	$^{+0.047}_{-0.036}$

Table 3: The estimated backgrounds for the entire signal region and the cleanest cell to be used in the analysis. The first error is the statistical uncertainty; the second error (when present) is the estimated systematic uncertainty. The total systematic uncertainty is taken as the linear sum of the uncertainties of each component as described in Section 10.5. The cleanest cell corresponds to the tight settings of the KIN, TD, PV and DELCO cuts. This table gives the backgrounds as used by the branching fraction calculation; that is, the estimated backgrounds for the entire signal region are the result of direct calculation and the estimated backgrounds in the cleanest signal region are the result of extrapolation into the signal region as described in Section 14. The components and total for the beam background are shown separately for the entire signal region, but only the total beam background in the cleanest cell is shown.

2 Summary of changes with respect to the 1/3 analysis note

A number of changes to the analysis were made subsequent to the 1/3 analysis note [1]. None of the changes had a significant effect on the background or acceptance estimates. The changes are

1. Fix to the CCDBADTIM cut. This cut requires consistency between the fitted first pulse and the global kaon time. Originally this cut was only placed on the first fitted pulse for fibers with double-pulse fits only. While searching by visual scan for evidence of K_{e4} contamination in the $K_{\pi 2}$ target-scatter 1/3 normalization branch, an event was observed that showed that the same requirements should be placed on the fitted pulse of single-pulse fits to avoid a possible loophole. Described fully in Section 2.1.

2. The evaluation of the single beam background revealed that an unused cut, E787_CCDPUL, had an unintended effect on the CCDPUL cut. Described fully in Section 2.2.

3. A coding error affected the muon normalization branch. Described fully in Section 2.3.

4. Deprecated cuts related to target dE/dx were inadvertently applied in the beam normalization branch. Described fully in Section 2.4.

5. The multiplexing of low-gain CCD fibers was not correctly taken into account. Described fully in Sections 2.5 and 2.6.

6. The TIMKF function inadvertantly used the incorrect fiber positions. Described fully in Section 2.7.

7. The evaluation of the background from $K^+ \to \pi^+\pi^o$ range stack scatters uses an improved evaluation of the efficiency of the range stack track quality cuts as described in Section 3.2.

8. As described in Sections 2.8, the tight PV cut was re-defined as the logical AND of PV30 and PV60 to ensure that the tight PV region was fully contained inside the loose PV region. The pass2 cut "PVCUT" was added to the definition of PV60 for consistency as defined in Section 2.9.

9. The signal region is defined as the logical OR of the SKIMs as described in Section 2.10.

2.1 CCDBADTIM fix

The CCDBADTIM was originally designed to remove events having incorrect double-pulse fit time values. During a visual scan of tg-scatter normalization events, an event like that found in Figure 1 was observed. The double-pulse fits were never performed on either the logain or the higain due to the single-fit probabilities for both gain channels being above 0.25. For both gain channels, the single-pulse time is consistent with *tpi* (global pion time) and not *tk* (global kaon time). Due to most of the energy being in the second pulse, the fitter found a reasonable solution for the single-pulse fit by fitting the second pulse. Observation of this type of event brought to our attention that the same conditions checked by CCDBADTIM on the first-pulse of the double-pulse fit also need to be applied to the single-pulse.

For each fiber, each of the two gain channels are checked to see if they have a single-fit probability above 0.25 and that the energy from ADC is above 1.25 MeV. If so, the same time conditions are checked for the single-pulse fit as are checked for the first-pulse on the double-pulse fit. If either of these conditions are met, that gain channel is flagged for possible rejection by CCDBADTIM:

- The single-pulse time is less than -9.98 This is the minimum value stored in the ntuple for the first-pulse times from the double-pulse fits;
- The single-pulse time (t_0) is not consistent with the global kaon time tk. The failing conditions are $t_0 - tk < -6$ or $t_0 - tk > 7$. Figure 2 shows that these conditions are suitable for times of both the single-pulse fit and the first pulse of the double-pulse fit.

A fiber having a gain channel that has been flagged for possible rejection by CCDBADTIM will cause the event to fail CCDBADTIM if

- Both gain channels have been flagged for possible rejection by CCDBADTIM;
- One gain channel has been flagged for possible rejection by and CCDBADTIM and the other gain channel has a double-pulse fit probability of zero;
- One gain channel has been flagged for possible rejection by and CCDBADTIM and data from the other gain channel is missing;

In addition to these new conditions on the single-pulse time, the previous conditions on the double-pules times are also checked.

2.2 E787_CCDPUL story

The routine `ccdpul_787.function` (the final version of CCDPUL used in E787) had routines and common blocks with the same name as `ccdpul.function`. Although `ccdpul_787.function` was no longer an "active" cut, the cut was available in Benji's scripts and functions for comparison purposes. The solution of replacing the cut function with a null cut was implemented. This would remove any other possible conflicts.

2.3 Muon background story

To require that only the loose version of TDCUT was inverted (to prevent looking into the box) a direct call to $TDCUT_{loose}$ was performed in Benji's muon-background function. However, during this special implementation an array was not initialized and so some events would be removed due to stale information in the array. After the situation was corrected, the end result did not change. Also, note that this error was not an issue during optimization of the TDCUTs. The error only appeared after the measurements of the tight regions began.

2.4 Beam background story

During E949-PNN2 beam background studies prior to the 2/3 note, the beam background cuts applied RTGHI, ETGHI, TGDEDX1, TGDEDX2 which were part of E949-PNN1's TGDEDX composite cut. TGDEDX cut differs for PNN2 analysis since the kinematic region is much larger than the PNN1 box. Since PNN2 analysis starting point was PNN1's cuts the initial analysis utilized what is now called `tgdedx_pnn1.function`. When the

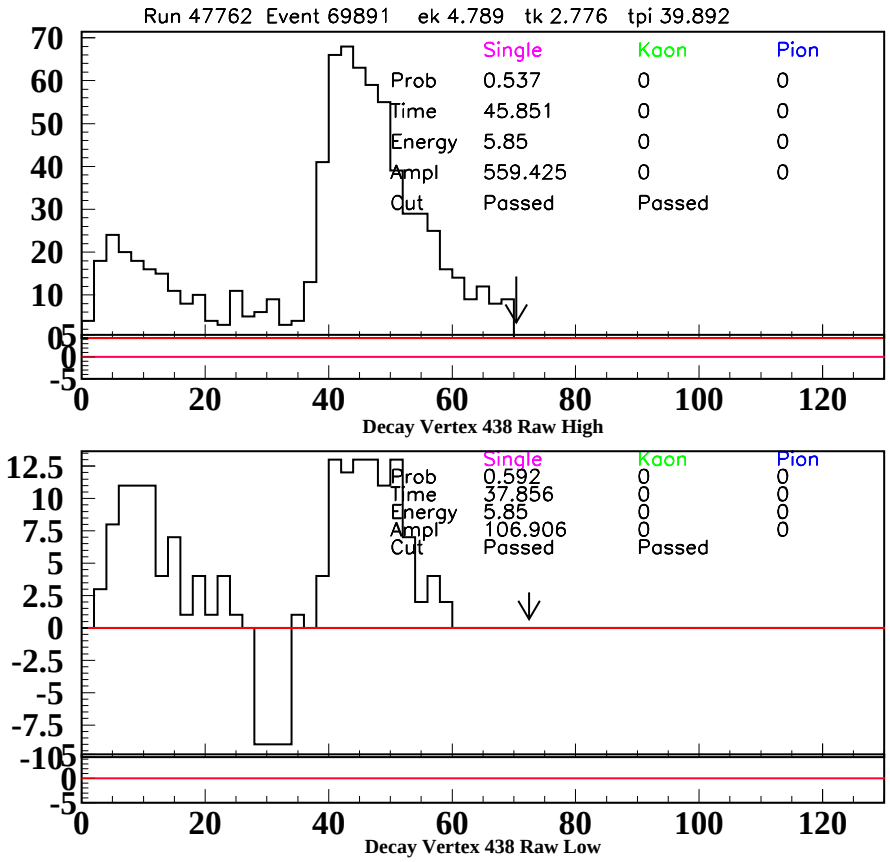

Figure 1: The type of event that motivated the CCDBADTIM fix.

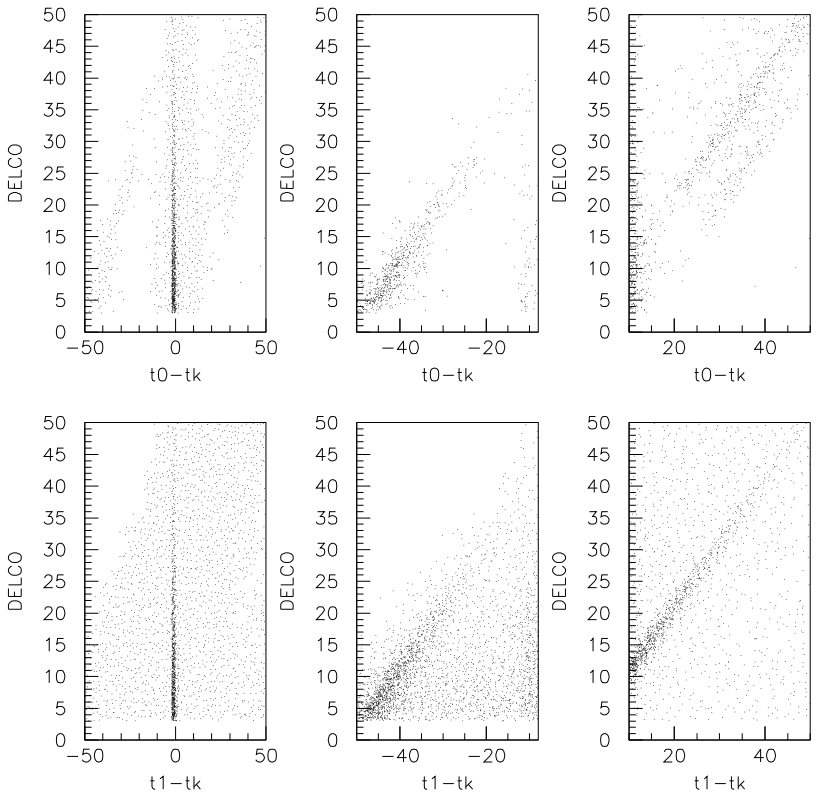

Figure 2: The plots show DELCO vs. the difference between the fitted single-pulse (t0, upper plots) or the first pulse of the double-pulse fit (t1, lower plots) and the global kaon time (tk). DELCO is the difference between the global pion and kaon times (tpi-tk). The central and right-most plots show narrowed x-axis time regions as compared to the left-most plots to emphasize some of the finer structure. The central band around a time of zero in the left-most plots represents good fits. In the upper-right plot, there are two distinct bands. The upper band is DELCO = t0-tk and comes from second (pion) pulses being fit as kaons. The lower band is a result of the 10 ns window around tpi used when fitting.

correct version of TGDEDX was implemented the cuts were not removed from the beam background branches. This oversight was corrected and had little to no effect on the measured beam background values.

2.5 CCD multiplexing story part 1

The routine `addmux.function` is employed by the target-CCD routines and is used to correctly account for multiplexed energy in the low-gain CCD fibers. The `addmux.function` did not correctly consider the time of Photon-Veto hits in the TG as stored in the array *tpvtg(i)*. The *tpvtg* hits were stored relative to *tpi* and other hits within the TG were stored relative to beam strobe. Corrective action was taken as follows:

```
Time = TPVTG(i)
```

became

```
Time = TPVTG(i) + tpi
```

This fixed the specific error which existed during E787-PNN2 analysis.

2.6 CCD multiplexing story part 2

A 1-cut failure (1/3 sample) revealed a mistake in the way low-gain CCD info was being de-multiplexed. Previously the ADC energy for all fibers multiplexed with a given fiber that were within 5ns of *tpi* were summed and subtracted from the fitted 2nd pulse energy. The multiplexed energy was then subtracted from the second pulse. This resulted in total energies between the first and second pulses that were less than the ADC energy of the fiber, which is a mistake since the ADC knows nothing of the multiplexing done with the low-gain CCDs. The algorithm was modified so that energy at both tk and tpi is correctly taken into account when assigning the energy of the 1st and 2d fitted pulse. Modifications were made to `ccdpul.function` and the demultiplexing function `addmux.function`. Additionally, the calls to `addmux.function` from the CCDBADTIM and CCDBADFIT cuts were removed as the amplitudes of the pulses are never actually used in CCDBADTIM and CCDBADFIT.

Here's what was done to `addmux.function`:

1. `addmux` retains the exact same method of determining the multiplexed energy associated with the second pulse, this energy is now considered the pion multiplexed energy;

2. `addmux` now looks for kaon fibers (5ns window around *tk*) that are multiplexed with the fiber in questions and returns a kaon multiplexed energy (in addition to the pion multiplexed energy);

3. Since some fibers can be assigned as both kaon and pion fibers, the pion multiplexed energy and kaon multiplexed energy are determined independently. It is possible for the same fiber to contribute to both types of multiplexed energies if the fiber is assigned as kaon and pion. The energy used to determine these energies are *ek_tg* and *epi_tg* respectively.

Here's what was done to CCDPUL:

1. The pion and kaon multiplexed energies are added to the adc energy to get a total energy as seen by the ccd;

	Before Fix	After Fix
Rejection	(from $\kappa_{\pi 2}$ target-scatter normalization branch)	
	2991/503 = 5.946	2991/500 = 5.982
Acceptance	(from Beam/Target acceptance measurement using km21)	
	669207/1262093 = 0.5302	666042/1262093 0.5277
Acceptance × Rejection		
	3.153	3.157

Table 4: Effects of demultiplexing fix on acceptance and rejection. Note that the values in this table do not agree with those from Table 19 as the fix of the TIMKF coding error (see Section 2.7) was performed after this demultiplexing fix.

2. The energy is split between the two pulses according to the ratio of the fitted amplitudes;

3. The pion and kaon multiplexed energies are then subtracted from their respective pulses;

4. If the resulting pulse energy is below 0.001 MeV, it is assigned an energy of 0.001 MeV. If the resulting pulse energy is above the initial ADC energy, it is assigned the initial ADC energy. Note that if a pulse meets one of these conditions, the other pulse will meet the other condition since the total energy between the two pulses will always equal the initial ADC energy in the kaon fiber.

Table 4 shows the resulting changes to the acceptance and rejection of CCDPUL as a result of the fix. This demultiplexing fix resulted in 3 additional events failing CCDPUL in the loose $K_{\pi 2}$ target-scatter normalization branch (see Table 19). These events are shown in Figures 3 4 and 5.

2.7 TIMKF coding error

TIMKF determines if the apparent path of the kaon in the TG is consistent with the measured kaon fiber times and energies. This is accomplished by looking at information on a fiber-by-fiber basis, the quantities of interest are time, energy, and position. The positions of these kaon fibers relative to the decay vertex (*tgx,tgy*) and the entering B4 position (*x_b4sw,y_b4sw*) are also important. We expect the reconstructed Kaon to deposit more energy/fiber as it slows down. The time of the first fiber hit should be earlier than the last fiber hit; the TG has sufficient timing resolution to accomplish this when there is enough energy deposited in a fiber.

The error was created when Benji modified all the cut routines to use the most up-to-date TG geometry file (determined in read_geom.function). After E949-PNN1 analysis, E949-PNN2 improved the TG geometry files and so Benji implemented changes to the read_geom.function to employ the same format as used by PASS2 source code. The error was the following:

- TIMKF code segment with error

```
ifib = elk_tg(ik)
```

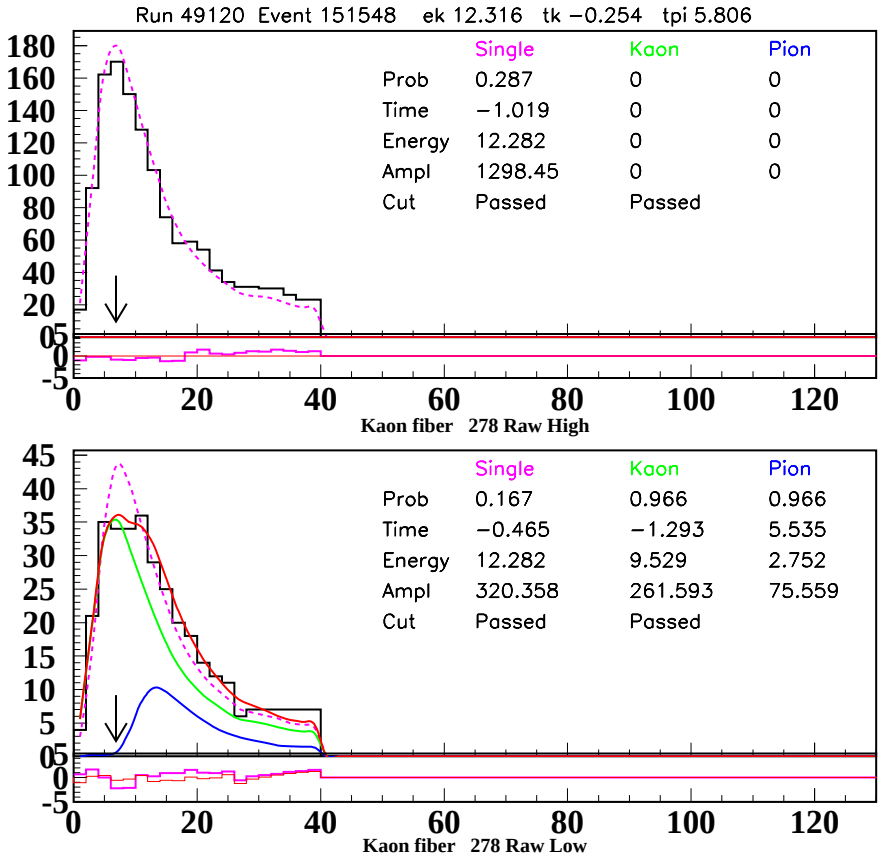

	Before Fix	After Fix
Energy from other multiplexed fibers (MeV)		
E_K(mux)	N/A	0.
E_π(mux)	1.58	1.58
Fitted pulse energy from ADC Energy (MeV)		
Total Energy	12.28	$12.28 + 0.00 + 1.58 = 13.86$
E_K	9.53	10.76
E_π	2.75	3.10
Energy corrected for multiplexed energy (MeV)		
$E_K(corr.)$	9.53	10.76
$E_\pi(corr.)$	$2.75 - 1.58 = 1.17$	$3.10 - 1.58 = 1.52$

Figure 3: Newly Rejected CCDPUL event: run 49120, event 151548. Before demultiplexing fix, the event was passing CCDPUL with 1.17 MeV in the second pulse ($E_\pi(corr.)$) which is below the CCDPUL pion energy threshold of 1.25 MeV. After the demultiplexing fix, the event fails with $E_\pi(corr.) = 1.52$ MeV. This kaon fiber (fiber 278) is multiplexed with a pion fiber with $t = 5.98$ and $E = 1.58$.

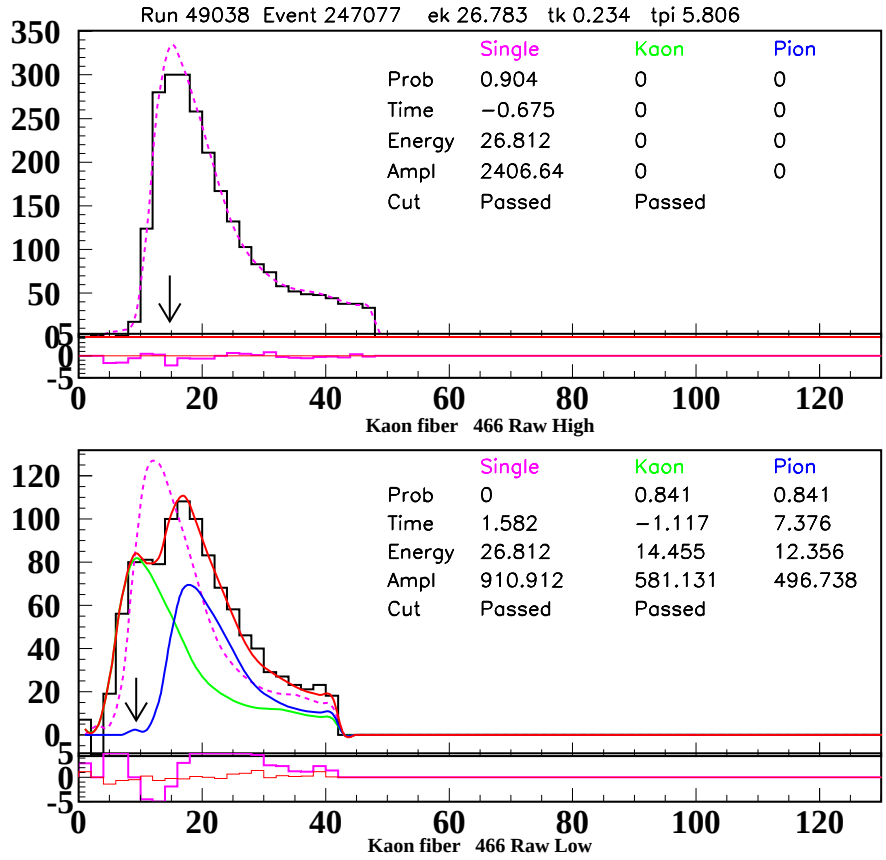

	Before Fix	After Fix
Energy from other multiplexed fibers (MeV)		
E_K(mux)	N/A	0.
E_π(mux)	17.68	17.68
Fitted pulse energy from ADC Energy (MeV)		
Total Energy	26.81	$26.81 + 0.00 + 17.68 = 44.49$
E_K	14.46	24.00
E_π	12.36	20.51
Energy corrected for multiplexed energy (MeV)		
$E_K(corr.)$	14.46	24.00
$E_\pi(corr.)$	$12.35 - 17.68 = -5.33$	$20.51 - 17.68 = 2.83$

Figure 4: Newly Rejected CCDPUL event: run 49038, event 247077. Before demultiplexing fix, the event was passing CCDPUL with 0.001 MeV in the second pulse ($E_\pi(corr.)$) which is below the CCDPUL pion energy threshold of 1.25 MeV. Note that corrected energies below 0.001 MeV are assigned an energy of 0.001 MeV. After the demultiplexing fix, the event fails with $E_\pi(corr.) = 2.83$ MeV. This kaon fiber (fiber 466) is multiplexed with a photon fiber with $t = 1.34$ and $E = 17.68$.

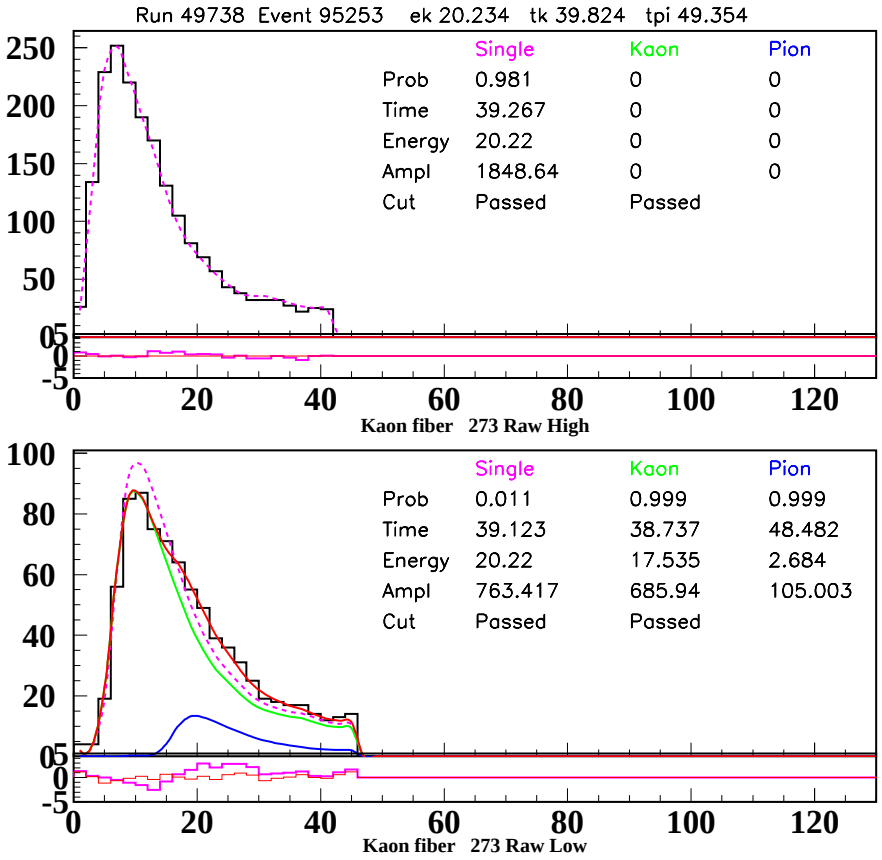

	Before Fix	After Fix
Energy from other multiplexed fibers (MeV)		
E_K(mux)	N/A	0.
E_π(mux)	1.49	1.49
Fitted pulse energy from ADC Energy (MeV)		
Total Energy	20.22	$20.22 + 0.00 + 1.49 = 21.71$
E_K	17.54	18.83
E_π	2.68	2.88
Energy corrected for multiplexed energy (MeV)		
$E_K(corr.)$	17.54	18.83
$E_\pi(corr.)$	$2.68 - 1.49 = 1.19$	$2.88 - 1.49 = 1.39$

Figure 5: Newly Rejected CCDPUL event: run 49738, event 95253.. Before demultiplexing fix, the event was passing CCDPUL with 1.19 MeV in the second pulse ($E_\pi(corr.)$) which is below the CCDPUL pion energy threshold of 1.25 MeV. After the demultiplexing fix, the event fails with $E_\pi(corr.) = 1.39$ MeV. This kaon fiber (fiber 273) is multiplexed with a pion fiber with $t = 48.56$ and $E = 1.49$.

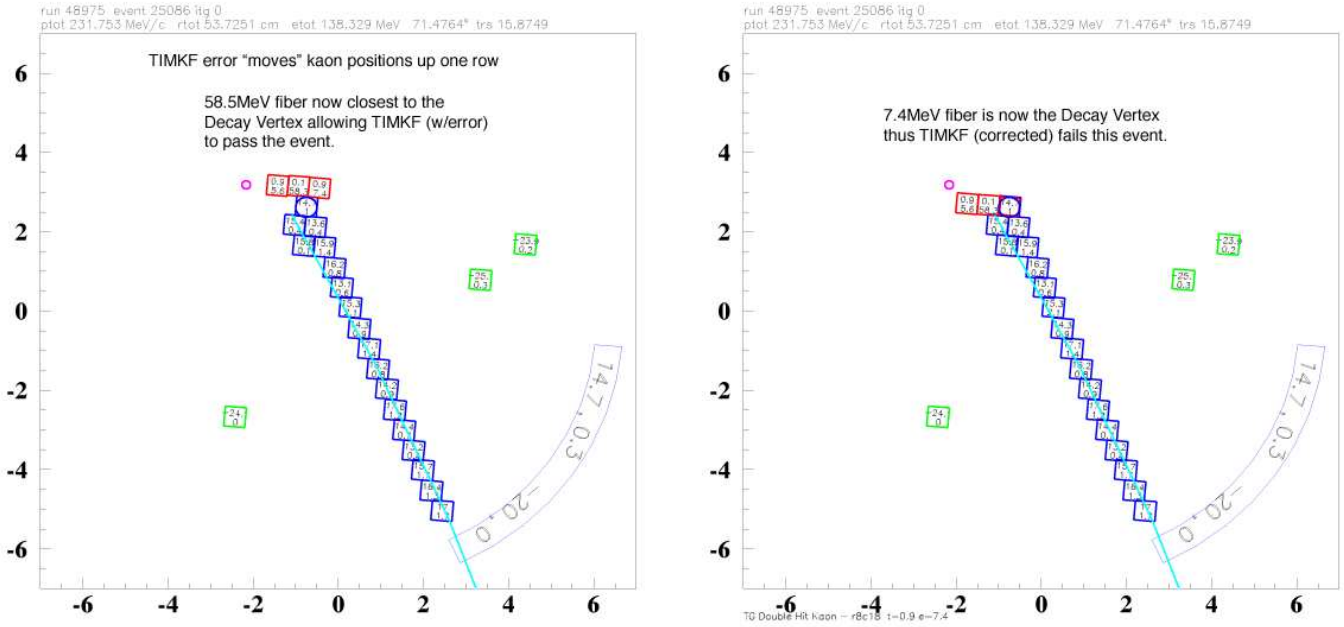

(a) Before Fix: Passes

(b) After Fix: Fails

Figure 6: **Display showing TIMKF Error**. These events fail after TIMKF is corrected. Display for (a) shows effect of error on kaon fiber positions relative to the kaon entry (stopping) position as determined by B4 (swathccd) as used by TIMKF. The error does not affect any other cut or the positions of the kaons used by the reconstruction. The kaon fibers are shifted in (a) for display purposes only.

```
...
xpos = t50h(ifib)
ypos = t50v(ifib)
```

- TIMKF code segment without error

```
....
xpos = t50h(ifib-24)
ypos = t50v(ifib-24)
```

Another similar segment within TIMKF was also corrected. As shown above, the indexing is incorrect. There is an offset of 24 between the indexing stored within the ntuple and the geometry file (tg_p50.02002). The correct indexing was implemented in all other cuts using target geometry information.

The error did not exist in E787 analysis or in E949-PNN1 since the TIMKF cut was not used by the PNN1 analysis.

Figures Fig. 6 and Fig. 7 demonstrates why events now fail, but with the error passed. As shown, the decay vertex (blue circle) is now further away from the largest energy kaon fiber (58.3 MeV or 42.4 MeV). The opposite is true of Figures Fig. 8 and Fig. 9 were the decay vertex is closer to the largest energy fiber.

The rejection from TIMKF comes mostly from two linear fits. The first is projection of the kaon path in the x-y plane as a function of time. The second is the range of the kaon in the target as a function of time. The range is determined from the energy deposited in the target. The quantities `xprob1` and `xprob2` are flat probability distributions from

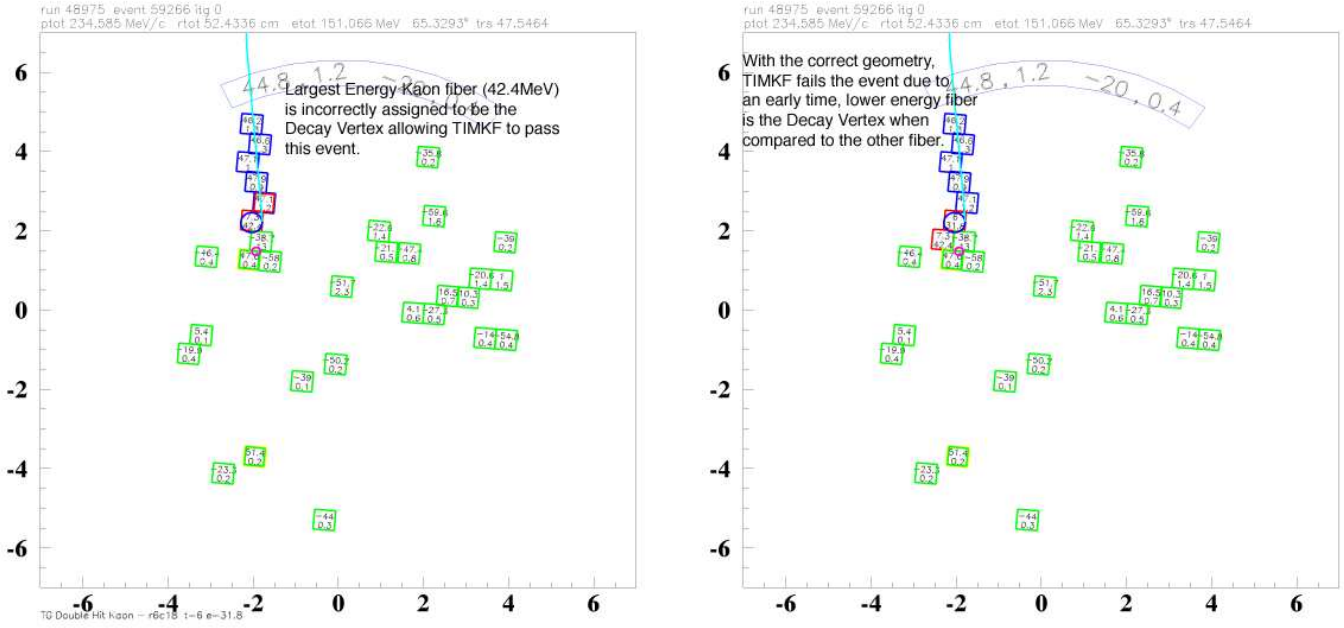

(a) Before Fix: Passes

(b) After Fix: Fails

Figure 7: **Display showing TIMKF Error**. These events, after TIMKF is corrected, fail. Display for (a) shows effect of error on kaon fiber positions relative to the kaon entry (stopping) position as determined by B4 (swathccd) as used by TIMKF. The error does not affect any other cut or the positions of the kaons used by the reconstruction. The kaon fibers are shifted in (a) for display purposes only.

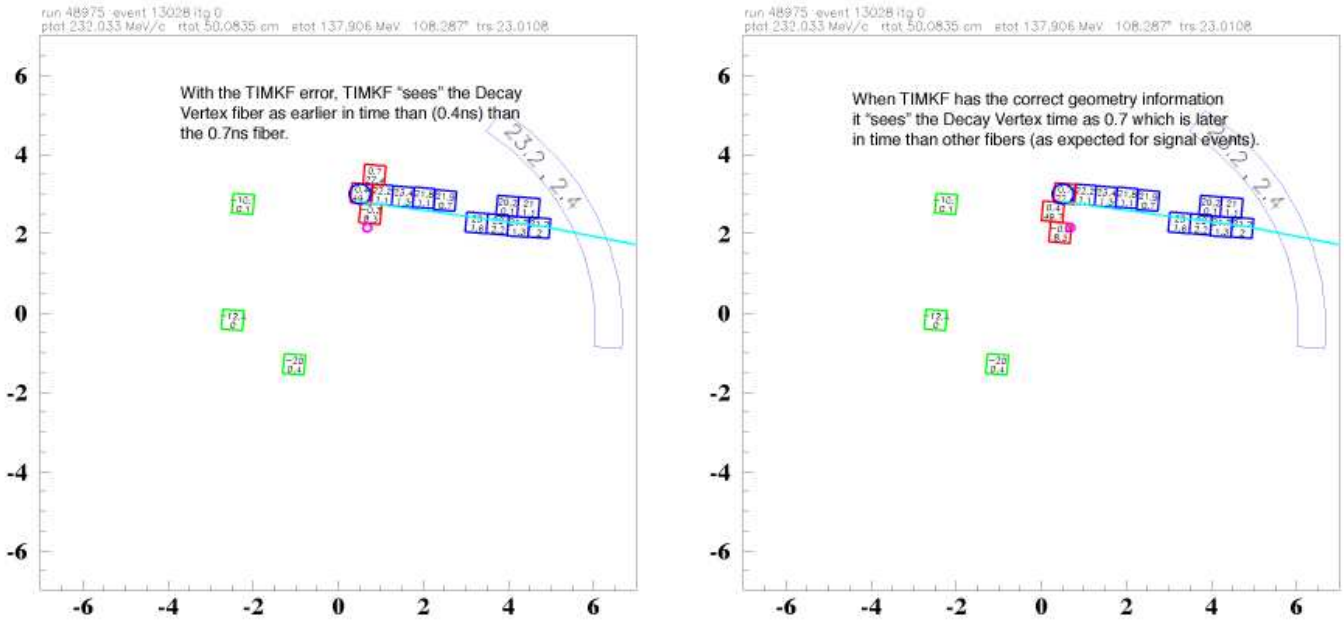

(a) Before Fix: Fails

(b) After Fix: Passes

Figure 8: **Display showing TIMKF Error**. These events, after TIMKF is corrected, pass. Display for (a) shows effect of error on kaon fiber positions relative to the kaon entry (stopping) position as determined by B4 (swathccd) as used by TIMKF. The error does not affect any other cut or the positions of the kaons used by the reconstruction. The kaon fibers are shifted in (a) for display purposes only.

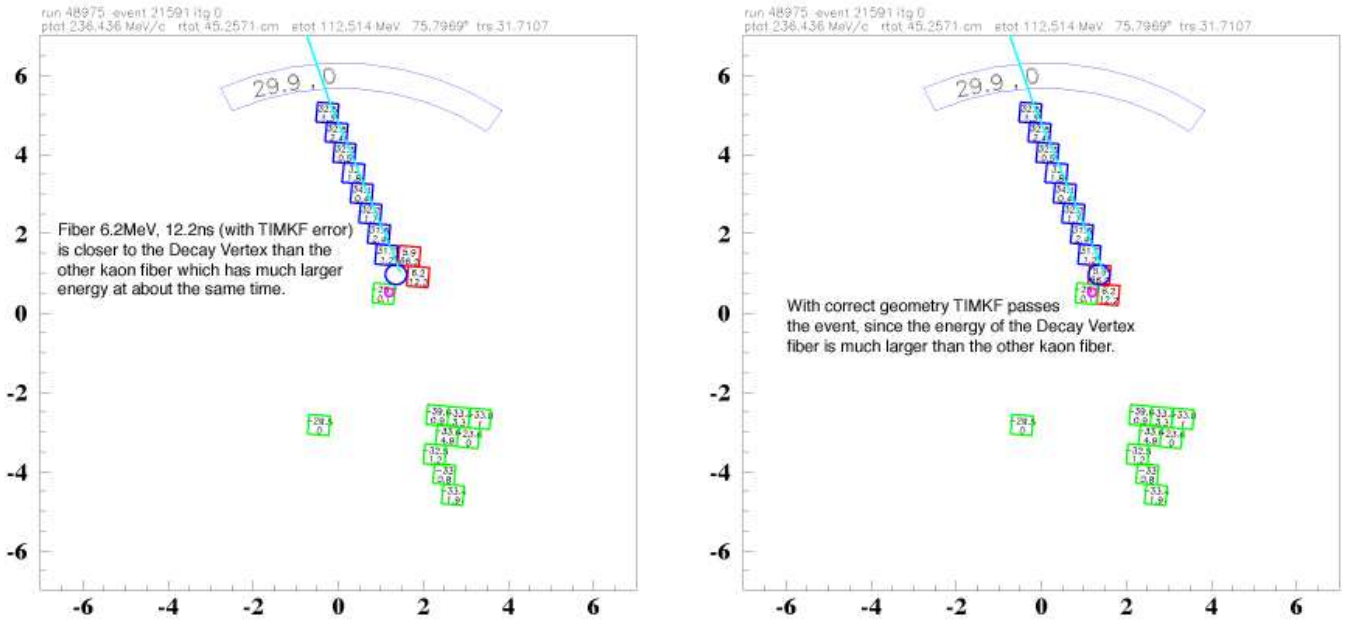

(a) Before Fix: Fails

(b) After Fix: Passes

Figure 9: **Display showing TIMKF Error**. These events, after TIMKF is corrected, pass. Display for (a) shows effect of error on kaon fiber positions relative to the kaon entry (stopping) position as determined by B4 (swathccd) as used by TIMKF. The error does not affect any other cut or the positions of the kaons used by the reconstruction. The kaon fibers are shifted in (a) for display purposes only.

	Before Fix	After Fix
Rejection	(from $\kappa_{\pi 2}$ target-scatter normalization branch)	
	6812/5542 = 1.229	6812/5702 1.195
Acceptance	(from Beam/Target acceptance measurement using km21)	
	0.9025	0.9205
Acceptance × Rejection		
	1.109	1.099

Table 5: Effects of fixing TIMKF bug

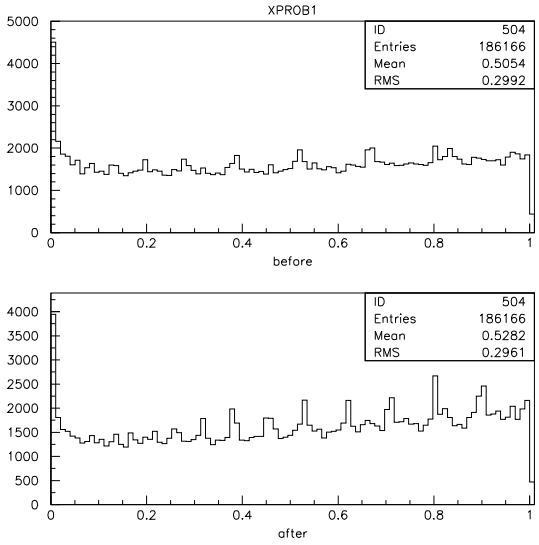

Figure 10: The distribution of TIMKF quantity `xprob1` before and after the TIMKF fix. TIMKF rejects events having `xprob1` less than 0.05.

the modified chi-square of the two fits. The distributions of these two quantities can be seen in Figures 10 and 11. The TIMKF fix caused these distributions to have a slight increasing slope as compared to a fairly flat distribution observed before the TIMKF fix. Events having a probability of less than 0.05 for either `xprob1` or `xprob2` are rejected. The effect of having slightly non-flat (sloped upward) distributions is that slightly less events are rejected, which is consistent with the observed change in performance of the cut.

The adjustable quantity used to cut events in TIMKF is the slope of the time versus kaon range fit which gives an inverse velocity of the kaon `velzk` in the z-direction. Plots of this quantity before and after the TIMKF fix are shown in Figure 12. Although it can be observed that the distribution became more narrow after the fix, the cut is set to reject only events beyond 5σ of the 'before' distribution. As a result, this cut on `velzk` is expected to cause a negligible change on the overall performance of the cut.

Note that there were previously two additional failing conditions in TIMKF based on the intercept of the two fits. These cutting conditions were removed to allow late kaons.

2.8 Change to Photon Veto

PVCUTPNN2, *pvcut02_new.function*, has three acc/rej points which were optimized by Ilektra. The chosen parameters had an approximate acceptance of 30% (tight PV, PV30), 60% (nominal PV, PV60), and 90% (loose PV, PV90); the parameters used in E949-PNN1 (PVPNN1) are also used in some cases when a very loose PV cut is required. In all studies prior to May 15, 2008 parts of the PV30 parameter space was outside PV60. This implied that an event could exist in the tight signal region and outside the loose signal region. Therefore, it was decided to redefine PV30 as the application of PV30 and PV60 parameters shown in Table 6. Henceforth, the notation PV30 (and subsystem cuts such as TGPV with PV30 parameters) will imply the application of PV30 and PV60 parameters. The acceptances of the offline PV cuts (the offline cuts comprising *pvcut02_new.function*) are the following:

- $A_{PV30} \equiv A_{PV30+PV60} = 0.3234 \pm 0.0022$

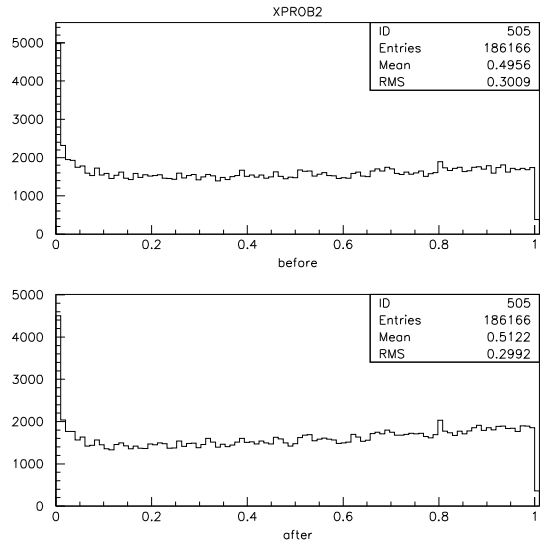

Figure 11: The distribution of TIMKF quantity `xprob2` before and after the TIMKF fix. TIMKF rejects events having `xprob2` less than 0.05.

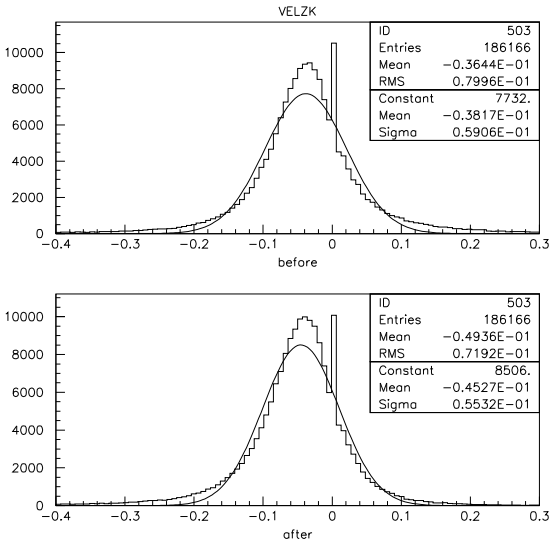

Figure 12: The distribution of TIMKF quantity `velzk` before and after the TIMKF fix. TIMKF rejects events having $|velzk + 0.036| > 0.75$ which is approximately 5σ.

- $A_{PV60} = 0.6199 \pm 0.0022$
- $A_{PV90} = 0.8855 \pm 0.0014$
- $A_{PVPNN1} = 0.925$

2.9 PVCUT

The PASS2 SKIM cut PVCUT has the parameters listed in Table 7. The acceptance of PVCUT is 0.9617 ± 0.00085.

2.10 OR versus AND of the SKIM cuts

It was decided that the signal region is comprised of the AND of the SKIMs, instead of the OR of the SKIMs. This implies that all cuts making up the SKIMs are applied. SKIMs 1-3 are the 2/3 sample and SKIMs 5-7 are the 1/3 sample. The SKIM cuts are define as follows:

- SKIM1(5) = FITPI, PSCUT, TGCUT
- SKIM2(6) = PSCUT, TGCUT, PVCUT, TGPVCUT, DELCO
- SKIM3(7) = FITPI, TGCUT, PVCUT, TGPVTR

This change impacts all normalization branches; since most normalization branches have 0 or 1 event no change will occur. This change does impact the 1-cut failure study, since PVCUT has some additional rejection after PV60 is applied.

3 $K_{\pi 2}$-Scatter background

3.1 $K^+ \to \pi^+\pi^o$ Target Scatters

The $K_{\pi 2}$ decay, where the π^+ scatters in the target, is the dominant background for the $\pi\nu\overline{\nu}(2)$ analysis [2]. As it has been shown with Monte Carlo simulations [4] , the photon distribution from the π^o decay is more uniform in polar angle for events where the π^+ has scattered in the target, than for unscattered ones. Therefore, the PV rejection for TG scatter events is expected to be different than that for $K_{\pi 2}$ events in the peak. The π^+ kinematics cannot be used in the bifurcation study, since the PV rejection has to be measured inside the $\pi\nu\overline{\nu}(2)$ kinematic box.

3.1.1 Rejection Branch

The other set of cuts used to suppress this background are the target quality cuts (TGCUT06). These eliminate events with evidence of a scattered pion in the target, either the scatter occurred outside the Kaon fibers (scatters visible in xy, or "xy-scatters") or inside them (events where the π^+ started in the beam direction and then scattered into the detector acceptance, or "z-scatters"). The two categories are not mutually exclusive. By inverting some of these cuts and applying others, samples with varying mixtures of xy- and z-scatters can be created for the rejection branch. These samples will be contaminated to an extent with K_{e4}, $K_{\pi 2\gamma}$ and Charge Exchange background, but the contamination is shown to be small [3]. Thirteen such "classes" were used, described in Table 8, and the PV rejection was measured on them in the $\pi\nu\overline{\nu}(2)$ kinematic box (Table 9) . The PV

Category	PV90 (Loose)			PV60 (Nominal)			PV30 (Tight)		
	Timing (ns)		Ener	Timing (ns)		Ener	Timing (ns)		Ener
	offset	window	(MeV)	offset	window	(MeV)	offset	window	(MeV)
BV	-0.15	4.00	0.50	2.25	7.95	0.20	1.35	8.85	0.70
early_{BV}	-19.15	15.0	30.0†	-20.7	15.0	30.00†	-22.5	15.0	30.0†
BVL	0.35	1.75	0.40	3.15	7.55	0.30	3.55	7.05	0.30
RS	-0.85	1.45	0.20	0.05	4.30	0.30	2.25	5.55	0.60
EC outer	0.15	1.80	2.20	1.80	6.15	0.40	1.75	7.75	0.20
EC inner	-0.35	2.30	1.00	0.99	4.64	0.20	-2.45	11.55	0.20
$\text{EC2}^{nd}\text{pulse}$	-2.75	0.32	18.80	-1.60	4.07	10.60	-1.51	4.19	1.70
TG	0.25	1.50	5.20	-0.25	2.40	2.00	-2.15	4.40	1.40
IC	-0.50	2.75	13.00	1.25	3.25	5.00	3.20	6.10	5.00
VC	-0.25	1.50	3.80	-2.40	4.15	6.80	-0.20	7.25	6.00
CO	2.60	1.23	1.80	2.90	2.95	0.60	2.15	2.95	1.60
μCO	-1.50	2.50	3.60	-1.60	3.90	3.00	-0.60	3.90	0.60
AD	3.00	5.00	0.60	3.00	5.00	0.60	3.00	5.00	0.60
DSPV	2.50	7.50	0.00	2.50	7.50	0.00	2.50	7.50	0.00
$\text{early}_{\text{BVL}}{}^{\ddagger}$	-3.50	1.50	10.00	-3.50	1.50	10.00	-3.50	1.50	10.00

Single-end hit categories

	hit-ends								
	E	t							
BV	B	S	0.55	13.05	0.40	3.05	15.95	1.00	0.55	13.05	0.40
BV	S	B	4.00	3.10	0.60	4.80	1.50	1.40	4.00	3.10	0.60
BV	S	S	-8.30	6.90	1.00	-8.10	8.50	1.60	-8.30	6.90	1.00
BVL	B	S	-5.65	11.80	8.19	-5.65	11.80	8.19	-5.65	11.80	8.19
RS	B	S	0.01	5.36	0.20	-2.85	0.70	5.20	0.01	5.36	0.20
RS	S	B	3.70	6.10	0.00	6.60	1.35	0.00	3.70	6.10	0.00
RS	S	S	-11.54	4.53	0.60	-6.80	1.22	3.40	-11.54	4.53	0.60

Table 6: PV30,60,90 photon cut parameters. The time window is shown in ns and energy threshold in MeV. An event is cut if the energy of all coincident hits sum to greater than the energy threshold. $|t - t_{RS} - t_{offset}| < t_{window}$ is defined as in coincidence for hit time t. EC inner are hits in the upstream inner ring ($elempvec \leq 13$) and EC outer are all other hits in the ECs($elempvec > 13$). † The energy threshold of early_{BV} is with respect to each hit (i.e. a hit within the time window must exceed 30MeV for the event to be cut). ‡ The additional time constraint of the time difference of the module is less than 4.0ns ($tzpvbl(i) < 4.0$). The BV, BVL, and RS photon cuts require both ends of the detector obtain a result for time and energy. Additional photon cuts are applied when the both-ends requirement in time and energy are not met. S=*single* refers to a hit in only one end of the detector observed in either *energy* or *time*. B=*both* means both ends were hit and *N* means a hit was not observed in either end.

	Timing (ns)		E
	offset	window	(MeV)
BV	0.0	2.0	1.5
RS	0.0	1.0	3.0
EC	0.0	1.5	3.5
TGPVCUT	0.8	1.0	5.0

Table 7: $|t - t_{RS} - t_{offset}| < t_{window}$ is defined as in coincidence for hit time t.

CLASS	TGCUTS
1	All cuts, KP2BOX
2	$\overline{CCDPUL}$, $\overline{EPIONK}$
3	$\overline{CCDPUL}$, $\overline{EPIONK}$, all others
4	CCDPUL, EPIONK, TGZFOOL, EIC, OPSVETO, $\overline{OTHERS}$
5	$\overline{CCDPUL}$, $\overline{EPIONK}$, $\overline{CHI567}$, $\overline{VERRNG}$
6	$\overline{CCDPUL}$, $\overline{EPIONK}$, $\overline{CHI567}$, $\overline{VERRNG}$, all others
7	$\overline{CHI567}$, $\overline{VERRNG}$
8	$\overline{CHI567}$, $\overline{VERRNG}$, all others
9	$\overline{CCDPUL}$, $\overline{EPIONK}$, $\overline{CHI567}$, $\overline{VERRNG}$, KIC, PIGAP, TARGF, TPICS
10	$\overline{B4EKZ}$
11	$\overline{B4EKZ}$, all others
12	$\overline{CCDPUL}$, $\overline{EPIONK}$, $\overline{B4EKZ}$
13	$\overline{CCDPUL}$, $\overline{EPIONK}$, $\overline{B4EKZ}$, all others

Table 8: Definition of the classes of events (2-13) used to measure the PV rejection in the $\pi\nu\overline{\nu}(2)$ kinematic box. Class 1 events have passed all the TG quality cuts, therefore they are required to be in the $K_{\pi 2}$ kinematic box as to not look in the signal region. All Classes that have either CCDPUL applied or CCDPUL inverted have the three associated safety cuts (CCDBADFIT, CCDBADTIM and CCD31FIB) applied. The nomenclature $\overline{CCDPUL}$, $\overline{EPIONK}$ means $\overline{CCDPUL} + \overline{EPIONK}$.

Loose Rejection Branch - Loose PNN2 Box + PV60

CLASS		bef. PV	af. PV	PV Rejection	Background
1	1/3	61410	36	1705.8±284.2	0.929±0.160
	2/3	122581	106	1156.4±112.3	1.468±0.149
2	1/3	24396	9	2710.7±903.4	0.585±0.197
	2/3	49032	21	2334.9±509.4	0.727±0.160
3	1/3	2776	3	925.3±534.0	1.714±0.993
	2/3	5495	2	2747.5±1942.4	0.618±0.437
4	1/3	4159	3	1386.3±800.1	1.143±0.662
	2/3	8092	1	8092.0±8091.5	0.210±0.210
5	1/3	29899	12	2491.6±719.1	0.636±0.186
	2/3	59871	22	2721.4±580.1	0.624±0.134
6	1/3	4170	3	1390.0±802.2	1.140±0.660
	2/3	8452	3	2817.3±1626.3	0.602±0.348
7	1/3	24574	6	4095.7±1671.8	0.387±0.159
	2/3	49636	18	2757.6±649.8	0.615±0.146
8	1/3	353	0	353.0±352.5	4.500±4.511
	2/3	644	0	644.0±643.5	2.638±2.642
9	1/3	23736	10	2373.6±750.4	0.668±0.213
	2/3	47463	19	2498.1±573.0	0.679±0.157
10	1/3	11037	4	2759.2±1379.4	0.574±0.288
	2/3	22037	10	2203.7±696.7	0.770±0.245
11	1/3	45	0	45.0±44.5	36.000±36.443
	2/3	64	0	64.0±63.5	26.929±27.154
12	1/3	26317	10	2631.7±832.1	0.602±0.192
	2/3	52621	22	2391.9±509.8	0.710±0.153
13	1/3	3319	3	1106.3±638.5	1.433±0.830
	2/3	6503	2	3251.5±2298.8	0.522±0.369

Table 9: The rejection branch for the $K_{\pi 2}$ TG scatter background in the loose box: PV rejection using the loose photon veto (PV60) for the $\pi\nu\overline{\nu}(2)$ box and the resulting background. The same setup cuts as in the loose normalization branch (Table 19) are applied.

Tight Rejection Branch - Loose PNN2 Box + PV30

CLASS		bef. PV	af. PV	PV Rejection	Background
1	1/3	61410	13	4723.9±1310.0	0.168±0.048
	2/3	122581	44	2785.9±419.9	0.276±0.043
2	1/3	24396	3	8132.0±4694.7	0.098±0.057
	2/3	49032	8	6129.0±2166.8	0.125±0.045
3	1/3	2776	1	2776.0±2775.5	0.286±0.287
	2/3	5495	1	5495.0±5494.5	0.140±0.140
4	1/3	4159	0	4159.0±4158.5	0.191±0.192
	2/3	8092	1	8092.0±8091.5	0.095±0.095
5	1/3	29899	4	7474.8±3737.1	0.106±0.054
	2/3	59871	8	7483.9±2645.8	0.103±0.037
6	1/3	4170	1	4170.0±4169.5	0.191±0.191
	2/3	8452	1	8452.0±8451.5	0.091±0.091
7	1/3	24574	1	24574.0±24573.5	0.032±0.032
	2/3	49636	7	7090.9±2679.9	0.108±0.041
8	1/3	353	0	353.0±352.5	2.259±2.266
	2/3	644	0	644.0±643.5	1.194±1.196
9	1/3	23736	3	7912.0±4567.7	0.100±0.058
	2/3	47463	7	6780.4±2562.6	0.113±0.043
10	1/3	11037	1	11037.0±11036.5	0.072±0.072
	2/3	22037	2	11018.5±7790.9	0.070±0.049
11	1/3	45	0	45.0±44.5	18.068±18.307
	2/3	64	0	64.0±63.5	12.191±12.299
12	1/3	26317	4	6579.2±3289.4	0.121±0.061
	2/3	52621	8	6577.6±2325.4	0.117±0.042
13	1/3	3319	1	3319.0±3318.5	0.240±0.240
	2/3	6503	1	6503.0±6502.5	0.118±0.118

Table 10: The rejection branch for the $K_{\pi 2}$ TG scatter background in the tight box: PV rejection using the tight photon veto (PV30) for the $\pi\nu\overline{\nu}(2)$ box and the resulting background. The same setup cuts as in the tight normalization branch (Table 20) are applied.

CLASS	Events	PV Rejection
1	122581(500)	245.162±10.9
2	49032(273)	179.604±10.8
3	5495 (34)	161.618±27.6
4	8092 (37)	218.703±35.9
5	59871(330)	181.427±10.0
6	8452 (53)	159.472±21.8
7	49636(256)	193.891±12.1
8	644 (5)	128.8±57.4
9	47463(274)	173.223±10.4
10	22037(141)	156.291±13.1
11	64 (1)	64±63.5
12	52621(302)	174.242±10.0
13	6503 (40)	162.575±25.6

Table 11: PV90 Rejection for the 13 $K_{\pi 2}$ TG scatter classes. The numbers in brackets are the statistical uncertainties.

CLASS	Events	PV Rejection
1	122581(1529)	80.1707±2.0
2	49032(1227)	39.9609±1.1
3	5495 (175)	31.4±2.3
4	8092 (171)	47.3216±3.6
5	59871(1456)	41.1202±1.1
6	8452 (269)	31.4201±1.9
7	49636(1136)	43.6937±1.3
8	644 (15)	42.9333±11.0
9	47463(1237)	38.3694±1.1
10	22037 (503)	43.8111±1.9
11	64 (2)	32±22.3
12	52621(1317)	39.9552±1.1
13	6503 (208)	31.2644±2.1

Table 12: PVPNN1 Rejection for the 13 $K_{\pi 2}$ TG scatter classes. The numbers in brackets are the statistical uncertainties.

rejections measured for different classes are consistent with each other within statistical uncertainties.

For the final PV rejection, class 12 was used, because it had adequate statistics and it is expected to be the richest in z-scatters, since the cuts that mainly attack them are inverted: CCDPUL and EPIONK cut events with large pulses in the kaon fibers at trs, and B4EKZ rejects events in which the z position of the decay vertex found by the UTC does not agree with the kaon energy deposit (and thus path length) in the target. Both these signatures are characteristic of a decay pion that started in the beam direction in the kaon fiber, and then scattered into the detector.

Updated May 31, 2008: The difference in PV rejection between the class with adequate statistics having the highest rejection and that of CLASS12 was used to estimate the upper bound on the the systematic uncertainty. The difference in PV rejection between CLASS12 and CLASS1 (the rejection of the Kp2-peak) was used to estimate the lower bound on the systematic uncertainty. The reason that CLASS1 is used to estimate the lower bound is that it should provide a reasonable estimate of the rejection of xy-scatters where CLASS12 provides a reasonable estimate of z-scatters.

Due to the loss of statistics in the rejection branch for the tight box [1], the rejection of the tight (30%) photon veto is measured on a rejection branch that uses the loose versions of the kinematic box, the TD cuts and DELCO. In doing this it is assumed that the rejection of the (30%) photon veto on these classes is the same for the loose and tight cuts. Tables 13 and 14 show that the rejection does not change within statistical error when applying the tight versions of these cuts to the 1/3 and 2/3 data sets respectively. Tables 22 and 23 summarize the photon veto rejections and other values used in the background estimation.

3.1.2 Normalization Branch

In the normalization branch (see Tables 19, 20 and 21), all the cuts in TGCUT06 were applied, and the PV was inverted. Some contamination from $K_{\pi 2}$-RS scatters and $K_{\pi 2\gamma}$ is expected, but these backgrounds are small compared to $K_{\pi 2}$-TG scatters. The ptot distribution of the events remaining in the normalization branch after the inversion of PVCUTPNN2, after the application of all the TGCUT06 except CCDPUL, and after the application of CCDPUL is shown in Figure 13. In the same figure, the ptot distribution of the events in class 12 of the rejection branch is also shown before and after PVCUTPNN2. Both of those distributions look adequately $K_{\pi 2}$-scatter-like. Tables 22 and 23 summarize the normalization values used for the background estimation.

Updated May 31, 2008: To estimate the target scatter background, the normalization numbers found in Tables 19 and 21 are corrected for range stack scatter contamination using Equation 5

3.1.3 Background

Updated May 31, 2008: An additional section (Section 3.1.4) was added discussing the correction due to $K_{\pi 2\gamma}$ contamination in the $K_{\pi 2}$ target scatter normalization branch. The background estimate performed in this section will be referred to as the uncorrected background estimate.

The uncorrected $K_{\pi 2}$ target scatter background for the loose box $n_{K_{\pi 2}-TGscat}$(loose, uncorrected) is given by

$$n_{K_{\pi 2}-TGscat}(\text{loose, uncorrected}) \;=\; \frac{N_{tg}}{R_{PV(60\%)} - 1} \qquad (1)$$

[1] Here, the tight box refers to the application of the tight KIN, TD and DELCO cuts

PV30 Rejection - 1/3 Sample

CLASS	All Loose	Ke4 Box	DELCO6	TDTIGHT	All Tight
2	24396/3 = 8132±4694.7	18325/3 = 6108.33±3526.4	21009/1 = 21009±21008.5	18205/1 = 18205±18204.5	11769/0 = 11769±11768.5
3	2776/1 = 2776±2775.5	2127/1 = 2127±2126.5	2229/1 = 2229±2228.5	2102/0 = 2102±2101.5	1293/0 = 1293±1292.5
4	4159/0 = 4159±4158.5	3210/0 = 3210±3209.5	3682/0 = 3682±3681.5	3087/0 = 3087±3086.5	2088/0 = 2088±2087.5
5	29899/4 = 7474.75±3737.1	22550/4 = 5637.5±2818.5	26049/2 = 13024.5±9209.4	22282/2 = 11141±7877.5	14625/1 = 14625±14624.5
6	4170/1 = 4170±4169.5	3232/1 = 3232±3231.5	3380/1 = 3380±3379.5	3152/0 = 3152±3151.5	1974/0 = 1974±1973.5
7	24574/1 = 24574±24573.5	18632/1 = 18632±18631.5	21929/1 = 21929±21928.5	18317/1 = 18317±18316.5	12376/1 = 12376±12375.5
8	353/0 = 353±352.5	292/0 = 292±291.5	302/0 = 302±301.5	252/0 = 252±251.5	183/0 = 183±182.5
9	23736/3 = 7912±4567.7	17851/3 = 5950.33±3435.1	20321/1 = 20321±20320.5	17658/1 = 17658±17657.5	11367/0 = 11367±11366.5
10	11037/1 = 11037±11036.5	7981/1 = 7981±7980.5	9876/1 = 9876±9875.5	8211/1 = 8211±8210.5	5292/1 = 5292±5291.5
11	45/0 = 45±44.5	40/0 = 40±39.5	37/0 = 37±36.5	31/0 = 31±30.5	23/0 = 23±22.5
12	26317/4 = 6579.25±3289.4	19741/4 = 4935.25±2467.4	22780/2 = 11390±8053.6	19624/2 = 9812±6937.8	12725/1 = 12725±12724.5
13	3319/1 = 3319±3318.5	2509/1 = 2509±2508.5	2655/1 = 2655±2654.5	2496/0 = 2496±2495.5	1507/0 = 1507±1506.5

Table 13: Rejection of the tight (30%) photon veto for the 1/3 sample for the various classes with different combinations of loose and tight versions of the setup cuts: kinematic box cut, TD cuts and DELCO. The "All Loose" and "All Tight" columns mean that those three sets of cuts were all loose or all tight. For the other three columns, all the cuts are loose except the one listed, which is tight. The numbers shown are the number of events before the photon veto is applied divided by the number of events remaining after the photon veto is applied and the resulting rejection with statistical error. If there are zero events remaining after the photon veto is applied, the rejection is determined assuming 1 event remained.

PV30 Rejection - 2/3 Sample

CLASS	All Loose	Ke4 Box	DELCO6	TDTIGHT	All Tight
2	49032/8 = 6129±2166.8	36782/7 = 5254.57±1985.9	42225/6 = 7037.5±2872.8	36610/6 = 6101.67±2490.8	23594/5 = 4718.8±2110.1
3	5495/1 = 5495±5494.5	4159/1 = 4159±4158.5	4386/1 = 4386±4385.5	4132/1 = 4132±4131.5	2516/1 = 2516±2515.5
4	8092/1 = 8092±8091.5	6217/0 = 6217±6216.5	7240/0 = 7240±7239.5	6028/1 = 6028±6027.5	4099/0 = 4099±4098.5
5	59871/8 = 7483.88±2645.8	45017/7 = 6431±2430.5	52195/6 = 8699.17±3551.2	44707/6 = 7451.17±3041.7	29228/5 = 5845.6±2614
6	8452/1 = 8452±8451.5	6504/1 = 6504±6503.5	6877/1 = 6877±6876.5	6397/1 = 6397±6396.5	4028/1 = 4028±4027.5
7	49636/7 = 7090.86±2679.9	37524/6 = 6254±2553	44381/4 = 11095.3±5547.4	37010/6 = 6168.33±2518	24929/4 = 6232.25±3115.9
8	644/0 = 644±643.5	512/0 = 512±511.5	561/0 = 561±560.5	491/0 = 491±490.5	343/0 = 343±342.5
9	47463/7 = 6780.43±2562.6	35430/7 = 5061.43±1912.9	40735/6 = 6789.17±2771.5	35500/5 = 7100±3175	22676/5 = 4535.2±2028
10	22037/2 = 11018.5±7790.9	15971/1 = 15971±15970.5	19757/1 = 19757±19756.5	16501/2 = 8250.5±5833.6	10710/1 = 10710±10709.5
11	64/0 = 64±63.5	49/0 = 49±48.5	53/0 = 53±52.5	44/0 = 44±43.5	30/0 = 30±29.5
12	52621/8 = 6577.63±2325.4	39481/7 = 5640.14±2131.6	45574/6 = 7595.67±3100.7	39287/6 = 6547.83±2672.9	25471/5 = 5094.2±2278
13	6503/1 = 6503±6502.5	4861/1 = 4861±4860.5	5218/1 = 5218±5217.5	4880/1 = 4880±4879.5	2956/1 = 2956±2955.5

Table 14: Rejection of the tight (30%) photon veto for the 2/3 sample for the various classes with different combinations of loose and tight versions of the setup cuts: kinematic box cut, TD cuts and DELCO. The "All Loose" and "All Tight" columns mean that those three sets of cuts were all loose or all tight. For the other three columns, all the cuts are loose except the one listed, which is tight. The numbers shown are the number of events before the photon veto is applied divided by the number of events remaining after the photon veto is applied and the resulting rejection with statistical error. If there are zero events remaining after the photon veto is applied, the rejection is determined assuming 1 event remained.

PV60 Rejection - 1/3 Sample

CLASS	All Loose	Ke4 Box	DELCO6	TDTIGHT	All Tight
2	24396/9 = 2710.67±903.4	18325/7 = 2617.86±989.3	21009/3 = 7003±4042.9	18205/4 = 4551.25±2275.4	11769/1 = 11769±11768.5
3	2776/3 = 925.333±534	2127/3 = 709±409.1	2229/2 = 1114.5±787.7	2102/1 = 2102±2101.5	1293/1 = 1293±1292.5
4	4159/3 = 1386.33±800.1	3210/1 = 3210±3209.5	3682/3 = 1227.33±708.3	3087/3 = 1029±593.8	2088/1 = 2088±2087.5
5	29899/12 = 2491.58±719.1	22550/8 = 2818.75±996.4	26049/6 = 4341.5±1772.2	22282/7 = 3183.14±1202.9	14625/2 = 7312.5±5170.4
6	4170/3 = 1390±802.2	3232/3 = 1077.33±621.7	3380/2 = 1690±1194.7	3152/1 = 3152±3151.5	1974/1 = 1974±1973.5
7	24574/6 = 4095.67±1671.8	18632/2 = 9316±6587.1	21929/4 = 5482.25±2740.9	18317/5 = 3663.4±1638.1	12376/2 = 6188±4375.2
8	353/0 = 353±352.5	292/0 = 292±291.5	302/0 = 302±301.5	252/0 = 252±251.5	183/0 = 183±182.5
9	23736/10 = 2373.6±750.4	17851/7 = 2550.14±963.7	20321/4 = 5080.25±2539.9	17658/5 = 3531.6±1579.2	11367/1 = 11367±11366.5
10	11037/4 = 2759.25±1379.4	7981/3 = 2660.33±1535.7	9876/2 = 4938±3491.3	8211/3 = 2737±1579.9	5292/2 = 2646±1870.7
11	45/0 = 45±44.5	40/0 = 40±39.5	37/0 = 37±36.5	31/0 = 31±30.5	23/0 = 23±22.5
12	26317/10 = 2631.7±832.1	19741/8 = 2467.63±872.3	22780/4 = 5695±2847.2	19624/5 = 3924.8±1755	12725/2 = 6362.5±4498.6
13	3319/3 = 1106.33±638.5	2509/3 = 836.333±482.6	2655/2 = 1327.5±938.3	2496/1 = 2496±2495.5	1507/1 = 1507±1506.5

Table 15: Rejection of the loose (60%) photon veto for the 1/3 sample for the various classes with different combinations of loose and tight versions of the setup cuts: kinematic box cut, TD cuts and DELCO. The "All Loose" and "All Tight" columns mean that those three sets of cuts were all loose or all tight. For the other three columns, all the cuts are loose except the one listed, which is tight. The numbers shown are the number of events before the photon veto is applied divided by the number of events remaining after the photon veto is applied and the resulting rejection with statistical error. If there are zero events remaining after the photon veto is applied, the rejection is determined assuming 1 event remained.

PV60 Rejection - 2/3 Sample

CLASS	All Loose	Ke4 Box	DELCO6	TDTIGHT	All Tight
2	49032/21 = 2334.86±509.4	36782/18 = 2043.44±481.5	42225/18 = 2345.83±552.8	36610/18 = 2033.89±479.3	23594/15 = 1572.93±406
3	5495/2 = 2747.5±1942.4	4159/2 = 2079.5±1470.1	4386/2 = 2193±1550.3	4132/2 = 2066±1460.5	2516/2 = 1258±889.2
4	8092/1 = 8092±8091.5	6217/0 = 6217±6216.5	7240/0 = 7240±7239.5	6028/1 = 6028±6027.5	4099/0 = 4099±4098.5
5	59871/22 = 2721.41±580.1	45017/18 = 2500.94±589.4	52195/19 = 2747.11±630.1	44707/19 = 2353±539.7	29228/15 = 1948.53±503
6	8452/3 = 2817.33±1626.3	6504/3 = 2168±1251.4	6877/3 = 2292.33±1323.2	6397/3 = 2132.33±1230.8	4028/3 = 1342.67±774.9
7	49636/18 = 2757.56±649.8	37524/13 = 2886.46±800.4	44381/13 = 3413.92±946.7	37010/16 = 2313.13±578.2	24929/10 = 2492.9±788.2
8	644/0 = 644±643.5	512/0 = 512±511.5	561/0 = 561±560.5	491/0 = 491±490.5	343/0 = 343±342.5
9	47463/19 = 2498.05±573	35430/17 = 2084.12±505.4	40735/17 = 2396.18±581	35500/16 = 2218.75±554.6	22676/14 = 1619.71±432.8
10	22037/10 = 2203.7±696.7	15971/4 = 3992.75±1996.1	19757/5 = 3951.4±1766.9	16501/9 = 1833.44±611	10710/4 = 2677.5±1338.5
11	64/0 = 64±63.5	49/0 = 49±48.5	53/0 = 53±52.5	44/0 = 44±43.5	30/0 = 30±29.5
12	52621/22 = 2391.86±509.8	39481/18 = 2193.39±516.9	45574/19 = 2398.63±550.2	39287/19 = 2067.74±474.3	25471/15 = 1698.07±438.3
13	6503/2 = 3251.5±2298.8	4861/2 = 2430.5±1718.3	5218/2 = 2609±1844.5	4880/2 = 2440±1725	2956/2 = 1478±1044.8

Table 16: Rejection of the loose (60%) photon veto for the 2/3 sample for the various classes with different combinations of loose and tight versions of the setup cuts: kinematic box cut, TD cuts and DELCO. The "All Loose" and "All Tight" columns mean that those three sets of cuts were all loose or all tight. For the other three columns, all the cuts are loose except the one listed, which is tight. The numbers shown are the number of events before the photon veto is applied divided by the number of events remaining after the photon veto is applied and the resulting rejection with statistical error. If there are zero events remaining after the photon veto is applied, the rejection is determined assuming 1 event remained.

PV90 Rejection - 1/3 Sample

CLASS	All Loose	Ke4 Box	DELCO6	TDTIGHT	All Tight
2	24396/125 = 195.168±17.4	18325/91 = 201.374±21.1	21009/92 = 228.359±23.8	18205/98 = 185.765±18.7	11769/57 = 206.474±27.3
3	2776/12 = 231.333±66.6	2127/12 = 177.25±51	2229/8 = 278.625±98.3	2102/8 = 262.75±92.7	1293/6 = 215.5±87.8
4	4159/29 = 143.414±26.5	3210/21 = 152.857±33.2	3682/25 = 147.28±29.4	3087/22 = 140.318±29.8	2088/12 = 174±50.1
5	29899/161 = 185.708±14.6	22550/117 = 192.735±17.8	26049/123 = 211.78±19.1	22282/126 = 176.841±15.7	14625/74 = 197.635±22.9
6	4170/13 = 320.769±88.8	3232/13 = 248.615±68.8	3380/9 = 375.556±125	3152/9 = 350.222±116.6	1974/7 = 282±106.4
7	24574/119 = 206.504±18.9	18632/89 = 209.348±22.1	21929/93 = 235.796±24.4	18317/94 = 194.862±20	12376/58 = 213.379±28
8	353/0 = 353±352.5	292/0 = 292±291.5	302/0 = 302±301.5	252/0 = 252±251.5	183/0 = 183±182.5
9	23736/123 = 192.976±17.4	17851/91 = 196.165±20.5	20321/91 = 223.308±23.4	17658/93 = 189.871±19.6	11367/54 = 210.5±28.6
10	11037/81 = 136.259±15.1	7981/55 = 145.109±19.5	9876/63 = 156.762±19.7	8211/66 = 124.409±15.3	5292/38 = 139.263±22.5
11	45/0 = 45±44.5	40/0 = 40±39.5	37/0 = 37±36.5	31/0 = 31±30.5	23/0 = 23±22.5
12	26317/140 = 187.979±15.8	19741/103 = 191.66±18.8	22780/105 = 216.952±21.1	19624/109 = 180.037±17.2	12725/66 = 192.803±23.7
13	3319/15 = 221.267±57	2509/15 = 167.267±43.1	2655/10 = 265.5±83.8	2496/11 = 226.909±68.3	1507/8 = 188.375±66.4

Table 17: Rejection of the very loose (90%) photon veto for the 1/3 sample for the various classes with different combinations of loose and tight versions of the setup cuts: kinematic box cut, TD cuts and DELCO. The "All Loose" and "All Tight" columns mean that those three sets of cuts were all loose or all tight. For the other three columns, all the cuts are loose except the one listed, which is tight. The numbers shown are the number of events before the photon veto is applied divided by the number of events remaining after the photon veto is applied and the resulting rejection with statistical error. If there are zero events remaining after the photon veto is applied, the rejection is determined assuming 1 event remained.

PV90 Rejection - 2/3 Sample

CLASS	All Loose	Ke4 Box	DELCO6	TDTIGHT	All Tight
2	49032/273 = 179.604±10.8	36782/197 = 186.711±13.3	42225/210 = 201.071±13.8	36610/207 = 176.86±12.3	23594/115 = 205.165±19.1
3	5495/34 = 161.618±27.6	4159/24 = 173.292±35.3	4386/22 = 199.364±42.4	4132/22 = 187.818±39.9	2516/11 = 228.727±68.8
4	8092/37 = 218.703±35.9	6217/29 = 214.379±39.7	7240/25 = 289.6±57.8	6028/29 = 207.862±38.5	4099/15 = 273.267±70.4
5	59871/330 = 181.427±10	45017/239 = 188.356±12.2	52195/251 = 207.948±13.1	44707/251 = 178.116±11.2	29228/135 = 216.504±18.6
6	8452/53 = 159.472±21.8	6504/38 = 171.158±27.7	6877/35 = 196.486±33.1	6397/38 = 168.342±27.2	4028/18 = 223.778±52.6
7	49636/256 = 193.891±12.1	37524/187 = 200.663±14.6	44381/200 = 221.905±15.7	37010/200 = 185.05±13	24929/110 = 226.627±21.6
8	644/5 = 128.8±57.4	512/4 = 128±63.7	561/3 = 187±107.7	491/3 = 163.667±94.2	343/1 = 343±342.5
9	47463/274 = 173.223±10.4	35430/196 = 180.765±12.9	40735/207 = 196.787±13.6	35500/208 = 170.673±11.8	22676/111 = 204.288±19.3
10	22037/141 = 156.291±13.1	15971/95 = 168.116±17.2	19757/111 = 177.991±16.8	16501/110 = 150.009±14.3	10710/61 = 175.574±22.4
11	64/1 = 64±63.5	49/1 = 49±48.5	53/1 = 53±52.5	44/1 = 44±43.5	30/1 = 30±29.5
12	52621/302 = 174.242±10	39481/213 = 185.357±12.7	45574/235 = 193.932±12.6	39287/230 = 170.813±11.2	25471/126 = 202.151±18
13	6503/40 = 162.575±25.6	4861/28 = 173.607±32.7	5218/26 = 200.692±39.3	4880/28 = 174.286±32.8	2956/15 = 197.067±50.8

Table 18: Rejection of the very loose (90%) photon veto for the 2/3 sample for the various classes with different combinations of loose and tight versions of the setup cuts: kinematic box cut, TD cuts and DELCO. The "All Loose" and "All Tight" columns mean that those three sets of cuts were all loose or all tight. For the other three columns, all the cuts are loose except the one listed, which is tight. The numbers shown are the number of events before the photon veto is applied divided by the number of events remaining after the photon veto is applied and the resulting rejection with statistical error. If there are zero events remaining after the photon veto is applied, the rejection is determined assuming 1 event remained.

Loose Normalization Branch

CUT	1/3	2/3
ALL_EVENTS	92709456	92709456
BAD_RUN,KERROR	90192888	90192888
SKIM2/5,RECON	2635077	5264890
PSCUT06	952180	1905107
DELCO3	945357	1891173
TDCUT02 loose	711847	1423458
KINCUT06	417199	833241
PNN2 KIN BOX loose	38835 (10.743)	77831 (10.706)
$\overline{\text{PV60}}$	38820 (1.000)	77796 (1.000)
B4EKZ(IC)	27787 (1.397)	55769 (1.395)
TGZFOOL	27396 (1.014)	55033 (1.013)
EPITG	17250 (1.588)	34860 (1.579)
EPIMAXK	17250 (1.000)	34860 (1.000)
TARGF	14700 (1.173)	29678 (1.175)
DTGTTP	14700 (1.000)	29678 (1.000)
RTDIF	14590 (1.008)	29425 (1.009)
DRP	14388 (1.014)	28983 (1.015)
TGKTIM	14144 (1.017)	28483 (1.018)
EIC	13847 (1.021)	27844 (1.023)
TIC	13847 (1.000)	27844 (1.000)
TGEDGE	13621 (1.017)	27395 (1.016)
TGDEDX	12809 (1.063)	25919 (1.057)
TGENR+TGER	12533 (1.022)	25404 (1.020)
PIGAP	12342 (1.015)	25038 (1.015)
TGB4	11082 (1.114)	22563 (1.110)
KIC	11076 (1.001)	22557 (1.000)
PHIVTX	8289 (1.336)	16873 (1.337)
OPSVETO	7238 (1.145)	14793 (1.141)
TGLIKE	6812 (1.063)	13863 (1.067)
TIMKF	5702 (1.195)	11743 (1.181)
NPITG	5702 (1.000)	11743 (1.000)
ALLKFIT	5450 (1.046)	11218 (1.047)
TPICS	5446 (1.001)	11217 (1.000)
EPIONK	5122 (1.063)	10551 (1.063)
CHI567	4282 (1.196)	8822 (1.196)
VERRNG	3586 (1.194)	7333 (1.203)
CHI5MAX	3585 (1.000)	7333 (1.000)
ANGLI	3576 (1.003)	7317 (1.002)
CCDBADFIT	3190 (1.121)	6450 (1.134)
CCDBADTIM	3098 (1.030)	6245 (1.033)
CCD31FIB	3098 (1.000)	6245 (1.000)
CCDPUL	528 (5.867)	1131 (5.522)

Table 19: The normalization branch for the loose $K_{\pi 2}$-TG scatter background: events after setup cuts and TGCUTS and their rejection (in brackets) in the $\pi\nu\overline{\nu}(2)$ loose box.

Tight Normalization Branch

CUT	1/3	2/3
ALL_EVENTS	92709456	92709456
BAD_RUN,KERROR	90192888	90192888
SKIM2/5,RECON	2635077	5264890
PSCUT06	952180	1905107
DELCO6	778661	1560187
TDCUT02 tight	428074	858447
KINCUT06	257607	516539
Ke4-phobic KIN BOX	18911 (13.622)	37733 (13.689)
$\overline{\text{PV60}}$	18907 (1.000)	37714 (1.000)
B4EKZ(IC)	13617 (1.388)	27008 (1.396)
TGZFOOL	13437 (1.013)	26631 (1.014)
EPITG	8228 (1.633)	16470 (1.617)
EPIMAXK	8228 (1.000)	16470 (1.000)
TARGF	6914 (1.190)	13831 (1.191)
DTGTTP	6914 (1.000)	13831 (1.000)
RTDIF	6870 (1.006)	13720 (1.008)
DRP	6791 (1.012)	13565 (1.011)
TGKTIM	6761 (1.004)	13502 (1.005)
EIC	6623 (1.021)	13237 (1.020)
TIC	6623 (1.000)	13237 (1.000)
TGEDGE	6535 (1.013)	13079 (1.012)
TGDEDX	6120 (1.068)	12360 (1.058)
TGENR+TGER	5988 (1.022)	12102 (1.021)
PIGAP	5883 (1.018)	11909 (1.016)
TGB4	5251 (1.120)	10663 (1.117)
KIC	5248 (1.001)	10660 (1.000)
PHIVTX	3826 (1.372)	7767 (1.372)
OPSVETO	3374 (1.134)	6872 (1.130)
TGLIKE	3176 (1.062)	6426 (1.069)
TIMKF	2690 (1.181)	5517 (1.165)
NPITG	2690 (1.000)	5517 (1.000)
ALLKFIT	2574 (1.045)	5282 (1.044)
TPICS	2571 (1.001)	5281 (1.000)
EPIONK	2388 (1.077)	4876 (1.083)
CHI567	1956 (1.221)	3989 (1.222)
VERRNG	1651 (1.185)	3286 (1.214)
CHI5MAX	1650 (1.001)	3286 (1.000)
ANGLI	1647 (1.002)	3279 (1.002)
CCDBADFIT	1481 (1.112)	2881 (1.138)
CCDBADTIM	1437 (1.031)	2789 (1.033)
CCD31FIB	1437 (1.000)	2789 (1.000)
CCDPUL	265 (5.423)	512 (5.447)

Table 20: The normalization branch for the tight $K_{\pi 2}$-TG scatter background: events after setup cuts and TGCUTS and their rejection (in brackets) in the $\pi\nu\overline{\nu}(2)$ ke4-phobic box. Note that it is the loose 60% photon veto that is inverted for the tight normalization branches.

Loose Normalization Branch in KP2 Kinematic Box

CUT	1/3	2/3
ALL_EVENTS	92709456	92709456
BAD_RUN,KERROR	90192888	90192888
SKIM2/5,RECON	2635077	5264890
PSCUT06	952180	1905107
DELCO3	945357	1891173
TDCUT02 loose	711847	1423458
KINCUT06	417199	833241
KP2 KIN BOX	337622 (1.236)	674203 (1.236)
$\overline{\text{PV60}}$	337381 (1.001)	673573 (1.001)
B4EKZ(IC)	307447 (1.097)	613761 (1.097)
TGZFOOL	302506 (1.016)	603837 (1.016)
EPITG	265782 (1.138)	529433 (1.141)
EPIMAXK	265782 (1.000)	529433 (1.000)
TARGF	256812 (1.035)	511739 (1.035)
DTGTTP	256805 (1.000)	511731 (1.000)
RTDIF	254620 (1.009)	507379 (1.009)
DRP	253748 (1.003)	505676 (1.003)
TGKTIM	251267 (1.010)	500828 (1.010)
EIC	247098 (1.017)	492289 (1.017)
TIC	247097 (1.000)	492284 (1.000)
TGEDGE	244794 (1.009)	487878 (1.009)
TGDEDX	243296 (1.006)	485103 (1.006)
TGENR+TGER	236835 (1.027)	472155 (1.027)
PIGAP	235173 (1.007)	468751 (1.007)
TGB4	221209 (1.063)	440996 (1.063)
KIC	221105 (1.000)	440799 (1.000)
PHIVTX	213727 (1.035)	425731 (1.035)
OPSVETO	204254 (1.046)	406813 (1.046)
TGLIKE	197705 (1.033)	393837 (1.033)
TIMKF	178944 (1.105)	357037 (1.103)
NPITG	178944 (1.000)	357037 (1.000)
ALLKFIT	172754 (1.036)	344685 (1.036)
TPICS	172725 (1.000)	344630 (1.000)
EPIONK	161704 (1.068)	322692 (1.068)
CHI567	140604 (1.150)	280130 (1.152)
VERRNG	131824 (1.067)	262670 (1.066)
CHI5MAX	131823 (1.000)	262670 (1.000)
ANGLI	131750 (1.001)	262529 (1.001)
CCDBADFIT	116443 (1.131)	231981 (1.132)
CCDBADTIM	113771 (1.023)	226730 (1.023)
CCD31FIB	113769 (1.000)	226730 (1.000)
CCDPUL	61374 (1.854)	122475 (1.851)

Table 21: The normalization branch for the $K_{\pi 2}$-TG scatter background in the KP2 box: events after setup cuts and TGCUTS and their rejection (in brackets) in the $K_{\pi 2}$ box.

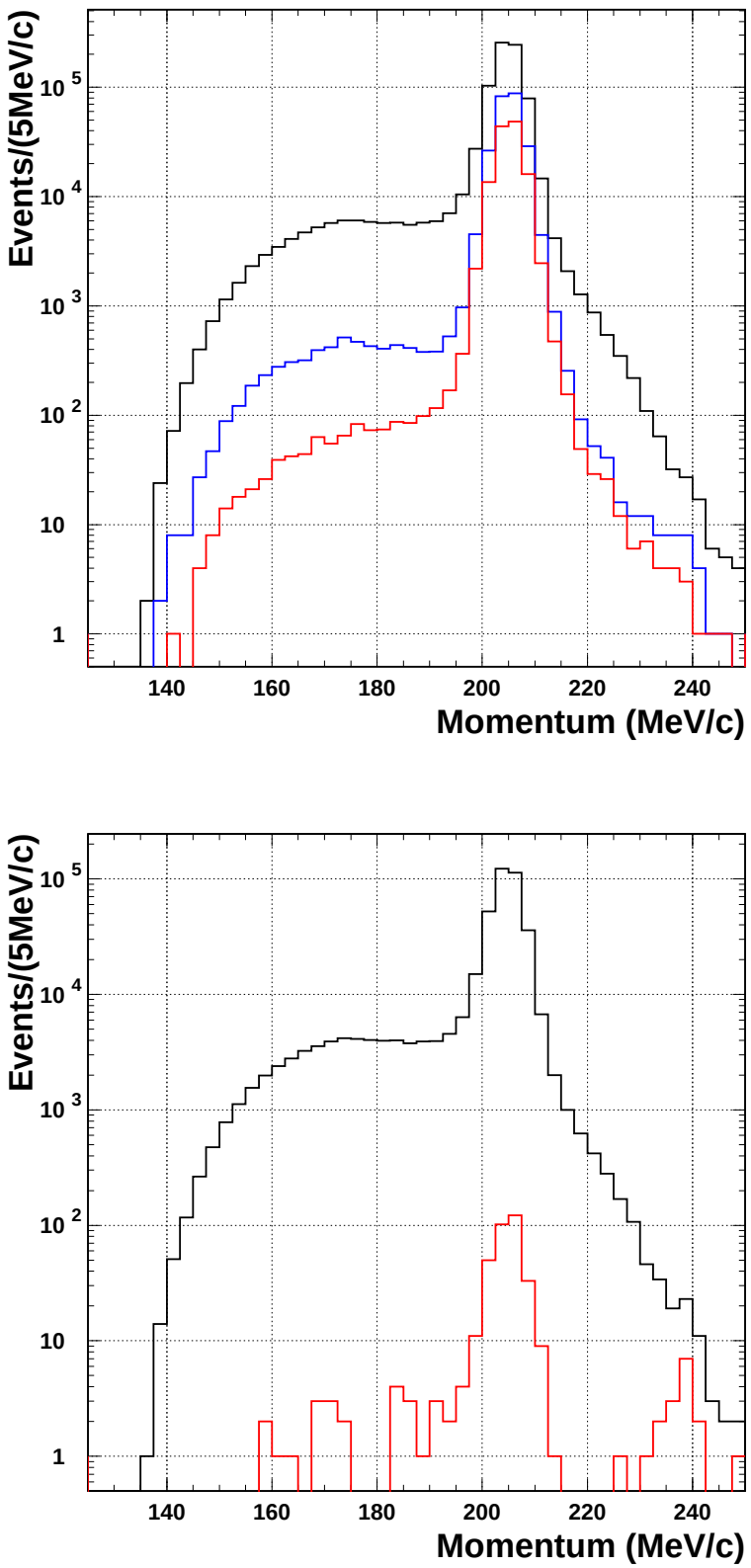

Figure 13: Top: The momentum (*ptot*) distribution of the events remaining in the loose normalization branch of the $K_{\pi 2}$ Target-scatter study after the inversion of the photon veto PVCUT60 (black), after the application of all the TGCUT06 except CCDPUL (blue), and after the application of CCDPUL (red). Bottom: The momentum (*ptot*) distribution of the events in CLASS12 of the loose rejection branch of the $K_{\pi 2}$ Target-scatter study before (black) and after (red) the photon veto PVCUT60.

, where the results from the 1/3 and 2/3 data sets are scaled to give results for the entire data set. The systematic error comes from the difference in background predicted by the class with the highest and lowest PV rejection, with respect to the central value from CLASS12. Only classes with adequate statistics are considered. The classes chosen for these systematic error bounds are shown in Tables 22 and 23.

For the tight box, the inverted photon veto used in the normalization branch was the loose (60%) photon veto as to not look in the box. Thus the the rejection branch required the use of the loose photon veto and the entire background was scaled by the ratio of the loose and tight (30%) photon vetoes. The uncorrected tight $K_{\pi 2}$ target scatter background $n_{K_{\pi 2}-TGscat}$(tight, uncorrected) is given by

$$n_{K_{\pi 2}-TGscat}(\text{tight, uncorrected}) = \frac{N_{tg}}{R_{PV(60\%)} - 1}\left(\frac{R_{PV(60\%)}}{R_{PV(30\%)}}\right), \quad (2)$$

where the results from the 1/3 and 2/3 data sets are scaled to give results for the entire data set. The lower and upper bounds on the systematic error again come from the difference in background predicted by the class with the highest and lowest PV rejections with respect to CLASS12. Only classes with adequate statistics are considered. For the purposes of determining the bounds on the systematic error, the difference in photon veto rejection for CLASS12 between the "All Loose" and "Ke4-phobic kinematic box" setups cuts (Table 13 and 14) is treated as another class.

Tables 22 and 23 show the summary of all values used to determine these loose and tight backgrounds respectively.

3.1.4 Correction for $K_{\pi 2\gamma}$ Contamination

Section 9.3 discusses the treatment of the potential contamination of the $K_{\pi 2}$ target scatter background due to $K_{\pi 2}$ Range-Stack scatter, K_{e4} and $K_{\pi 2\gamma}$ contamination. This section deals with the correction of the $K_{\pi 2}$ target scatter background, as estimated in Section 3.1.3, for $K_{\pi 2\gamma}$ contamination in the normalization branch.

To remove double-counting of the $K_{\pi 2\gamma}$ background, it is subtracted from $K_{\pi 2}$ target scatter background to estimate a final $K_{\pi 2}$ target scatter background corrected for contamination. The values are given as the "Final Corrected Background" in Tables 22 and 23.

Loose $K_{\pi 2}$ Target Scatter Summary

	1/3	2/3
	Normalization	
N_{tg}	$515.5 \pm 23.1\,^{+1.16}_{-1.12}$	$1107.7 \pm 33.8^{+2.89}_{-2.79}$
	Photon Veto Rejection R_{PV60}	
R_{PV60}(CLASS12)	2631.7±832.1	2391.9±509.8
R_{PV60}(max.)	4095.7±1671.8 (CLASS7)	2757.6±649.8 (CLASS7)
R_{PV60}(min.)	2373.6±750.4 (CLASS9)	2203.7±696.7 (CLASS10)
R_{PV60}	$2631.7 \pm 832.1^{+1464.0}_{-258.1}$	$2391.9 \pm 509.8^{+365.7}_{-188.2}$
	Background (Not corrected for $K_{\pi 2\gamma}$)	
$n_{\rm bg}$(uncorrected)	$0.588 \pm 0.188\,^{+0.065}_{-0.211}$	$0.695 \pm 0.150^{+0.061}_{-0.094}$
	$K_{\pi 2\gamma}$ Background	
$n_{\rm bg}^{K_{\pi 2\gamma}}$	$0.0514 \pm 0.0086\,^{+0.0042}_{-0.0038}$	$0.0757 \pm 0.0073\,^{+0.0062}_{-0.0056}$
	Final Corrected Background	
$n_{\rm bg}$	$0.537 \pm 0.188\,^{+0.069}_{-0.215}$	$0.619 \pm 0.150\,^{+0.067}_{-0.100}$

Table 22: The summary of the loose $K_{\pi 2}$ target-scatter background estimation. For the photon veto rejection R_{PV60} and background estimate n_{bg}, the first error is statistical and the second error systematic. The maximum and minimum 60% photon veto rejections are labeled to show which class was used to determine the systematic errors in R_{PV60} and n_{bg}.

Tight $K_{\pi 2}$ Target Scatter Summary

	1/3	2/3
	Normalization	
N_{tg}	$259.1 \pm 16.4\,^{+0.55}_{-0.66}$	$499.7 \pm 22.8\,^{+1.07}_{-1.28}$
	Photon Veto Rejection R_{PV30}	
R_{PV30}(CLASS12)	6579.2±3289.4	6577.6±3289.4
R_{PV30}(max.)	8132.0±4694.7 (CLASS2)	7483.9±2645.8 (CLASS5)
R_{PV30}(min.)	4935.2±2467.4 (KE4-PHOBIC)	5640.1±2131.6 (KE4-PHOBIC)
R_{PV30}	$6579.2 \pm 3289.4\,^{+1552.8}_{-1644.0}$	$6577.6 \pm 2325.4\,^{+906.3}_{-937.5}$
	Photon Veto Rejection R_{PV60}	
R_{PV60}	$2631.7 \pm 832.1^{+1464.0}_{-258.1}$	$2391.9 \pm 509.8^{+365.7}_{-188.2}$
	Background (Not corrected for $K_{\pi 2\gamma}$)	
	$n_{\rm bg} = \frac{N_{tg}}{R_{PV60}-1}\left(\frac{R_{PV60}}{R_{PV30}}\right)$	
$n_{\rm bg}$(uncorrected)	$0.118 \pm 0.059\,^{+0.075}_{-0.023}$	$0.114 \pm 0.041^{+0.019}_{-0.014}$
	$K_{\pi 2\gamma}$ Background	
$n_{\rm bg}^{K_{\pi 2\gamma}}$	$0.0122 \pm 0.0038\,^{+0.0010}_{-0.0010}$	$0.0188 \pm 0.0034\,^{+0.0016}_{-0.0014}$
	Final Corrected Background	
$n_{\rm bg}$	$0.106 \pm 0.059\,^{+0.076}_{-0.024}$	$0.095 \pm 0.041\,^{+0.020}_{-0.016}$

Table 23: The summary of the tight $K_{\pi 2}$ target-scatter background estimation. For the photon veto rejection R_{PV60} and background estimate n_{bg}, the first error is statistical and the second error systematic. The maximum and minimum 30% photon veto rejections are labeled to show which class was used to determine the systematic errors in R_{PV60} and n_{bg}. The rejection for the 60% photon veto is taken from Table 22

RS-Scat Rejection Branch - Loose Box

CUT	KP2BOX		KP2-PBOX PNN2-REBOX	
	1/3	2/3	1/3	2/3
PBOX from KP2BOX	93824	187638	728	1555
LAYER14	93772	187534	728	1555
FIDUCIAL	86512	172935	655	1403
UTCQUAL	83790	167397	642	1355
RNGMOM	83076	166017	642	1355
RSDEDX	72492	145014	112	270
PRRF	61410	122581	80	192
PVCUT	36	106	0	0

Table 24: The loose rejection branch for $K_{\pi 2}$-RS scatters. PBOX is the momentum cut and RE BOX the range and energy cut.

3.2 $K^+ \to \pi^+\pi^o$ Range Stack Scatters

3.2.1 Background

Pions from the $K_{\pi 2}$ decay can also undergo inelastic scattering in the Range Stack and fall into the $\pi\nu\overline{\nu}(2)$ kinematic box by losing energy in the scattering process. However, for these events to be a background for this analysis, the pion momentum also has to be mis-measured and the photons from the π^o decay have to be missed. Therefore, this background is expected to be smaller compared to the $K_{\pi 2}$ target scattered background. It should be noted that these background events are already included in the normalization branches in Tables 19 and 20[2], but they are not included in the rejection branch in Table 9 because the target cuts were reversed to measure this PV rejection. The $K_{\pi 2}$ events which scattered in the RS should be assigned the same Photon Veto rejection as the $K_{\pi 2}$ peak events, since the pion did not scatter in the target. The method used to determine this background was originally formulated by Milind et al. [2].

The most effective cuts against this background are the Range Stack track quality cuts RSDEDX and PRRF (collectively referred to as RSCT), the BOX cut on *ptot* and the Photon Veto cut. The SETUP cuts are the same as the $K_{\pi 2}$ target scatter normalization branch. Tables 24 and 25 contain events in the $K_{\pi 2}$ momentum peak. Events with the momentum of the $K_{\pi 2}$ peak events, but lowered in range and energy are assumed to have scattered in the Range Stack.

The rejection R_{RSCT} of the RSCT cuts can be determined from the RS-Scatter Rejection Tables 24 and 25. The rejection R_{RSCT} is determined from the "KP2-PBOX PNN2-REBOX" column.

$$R_{RSCT} \quad = N_{\mathrm{RNGMOM}}/N_{\mathrm{PRRF}} \tag{3}$$

The method in which the efficiency ϵ_{RSCT} is determined has changed from [1]. Previously, the efficiency was determined from the "KP2BOX" column of Tables 24 and 25. Instead, the efficiency will now be taken from the Range-Stack kinematic acceptance measurements (Section 11.3), with systematic errors determined in the same way as described in that section. This change gives non-zero values for the number of range-stack scatter

[2]Correcting the normalization of $K_{\pi 2}$-TG scatters for $K_{\pi 2}$-RS scatters does not make a significant difference in the background, given the statistical uncertainty.

RS-Scat Rejection Branch - Tight Box

CUT	KP2BOX		KP2-PBOX KE4-PHOBIC REBOX	
	1/3	2/3	1/3	2/3
PBOX from KP2BOX	62375	125147	351	839
LAYER14	62341	125080	351	839
FIDUCIAL	57570	115407	312	767
UTCQUAL	55744	111727	307	739
RNGMOM	55262	110833	307	739
RSDEDX	48348	97120	63	167
PRRF	41103	82387	44	118
PVCUT	10	31	0	0

Table 25: The tight rejection branch for $K_{\pi 2}$-RS scatters. PBOX is the momentum cut and RE BOX the range and energy cut.

RS-Scat Normalization Branch - Loose Box

CUT	KP2BOX		PNN2BOX	
	1/3	2/3	1/3	2/3
$\overline{\text{RSDEDX}}$.or.$\overline{\text{PRRF}}$	25328	50617	217	407
LAYER14	25309	50579	217	407
FIDUCIAL	22811	45731	202	384
UTCQUAL	21894	43905	179	347
RNGMOM	21666	43436	153	281
$\overline{\text{PVCUT60}}$	21657	43410	153	281

Table 26: The loose normalization branch for $K_{\pi 2}$-RS scatters.

RS-Scat Normalization Branch - Tight Box

CUT	KP2BOX		KE4-PHOBIC BOX	
	1/3	2/3	1/3	2/3
$\overline{\text{RSDEDX}}$.or.$\overline{\text{PRRF}}$	16566	33191	81	159
LAYER14	16554	33167	81	159
FIDUCIAL	14932	29939	75	152
UTCQUAL	14318	28751	68	136
RNGMOM	14159	28446	66	124
$\overline{\text{PVCUT60}}$	14152	28432	66	124

Table 27: The tight normalization branch for $K_{\pi 2}$-RS scatters.

$K_{\pi 2}$ Range Stack Scatter Summary

	Loose		Tight	
	1/3	2/3	1/3	2/3
	Acceptance of $RSCT$			
A_{RSCT}	$0.888 \pm 0.001 \pm 0.012$		$0.894 \pm 0.002\,^{+0.010}_{-0.012}$	
	Rejection of $RSCT$			
$N_{\rm RNGMOM}$	642	1355	307	739
$N_{\rm PRRF}$	80	192	44	118
R_{RSCT}	8.025±0.839	7.057±0.472	6.977±0.974	6.263±0.528
	Normalization Numbers			
$norm\_tg$	528	1131	265	512
$norm\_rs$	153	281	66	124
$N_{rs}(1/3)$	$12.52 \pm 2.39\,^{+1.18}_{-1.21}$		$5.90 \pm 1.73\,^{+0.58}_{-0.70}$	
$N_{rs}(2/3)$	$23.33 \pm 3.46\,^{+2.93}_{-2.99}$		$12.30 \pm 2.56\,^{+1.27}_{-1.54}$	
	Photon Veto Rejection R_{PV60} ($K_{\pi 2}$ peak)			
Before PV	61410	122581	41103	82387
After PV	36	106	10	31
R_{PV60}	1705.8±284.2	1156.4±112.3	4110.3±1299.6	2657.7±477.2
	Background Estimate			
$n_{\rm bg}(1/3)$	$0.0220 \pm 0.0056\,^{+0.0021}_{-0.0021}$		$0.0043 \pm 0.0019\,^{+0.0004}_{-0.0005}$	
$n_{\rm bg}(2/3)$	$0.0303 \pm 0.0054\,^{+0.0038}_{-0.0039}$		$0.0069 \pm 0.0019\,^{+0.0007}_{-0.0009}$	

Table 28: The summary of the $K_{\pi 2}$ range-stack scatter background estimation. For values having two sets of errors, the first is statistical and the second systematic.

normalization events N_{rs} and for the resulting background. This change is also justified due to the fact that the kinematics of target-scatter events in the PNN2 kinematic box are much more similar to piscat monitors in the PNN2 kinematic box than to $K_{\pi 2}$-peak events. Additionally, the piscat sample used has the Range Stack portion of the photon veto applied, where the $K_{\pi 2}$-peak did not.

Tables 26 and 27 show the normalization branch. The RSCT cut is reversed and all other cuts are applied. The various contributions to the total $norm\_rs$ events left at the the end of the branch have to be considered in order to calculate the background of interest. The largest component of this sample comes from scattering in the target that contaminated the RSCT reversed sample because of the inefficiency of the RSCT cuts. On the other hand, the total $norm\_tg$ events left at the end of the $K_{\pi 2}$ target scatter normalization branch (Tables 19 and 20) have a target scattered (N_{tg}) and a RS scattered (N_{rs}) component. We can write

$$N_{tg} + N_{rs} = norm\_tg \quad (4)$$

$$\frac{1-\epsilon_{RSCT}}{\epsilon_{RSCT}} \times N_{tg} + (R_{RSCT} - 1) \times N_{rs} = norm\_rs \quad (5)$$

Note that the form of the second equation has been corrected from that as used by Milind et al. [2].

The final background from the RS scattered events can be determined from N_{rs} and the $K_{\pi 2}$-peak Photon Veto rejection from CLASS1 as shown:

$$n^{loose}_{K_{\pi 2}-RSscat} = \frac{N^{loose}_{rs}}{R_{PV60-K_{\pi 2}-peak} - 1} \tag{6}$$

$$n^{tight}_{K_{\pi 2}-RSscat} = \frac{N^{tight}_{rs}}{R_{PV60-K_{\pi 2}-peak} - 1} \times \frac{R_{PV60-K_{\pi 2}-peak}}{R_{PV30-K_{\pi 2}-peak}} \tag{7}$$

where a normalization factor of 3 is used for the 1/3 data sample and a normalization factor of 3/2 for the 2/3 data sample.

4 $K_{\pi 2\gamma}$ Background

$K_{\pi 2\gamma}$ background is estimated with the same approach as in 1/3 note.

$$N_{Kp2\gamma} = \frac{N_{Kp2-peak}}{\kappa \cdot R_{\gamma}} \ . \tag{8}$$

The results are summarized in Tab. 29.

	Tight cuts 1/3	Loose cuts 1/3	Tight cuts 2/3	Loose cuts 2/3
$N_{Kp2-peak}$	10	36	31	106
κ	483 ± 28	417 ± 24	483 ± 28	417 ± 24
R_γ	5.11 ± 0.11	5.04 ± 0.10	5.11 ± 0.11	5.04 ± 0.10
$N_{Kp2\gamma}$	$0.0121 \pm 0.0038\,^{+0.0010}_{-0.0010}$	$0.0514 \pm 0.0086\,^{+0.0042}_{-0.0038}$	$0.0188 \pm 0.0034\,^{+0.0016}_{-0.0014}$	$0.0757 \pm 0.0073\,^{+0.0062}_{-0.0056}$

Table 29: $K\pi 2\gamma$ background number normalized to 3/3 data. The first error of $N_{Kp2\gamma}$ is statistical and the second error is from κ and R_γ.

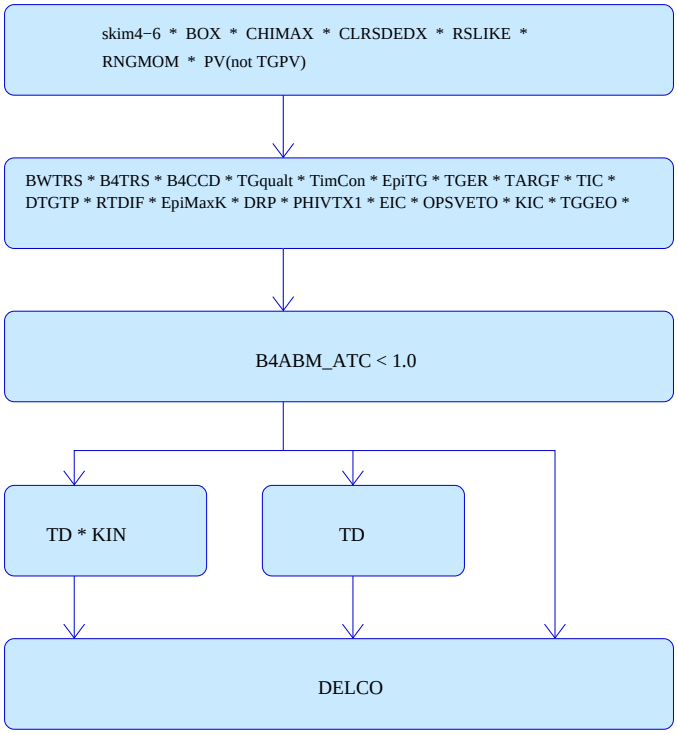

Figure 14: **1-Beam Rejection Bifurcation**. The additional branches in this rejection bifurcation are cleaning up the sample with additional cuts at the expense of reducing statistics. *DELCO*=DEL3 OR DELC6 depending on what signal region is being studied.

5 Beam Background

For comparison, the beam background is explicitly measured in the tight region in the following sections. However, PNN2 will be utilizing the value from scaling the background in the loose region. Further, details of the beam background were written in Ref. [5].

5.1 Single-Beam Background

The single-beam background is bifurcated using DELCO. To preserve the blind analysis the loosest delayed-coincidence cut (DELC3) is used when measuring the background in the tight region. The rejection bifurcation has three samples as shown in Fig. 14 of varying purity. The two looser branches do not apply kinematic (KIN) and/or TD cuts. The cleanest sample (additionally applying both KIN and TD cuts) to measure the rejection of DELCO has much lower statistics.

The samples with larger statistics have a large amount of contamination. The 16 events (2 from 1/3 and 14 from 2/3 samples) which survived all cuts in the rejection branch were studied. 14 of the 16 events failed CCDPUL (many also failed and EC PV cut). It was concluded that $K_{\pi 2}$ TG-scatters were contaminating the 1-beam rejection sample. Therefore, the cleanest sample was chosen for the final measurement.

The value of R_{DELCO}^{Tight} was taken as R_{DELCO}^{Loose}, since the lower value in the tight sample is due to reduction of the sample size.

$$N_{1bm}^{1/3} = 3 \times \frac{Norm_{1bm}^{1/3}}{R_{1bm}^{1/3} - 1} \tag{9}$$

1BM Rej Branches	Loose 1/3		Loose 2/3		Tight 1/3		Tight 2/3	
R_{1bm}^{Loose}	10582.5 ± 7482.6	(2)	3032.4 ± 810.3	(14)	17793.0 ± 17792.5	(1)	5088.3 ± 1923.0	(7)
R_{1bm}^{TD}	17608.0 ± 17607.5	(1)	4416.0 ± 1561.1	(8)	10738.0 ± 10737.5	(0)	5353.0 ± 2676.2	(4)
$\mathbf{R_{1bm}^{TD \cdot KIN}}$	$\mathbf{6483.0 \pm 6482.5}$	(0)	$\mathbf{6425.0 \pm 4542.8}$	(2)	$\mathbf{6483.0 \pm 6482.5}$	(0)	$\mathbf{7780.0 \pm 7779.5}$	(1)
$\mathbf{Norm_{1bm}}$	$\mathbf{1.0 \pm 1.0}$		$\mathbf{1.0 \pm 1.0}$		$\mathbf{1.0 \pm 1.0}$		$\mathbf{1.0 \pm 1.0}$	

Table 30: **1-Beam Rejection Summary and Normalization**. Each row is a different branch to measure the DELCO rejection with samples becoming cleaner for each subsequent row. First number is the rejection. The number is parenthesis is the number of events remaining that the rejection is based upon. The difference between loose and tight columns are the application of the loose or tight version of DELCO, PV, TD, and BOX. The rejection denoted in bold typeface is rejection employed in measured values. To avoid looking into the signal region, the normalization was measured from a inverted DELC3 (loose version of DELCO) sample for both loose and tight measurements. $\mathbf{R_{1bm}^{TD \cdot KIN}}$ for the 1/3 tight column was actually 3913.0 ± 3912.5, but 6483.0 ± 6482.5 was used since the sample was further limited in statistics when tight cuts were applied.

$$N_{1bm}^{2/3} = \frac{3}{2} \times \frac{Norm_{1bm}^{2/3}}{R_{1bm}^{2/3} - 1} \quad (10)$$

Eq. (9) and Eq. (10) are used to calculate the one-beam background values shown in Table 39. However, the method to measure the signal region uses Eq. (11). The scaling method and direct measurement provides an overestimate of the tight region 1-beam background; this is due to the fact that the tight DELCO should provide a greater reduction of 1-beam background than the measured rejection can provide (i.e R_{DELCO}^{tight} is statistically limited). The good news is that the background is very small and thus an overestimate of a small number is still a small number.

$$N_{1bm}^{scaled} = \frac{A_{PV_{tight}}}{A_{PV_{loose}}} \times \frac{A_{BOX_{tight}}}{A_{BOX_{loose}}} \times \frac{A_{TD_{tight}}}{A_{TD_{loose}}} \times \frac{R_{1bm}^{Loose}}{R_{1bm}^{Tight}} \times N_{1bm} \quad (11)$$

$$N_{1bm}^{1/3\ scaled} = \left(\frac{0.360}{0.619}\right) \times \left(\frac{0.385}{0.474}\right) \times \left(\frac{0.3897}{0.4805}\right) \times \left(\frac{6483}{6483}\right) \times 0.00046$$

$$= (0.18 \pm 0.18) \times 10^{-3} \quad (12)$$

$$N_{1bm}^{2/3\ scaled} = \left(\frac{0.360}{0.619}\right) \times \left(\frac{0.385}{0.474}\right) \times \left(\frac{0.3897}{0.4805}\right) \times \left(\frac{6425}{7780}\right) \times 0.00023$$

$$= (0.073 \pm 0.073) \times 10^{-3} \quad (13)$$

1BM Rej	Loose		Tight (measured)	
Branch	1/3	2/3	1/3	2/3
BAD_RUN	1535485 (0.00)	3067491 (0.00)	1080842 (0.00)	2160149 (0.00)
TRIGGER	1535485 (1.00)	3067491 (1.00)	1080842 (1.00)	2160149 (1.00)
BOX	1535485 (1.00)	3067491 (1.00)	1080842 (1.00)	2160149 (1.00)
RSDEDXMAX	1535485 (1.00)	3067491 (1.00)	1080842 (1.00)	2160149 (1.00)
RSDEDXCL	1535485 (1.00)	3067491 (1.00)	1080842 (1.00)	2160149 (1.00)
RSLIKE	1535485 (1.00)	3067491 (1.00)	1080842 (1.00)	2160149 (1.00)
RNGMOM	986914 (1.56)	1973636 (1.55)	721828 (1.50)	1443507 (1.50)
PV(not TG AD)	470206 (2.10)	940856 (2.10)	355627 (2.03)	710313 (2.03)
BWTRS	342393 (1.37)	685287 (1.37)	256137 (1.39)	512130 (1.39)
B4TRS	297348 (1.15)	595198 (1.15)	222297 (1.15)	444437 (1.15)
B4CCD	296526 (1.00)	593547 (1.00)	221768 (1.00)	443354 (1.00)
TGQUALT	268744 (1.10)	537609 (1.10)	205388 (1.08)	410373 (1.08)
TIMCON	267096 (1.01)	534309 (1.01)	204214 (1.01)	408046 (1.01)
EPITG	203834 (1.31)	407378 (1.31)	155496 (1.31)	310202 (1.32)
TGER	201702 (1.01)	403220 (1.01)	154189 (1.01)	307604 (1.01)
TARGF	190314 (1.06)	380857 (1.06)	145356 (1.06)	290285 (1.06)
TICCON	190310 (1.00)	380849 (1.00)	145354 (1.00)	290279 (1.00)
DTGTTP	190280 (1.00)	380790 (1.00)	145331 (1.00)	290246 (1.00)
RTDIF	183958 (1.03)	368071 (1.03)	140705 (1.03)	281030 (1.03)
EPIMAXK	183958 (1.00)	368071 (1.00)	140705 (1.00)	281030 (1.00)
DRP	177735 (1.04)	355930 (1.03)	136979 (1.03)	273784 (1.03)
1BM Rej. Branch continued on next page				

1BM Rej. Branch continued from previous page				
	Loose		Tight (measured)	
	1/3	2/3	1/3	2/3
PHIVTX	141265 (1.26)	282492 (1.26)	109410 (1.25)	218101 (1.26)
EICCON	137303 (1.03)	274453 (1.03)	106639 (1.03)	212502 (1.03)
OPSVETO	100924 (1.36)	201685 (1.36)	80469 (1.33)	160506 (1.32)
KIC	90655 (1.11)	181329 (1.11)	72642 (1.11)	145012 (1.11)
TGGEO	76579 (1.18)	153708 (1.18)	62309 (1.17)	124629 (1.16)
TGEDGE	71885 (1.07)	144252 (1.07)	58484 (1.07)	116956 (1.07)
TGZFOOL	52579 (1.37)	105340 (1.37)	42786 (1.37)	85554 (1.37)
UPVTRS	46435 (1.13)	93169 (1.13)	37698 (1.13)	75475 (1.13)
RVTRS	46240 (1.00)	92716 (1.00)	37537 (1.00)	75117 (1.00)
TGTCON	43605 (1.06)	87336 (1.06)	35533 (1.06)	71033 (1.06)
B4ETCON	42541 (1.03)	85121 (1.03)	34663 (1.03)	69201 (1.03)
$B4ABM < 1.0$	21165 (2.01)	42454 (2.01)	17793 (1.95)	35618 (1.94)
PIFLG	21111 (1.00)	42371 (1.00)	17750 (1.00)	35552 (1.00)
ELVETO	19215 (1.10)	38617 (1.10)	13069 (1.09)	26250 (1.09)
TDFOOL	19166 (1.00)	38521 (1.00)	13038 (1.00)	26183 (1.00)
TDNN	17608 (1.09)	35328 (1.09)	10738 (1.21)	21412 (1.22)
LAYER14	17608 (1.00)	35328 (1.00)	10738 (1.00)	21412 (1.00)
COS3D	16795 (1.05)	33738 (1.05)	10217 (1.05)	20400 (1.05)
LAYV4	16795 (1.00)	33738 (1.00)	10217 (1.00)	20400 (1.00)
ZFRF	16784 (1.00)	33701 (1.00)	10212 (1.00)	20378 (1.00)
ZUTOUT	16780 (1.00)	33686 (1.00)	10209 (1.00)	20371 (1.00)
UTCQUAL	16116 (1.04)	32336 (1.04)	9813 (1.04)	19590 (1.04)
PRRF1	15920 (1.01)	31959 (1.01)	9682 (1.01)	19369 (1.01)
PRRFZ	15152 (1.05)	30350 (1.05)	9194 (1.05)	18374 (1.05)
TGDEDX	14843 (1.02)	29729 (1.02)	9003 (1.02)	17987 (1.02)
TGLIKE1	14204 (1.04)	28433 (1.05)	8640 (1.04)	17233 (1.04)
TGLIKE2	13614 (1.04)	27291 (1.04)	8269 (1.04)	16543 (1.04)
TBDB4	12051 (1.13)	24144 (1.13)	7314 (1.13)	14616 (1.13)
TGDB4TIP	8339 (1.45)	16630 (1.45)	5061 (1.45)	10101 (1.45)
TGDVXTIP	7299 (1.14)	14524 (1.15)	4434 (1.14)	8850 (1.14)
TGDVXPI	6590 (1.11)	13057 (1.11)	3979 (1.11)	7915 (1.12)
PIGAP	6483 (1.02)	12850 (1.02)	3913 (1.02)	7780 (1.02)
DELCO	**0** (6483.00)	**2** (6425.00)	**0** (3913.00)	**1** (7780.00)
Rej_{DELCO}	$\mathbf{6483.0 \pm 6482.5}$	$\mathbf{6425.0 \pm 4542.8}$	$\mathbf{3913.0 \pm 3912.5}$	$\mathbf{7780.0 \pm 7779.5}$

Table 31: Beam Background Rejection Branch. Shown are the number of events remaining after applying the cut in the first column; number in parenthesis is the rejection of the cut within this sample.

1BM Norm. Branch	Loose 1/3	Loose 2/3	Tight (measured) 1/3	Tight (measured) 2/3
BAD_RUN	1535485 (0.00)	3067491 (0.00)	1080842 (0.00)	2160149 (0.00)
TRIGGER	1535485 (1.00)	3067491 (1.00)	1080842 (1.00)	2160149 (1.00)
BOX	1535485 (1.00)	3067491 (1.00)	1080842 (1.00)	2160149 (1.00)
RSDEDXMAX	1535485 (1.00)	3067491 (1.00)	1080842 (1.00)	2160149 (1.00)
RSDEDXCL	1535485 (1.00)	3067491 (1.00)	1080842 (1.00)	2160149 (1.00)
RSLIKE	1535485 (1.00)	3067491 (1.00)	1080842 (1.00)	2160149 (1.00)
RNGMOM	986914 (1.56)	1973636 (1.55)	721828 (1.50)	1443507 (1.50)
LAYER14	986914 (1.00)	1973632 (1.00)	721828 (1.00)	1443504 (1.00)
COS3D	900053 (1.10)	1800056 (1.10)	652711 (1.11)	1305559 (1.11)
LAYV4	900053 (1.00)	1800056 (1.00)	652711 (1.00)	1305559 (1.00)
ZFRF	898843 (1.00)	1797638 (1.00)	651751 (1.00)	1303605 (1.00)
ZUTOUT	898335 (1.00)	1796646 (1.00)	651367 (1.00)	1302855 (1.00)
UTCQUAL	821014 (1.09)	1641598 (1.09)	602882 (1.08)	1205528 (1.08)
PRRF1	812359 (1.01)	1624636 (1.01)	595824 (1.01)	1191612 (1.01)
PRRFZ	765804 (1.06)	1532226 (1.06)	560676 (1.06)	1121926 (1.06)
TGDEDX	670068 (1.14)	1339412 (1.14)	498202 (1.13)	995858 (1.13)
TGLIKE1	583669 (1.15)	1166794 (1.15)	439603 (1.13)	878815 (1.13)
TGLIKE2	549113 (1.06)	1097809 (1.06)	414369 (1.06)	828378 (1.06)
TBDB4	460113 (1.19)	921030 (1.19)	345928 (1.20)	692595 (1.20)
TGDB4TIP	343810 (1.34)	686621 (1.34)	255122 (1.36)	509965 (1.36)
TGDVXTIP	312096 (1.10)	623341 (1.10)	231027 (1.10)	461623 (1.10)
TGDVXPI	285768 (1.09)	570747 (1.09)	209302 (1.10)	418248 (1.10)
PIGAP	273968 (1.04)	547289 (1.04)	199627 (1.05)	398922 (1.05)
TGPV	170043 (1.61)	339461 (1.61)	128389 (1.55)	256815 (1.55)
BWTRS	153318 (1.11)	306121 (1.11)	115503 (1.11)	231193 (1.11)
B4TRS	143373 (1.07)	285980 (1.07)	107965 (1.07)	215949 (1.07)
B4CCD	142094 (1.01)	283379 (1.01)	107085 (1.01)	214117 (1.01)
TGQUALT	136614 (1.04)	272763 (1.04)	103399 (1.04)	206880 (1.03)
TIMCON	135650 (1.01)	270739 (1.01)	102842 (1.01)	205674 (1.01)
EPITG	110388 (1.23)	220227 (1.23)	82548 (1.25)	165276 (1.24)
TGER	110270 (1.00)	219965 (1.00)	82464 (1.00)	165093 (1.00)
TARGF	105258 (1.05)	209803 (1.05)	78577 (1.05)	157130 (1.05)
TICCON	105256 (1.00)	209800 (1.00)	78575 (1.00)	157129 (1.00)
DTGTTP	105256 (1.00)	209799 (1.00)	78575 (1.00)	157128 (1.00)
RTDIF	103457 (1.02)	206094 (1.02)	77472 (1.01)	154956 (1.01)
EPIMAXK	103457 (1.00)	206094 (1.00)	77472 (1.00)	154956 (1.00)
DRP	102447 (1.01)	204083 (1.01)	76908 (1.01)	153838 (1.01)
PHIVTX	84358 (1.21)	167556 (1.22)	62941 (1.22)	125517 (1.23)
EICCON	82421 (1.02)	163636 (1.02)	61623 (1.02)	122774 (1.02)
OPSVETO	66978 (1.23)	133102 (1.23)	50754 (1.21)	101158 (1.21)
KIC	60426 (1.11)	120425 (1.11)	45506 (1.12)	90895 (1.11)
TGGEO	49466 (1.22)	98704 (1.22)	37718 (1.21)	75216 (1.21)
TGEDGE	48178 (1.03)	96121 (1.03)	36733 (1.03)	73244 (1.03)

1BM Norm. Branch continued on next page

1BM Norm. Branch continued from previous page				
	Loose		Tight (measured)	
	1/3	2/3	1/3	2/3
TGZFOOL	40692 (1.18)	80857 (1.19)	30793 (1.19)	61236 (1.20)
UPVTRS	37692 (1.08)	75206 (1.08)	28381 (1.08)	56689 (1.08)
RVTRS	37574 (1.00)	74973 (1.00)	28292 (1.00)	56511 (1.00)
TGTCON	31423 (1.20)	62763 (1.19)	24487 (1.16)	48936 (1.15)
B4ETCON	30990 (1.01)	61824 (1.02)	24131 (1.01)	48183 (1.02)
B4EKZ	12771 (2.43)	25821 (2.39)	9867 (2.45)	19934 (2.42)
TGKTIM	8522 (1.50)	17282 (1.49)	6680 (1.48)	13502 (1.48)
TGENR	8344 (1.02)	16968 (1.02)	6539 (1.02)	13266 (1.02)
CHI567	7118 (1.17)	14566 (1.16)	5526 (1.18)	11244 (1.18)
NPITG	7118 (1.00)	14566 (1.00)	5526 (1.00)	11244 (1.00)
VERRNG	6015 (1.18)	12293 (1.18)	4686 (1.18)	9536 (1.18)
CHI5MAX	6014 (1.00)	12293 (1.00)	4685 (1.00)	9536 (1.00)
ANGLI	5998 (1.00)	12264 (1.00)	4676 (1.00)	9518 (1.00)
ALLKFIT	5693 (1.05)	11662 (1.05)	4457 (1.05)	9043 (1.05)
TPICS	5687 (1.00)	11661 (1.00)	4452 (1.00)	9042 (1.00)
EPIONK	5412 (1.05)	11131 (1.05)	4237 (1.05)	8614 (1.05)
CCDPUL CCDBADFIT CCDBADTIM CCD31FIB	801 (6.76)	1716 (6.49)	655 (6.47)	1387 (6.21)
TIMKF	745 (1.08)	1586 (1.08)	612 (1.07)	1284 (1.08)
$\overline{DELC3}$	109 (6.83)	231 (6.87)	89 (6.88)	193 (6.65)
CPITRS	106 (1.03)	226 (1.02)	86 (1.03)	189 (1.02)
CPITAIL	106 (1.00)	226 (1.00)	86 (1.00)	189 (1.00)
B4DEDX	106 (1.00)	225 (1.00)	86 (1.00)	188 (1.01)
CKTRS	88 (1.20)	182 (1.24)	71 (1.21)	151 (1.25)
CKTAIL	69 (1.28)	148 (1.23)	55 (1.29)	124 (1.22)
PV_{PNN1}	2 (34.50)	9 (16.44)	2 (27.50)	9 (13.78)
PIFLG	2 (1.00)	9 (1.00)	2 (1.00)	9 (1.00)
EV5	2 (1.00)	9 (1.00)	1 (2.00)	8 (1.12)
ELVETO	1 (2.00)	9 (1.00)	1 (1.00)	8 (1.00)
TDFOOL	1 (1.00)	9 (1.00)	1 (1.00)	8 (1.00)
TDNN	1 (1.00)	8 (1.12)	1 (1.00)	7 (1.14)
PV_{PNN2}	1 (1.00)	0 (8.00)	1 (1.00)	0 (7.00)
$Norm_{1bm}$	**1**	**0**	**1**	**0**

Table 32: 1-Beam Background Normalization Branch. Shown are the number of events remaining after applying the cut in the first column; number in parenthesis is the rejection of the cut within this sample.

5.2 Double-Beam Background

The normalization branches of KK and Kpi beam background changed slightly from the 1/3 TN. Some TG cuts were being applied as setup cuts before ADPV was bifurcated and the rejection measured; ADPV has rejection beyond acceptance loss for double-beam background. These TG cuts were removed as setups and applied after the rejection of ADPV was measured. This allowed for a better estimate of the rejection of ADPV. In

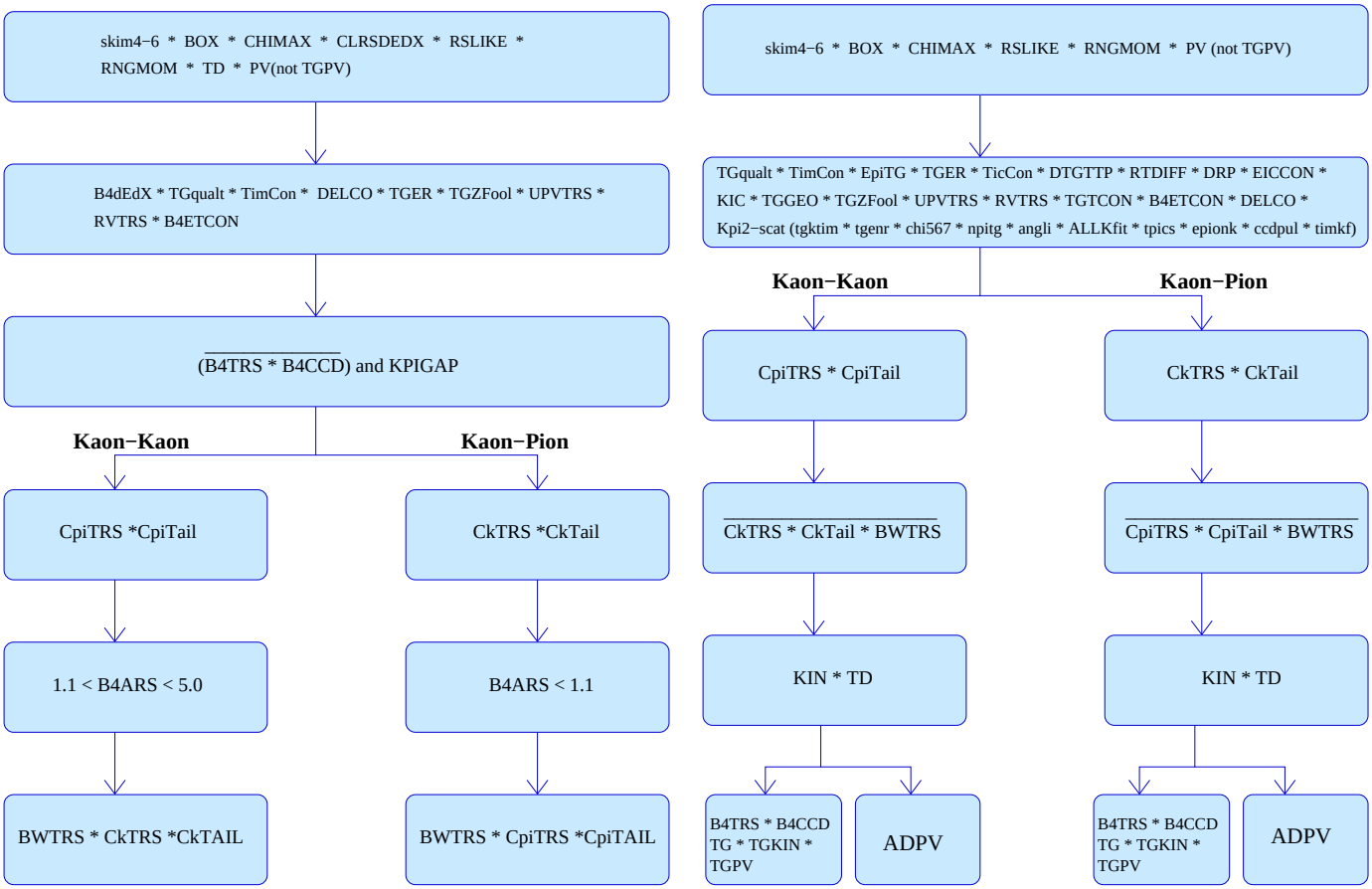

(a) Rejection (b) Normalization

Figure 15: **2-Beam Bifurcations (Kaon-Kaon and Kaon-Pion).** *DELCO* changes depending on the study. *DELCO*=DEL3 OR DELC6 depending on what signal region is being studied.

addition, PV_{PNN2} (w/o ADPV) was applied instead of PV_{PNN1}. Since the background within the different cells are calculated based upon scaling of acceptance loss and rejection of tight versus loose cuts, having an additional scaling of the background measurement by applying looser cuts is bad practice.

Tables 35 and 36 are summarized in Table 33 and is diagramed in Fig. 15(a). Tables 37 and 38 are summarized in Table 34 and is diagramed in Fig. 15(b). The "Tight" columns display results with the application of the tighter cuts (if applied); this is shown for comparison purposes only, as the background in the tight cell is measured by scaling the loosest cell. The scaling of the two-beam background includes a factor related to the tightening of DELCO. This is assumed to be one, and so is omitted from the scaling equations, as this background is a function of the beam rate rather than the kaon life-time. Since the beam rate is slow compared to the difference between the tight and loose DELCO, we are assuming the factor is 1.0 to be conservative. The background values are shown in Table 39.

5.2.1 2-beam results

5.2.2 KK-beam background

- ADPV has additional rejection on KK background. The normalization branch is bifurcated to measure this rejection and thus the normalization brach is equlivant to $\frac{n_{KK}}{r_{KK}}$.

2BM Rej Branches	Loose 1/3	Loose 2/3	Tight 1/3	Tight 2/3
R_{KK}	112.9 ± 42.5 (7)	394.0 ± 196.8 (4)	148.0 ± 147.5 (1)	269.0 ± 268.5 (1)
R_{Kpi}	589.5 ± 416.5 (2)	616.8 ± 308.1 (4)	261.0 ± 260.5 (1)	541.0 ± 540.5 (1)

Table 33: **2-Beam Rejection Summary**. First number is the rejection. The number in parenthesis is the number of events remaining that the rejection is based upon. K-K is the case where two Kaons are entering the beam. K-pi is the case where we have a Kaon and a Pion entering. $\overline{B4TRS \cdot B4CCD}\ AND\ KPIGAP$ is applied to select the rejection sample. KIN, TD and many other cuts listed in these flow charts are composite cuts.

2BM Norm Branches	Loose 1/3	Loose 2/3	Tight 1/3	Tight 2/3
$n_{KK} : TG \cdot TGPV \cdot B4$	1.0 ± 1.0	1.0 ± 1.0	1.0 ± 1.0	1.0 ± 1.0
$r_{KK} : ADPV$	7.49 ± 0.52	8.30 ± 0.432	9.64 ± 1.94	9.63 ± 1.32
$Norm_{KK}$	0.134 ± 0.134	0.120 ± 0.120	0.104 ± 0.104	0.104 ± 0.104
$n_{Kpi} : TG \cdot TGPV \cdot B4$	1.0 ± 1.0	1.0 ± 1.0	1.0 ± 1.0	1.0 ± 1.0
$r_{Kpi} : APPV$	10.36 ± 0.66	9.56 ± 0.42	13.72 ± 2.20	10.21 ± 1.01
$Norm_{Kpi}$	0.097 ± 0.097	0.105 ± 0.105	0.073 ± 0.073	0.098 ± 0.098

Table 34: **2-Beam Normalization Summary**. The 2-BM Normalization has 2 branches that are further bifurcated. $K\text{-}K_{r,n}$, $K\text{-}pi_{r,n}$ are the results of the bifurcations, r=rejection, n=normalization, which we used to determine the last two rows. N_{K-K} *and* N_{K-pi} are the 2-BM normalization values which are employed in the calculation of the beam-background. For KK (Kpi), $\overline{CkTRS \cdot CkTAIL \cdot BWTRS}$ ($\overline{CpiTRS \cdot CpiTAIL \cdot BWTRS}$) is applied

$$N_{KK}^{1/3} = 3 \times \frac{\left(\frac{n_{KK}^{1/3}}{r_{KK}^{1/3}}\right)}{R_{KK}^{1/3} - 1} \tag{14}$$

$$N_{KK}^{2/3} = \frac{3}{2} \times \frac{\left(\frac{n_{KK}^{2/3}}{r_{KK}^{2/3}}\right)}{R_{KK}^{2/3} - 1} \tag{15}$$

$$N_{KK}^{scaled} = \frac{A_{PV_{tight}}}{A_{PV_{loose}}} \times \frac{A_{BOX_{tight}}}{A_{BOX_{loose}}} \times \frac{A_{TD_{tight}}}{A_{TD_{loose}}} \times N_{KK} \quad (16)$$

$$N_{KK}^{1/3\ scaled} = \left(\frac{0.360}{0.619}\right) \times \left(\frac{0.385}{0.474}\right) \times \left(\frac{0.3897}{0.4805}\right) \times 0.00599 \pm 0.00599$$

$$= (2.29 \pm 2.29) \times 10^{-3} \quad (17)$$

$$N_{KK}^{2/3\ scaled} = \left(\frac{0.360}{0.619}\right) \times \left(\frac{0.385}{0.474}\right) \times \left(\frac{0.3897}{0.4805}\right) \times 0.00343 \pm 0.00343$$

$$= (1.31 \pm 1.31) \times 10^{-3} \quad (18)$$

5.2.3 $K\pi$-beam background

- Only measure the background in the data before the $\pi\nu\nu(2)$ C_π trigger change. This entails scaling by 2.54 to extrapolate to the full running period.
- ADPV has additional rejection on Kpi background. The normalization branch is bifurcated to measure this rejection and thus the normalization brach is equlivant to $\frac{n_{Kpi}}{r_{Kpi}}$.

$$N_{K\pi}^{1/3} = 3 \times 2.54 \times \frac{\left(\frac{n_{K\pi}^{1/3}}{r_{K\pi}^{1/3}}\right)}{R_{K\pi}^{1/3} - 1} \quad (19)$$

$$N_{K\pi}^{2/3} = \frac{3}{2} \times 2.54 \times \frac{\left(\frac{n_{K\pi}^{2/3}}{r_{K\pi}^{2/3}}\right)}{R_{K\pi}^{2/3} - 1} \quad (20)$$

$$N_{K\pi}^{scaled} = \frac{A_{PV_{tight}}}{A_{PV_{loose}}} \times \frac{A_{BOX_{tight}}}{A_{BOX_{loose}}} \times \frac{A_{TD_{tight}}}{A_{TD_{loose}}} \times N_{K\pi} \quad (21)$$

$$N_{K\pi}^{1/3\ scaled} = \left(\frac{0.360}{0.619}\right) \times \left(\frac{0.385}{0.474}\right) \times \left(\frac{0.3897}{0.4805}\right) \times 0.00245 \pm 0.00245$$

$$= (0.00094 \pm 0.00094) \times 10^{-3} \quad (22)$$

$$N_{K\pi}^{2/3\ scaled} = \left(\frac{0.360}{0.619}\right) \times \left(\frac{0.385}{0.474}\right) \times \left(\frac{0.3897}{0.4805}\right) \times 0.00157 \pm 0.00157$$

$$= (0.00060 \pm 0.00060) \times 10^{-3} \quad (23)$$

5.2.4 KK/Kpi Cut Tables

KK Rej.	Loose		Tight (measured)	
Branch	1/3	2/3	1/3	2/3
BAD_RUN TRIGGER BOX RSDEDXMAX RSDEDXCL RSLIKE	1535485 (0.00)	3067491 (0.00)	1080842 (0.00)	2160149 (0.00)
RNGMOM	986914 (1.56)	1973636 (1.55)	721828 (1.50)	1443507 (1.50)
PV(not TG AD)	177919 (5.55)	357034 (5.53)	47050 (15.34)	94320 (15.30)
PIFLG	177099 (1.00)	355394 (1.00)	46857 (1.00)	93935 (1.00)
EV5	-	-	37913 (1.24)	75955 (1.24)
ELVETO	161595 (1.10)	324198 (1.10)	35148 (1.08)	70326 (1.08)
TDFOOL	161170 (1.00)	323304 (1.00)	35057 (1.00)	70165 (1.00)
TDNN	147389 (1.09)	295450 (1.09)	28711 (1.22)	57337 (1.22)
TDCUT	147389 (1.00)	295450 (1.00)	28614 (1.00)	57131 (1.00)
B4DEDX	87013 (1.69)	174170 (1.70)	16017 (1.79)	32166 (1.78)
TGQUALT	78007 (1.12)	156460 (1.11)	14689 (1.09)	29518 (1.09)
TIMCON	77243 (1.01)	154838 (1.01)	14540 (1.01)	29222 (1.01)
DELCO	22167 (3.48)	44482 (3.48)	4259 (3.41)	8626 (3.39)
TGER	21228 (1.04)	42520 (1.05)	4119 (1.03)	8372 (1.03)
TGZFOOL	15039 (1.41)	30245 (1.41)	2917 (1.41)	5988 (1.40)
UPVTRS	13363 (1.13)	26750 (1.13)	2566 (1.14)	5231 (1.14)
RVTRS	13232 (1.01)	26475 (1.01)	2547 (1.01)	5189 (1.01)
B4ETCON	13025 (1.02)	26004 (1.02)	2512 (1.01)	5111 (1.02)
$\overline{b4trs \cdot b4ccd} \cdot kpigap$	4141 (3.15)	8153 (3.19)	876 (2.87)	1722 (2.97)
CPITRS	1075 (3.85)	2095 (3.89)	204 (4.29)	382 (4.51)
CPITAIL	1073 (1.00)	2090 (1.00)	204 (1.00)	380 (1.01)
$1.1 < b4ars\_atc < 5.0$	**790** (1.36)	**1576** (1.33)	**148** (1.38)	**269** (1.41)
CKTRS	46 (17.17)	78 (20.21)	5 (29.60)	10 (26.90)
CKTAIL	31 (1.48)	57 (1.37)	3 (1.67)	8 (1.25)
BWTRS	**7** (4.43)	**4** (14.25)	**1** (3.00)	**1** (8.00)
R_{KK}	**112.86**	**394.00**	**148.00**	**269.00**

Table 35: KK Rejection. Branch.

Kπ Rej.	Loose		Tight (measured)	
Branch	1/3	2/3	1/3	2/3
BAD_RUN	1535485 (0.00)	3067491 (0.00)	1080842 (0.00)	2160149 (0.00)
TRIGGER BOX RSDEDXMAX RSDEDXCL RSLIKE $Run \leq 49151$	753980 (2.04)	1504842 (2.04)	540485 (2.00)	1078925 (2.00)
RNGMOM	533898 (1.41)	1067802 (1.41)	396676 (1.36)	793454 (1.36)
PV(not TG AD)	111565 (4.79)	223614 (4.78)	29797 (13.31)	59918 (13.24)
Kπ Rej. Branch continued on next page				

Kπ Rej. Branch continued from previous page				
	Loose		Tight (measured)	
	1/3	2/3	1/3	2/3
PIFLG	111134 (1.00)	222761 (1.00)	29694 (1.00)	59726 (1.00)
EV5	111134 (1.00)	222761 (1.00)	23597 (1.26)	47474 (1.26)
ELVETO	101398 (1.10)	203515 (1.09)	21826 (1.08)	43979 (1.08)
TDFOOL	101143 (1.00)	202964 (1.00)	21777 (1.00)	43880 (1.00)
TDNN	92467 (1.09)	185299 (1.10)	17843 (1.22)	35796 (1.23)
B4DEDX	46998 (1.97)	93984 (1.97)	8528 (2.09)	17222 (2.07)
TGQUALT	43233 (1.09)	86663 (1.08)	8059 (1.06)	16314 (1.06)
TIMCON	42833 (1.01)	85820 (1.01)	7984 (1.01)	16160 (1.01)
DELCO	10946 (3.91)	22167 (3.87)	2029 (3.93)	4248 (3.80)
TGER	10400 (1.05)	21006 (1.06)	1935 (1.05)	4104 (1.04)
TGZFOOL	7253 (1.43)	14882 (1.41)	1345 (1.44)	2897 (1.42)
UPVTRS	6307 (1.15)	12801 (1.16)	1172 (1.15)	2463 (1.18)
RVTRS	6240 (1.01)	12670 (1.01)	1163 (1.01)	2443 (1.01)
B4ETCON	6146 (1.02)	12446 (1.02)	1146 (1.01)	2411 (1.01)
$\overline{b4trs \cdot b4ccd \cdot kpigap}$	2207 (2.78)	4476 (2.78)	461 (2.49)	934 (2.58)
CKTRS	1834 (1.20)	3730 (1.20)	391 (1.18)	810 (1.15)
CKTAIL	1819 (1.01)	3695 (1.01)	388 (1.01)	804 (1.01)
$b4ars\_atc < 1.1$	**1179** (1.54)	**2467** (1.50)	**261** (1.49)	**541** (1.49)
CPITRS	17 (69.35)	23 (107.26)	4 (65.25)	5 (108.20)
CPITAIL	17 (1.00)	21 (1.10)	4 (1.00)	4 (1.25)
BWTRS	**2** (8.50)	**4** (5.25)	**0** (4.00)	**0** (4.00)
R_{Kpi}	**589.50**	**616.75**	**261.00**	**541.00**

Table 36: Kpi Rejection. Branch.

KK Norm. Branch	Loose 1/3	Loose 2/3	Tight (measured) 1/3	Tight (measured) 2/3
BAD_RUN	1535485 (0.00)	3067491 (0.00)	1080842 (0.00)	2160149 (0.00)
TRIGGER BOX RSDEDXMAX RSDEDXCL RSLIKE PV(not TG AD)	397178 (3.87)	794492 (3.86)	107156 (10.09)	214497 (10.07)
TGQUALT	370184 (1.07)	741330 (1.07)	101820 (1.05)	203689 (1.05)
TIMCON	367052 (1.01)	734731 (1.01)	101063 (1.01)	202174 (1.01)
EPITG	291482 (1.26)	582642 (1.26)	79985 (1.26)	159822 (1.26)
TGER	286430 (1.02)	572404 (1.02)	78986 (1.01)	157856 (1.01)
TICCON	286427 (1.00)	572390 (1.00)	78985 (1.00)	157853 (1.00)
DTGTTP	286387 (1.00)	572315 (1.00)	78978 (1.00)	157836 (1.00)
RTDIF	280898 (1.02)	561297 (1.02)	77509 (1.02)	154973 (1.02)
DRP	276717 (1.02)	553065 (1.01)	76598 (1.01)	153262 (1.01)
EICCON	272205 (1.02)	543827 (1.02)	75528 (1.01)	151096 (1.01)
KIC	232562 (1.17)	464232 (1.17)	65645 (1.15)	131207 (1.15)
KK Norm. Branch continued on next page				

KK Norm. Branch continued from previous page				
	Loose		Tight (measured)	
	1/3	2/3	1/3	2/3
UPVTRS	216575 (1.07)	432489 (1.07)	61168 (1.07)	122183 (1.07)
RVTRS	214069 (1.01)	427417 (1.01)	60667 (1.01)	121164 (1.01)
TGTCON	203722 (1.05)	406388 (1.05)	57939 (1.05)	115505 (1.05)
B4ETCON	198850 (1.02)	396614 (1.02)	56614 (1.02)	112892 (1.02)
DELCO	38022 (5.23)	75997 (5.22)	9106 (6.22)	18221 (6.20)
CPITRS	31092 (1.22)	62303 (1.22)	7039 (1.29)	14048 (1.30)
CPITAIL	31084 (1.00)	62282 (1.00)	7039 (1.00)	14042 (1.00)
$\overline{cktrs \cdot cktail \cdot bwtrs}$	26116 (1.19)	52543 (1.19)	6104 (1.15)	12254 (1.15)
LAYER14	26116 (1.00)	52543 (1.00)	6104 (1.00)	12254 (1.00)
COS3D	25354 (1.03)	51008 (1.03)	5900 (1.03)	11875 (1.03)
LAYV4	25354 (1.00)	51008 (1.00)	5900 (1.00)	11875 (1.00)
ZFRF	25340 (1.00)	50973 (1.00)	5896 (1.00)	11866 (1.00)
ZUTOUT	25329 (1.00)	50937 (1.00)	5894 (1.00)	11859 (1.00)
UTCQUAL	23711 (1.07)	47549 (1.07)	5579 (1.06)	11245 (1.05)
RNGMOM	1747 (13.57)	3413 (13.93)	358 (15.58)	739 (15.22)
PRRF1	1731 (1.01)	3381 (1.01)	355 (1.01)	734 (1.01)
PRRFZ	1651 (1.05)	3260 (1.04)	344 (1.03)	705 (1.04)
PIFLG	1633 (1.01)	3237 (1.01)	342 (1.01)	703 (1.00)
EV5	-	-	290 (1.18)	609 (1.15)
ELVETO	1514 (1.08)	2966 (1.09)	273 (1.06)	571 (1.07)
TDFOOL	1509 (1.00)	2961 (1.00)	272 (1.00)	569 (1.00)
TDNN	1363 (1.11)	2699 (1.10)	213 (1.28)	464 (1.23)
TDCUT	**1363** (1.00)	**2699** (1.00)	**212** (1.00)	**462** (1.00)
r_{KK} branch				
ADPV	**182** (7.49)	**325** (8.30)	**22** (9.64)	**48** (9.62)
r_{KK}	**7.49**	**8.30**	**9.64**	**9.62**
n_{KK} branch				
TGKTIM	1319 (1.03)	2607 (1.04)	208 (1.02)	443 (1.04)
TGENR	1309 (1.01)	2579 (1.01)	207 (1.00)	442 (1.00)
CHI567	545 (2.40)	1081 (2.39)	84 (2.46)	183 (2.42)
NPITG	545 (1.00)	1081 (1.00)	84 (1.00)	183 (1.00)
VERRNG	173 (3.15)	361 (2.99)	20 (4.20)	58 (3.16)
CHI5MAX	173 (1.00)	361 (1.00)	20 (1.00)	58 (1.00)
ANGLI	173 (1.00)	357 (1.01)	20 (1.00)	56 (1.04)
ALLKFIT	151 (1.15)	319 (1.12)	18 (1.11)	47 (1.19)
TPICS	151 (1.00)	319 (1.00)	18 (1.00)	47 (1.00)
EPIONK	99 (1.53)	214 (1.49)	12 (1.50)	32 (1.47)
CCDPUL CCDBADFIT CCDBADTIM CCD31FIB	25 (3.96)	65 (3.29)	6 (2.00)	9 (3.56)
TIMKF	20 (1.25)	51 (1.27)	5 (1.20)	7 (1.29)
TGGEO	13 (1.54)	38 (1.34)	4 (1.25)	5 (1.40)
TGZFOOL	7 (1.86)	17 (2.24)	2 (2.00)	2 (2.50)
B4DEDX	6 (1.17)	17 (1.00)	2 (1.00)	2 (1.00)
KK Norm. Branch continued on next page				

KK Norm. Branch continued from previous page				
	Loose		Tight (measured)	
	1/3	2/3	1/3	2/3
B4TRS	0 (6.00)	1 (17.00)	0 (2.00)	0 (2.00)
B4CCD	0 (0.00)	1 (1.00)	0 (0.00)	0 (0.00)
TARGF	0 (0.00)	1 (1.00)	0 (0.00)	0 (0.00)
B4EKZ	0 (0.00)	0 (1.00)	0 (0.00)	0 (0.00)
EPIMAXK	0 (0.00)	0 (0.00)	0 (0.00)	0 (0.00)
PHIVTX	0 (0.00)	0 (0.00)	0 (0.00)	0 (0.00)
OPSVETO	0 (0.00)	0 (0.00)	0 (0.00)	0 (0.00)
TGEDGE	0 (0.00)	0 (0.00)	0 (0.00)	0 (0.00)
TGDEDX	0 (0.00)	0 (0.00)	0 (0.00)	0 (0.00)
TGLIKE1	0 (0.00)	0 (0.00)	0 (0.00)	0 (0.00)
TGLIKE2	0 (0.00)	0 (0.00)	0 (0.00)	0 (0.00)
TBDB4	0 (0.00)	0 (0.00)	0 (0.00)	0 (0.00)
TGDB4TIP	0 (0.00)	0 (0.00)	0 (0.00)	0 (0.00)
TGDVXTIP	0 (0.00)	0 (0.00)	0 (0.00)	0 (0.00)
TGDVXPI	0 (0.00)	0 (0.00)	0 (0.00)	0 (0.00)
PIGAP	0 (0.00)	0 (0.00)	0 (0.00)	0 (0.00)
TGPV	0 (0.00)	0 (0.00)	0 (0.00)	0 (0.00)
n_{KK}	$\mathbf{1.0 \pm 1.0}$	$\mathbf{1.0 \pm 1.0}$	$\mathbf{1.0 \pm 1.0}$	$\mathbf{1.0 \pm 1.0}$

Table 37: 2-Beam KK Normalization Branches. First number in each cell is the number of events remaining after cut is applied. Number in parenthesis is the rejection of the cut. After the TDNN cut is applied the normalization branch is bifurcated and the rejection of ADPV is measured; this is denoted within this table. ADPV is not applied for the sample of events that follow the ADPV-row.

Kπ Norm. Branch	Loose		Tight (measured)	
	1/3	2/3	1/3	2/3
BAD_RUN TRIGGER BOX RSDEDXMAX RSDEDXCL RSLIKE	1535485 (0.00)	3067491 (0.00)	1080842 (0.00)	2160149 (0.00)
$Run \leq 49151$	753980 (2.04)	1504842 (2.04)	540485 (2.00)	1078925 (2.00)
PV(not TG AD)	196884 (3.83)	392721 (3.83)	52730 (10.25)	105760 (10.20)
TGQUALT	185037 (1.06)	369660 (1.06)	50595 (1.04)	101363 (1.04)
TIMCON	183607 (1.01)	366643 (1.01)	50243 (1.01)	100685 (1.01)
EPITG	143765 (1.28)	286585 (1.28)	39038 (1.29)	78181 (1.29)
TGER	141255 (1.02)	281616 (1.02)	38554 (1.01)	77253 (1.01)
TICCON	141253 (1.00)	281613 (1.00)	38553 (1.00)	77253 (1.00)
DTGTTP	141226 (1.00)	281573 (1.00)	38549 (1.00)	77247 (1.00)
RTDIF	137649 (1.03)	274502 (1.03)	37580 (1.03)	75377 (1.02)
DRP	135573 (1.02)	270426 (1.02)	37126 (1.01)	74575 (1.01)
EICCON	133056 (1.02)	265434 (1.02)	36533 (1.02)	73390 (1.02)
Kπ Norm. Branch continued on next page				

Kπ Norm. Branch continued from previous page				
	Loose		Tight (measured)	
	1/3	2/3	1/3	2/3
KIC	114175 (1.17)	227822 (1.17)	31890 (1.15)	64011 (1.15)
UPVTRS	103767 (1.10)	207216 (1.10)	28977 (1.10)	58142 (1.10)
RVTRS	102582 (1.01)	204809 (1.01)	28733 (1.01)	57664 (1.01)
TGTCON	97293 (1.05)	193863 (1.06)	27330 (1.05)	54675 (1.05)
B4ETCON	94765 (1.03)	188878 (1.03)	26667 (1.02)	53313 (1.03)
DELCO	14673 (6.46)	29403 (6.42)	3413 (7.81)	6933 (7.69)
CKTRS	6036 (2.43)	11987 (2.45)	1416 (2.41)	2832 (2.45)
CKTAIL	5787 (1.04)	11497 (1.04)	1393 (1.02)	2777 (1.02)
$\overline{cpitrs \cdot cpitail \cdot bwtrs}$	3901 (1.48)	7933 (1.45)	1051 (1.33)	2148 (1.29)
LAYER14	3901 (1.00)	7933 (1.00)	1051 (1.00)	2148 (1.00)
COS3D	3511 (1.11)	7084 (1.12)	957 (1.10)	1882 (1.14)
LAYV4	3511 (1.00)	7084 (1.00)	957 (1.00)	1882 (1.00)
ZFRF	3509 (1.00)	7083 (1.00)	957 (1.00)	1881 (1.00)
ZUTOUT	3507 (1.00)	7080 (1.00)	956 (1.00)	1881 (1.00)
UTCQUAL	3320 (1.06)	6665 (1.06)	914 (1.05)	1779 (1.06)
RNGMOM	2848 (1.17)	5710 (1.17)	820 (1.11)	1625 (1.09)
PRRF1	2819 (1.01)	5657 (1.01)	811 (1.01)	1610 (1.01)
PRRFZ	2687 (1.05)	5357 (1.06)	784 (1.03)	1537 (1.05)
PIFLG	2682 (1.00)	5341 (1.00)	784 (1.00)	1534 (1.00)
EV5	-	-	638 (1.23)	1240 (1.24)
ELVETO	2482 (1.08)	4899 (1.09)	587 (1.09)	1163 (1.07)
TDFOOL	2475 (1.00)	4886 (1.00)	587 (1.00)	1158 (1.00)
TDNN	2289 (1.08)	4435 (1.10)	497 (1.18)	943 (1.23)
TDCUT	**2289** (1.00)	**4435** (1.00)	**494** (1.01)	**939** (1.00)
$r_{K\pi}$ branch				
ADPV	**221** (10.36)	**464** (9.56)	**36** (13.72)	**92** (10.21)
$\mathbf{r_{K\pi}}$	**10.36**	**9.56**	**13.72**	**10.21**
$n_{K\pi}$ branch				
TGKTIM	2230 (1.03)	4328 (1.02)	485 (1.02)	924 (1.02)
TGENR	2192 (1.02)	4276 (1.01)	475 (1.02)	910 (1.02)
CHI567	1022 (2.14)	2010 (2.13)	217 (2.19)	409 (2.22)
NPITG	1022 (1.00)	2010 (1.00)	217 (1.00)	409 (1.00)
VERRNG	303 (3.37)	632 (3.18)	73 (2.97)	136 (3.01)
CHI5MAX	303 (1.00)	632 (1.00)	73 (1.00)	136 (1.00)
ANGLI	299 (1.01)	629 (1.00)	73 (1.00)	136 (1.00)
ALLKFIT	262 (1.14)	550 (1.14)	62 (1.18)	122 (1.11)
TPICS	262 (1.00)	550 (1.00)	62 (1.00)	122 (1.00)
EPIONK	177 (1.48)	366 (1.50)	40 (1.55)	77 (1.58)
CCDPUL CCDBADFIT CCDBADTIM CCD31FIB	67 (2.64)	109 (3.36)	15 (2.67)	28 (2.75)
TIMKF	52 (1.29)	81 (1.35)	11 (1.36)	22 (1.27)
TGGEO	32 (1.62)	51 (1.59)	6 (1.83)	14 (1.57)
TGZFOOL	22 (1.45)	36 (1.42)	3 (2.00)	10 (1.40)
				Kπ Norm. Branch continued on next page

Kπ Norm. Branch continued from previous page				
	Loose		Tight (measured)	
	1/3	2/3	1/3	2/3
B4DEDX	21 (1.05)	34 (1.06)	3 (1.00)	9 (1.11)
B4TRS	0 (21.00)	1 (34.00)	0 (3.00)	0 (9.00)
B4CCD	0 (0.00)	0 (1.00)	0 (0.00)	0 (0.00)
TARGF	0 (0.00)	0 (0.00)	0 (0.00)	0 (0.00)
B4EKZ	0 (0.00)	0 (0.00)	0 (0.00)	0 (0.00)
EPIMAXK	0 (0.00)	0 (0.00)	0 (0.00)	0 (0.00)
PHIVTX	0 (0.00)	0 (0.00)	0 (0.00)	0 (0.00)
OPSVETO	0 (0.00)	0 (0.00)	0 (0.00)	0 (0.00)
TGEDGE	0 (0.00)	0 (0.00)	0 (0.00)	0 (0.00)
TGDEDX	0 (0.00)	0 (0.00)	0 (0.00)	0 (0.00)
TGLIKE1	0 (0.00)	0 (0.00)	0 (0.00)	0 (0.00)
TGLIKE2	0 (0.00)	0 (0.00)	0 (0.00)	0 (0.00)
TBDB4	0 (0.00)	0 (0.00)	0 (0.00)	0 (0.00)
TGDB4TIP	0 (0.00)	0 (0.00)	0 (0.00)	0 (0.00)
TGDVXTIP	0 (0.00)	0 (0.00)	0 (0.00)	0 (0.00)
TGDVXPI	0 (0.00)	0 (0.00)	0 (0.00)	0 (0.00)
PIGAP	0 (0.00)	0 (0.00)	0 (0.00)	0 (0.00)
TGPV	0 (0.00)	0 (0.00)	0 (0.00)	0 (0.00)
$n_{K\pi}$	$\mathbf{1.0 \pm 1.0}$	$\mathbf{1.0 \pm 1.0}$	$\mathbf{1.0 \pm 1.0}$	$\mathbf{1.0 \pm 1.0}$

Table 38: 2-Beam Kπ Normalization Branches. First number in each cell is the number of events remaining after cut is applied. Number in parenthesis is the rejection of the cut. After the TDNN cut is applied the normalization branch is bifurcated and the rejection of ADPV is measured; this is denoted within this table. ADPV is not applied for the sample of events that follow the ADPV-row.

5.3 Beam Background Summary

Bkgrnd	Loose		Tight (measured)		Tight (scaled)	
($\times 10^{-3}$)	1/3	2/3	1/3	2/3	1/3	2/3
1-BM	0.46 ± 0.46	0.23 ± 0.23	0.46 ± 0.46	0.19 ± 0.19	0.18 ± 0.18	0.073 ± 0.073
N_{KK}	3.59 ± 3.59	0.458 ± 0.458	2.12 ± 2.12	0.58 ± 0.58	2.29 ± 2.29	1.31 ± 1.31
$N_{K\pi}$	1.26 ± 1.26	0.650 ± 0.650	0.945 ± 0.945	0.69 ± 0.69	0.94 ± 0.94	0.60 ± 0.60
2-BM	4.85 ± 3.80	1.11 ± 0.80	3.07 ± 2.32	1.27 ± 0.90	3.23 ± 2.48	1.91 ± 1.44
N_{Beam}	5.31 ± 3.83	1.34 ± 0.83	3.53 ± 2.37	1.46 ± 0.92	3.41 ± 2.48	1.98 ± 1.44

Table 39: **Beam Background Summary.** Scaled to the 3/3 sample. The "Tight (measured)" column is the direct measurement of the tight signal region while inverting the loose cut (if applicable); When the statistics of the tight region is limited, so the loose-region rejection is used. The "Tight (scaled)" is the background measurement used in the final BR measurement.

6 Muon Background

The muon background is expected to come mainly from $K^+ \to \mu^+\nu\gamma$ and $K^+ \to \pi^0\mu^+\nu$ decays ($K_{\mu 2\gamma}$) in the PNN2 kinematic region. This background is expected to be small, because for these processes to be confused with signal, both the muon has to be misidentified as a π^+ and the photon(s) have to be missed. The cuts used to suppress the muon background are the $\pi^+ \to \mu^+ \to e^+$ decay sequence cuts (TDCUT02) and the π/μ kinematic separation cut, RNGMOM. The rejection of TDCUT02 is measured by inverting RNGMOM on an appropriate sample of muon decays. The normalization is measured after applying the loose TDCUT02; this is also done in the tight background measurement, to avoid looking in the box.

Table 40 shows the measured rejection and normalization values for the 1/3 and 2/3 data sets and the loose and tight signal region. Also, listed are additional rejection measurements on cleaner samples by applying $ERBox$, PV_{PNN2}, or $ERBox \cdot PV_{PNN2}$. The cleaner samples have much less statistics and it was decided to utilize the large sample (bold values) due to the lower statistical uncertainty. The measured rejections for the various samples are consistent within 2σ.

	Loose		Tight	
	1/3	2/3	1/3	2/3
$\mathbf{R_\mu}$	$\mathbf{122.95 \pm 13.36}$	$\mathbf{133.04 \pm 10.68}$	$\mathbf{545.71 \pm 132.23}$	$\mathbf{409.13 \pm 60.92}$
R_μ^{ERbox}	96.69 ± 26.68	126.84 ± 28.98	375.33 ± 216.41	1088.00 ± 768.98
R_μ^{PV}	215.67 ± 62.11	182.32 ± 34.36	2321.00 ± 2320.50	901.40 ± 402.89
$R_\mu^{PV \cdot ERbox}$	37.50 ± 26.16	127.00 ± 126.50	59.00 ± 58.50	112.00 ± 111.50
$\mathbf{Norm_\mu}$	$\mathbf{0}$	$\mathbf{1. \pm 1.}$	$\mathbf{0}$	$\mathbf{1 \pm 1.}$

Table 40: Rejection and Normalization for Muon Background. R=Rej, Norm=Normalization, PV= PV_{PNN2} cut. The rejection for additional samples are displayed, such that the additional cuts are listed (ERbox= $EBOX \cdot RBOX$) and PV_{PNN2}. The difference between loose and tight columns are the application of the loose or tight version of DELCO, PV, TD, and BOX. Bold indicates that the value is used in the final measurement. Tables 43 and 43 details the cuts employed in the rows with bold numbers.

The background is calculated by Eq. (24) and Eq. (25). Table 41 is obtained by using these equations and the measured values from Table 40. The muon background in the tight signal region is determined by using a scaling method as shown in Eq. (26). The values determined by the scaling method is used in the final determination of the branching ratio. The directly measured background is also shown in Table 41 for comparison purposes.

$$N_\mu^{1/3} = 3 \times \frac{Norm_\mu^{1/3}}{R_\mu^{1/3} - 1} \tag{24}$$

$$N_\mu^{2/3} = \frac{3}{2} \times \frac{Norm_\mu^{2/3}}{R_\mu^{2/3} - 1} \tag{25}$$

$$N_\mu^{scaled} = \frac{A_{PV_{tight}}}{A_{PV_{loose}}} \times \frac{A_{BOX_{tight}}}{A_{BOX_{loose}}} \times \frac{A_{beam_{tight}}}{A_{beam_{loose}}} \times \frac{R_\mu^{Loose}}{R_\mu^{Tight}} \times N_\mu \quad (26)$$

$$N_\mu^{1/3\ scaled} = \left(\frac{0.360}{0.619}\right) \times \left(\frac{0.385}{0.474}\right) \times \left(\frac{0.137}{0.151}\right) \times \left(\frac{64.94}{221.26}\right) \times 0.0469$$

$$= 0.00590 \pm 0.00590 \quad (27)$$

$$N_\mu^{2/3\ scaled} = \left(\frac{0.360}{0.619}\right) \times \left(\frac{0.385}{0.474}\right) \times \left(\frac{0.137}{0.151}\right) \times \left(\frac{62.49}{230.99}\right) \times 0.0244$$

$$= 0.00283 \pm 0.00283 \quad (28)$$

	Loose		Tight (measured)		Tight (scaled)	
$\times 10^{-3}$	1/3	2/3	1/3	2/3	1/3	2/3
$\mathbf{N_\mu}$	$\mathbf{24.6 \pm 24.6}$	$\mathbf{11.4 \pm 11.4}$	$\mathbf{5.51 \pm 5.51}$	$\mathbf{3.68 \pm 3.68}$		
N_μ^{ERbox}	31.4 ± 31.4	11.9 ± 11.9	8.01 ± 8.01	1.38 ± 1.38		
N_μ^{PV}	13.9751 ± 14.0	8.27 ± 8.27	1.29 ± 1.29	1.67 ± 1.67		
$N_\mu^{PV \cdot ERbox}$	82.2 ± 82.2	11.9 ± 11.9	51.7 ± 51.7	13.5 ± 13.5		

Table 41: Muon Background. All values are scaled to the 3/3 and expressed in units of $\times 10^{-3}$ events. Bold indicate that the value used in the final measurements. The values are obtained by using Eq. (24) and Eq. (25).

Rej	Loose		Tight (measured)	
Branch	1/3	2/3	1/3	2/3
BAD_RUN	12892493 (0.00)	25768044 (0.00)	12892493 (0.00)	25768040 (0.00)
TRIGGER	12823737 (1.01)	25631012 (1.01)	12823737 (1.01)	25631012 (1.01)
DUPL_EVT	12823737 (1.00)	25631012 (1.00)	12823737 (1.00)	25631012 (1.00)
RD_TRK	12823737 (1.00)	25631012 (1.00)	12823737 (1.00)	25631012 (1.00)
TRKTIM	12823737 (1.00)	25631012 (1.00)	12823737 (1.00)	25631012 (1.00)
TARGET	12823737 (1.00)	25631012 (1.00)	12823737 (1.00)	25631012 (1.00)
STLAY	12823737 (1.00)	25631012 (1.00)	12823737 (1.00)	25631012 (1.00)
UTC	12823737 (1.00)	25631012 (1.00)	12823737 (1.00)	25631012 (1.00)
RDUTM	12823737 (1.00)	25631012 (1.00)	12823737 (1.00)	25631012 (1.00)
BADSTC	12823737 (1.00)	25631012 (1.00)	12823737 (1.00)	25631012 (1.00)
PDC	12823737 (1.00)	25631012 (1.00)	12823737 (1.00)	25631012 (1.00)
B4DEDX	11409696 (1.12)	22803548 (1.12)	11409696 (1.12)	22803548 (1.12)
BWTRS	8868972 (1.29)	17724326 (1.29)	8868972 (1.29)	17724324 (1.29)
B4TRS	8220794 (1.08)	16427904 (1.08)	8220794 (1.08)	16427903 (1.08)
B4ETCON	8135020 (1.01)	16256902 (1.01)	8135020 (1.01)	16256901 (1.01)
Rej. Branch continued on next page				

Rej. Branch continued from previous page

	Loose		Tight (measured)	
	1/3	2/3	1/3	2/3
B4CCD	8036604 (1.01)	16060975 (1.01)	8036604 (1.01)	16060974 (1.01)
CPITRS	7688327 (1.05)	15362723 (1.05)	7688327 (1.05)	15362722 (1.05)
CPITAIL	7684992 (1.00)	15355998 (1.00)	7684992 (1.00)	15355997 (1.00)
CKTRS	5335463 (1.44)	10660536 (1.44)	5335463 (1.44)	10660535 (1.44)
CKTAIL	5062839 (1.05)	10118608 (1.05)	5062839 (1.05)	10118607 (1.05)
TGQUALT	4815371 (1.05)	9625818 (1.05)	4815371 (1.05)	9625817 (1.05)
TIMCON	4789227 (1.01)	9573254 (1.01)	4789227 (1.01)	9573253 (1.01)
TGTCON	4683555 (1.02)	9361755 (1.02)	4683555 (1.02)	9361754 (1.02)
RVTRS	4666832 (1.00)	9328367 (1.00)	4666832 (1.00)	9328366 (1.00)
UPVTRS	4585317 (1.02)	9165183 (1.02)	4585317 (1.02)	9165182 (1.02)
DELCO	3976305 (1.15)	7947312 (1.15)	3311966 (1.38)	6622308 (1.38)
TGGEO	2926088 (1.36)	5848653 (1.36)	2429497 (1.36)	4859101 (1.36)
$\overline{RNGMOM}$	1209061 (2.42)	2414194 (2.42)	1004904 (2.42)	2007254 (2.42)
B4EKZ	1014599 (1.19)	2025353 (1.19)	841842 (1.19)	1681767 (1.19)
EPITG	844535 (1.20)	1685549 (1.20)	700195 (1.20)	1398422 (1.20)
EPIMAXK	844535 (1.00)	1685549 (1.00)	700195 (1.00)	1398422 (1.00)
TARGF	806399 (1.05)	1610360 (1.05)	668510 (1.05)	1336053 (1.05)
TGER	804818 (1.00)	1607188 (1.00)	667089 (1.00)	1333214 (1.00)
DTGTTP	804809 (1.00)	1607170 (1.00)	667080 (1.00)	1333203 (1.00)
RTDIF	797785 (1.01)	1592799 (1.01)	661169 (1.01)	1321157 (1.01)
DRP	796019 (1.00)	1589231 (1.00)	659637 (1.00)	1318057 (1.00)
TGKTIM	789942 (1.01)	1577192 (1.01)	658244 (1.00)	1315468 (1.00)
EICCON	755694 (1.05)	1508824 (1.05)	629671 (1.05)	1258394 (1.05)
TICCON	755690 (1.00)	1508815 (1.00)	629667 (1.00)	1258386 (1.00)
TGEDGE	750037 (1.01)	1497404 (1.01)	626047 (1.01)	1251032 (1.01)
TGENR	731229 (1.03)	1459572 (1.03)	609732 (1.03)	1218178 (1.03)
PIGAP	721184 (1.01)	1439511 (1.01)	601284 (1.01)	1201394 (1.01)
TGLIKE	687003 (1.05)	1371135 (1.05)	572485 (1.05)	1143743 (1.05)
TBDB4	670474 (1.02)	1338069 (1.02)	558506 (1.03)	1115756 (1.03)
TGDB4TIP	667741 (1.00)	1332645 (1.00)	556160 (1.00)	1111135 (1.00)
TGDVXTIP	666148 (1.00)	1329452 (1.00)	554824 (1.00)	1108455 (1.00)
TGDVXPI	644754 (1.03)	1286459 (1.03)	538467 (1.03)	1075438 (1.03)
PHIVTX	621056 (1.04)	1239008 (1.04)	516196 (1.04)	1030809 (1.04)
OPSVETO	609426 (1.02)	1216002 (1.02)	506253 (1.02)	1011139 (1.02)
TIMKF	554815 (1.10)	1106913 (1.10)	460804 (1.10)	920542 (1.10)
NPITG	554815 (1.00)	1106913 (1.00)	460804 (1.00)	920542 (1.00)
KIC	554684 (1.00)	1106656 (1.00)	460685 (1.00)	920321 (1.00)
TGZFOOL	540905 (1.03)	1078953 (1.03)	449378 (1.03)	897519 (1.03)
LAYV4	540901 (1.00)	1078937 (1.00)	449374 (1.00)	897503 (1.00)
LAYER14	508124 (1.06)	1013162 (1.06)	422058 (1.06)	842848 (1.06)
TGPVCUT	504326 (1.01)	1005715 (1.01)	418866 (1.01)	836630 (1.01)
CCDPUL	225452 (2.24)	450396 (2.23)	203353 (2.06)	406666 (2.06)
EPIONK	224362 (1.00)	448118 (1.01)	202263 (1.01)	404388 (1.01)
CCDBADTIM	223005 (1.01)	445314 (1.01)	201028 (1.01)	401797 (1.01)
CCD31FIB	223005 (1.00)	445313 (1.00)	201028 (1.00)	401796 (1.00)

Rej. Branch continued on next page

Rej. Branch continued from previous page				
	Loose		Tight (measured)	
	1/3	2/3	1/3	2/3
VERRNG	205833 (1.08)	411064 (1.08)	185478 (1.08)	370716 (1.08)
ANGLI	205739 (1.00)	410874 (1.00)	185389 (1.00)	370540 (1.00)
ALLKFIT	203518 (1.01)	406444 (1.01)	183335 (1.01)	366394 (1.01)
TPICS	203469 (1.00)	406344 (1.00)	183286 (1.00)	366296 (1.00)
COS3D	185183 (1.10)	369023 (1.10)	166870 (1.10)	332720 (1.10)
ZFRF	166944 (1.11)	332289 (1.11)	150569 (1.11)	299967 (1.11)
ZUTOUT	166803 (1.00)	332022 (1.00)	150443 (1.00)	299722 (1.00)
RSDEDXMAX	120467 (1.38)	239910 (1.38)	108580 (1.39)	216439 (1.38)
RSDEDXCL	69911 (1.72)	138531 (1.73)	63003 (1.72)	124943 (1.73)
RSLIKE	67539 (1.04)	133668 (1.04)	60872 (1.04)	120552 (1.04)
UTCQUAL	64542 (1.05)	127573 (1.05)	58194 (1.05)	115078 (1.05)
PRRF1	38366 (1.68)	75729 (1.68)	34602 (1.68)	68257 (1.69)
PRRFZ	32906 (1.17)	64883 (1.17)	29684 (1.17)	58456 (1.17)
TGGEO	32906 (1.00)	64883 (1.00)	29684 (1.00)	58456 (1.00)
TGDEDX	32631 (1.01)	64304 (1.01)	29443 (1.01)	57939 (1.01)
PV_{PNN1}	**10328** (3.16)	**20488** (3.14)	**9277** (3.17)	**18411** (3.15)
TDCUT	794 (13.01)	1561 (13.12)	721 (12.87)	1400 (13.15)
PIFLG	785 (1.01)	1550 (1.01)	713 (1.01)	1392 (1.01)
ELVETO	638 (1.23)	1208 (1.28)	584 (1.22)	1091 (1.28)
TDFOOL	619 (1.03)	1187 (1.02)	565 (1.03)	1072 (1.02)
TDNN	84 (7.37)	154 (7.71)	37 (15.27)	87 (12.32)
EV5	84 (1.00)	154 (1.00)	17 (2.18)	45 (1.93)
TD Rej.	122.95 ± 13.36	133.04 ± 10.68	545.71 ± 132.23	409.13 ± 60.92

Table 42: Muon Background Rejection Branch. Shown are the number of events remaining after applying the cut in the first column; number in parenthesis is the rejection of the cut within this sample.

Norm	Loose		Tight (measured)	
Branch	1/3	2/3	1/3	2/3
BAD_RUN	12892493 (0.00)	25768044 (0.00)	12892493 (0.00)	25768044 (0.00)
TRIGGER	12823737 (1.01)	25631012 (1.01)	12823737 (1.01)	25631012 (1.01)
DUPL_EVT	12823737 (1.00)	25631012 (1.00)	12823737 (1.00)	25631012 (1.00)
RD_TRK	12823737 (1.00)	25631012 (1.00)	12823737 (1.00)	25631012 (1.00)
TRKTIM	12823737 (1.00)	25631012 (1.00)	12823737 (1.00)	25631012 (1.00)
TARGET	12823737 (1.00)	25631012 (1.00)	12823737 (1.00)	25631012 (1.00)
STLAY	12823737 (1.00)	25631012 (1.00)	12823737 (1.00)	25631012 (1.00)
UTC	12823737 (1.00)	25631012 (1.00)	12823737 (1.00)	25631012 (1.00)
RDUTM	12823737 (1.00)	25631012 (1.00)	12823737 (1.00)	25631012 (1.00)
BADSTC	12823737 (1.00)	25631012 (1.00)	12823737 (1.00)	25631012 (1.00)
PDC	12823737 (1.00)	25631012 (1.00)	12823737 (1.00)	25631012 (1.00)
B4DEDX	11409696 (1.12)	22803548 (1.12)	11409696 (1.12)	22803548 (1.12)
Norm. Branch continued on next page				

Norm. Branch continued from previous page

	Loose		Tight (measured)	
	1/3	2/3	1/3	2/3
BWTRS	8868972 (1.29)	17724326 (1.29)	8868972 (1.29)	17724326 (1.29)
B4TRS	8220794 (1.08)	16427904 (1.08)	8220794 (1.08)	16427904 (1.08)
B4ETCON	8135020 (1.01)	16256902 (1.01)	8135020 (1.01)	16256902 (1.01)
B4CCD	8036604 (1.01)	16060975 (1.01)	8036604 (1.01)	16060975 (1.01)
CPITRS	7688327 (1.05)	15362723 (1.05)	7688327 (1.05)	15362723 (1.05)
CPITAIL	7684992 (1.00)	15355998 (1.00)	7684992 (1.00)	15355998 (1.00)
CKTRS	5335463 (1.44)	10660536 (1.44)	5335463 (1.44)	10660536 (1.44)
CKTAIL	5062839 (1.05)	10118608 (1.05)	5062839 (1.05)	10118608 (1.05)
TGQUALT	4815371 (1.05)	9625818 (1.05)	4815371 (1.05)	9625818 (1.05)
TIMCON	4789227 (1.01)	9573254 (1.01)	4789227 (1.01)	9573254 (1.01)
TGTCON	4683555 (1.02)	9361755 (1.02)	4683555 (1.02)	9361755 (1.02)
RVTRS	4666832 (1.00)	9328367 (1.00)	4666832 (1.00)	9328367 (1.00)
UPVTRS	4585317 (1.02)	9165183 (1.02)	4585317 (1.02)	9165183 (1.02)
DELCO	3976305 (1.15)	7947312 (1.15)	3311966 (1.38)	6622309 (1.38)
TGGEO	2926088 (1.36)	5848653 (1.36)	2429497 (1.36)	4859102 (1.36)
$\overline{TDcutloose}$	2121654 (1.38)	4239416 (1.38)	1761178 (1.38)	3520415 (1.38)
BOX	64902 (32.69)	130019 (32.61)	29392 (59.92)	59045 (59.62)
B4EKZ	51753 (1.25)	104333 (1.25)	22683 (1.30)	46090 (1.28)
EPITG	42815 (1.21)	86699 (1.20)	18186 (1.25)	37093 (1.24)
EPIMAXK	42815 (1.00)	86699 (1.00)	18186 (1.00)	37093 (1.00)
TARGF	40098 (1.07)	80897 (1.07)	16765 (1.08)	34060 (1.09)
TGER	40050 (1.00)	80753 (1.00)	16754 (1.00)	34021 (1.00)
DTGTTP	40048 (1.00)	80753 (1.00)	16754 (1.00)	34021 (1.00)
RTDIF	39715 (1.01)	80095 (1.01)	16617 (1.01)	33723 (1.01)
DRP	39402 (1.01)	79484 (1.01)	16527 (1.01)	33547 (1.01)
TGKTIM	38977 (1.01)	78645 (1.01)	16473 (1.00)	33422 (1.00)
EICCON	38147 (1.02)	77034 (1.02)	16095 (1.02)	32718 (1.02)
TICCON	38147 (1.00)	77034 (1.00)	16095 (1.00)	32718 (1.00)
TGEDGE	37730 (1.01)	76147 (1.01)	15950 (1.01)	32383 (1.01)
TGENR	37024 (1.02)	74676 (1.02)	15632 (1.02)	31763 (1.02)
PIGAP	36676 (1.01)	74019 (1.01)	15459 (1.01)	31436 (1.01)
TGLIKE	34132 (1.07)	68680 (1.08)	14363 (1.08)	29156 (1.08)
TBDB4	33210 (1.03)	66854 (1.03)	13999 (1.03)	28375 (1.03)
TGDB4TIP	32814 (1.01)	66016 (1.01)	13771 (1.02)	27922 (1.02)
TGDVXTIP	32612 (1.01)	65664 (1.01)	13676 (1.01)	27734 (1.01)
TGDVXPI	32154 (1.01)	64684 (1.02)	13428 (1.02)	27206 (1.02)
PHIVTX	30046 (1.07)	60326 (1.07)	12271 (1.09)	24806 (1.10)
OPSVETO	28290 (1.06)	56836 (1.06)	11578 (1.06)	23507 (1.06)
TIMKF	25383 (1.11)	51220 (1.11)	10367 (1.12)	21144 (1.11)
NPITG	25383 (1.00)	51220 (1.00)	10367 (1.00)	21144 (1.00)
KIC	25376 (1.00)	51209 (1.00)	10363 (1.00)	21140 (1.00)
TGZFOOL	24923 (1.02)	50352 (1.02)	10184 (1.02)	20783 (1.02)
LAYV4	24923 (1.00)	50352 (1.00)	10184 (1.00)	20783 (1.00)
LAYER14	24923 (1.00)	50352 (1.00)	10184 (1.00)	20783 (1.00)
TGPVCUT	24174 (1.03)	48813 (1.03)	9829 (1.04)	20041 (1.04)

Norm. Branch continued on next page

Norm. Branch continued from previous page				
	Loose		Tight (measured)	
	1/3	2/3	1/3	2/3
RNGMOM	1828 (13.22)	3725 (13.10)	1121 (8.77)	2320 (8.64)
COS3D	1766 (1.04)	3575 (1.04)	1080 (1.04)	2224 (1.04)
ZFRF	1764 (1.00)	3562 (1.00)	1079 (1.00)	2213 (1.00)
ZUTOUT	1754 (1.01)	3530 (1.01)	1071 (1.01)	2195 (1.01)
RSDEDXMAX	1550 (1.13)	3109 (1.14)	953 (1.12)	1979 (1.11)
RSDEDXCL	1385 (1.12)	2795 (1.11)	861 (1.11)	1790 (1.11)
RSLIKE	1385 (1.00)	2795 (1.00)	861 (1.00)	1790 (1.00)
UTCQUAL	1255 (1.10)	2565 (1.09)	780 (1.10)	1656 (1.08)
PRRF1	1242 (1.01)	2535 (1.01)	774 (1.01)	1638 (1.01)
PRRFZ	1143 (1.09)	2330 (1.09)	709 (1.09)	1511 (1.08)
TGGEO	1143 (1.00)	2330 (1.00)	709 (1.00)	1511 (1.00)
TGDEDX	1118 (1.02)	2273 (1.03)	694 (1.02)	1468 (1.03)
CCDPUL	204 (5.48)	395 (5.75)	137 (5.07)	266 (5.52)
EPIONK	202 (1.01)	393 (1.01)	135 (1.01)	265 (1.00)
CCDBADTIM	195 (1.04)	383 (1.03)	131 (1.03)	257 (1.03)
CCD31FIB	195 (1.00)	383 (1.00)	131 (1.00)	257 (1.00)
VERRNG	146 (1.34)	284 (1.35)	95 (1.38)	191 (1.35)
ANGLI	146 (1.00)	283 (1.00)	95 (1.00)	191 (1.00)
ALLKFIT	141 (1.04)	274 (1.03)	92 (1.03)	185 (1.03)
TPICS	141 (1.00)	274 (1.00)	92 (1.00)	185 (1.00)
TGDEDX	141 (1.00)	274 (1.00)	92 (1.00)	185 (1.00)
CHI567	115 (1.23)	231 (1.19)	77 (1.19)	155 (1.19)
CHI5MAX	115 (1.00)	231 (1.00)	77 (1.00)	155 (1.00)
PV_{PNN2}	**0** (115.00)	**1** (231.00)	**0** (77.00)	**1** (155.00)
Norm.	1 ± 1.00	1 ± 1.00	1 ± 1.00	1 ± 1.00

Table 43: Muon Background Normalization Branch. Shown are the number of events remaining after applying the cut in the first column; number in parenthesis is the rejection of the cut within this sample

7 Charge exchange background

7.1 Semi-leptonic Decay of K_L^0

The pass2 cuts history is tabulated in Tab. 44 along with the result from 1/3 sample. The result are consistent within statistical uncertainty. With the following formula:

$$N_{CEX} = N_{norm,\ data} \times \frac{N_{targf,\ UMC}}{N_{kpigap,\ UMC}} \times ACC_{unapplied}\ , \tag{29}$$

The background numbers are estimated and summarized in Tab. 45. $ACC_{unapplied}$ is 70% where the contribution of CCDBADFIT was missed in 1/3 note.

7.2 Hyperon Production

Following the charge exchange interaction of K^+, hyperon production could be another background source besides semi-leptonic decay of K_L^0. The product, K^0, of the CEX

	Tight cuts 1/3	Loose cuts 1/3	Tight cuts 2/3	Loose cuts 2/3
skim123,567	12621399	12621399	25768044	25768044
delco2	7716700	7716700	15743575	15743575
KCUTS	206709	289592	423053	592084
CKTRS	182952(0.885)	256241(0.884)	374726(0.885)	524435(0.885)
CKTAIL	178646(0.976)	250182(0.976)	366054(0.976)	512270(0.976)
CPITRS	126363(0.707)	186280(0.744)	259740(0.709)	382042(0.745)
CPITAIL	126224(0.998)	186108(0.999)	259442(0.998)	381643(0.998)
BWTRS	119382(0.945)	176467(0.948)	245502(0.946)	362127(0.948)
B4DEDX	118158(0.989)	174641(0.989)	242944(0.989)	358323(0.989)
B4TRS	108812(0.920)	161046(0.922)	224029(0.922)	330320(0.921)
B4CCD	107089(0.984)	158536(0.984)	220373(0.983)	325020(0.983)
TIMCON	106186(0.991)	156924(0.989)	218457(0.991)	321662(0.989)
IPIFLG	105642(0.994)	156112(0.994)	217349(0.994)	320044(0.994)
ELVETO	98219(0.929)	145296(0.930)	202144(0.930)	298045(0.931)
TDFOOL	98051(0.998)	145025(0.998)	201803(0.998)	297521(0.998)
TDVARNN	67226(0.685)	133473(0.920)	137530(0.681)	273819(0.920)
PVCUT	188(0.002)	1395(0.010)	426(0.003)	2938(0.010)
KPIGAP	12(0.063)	62(0.044)	15(0.035)	98(0.033)
TGZFOOL	8(0.666)	50(0.806)	13(0.866)	79(0.806)
EPITG	3(0.375)	29(0.580)	5(0.384)	55(0.696)
EPIMAXK	3(1.000)	29(1.000)	5(1.000)	55(1.000)
EPIONK	3(1.000)	29(1.000)	5(1.000)	55(1.000)
TIMKF	2(0.666)	18(0.620)	3(0.600)	39(0.709)
KIC	2(1.000)	14(0.777)	2(0.666)	30(0.769)
TGQUALT	2(1.000)	14(1.000)	2(1.000)	30(1.000)
NPITG	2(1.000)	14(1.000)	2(1.000)	30(1.000)
TGER	2(1.000)	14(1.000)	2(1.000)	29(0.966)
DTGTTP	2(1.000)	14(1.000)	2(1.000)	29(1.000)
RTDIF	2(1.000)	14(1.000)	2(1.000)	29(1.000)
DRP	2(1.000)	14(1.000)	2(1.000)	29(1.000)
TGKTIM	2(1.000)	14(1.000)	2(1.000)	28(0.965)
TGEDGE	2(1.000)	13(0.928)	2(1.000)	27(0.964)
TGDEDX	2(1.000)	13(1.000)	2(1.000)	25(0.925)
TGENR	2(1.000)	13(1.000)	2(1.000)	23(0.920)
PIGAP	2(1.000)	13(1.000)	2(1.000)	22(0.956)
TGLIKE	2(1.000)	9(0.692)	2(1.000)	16(0.727)
TGB4	2(1.000)	5(0.555)	0(0.000)	7(0.437)
PHIVTX	1(0.500)	5(1.000)	0( )	7(1.000)
TPICS	1(1.000)	5(1.000)	0( )	7(1.000)
TGTCON	1(1.000)	5(1.000)	0( )	7(1.000)
B4ETCON	1(1.000)	5(1.000)	0( )	7(1.000)
TGGEO	1(1.000)	3(0.600)	0( )	0(0.000)

Table 44: The pass2 cuts history of the normalization branch of the 1/3 and 2/3 data for the CEX study.

	Tight cuts 1/3	Loose cuts 1/3	Tight cuts 2/3	Loose cuts 2/3
N_{norm}	1	3	1	1
$N_{targf,\ UMC}$	6^{+6}_{-2}	50^{+33}_{-10}	6^{+6}_{-2}	50^{+33}_{-10}
$N_{kpigap,\ UMC}$	3332	4136	3332	4136
N_{CEX}	$0.0038 \pm 0.0038^{+0.0038}_{-0.0013}$	$0.076 \pm 0.044^{+0.058}_{-0.015}$	$0.0019 \pm 0.0019^{+0.0019}_{-0.0006}$	$0.013 \pm 0.013^{+0.010}_{-0.003}$

Table 45: CEX background number normalized to 3/3 data. The first error of N_{CEX} is statistical and the second error is the estimated systematic uncertainty due to TGPV, OPSVETO and CCDPUL.

of K^+ can oscillate to $\overline{K^0}$ through the famous $W^\pm$ box diagram [9]. Suppose to start off with a pure K^0 beam of unit intensity at t=0. Without any consideration of strong interaction after time t the K^0 intensity will be

$$I(K^0) = \frac{1}{4}[e^{-\Gamma_S t} + e^{-\Gamma_L t} + 2e^{-(\Gamma_S+\Gamma_L)t/2} cos\Delta m t] \tag{30}$$

where $\Delta m = m_S - m_L$. Current measurement gives $\Delta m = 0.5/\tau_S$. Similarly

$$I(\overline{K^0}) = \frac{1}{4}[e^{-\Gamma_S t} + e^{-\Gamma_L t} - 2e^{-(\Gamma_S+\Gamma_L)t/2} cos\Delta m t] \tag{31}$$

The intensity of K^0_S and K^0_L will be:

$$\begin{aligned} I(K^0_S) &= \frac{1}{2}e^{-\Gamma_S t} \\ I(K^0_L) &= \frac{1}{2}e^{-\Gamma_L t} \end{aligned} \tag{32}$$

After about $3 \times \tau_S$ (τ_S is the lifetime of K^0_S, $0.8958 \times 10^{-10} s$) the intensity of the K^0 will be comparable to $\overline{K^0}$.

Since $\overline{K^0}$ contains a strange quark as opposed to a anti strange quark, it can interact with a nucleon and produce a strange baryon like:

$$\overline{K^0} + N \rightarrow Y + \pi \tag{33}$$

where N is a nucleon and Y is a hyperon.

The actual processes involved in E949's low energy range are:

$$\begin{aligned} \overline{K^0} + p &\rightarrow \pi^0 + \Sigma^+ \rightarrow \pi^0 + (p^+\pi^0\ or\ n\pi^+) \\ &... \rightarrow \pi^+ + \Sigma^0 \rightarrow \pi^+ + (\Lambda^0\gamma) \rightarrow \pi^+ + ((p^+\pi^-\ or\ n\pi^0)\gamma) \\ &... \rightarrow \pi^+ + \ \Lambda\ \rightarrow \pi^+ + (p^+\pi^-\ or\ n\pi^0) \\ \overline{K^0} + n &\rightarrow \pi^0 + \Sigma^0\ \rightarrow \pi^0 + (\Lambda^0\gamma) \rightarrow \pi^+ + ((p^+\pi^-\ or\ n\pi^0)\gamma) \\ &... \rightarrow \pi^0 + \ \Lambda\ \rightarrow \pi^0 + (p^+\pi^-\ or\ n\pi^0) \\ &... \rightarrow \pi^- + \Sigma^+ \rightarrow \pi^- + (p^+\pi^0\ or\ n\pi^+) \\ &... \rightarrow \pi^+ + \Sigma^- \rightarrow \pi^+ + (n\pi^-) \end{aligned} \tag{34}$$

Σ^- is often absorbed through $\Sigma^- + p \rightarrow \Lambda + n$. One measurement of the absorption probability is 0.52 ± 0.10 [10].

In addition to the hyperon production by the $\overline{K^0}$, the following two charge exchange processes can also reduce the intensity of K^0 and $\overline{K^0}$.

$$\begin{aligned} K^0 + p &\rightarrow K^+ + n \\ \overline{K^0} + n &\rightarrow K^- + p \end{aligned} \tag{35}$$

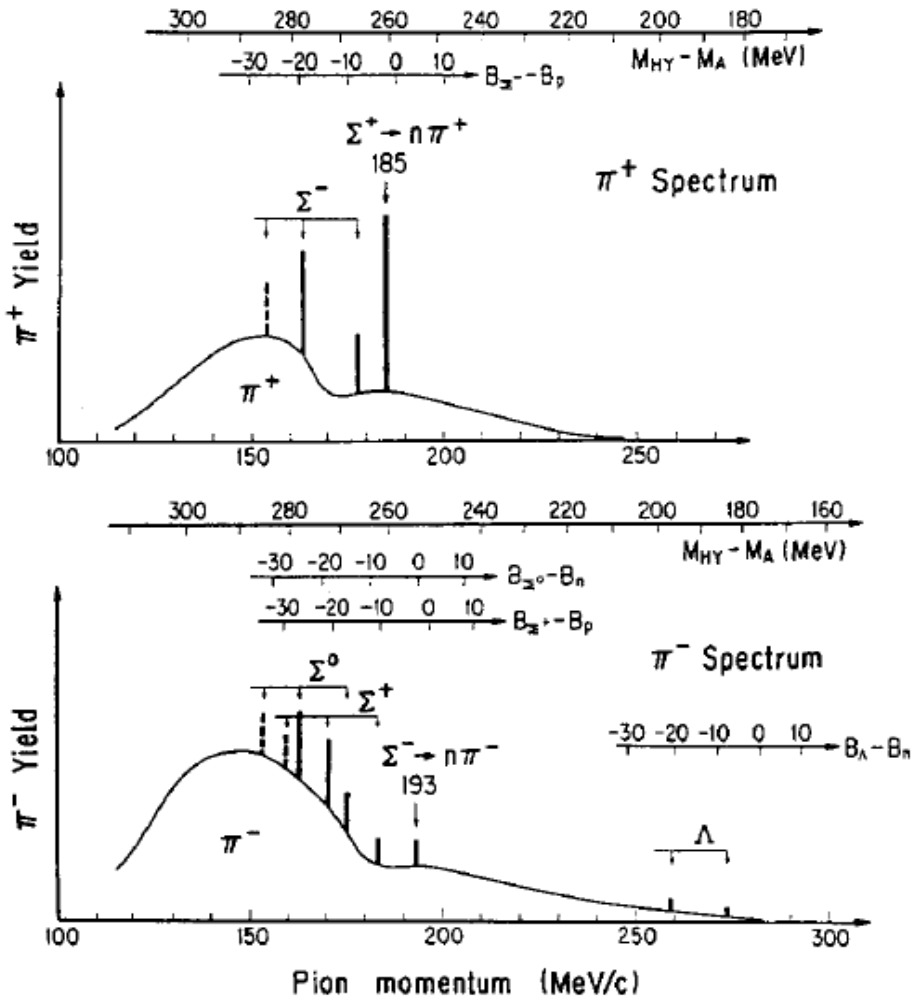

Fig. 1. Expected spectra of π^+ and π^- when K^-'s are stopped in a nuclear target. The corresponding mass scale $M_{HY} - M_A$ and the binding-energy differences $B_N - B_{HY}$ are shown.

Figure 16: Expected spectra of π^+ and π^- when K^-'s are stopped in a nuclear target [12].

The cross section of charge exchange is usually less than 3 mb for momentum of $K^\pm < 100 MeV/c$ [11]. From the discussion below it is known that its cross section is much lower than hyperon production and has only some minor contribution to the total cross section.

The expected momentum spectrum of $\pi^\pm$ from K^- captured at rest and hyperons are displayed in Fig. 16 [12]. The CEX process for K^0 production from K^+ could happen at rest or in flight which will boost the daughter particles a little. For a K^+ with momentun of 100 MeV hitting a nucleon which is at rest in lab frame $\beta = 0.07$. It can be seen almost all processes in Equ. 34 can be a background process

It is not trivial to figure out the cross section of hyperon production, however one can use the knowledge of isospin symmetry of u and d quarks to get a rough estimation from K^-'s hyperon production. For instance some early measurements carried on bubble chamber gives a total hyperon production cross section 90 mb per proton at K^- momentum of 160 MeV/c [13] which is consistent with the measurement of K_L^0 total cross section on protons [14]. In [13] and [14] the measured cross sections on H at other momentum points are also available, and they agree very well. Unfortunately the measurement of K_L^0 only goes down to the momentum of 168 MeV/c that is still higher than the interesting region

(0–100 MeV/c). The total cross section of 481 mb/(carbon nucleus) and 70 mb/H as measured in [14] is used to estimate the mean free path of $\overline{K^0}$ in E949 target (polystyrene with 3% acrylic cladding). In addition from the extrapolation in [13] it is known that these cross sections are doubled at low energy. With pure polystyrene assumption the mean free path is 37.3-74.6 cm which tells the survival probability of $\overline{K^0}$ after 6 cm of target is 73% – 85%.

As explained in 1/3 note [1], CEX section, semi-leptonic decay of K_L^0, a normalization branch is created mainly with KPIGAP and without DELCO, B4EKZ, TGPV, OPSVETO and CCDPUL. After scanning the remaing events in the loose setup cuts normalization sample, one can conclude that it is compatible with selection of hyperon background and that is a normalization branch for both K_L^0 semi-leptonic decay and hyperon background.

Before the semi-leptonic decay or hyperon production, these two backgound processes are identical which means the rejection of B4EKZ should be the same for both.

Another interesting issue is that it is very hard to get the time profile of $K^0(\overline{K^0})$ with the consideration of hadronic interaction. To avoid solving a differential equation to get the intensity of $K^0(\overline{K^0})$ as a function of time one can find out the rejection of offline DELCO against hyperon background is roughly the same with K_L^0 semi-leptonic decay. Note that a DC trigger (2 ns) is applyed online. This 2 ns, when being converted to c.m., is far beyond $3 \times \tau_S$ even some boost exists. The significantly different parts of K^0 and $\overline{K^0}$ intensity functions in the early time range is already over. This difference is included in normalization branch. While for the rest of time the time characteristics of the intensity of K_L^0 and $\overline{K^0}$ will be the same except for the fast oscillation term as expressed in Equ 31 and Equ 32. The period of the oscillation is $2 \times \tau_S$ and its amplitude is very small so that our measurement is not sensitive to that at all. In [1], CEX section, due to the less of hyperson production knowledge, the DELCO rejection is simulated and estimated without any strong interaction. The rejection of DELCO is underestimated for K_L^0's semi-leptonic decay and hyperon prodcution.

The rejection of TGPV, OPSVETO and CCDPUL of K_L^0 semi-leptonic decay is 7.54 estimated by UMC with all the other cuts applyed. Accompanying π^+ production, π^0, π^-, Σ and Λ are generated. Their lifetime is relatively short. π^- absorption probability is about 10% as used in [10] which is consistent with our $Ke4$ study. Although Σ^- can be absorbed, it emits a Λ again. Considering the lowest pion momentum in Fig. 16 and $\beta = 0.07$ the final pion have at least 25 MeV of kinetic energy. The rejection of TGPV, OPSVETO and CCDPUL for K_L^0 semi-leptonic decay is a modest estimation for this background.

Based on the discussion above no separated study is going to be made for hyperon background.

8 K_{e4} background

K_{e4} background is estimated with 2/3 sample. The normalization branching of 2/3 sample as well as that from 1/3 sample where the bug of multiplexing is cleared are tabulated in Tab. 46. The background number is summarized in Tab. 47.

9 Background Contamination Studies

This study was initially prompted by Toshio asking how much additional muon contamination was introduced into the $K_{\pi 2}$ target-scatter normalization and rejection branches due to using a set of TD cuts that are looser than the E949 PNN1 ones.

	Tight cuts 1/3	Loose cuts 1/3	Tight cuts 2/3	Loose cuts 2/3
skim123,456	12892493	12892493	25768044	25768044
KCUTS	565304	764574	1131416	1249551
PCUTS	120637	179885	242199	296647
TDCUTS	76142	152880	152260	247183
PVCUT	516	3011	1020	5789
DELC	268(0.519)	1648(0.547)	554(0.543)	3262(0.563)
DELC3	235(0.876)	1644(0.997)	481(0.868)	3252(0.996)
TGZFOOL	224(0.953)	1579(0.960)	463(0.962)	3138(0.964)
R-cut	222(0.991)	1554(0.984)	446(0.963)	3067(0.977)
PVICVC	138(0.621)	1118(0.719)	311(0.697)	2289(0.746)
B4EKZ	118(0.855)	933(0.834)	254(0.816)	1814(0.792)
EPITG	78(0.661)	569(0.609)	131(0.515)	1056(0.582)
EPIMAXK	78(1.000)	569(1.000)	131(1.000)	1056(1.000)
TIMKF	59(0.756)	422(0.741)	103(0.786)	823(0.779)
KIC	58(0.983)	410(0.971)	102(0.990)	811(0.985)
TGQUALT	56(0.965)	374(0.912)	94(0.921)	719(0.886)
NPITG	56(1.000)	374(1.000)	94(1.000)	719(1.000)
TGER	56(1.000)	374(1.000)	94(1.000)	717(0.997)
TARGF	53(0.946)	359(0.959)	85(0.904)	673(0.938)
DTGTTP	53(1.000)	359(1.000)	85(1.000)	673(1.000)
RTDIF	53(1.000)	356(0.991)	85(1.000)	665(0.988)
DRP	47(0.886)	327(0.918)	80(0.941)	600(0.902)
TGKTIM	47(1.000)	327(1.000)	80(1.000)	596(0.993)
TGEDGE	45(0.957)	312(0.954)	79(0.987)	562(0.942)
TGDEDX	41(0.911)	287(0.919)	64(0.810)	508(0.903)
TGENR	40(0.975)	282(0.982)	63(0.984)	500(0.984)
PIGAP	38(0.950)	277(0.982)	62(0.984)	492(0.984)
TGLIKE	34(0.894)	257(0.927)	57(0.919)	448(0.910)
TGB4	34(1.000)	250(0.972)	55(0.964)	436(0.973)
PHIVTX	14(0.411)	105(0.420)	25(0.454)	183(0.419)
CHI567	13(0.928)	93(0.885)	15(0.600)	153(0.836)
CHI5MAX	13(1.000)	93(1.000)	15(1.000)	153(1.000)
VERRNG	10(0.769)	81(0.870)	14(0.933)	134(0.875)
ANGLI	10(1.000)	81(1.000)	14(1.000)	134(1.000)
TGFITALLK	10(1.000)	80(0.987)	14(1.000)	128(0.955)
TPICS	10(1.000)	80(1.000)	14(1.000)	128(1.000)
TGTCON	10(1.000)	80(1.000)	14(1.000)	128(1.000)
B4ETCON	10(1.000)	80(1.000)	14(1.000)	127(0.992)
CCDBADTIM	9(0.900)	76(0.950)	13(0.928)	121(0.952)
CCDBADFIT	6(0.666)	66(0.868)	13(1.000)	110(0.909)
CCD31FIB	6(1.000)	66(1.000)	13(1.000)	110(1.000)
CCDPUL	1(0.166)	4(0.060)	0(0.000)	6(0.054)
EPIONK	1(1.000)	4(1.000)	0( )	6(1.000)

Table 46: The pass2 cuts history of the normalization branch of the 1/3 and 2/3 data for K_{e4} study. R-cut is $\overline{\text{TGPV} \cdot \text{OPSVETO}}$.

	Tight cuts 1/3	Loose cuts 1/3	Tight cuts 2/3	Loose cuts 2/3
N_{norm}	1	4	1	6
$R_{TGPV\cdot OPSVETO}$	88^{+263}_{-70}	52^{+121}_{-29}	88^{+263}_{-70}	52^{+121}_{-29}
$N_{K_{e4}}$	$0.034 \pm 0.034^{+0.142}_{-0.026}$	$0.235 \pm 0.118^{+0.310}_{-0.166}$	$0.017 \pm 0.017^{+0.071}_{-0.013}$	$0.176 \pm 0.072^{+0.233}_{-0.124}$

Table 47: K_{e4} background number normalized to 3/3 data. The first error of $N_{K_{e4}}$ is statistical and the second error is from $R_{TGPV\cdot OPSVETO}$.

As discussed in [1], three of the ten events remaining at the end of the loose $K_{\pi 2}$ target-scatter rejection branch (1/3 data) were classified as being non $K_{\pi 2}$ target-scatter. One of these events was 2-beam, one was K_{e4} and one was likely K_{e4}.

Quantification of the contamination of the $K_{\pi 2}$ target-scatter branches by these three background processes (K_{e4}, muon and 2-beam) would allow corrections to be made to the $K_{\pi 2}$ target-scatter background to remove the double counting of these backgrounds. Generally, the effect of these contaminations will be to cause the backgrounds to be overestimated.

The general method of estimating a background is to identify two sets of uncorrelated cuts (CUT1 and CUT2, collectively known as bifurcation cuts) which provide a large rejection for the background in question. The normalization branch is a sample created by inverting one of these sets of bifurcation cuts (CUT1) to create a sample rich in the background being studied and applying the rest of the cuts to purify the sample. The number of events left after all cuts have been applied in the normalization branch is known as the normalization N. The rejection branch is created by inverting the second set of bifurcation cuts (CUT2) to create another sample rich in the studied background with which to measure the rejection R of the set of cuts inverted to created the normalization branch. The background bg is estimated by the equation

$$bg = \frac{N}{R-1}.$$

Contamination from another background process will usually inflate the value estimated by this method. The normalization N will contain contamination events in addition to the background events. The rejection of the bifurcation cuts on the contamination events will generally be significantly lower than on the background being measured. The contamination events in the rejection branch will usually result in a measured rejection R that is lower than the rejection would be for an uncontaminated sample.

The typical effect of the contamination in both the normalization N and the rejection R values is that they inflate the background estimate in question. Since background estimates are made for each of the contamination processes, this contamination ends up inflating the total background estimate by double counting the contribution of the contamination processes. This inflated total background estimate reduces the central value of the branching fraction calculated from this analysis.

The contamination estimates in this section were measured only on the 2/3 data sample.

9.1 Muon Contamination in the $K_{\pi 2}$ Target-Scatter Background

The bifurcation cuts used to estimate the muon background are (CUT1) the collection of cuts known as TDCUT02 and (CUT2) RNGMOM.

9.1.1 Acceptance and Rejection of the Muon Bifurcation Cuts

The rejection of RNGMOM (R_{RNGMOM}) for muon events was measured in the muon background normalization branch by inverting TDCUT02. The rejection found in this section is larger than that found in Table 43 as it was measured with tighter setup cuts for this study. The rejection of TDCUT02 (R_{TDCUT02}) for muon events was measured in the muon background rejection branch 42 by inverting RNGMOM. The combined rejection of these cuts R_μ can be calculated

$$\begin{aligned} R_\mu &= R_{\mathrm{RNGMOM}} \times R_{\mathrm{TDCUT02}} \\ &= (28.29 \pm 1.06) \times (133.04 \pm 10.68) \\ &= 3764 \pm 333 \end{aligned} \tag{36}$$

The acceptance of these cuts for pion events was measured directly using a modified version of the rejection branch for the $K_{\pi 2}$ target-scatter background estimate. The modifications are that TDCUT02 and RNGMOM were removed from the setup cuts and the kinematic box was changed from the PNN2 loose kinematic box to the $K_{\pi 2}$-peak kinematic box. The setup cuts are shown in Table 48.

Setup cuts for measuring acceptance of RNGMOM and TDCUT
P2PSCUT, P2TGCUT, P2TGPVCUT, STLAY, VALID_TRIG, HEX_AFTER, PSCUT06, DELC3 KINCUT06 (without RNGMOM), KP2-PEAK KINEMATIC BOX

Table 48: The setup cuts for measuring acceptance of RNGMOM and TDCUT.

After the setup cuts have been applied, the 12 classes (2-13) described in Table 8 are applied and the performance of the cuts RNGMOM and TDCUT02 are measured before and after application of the photon veto as shown in Table 49. For each of the classes with sufficient statistics in the 'AFTER PV60' column the measured acceptance of these muon bifurcation cuts is equal before and after the application of the photon veto cut within statistical error. The extracted acceptance A_π can be taken as the average of the highest and lowest acceptances measured before the application of the photon veto with the difference between these extreme values setting the bounds for the error:

$$A_\pi = 0.8813 \pm 0.0035. \tag{37}$$

9.1.2 Muon Contamination in the Normalization Branch

To determine the amount of muon contamination in the normalization branch, the number of events N left at the end of the normalization branch is treated as being made up of either muon N_μ or pion N_π events. Written in equation form, this looks like

$$N = N_\pi + N_\mu \tag{38}$$

Since we know the performance of the muon bifurcation cuts (RNGMOM and TDCUT02) with respect to pions (A_π) and muons (R_μ), we can move these cuts to the

Acceptances of RNGMOM×TDCUT02 for $K_{\pi 2}$-peak events

CLASS	BEFORE PV60		AFTER PV60
2	293455/363196 = 0.8080 ± 0.0007	280/343	0.8163 ± 0.0209 =
3	120164/148540 = 0.8090 ± 0.0010	115/140	0.8214 ± 0.0324 =
4	120568/149124 = 0.8085 ± 0.0010	109/138	0.7899 ± 0.0347 =
5	364667/451267 = 0.8081 ± 0.0006	346/428	0.8084 ± 0.0190 =
6	175663/217075 = 0.8092 ± 0.0008	159/199	0.7990 ± 0.0284 =
7	179337/222017 = 0.8078 ± 0.0008	166/214	0.7757 ± 0.0285 =
8	27644/34214 = 0.8080 ± 0.0021	16/25	0.6400 ± 0.0960 =
9	343309/424682 = 0.8084 ± 0.0006	331/412	0.8034 ± 0.0196 =
10	59863/74471 = 0.8038 ± 0.0015	58/72	0.8056 ± 0.0466 =
11	5883/7383 = 0.7968 ± 0.0047	5/5	1.0000 ± 0.0000 =
12	316971/392405 = 0.8078 ± 0.0006	303/368	0.8234 ± 0.0199 =
13	132619/164163 = 0.8078 ± 0.0010	127/152	0.8355 ± 0.0301 =

Table 49: The acceptance of RNGMOM×TDCUT02 is measured for $K_{\pi 2}$-peak events before and after the application of the photon veto cut at the 60% level (PV60) for each of the 12 classes (2-13) from the $K_{\pi 2}$ target-scatter rejection branch.

bottom of the $K_{\pi 2}$ target-scatter normalization branch and measure the number of events n remaining before these cuts are applied. This allows us to write the following equation

$$n = \frac{N_\pi}{A_\pi} + R_\mu N_\mu \tag{39}$$

The amount of muon contamination left at the end of the normalization branch can be represented by the quantity f,

$$f = \frac{N_\mu}{N} \tag{40}$$

$$= \frac{A_\pi \frac{n}{N} - 1}{A_\pi R_\mu - 1} \tag{41}$$

Taking the values from Section 9.1.1 ($A_\pi = 0.8821 \pm 0.0043$ and $R_\mu = 3764 \pm 333$) and the measured values $N = 1131$ and $n = 12980$, we can solve for the value f,

$$f = (2.76 \pm 0.26) \times 10^{-3} \tag{42}$$

Using these conventions, the corrected (uncontaminated) normalization number N', which is the number of pions at the end of the normalization branch can be written as

$$N' = N(1 - f) \tag{43}$$

$$= 1127.9 \pm 33.5. \tag{44}$$

Correcting this for the Range-Stack contamination n_{rs} gives the final corrected normalization:

$$N'_{tg} = N' - n_{rs} \tag{45}$$

$$= (1127.9 \pm 33.5) - (23.33 \pm 3.46) \tag{46}$$

$$= 1104.6 \pm 33.7. \tag{47}$$

9.1.3 Muon Contamination in the Rejection Branch

The method used to determine the amount of muon contamination in the rejection branch is very similar to that for the normalization branch except the amount of contamination has to be measured before and after the bifurcation cut (CUT1) for which the rejection is being measured. For $K_{\pi 2}$ target-scatter, this cut is the photon veto.

Again, we will call the number of events left at the end of the branch N where each class is its own branch and the end of the branch is considered to be after the photon veto has been applied. The number of events before the photon veto is applied will be denoted M. Using these conventions, the photon veto rejection $R_{\rm PV}$ is given by

$$R_{\rm PV} = \frac{M}{N} \tag{48}$$

We can examine the amount of muon contamination both before and after the photon veto has been applied by treating M and N as being made up of muon and pion events as with the normalization branch method:

$$M = M_\pi + M_\mu, \tag{49}$$
$$N = N_\pi + N_\mu. \tag{50}$$

Again we can use the known performance of the muon bifurcation cuts (RNGMOM and TDCUT02) with respect to pions (A_π) and muons (R_μ) to solve for the fraction of the events which are muon contamination. These muon bifurcation cuts can be applied immediately before the end of the branch (after the photon veto) giving a value n before the muon bifurcation cuts and N after the bifurcation cuts. The same can be done by applying these muon bifurcation cuts immediately before the photon veto is applied giving a value m before the muon bifurcation cuts and M after the bifurcation cuts.

$$m = \frac{M_\pi}{A_\pi} + R_\mu M_\mu, \tag{51}$$
$$n = \frac{N_\pi}{A_\pi} + R_\mu N_\mu. \tag{52}$$

The amount of muon contamination before and after the photon veto are applied can be represented by the quantities f_M and f_N respectively,

$$f_M = \frac{A_\pi \frac{m}{M} - 1}{A_\pi R_\mu - 1}, \tag{53}$$
$$f_N = \frac{A_\pi \frac{n}{N} - 1}{A_\pi R_\mu - 1} \tag{54}$$

Using these conventions, the corrected (uncontaminated) photon veto rejection is given by

$$R'_{\rm PV} = \frac{M(1-f_M)}{N(1-f_N)} \tag{55}$$
$$= 2665.9 \pm 843.3 \tag{56}$$

Table 50 shows the values used to arrive at a corrected value for the photon veto rejection.

Quantity	Before PV60	After PV60
Muon bifurcation cuts not applied	$m = 94424$	$n = 652$
Muon bifurcation cuts applied	$M = 52621$	$N = 22$
f-value	$f_M = (1.76 \pm 0.16) \times 10^{-4}$	$f_N = (7.63 \pm 1.80) \times 10^{-3}$
Corrected value	$M' = M(1 - f_M)$ $= 52611.8 \pm 229.4$	$N' = N(1 - f_N)$ $= 21.83 \pm 4.66$
$R'_{\rm PV} = M'/N'$	2409.9 ± 513.9	

Table 50: This table shows the values used to arrive at a photon veto rejection after the effects of muon contamination have been removed.

9.1.4 Background Estimate Corrected for Muon Contamination

Numbers from the previous two sections can be used to estimate the background without muon contamination.

$$bg' = \frac{\frac{3}{2}N'}{R'_{\rm PV} - 1} \quad (57)$$

$$= \frac{\frac{3}{2}(1104.6 \pm 33.7)}{(2409.9 \pm 513.9) - 1} \quad (58)$$

$$= 0.688 \pm 0.148 \quad (59)$$

The nominal value is $0.695 \pm 0.150\,^{+0.061}_{-0.094}$.

Since the central values of these two quantities agree to approximately 1%, we can consider the muon contamination in the $K_{\pi 2}$ target-scatter background to be negligible.

9.2 Double-Beam Contamination in the $K_{\pi 2}$ Target-Scatter Background

Due to a lack of acceptance and rejection information for the rejection branch bifurcation cuts for double-beam background, only the normalization branch bifurcation cuts will be used in the study.

The rejection of CKTRS, CKTAIL and BWTRS will be denoted R_{KK} and the rejection of CPITRS, CPITAIL and BWTRS will be denoted R_{KP}. These rejections are taken from the double-beam rejection branch (see Table 33). The acceptance of these cuts for pion events was taken from the beam acceptance (Table 46 of [1]) which uses $K_{\mu 2}$ monitors which have had cuts applied to ensure it looks like a single K^+ decay with no photons. These values are summarized in Table 51

	KK Branch	KP Branch
Cuts	CKTRS·CKTAIL·BWTRS	CPITRS·CPITAIL·BWTRS
Acceptance	$A_{KK} = 0.8973 \pm 0.0002$	$A_{KP} = 0.9159 \pm 0.0002$
Rejection	$R_{KK} = 394.0 \pm 196.8$	$R_{KP} = 616.8 \pm 308.1$

Table 51: Acceptances and rejections of double-beam bifurcation cuts

9.2.1 Double-Beam Contamination in the Normalization Branch

The method for determining the double-beam contamination in the $K_{\pi 2}$ target-scatter normalization branch is the same as that described for muon contamination, but with with a different set of cuts for each of the KK and KP double-beam contamination. Since the contamination due to each of these backgrounds is expected to be very small, the KK contamination will be ignored for the KP contamination study and the KP contamination ignored for the KK contamination study.

The following discussion lays out the equations used to determine the amount of KK double-beam contamination, but the same equations all apply for the KP double-beam contamination with the KP notation replacing the KK notation. To determine the amount of KK contamination in the normalization branch, the number of events N left at the end of the normalization branch is treated as being made up of either $K_{\pi 2}$ pion N_π or KK double-beam N_{KK} events. Note that these pion events could be target-scatter, range-stack scatter or $K_{\pi 2\gamma}$. Written in equation form, this looks like:

$$N = N_\pi + N_{KK}. \tag{60}$$

Since we know the performance of the KK double-beam rejection branch bifurcation cuts (CKTRS, CKTAIL and BWTRS) with respect to kp2 target-scatter events (A_{KK}) and KK double-beam (R_{KK}), we can move these cuts to the bottom of the kp2 target-scatter normalization branch and measure the number of events n remaining before these cuts are applied. This allows us to write the following equation

$$n = \frac{N_\pi}{A_{KK}} + R_{KK} N_{KK} \tag{61}$$

The amount of KK contamination left at the end of the normalization branch can be represented by the quantity f,

$$f = \frac{A_{KK}\frac{n}{N} - 1}{A_{KK} R_{KK} - 1} \tag{62}$$

Table 52 shows the values used to determine the fractional contamination for KK and KP double-beam in the normalization branch. Note that the final corrected normalization N' is corrected for both the f-value and the range-stack scatter component N_{rs} (Section 3.2).

	KK Branch	KP Branch
n	1186	1160
N	1131	1131
f-value	$f_{KK} = -0.00017 \pm 0.00009$	$f_{KP} = -0.00011 \pm 0.00005$
TG-Scatter Normalization corrected for f-value and N_{rs}		
$N' = N(1-f) - N_{rs}$	$N'_{KK} = 1107.9 \pm 22.8$	$N'_{KP} = 1107.8 \pm 33.8$

Table 52: Correcting for double-beam contamination in the $K_{\pi 2}$ normalization branch.

9.2.2 Double-Beam Contamination in the Rejection Branch

The method for determining the double-beam contamination in the kp2 target scatter rejection branch is also similar to that described for muon contamination with the bifurcation cuts from the KK or KP double-beam contamination instead of the muon

bifurcation cuts. Again contamination due to one type of double-beam process (KK or KP) can be ignored when studying the other.

The following discussion lays out the equations used to determine the amount of KK double-beam contamination, but the same equations all apply for the KP double-beam contamination with the KP notation replacing the KK notation. As with the muon contamination in the rejection branch, the amount of contamination has to be measured before and after the photon veto is applied at then end of the rejection branch.

The definitions for M and N can be found in Section 9.1.3. We can examine the amount of KK double-beam contamination both before and after the photon veto has been applied by treating M and N as being made up of muon and pion events as with the normalization branch method:

$$M = M_\pi + M_{KK}, \tag{63}$$
$$N = N_\pi + N_{KK}. \tag{64}$$

These KK double-beam bifurcation cuts can be applied immediately before the end of the branch (after the photon veto) giving a value n before the KK double-beam bifurcation cuts and N after the bifurcation cuts. The same can be done by applying these KK double-beam bifurcation cuts immediately before the photon veto is applied giving a value m before the KK double-beam bifurcation cuts and M after the bifurcation cuts.

$$m = \frac{M_\pi}{A_{KK}} + R_{KK} M_{KK}, \tag{65}$$
$$n = \frac{N_\pi}{A_{KK}} + R_{KK} N_{KK}. \tag{66}$$

The amount of KK double-beam contamination before and after the photon veto are applied can be represented by the quantities f_M and f_N respectively, as defined in Section 9.1.3. Tables 53 and 54 show the values used to arrive at values for the photon veto rejection after being corrected for each of the double-beam processes.

Quantity	Before PV60	After PV60
Double-beam bifurcation cuts not applied	$m = 55873$	$n = 25$
Double-beam bifurcation cuts applied	$M = 52621$	$N = 22$
f-value	$f_M = (-13.3 \pm 6.7) \times 10^{-5}$	$f_N = (5.48 \pm 2.16) \times 10^{-5}$
Corrected value	$M' = M(1 - f_M)$ $= 52628.0 \pm 229.5$	$N' = N(1 - f_N)$ $= 22.00 \pm 4.69$
$R'_{\rm PV}(KK) = M'/N'$	2392.3 ± 510.1	

Table 53: The KK Double-Beam Contamination in Photon Veto Rejection in the $K_{\pi 2}$ target-scatter rejection branch. This table shows the values used to arrive at a photon veto rejection after the effects of KK double-beam contamination have been removed.

9.2.3 Background Estimates Corrected for Double-Beam Contamination

Numbers from the previous two sections can be used to estimate the background after being corrected for each of the double-beam processes.

Quantity	Before PV60	After PV60
Double-beam bifurcation cuts not applied	$m = 54563$	$n = 25$
Double-beam bifurcation cuts applied	$M = 52621$	$N = 22$
f-value	$f_M = (-8.90 \pm 4.46) \times 10^{-5}$	$f_N = (-7.18 \pm 14.11) \times 10^{-5}$
Corrected value	$M' = M(1 - f_M)$ $= 52625.7 \pm 229.4$	$N' = N(1 - f_N)$ $= 22.00 \pm 4.69$
$R'_{\rm PV}(KP) = M'/N'$	2392.3 ± 510.1	

Table 54: The KP Double-Beam Contamination in Photon Veto Rejection in the $K_{\pi 2}$ target-scatter rejection branch. This table shows the values used to arrive at a photon veto rejection after the effects of KP double-beam contamination have been removed.

$$bg'_{KK} = \frac{\frac{3}{2}N'}{R'_{\rm PV} - 1} \quad (67)$$

$$= \frac{\frac{3}{2}(1107.9 \pm 33.6)}{(2392.3 \pm 510.1) - 1} \quad (68)$$

$$= 0.695 \pm 0.150 \quad (69)$$

$$bg'_{KP} = \frac{\frac{3}{2}N'}{R'_{\rm PV} - 1} \quad (70)$$

$$= \frac{\frac{3}{2}(1107.8 \pm 33.6)}{(2392.3 \pm 510.1) - 1} \quad (71)$$

$$= 0.695 \pm 0.150 \quad (72)$$

Since the central values of these two quantities agree to better than 1% with the uncorrected for $K_{\pi 2\gamma}$ contamination value from Section 3.1.3 of 0.695 ± 0.150 we can consider both of the double-beam contaminations in the $K_{\pi 2}$ target-scatter background to be negligible.

9.2.4 Double-Beam Contamination Follow-Up Study

A follow-up study was performed to test the assumption that the KP contamination could be ignored for the KK contamination study and vice versa. In this study, Equations 60 and 61 were replaced with a set of 3 equations:

$$N = N_\pi + N_{KK} + N_{KP}, \quad (73)$$

$$n_1 = \frac{N_\pi}{A_{KK}} + N_{KK}R_{KK} + \frac{N_{KP}}{A'_{KK}}, \quad (74)$$

$$n_2 = \frac{N_\pi}{A_{KP}} + \frac{N_{KK}}{A'_{KP}} + N_{KP}R_{KP}. \quad (75)$$

For these equations n_1 and n_2 are the n-values from Table 52 for the KK and KP branches respectively. The acceptance A'_{KK} (A'_{KP}) is the same as A_{KK} (A_{KP}) except the acceptance of BWTRS was replaced with the inverse of the rejection for BWTRS for that specific background, from the double-beam rejection branch. To determine the amount

of KK (KP) contamination, the value N_{KK} (N_{KP}) was determined from the set of 3 equations and the f-value determined as N_{KK}/N (N_{KP}/N). This method was repeated to determine the equivalent f-values to those found in Tables 53 and 54.

The results from this follow-up study were consistent with the original double-beam contamination studies, showing it was reasonable to assume that KP contamination could be ignored for the KK contamination study and vice versa.

9.3 Treatment of contamination of $K_{\pi 2}$-scatter samples

9.3.1 $K_{\pi 2}$-TT-scatter normalization sample

The $K_{\pi 2}$-TT-scatter normalization sample is formed from the inversion of the PV cut and may contain $K_{\pi 2}$-RS-scatter, $K_{\pi 2\gamma}$ and K_{e4} contamination.

$K_{\pi 2}$-RS-scatter contamination

The amount of $K_{\pi 2}$-RS-scatter contamination of the "$K_{\pi 2}$-TT-scatter" normalization sample can be determined from the methodology of Section 3.2 and directly subtracted.

$K_{\pi 2\gamma}$ contamination

- The $K_{\pi 2\gamma}$ background estimate is derived from the $K_{\pi 2}$ peak rate, the relative $K_{\pi 2\gamma}$ to $K_{\pi 2}$ acceptance from UMC, and the estimated PV rejection on the radiative photon as described in Section 10 of [1].
- An upper limit on the $K_{\pi 2\gamma}$ contamination of $30.0 \pm 7.5\%$ has been made using KP21 monitors and assuming all events in PNN2 box are due to $K_{\pi 2\gamma}$ (see Section 9.4 for details). An analogous estimate from E787 pnn2 analysis in TN-385 was $< 20\%$.
- We expect an increase in $K_{\pi 2\gamma}$ contamination due to the increase in the upper limit of the PNN2 box.

K_{e4} contamination

The following demonstrates that K_{e4} contamination is negligible. Note that K_{e4} events differ from $K_{\pi 2}$ and $K_{\pi 2\gamma}$ events in that there are no photons in the final state. Thus the products of K_{e4} decay are much more likely to leave energy in the target and allow K_{e4} to be readily suppressed by CCDPUL $\cdot$ OPSVETO.

The K_{e4} normalization branch is defined by the inversion of TGPV and OPSVETO. The events remaining before the application of the CCDPUL near the bottom of the normalization branch (Table 46) were examined visually for the 1/3 sample. These events look like K_{e4} events. In addition, the momentum distribution of these events (Figure 7 of [1]) is consistent with the expected distribution for K_{e4} events (Figure 8 of [1]). Thus we are confident that the events in the K_{e4} normalization branch are dominated by K_{e4}.

After the application of CCDPUL and EPIONK, only 4(7) events remain in the 1/3(2/3) K_{e4} normalization branch. The K_{e4} normalization branch can be characterized as $(\overline{\text{TGPV}} + \overline{\text{OPSVETO}}) \cdot$ CCDPUL and can be compared with the $K_{\pi 2}$-TT-scatter normalization branch $\overline{\text{PV}} \cdot$ OPSVETO $\cdot$ CCDPUL. Since $\overline{\text{TGPV}} \cdot$ OPSVETO $\cdot$ CCDPUL is a subset of the $K_{\pi 2}$-TT-scatter normalization branch, we conclude that the contamination of the $K_{\pi 2}$-TT-scatter normalization branch by K_{e4} must be less than the number of events selected in the K_{e4} normalization and thus negligible.

9.3.2 $K_{\pi 2}$-TT-scatter rejection sample

- The $K_{\pi 2}$-TT-scatter rejection sample is formed from inversion of combinations of CCDPUL, B4EKZ and other target cuts.
- Contamination by $K_{\pi 2}$-RS-scatter and $K_{\pi 2\gamma}$ is suppressed by selecting on scatters in the target.
- The 12 classes and different kinematic regions have different amounts of K_{e4} contamination. In particular, the consistency between the PV rejection measured inside the K_{e4}-phobic box and in the full kinematic region indicates that the effect of K_{e4} contamination is small. We use the range of measured rejection for these classes and regions to estimate the uncertainty on the PV rejection of target scatters.

Thus we expect that the affect of the contamination in the photon veto $K_{\pi 2}$-TT-scatter rejection is currently taken into account.

9.3.3 Procedure

1. Subtract the known $K_{\pi 2}$-RS-scatter contribution to the $K_{\pi 2}$-TT-scatter normalization branch.
2. Subtract the estimated $K_{\pi 2\gamma}$ backgrounds from the current $K_{\pi 2}$-TT-scatter background estimate.
3. We have demonstrated in Section 9.3.1 that the rate of K_{e4} contamination is negligible in the normalization branch and taken into account in the rejection branch, so no adjustment needs to be made.

9.4 Upper Limit of $K_{\pi 2\gamma}$ Contamination in $K_{\pi 2}$-tgscat

This study estimates the upper limit of $K_{\pi 2\gamma}$ contamination in the $K_{\pi 2}$-tgscat normalization branch using kp21 monitor data. The Table 55 is our reproduction of Table 7 (Pg. 50) of TN-385.

This estimation is based on the the assumption that the $K_{\pi 2\gamma}$ contamination in the kp21 monitors is large enough that events in the PNN2 box will be entirely $K_{\pi 2\gamma}$ events (tail) and the events in the kp2-peak will be kp2 events (peak).

The fraction of $K_{\pi 2\gamma}$ events in the $K_{\pi 2}$-tgscat normalization branch is

$$g = \frac{N_g}{N_s + N_g} \tag{76}$$

where N_g is the number of $K_{\pi 2\gamma}$ events in $K_{\pi 2}$-tgscat normalization branch and N_s is number of $K_{\pi 2}$-scatter events in the $K_{\pi 2}$-tgscat normalization branch. The value of N_s+N_g is 1131 for the 2/3 sample from Table 19.

Assuming

$$N_g = f \times N_p \tag{77}$$

where N_p is the number of $K_{\pi 2}$ events in the KP2BOX normalization branch and f is the relative rate of $K_{\pi 2\gamma}$ events in the PNN2BOX to $K_{\pi 2}$ events in the KP2BOX. The value of N_p is 122475 for the 2/3 sample from Table 21. The value of the relative rate f is $1/(361.12 \pm 90.15)$ from Table 55.

Using the numbers above, the upper limit on the $K_{\pi 2\gamma}$ contamination in the $K_{\pi 2}$-tgscat normalization branch is

$$g = \frac{122473/361.12}{1131} = 0.300 \pm 0.075. \quad (78)$$

This upper limit is consistent with the estimated $K_{\pi 2}$ and $K_{\pi 2\gamma}$ backgrounds given in Table 22:

$$\frac{0.0757 \pm 0.0073}{0.695 \pm 0.150} = 0.109 \pm 0.026 \quad (79)$$

where the systematic uncertainty has been assumed to be fully correlated between the background estimates and thus not relevant for the ratio.

10 Outside-the-Box Studies

Three sets of outside-the-box studies were performed:

1. Loosening of the photon veto from PV60 to PV90
2. Loosening of the photon veto from PV60 to PVPNN1
3. Loosening of the energy threshold in the cuts CCDBADFIT, CCDBADTIM, CCDPUL and EPIONK from 1.25 MeV to 2.5 MeV.

10.1 Loosening from PV60 to PV90

For this outside-the-box study, each of PV60 and PV90 actually refer to the combination of that cut and the PASS2 cut PVCUT. For many of the backgrounds, loosening the photon veto will increase the background by the ratio of the acceptance of PV90 to PV60. These backgrounds are K_{e4}, CEX, muon and beam and the scaling factor is A(PV90)/A(PV60) = 0.8855/0.6199 = 1.428. For the remaining backgrounds, the new background due to loosening of the photon veto is evaluated with PV90 applied instead of PV60. Table 56 shows the backgrounds due to PV60, PV90 and the resulting outside-the-box background. Note that due to the correction of the $K_{\pi 2}$ background from $K_{\pi 2\gamma}$ contamination, the $K_{\pi 2\gamma}$ background only contributes to the total uncertainty and not the central value.

The total number of background events expected from the PV90 outside-the-box study is $9.09 \pm 0.65(stat.)\,^{+1.38}_{-1.15}(sys.)$. When the number of events in this region was measured directly, 3 events were found. If we treat the central value of 9.09 events as the mean of a Poisson distribution, we have a 1.99% chance of observing 3 or less events. If we shift the mean down by an amount equal to the lower bound of the systematic error $(9.09 - 1.15 = 7.94)$, we have a 4.4% chance of observing 3 or less events.

To help determine if this lower than expected number of events was a statistical anomaly or an indication of strong anti-correlation between the photon veto and CCDPUL cuts, this outside the box study was repeated looking at the region between the PV90 and the PNN1-level photon veto.

10.2 The Outside-the-Box Region Between PV90 and PVPNN1

This study examines the outside-the-box region between the PVPNN1 and PV90 regions. For this study, scaling is used to determine the background level in the expanded box for K_{e4}, CEX, muon and beam. The scaling factor is

$$\frac{A(PVPNN1)}{A(PV60)} - \frac{A(PV90)}{A(PV60)} = \frac{0.9248}{0.6199} - \frac{0.8855}{0.6199} = 0.064 \quad (80)$$

CUT	KP2 box	PNN2 box	Peak/Tail
START	1913712	1913712	1.00±0.00
BOX	473271 (4.04)	128734 (14.87)	3.68±0.01
LEV11	473121 (1.00)	126739 (1.02)	3.73±0.01
LEV12	473085 (1.00)	126538 (1.00)	3.74±0.01
PSCUT	443561 (1.07)	104451 (1.21)	4.25±0.01
TGCUT	438030 (1.01)	83008 (1.26)	5.28±0.02
TGPVCUT	396391 (1.11)	68873 (1.21)	5.76±0.02
TDCUT	283529 (1.40)	13835 (4.98)	20.49±0.17
STLAY	263217 (1.08)	11726 (1.18)	22.45±0.20
TARGET	263217 (1.00)	11726 (1.00)	22.45±0.20
ICBIT	263149 (1.00)	11724 (1.00)	22.45±0.20
DCBIT	232378 (1.13)	5421 (2.16)	42.87±0.58
LHEX	75693 (3.07)	2189 (2.48)	34.58±0.73
PSCUT06	48461 (1.56)	912 (2.40)	53.14±1.74
DELCO3	48102 (1.01)	907 (1.01)	53.03±1.74
TDCUT02	39967 (1.20)	625 (1.45)	63.95±2.54
ICODEL14	39950 (1.00)	625 (1.00)	63.92±2.54
FIDUCIAL	37699 (1.06)	599 (1.04)	62.94±2.55
UTCQUAL	36738 (1.03)	568 (1.05)	64.68±2.69
RSDEDX	33574 (1.09)	512 (1.11)	65.57±2.88
RNGMOM	33288 (1.01)	500 (1.02)	66.58±2.96
PRRF	29842 (1.12)	473 (1.06)	63.09±2.88
B4EKZ	27482 (1.09)	383 (1.23)	71.75±3.64
TGZFOOL	27109 (1.01)	379 (1.01)	71.53±3.65
EPITG	23842 (1.14)	272 (1.39)	87.65±5.28
EPIMAXK	23842 (1.00)	272 (1.00)	87.65±5.28
TARGF	23088 (1.03)	216 (1.26)	106.89±7.24
DTGTTP	23088 (1.00)	216 (1.00)	106.89±7.24
RTDIF	22899 (1.01)	216 (1.00)	106.01±7.18
DRP	22834 (1.00)	213 (1.01)	107.20±7.31
TGKTIM	22592 (1.01)	210 (1.01)	107.58±7.39
EIC	22252 (1.02)	205 (1.02)	108.55±7.55
TIC	22252 (1.00)	205 (1.00)	108.55±7.55
TGEDGE	22117 (1.01)	203 (1.01)	108.95±7.61
TGDEDX	22013 (1.00)	196 (1.04)	112.31±7.99
TGENR	21418 (1.03)	192 (1.02)	111.55±8.01
TGER	21418 (1.00)	192 (1.00)	111.55±8.01
PIGAP	21276 (1.01)	188 (1.02)	113.17±8.22
TGB4	20130 (1.06)	170 (1.11)	118.41±9.04
KIC	20127 (1.00)	169 (1.01)	119.09±9.12
PHIVTX	19504 (1.03)	120 (1.41)	162.53±14.79
OPSVETO	18995 (1.03)	99 (1.21)	191.87±19.23
TGLIKE	18425 (1.03)	92 (1.08)	200.27±20.83
TIMKF	16657 (1.11)	77 (1.19)	216.32±24.59
NPITG	16657 (1.00)	77 (1.00)	216.32±24.59
ALLKFIT	16044 (1.04)	71 (1.08)	225.97±26.76
TPICS	16042 (1.00)	71 (1.00)	225.94±26.75
EPIONK	15041 (1.07)	68 (1.04)	221.19±26.76
CHI567	13129 (1.15)	54 (1.26)	243.13±33.02
VERRNG	12357 (1.06)	45 (1.20)	274.60±40.86
CHI5MAX	12357 (1.00)	45 (1.00)	274.60±40.86
ANGLI	12348 (1.00)	45 (1.00)	274.40±40.83
CCDBADFIT	10937 (1.13)	38 (1.18)	287.82±46.61
CCDBADTIM	10743 (1.02)	37 (1.03)	290.35±47.65
CCD31FIB	10743 (1.00)	37 (1.00)	290.35±47.65
CCDPUL	5778 (1.86)	16 (2.31)	361.12±90.15

Table 55: The relative rate of $K_{\pi 2\gamma}$ events in the PNN2BOX to $K_{\pi 2}$ events in the KP2BOX using KP21 monitors.

Background	PV60	PV90	OTB
$K_{\pi 2}$-tgscat	$0.695 \pm 0.150\,^{+0.061}_{-0.094}$	$9.584 \pm 0.626\,^{+1.133}_{-1.000}$	$8.889 \pm 0.644\,^{+1.227}_{-1.061}$
$K_{\pi 2}$-rsscat	$0.030 \pm 0.005\,^{+0.004}_{-0.004}$	$0.143 \pm 0.022\,^{+0.018}_{-0.018}$	$0.113 \pm 0.023\,^{+0.022}_{-0.022}$
$K_{\pi 2\gamma}$	$0.076 \pm 0.007\,^{+0.006}_{-0.006}$	$0.357 \pm 0.016\,^{+0.029}_{-0.026}$	$0.281 \pm 0.018\,^{+0.023}_{-0.020}$
K_{e4}	$0.176 \pm 0.072\,^{+0.233}_{-0.124}$	$0.251 \pm 0.103\,^{+0.333}_{-0.177}$	$0.075 \pm 0.031\,^{+0.100}_{-0.053}$
CEX	$0.013 \pm 0.013\,^{+0.010}_{-0.003}$	$0.019 \pm 0.019\,^{+0.014}_{-0.004}$	$0.006 \pm 0.006\,^{+0.004}_{-0.001}$
Muon	0.0114 ± 0.0114	0.0163 ± 0.0163	0.0049 ± 0.0049
1bm	0.00023 ± 0.00023	0.00033 ± 0.00033	0.00010 ± 0.00010
2bm-KK	0.00046 ± 0.00046	0.00065 ± 0.00065	0.00020 ± 0.00020
2bm-KP	0.00065 ± 0.00065	0.00093 ± 0.00093	0.00028 ± 0.00028
Total	$0.93 \pm 0.17\,^{+0.31}_{-0.23}$	$10.02 \pm 0.64\,^{+1.53}_{-1.23}$	$9.09 \pm 0.65\,^{+1.38}_{-1.15}$

Table 56: Summary of PV90 Outside-the-Box Study. Scaling by a factor of A(PV90)/A(PV60) = 0.8855/0.6199 = 1.428 was used for the backgrounds K_{e4}, CEX, muon and beam. The remaining backgrounds were re-evaluated using PV90. For values having two sets of uncertainties, the first is statistical and the second systematic. The central value for $K_{\pi 2\gamma}$ is treated as zero as the contribution due to this background is included in the $K_{\pi 2}$-tgscat value.

As with the PV90 outside-the-box study, the $K_{\pi 2}$ scatter backgrounds and $K_{\pi 2\gamma}$ were re-evaluated for the expanded regions. Table 57 shows the backgrounds due to PV90, PVPNN1 and the resulting outside-the-box background. Again, note that due to the correction of the $K_{\pi 2}$ background from $K_{\pi 2\gamma}$ contamination, the $K_{\pi 2\gamma}$ background only contributes to the total uncertainty and not the central value.

The total number of background events expected from the PVPNN1 outside-the-box study is $32.4 \pm 1.85(stat.)\,^{+12.2}_{-7.9}(sys.)$. When the number of events in this region was measured directly, 34 events were found. This number of observed events agrees with the predicted number within statistical error. The probability to observe 34 or fewer events when 32.36 are expected is 61.3% assuming a Poisson distribution of mean 32.36 can be approximated by a Gaussian of mean 32.36 and $\sigma = \sqrt{32.36}$. For the lower bound of the systematic uncertainty, the probability to observed 34 or fewer events is 97.3%.

10.3 Loosening the Pion Energy Under Kaon Fiber Cuts

For the purpose of this study, the cuts CCDBADFIT, CCDBADTIM, CCDPUL and EPIONK will be called "EPI" cuts. The pion energy threshold for these cuts was loosened from 1.25 MeV ("EPI=1.25") to 2.5 MeV ("EPI=2.5") for this outside-the-box study.

For this study, scaling by a factor of A(EPI=2.5)/A(EPI=1.25) = 0.6862/0.4576 = 1.4995 was used to determine the K_{e4}, CEX, muon and beam backgrounds in the expanded box. The normalization branch for $K_{\pi 2\gamma}$ was re-evaluated and the $K_{\pi 2}$-scatter backgrounds completely re-evaluated to determine the background levels in the expanded box.

Table 58 shows the backgrounds due to EPI=1.25, EPI=2.5 and the resulting outside-the-box background. Yet again, note that due to the correction of the $K_{\pi 2}$ background from $K_{\pi 2\gamma}$ contamination, the $K_{\pi 2\gamma}$ background only contributes to the total uncertainty and not the central value.

Background	PV90	PVPNN1	OTB
$K_{\pi 2}$-tgscat	$9.584 \pm 0.626\,^{+1.133}_{-1.000}$	$41.627 \pm 1.741\,^{+12.092}_{-6.651}$	$32.043 \pm 1.850\,^{+13.092}_{-7.784}$
$K_{\pi 2}$-rsscat	$0.143 \pm 0.022\,^{+0.018}_{-0.018}$	$0.449 \pm 0.067\,^{+0.054}_{-0.056}$	$0.305 \pm 0.070\,^{+0.073}_{-0.074}$
$K_{\pi 2\gamma}$	$0.357 \pm 0.016\,^{+0.029}_{-0.026}$	$1.091 \pm 0.028\,^{+0.090}_{-0.079}$	$0.734 \pm 0.018\,^{+0.061}_{-0.053}$
K_{e4}	$0.251 \pm 0.103\,^{+0.333}_{-0.177}$	$0.266 \pm 0.107\,^{+0.348}_{-0.185}$	$0.011 \pm 0.005\,^{+0.015}_{-0.008}$
CEX	$0.0186 \pm 0.0186\,^{+0.0143}_{-0.0043}$	$0.0194 \pm 0.0194\,^{+0.0149}_{-0.0045}$	$0.0008 \pm 0.0008\,^{+0.0006}_{-0.0002}$
Muon	0.0163 ± 0.0163	0.0170 ± 0.0170	0.0007 ± 0.0007
1bm	0.00033 ± 0.00033	0.00034 ± 0.00034	0.00001 ± 0.00001
2bm-KK	0.00065 ± 0.00065	0.00068 ± 0.00068	0.00003 ± 0.00003
2bm-KP	0.00093 ± 0.00093	0.00097 ± 0.00097	0.00004 ± 0.00004
Total	$10.02 \pm 0.64\,^{+1.53}_{-1.23}$	$42.38 \pm 1.75\,^{+12.60}_{-6.98}$	$32.36 \pm 1.85\,^{+13.24}_{-7.92}$

Table 57: Summary of the PVPNN1 to PV90 Outside-the-Box Study. Scaling was used for the backgrounds K_{e4}, CEX, muon and beam. The remaining backgrounds were re-evaluated in both the PVPNN1 and PV90 regions. For values having two sets of uncertainties, the first is statistical and the second systematic. The central value for $K_{\pi 2\gamma}$ is treated as zero as the contribution due to this background is included in the $K_{\pi 2}$-tgscat value.

The total number of background events expected from the EPI outside-the-box study is $0.79 \pm 0.35(stat.)\,^{+0.30}_{-0.37}(sys.)$. When the number of events in this region was measured directly, 0 events were found. If we treat the central value of 0.79 events as the mean of a Poisson distribution, we have a 45.2% chance of observing 0 events. If we shift the mean down by an amount equal to the lower bound of the systematic error ($0.79 - 0.37 = 0.42$), we have a 65.4% chance of observing 0 events.

10.4 Consistency of Outside-the-Box Results

Given the probabilities p_1 and p_2 of two outside-the-box studies, the combined probability is given by $p_{12} = p_1 p_2(1 - \ln p_1 p_2)$ [17]. For the outside-the-box regions described in the Sections 10.1 and 10.3, $p_1 = 0.0199$ and $p_2 = 0.452$, respectively, the combined probability is $p_{12} = 0.0513$. Including the result of the outside-the-box region described in Section 10.2 of $p = 0.613$ gives an overall probability of 0.140.

The overall probability of 14% indicates that the outside-the-box results are generally consistent, although the 5.1% probability for the two regions nearest the signal region may indicate that the background is over-estimated. This result is consistent with the general philosophy of background estimation for this analysis in that some level of contamination of background samples is inevitable and generally inflates the background estimates. As described in Section 10.5, the assigned systematic uncertainty is intended to define a range that contains the actual value of the background. Taking the lower limit of the range specified for the three outside-the-box regions, the probability is 13% for the results in the two nearest regions and 39% for all three regions. We take this as an indication that the assigned systematic uncertainties are adequate.

Background	EPI=1.25	EPI=2.5	OTB
$K_{\pi 2}$-tgscat	$0.695 \pm 0.150\,^{+0.061}_{-0.094}$	$1.361 \pm 0.314\,^{+0.066}_{-0.229}$	$0.666 \pm 0.348\,^{+0.160}_{-0.290}$
$K_{\pi 2}$-rsscat	$0.030 \pm 0.005\,^{+0.004}_{-0.004}$	$0.057 \pm 0.008\,^{+0.008}_{-0.008}$	$0.026 \pm 0.009\,^{+0.011}_{-0.011}$
$K_{\pi 2\gamma}$	$0.076 \pm 0.007\,^{+0.006}_{-0.006}$	$0.121 \pm 0.009\,^{+0.010}_{-0.009}$	$0.045 \pm 0.012\,^{+0.004}_{-0.003}$
K_{e4}	$0.176 \pm 0.072\,^{+0.233}_{-0.124}$	$0.264 \pm 0.108\,^{+0.349}_{-0.186}$	$0.088 \pm 0.036\,^{+0.116}_{-0.062}$
CEX	$0.013 \pm 0.013\,^{+0.010}_{-0.003}$	$0.019 \pm 0.019\,^{+0.015}_{-0.005}$	$0.006 \pm 0.006\,^{+0.005}_{-0.002}$
Muon	0.0114 ± 0.0114	0.0171 ± 0.0171	0.0057 ± 0.0057
1bm	0.00023 ± 0.00023	0.00034 ± 0.00034	0.00011 ± 0.00011
2bm-KK	0.00046 ± 0.00046	0.00069 ± 0.00069	0.00023 ± 0.00023
2bm-KP	0.00065 ± 0.00065	0.00097 ± 0.00097	0.00032 ± 0.00032
Total	$0.93 \pm 0.17\,^{+0.31}_{-0.23}$	$1.72 \pm 0.33\,^{+0.45}_{-0.44}$	$0.79 \pm 0.35\,^{+0.30}_{-0.37}$

Table 58: Summary of the pion energy in kaon fibers outside-the-box study. Scaling by a factor of A(EPI-2.5)/A(EPI-1.25) = 1.499 was used for the backgrounds K_{e4}, CEX, muon and beam. The remaining backgrounds were re-evaluated using the loosened CCDPUL, CCDBADFIT, CCDBADTIM and EPIONK cuts. For values having two sets of uncertainties, the first is statistical and the second systematic. The central value for $K_{\pi 2\gamma}$ is treated as zero as the contribution due to this background is included in the $K_{\pi 2}$-tgscat value.

10.5 The Range-of-Values Systematic Uncertainty Method

The systematic uncertainties in the outside-the-box studies were determined using a range-of-values method. This section discusses that method and the specific details of how it was implemented to determine the systematic uncertainties of each background in the outside-the-box regions. All mentions of uncertainties in these discussions refer only to systematic uncertainties.

In these analyses, the systematic errors generally represent the range over which it is more or less equally probably that the central value actually falls. Given a measured number of events in the normalization branch with systematic errors $N^{+dN_{hi}}_{-dN_{lo}}$ and a rejection $R^{+dR_{hi}}_{-dR_{lo}}$, the equation for a typical background estimate is given by

$$n = \frac{N}{R-1}. \tag{81}$$

Since these uncertainties do not represent a gaussian shape and are typically quite large relative to their central values, a range-of-values method is used to determine the total systematic uncertainties for a calculated value. For the background equation above, the upper and lower bounds on the systematic error are determined by maximizing and minimizing the the quantity n_{bg} using the systematic uncertainties of N and R:

$$dn_{hi} = \frac{(N + dN_{hi})}{(R - dR_{lo}) - 1} - n, \tag{82}$$

$$dn_{lo} = n - \frac{(N - dN_{lo})}{(R + dR_{hi}) - 1}. \tag{83}$$

Normalization and Rejection Branches Change Outside-the-Box

For backgrounds such as $K_{\pi 2}$-tgscat and $K_{\pi 2}$-rsscat where loosening the photon veto changes both the normalization and the rejection, the following method is used.

The estimated background in the outside-the-box region n_{otb} is the difference between the background estimate in the expanded (loosened photon veto) region n_{exp} and the background estimate at the regular cut levels n_{reg}. To represent the true range of values that can be found using the systematic uncertainties on both n_{exp} and n_{reg}, we need to maximize (minimize) the systematic uncertainties for n_{otb}:

$$dn_{otb}^{hi} = dn_{exp}^{hi} + dn_{reg}^{lo}, \tag{84}$$

$$dn_{otb}^{lo} = dn_{exp}^{lo} + dn_{reg}^{hi}. \tag{85}$$

Scaled Backgrounds

For backgrounds such as beam, muon, Ke4 and CEX where scaling was used to determine the background estimate in the outside-the-box region, the following method was used.

The scaling factor to go from the region with regular cut levels to the expanded region is given by

$$S_{exp} = \frac{A_{exp}}{A_{reg}}, \tag{86}$$

where A_{exp} and A_{reg} are the acceptances of the cut being loosened at the loosened (expanded) and regular levels respectively.

The scaling factor to directly from the regular background level estimate to the estimate for the outside-the-box region is simply $S_{exp} - 1$ or

$$S_{otb} = \frac{A_{exp}}{A_{reg}} - 1. \tag{87}$$

The resulting systematic uncertainties are then

$$dn_{otb}^{hi} = dn_{reg}^{hi} \times S_{otb}, \tag{88}$$

$$dn_{otb}^{lo} = dn_{reg}^{lo} \times S_{otb}. \tag{89}$$

Only Normalization Changes for Outside-the-Box

For backgrounds such as $K_{\pi 2\gamma}$ where loosening the photon veto changes only the normalization branch, the following method is used. Here it is important to note that there is no systematic uncertainty associated with the normalization number.

For $K_{\pi 2\gamma}$ the systematic error comes completely from the terms R_γ and κ in the denominator and not at all from the normalization number.

The central value of the outside-the-box estimate for $K_{\pi 2\gamma}$ looks like

$$n_{otb} = \frac{N_{exp} - N_{reg}}{R_\gamma \times \kappa}. \tag{90}$$

Using the range-of-values method to maximize (minimize) the systematic uncertainties for n_{otb}:

$$dn_{otb}^{hi} = \frac{N_{exp} - N_{reg}}{(R_\gamma - dR_\gamma^{lo}) \times (\kappa - d\kappa^{lo})} - n_{otb}, \tag{91}$$

$$dn_{otb}^{lo} = \frac{N_{exp} - N_{reg}}{(R_\gamma + dR_\gamma^{hi}) \times (\kappa + d\kappa^{hi})} - n_{otb}. \tag{92}$$

$K_{\mu 2}$ **Setups**	**Component cuts**
$Setup_{RS\ track}$	TRIGGER, ICBIT, $t_{IC} - t_{Ck} > 5$ ns, B4DEDX, UTC, UTC_QUAL
$Setup_{recon}$	TRIGGER, ICBIT, $t_{IC} - t_{Ck} > 5$ ns, B4DEDX, CPITRS, CPITAIL, CKTRS, CKTAIL, BWTRS, RDTRK, TRKTIM, $\lvert t_{IC} - t_{RS}\rvert < 5$ ns, PVCUTPNN2(noBV+BVL)
$Setup_{beam}$	TRIGGER, ICBIT, RDTRK, TRKTIM, RDUTM, KM2PBOX, COS3D
$Setup_{PV}$	$Setup_{beam}$, A_{beam} cuts, stopping layer< 19

Table 59: Setup cuts used for the $K_{\mu 2}$-based acceptance measurements. "A_{beam} cuts" are the cuts whose acceptance is measured in "beam" category. ICBIT is the online-IC-trigger bit, KM2PBOX selects events with 226 MeV/c $< ptot <$ 246 MeV/c.

Cut	Loose Box		Tight Box	
	Events	**Acceptance**	**Events**	**Acceptance**
$Setup_{RS\ track}$	2967140		2967140	
RD_TRK	2967140	1.0000 ± 0.00000	2967140	1.0000 ± 0.00000
TRKTIM	2966943	0.9999 ± 0.00000	2966943	0.9999 ± 0.00000
A_{RS}	0.99993 ± 0.000005		0.99993 ± 0.000005	

Table 60: RS reconstruction acceptance using $K_{\mu 2}(1)$ monitor events.

Systematic Uncertainty of the Total Outside-the-Box Background

When performing a sum of all the outside-the-box backgrounds to determine the total outside-the-box background estimate, the range-of-values method of determining the systematic uncertainty is the same as doing a linear sum of the upper (lower) bounds dn_{hi} (dn_{lo}) from each of the individual backgrounds. This is the same method that is used to determine the total background in the regular signal region.

11 Acceptance

11.1 Acceptance Factors from $K_{\mu 2}$ Events

$K_{\mu 2}$ events which have an incoming K^+, one charged track entering the fiducial region, and no photons products are ideal in emulating signal event criteria for beam conditions, target reconstruction, tracking, and photons. To obtain appropriate samples for these aspects of the $K^+ \to \pi^+ \nu \bar{\nu}$ decay, setup cuts listed in Table 59 were employed.

To measure event reconstruction in the RS, see Table 60, the setup cuts chosen, $Setup_{Recon}$, created a sample with good tracks by requiring that the TG and UTC, which are independent of the RS, have a valid reconstruction, a delayed-coincidence style cut using $\check{C}_K$ and IC, K^+ entering the TG (B4DEDX). Measuring the reconstruction efficiency of the TG and UTC, see Table 61, requires a sample with a single K^+ (B4DEDX) and no beam π^+'s entering the detector (CPITRS, CPITAIL, CKTRS, CKTAIL, BWTRS). A requirement that insures a delayed coincidence using $\check{C}_K$ and IC[3] ($t_{IC} - t_{Ck} > 5$ ns), a good

[3]DELCO could not be used in here because DELCO requires a TG reconstruction which in turn requires a reconstructed track from the UTC and RS.

Cut	Loose Box		Tight Box	
	Events	**Acceptance**	**Events**	**Acceptance**
$Setup_{recon}$	1542443		759060	
RDUTM	1541571	0.9994 ± 0.00002	758792	0.9996 ± 0.00002
TARGET	1541571	1.0000 ± 0.00000	758792	1.0000 ± 0.00000
A_{recon}	0.99943 ± 0.000019		0.99965 ± 0.000022	

Table 61: TG and UTC reconstruction acceptance using $K_{\mu 2}(1)$ monitor events.

charged track traversing the UTC detector ($|t_{IC} - t_{RS}| < 5$ ns, RD_TRK, TRKTIM), and no photons (PVCUTPNN2(noBV+BVL)). BV and BVL photon-vetoing criteria is not used for the A_{RS} sample, so that the sample will not remove events with μ^+'s traversing the entire RS and entering the BVL and BV.

The acceptances associated with the beam and target-region cuts require a sample which is definitely a single K^+ decay with no photons. So the $K_{\mu 2}$ decay was chosen with requirements on the track momentum (KM2PBOX), on the quality of the track (RD_TRK, TRKTIM, RDUTM), and on the fiducial region (COS3D). The cuts in Table 62 were ordered in a way that would allow for a more meaningful acceptance value for each cut (e.g. TGQUALT was placed at the beginning because many of the following cuts require a successful TG reconstruction before they work properly.)

Cut	Loose Box		Tight Box	
	Events	**Acceptance**	**Events**	**Acceptance**
$Setup_{beam}$	3824854		3824854	
TGCUT	3741291	0.9782 ± 0.00007	3741291	0.9782 ± 0.00007
TGQUALT	3610937	0.9652 ± 0.00009	3610937	0.9652 ± 0.00009
NPITG	3610937	1.0000 ± 0.00000	3610937	1.0000 ± 0.00000
TIMCON	3605667	0.9985 ± 0.00002	3605667	0.9985 ± 0.00002
TGTCON	3566647	0.9892 ± 0.00005	3566647	0.9892 ± 0.00005
B4ETCON	3531329	0.9901 ± 0.00005	3531329	0.9901 ± 0.00005
DCBIT	3110649	0.8809 ± 0.00017	3110649	0.8809 ± 0.00017
DELCO	2665661	0.8569 ± 0.00020	2191189	0.7044 ± 0.00026
PSCUT	2528550	0.9486 ± 0.00014	2074552	0.9468 ± 0.00015
B4DEDX	2514694	0.9945 ± 0.00005	2063095	0.9945 ± 0.00005
BWTRS	2308180	0.9179 ± 0.00017	1892260	0.9172 ± 0.00019
CPITRS	2304287	0.9983 ± 0.00003	1889137	0.9983 ± 0.00003
CPITAIL	2303213	0.9995 ± 0.00001	1888271	0.9995 ± 0.00002
CKTRS	2288540	0.9936 ± 0.00005	1878953	0.9951 ± 0.00005
CKTAIL	2251649	0.9839 ± 0.00008	1867769	0.9940 ± 0.00006
B4TRS	2193877	0.9743 ± 0.00011	1818255	0.9735 ± 0.00012
B4CCD	2164219	0.9865 ± 0.00008	1798933	0.9894 ± 0.00008
UPVTRS	2128633	0.9836 ± 0.00009	1770430	0.9842 ± 0.00009
RVTRS	2126603	0.9990 ± 0.00002	1768838	0.9991 ± 0.00002
TGGEO	2041316	0.9599 ± 0.00013	1696457	0.9591 ± 0.00015
B4EKZ	1861055	0.9117 ± 0.00020	1544226	0.9103 ± 0.00022
TGZFOOL	1838070	0.9876 ± 0.00008	1525163	0.9877 ± 0.00009
TARGF	1778937	0.9678 ± 0.00013	1475963	0.9677 ± 0.00014
DTGTTP	1778930	1.0000 ± 0.00000	1475956	1.0000 ± 0.00000
RTDIF	1761888	0.9904 ± 0.00007	1461737	0.9904 ± 0.00008
TGKTIM	1744527	0.9901 ± 0.00007	1456412	0.9964 ± 0.00005
EICCON	1697720	0.9732 ± 0.00012	1417410	0.9732 ± 0.00013

Table 62 continued on next page

Table 62 continued from previous page				
Cut	Loose Box		Tight Box	
	Events	**Acceptance**	**Events**	**Acceptance**
TICCON	1697716	1.0000 ± 0.00000	1417407	1.0000 ± 0.00000
PIGAP	1682926	0.9913 ± 0.00007	1405081	0.9913 ± 0.00008
TBDB4	1637496	0.9730 ± 0.00012	1366451	0.9725 ± 0.00014
TGDB4TIP	1629171	0.9949 ± 0.00006	1359267	0.9947 ± 0.00006
TGDVXTIP	1624888	0.9974 ± 0.00004	1355631	0.9973 ± 0.00004
TGDVXPI	1588984	0.9779 ± 0.00012	1327709	0.9794 ± 0.00012
PHIVTX	1541372	0.9700 ± 0.00014	1283527	0.9667 ± 0.00016
CCDPUL CCDBADFIT	694731	0.4507 ± 0.00040	633868	0.4938 ± 0.00044
EPIONK	691595	0.9955 ± 0.00008	630732	0.9951 ± 0.00009
CCDBADTIM	684667	0.9900 ± 0.00012	624344	0.9899 ± 0.00013
CCD31FIB	684658	1.0000 ± 0.00000	624335	1.0000 ± 0.00000
TIMKF	628179	0.9175 ± 0.00033	572339	0.9167 ± 0.00035
VERRNG	585499	0.9321 ± 0.00032	533386	0.9319 ± 0.00033
ANGLI	585135	0.9994 ± 0.00003	533050	0.9994 ± 0.00003
ALLKFIT	577756	0.9874 ± 0.00015	526144	0.9870 ± 0.00015
TPICS	577003	0.9987 ± 0.00005	525413	0.9986 ± 0.00005
KIC	576825	0.9997 ± 0.00002	525245	0.9997 ± 0.00002
A_{beam}	0.15081 ± 0.000183		0.13732 ± 0.000176	

Table 62: Target and Beam acceptance based on $K_{\mu 2}(1)$ events

Cut	Loose Box		Tight Box	
	Events	**Acceptance**	**Events**	**Acceptance**
$Setup_{PV}$	62556		56294	
LHEX	58388	0.9334 ± 0.00100	52530	0.9331 ± 0.00105
HEXAFTER	56244	0.9633 ± 0.00078	50621	0.9637 ± 0.00082
PVONLINE	53832	0.9571 ± 0.00085	48449	0.9571 ± 0.00090
LAY20or21	53413	0.9922 ± 0.00038	48069	0.9922 ± 0.00040
STLAY	52910	0.9906 ± 0.00042	47609	0.9904 ± 0.00044
RSHEX	50992	0.9637 ± 0.00081	45855	0.9632 ± 0.00086
PVCUT	49039	0.9617 ± 0.00085	44092	0.9616 ± 0.00090
TGPVCUT	48558	0.9902 ± 0.00045	43661	0.9902 ± 0.00047
TGPVTR	48558	1.0000 ± 0.00000	43661	1.0000 ± 0.00000
TGPV	47044	0.9688 ± 0.00079	40121	0.9189 ± 0.00131
ICPV	46996	0.9990 ± 0.00015	40007	0.9972 ± 0.00027
VCPV	46966	0.9994 ± 0.00012	39933	0.9981 ± 0.00021
COPV	46707	0.9945 ± 0.00034	39778	0.9961 ± 0.00031
MCPV	46702	0.9999 ± 0.00005	39768	0.9997 ± 0.00008
ECinner	43191	0.9248 ± 0.00122	31655	0.7960 ± 0.00202
ECouter	37652	0.8718 ± 0.00161	25258	0.7979 ± 0.00226
EC 2nd	37390	0.9930 ± 0.00043	23395	0.9262 ± 0.00164
RSPV	34680	0.9275 ± 0.00134	16681	0.7130 ± 0.00296
BVPV	32182	0.9280 ± 0.00139	15318	0.9183 ± 0.00212
BVLPV	31668	0.9840 ± 0.00070	15108	0.9863 ± 0.00094
ADPV	30132	0.9515 ± 0.00121	14439	0.9557 ± 0.00167
EARLY_{BV}	30106	0.9991 ± 0.00017	14433	0.9996 ± 0.00017
DSPV	30103	0.9999 ± 0.00006	14432	0.9999 ± 0.00007
EARLY_{BVL}	30103	1.0000 ± 0.00000	14432	1.0000 ± 0.00000
PV60	-	-	14120	0.9784 ± 0.00121
PV_{PNN2}	0.6199 ± 0.0022		0.3234 ± 0.0022	
A_{PV}	0.48122 ± 0.001998		0.25083 ± 0.001827	

Table 63: Online and offline photon-veto acceptance using $K_{\mu 2}(1)$ monitor events. PV_{PNN2} is not an additional cut, but simply the offline acceptance of the PV cuts from TGPV to $\text{EARLY}_{\text{BVL}}$ inclusive. A_{PV} is the acceptance of all the cuts listed in the table.

Measuring the photon-veto criteria required a valid decay and successfully reconstructed $K_{\mu 2}$ event without any additional secondary beam particles at decay time ($Setup_{beam}$, A_{beam}). Since a μ^+ from a $K_{\mu 2}$ decay could penetrate the whole RS and reach the BVL or BV photon detector, a requirement of *stopping layer* < 19 was imposed. Both the online and offline PV cuts are measured with $K_{\mu 2}(1)$ since there was no online PV requirement in the trigger.

The total acceptance measured using $K_{\mu 2}$-monitor events is calculated via Eq. (93) and is summarized in Table 64.

$$A_{K_{\mu 2}} = A_{RS} \times A_{recon} \times A_{beam} \times A_{PV} \tag{93}$$

11.2 Acceptance Factors from $\pi_{scatter}$ Events

Since the π^+ from $K^+ \to \pi^+ \nu\bar{\nu}$ events has a spectrum of energy and range values, unlike π^+'s from $K_{\pi 2}$, π_{scat}'s are ideal to measure acceptances dealing with RS kinematics. The π^+ from π_{scat} events have a continuous stopping-layer distribution, as is expected with $K^+ \to \pi^+ \nu\bar{\nu}$ events, which is advantageous in considering possible layer dependences within the RS (such as the TD cuts). The setup cuts used to create these samples are listed in Table 65.

	Loose Box	Tight Box
A_{RS}	0.99993 ± 0.000005	0.99993 ± 0.000005
A_{recon}	0.99943 ± 0.000019	0.99965 ± 0.000022
A_{beam}	0.15081 ± 0.000183	0.13732 ± 0.000176
A_{PV}	0.48122 ± 0.001998	0.25083 ± 0.001827
$A_{K_{\mu 2}}$	0.07253 ± 0.00031	0.03443 ± 0.00025

Table 64: $K_{\mu 2}$ acceptance summary.

$\pi_{scatter}$ **Setups**	**Component cuts**
$Setup_{bad\_stc}$	RD_TRK, TRKTIM, STLAY, UTC, RDUTM, PDC, ICBIT, $b4abm2 < 1.3MeV$, $\|t_\pi - t_{RS}\| < 5$ ns, $\|t_{IC} - t_{RS}\| < 5$ ns, TARGF, DTGTTP, RTDIF, TGQUALT, TGZFOOL, CKTRS, CKTAIL, PVCUTPNN2(only RS), COS3D, LAYV4, PNN2BOX
$Setup_{RSkin}$	$Setup_{bad\_stc}$, BAD_STC, TDCUT02
$Setup_{\pi\to\mu\to e}$	$Setup_{bad\_stc}$, BAD_STC, RNGMOM, ZFRF, ZUTOUT, LAYER14, UTC_QUAL, EIC

Table 65: Setup cuts used for the $\pi_{scatter}$ based acceptance measurements. $b4abm2$ is the energy of the B4 hit near beam time.

Creating a sample of single-beam π^+'s which scatter in the TG required removing events with K^+ particles in the beam ($b4abm2 < 1.3MeV$, CKTRS, CKTAIL); the requirement $|t_\pi - t_{RS}| < 5$ ns requires a scattering of the incoming particle and $|t_{IC} - t_{RS}| < 5$ ns requires that the track in the RS and TG are from the same particle. The RS photon-vetoing requirements are applied so as to remove coincident activity within the RS that would otherwise artificially lower the acceptance. PVPNN2 was not applied due to the photon cuts removing events with additional activity at decay time; since a decay does not occur, timing used by the photon cuts are not as meaningful. The remaining cuts which make up $Setup_{bad\_stc}$ require a nicely reconstructed track.

BADSTC, as discussed in Section 8 of [1], removes events when the TD in the determined stopping counter was not working properly.

Cut	Loose Box		Tight Box	
	Events	**Acceptance**	**Events**	**Acceptance**
$Setup_{bad\_stc}$	153716		74214	
BADSTC	153474	0.9984 ± 0.00010	74093	0.9984 ± 0.00015
A_{badstc}	0.99843 ± 0.000101		0.99837 ± 0.000148	

Table 66: BADSTC acceptance using $\pi_{scatter}$ monitor events.

11.3 Range-Stack-Kinematic Acceptance

Measuring the kinematic acceptance in the RS (A_{RSkin}) required further refinements to the sample employed by the A_{badstc} measurement. The particle-identification cuts TDCUT02 were utilized, requiring a stopped π^+ in the RS. Without the TDCUT02 requirement a

π^+, after entering the RS, could decay in flight yielding kinematics similar to a μ^+ or e^+. A sample with decay-in-flight π^+'s included would artificially lower A_{RSkin}.

Cut	Loose Box		Tight Box	
	Events	**Acceptance**	**Events**	**Acceptance**
$Setup_{RSkin}$	88719		32932	
UTCQUAL	84373	0.9510 ± 0.00072	31672	0.9617 ± 0.00106
RNGMOM	82845	0.9819 ± 0.00046	31161	0.9839 ± 0.00071
RSDEDXMAX	80449	0.9711 ± 0.00058	30355	0.9741 ± 0.00090
RSDEDXCL	76828	0.9550 ± 0.00073	29048	0.9569 ± 0.00117
RSLIKE	76828	1.0000 ± 0.00000	29048	1.0000 ± 0.00000
PRRF1	76196	0.9918 ± 0.00033	28841	0.9929 ± 0.00049
PRRFZ	73596	0.9659 ± 0.00066	27862	0.9661 ± 0.00107
A_{RSkin}	0.82954 ± 0.001262		0.84605 ± 0.001989	

Table 67: RS-kinematic acceptance using $\pi_{scatter}$ monitor events.

In order to account for the systematics associated with poor target reconstruction of the π_{scat} events, which is a function of the kinematics, the kinematic box cut was varied. The PNN2BOX was the nominal box cut. The size of the smaller and larger box cut was a shrunken or expanded PNN2BOX.

The difference in reconstruction quality for $\pi_{scatter}$ events and $K_{\pi 2}$ events was evaluated from the resolution of the reconstructed π^+ mass, $m_\pi = \frac{ptot^2 - etot^2}{2 \cdot etot}$, of the two samples. The distributions from π_{scat} and $K_{\pi 2}$ samples, shown in Fig. 17, have resolutions of 13.8 and 8.4 respectively. The fractional uncertainty in $\pi_{scatter}$-target-track reconstruction is therefore $\sqrt{13.8^2 - 8.4^2}/140.0 \simeq 7.8\%$.

Since *ptot* and *etot* contribute roughly equally to the resolution, their uncertainties are $7.8\%/\sqrt{2} = 5.5\%$. *rtot* scales approximately linearly with *etot*, so its uncertainty is also 5.5%. The boundaries of the nominal PNN2 kinematic box were varied by 5.5% yielding the following small and large boxes:

$$
\begin{aligned}
&\text{Small box :} \\
147.7 \text{ MeV/c} &< ptot < 188.1 \text{ MeV/c} \\
12.7 \text{ cm} &< rtot < 26.5 \text{ cm} \\
63.3 MeV &< etot < 95.0 MeV \\
&\text{Large box :} \\
132.3 \text{ MeV/c} &< ptot < 209.9 \text{ MeV/c} \\
11.3 \text{ cm} &< rtot < 29.5 \text{ cm} \\
56.7 MeV &< etot < 106.0 MeV
\end{aligned}
$$

The variation in the kinematic box determines the systematic error associated with the RS-kinematic cuts, as determined in Eq. (94).

$$\Delta A^{sys}_{RSkin} = \frac{|A^{large\ box}_{RSkin} - A^{small\ box}_{RSkin}|}{2} \tag{94}$$

Hence, the RS-kinematic acceptance is

$$A^{loose}_{RSkin} = 0.82954 \pm 0.001262 \pm 0.012 \tag{95}$$

$$A^{tight}_{RSkin} = 0.84605 \pm 0.001989^{+0.003}_{-0.020} \tag{96}$$

Cut	Loose Box		Tight Box	
	Events	**Acceptance**	**Events**	**Acceptance**
$Setup_{RSkin}^{small}$	63400		29195	
UTCQUAL	60350	0.9519 ± 0.00085	27906	0.9558 ± 0.00120
RNGMOM	59251	0.9818 ± 0.00054	27396	0.9817 ± 0.00080
RSDEDXMAX	57778	0.9751 ± 0.00064	26746	0.9763 ± 0.00092
RSDEDXCL	55375	0.9584 ± 0.00083	25685	0.9603 ± 0.00119
RSLIKE	55375	1.0000 ± 0.00000	25685	1.0000 ± 0.00000
PRRF1	55017	0.9935 ± 0.00034	25548	0.9947 ± 0.00045
PRRFZ	53324	0.9692 ± 0.00074	24778	0.9699 ± 0.00107
LAYER14	53324	1.0000 ± 0.00000	24778	1.0000 ± 0.00000
$A_{RSkin}^{small\ box}$	0.84107 ± 0.001452		0.84871 ± 0.002097	

Table 68: RS kinematic acceptance in the small box using $\pi_{scatter}$ monitor events. The "Tight box" of the rightmost two columns refers to tight PV and TD cuts.

Cut	Loose Box		Tight Box	
	Events	**Acceptance**	**Events**	**Acceptance**
$Setup_{RSkin}^{large}$	110317		51078	
UTCQUAL	104830	0.9503 ± 0.00065	48730	0.9540 ± 0.00093
RNGMOM	102909	0.9817 ± 0.00041	47846	0.9819 ± 0.00060
RSDEDXMAX	99517	0.9670 ± 0.00056	46347	0.9687 ± 0.00080
RSDEDXCL	94726	0.9519 ± 0.00068	44201	0.9537 ± 0.00098
RSLIKE	94726	1.0000 ± 0.00000	44201	1.0000 ± 0.00000
PRRF1	93737	0.9896 ± 0.00033	43806	0.9911 ± 0.00045
PRRFZ	90176	0.9620 ± 0.00062	42205	0.9635 ± 0.00090
LAYER14	90176	1.0000 ± 0.00000	42205	1.0000 ± 0.00000
$A_{RSkin}^{large\ box}$	0.81743 ± 0.001163		0.82629 ± 0.001676	

Table 69: RS kinematic acceptance in the large box using $\pi_{scatter}$ monitor events. The "Tight box" of the rightmost two columns refers to tight PV and TD cuts.

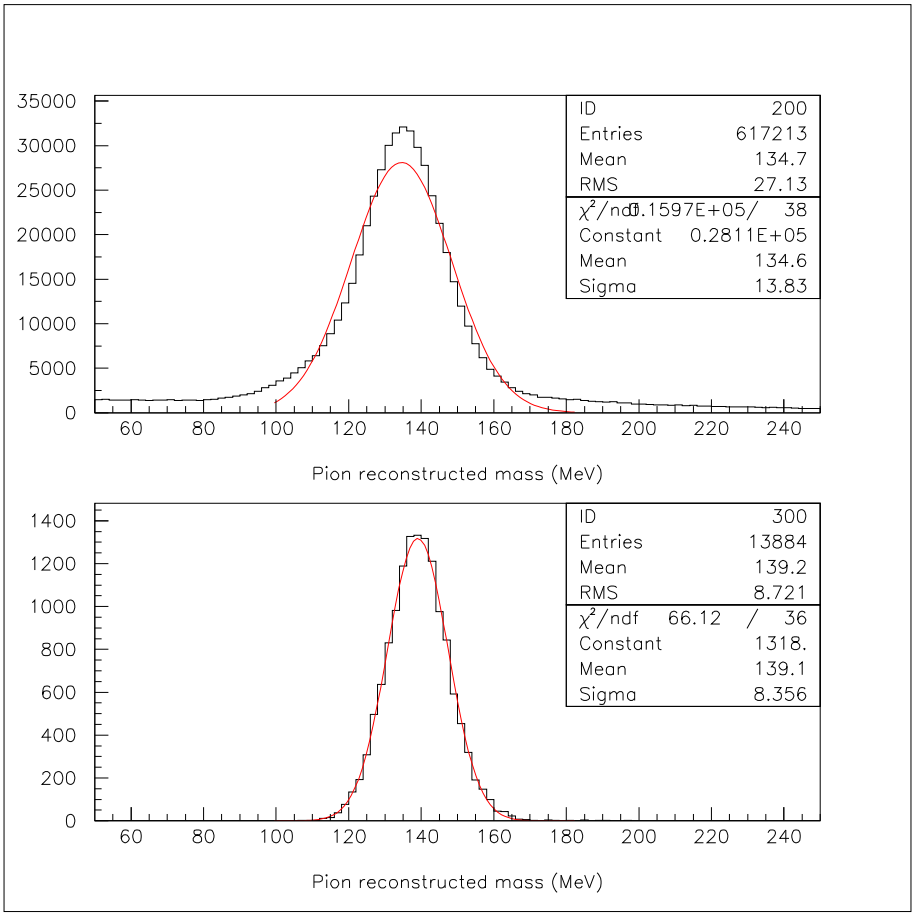

Figure 17: Distributions of the reconstructed π^+ mass from $\pi_{scatter}$ (top) and $K_{\pi 2}$ events (bottom).

11.4 $\pi^+ \to \mu^+ \to e^+$ Identification Acceptance

In an analogous way as the RS-kinematic-acceptance sample was created, the $\pi^+ \to \mu^+ \to e^+$ acceptance ($A_{\pi\to\mu\to e}$) requires the sample to be purified via cuts which are uncorrelated to the $\pi \to \mu \to e$ criteria (or simply TD cuts) being measured. RS-kinematic requirements were used to insure that the track was from a π^+. Since the $\pi_{scatter}$ did not include the online LEV1.1 and LEV1.2, the acceptances of these online requirements on the $\pi\nu\bar{\nu}(1)$ and $\pi\nu\bar{\nu}(2)$ could also be measured.

RSDEDX is correlated with EV5 due to μ^+ accidentals along the track causing EV5 to reject the event along with RSDEDX rejecting the event due to incorrect dE/dX value. PRRF1's dependence on the stopping-counter energy correlates it to the TD-pulse fitting utilized by TDNN. Tables 70 and 71 show the measured acceptances without and with RSDEDX and PRRF1,PRRFZ included in the setup cuts (A_{TD1}, A_{TD2}), respectively.

$A_{\pi\to\mu\to e}$ will be determined by the average of A_{TD1} and A_{TD2} and the systematic error is calculated from the difference. A 1.014% correction for π^+ decay-in-flight and π^+ absorption in the stopping counter, estimated from Monte Carlo, was applied to A_{TD2}.

The $\pi^+ \to \mu^+ \to e^+$ and total acceptance measured using $\pi_{scatter}$-monitor events is calculated via Eq. (97) and is summarized in Table 72

$$A_{\pi_{scat}} = A_{badstc} \times A_{RSkin} \times A_{\pi\to\mu\to e} \tag{97}$$

Cut	Loose Box		Tight Box	
	Events	**Acceptance**	**Events**	**Acceptance**
$Setup_{\pi\to\mu\to e}$	126239		64210	
PIFLG	104055	0.8243 ± 0.00107	53280	0.8298 ± 0.00148
RSHEX2	102123	0.9814 ± 0.00042	52271	0.9811 ± 0.00059
LEV1.1	82659	0.8094 ± 0.00123	42382	0.8108 ± 0.00171
LEV1.2	69374	0.8393 ± 0.00128	38160	0.9004 ± 0.00145
TDCUT	65186	0.9396 ± 0.00090	35907	0.9410 ± 0.00121
ELVETO	62425	0.9576 ± 0.00079	34453	0.9595 ± 0.00104
TDFOOL	62208	0.9965 ± 0.00024	34343	0.9968 ± 0.00030
TDNN	58607	0.9421 ± 0.00094	29016	0.8449 ± 0.00195
EV5	58607	1.0000 ± 0.00000	24264	0.8362 ± 0.00217
A_{TD1}	0.46425 ± 0.001404		0.37789 ± 0.001913	

Table 70: $\pi^+ \to \mu^+ \to e^+$ acceptance using $\pi_{scatter}$ monitor events.

Cut	Loose Box		Tight Box	
	Events	**Acceptance**	**Events**	**Acceptance**
$Setup_{\pi\to\mu\to e}$	126239		64210	
RSDEDXMAX				
RSDEDXCL				
RSLIKE				
PRRF1				
PRRFZ	107124		55113	
PIFLG	90161	0.8417 ± 0.00112	46466	0.8431 ± 0.00155
RSHEX2	88616	0.9829 ± 0.00043	45640	0.9822 ± 0.00061
LEV1.1	72545	0.8186 ± 0.00129	37347	0.8183 ± 0.00180
LEV1.2	61913	0.8534 ± 0.00131	34125	0.9137 ± 0.00145
TDCUT	58288	0.9415 ± 0.00094	32155	0.9423 ± 0.00126
ELVETO	55833	0.9579 ± 0.00083	30859	0.9597 ± 0.00110
TDFOOL	55655	0.9968 ± 0.00024	30774	0.9972 ± 0.00030
TDNN	52472	0.9428 ± 0.00098	26060	0.8468 ± 0.00205
EV5	52472	1.0000 ± 0.00000	21820	0.8373 ± 0.00229
$A_{uncorr\ TD2}$	0.48983 ± 0.001527		0.39591 ± 0.002083	
π^+ DIF/abs	$\times 1.014$			
A_{TD2}	0.4967 ± 0.0015		0.4015 ± 0.0021	

Table 71: $\pi^+ \to \mu^+ \to e^+$ acceptance using $\pi_{scatter}$ monitor events. $A_{uncorr\ TD2}$ is the acceptance before the correction factor for decay-in-flight (DIF) and π^+ absorption (abs) in the stopping counter (π^+ DIF/abs).

	Loose	Tight Box
A_{badstc}	0.99843 ± 0.000101	0.99837 ± 0.000148
A_{RSkin}	$0.82954 \pm 0.001262 \pm 0.012$	$0.84605 \pm 0.001989^{+0.003}_{-0.020}$
$A_{\pi\to\mu\to e}$	$0.4805 \pm 0.0015 \pm 0.016$	$0.3897 \pm 0.0021 \pm 0.012$
$A_{\pi_{scat}}$	$0.3980 \pm 0.0014 \pm 0.014$	$0.3292 \pm 0.0020^{+0.010}_{-0.013}$

Table 72: $\pi_{scatter}$ acceptance summary for loose and tight regions.

11.5 Acceptance Factors from $K_{\pi 2}$ Events

Within the E949 analysis, events from $K_{\pi 2}(1)$ monitors are similar to $K^+ \to \pi^+\nu\bar{\nu}$ events in a few aspects: (1) They both have a single π^+ track emerging from a single incoming K^+. (2) The π^+ within the TG is minimum ionizing. Condition (1) allows for a valid target reconstruction with a good decay-vertex determination. These properties allow acceptances to be measured for target kinematics.

$K_{\pi 2}$ **Setups**	**Component cuts**
$Setup_{utc}$	TRIGGER, RD_TRK, TRKTIM, STLAY, BAD_STC
$Setup_{ops}$	$Setup_{utc}$, UTC, RDUTM, PDC, PSCUT06, KCUTS, TGCUT06 without the ones measured, TDCUT02, KP2BOX
$Setup_{TGkin}$	$Setup_{ops}$, OPSVETO, TGPVCUT

Table 73: Setup cuts used for the $K_{\pi 2}$-based acceptance measurements.

To obtain a sample of PNN2 signal-like events, setup cut in Table 73 were utilized on $K_{\pi 2}(1)$ triggers. Measuring the acceptance of the PASS1 UTC cuts required reconstructing the TG and RS.

Cut	**Events**	**Acceptance**
$Setup_{utc}$	1502895	
UTC	1417906	0.9435 ± 0.00019
A_{utc}	0.94345 ± 0.000188	

Table 74: UTC acceptance using $K_{\pi 2}(1)$ monitor events.

The acceptance measurement of OPSVETO, Table 75, requires a sample with valid reconstruction within the TG and RS along with the requirement that there are no secondary beam particles (PSCUT06). Applying KP2BOX and TDCUT02 further purifies the sample to be valid $K_{\pi 2}$ decays.

Obtaining the best sample to measure acceptance of target kinematics is a combination of (1) good TG reconstruction, which is not available in a $\pi_{scatter}$ sample due to poor reconstruction of the TG at very small delayed-coincidence, and (2) π^+'s with kinetic energies spread throughout the PNN2 signal region ($60.0\text{M}eV \leq E_{\pi^+} \leq 100.5\text{M}eV$), which is not available in a $K_{\pi 2}(1)$ sample. That is, E949 montior samples do not satisfy both (1) and (2). In the $\pi_{scatter}$ sample, TG fiber hits may be identified as a π^+-fiber near the scattering point (ideally reconstructed as the decay vertex) could have energy much

Cut	Events	Acceptance
$Setup_{ops}$	64024	
OPSVETO	62370	0.9742 ± 0.00063
A_{tgkin}	0.97417 ± 0.000627	

Table 75: OPSVETO acceptance using $K_{\pi 2}(1)$ monitor events.

greater than a normal π^+ from a $K^+ \to \pi^+ \nu\bar{\nu}$ decay. Thus, using a $\pi_{scatter}$ sample would yield a TG kinematic acceptance systematically lower than the true value.

Measuring the acceptance of TGDEDX with the sample used for calibration, $\pi_{scatter}$, would bias the acceptance measurement (see [1]). Therefore, the clean $K_{\pi 2}$ sample obtained by applying $Setup_{TGkin}$ is employed. The rest of the cuts in Table 76 employed the $K_{\pi 2}$ sample due to their dependence on good determination of the decay vertex and assuming no π^+ energy dependence.

Cut	Loose Box		Tight Box	
	Events	**Acceptance**	**Events**	**Acceptance**
$Setup_{TGkin}$	61687		37295	
TGDEDX	61017	0.9891 ± 0.00042	36883	0.9890 ± 0.00054
TGER	61000	0.9997 ± 0.00007	36873	0.9997 ± 0.00009
TGENR	58984	0.9670 ± 0.00072	35594	0.9653 ± 0.00095
TGLIKE1	57931	0.9821 ± 0.00055	34946	0.9818 ± 0.00071
TGLIKE2	57005	0.9840 ± 0.00052	34381	0.9838 ± 0.00067
EPITG	51086	0.8962 ± 0.00128	30874	0.8980 ± 0.00163
EPIMAXK	51086	1.0000 ± 0.00000	30874	1.0000 ± 0.00000
TGEDGE	50802	0.9944 ± 0.00033	30715	0.9949 ± 0.00041
DRP	50716	0.9983 ± 0.00018	30658	0.9981 ± 0.00025
CHI567	44324	0.8740 ± 0.00147	26823	0.8749 ± 0.00189
CHI5MAX	44323	1.0000 ± 0.00002	26822	1.0000 ± 0.00004
A_{tgkin}	0.71851 ± 0.001811		0.71918 ± 0.002327	

Table 76: TG kinematic acceptance using $K_{\pi 2}(1)$ monitor events.

The total acceptance of cuts measured using $K_{\pi 2}$-monitor events, as shown in Eq. (98), is summarized in Table 77.

$$A_{K_{\pi 2}} = A_{utc} \times A_{opsveto} \times A_{TGkin} \tag{98}$$

	Loose Box	Tight Box
A_{utc}	0.94345 ± 0.000188	0.94345 ± 0.000188
$A_{opsveto}$	0.97417 ± 0.000627	0.97354 ± 0.000815
A_{TGkin}	0.71851 ± 0.001811	0.71918 ± 0.002327
$A_{K_{\pi 2}}$	0.6604 ± 0.0018	0.6606 ± 0.0023

Table 77: $K_{\pi 2}$ acceptance summary.

11.6 UMC based acceptance

The acceptance of the online trigger and the phase space and solid angle cuts and the acceptance loss due to pion decay-in-flight and pion nuclear interactions ("NIDIF") are calculated with $K^+ \to \pi^+\nu\bar{\nu}$ Monte Carlo simulated events. About 10^5 signal events were generated with NIDIF on and another 10^5 with NIDIF off. The trigger A_{tr} and phase space A_{ps} acceptance are measured with NIDIF-off sample, and then are corrected for NIDIF by comparing with the NIDIF-on sample (A_{NIDIF}). The results are shown in Tab. 78. UFATE, USTMED and USTOP_HEX cuts are based on UMC truth variables. UFATE requires that the pion stopped without decay or interaction. USTMED requires that the pion stopped in the RS scintillator, and USTOP_HEX requires that the offline reconstructed stopping counter agrees with the real one. The SETUP cut is $ptot < 300\ MeV$.

	NIDIF on	NIDIF off
	99999	100000
T•2	39227	41036
$3_{ct} \cdot 4_{ct} \cdot 5_{ct} \cdot 6_{ct}$	27575	33742
pnn1 or pnn2	26288	32914
A_{tr}	0.2629 ± 0.0014	0.3291 ± 0.0015
SETUP	25793	32887
UFATE	22688	32887
USTMED	22517	32620
USTOP_HEX	21743	32500
COS3D	20870	31294
LAYER14	20838	31282
ZFRF	20175	30083
ZUTOUT	20148	30063
Ke4 BOX	7758	10812
A_{Ke4}	0.3008 ± 0.0029	0.3288 ± 0.0026
Loose BOX	9552	13334
A_{loose}	0.3703 ± 0.0030	0.4054 ± 0.0027

Table 78: UMC based acceptance.

11.7 Acceptance Summary

The total acceptance is summarized in Table 79.

	Loose Box	Tight Box	From Table
$A_{K_{\mu 2}}$	0.07253 ± 0.00031	0.03443 ± 0.00025	64
$A_{\pi_{scat}}$	$0.3980 \pm 0.0014 \pm 0.014$	$0.3292 \pm 0.0020^{+0.010}_{-0.013}$	72
$A_{K_{\pi 2}}$	0.6604 ± 0.0018	0.6606 ± 0.0023	77
A_{UMC}	0.0974 ± 0.0009	0.0791 ± 0.0009	78
A_{tot}	$\mathbf{(1.857 \pm 0.021 \pm 0.065) \times 10^{-3}}$	$\mathbf{(0.592 \pm 0.009^{+0.018}_{-0.024}) \times 10^{-3}}$	-

Table 79: Total acceptance for PNN2.

12 Kaon exposure

As described in the 1/3 analysis note [1], The total KB_{Live} was measured to be 1.7096×10^{12}.

13 Single Cut Failure Study

13.1 Overview

Group	1/3	2/3
BOX	41 (0)	114 (0)
PV(no AD, no TG)	221 (1/22)	494 (6/38)
ADPV	0	2 (2)
DELC3	0	0
B4EKZ	0	0
TGZFOOL	0	0
Extra TG Energy	1 (0)	3 (0)
π^+ energy in K^+ fiber	3 (2)	3 (3)
TG/IC	1 (1)	0
TD	0	1 (1)
Kinematics	3 (2)	1 (0)
Beam	0	0
Other	3 (1)	1 (1)
Total	273 (7/28)	619 (13/45)

Table 80: 2/3 NOT UPDATED. Number of single-cut failures listed by grouped-cuts. "true" single-cut failures are listed in parenthesis and refer to events which only fail one individual cut within the cut group. Since PVCUT is composed of EC,RD,BV components, an event failing PVCUT would likely fail 2 or more cuts. So the second number in parenthesis show the number of events not including the PVCUT component. The definition of "Group" can be found in Section 17 of the 1/3 note [1].

The results for the 1/3 and 2/3 samples in Table 80 differ from the 1/3 note (and previous 2/3 draft) due to modifications to cuts as described in Section 2. The BOX group lost 1 event (42 to 41) compared to the 2/3 TN draft; this was due to the addition of PVCUT, run 49553 event 70188 now fails both BOX and PV(no AD, no TG) because it fails PVCUT. The PV(no AD, no TG) group lost 1 event (222 to 221) compared to the draft of the 2/3 TN; this was due to the addition of TDCUT to the TD cut group, run 49335 event 181587 now fails the PV group and the TD group.

The 2/3 numbers changed from 116 to 114 in the BOX category. The PV group changed from 498 to 494 and the true 1-cut PV failures decreased from 38 to 37. All other groups were unchanged. The following details what happened to these events:

- Run 49298 Event 83783 1-cut BOX becomes a 2-cut BOX and PVCUT failure.
- Run 50194 Event 49417 1-cut BOX becomes a 2-cut BOX and PVCUT failure.
- Run 49169 Event 232415 1-cut PV becomes a 2-cut PV and TDCUT failure.
- Run 49348 Event 160561 1-cut PV becomes a 2-cut PV and TDCUT failure.

- Run 49625 Event 242384 1-cut PV becomes a 2-cut PV and TDCUT failure.
- Run 49750 Event 22354 1-cut PV becomes a 2-cut PV and TDCUT failure.

13.2 Double-cut Failures

The vast majority of double-cut failures (events which are cut by only two groups of cuts) fail Box and/or PV(no TG, no AD). The 1/3 and 2/3 2-cut failures are very consistent in the quick summary shown in Table 81. Detailed 2-cut failures are shown in Tables 82 and 83.

Group	1/3	2/3
BOX & PV	47518	94557
BOX OR PV	4469	9053
w/o BOX & PV	213	442
Total	52200	104052

Table 81: Number of double-cut failures listed by grouped-cuts. "BOX OR PV" means either BOX or PV(no AD, no TG) is one of the two groups which cut the event, but not both (i.e. exclusive or). "w/o BOX & PV" means the two groups which cut the event were from groups other than BOX and PV(no AD, no TG). The definition of "Group" can be found in Section 17 of the 1/3 note [1].

Groups	Box	PV	AD	Del	B4	TGZ	TGE	EK	IC	TD	Kin	Bm	Ot
BOX	-	47518	61	2	3	1	176	79	11	353	934	3	26
PV	47518	-	233	39	17	8	93	1328	30	48	179	37	808
ADPV	61	233	-	1			3	9		2	2		2
Del	2	39	1	-							1		2
B4Ekz	3	17			-						1		
TGZ	1	8				-							
TGE	176	93	3				-	36	3		1		19
Ekaon	79	1328	9					-			1		5
IC	11	30							-				1
TD	353	48	2							-	121		1
Kin	934	179	2	1	1			1		121	-		1
Beam	3	37										-	1
Other	26	808	2	2				5	1	1	1	1	-
Total	49167	50338	313	45	21	9	9	1458	45	525	1241	41	866

Table 82: 1/3 sample, number of double-cut failures listed by grouped-cuts. The definition of "Group" can be found in Section 17 of the 1/3 note [1]. PV=PV(no TG, no AD), AD=ADPV, Del=DELCO, TGE= extra TG energy, EK=Ekaon=π^+ energy in K^+ fiber, IC=TG/IC, Kin=Kinematics, Ot=Other.

13.3 Reading Paw Photo Events

The following sections detail the events in the single-cut failure study. Earlier iterations of the 1-cut study found mistakes which were fixed. The current study finds no indication

	Box	PV	AD	Del	B4	TGZ	TGE	EK	IC	TD	Kin	Bm	Ot
BOX	-	94557	141	9	6	2	352	187	23	731	1885	16	95
PV	94557	-	533	96	32	4	182	2557	82	113	372	60	1575
ADPV	141	533	-					6			8		7
Del	9	96		-	1			1				2	8
B4Ekz	6	32		1	-			1			2		
TGZ	2	4				-							
TGE	352	182					-	56	3	2	1	1	30
Ekaon	187	2557	6	1	1			-	2	3	4	2	25
IC	23	82						2	-				2
TD	731	113						3		-	268		
Kin	1885	372	8		2			4		268	-	1	4
Beam	16	60		2				2			1	-	2
Other	95	1575	7	8				25	2		4	2	-
Total	98004	100163	695	117	42	6	6	2844	112	1117	2545	84	1748

Table 83: 2/3 sample, number of double-cut failures listed by grouped-cuts. The definition of "Group" can be found in Section 17 of the 1/3 note [1]. PV=PV(no TG, no AD), AD=ADPV, Del=DELCO, TGE= extra TG energy, EK=Ekaon=π^+ energy in K^+ fiber, IC=TG/IC, Kin=Kinematics, Ot=Other.

of problems with coding mistakes or background loopholes.

How to read hit *pawphoto* event reconstruction information:

- Blue generally means Pion or pion trajectory
- Red generally means Kaon
- Green generally means PV
- PV hits are relative to trs (or tpi)
- For clarity, some 2nd hits are not displayed.
- Time (ns) is either the first, top, or outside number
- Energy (MeV) is either the second, bottom, or inner number
- Energy in Active Degrader is displayed in ADC counts

CCDFITS:

- The "Cut" row (passed/failed cut):

  1st column: CCDPUL cut (on a fiber by fiber basis)

  2nd column: CCDBADFIT cut (on a fiber by fiber basis)

  3rd column: CCDBADTIM cut (on a event basis)

- The "Emux" row:

  Will not be displayed unless Emux energy exists.

  1st column: Total (Pi+Kaon) multiplexed energy

  2nd column: multiplexed energy from kaon fibers

(within 5ns of tk)

3rd column: multiplexed energy from Pi,OPS-PI,PV

(within 5ns of tpi)

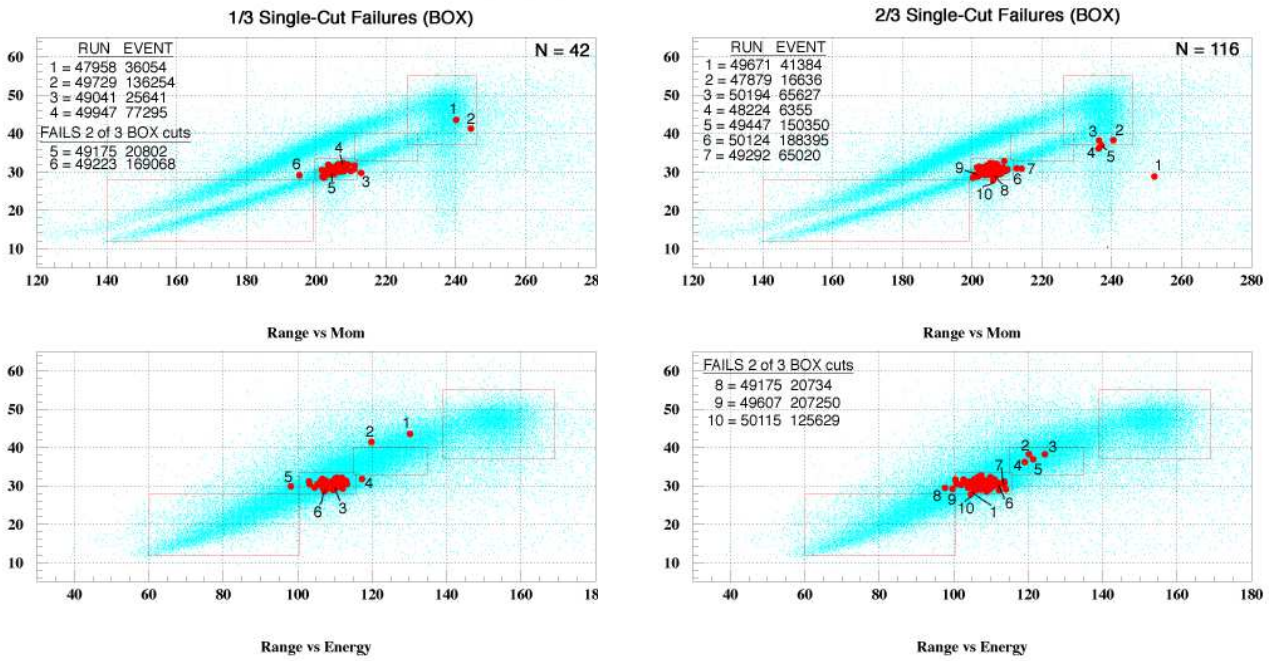

(a) 1/3 (b) 2/3

Figure 18: Kinematics of Single-Cut Box Failures for the 1/3 and 2/3 samples. The red boxes, starting from the bottom left to the upper right, are PNN2, KPI2, PNN1, KMU2. The blue points are events from the $pnn1 \cdot pnn2$ trigger.

13.4 Single-cut BOX Failures

There were 42 (116) events which failed only the BOX group (EBOX,PBOX,RBOX) in the 1/3 (2/3) sample. The 2/3 measured value is within 1.6 sigma of the expected. An excess was expected since the PV parameters were optimized using the 1/3 sample, so that 2/3 events that are near PV thresholds will likely fail the BOX cuts.

The events displayed in Fig. 18 are all the events which only failed the BOX cut. The events within the Kpi2 box are $K_{\pi 2}$ events in which the photons were not found by the loose PV cuts. The remaining events are possibility due to mismeasurement by the detector, an accidental, or a scattering. The events which have an abnormally large momentum, for the range and energy, are detailed in the following subsections. There were no indication of a problem which would lead to background or acceptance loss that is not already being taken into account.

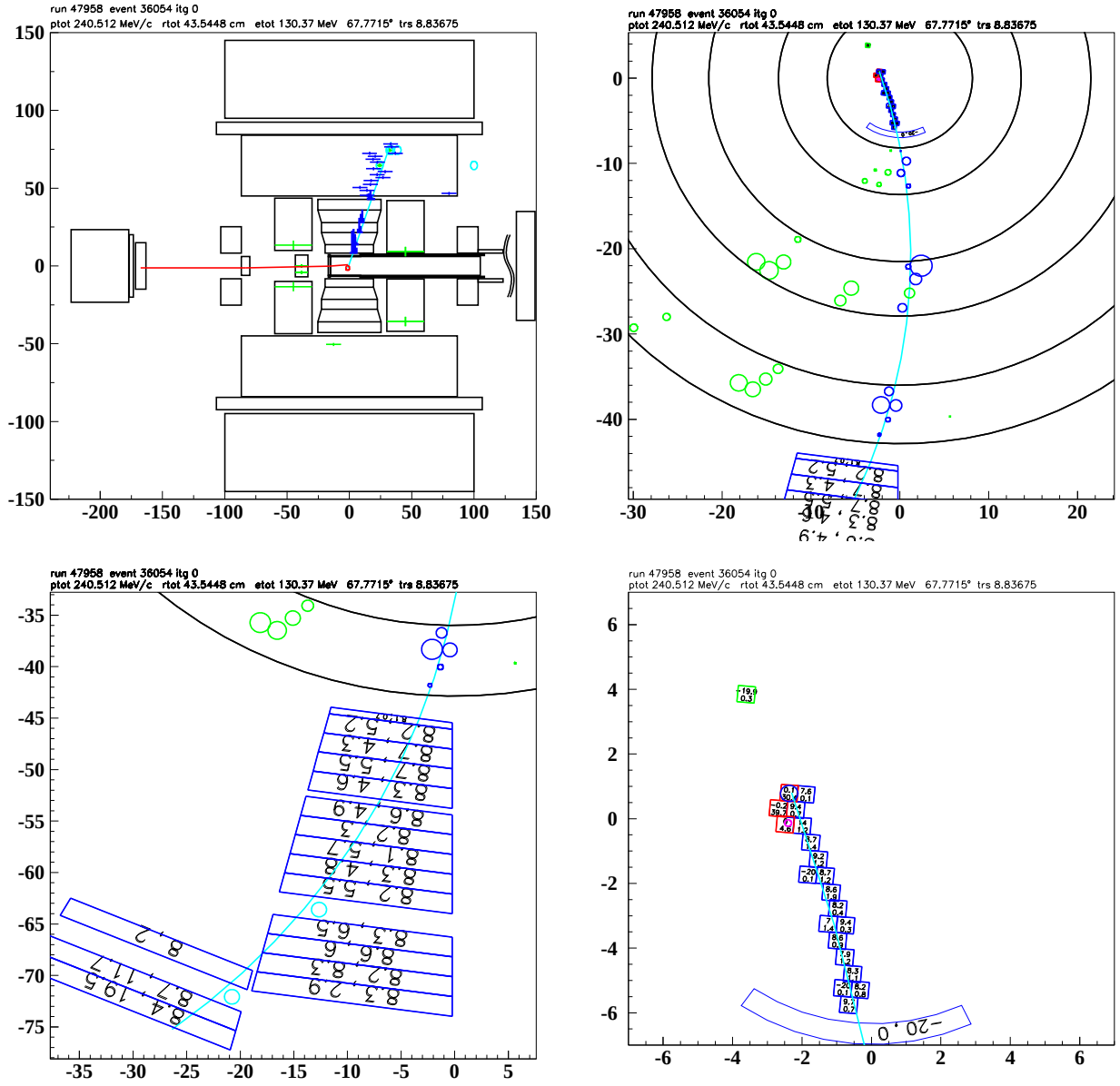

Figure 19: Range Stack, UTC, and Target reconstruction of event failing only the BOX cut. This event had an abnormally large momentum. This is tagged as "no.1" in Fig. 18(a).

13.4.1 1/3 box event no. 1, Run 47958 Event 36074

The reconstruction as seen in Fig. 19 does not lead me to conclude there was a bad reconstruction, mistake, or loophole. Although, the anomalously large momentum for the given range and energy, the fitted track seems to correspond well to the hits in the TG, UTC, RS, and RSSCs.

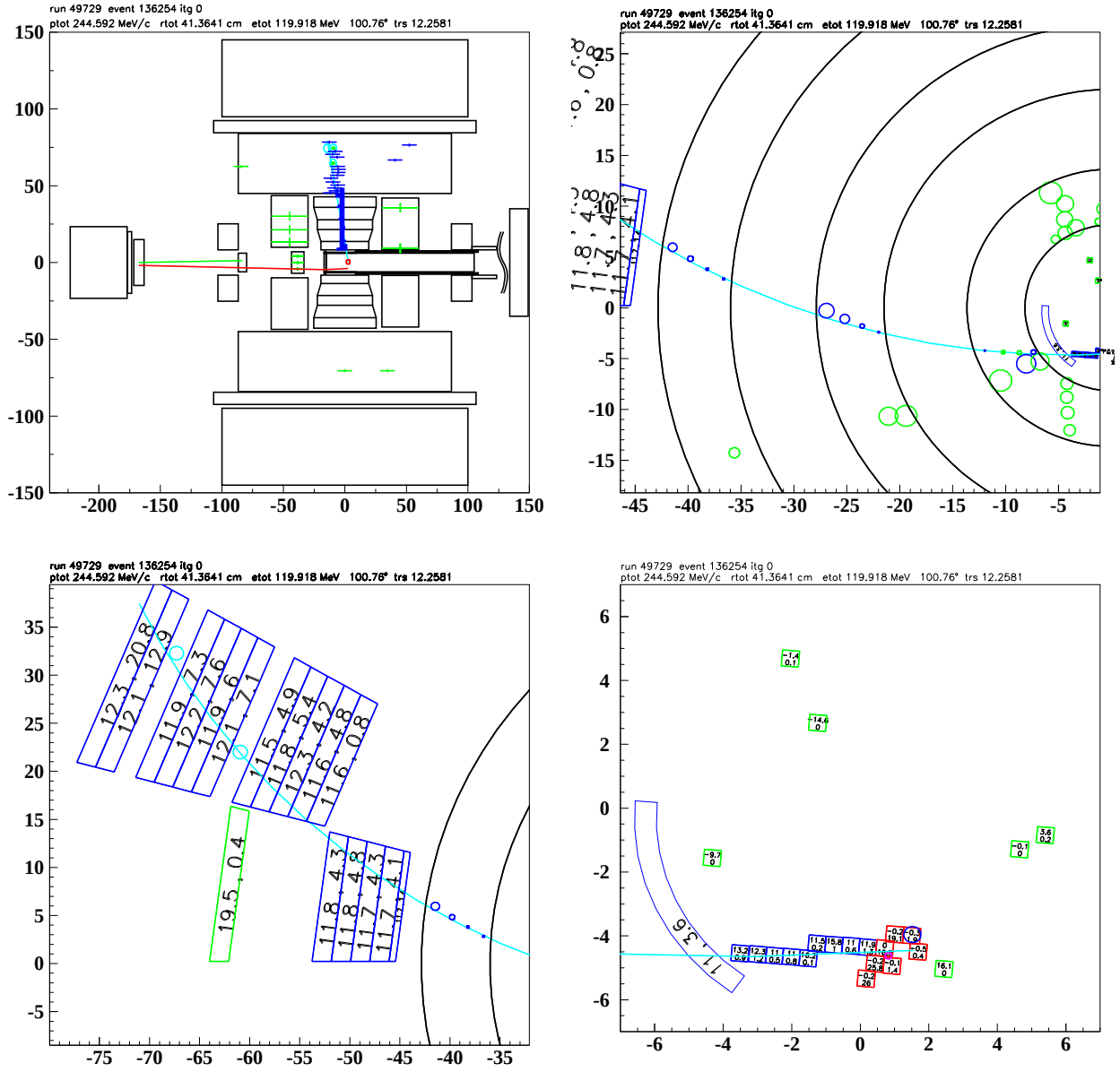

Figure 20: Range Stack, UTC, and Target reconstruction of event failing only the BOX cut. This event had an abnormally large momentum. This is tagged as "no.2" in Fig. 18(a).

13.4.2 1/3 box event no. 2, Run 49729 Event 136254

As shown in Target blow-up of Fig. 20, the range should have been about 1cm smaller. Thus, this event would have been in the PNN1 range-energy box with a correctly reconstructed decay vertex. The RS and UTC reconstruction of run 49729 event 136254 does not show conclusively why the momentum is very large. If the utc reconstruction placed a few utc hits on different sides (left-right ambiguity) of the fitted track, the momentum may have been smaller. The utc track traverses the TG fibers, so the addition of these fibers to the utc track fit would have had little to no impact in the resulting momentum. Although this event has unusual kinematic variables, there is no evidence of a mistake or a loophole for new backgrounds.

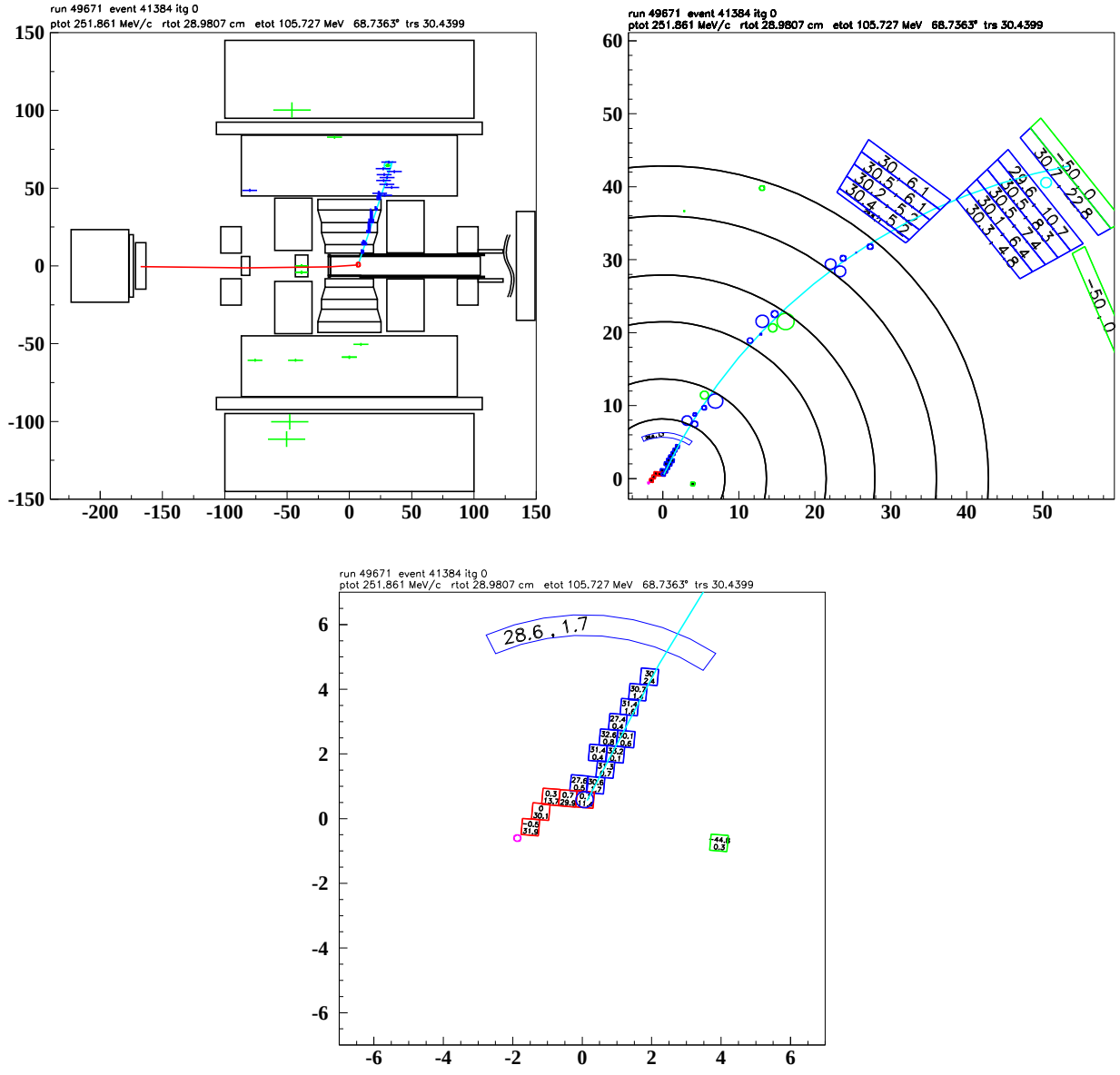

Figure 21: Range Stack, UTC, and Target reconstruction of event failing only the BOX cut. This event had an abnormally large momentum. This is tagged as "no.1" in Fig. 18(b).

13.4.3 2/3 box event no. 1, Run 49671 Event 41384

As shown in Fig. 21, the UTC track has a good fit to hits from the TG, UTC, RS, and RSSCs. Therefore, there is no indication that there is a problem to explain the abnormally large momentum.

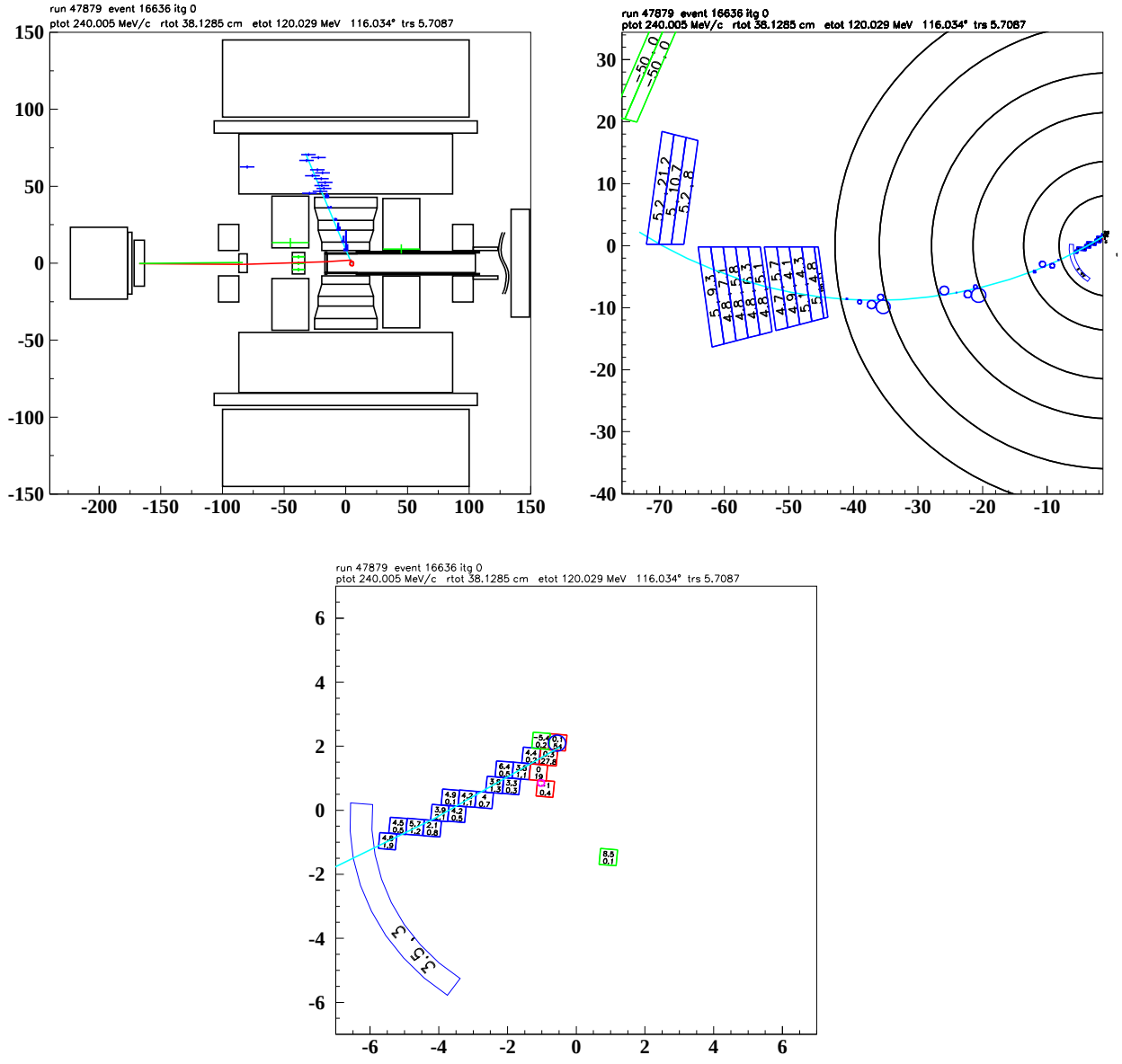

Figure 22: Range Stack, UTC, and Target reconstruction of event failing only the BOX cut. This event had an abnormally large momentum. This is tagged as "no.2" in Fig. 18(b).

13.4.4 2/3 box event no. 2, Run 47879 Event 16636

As seen in Fig. 22, the UTC track does not fit the RS hits well. The poor RS-fit is most likely due to no RSSC hits. Without RSSC hits included in the track fit, the momentum will be larger than the true value. This effect would push the kinematics away from the kinematic signal region, i.e. an acceptance loss, not a background.

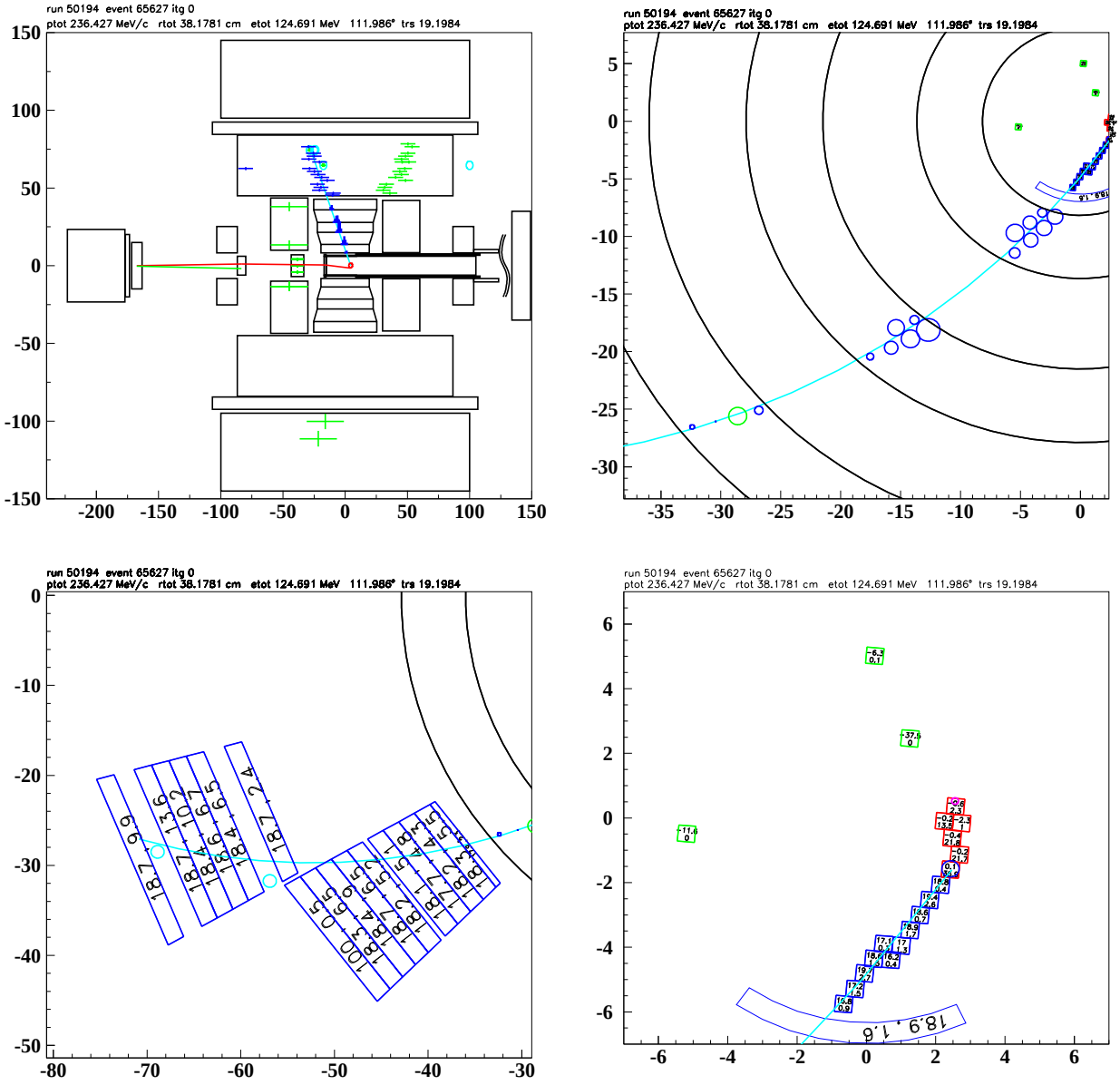

Figure 23: Range Stack, UTC, and Target reconstruction of event failing only the BOX cut. This event had an abnormally large momentum. This is tagged as "no.3" in Fig. 18(b).

13.4.5 2/3 box event no. 3, Run 50194 Event 65627

Fig. 23 does not indicate a obvious reason why the momentum of this event is abnormally large. Comparing the track fit to the RS-hits, one could come to the conclusion that the momentum should be slightly larger to obtain a better fit. However, there is no indication of a mistake.

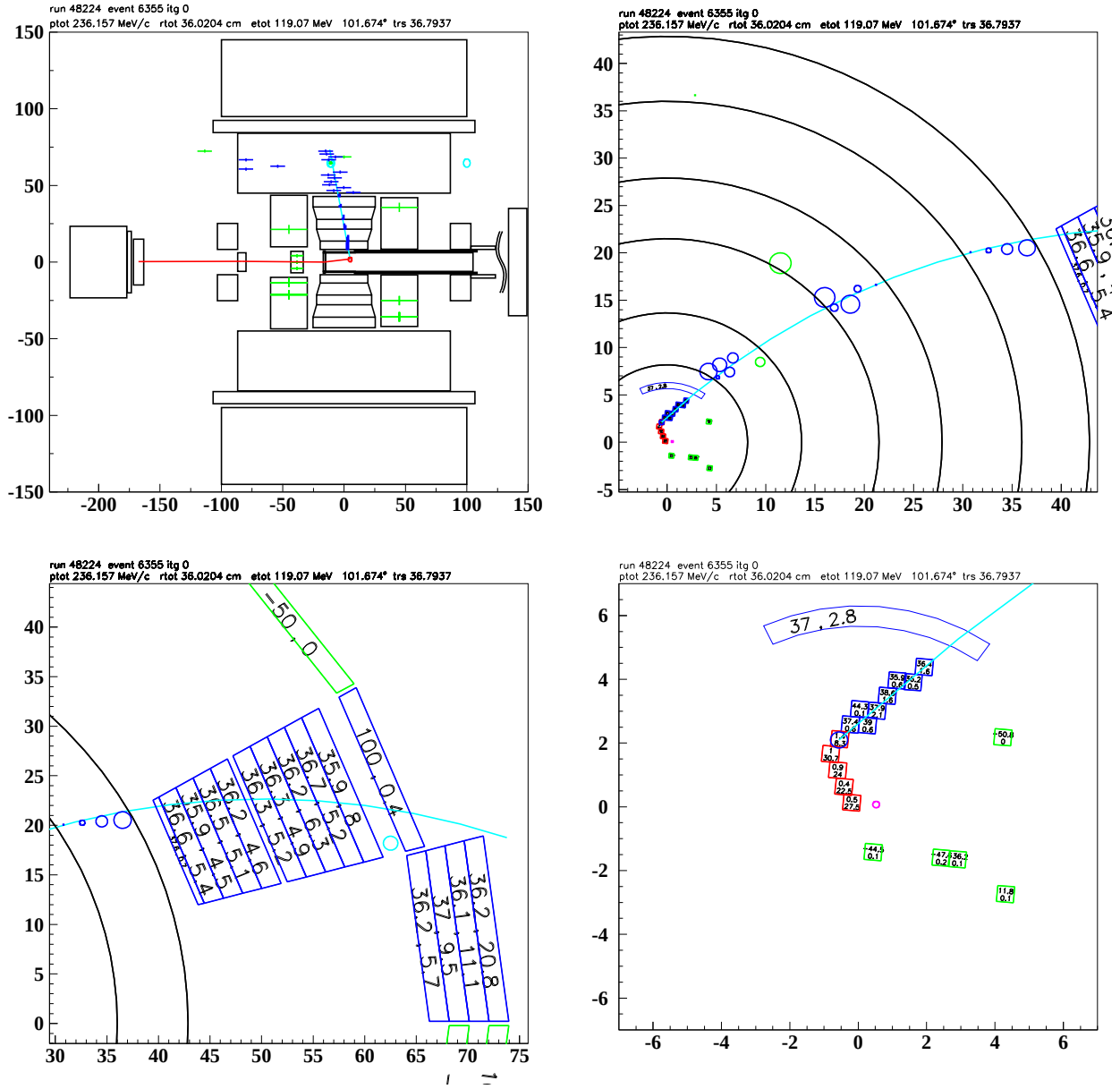

Figure 24: Range Stack, UTC, and Target reconstruction of event failing only the BOX cut. This event had an abnormally large momentum. This is tagged as "no.4" in Fig. 18(b).

13.4.6 2/3 box event no. 4, Run 48224 Event 6355

Fig. 24 does show a poor RS track fit leading to a momentum which is larger than what is expected. However, there is not evidence to lead us to believe there is a mistake within the fitter.

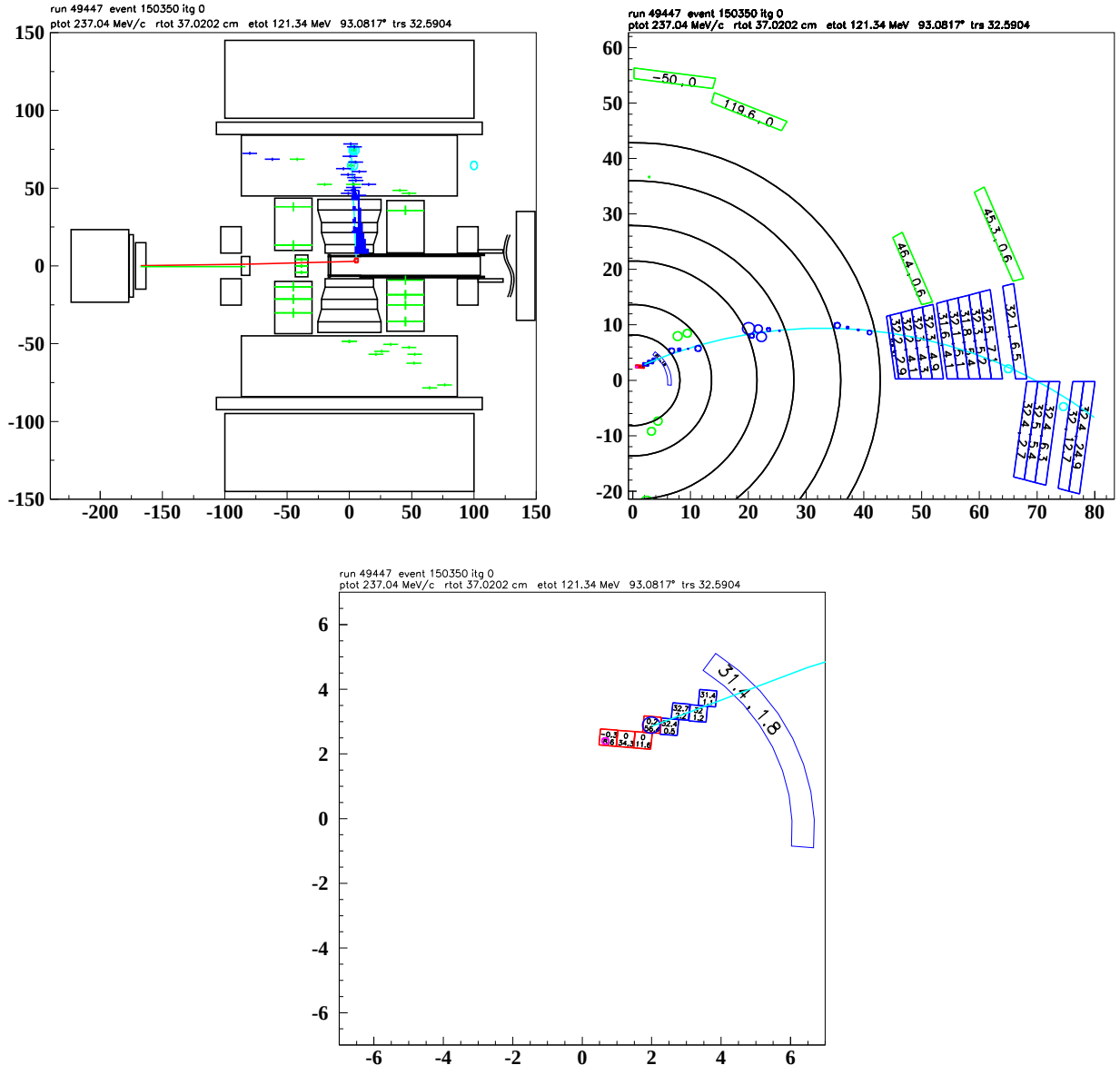

Figure 25: Range Stack, UTC, and Target reconstruction of event failing only the BOX cut. This event had an abnormally large momentum. This is tagged as "no.5" in Fig. 18(b).

13.4.7 2/3 box event no. 5, Run 49447 Event 150350

Fig. 25 shows no evidence, with respect to the track fit, to explain the larger than expected momentum as seen in Fig. 18(b).

13.5 Single-cut PV Failures

The PV group does not contain the Target PV nor the ADPV. There were 222 (498) event in the 1/3 (2/3 sample which only failed the PV-group. The events that only fail one subsystem ("true" 1-cut failures) were of the most concern for the analysis. There are 22 (38) "true" 1-cut failures within the 1/3 (2/3) sample; 18 (21) of these are from ECout, 1 (4) from BV, 2 (8) from RD (Range Stack), 1 (4) from CO (Collar).

Fig. 26 shows the kinematic distribution of events that are classified as true 1-cut failures. The plots show no grouping near the edges of the kinematic box which could

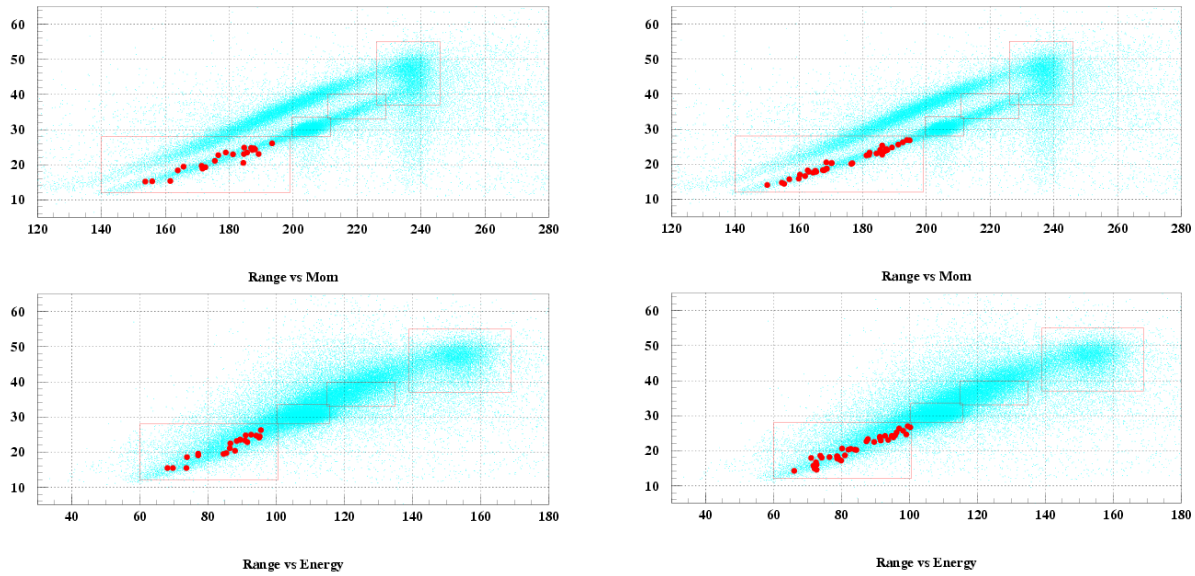

c

Figure 26: Kinematic plots of all events classified as a true 1-cut PV failure. 1/3 (2/3) sample is on the left (right).

indicate mistakes in the PV leading to excessive background. There were no indications from the 1-cut study that no further problem existed in regard to the PV 1-cut events; all 22+38 "true" 1-cut failure events were visually inspected; in addition, to many of the other 222+498 PV-group 1-cut failure events.

13.6 Single-cut ADPV Failures

There were 0 ADPV only events in the 1/3 sample and 2 ADPV only events in the 2/3 sample. The 2 events almost failed other PV subsystems and were well above the ADPV threshold. So there is nothing within the 1-cut failure study to show problems within the ADPV cut. The following subsections detail the two ADPV events.

13.6.1 Run 49113 Event 13361

As seen in Fig. 27, this event almost failed the ECout(ter) section of the PV cuts by having $E = 0.391 MeV$ where the threshold is 0.4MeV (upstream hits). The ADPV had 276.2 units of in-time energy (threshold=5.) from 3 hits.

13.6.2 Run 50024 Event 56470

As seen in Fig. 28, this event almost failed the ECin(ner) section of the PV cuts by a hit at 6.3ns (E=0.3MeV) with a threshold of 0.2MeV and the upper time window being 5.63ns. There was another slightly out-of-time hit within the RDoff subsystem which was above the energy threshold. The ADPV had 193 units of in-time energy (threshold=5.) from 3 hits.

13.7 Single-cut Extra-TG-Energy Failures

There was one event in the 1/3 sample and three in the 2/3 sample which failed only the group of cuts that deal with extra energy within the TG (TGPV,OPSVETO).

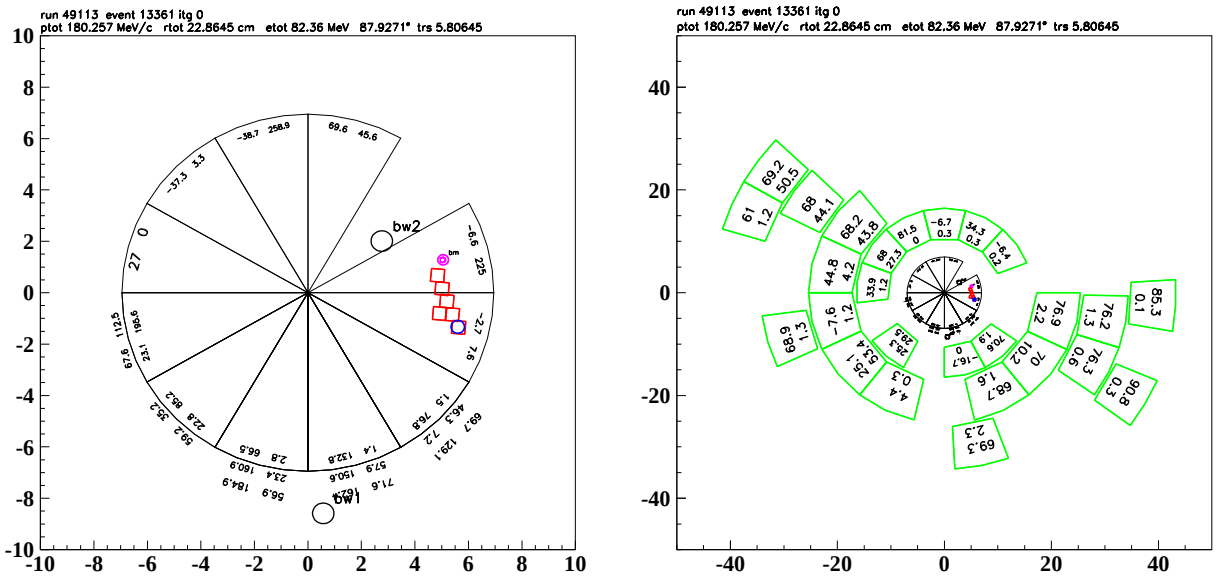

Figure 27: Run 49113 Event 13361 only failed the ADPV cut.

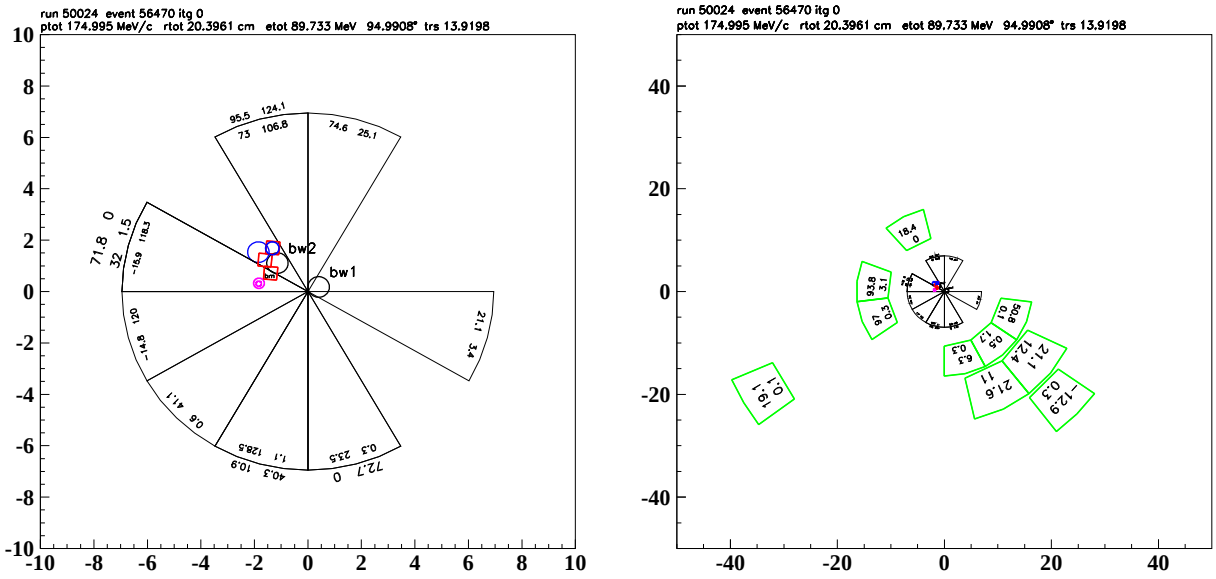

Figure 28: Run 50024 Event 56470 only failed the ADPV cut.

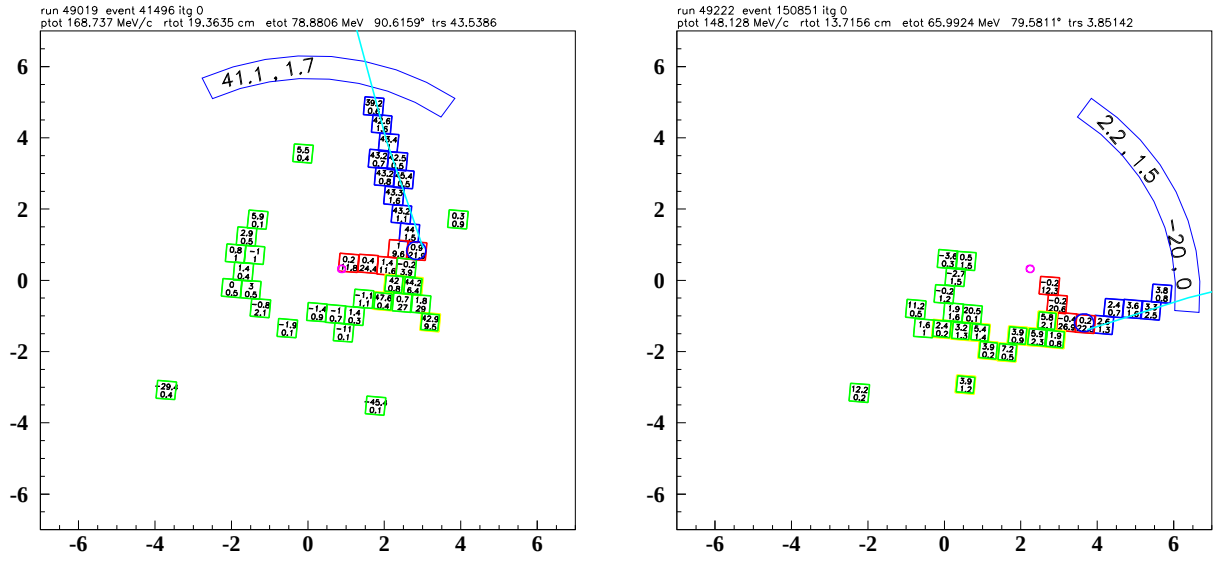

Figure 29: (Left) Run 49019 Event 41496 (Right) Run 49222 Event 150851 failed only the Extra-TG Energy cut-group.

13.7.1 1/3 TGE Event, Run 49019 Event 41496

As observed in Fig. 29, there is 87MeV of PV energy within the TG (threshold is 2MeV). This in-time energy was due to a multiple-body decay where the extra particles are contained within the TG.

13.7.2 2/3 TGE Event, Run 49222 Event 150851

As observed in Fig. 29, there is 10.7MeV of PV energy within the TG (threshold is 2MeV). This in-time energy was due to a multiple-body decay where the extra particles are contained within the TG. This event also had $tpi - tk < 4ns$ and the kinematics of the event placed it at the lower-left corner of the BOX cut; therefore, the event would fail the tight version of DELCO and BOX.

13.7.3 2/3 TGE Event, Run 49545 Event 100682

As observed in Fig. 30 (left-side), there is 62.2MeV of PV energy within the TG (threshold is 2MeV). This in-time energy was due to a multiple-body decay where the extra particles are contained within the TG. The kinematics of the event placed it at the lower-left corner of the BOX cut; therefore, the event would fail the tight version of BOX; this event also fails the tight version of TDNN. In addition, the energy under the kaon is 1.213MeV and the CCDPUL threshold is 1.25MeV. So this event fails two tighter cuts and almost fails CCDPUL. These types of events which are near a threshold are expected.

13.7.4 2/3 TGE Event, Run 50028 Event 112771

As observed in Fig. 30 (right-side), there is 59MeV of PV energy within the TG (threshold is 2MeV). This in-time energy was due to a PV conversion in the TG. The $Prob(\chi_{567})$ value, from the TG fitter, was low.

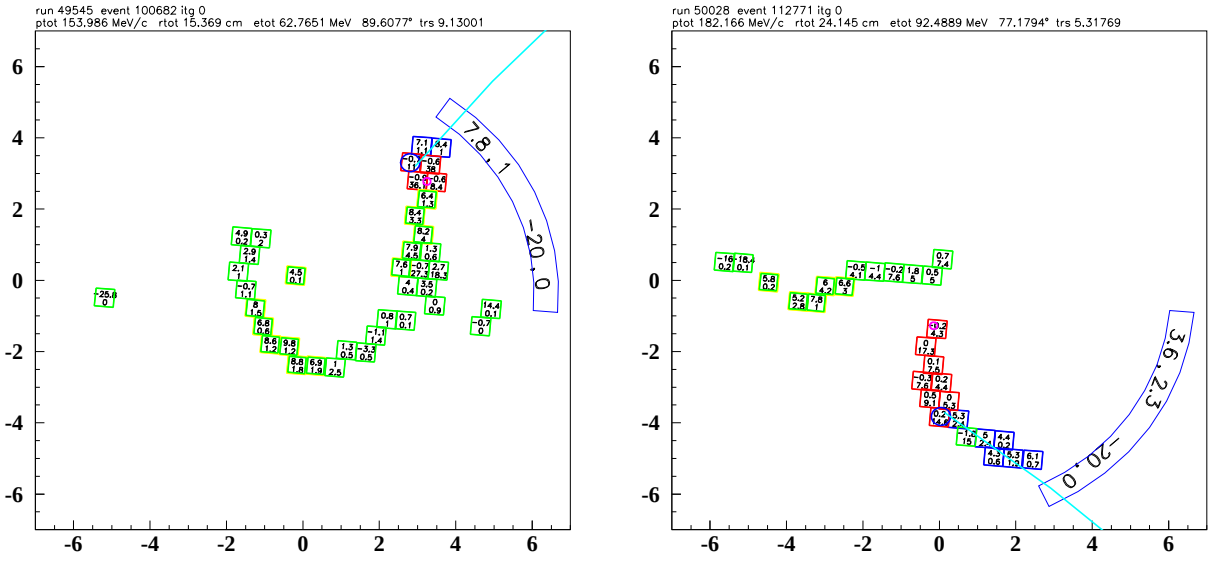

Figure 30: (Left) Run 49545 Event 100682, (Right) Run 50028 Event 112771 failed only the Extra-TG Energy cut-group.

13.8 Single-cut π^+ energy in K^+ fiber Failures

This group consist of CCDPUL·CCDBADFIT, CCDBADTIM, CCD31FIB , EPIONK, TIMKF. There were 3 events in each of the 1/3 and 2/3 samples; 2 (3) were "true" 1-cut failures in the 1/3 (2/3) sample.

13.8.1 1/3 sample: Run 48237 Event 94557

This event failed only CCDPUL. This event came close to failing the PV-subsystem EC outer (ECout) by having E=0.391MeV (threshold=0.4). As seen in Fig. 31, the 2nd pulse energy found in the kaon fiber was 30MeV far above the threshold of 1.25MeV.

13.8.2 1/3 sample: Run 49467 Event 14793

This event failed CCDPUL and EPIONK. As seen in Fig. 31, the 2nd pulse energy found in the kaon fiber was 3.1MeV (in the low gain - which is what was used by CCPUL) far above the threshold of 1.25MeV.

13.8.3 1/3 sample: Run 50020 Event 35133

This event fails CCDPUL. There are two fibers which fail CCDPUL in this event, as shown in Fig. 31. There is some End-Cap PV activity ($< 0.3 MeV$), but not enough to exceed the set threshold.

13.8.4 2/3 sample: Run 49306 Event 106589

This event fails only CCDPUL, in three separate kaon fibers. There is no indication of a photon - all activity is out-of-time. The three fits are shown in Fig. 32.

13.8.5 2/3 sample: Run 50026 Event 96664

As shown in Fig. 33, the 12.5MeV 2nd pulse as determined by the CCD fitter, forces the event to fail CCDPUL. The event is a late kaon ($tk = 43ns$).

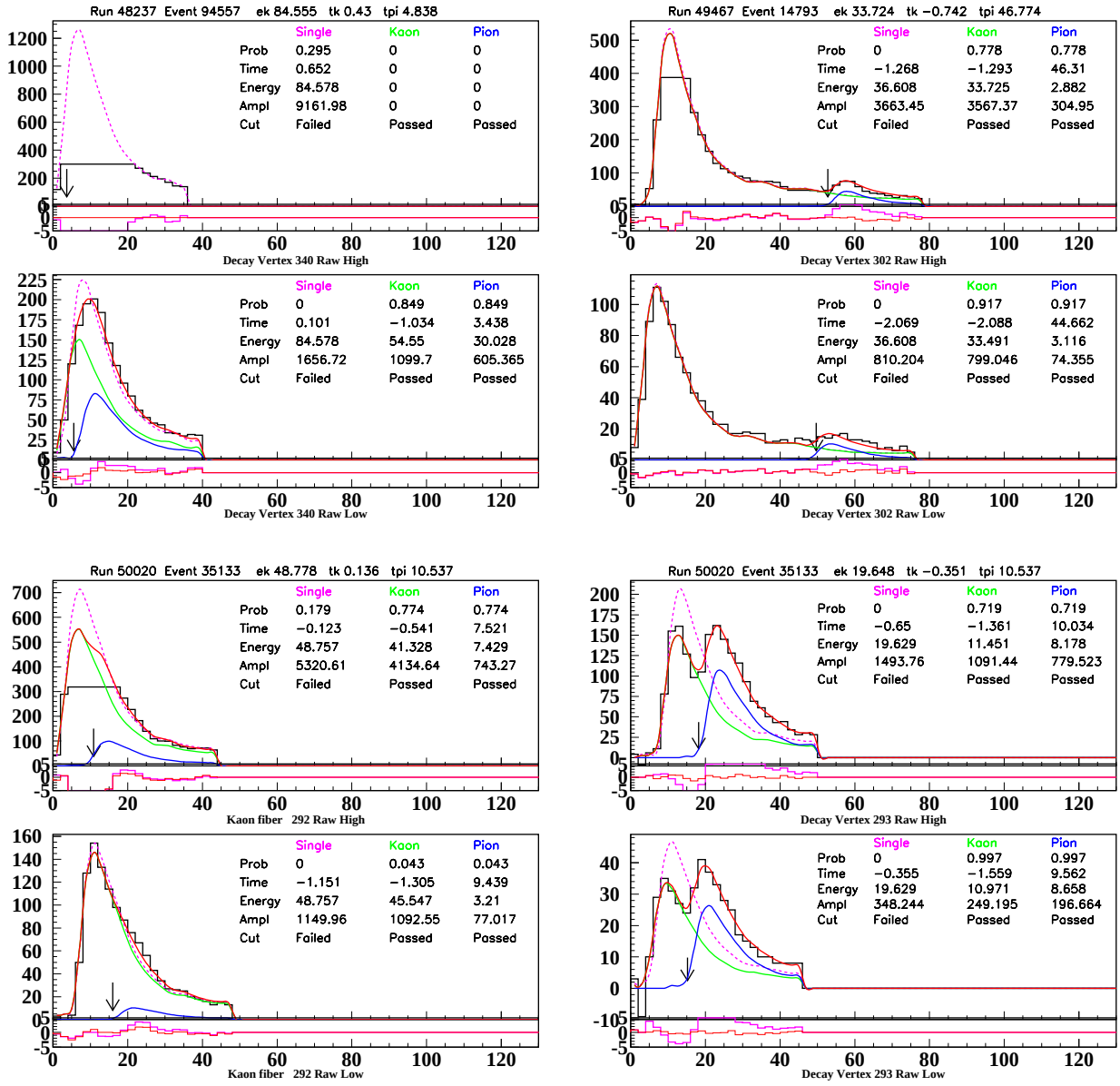

Figure 31: (Top-Left) CCD fit of Run 48237 Event 94557 which fails with an 2nd pulse energy of 30MeV. (Top-Right) CCD fit of Run 49467 Event 14793 which fails with 3.1MeV detected as the 2nd pulse. (Bottom) CCD fits of Run 50020 Event 35133 fail CCDPUL in two fibers, one with 3.21MeV and the other with over 8MeV.

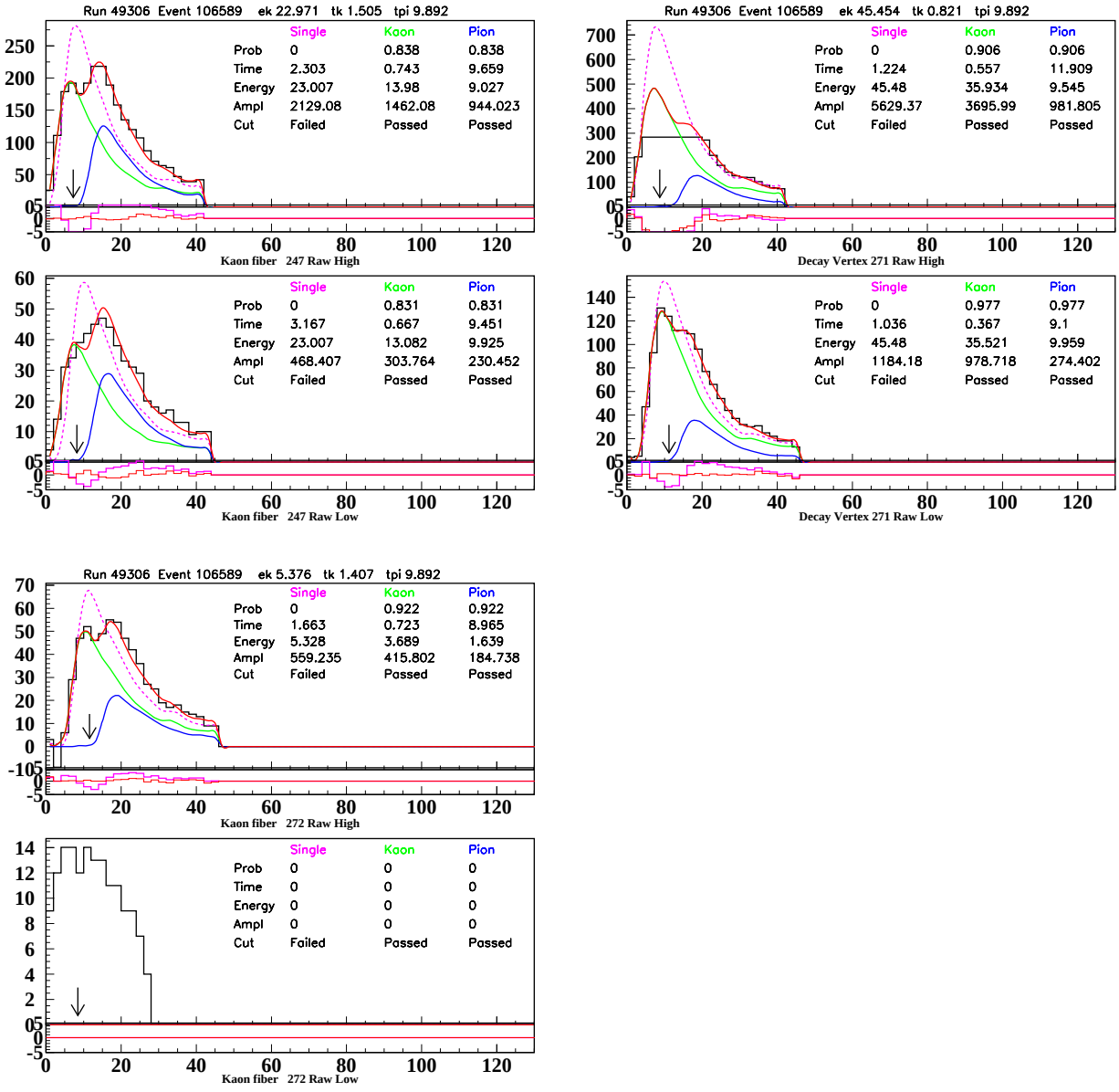

Figure 32: Run 49306 Event 106589 CCD fits of 3 fibers which all fail CCDPUL.

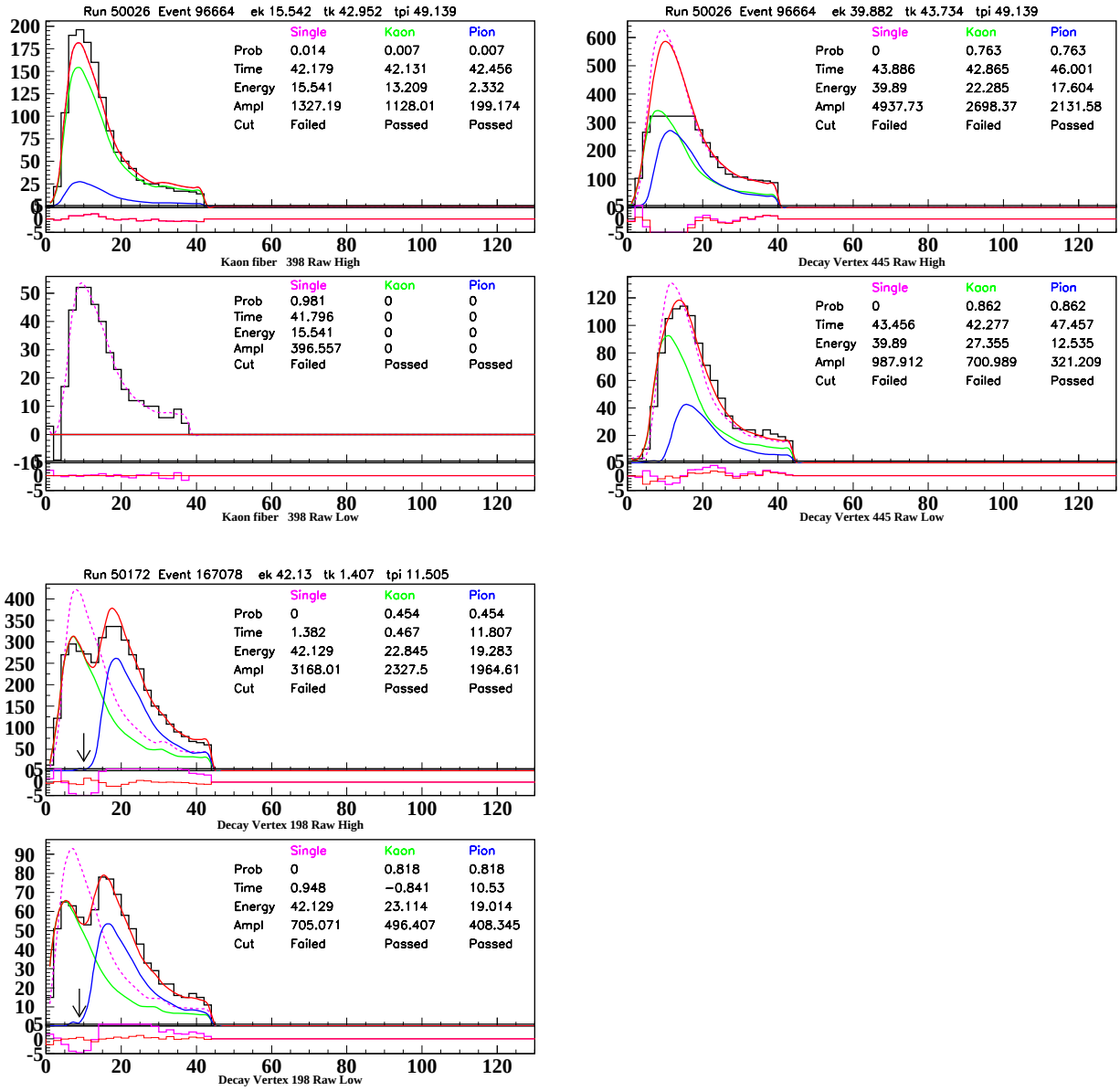

Figure 33: (Top) Run 50026 Event 96664, two fibers fail CCDPUL requirements. (Bottom) Run 50172 Event 167078 fails CCDPUL.

13.8.6 2/3 sample: Run 50172 Event 167078

As shown in Fig. 33, there is 19MeV pulse detected in a kaon fiber that is in time with the pion, which is far larger than the 1.25MeV threshold.

13.9 Single-cut TG/IC Failures

The TG/IC group is composed of TGGEO and KIC. There was only one event which within the 1/3 sample and no events within the 2/3 sample. Run 49856 Event 17346 failed only TGGEO, specifically TGGEO returned a value of 1. for *geocut4*. This means that the cut was regarding the VC. The in-time ($-5.25 \leq t_{VC} \leq 4.25$) energy in the V-counter was greater than threshold of 0.35MeV; the energy was 1.57MeV.

From the TG reconstruction shown in Fig. 34, it appears that the decay vertex position is off by one fiber (should be the fiber with E=52.6MeV); if so, the event would appear to be a TG-scatter or some other pathological event. This conclusion is due to comparing

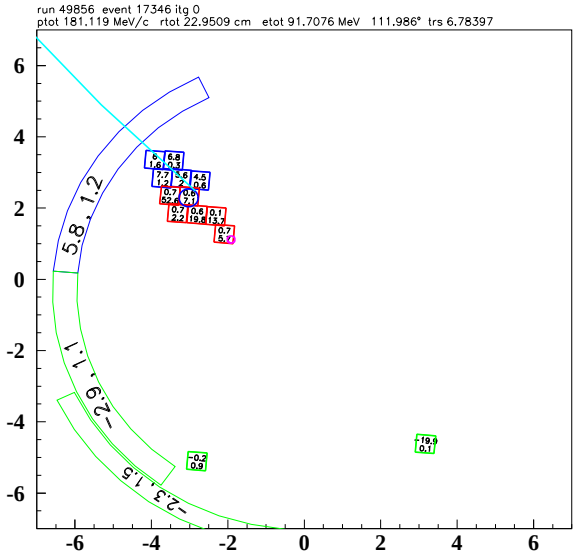

Figure 34: Run 49856 Event 17346 failed only TGGEO of the TG/IC cut-group.

the decay vertex, the position of the pion fibers and utc track. This is supported by the low $Prob(\chi_{567})$ value (although large enough to pass CHI567).

13.10 Single-cut TD Failures

This group is composed of IPIFLG, ELVETO, TGFOOL, TDNN (loose). No event was in the TD-only group in the 1/3 sample and only one event was in this group for the 2/3 sample. Run 48379 Event 55909 failed only ELVETO. This event also passed the tight version of TDNN and also passed EV5 (which is part of the TD-tight cuts), as seen in Fig. 35. The value used in the RNGMOM cut is far from the threshold.

13.11 Single-cut Kinematic Failures

This cut group contains the following cuts: COS3D, ZFRF, ZUTOUT, UTCQUAL, TIC, EIC, LAYV4, ICODEL14, RNGMOM, PRRF1, PRRFZ, RSDEDXCL, RSDEDXMAX, RSLIKE. There were 3 events within the 1/3 sample and one within the 2/3 sample; of those, 2 events in the 1/3 sample were a "true" 1-cut failure. The single-cut failure study did not find any additional problems within the kinematic group of cuts. The 1-cut kinematic events show the expected, such as failing the tighter signal-region cuts or fails multiple cuts within the group.

13.11.1 Run 49488 Event 180150

This "true" 1-cut event failed only RNGMOM with a value far larger than the threshold. This cut passes even the tight TDNN cut, as seen in Fig. 36. However, it fails EV5 (applied in the tight signal region). The kinematic plot in Fig. 36 shows the event in the muon band.

13.11.2 Run 49238 Event 95361

This "true" 1-cut event failed only RNGMOM with a value far larger than the threshold. This cut fails the tight TDNN cut, as shown in Fig. 37.

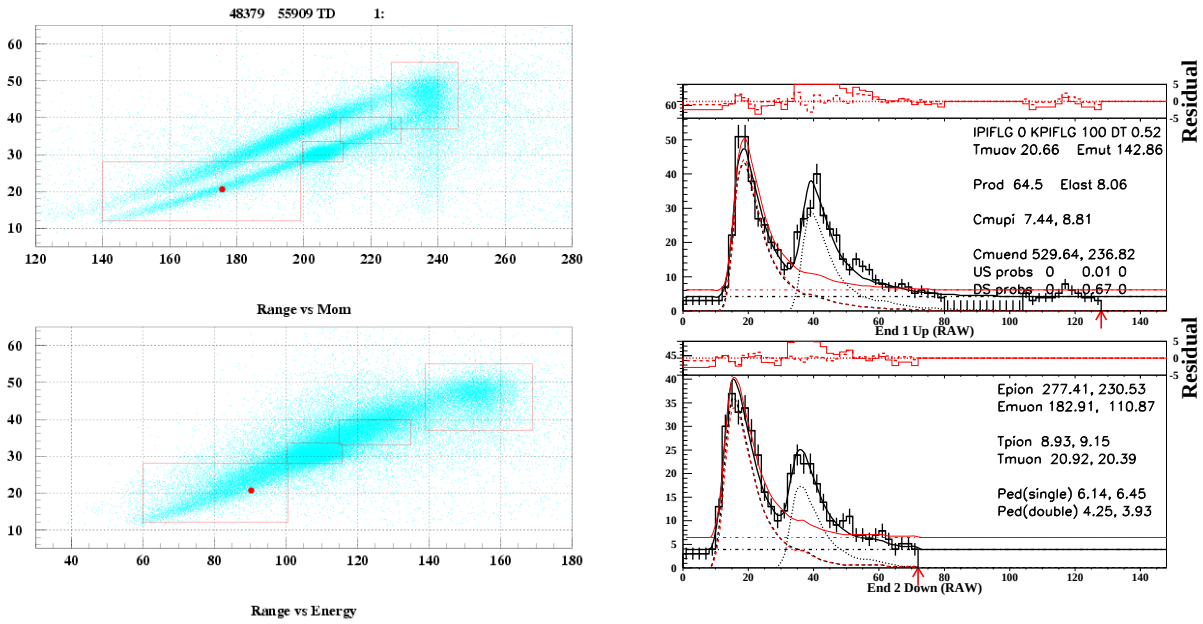

Figure 35: Run 48379 Event 55909 only failed ELVETO of the TD cut-group. These kinematic plots (left) show that it lies within the pion-band. This plot of the TDs show that it appears to be a pion.

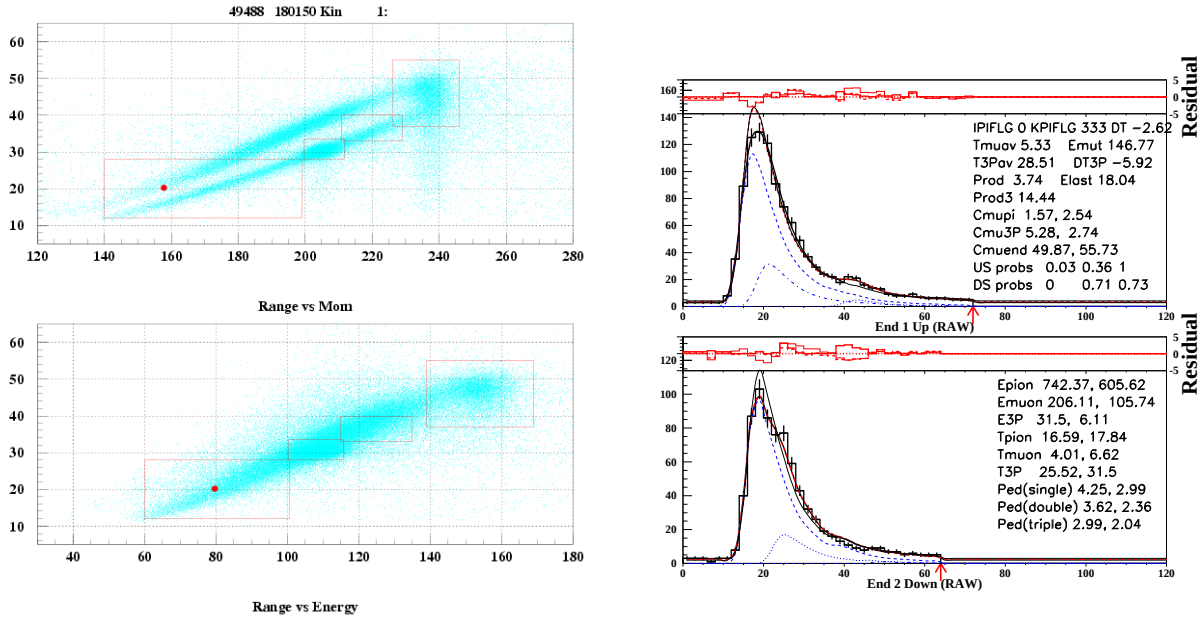

Figure 36: Run 49488 Event 180150 failed only the RNGMOM cut with the Kinematic cut-group. The left plot shows the kinematics of the event; notice that it is in the muon band. The TD plot (right) shows that the TD fit satisfies the TDNN cut.

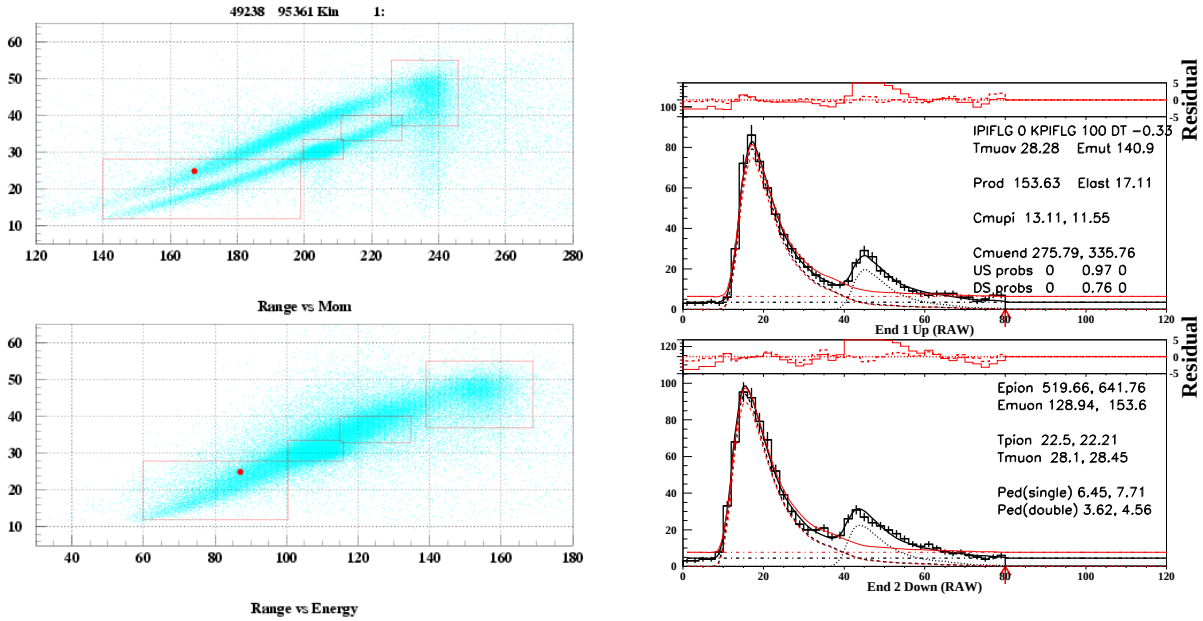

Figure 37: Run 49238 Event 95361 failed only the RNGMOM cut with the Kinematic cut-group. The left plot shows the kinematics of the event; notice that it is in the muon band. The TD plot (right) shows that the TD fit satisfies the TDNN cut.

13.11.3 Run 47936 Event 26190

This event fails COS3D, ZUTOUT, RSDEDXCL, RSDEDXMAX. It comes close to failing the energy requirement of the BOX cut; E=100.39MeV ($E_{threshold} = 100.5 MeV$). The track escapes thru the edge of the UTC detector before entering the RS.

13.11.4 Run 49728 Event 84575

This event failed UTCQUAL, PRRF1, PRRFZ, RSDEDXCL. It was very close to the 2.2 threshold of RNGMOM. The fitted track was very poor within the RS, as seen in Fig. 38, due to the outer utc superlayer having no xy-hits. This poor reconstruction makes the event lie off the pion band.

13.12 Single-cut Other Failures

The "Other" 1-cut group is a list of all other cuts which are the following: TGQUALT, NPITG, EPITG, EPIMAX, TGER, TARGF, DTGTTP, RTDIF, DRP, TGKTIM, TGEDGE, TGDEDX, TGENR, PIGAP, TGLIKE1, TGLIKE2, TGDB4, TGDB4TIP, TGDVXTIP, TGDVXPI, PHIVTX, CHI567, CHI5MAX, VERRNG, ANGLI, TGFITALLK, TPICS, TGTCON, B4ETCON. There were 3 events (1 of which was a true 1-cut failure) in the 1/3 sample and 1 (which was also a true 1-cut failure) in the 2/3 sample. The following subsection detail these events. There was no indication of backgrounds not yet considered.

13.12.1 Run 48730 Event 262365

This event fails many TG cuts (EPITG, EPIMAX, TARGF, TGLIK1, TGDVXPI, CHI567, VERRNG). As seen in Fig. 39, the TG reconstruction has a large gap between the kaon and pion fibers making it a candidate for a CEX event. The K/Pi gap forces other cuts to also remove this event. *tgz* for this event is -2.83cm, very close to the center of the fiducial region.

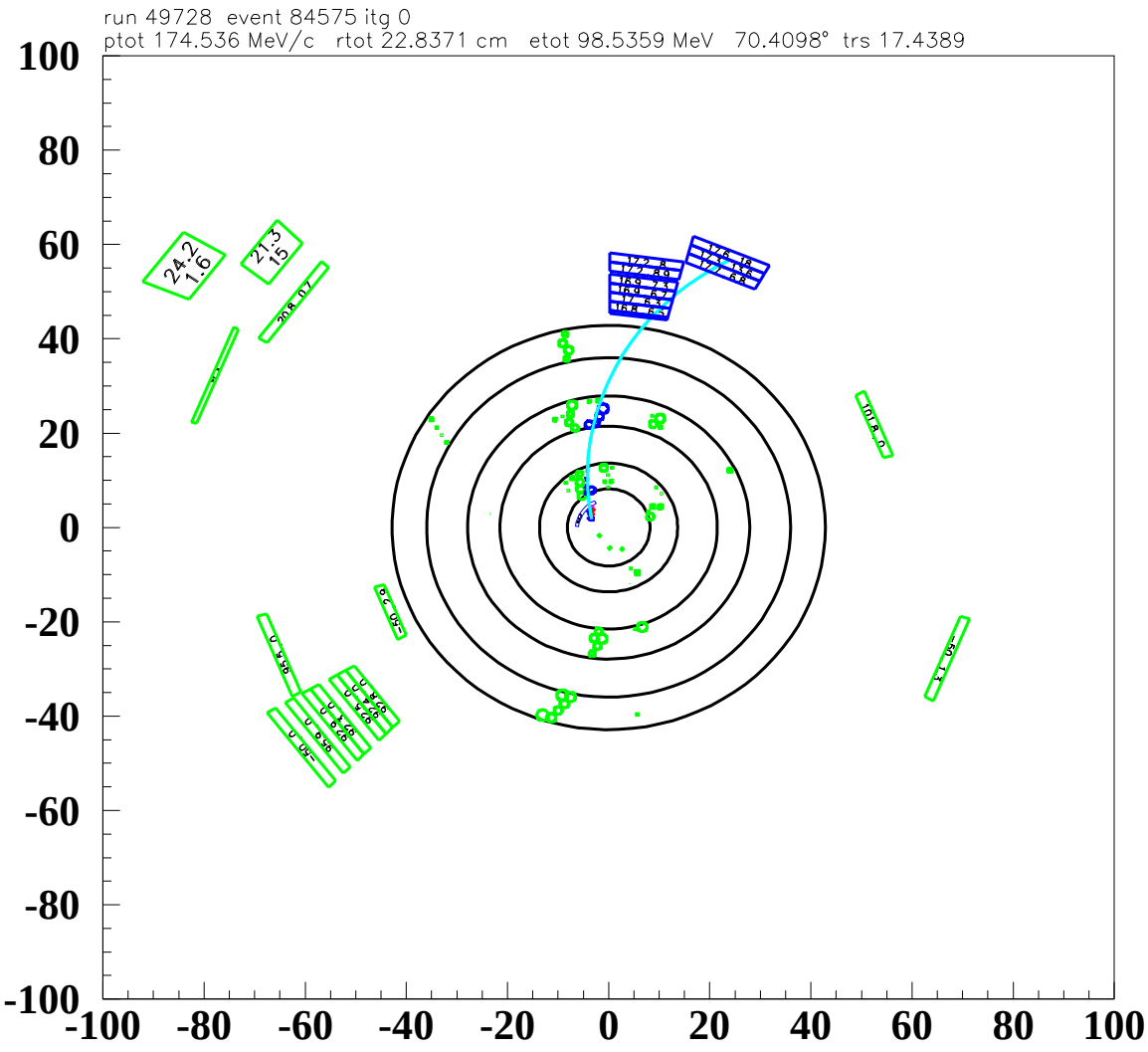

Figure 38: Run 49728 Event 84575 only failed the KIN cut-group. This picture shows the poor reconstruction of the track.

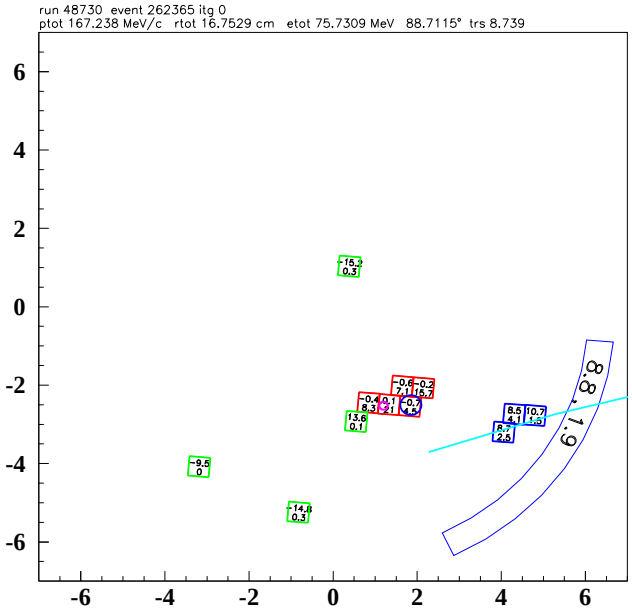

Figure 39: Run 48730 Event 262365 fails the OTHER 1-cut group including many TG cuts. Shown here is the TG reconstruction.

13.12.2 Run 49414 Event 141984

This event is very clean and only fails TARGF. As shown in Fig. 40, the gap is due to not including the edge fibers. Ideally the reconstruction would include the TG edge fibers, however, we do not have good geometry information from these fibers and they are highly multiplexed. The effort to include these fibers in the analysis in this way is not productive considering the effort required.

13.12.3 Run 49948 Event 93492

This event fails EPITG, TGDEDX, PHIVTX, CHI567, VERRNG. As seen in Fig. 41, there are many high-energy pion fibers in the TG. This indicates a possible TG scatter.

13.12.4 Run 49276 Event 106042

This event fails only PHIVTX. As seen in Fig. 42(left), it is kinematically very close to failing all there parameters; E=100.08MeV (100.5), P=196.9MeV/c (199.), R=27.49cm (28.), such that the number in parenthesis is the threshold of the loose box. As shown in Fig. 42(right), there is also a hit located on the opposite-side of the kaon blob which is classified as a pion; the fiber has an energy of 1.8MeV and a time of 4.8ns ($trs = 4.9ns$). There is a gap in the pion track of 1.483cm; the cut threshold is 1.5cm.

If the fiber (1.8MeV, 4.8ns) was instead a PV fiber and the TGPV threshold is 2.0MeV, it would pass the TGPV cut. However, it would have failed OPSVETO (threshold=1.0MeV) if it was classified as a opposite-side pion. *swatccd*, the TG reconstruction routine, classifies this fiber as a CCW (counter-clockwise or opposite-side pion) fiber biased upon the nominal method. However, at the time it was classified as a CCW-fiber it was also tagged as a possible fiber to mend into the pion cluster. This particular mending process is based upon the distance from the fiber to the stopping kaon fiber being less than 0.6cm. Later in reconstruction, when the mending was performed, the routine decided it was a pion instead of a opposite-side pion.

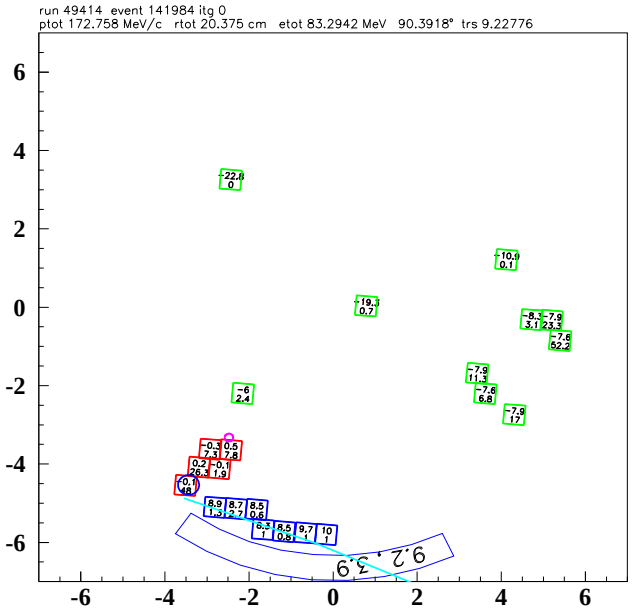

Figure 40: Run 49414 Event 141984 fails only TARGF in the OTHER 1-cut group. Shown here is the TG reconstruction.

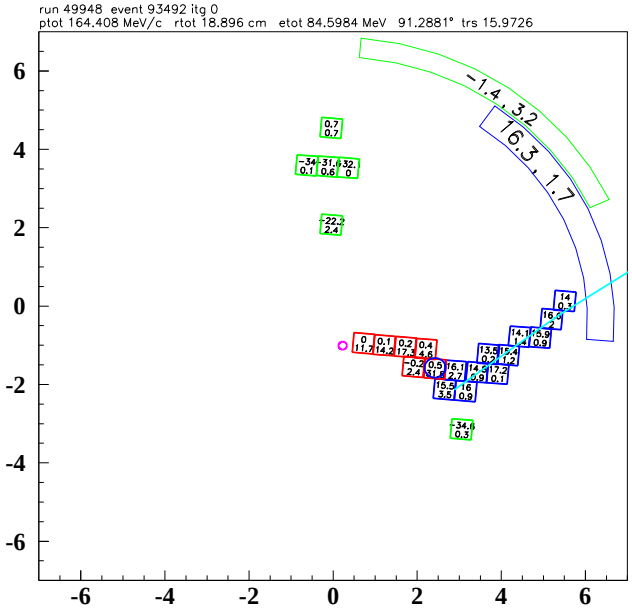

Figure 41: Run 49948 Event 93492 fails the OTHER 1-cut group including many TG cuts. Shown here is the TG reconstruction.

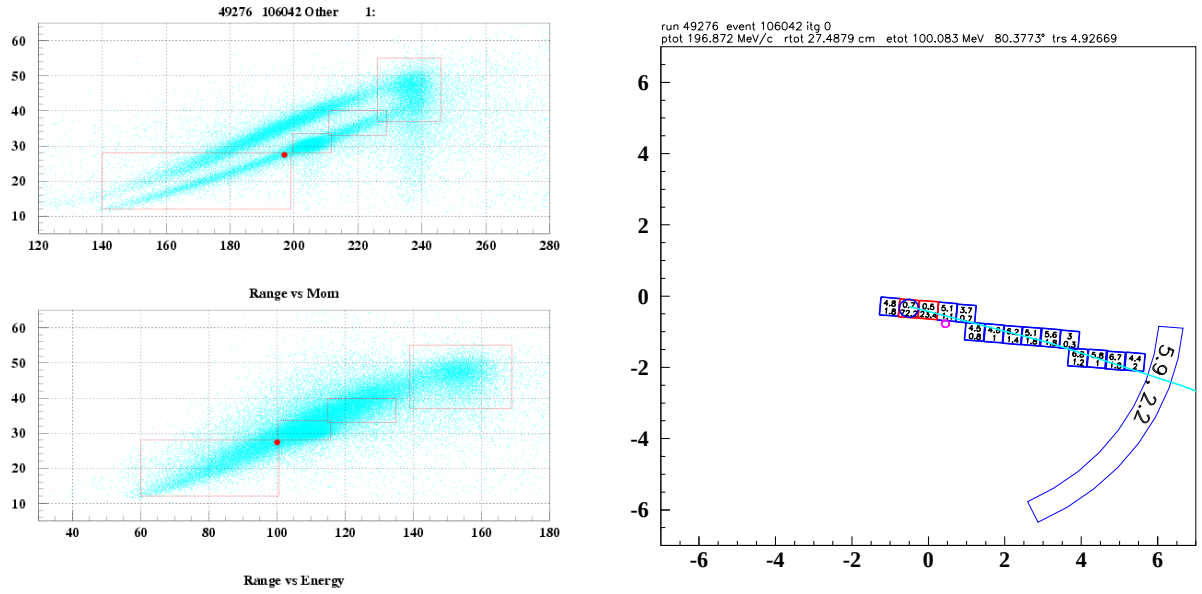

Figure 42: Run 49276 Event 106042 failed only the PHIVTX cut. The left plot shows how close the event is to failing the BOX cut. The right plot shows the TG reconstruction.

14 Sensitivity

14.1 Single event sensitivity

Single event sensitivity (SES) is defined as

$$SES = A_{tot} \times \epsilon_{T\bullet 2} \times f_s \times KB_{live}.$$

In the absence of background, the SES^{-1} is the lowest branching ratio that could be measured by this analysis.

	value	Reference
A_{tot}(entire)	$(1.857 \pm 0.021 \pm 0.065) \times 10^{-3}$	Table 79
A_{tot}(tight)	$(0.592 \pm 0.009^{+0.018}_{-0.024}) \times 10^{-3}$	Table 79
$\epsilon_{T\bullet 2}$	$0.9505 \pm 0.0012 \pm 0.0143$	[6, 16]
f_s	0.7740 ± 0.0011	[6, 16]
KB_{live}	1.7096×10^{12}	Section 12
A_{tot}(entire) $\times \epsilon_{T\bullet 2} \times f_s$	$(1.366 \pm 0.016 \pm 0.052) \times 10^{-3}$	
A_{tot}(tight) $\times \epsilon_{T\bullet 2} \times f_s$	$(0.436 \pm 0.007^{+0.015}_{-0.019}) \times 10^{-3}$	
SES(entire)$^{-1}$	$(4.28 \pm 0.43) \times 10^{-10}$	
SES(tight)$^{-1}$	$(13.42 \pm 1.34) \times 10^{-10}$	

Table 84: Values used in SES determination.

The total acceptance, including the $T\bullet 2$ efficiency and stopping fraction f_s, are given in Table 84 for both the entire signal region and the tight region. For the E949 pnn1 analysis, the total acceptance of the extended signal region was $(2.22 \pm 0.07 \pm 0.15) \times 10^{-3}$ [16] or 1.63 times as large as the pnn2 acceptance.

As described in the 1/3 note [1], there is a 6% difference between the measured $K_{\pi 2}$ branching fraction and the world average. In light of this discrepancy, we set the relative uncertainty on the total acceptance to be 10%. The SES^{-1} for the entire signal region and the tight region are given in Table 84 For comparison, the SES^{-1} for the extended signal region used in the E949 pnn1 analysis was $(2.55 \pm 0.08 \pm 0.18) \times 10^{-10}$ [16].

14.2 E949 pnn2 Cell definition

Nine cells are defined for E949 pnn2 analysis. They are based on the combinations of the following four cuts.

- KIN: Ke4 phobic box,
- PV: Tight PV, at 30% offline acceptance,
- DELCO: DELCO6,
- TD: The tight cut corresponds to the E949 PNN1-level TDCUTS. For the loose cut, EV5 is removed and the TDVARNN cut is loosened.

We present the following description of the calculation of each background component to each cell.

The Ke4 phobic box was defined to effectively suppress K_{e4} and $K_{\pi 2}$ background (Section 5 of [1]). The rejection of Ke4 phobic box on K_{e4} background is estimated with UMC sample like in Sec.5.2 of [1], while the rejection on $K_{\pi 2}$ background is estimated with its normalization branch. Here the rejection of TGPV·OPSVETO for K_{e4} background and the rejection of PVCUT for $K_{\pi 2}$ are assumed to be not sensitive for this change of kinematic range. The assumption on PVCUT is confirmed by the results in Table 14. When tightening the upper bound of kinematic cut, the possible momentum of π^+ from $K_{\pi 2\gamma}$ decay will decrease. Correspondingly the minimum energy of the inner bremsstrahlung increases. The higher the energy of the gamma is, the higher rejection of PVCUT. So besides shrinking the effective phase space of $K_{\pi 2\gamma}$ background, tightening kinematic cut also contributes more rejection. This rejection factor is estimated with the UMC sample. However its rejection is almost the same with acceptance loss. Muon, beam and CEX background are thought to be not dramatically affected by this cut. Acceptance loss is used to account for the decrease of these background.

Only muon background situation is significantly improved by tightening TDCUTS. The rejection when tightening TDCUTS on muon background is taken from Tab. 40 We assume that the rejection of TDCUTS has no or very weak correlation with KIN, DELCO and PV. So the rejection increase mainly comes from TDCUTS itself. Acceptance loss is used to explain the decrease of the other backgrounds.

DELCO will suppress single beam and CEX backgrond. Some cuts is correlated with DELCO, like CCDPUL which has better acceptance with tight DELCO. The acceptance loss of DELCO is the ratio of $A_{beam(tight)}/A_{beam(loose)}$. As single beam background is only several percents of total beam background, it is not put into further calculation. Attention is only put onto CEX background and is evaluated with UMC. Tighting DELCO cut also does not show any significant rejection increase for double beam backgound.

Tight PV cut also suppress $K_{\pi 2}$ and $K_{\pi 2\gamma}$ background. The rejection increasing when tightening PV is estimated with Tab. 22 and 23. Acceptance loss are calculated for the other background.

The rejections of these cuts and the acceptance losses of them are summarized in Table 85.

The low statistics in pnn2 background study does not allow a more intensive analysis for these four cuts and does not allow to have too more cells. From the material shown in the following sections one can find that more cells also does not provide more useful information for signal search and final BR measurement. Tab. 86 gives a summary for the acceptance and background. Tab. 87 is a breakdown of each kind of backgrounds in each cells. Loose is for entire E949 pnn2 search region. Shorthand KIN means KIN is applied in addition to the loose cuts. And KIN* means the counterpart of KIN is applied in

	KIN	TD	DELCO	PV
Acc loss	81.2%	81.2%	91.1%	52.2%
Rej for specific bkg	1.63 (Kp2) 2.7 (Ke4) 1.2 (Kp2g)	3.08 (Muon)	6.7 (CEX) 1 (beam)	2.75 (kp2,kp2g)

Table 85: Assumed acceptance loss and rejection for each background for each of the 4 cuts. More details can be found in the text.

addtion to the loose cuts. (KIN* = Loose kinematic box - tight kinematic box) The same definitions is also applied to TD, TD*, DC, DC*, PV and PV*. The 9th cell is defined to the cell with KIN* since it has low acceptance and poor Acc/Bkg. No separation is done for that cell.

Cell	Cuts	Acc	Total bkg	Acc/Bkg	S/B	S/B
	Loose	1.000	$0.927 \pm 0.168^{+0.320}_{-0.237}$	1.079		
9	**KIN***	**0.188**	$\mathbf{0.379 \pm 0.074^{+0.177}_{-0.120}}$	**0.496**	**0.17**	0.20
	KIN	0.812	$0.548 \pm 0.097^{+0.143}_{-0.113}$	1.483		
1	KIN +TD +DC +PV	0.314	$0.152 \pm 0.027^{+0.047}_{-0.035}$	2.065	0.71	0.84
2	**KIN +TD +DC +PV***	**0.287**	$\mathbf{0.243 \pm 0.044^{+0.054}_{-0.047}}$	**1.183**	**0.41**	0.47
3	KIN +TD +DC*+PV	0.031	$0.019 \pm 0.005^{+0.007}_{-0.004}$	1.653	0.56	0.66
4	**KIN +TD +DC*+PV***	**0.028**	$\mathbf{0.027 \pm 0.006^{+0.008}_{-0.005}}$	**1.036**	**0.36**	0.42
5	KIN +TD*+DC +PV	0.073	$0.038 \pm 0.007^{+0.011}_{-0.008}$	1.921	0.66	0.78
6	KIN +TD*+DC +PV*	0.066	$0.059 \pm 0.011^{+0.012}_{-0.011}$	1.135	0.38	0.45
7	KIN +TD*+DC*+PV	0.007	$0.005 \pm 0.001^{+0.002}_{-0.001}$	1.559	0.48	0.57
8	KIN +TD*+DC*+PV*	0.006	$0.007 \pm 0.001^{+0.002}_{-0.001}$	0.998	0.29	0.35
Cand.						
02A					0.9	1.1
98C					7	8
95A					50	59
96B					0.17	0.20

Table 86: Acceptance and background summary of each cell. All the acceptance is normalized to that in loose cuts. Note that KIN* $\equiv$ Loose kinematic box - tight kinematic box, etc. See text for additional details. The rows in **bold** denote the cells that contain one candidate each. When calculating S/B, a branching fraction of 1.47×10^{-10} or 1.73×10^{-10} is assumed. The S/B of previous pnn1 candidates 02A, 98C, 95A and pnn2 candidate 96B are included for comparison.

14.3 Junk method

When the Pnn2 analysis goes to its final stage the features of junk method were studied intensively. It inherited some nice similar behavior from the one cell Bayesian theorem. Problems with multi cells case seems get an easy approximate solution. However some hidden issues have to pop up when too many expectation is given to it. Past pnn results were published with junk method. It is not recommended to switch to another approach. But people should have better understanding of the result.

cuts	kp2 TG	kp2 RS	Beam	Muon	Ke4	Kp2g	CEX
Loose	$0.619 \pm 0.150^{+0.067}_{-0.100}$	$0.030 \pm 0.005^{+0.004}_{-0.004}$	0.001 ± 0.001	0.011 ± 0.011	$0.176 \pm 0.072^{+0.233}_{-0.124}$	$0.076 \pm 0.007^{+0.006}_{-0.006}$	$0.013 \pm 0.013^{+0.010}_{-0.003}$
KIN*	$0.239 \pm 0.058^{+0.026}_{-0.039}$	$0.012 \pm 0.002^{+0.001}_{-0.002}$	0.000 ± 0.000	0.002 ± 0.002	$0.111 \pm 0.045^{+0.147}_{-0.078}$	$0.013 \pm 0.001^{+0.001}_{-0.001}$	$0.002 \pm 0.002^{+0.002}_{-0.001}$
KIN	$0.380 \pm 0.092^{+0.041}_{-0.061}$	$0.019 \pm 0.003^{+0.002}_{-0.002}$	0.001 ± 0.001	0.009 ± 0.009	$0.065 \pm 0.027^{+0.086}_{-0.046}$	$0.063 \pm 0.006^{+0.005}_{-0.001}$	$0.011 \pm 0.011^{+0.008}_{-0.002}$
KIN +TD +DC +PV	$0.102 \pm 0.025^{+0.011}_{-0.017}$	$0.005 \pm 0.001^{+0.001}_{-0.001}$	0.000 ± 0.000	0.001 ± 0.001	$0.025 \pm 0.010^{+0.033}_{-0.018}$	$0.017 \pm 0.002^{+0.001}_{-0.000}$	$0.001 \pm 0.001^{+0.001}_{-0.000}$
KIN +TD +DC +PV*	$0.179 \pm 0.043^{+0.019}_{-0.029}$	$0.009 \pm 0.002^{+0.001}_{-0.001}$	0.000 ± 0.000	0.001 ± 0.001	$0.023 \pm 0.009^{+0.031}_{-0.016}$	$0.030 \pm 0.003^{+0.002}_{-0.000}$	$0.001 \pm 0.001^{+0.000}_{-0.000}$
KIN +TD +DC*+PV	$0.010 \pm 0.002^{+0.001}_{-0.002}$	$0.000 \pm 0.000^{+0.000}_{-0.000}$	0.000 ± 0.000	0.000 ± 0.000	$0.002 \pm 0.001^{+0.003}_{-0.002}$	$0.002 \pm 0.000^{+0.000}_{-0.000}$	$0.004 \pm 0.004^{+0.003}_{-0.001}$
KIN +TD +DC*+PV*	$0.017 \pm 0.004^{+0.002}_{-0.003}$	$0.001 \pm 0.000^{+0.000}_{-0.000}$	0.000 ± 0.000	0.000 ± 0.000	$0.002 \pm 0.001^{+0.003}_{-0.002}$	$0.003 \pm 0.000^{+0.000}_{-0.000}$	$0.003 \pm 0.003^{+0.003}_{-0.001}$
KIN +TD*+DC +PV	$0.024 \pm 0.006^{+0.003}_{-0.004}$	$0.001 \pm 0.000^{+0.000}_{-0.000}$	0.000 ± 0.000	0.003 ± 0.003	$0.006 \pm 0.002^{+0.008}_{-0.004}$	$0.004 \pm 0.000^{+0.000}_{-0.000}$	$0.000 \pm 0.000^{+0.000}_{-0.000}$
KIN +TD*+DC +PV*	$0.041 \pm 0.010^{+0.004}_{-0.007}$	$0.002 \pm 0.000^{+0.000}_{-0.000}$	0.000 ± 0.000	0.003 ± 0.003	$0.005 \pm 0.002^{+0.007}_{-0.004}$	$0.007 \pm 0.001^{+0.001}_{-0.000}$	$0.000 \pm 0.000^{+0.000}_{-0.000}$
KIN +TD*+DC*+PV	$0.002 \pm 0.001^{+0.000}_{-0.000}$	$0.000 \pm 0.000^{+0.000}_{-0.000}$	0.000 ± 0.000	0.000 ± 0.000	$0.001 \pm 0.000^{+0.001}_{-0.000}$	$0.000 \pm 0.000^{+0.000}_{-0.000}$	$0.001 \pm 0.001^{+0.001}_{-0.000}$
KIN +TD*+DC*+PV*	$0.004 \pm 0.001^{+0.000}_{-0.001}$	$0.000 \pm 0.000^{+0.000}_{-0.000}$	0.000 ± 0.000	0.000 ± 0.000	$0.001 \pm 0.000^{+0.001}_{-0.000}$	$0.001 \pm 0.000^{+0.000}_{-0.000}$	$0.001 \pm 0.001^{+0.001}_{-0.000}$

Table 87: Detailed background information of each cell.

14.3.1 Bayesian theorem

Basic

$$\begin{aligned} P(s|n) &= \frac{P(n|s)P(s)}{P(n)} \\ &= \frac{P(n|s)P(s)}{\int_0^\infty P(n|s)P(s)ds} \end{aligned} \tag{99}$$

- n: number of observed events.
- s: expected signal.
- $P(s)$: prior distribution.
- $P(s|n)$: the probability of s signal with n events observed.

Single channel Assuming a poisson process with signal and background, corresponding to a upper limit N of s the confidence level is:

$$\begin{aligned} 1-\epsilon = 1 - & \frac{e^{-(b+N)}\sum_{n=0}^{n_0}\frac{(b+N)^n}{n!}}{e^{-b}\sum_{n=0}^{n_0}\frac{b^n}{n!}} \\ &= 1 - \frac{\sum_{n=0}^{n_0} P(n|b+N)}{\sum_{n=0}^{n_0} P(n|b)} \\ CL &= 1 - CL_s \\ &= 1 - \frac{CL_{s+b}}{CL_b} \end{aligned} \tag{100}$$

- N: upper limit of signal
- b: background prediction
- n_0: observed events

Here a uniform prior distribution is assumed for $P(s)$ if nothing is known about the signal, like searching for a new phenomena. However it is not the only one choice of that. This presents an analytic, exact solution. In the last two lines of this equations some expression is replaced by some shorthand words, ie. CL, CL_{s+b}, CL_b. CL_{s+b} stands for the poisson probability of observing n event with signal plus background $(b+N)$ assumption. CL_b is the one for background only assumption.

What is CL?

- Given observed events n_0, the probability of $s <= N$ is CL.
- If $s = N$, the probability to find more than n_0 events is CL.

The above two explanations are equivalent. But the form of CL equals the ratio of CL_{s+b} over CL_b is quite accidental. As far as my ability can reach there is no primary physics reason for that.

14.3.2 Junk method (Extended Bayesian limit for multi cells)

- It is based on the last two lines of Equ. 100.
- The CL of this result cannot be understood as a usual probability.
- It can combine the results from multi cells.
- Some reviews tells its ability to distinguish background and signal.

Assume there are many cells, from 1 to m, and each of them have its expected signal s_i and background b_i where i is the index for cells. Then some events ($0 \to \infty$) are observed in some of these cells. To distribute these events into each cell there are lots of combinations. For each of the combination, α is used for the index of combinations and d_i is used to denote the number of observed events in the ith cell then three quantities are defined:

- X_α, test statistic. One choice of that is likelihood ratio.
- $P_\alpha(s+b)$, the probability of the appearance this combination with the assumption of signal and background.
- $P_\alpha(b)$, the probability of the appearance this combination with the assumption of background only.

$$\begin{aligned} X_\alpha &= \prod_{i=1}^{m} \frac{e^{-(b_i+s_i)}\dfrac{(b_i+s_i)^{d_i}}{d_i!}}{e^{-b_i}\dfrac{b_i^{d_i}}{d_i!}} \\ &= \prod_{i=1}^{m} e^{-s_i}(1+\frac{s_i}{b_i})^{d_i} \end{aligned} \tag{101}$$

A sequence of combinations can be defined as the ascending order of X_α. Here comes two definitions which are analogs of Equ. 100. "obs" refers to the real experimental yield.

$$\begin{aligned} P_{s+b}(X_\alpha \le X_{obs}) &= \sum_{X_\alpha \le X_{obs}} P_\alpha(s+b) \\ P_b(X_\alpha \le X_{obs}) &= \sum_{X_\alpha \le X_{obs}} P_\alpha(b) \end{aligned} \tag{102}$$

A CL is defined as

$$\begin{aligned} CL &= 1 - CL_s \\ &= 1 - \frac{CL_{s+b}}{CL_b} \end{aligned} \tag{103}$$

Of course it's identical to the single cell case.

14.3.3 BR in junk method

The interesting quantity to be estimated is branching fraction, BR. It is separated from s to make the following discussion more straightforward. SES_i is the single event sensitivity for the ith cell. X_α and CLs will be functions of BR.

$$s_i = SES_i \times BR \tag{104}$$

For pnn analysis the BR which makes X_{obs} reach its maximum is used as the central value of branching fraction. The BR range corresponding to CL_s interval $(50 \pm 34)\%$ is referred to as 68% coverage.

14.3.4 Uncorrelated and correlated uncertainties

Uncorrelated uncertainties of signal and background prediction are treated as a gaussian function in this approach. A gaussian convolution is going to be calculated in junk's code through a numerical integration, see [15]. A global gaussian distribution is generated for every correlated uncertainty. Every correlated variable is changing according that with the same phase, for instance:

$$\begin{aligned} x &\sim Gauss(0,1) \\ SES_1 &= \sigma_1 * x \\ SES_2 &= \sigma_2 * x \\ &... \end{aligned} \tag{105}$$

where x is gaussian variable, σ_i is one standard deviation of SES_i and here SES_1 and SES_2 are 100 percent correlated. In junk's code the negative numbers are truncated. In the following sections the integrations steps are tried to be broken down to get better understanding of that.

14.3.5 An example for one cell

An example of one cell case is given which is of the strict statistic meaning. It is the basic step to understand more complicated multi cells situation.

For one cell:

$$\begin{aligned} X &= e^{-s}(1+\frac{s}{b})^d \\ CL_s &= \frac{\sum_{n=0}^{d} P(n|b+s)}{\sum_{n=0}^{d} P(n|b)} = \frac{e^{-s}\sum_{n=0}^{d}\frac{(b+s)^n}{n!}}{\sum_{n=0}^{d}\frac{b^n}{n!}} \\ &= \frac{e^{-s}(1+(b+s)+(b+s)^2/2+...)}{1+b+b^2/2+...} \end{aligned} \tag{106}$$

Increase of candidates The first test is done by varying the possible candidate, see Fig. 43. (Assuming SES=0.5, b=0.2, no error for SES and b, and d changing from 0 through 5.) With the increasing of d the central value also increase. As well the 68% coverage position and interval also increases. However the relative error will decrease (error/central value).

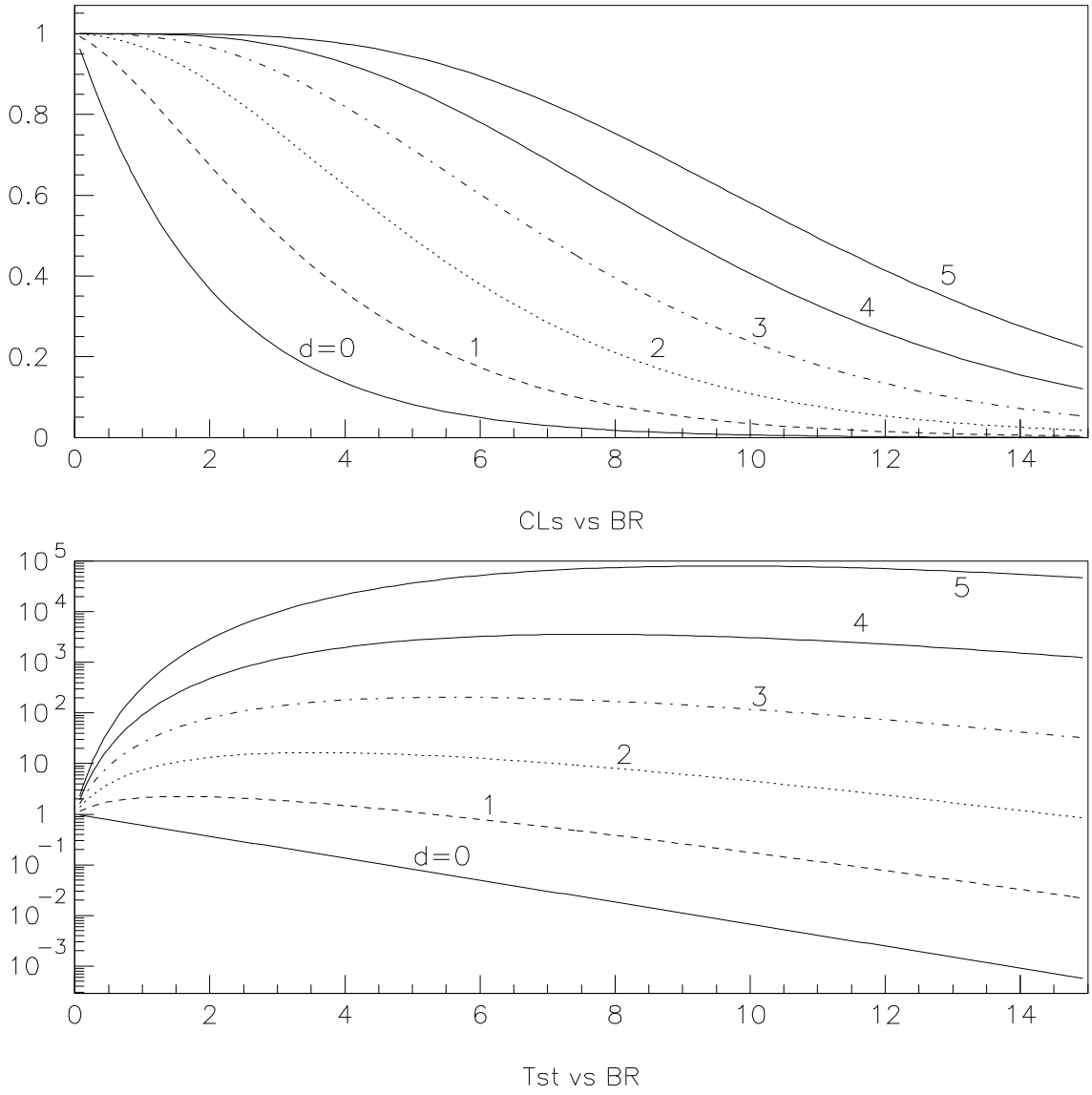

Figure 43: One cell with different number of event observed. The different d is labeled in each curve. The plot on the top is for CL_s, the one on the bottom is for test statistics.

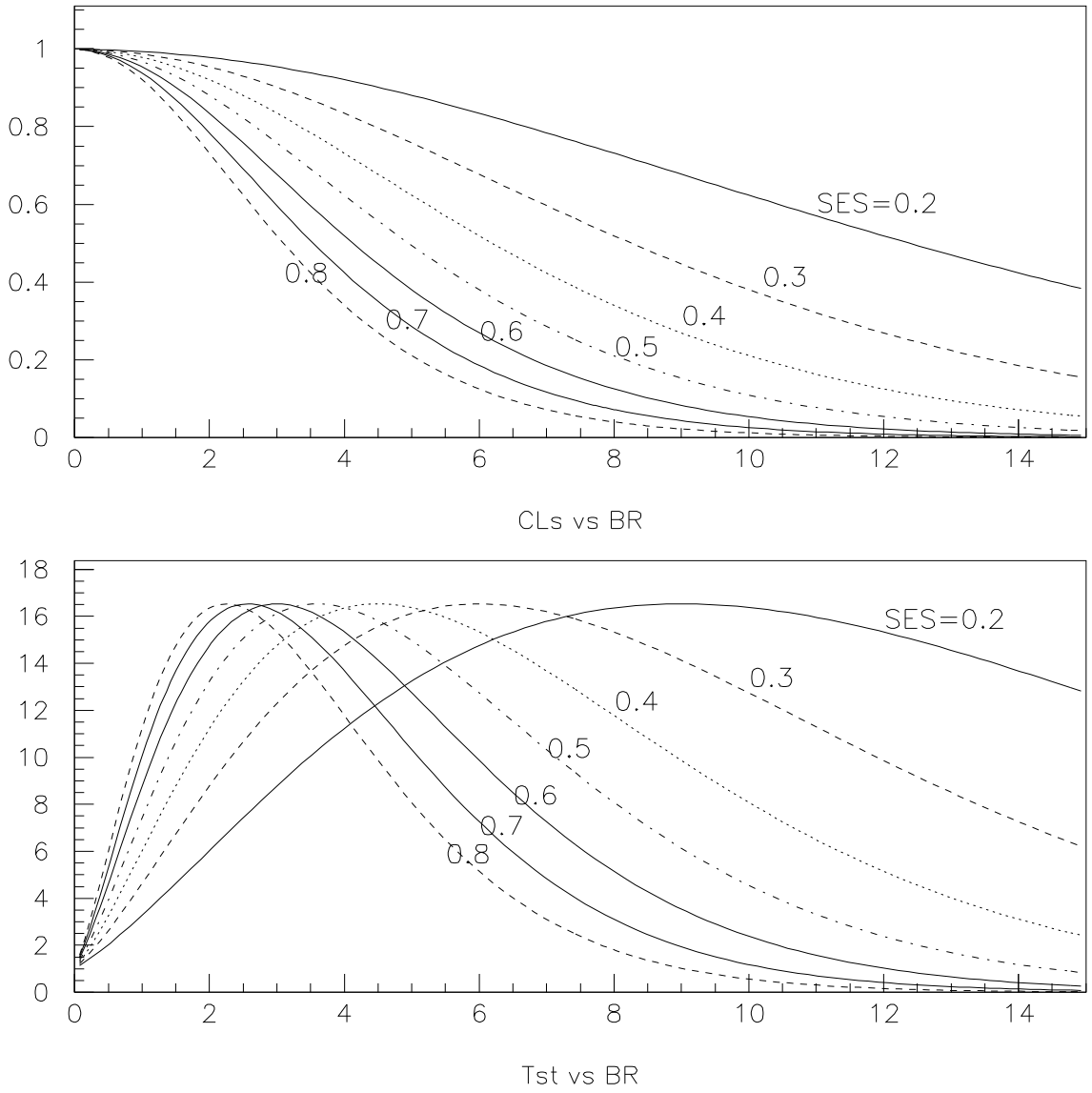

Figure 44: One cell with different SES. The SES for each curve is labeled in the plots. The plot on the top is for CL_s, the one on the bottom is for test statistics.

Increase of SES This test is done with b=0.2, d=2. The SES is set to 0.2, 0.3 ... 0.8. No error is assumed in this test. See Fig. 44 For two candidates the formulas is quite simple.

$$\begin{aligned} X &= e^{-s}(1+\frac{s}{b})^d \\ CL_s &= \frac{e^{-s}(1+(b+s)+(b+s)^2/2)}{1+b+b^2/2} \end{aligned} \tag{107}$$

SES **uncertainty** This is an example very close to reality. Suppose b=0.2 and no error for it. The SES is 0.5 ± 0.1 where 0.1 is one time of deviation. Just image the coarsest approximation for the integration is going to be made. Only take the three point in the gaussian curve, one in the central, the other two ones are at one time of positive deviation and negative deviation respectively. This could be accomplished by taking three curves in Fig. 44, SES=0.4, 0.5 and 0.6 and then get an average of them. So the new test statistics

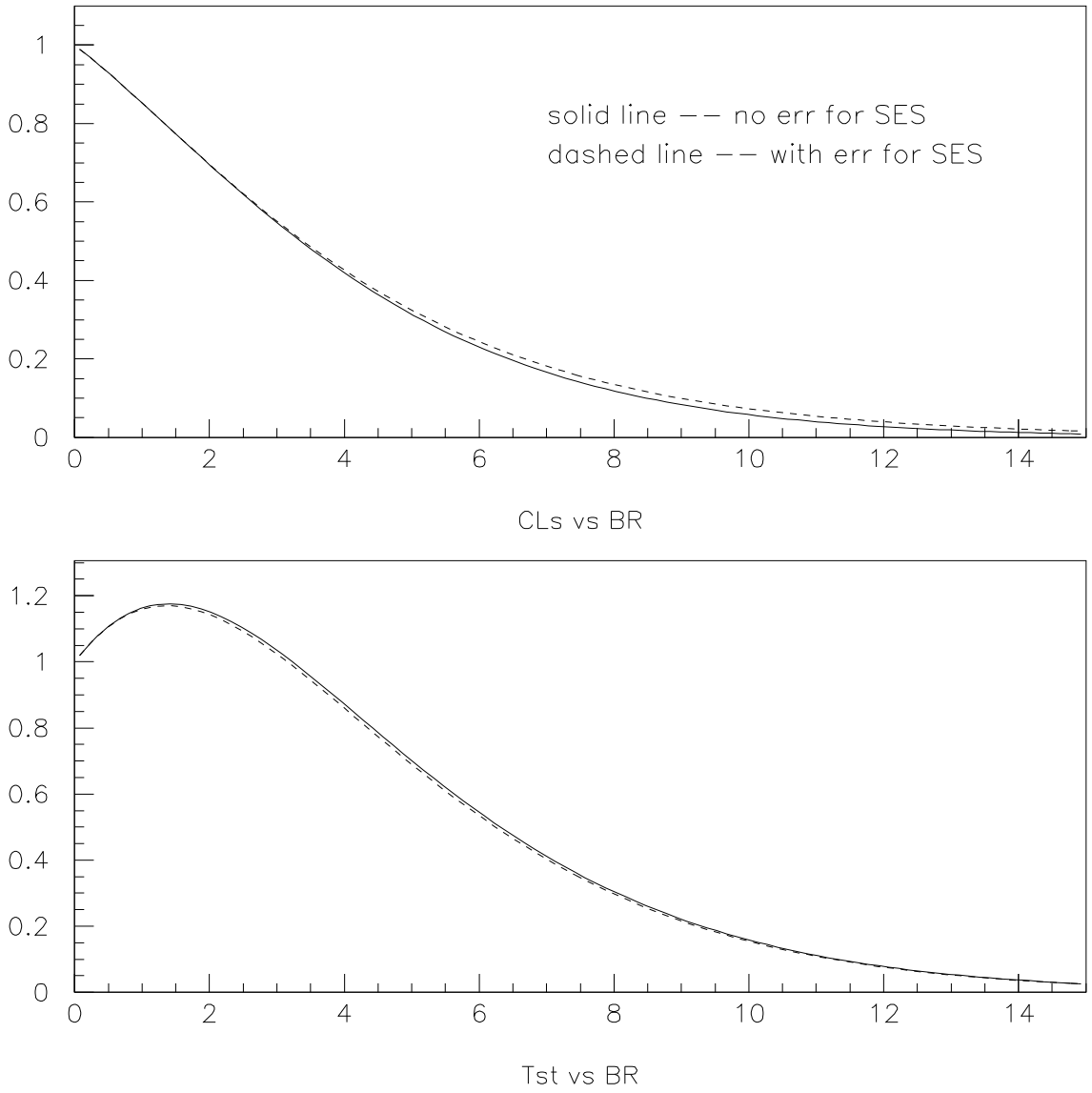

Figure 45: One cell with SES uncertainty. The plot on the top is for CL_s, the one on the bottom is for test statistics.

will shifted and the CL_s curve will intersect with the old one (SES=0.5, no error) at some place.

Put this example into code (61 steps for integration approximation), it gives Fig. 45. The 68% interval is larger than that without error as expected.

Increase of background The case of with different background prediction can also be understood by Equ. 107. The understanding of increasing background will help to get a feeling of with the result with background uncertainty. In this example $SES = 0.5$ and $d = 2$. The background prediction goes from 0.1 to 2.5. See Fig. 46 for the result. Some conclusion can be drawn in this paragraph. Less background gives larger test statistics and central value of BR. The CL_s curve with less background is always on the right side of one with higher background. In addition less background usually gives smaller 68% confidence interval like the way implemented in this note. If the 68% interval is chosen as $CL_s \in [0.32, 1]$ it will gives larger range in BR.

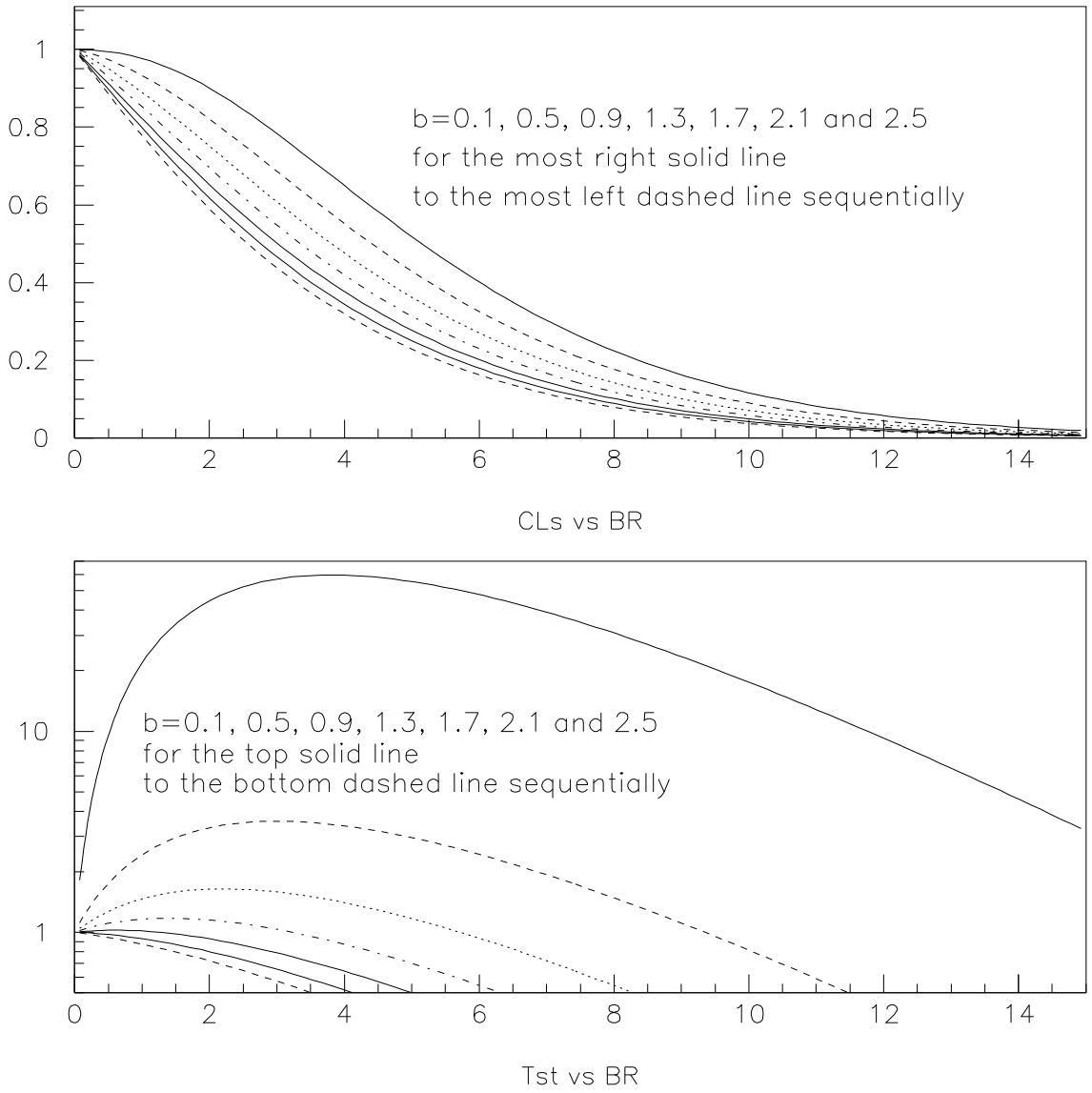

Figure 46: One cell with increasing background. The plot on the top is for CL_s, the one on the bottom is for test statistics.

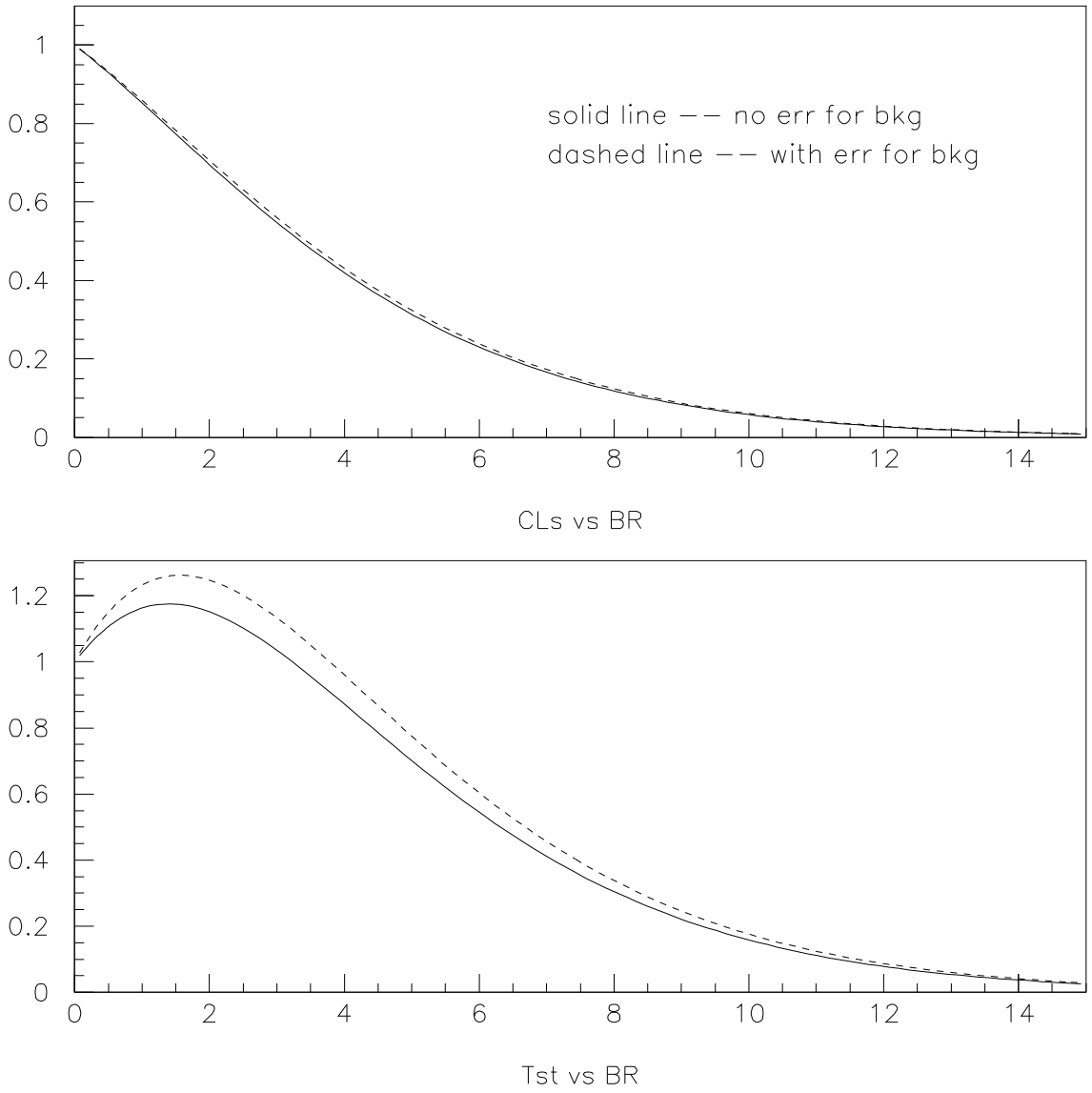

Figure 47: One cell with background error. The plot on the top is for CL_s, the one on the bottom is for test statistics.

Background uncertainty Do another imaginary integral for background uncertainty. Set $SES = 0.5$, $b = 1.3 \pm 0.4$ and no error for SES which will give a plot shown in Fig. 47. The curve with background uncertainty is always on the right side of the one without background error, however it does not make sure the one with background error will give a larger confidence interval. For example for this case if choosing $CL_s \in [0.2, 0.4]$ a smaller interval is got.

14.3.6 An example for two cells

Two cells situation is simplest case to study junk method. Some problems with junk method will appear here. They will give a hint on how to understand the final pnn result.

Increase of candidates in one of two cells This test is very simple. Cell 1 and 2 both have $SES = 0.5$ and $b = 0.2$ whose error are all 0. Cell 2 has 0 candidate. Cell 2 has 0 to 5 candidates. See Fig. 48 for the result. With the increase of candidates number the central value and 68% interval position both increase simultaneously.

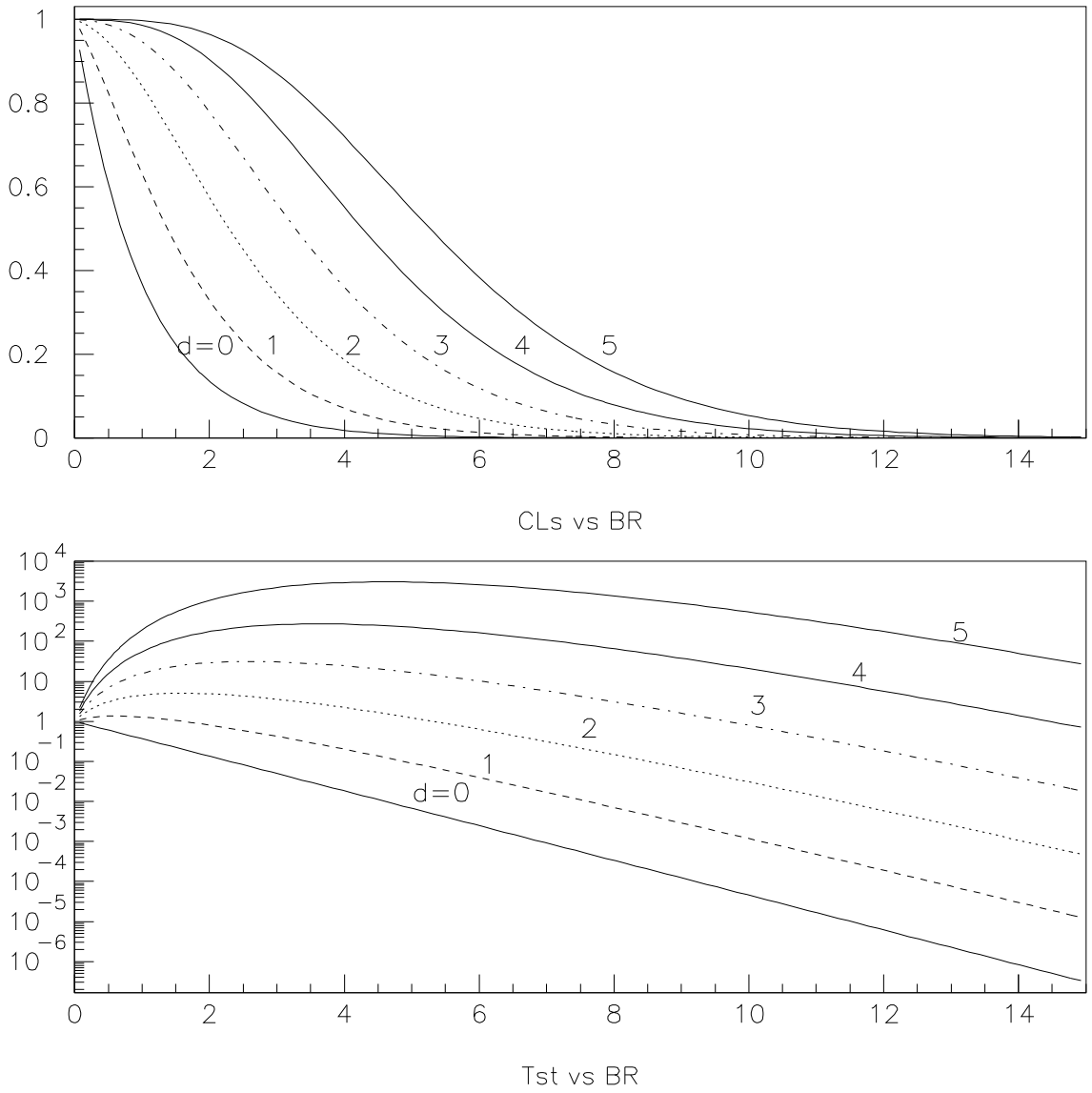

Figure 48: Increase of candidates in one of two cells. The plot on the top is for CL_s, the one on the bottom is for test statistics. Candidates number is labeled on each curve.

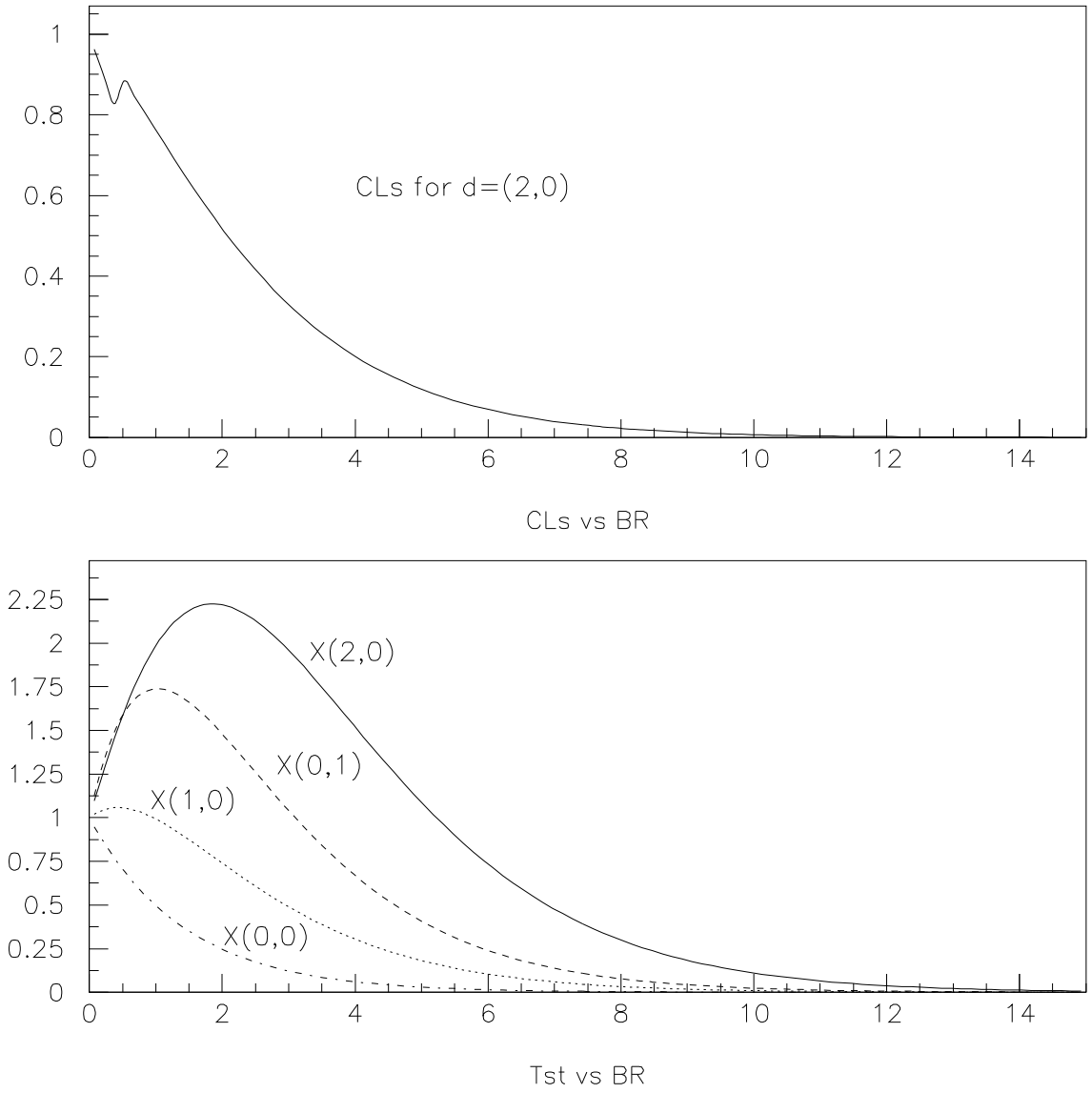

Figure 49: CL_s curve may not be continuous. The plot on the top is for CL_s, the one on the bottom is for test statistics. See text for detailed explanation.

CL_s curve may not be continuous CL_s curve is supposed to be continuous. So the confidence interval can be figured out through it. However in junk method this requirement is not perfectly met. There will be some ambiguity when trying to get the final result. When the cell numbers increase or the uncertainty is considered in the calculation this behavior will be not very obvious, but it still exist.

When evaluating $P(s+b)$ and $P(b)$ (see Equ. 102) the test statistic of each candidates combination X_α is compared with the observed one X_{obs}. With the increase of s (for a fixed SES with the increase of BR) the X_α might cross X_{obs} at some point. So the sum of $P(s+b)$ or $P(b)$ will suddenly include or drop the contribution from one combination. Now the choice of X is likelihood ratio which probably is not the best option. However choosing a new X may not the essential solution of junk method.

Here an example is given to get some feeling about this issue. Assume $SES_1 = 0.2$, $b_1 = 0.2$, $d_1 = 2$, $SES_2 = 0.5$, $b_2 = 0.2$ and $d_2 = 0$. Result is shown in Fig. 49. The CL_s curve for (2,0) is not continuous. The reason is that $X(2,0)$ and $X(0,1)$ intersect. (In this paragraph the two integers in parentheses is the candidates number in the 1st and 2nd cell respectively.)

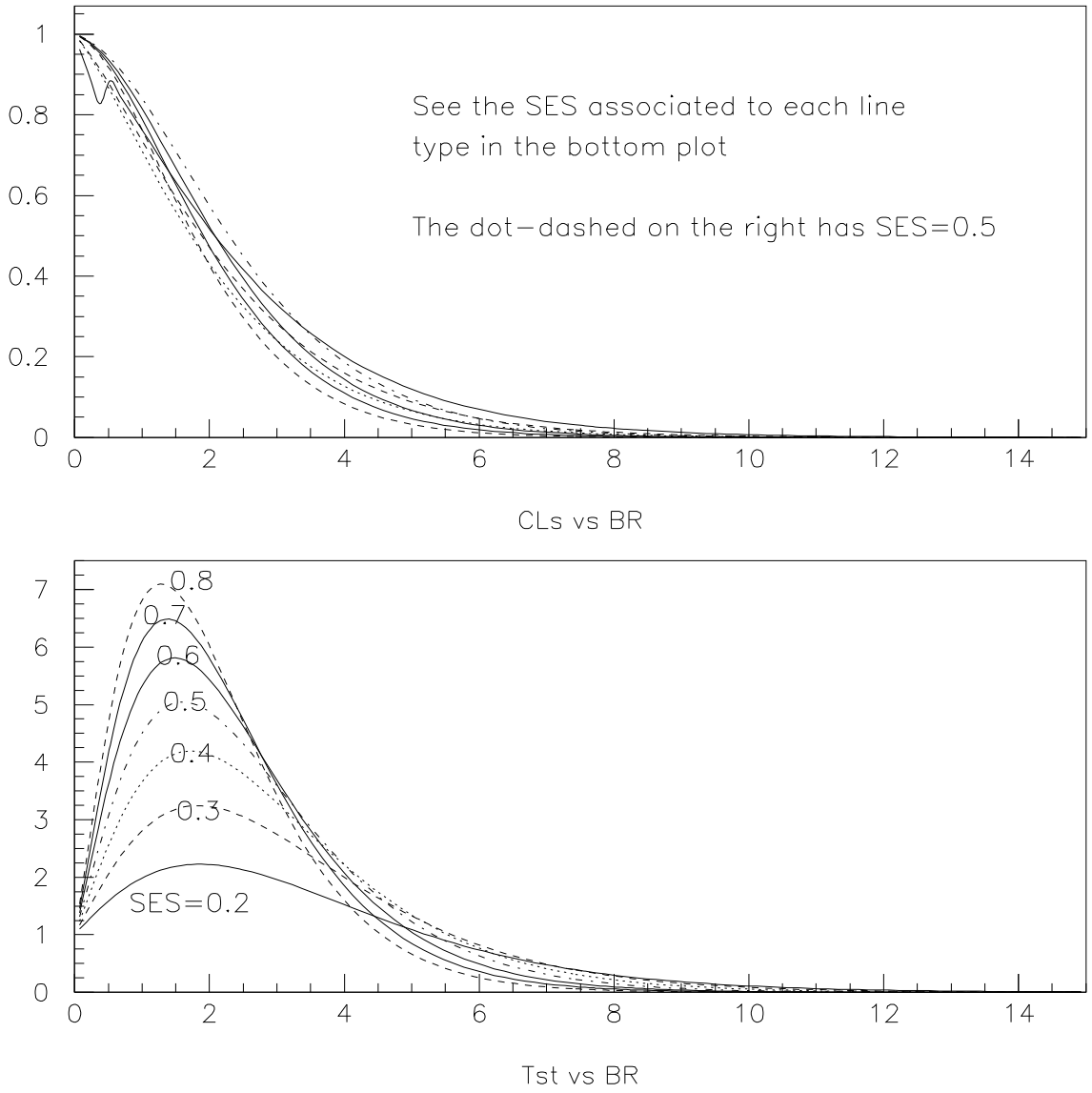

Figure 50: Two cells with different SES. The plot on the top is for CL_s, the one on the bottom is for test statistics. See text for detailed explanation.

Increase of SES Here a simple example is given on two cells case with different SES. The specific number using in this test are: $SES_1 = 0.2, 0.3, 0.4, 0.5, 0.6, 0.7, 0.8$, $b_1 = 0.2$, $d_1 = 2$, $SES_2 = 0.5$, $b_2 = 0.2$ and $d_2 = 0$. See Fig. 50 for the CL_s and test statistics curves of them. An obvious defect is when BR is around 2 all the CL_s curves are on the left side of the one with $SES = 0.5$. No matter SES increase or decrease they all lead to smaller CL_s. And they don't show any possible regular pattern. This is against the intuition. The surface reason is the choice of test statistic. The way of calculating P_{s+b} or CL_s is also questionable. Following this property is that the behavior of CL_s curves with uncertainties will be out of control and show some 'random' character. When the number of observed candidates is small this is not serious problem. The test statistic still works well like one cell case.

SES **uncertainty** In this example every setting is the same with previous test, ie. $b_1 = 0.2$, $d_1 = 2$, $SES_2 = 0.5$, $b_2 = 0.2$ and $d_2 = 0$, except that $SES_1 = 0.5 \pm 0.1$. The CL_s and test statistic curves is shown in Fig. 51. Obviously the one with uncertainty gives smaller 68% interval.

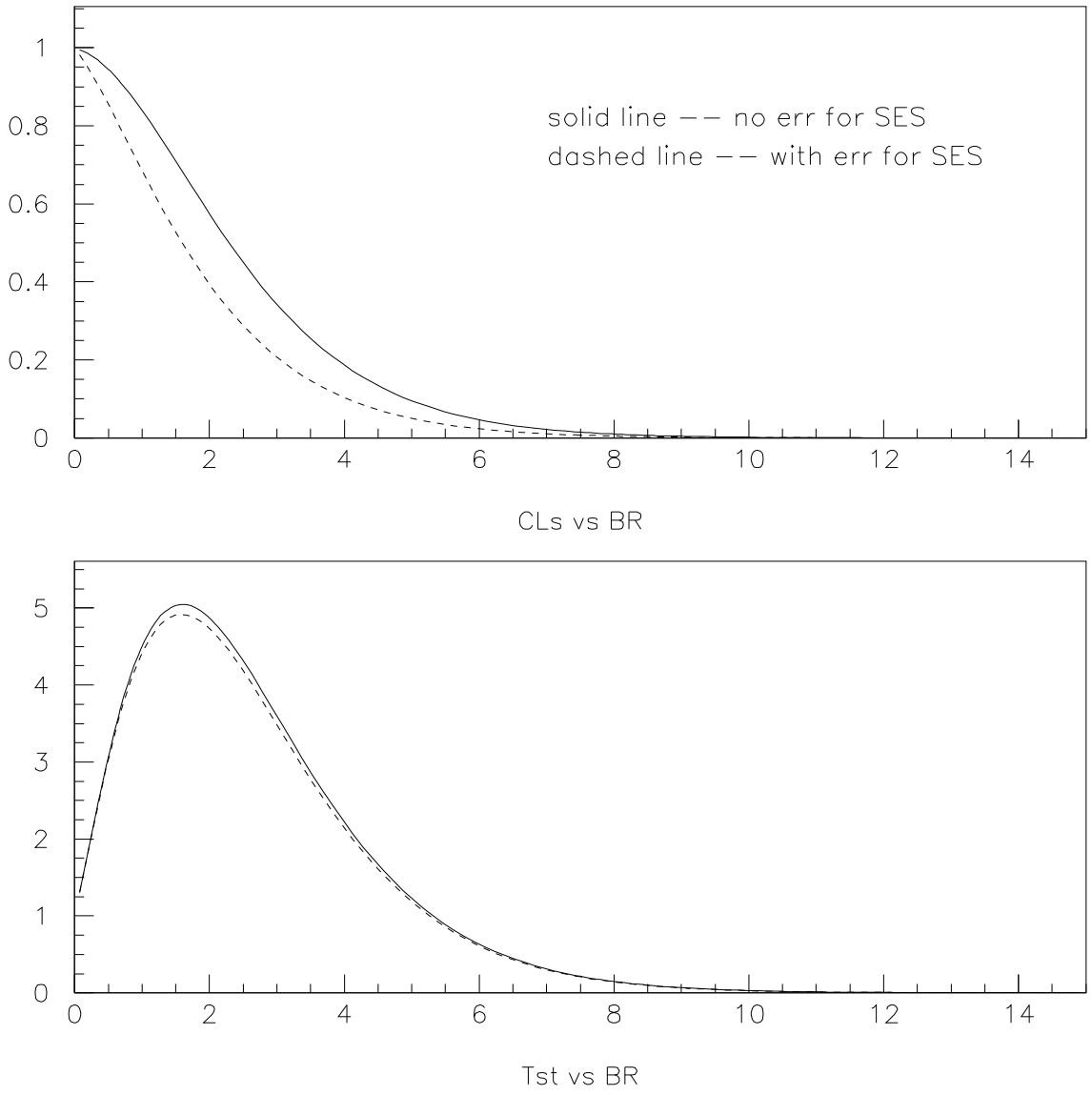

Figure 51: Two cells with SES error. The plot on the top is for CL_s, the one on the bottom is for test statistics.

Different background and background error The same work is done with background numbers. There is no transparent conclusion. b appears in numerator and denominator. CL_s and X are both complex functions of that.

Other comment Another interesting plot is shown in [16], Fig. 88. The so-called "pdf" is not consistent with X_{obs} as a function of branching ratio.

14.4 BR measurement

The branching fraction of pnn rare decay is calculated with junk method. The error of branching fraction is dominated by statistical uncertainty of candidates number. When taking the error of background and sensitivity into account the central value of BR will change only one or two percent and it has minor impact on 68% interval.

Background and sensitivity numbers are collected from previous E787 and E949 publications. When they are not interpreted there previous analysis notes are scanned to find the number. Some help are provided by previous E949 pnn1 analysis junk code for the detailed information of the 98's 486 and 2002's 3781 cells.

In this analysis 7 cells are defined for all pnn1 result like presented in 2002 pnn1 paper. Two cells are for 95 97 data. 486+3781 cells are sorted according to their Acc/Bkg and they are grouped into five cells. Two are for candidates cells and three empty cells. One empty cell is the sum of all the empty cells with Acc/Bkg less than candidate cell 1, one is with Acc/Bkg greater than candidate cell 2 while another one is in between. One cell is defined for each of 96 and 97 pnn2 data. So there are totally 9 cells for previous analysis. 9 cells for this E949 pnn2 study. They add up to 18 cells in this estimation.

Background uncertainties is considered in this calculation as independent gaussian fluctuation. Correlated 10% uncertainty is assigned to every year's sensitivity result.

14.4.1 1/3 sample result

See Tab. 88 for the result with or with any errors for sensititity and background prediction. For current analysis the error is still dominated by the low statistic. In addition Fig. 52 presents the CL_s and test statistics curves for the case with errors.

$\times 10^{-10}$	BR (1/3 with err)	BR (1/3 without err)	BR (2/3 with err)
pnn1	$1.46^{+1.36}_{-0.87}$	$1.47^{+1.34}_{-0.89}$	$1.46^{+1.36}_{-0.87}$
pnn1+E787,pnn2	$1.41^{+1.33}_{-0.82}$	$1.42^{+1.34}_{-0.83}$	$1.41^{+1.33}_{-0.82}$
all, 9 empty cells	$1.21^{+1.31}_{-0.63}$	$1.22^{+1.32}_{-0.63}$	$1.21^{+1.32}_{-0.63}$
one Can in cell 9 (worst)	$1.29^{+1.29}_{-0.71}$	$1.29^{+1.30}_{-0.70}$	$1.27^{+1.30}_{-0.69}$
one Can in cell 1 (best)	$1.50^{+1.26}_{-0.85}$	$1.50^{+1.26}_{-0.84}$	$1.44^{+1.27}_{-0.83}$
one Can in cell 2	$1.43^{+1.27}_{-0.82}$	$1.43^{+1.28}_{-0.81}$	$1.39^{+1.28}_{-0.80}$
one Can in cell 3	$1.32^{+1.29}_{-0.73}$	$1.31^{+1.30}_{-0.72}$	$1.42^{+1.28}_{-0.81}$
one Can in cell 4	$1.31^{+1.29}_{-0.72}$	$1.30^{+1.30}_{-0.72}$	$1.38^{+1.28}_{-0.79}$
one Can in cell 5	$1.46^{+1.26}_{-0.83}$	$1.46^{+1.27}_{-0.82}$	$1.42^{+1.28}_{-0.81}$
one Can in cell 6	$1.41^{+1.27}_{-0.81}$	$1.40^{+1.28}_{-0.80}$	$1.38^{+1.28}_{-0.79}$
one Can in cell 7	$1.31^{+1.29}_{-0.72}$	$1.30^{+1.30}_{-0.72}$	$1.41^{+1.29}_{-0.80}$
one Can in cell 8	$1.30^{+1.29}_{-0.72}$	$1.30^{+1.30}_{-0.71}$	$1.36^{+1.29}_{-0.77}$

Table 88: BR measurement of 1/3 sample with or without uncertainties and BR result of 2/3 sample.

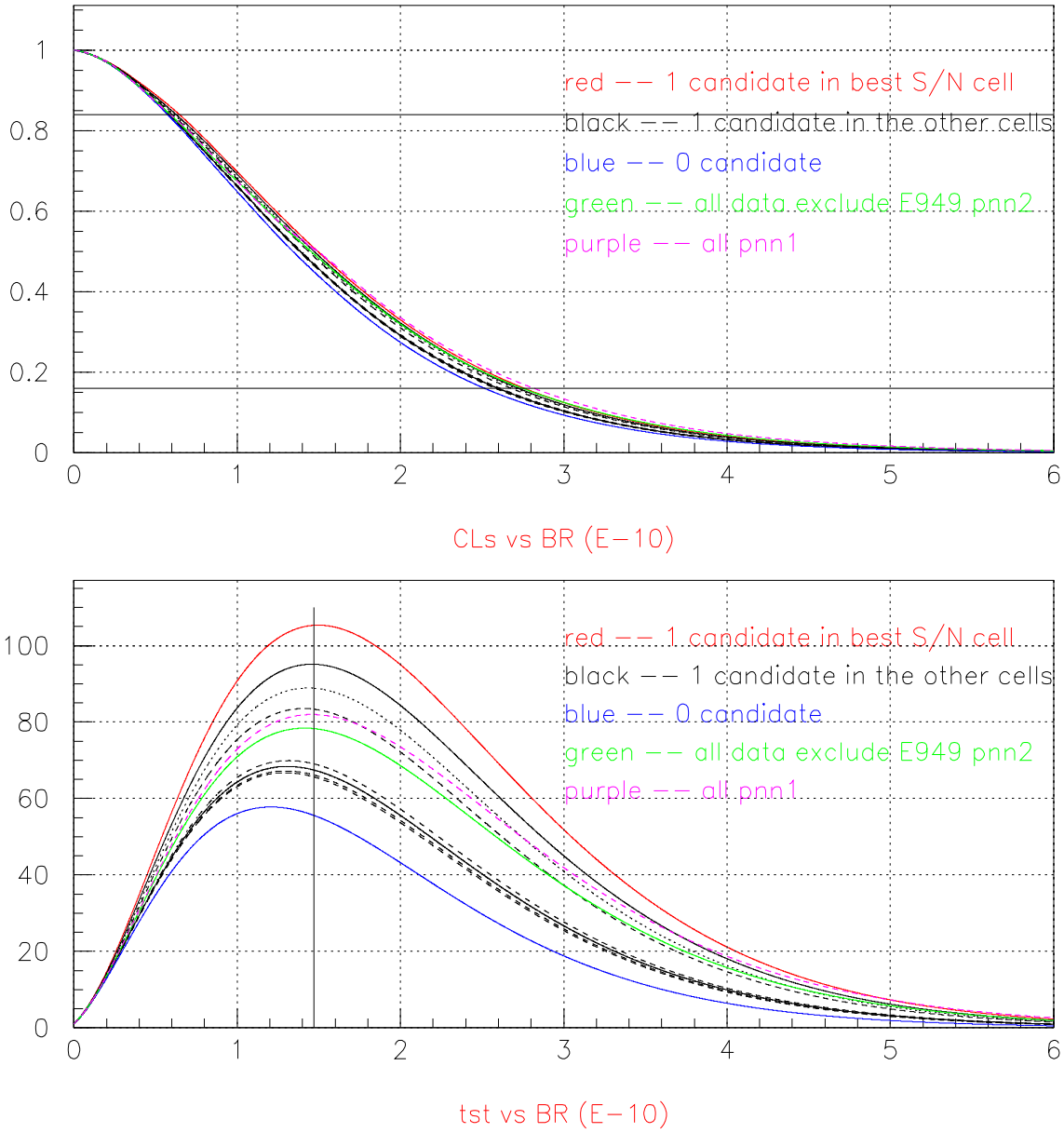

Figure 52: CL_s and test statistic curves for BR measurement in 1/3 sample. The two horizontal lines in the upper plot indicates the 68% coverage and the vertical line in the bottom plot indicates the published central value in 2002 pnn1 paper.

14.4.2 2/3 sample result

Tab. 88 also gives the predicted BR for 9 empty cells and finding one candidate in one of the cells. Correspondingly Fig. 53 shows the CL_s and test statistics curves.

14.4.3 After box opening

With the observation of three candidates in cell 2, 4 and 9 the branching ratios (68% CL) and upper limits (90% CL) are calculated and summurized in Tab. 89 with almost all kinds of possible situation. Cls curves and test statistic are shown in Fig. 54 and Fig. 55 for each case. They are seperated into two plots due to different scales. The Cls curves and test statistic for all pnn result combined are brought out in Fig. 56.

($\times 10^{-10}$)	sample	BR (68% CL)	Upper Limit (90% CL)
pnn1 publication [20]	pnn1:9597, 98 and 02	$1.47^{+1.30}_{-0.89}$	3.22
E949 pnn1 only [23]	pnn1:02	$0.96^{+4.09}_{-0.47}$	
All E787	pnn1:9597, 98; pnn2:9697	$1.49^{+1.61}_{-0.79}$	3.66
All E949	pnn1:02; pnn2:02this	$2.80^{+2.24}_{-2.32}$	6.22
All pnn1 result	pnn1:9597, 98 and 02	$1.46^{+1.36}_{-0.87}$	3.29
E949 pnn2 only	pnn2:02this	$7.89^{+9.26}_{-5.10}$	20.3
All pnn2 analysis	pnn2:9697, 02this	$5.11^{+7.04}_{-3.14}$	14.4
All pnn result	ALL	$1.73^{+1.15}_{-1.05}$	3.35
SM prediction [20]		0.80 ± 0.11	–

Table 89: BR and upper limit measurement after box opening.

Given the background prediction presented in early chapters a background alone probability is calculated. Assume the background of each cell is b_i $(i = 1, ..., 9)$, then due to statistical fluctuation of poisson distribution the probability of finding n_i candidates in the ith cell is $P(n_i, b_i)$. The associated probability is defined as

$$P_{asso} = \prod_{i=1}^{9} P(n_i, b_i) \tag{108}$$

Three candidates are found in the 2nd, 4th and 9th cell while zero in the others. The corresponding probability, P_{obs}, is

$$P_{obs} = P(0, b_1) \times P(1, b_2) \times P(0, b_3) \times P(1, b_4) \times ... \times P(1, b_9) \tag{109}$$

Then the background alone probability is

$$P_{bkg} = \sum_{P_{asso} \leq P_{obs}} P_{asso} \tag{110}$$

where $P_{asso} \leq P_{obs}$ means a more signal like yield and the sum will go over all possible cases. Within this scheme the background alone probability of this analysis is 0.037.

Another test is done on BR calculation to double check the result from junk code. When the first derivative of Eq. 101 equals zero it gives the mean of BR. Apperantly without the consideration of error information it can be done analytically. The result for all pnn result calculated by hand is 1.69×10^{-10} which is totally consistent with junk code 1.73×10^{-10}.

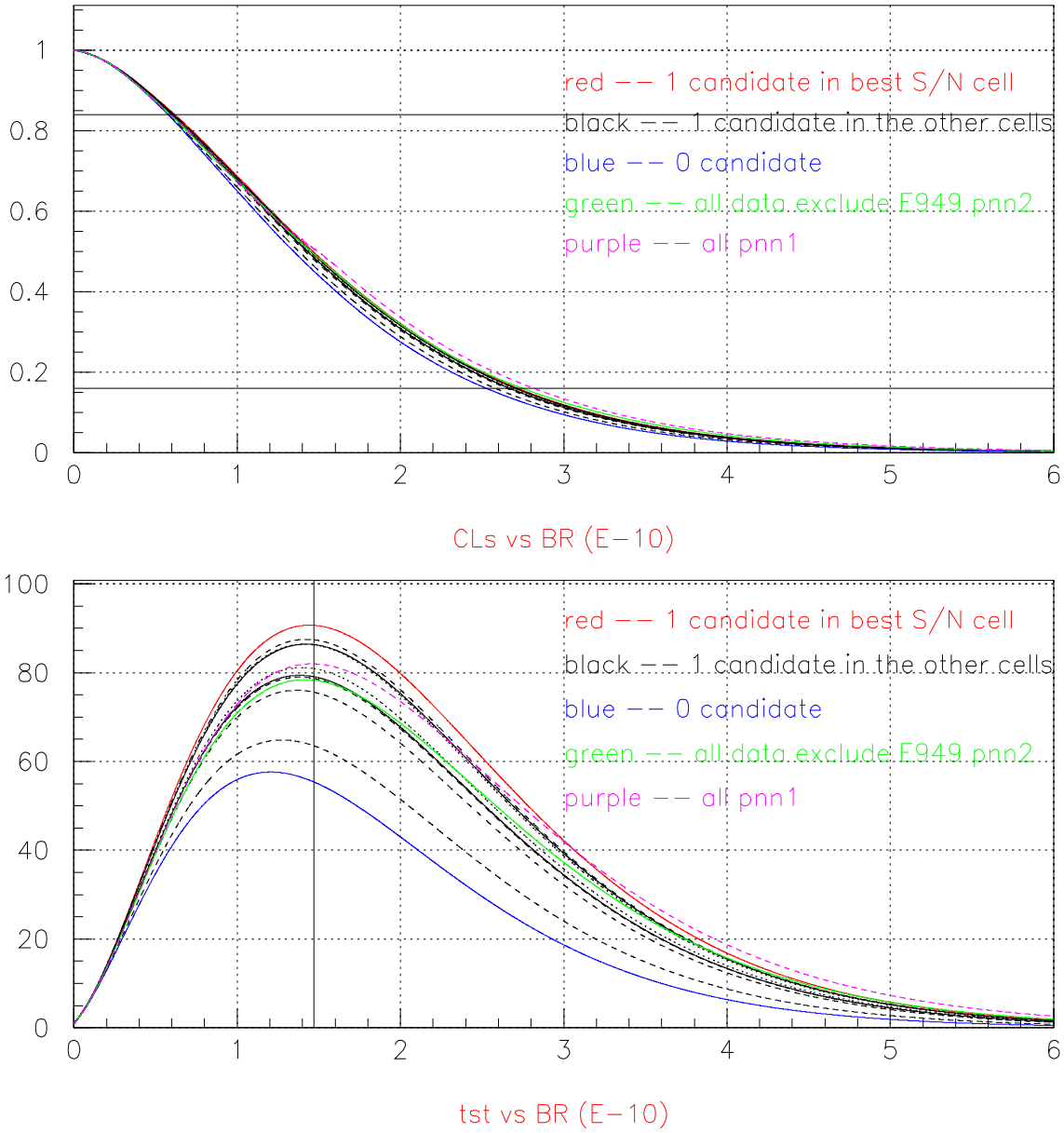

Figure 53: CL_s and test statistic curves for BR measurement in 2/3 sample. The two horizontal lines in the upper plot indicates the 68% coverage and the vertical line in the bottom plot indicates the published central value in 2002 pnn1 paper.

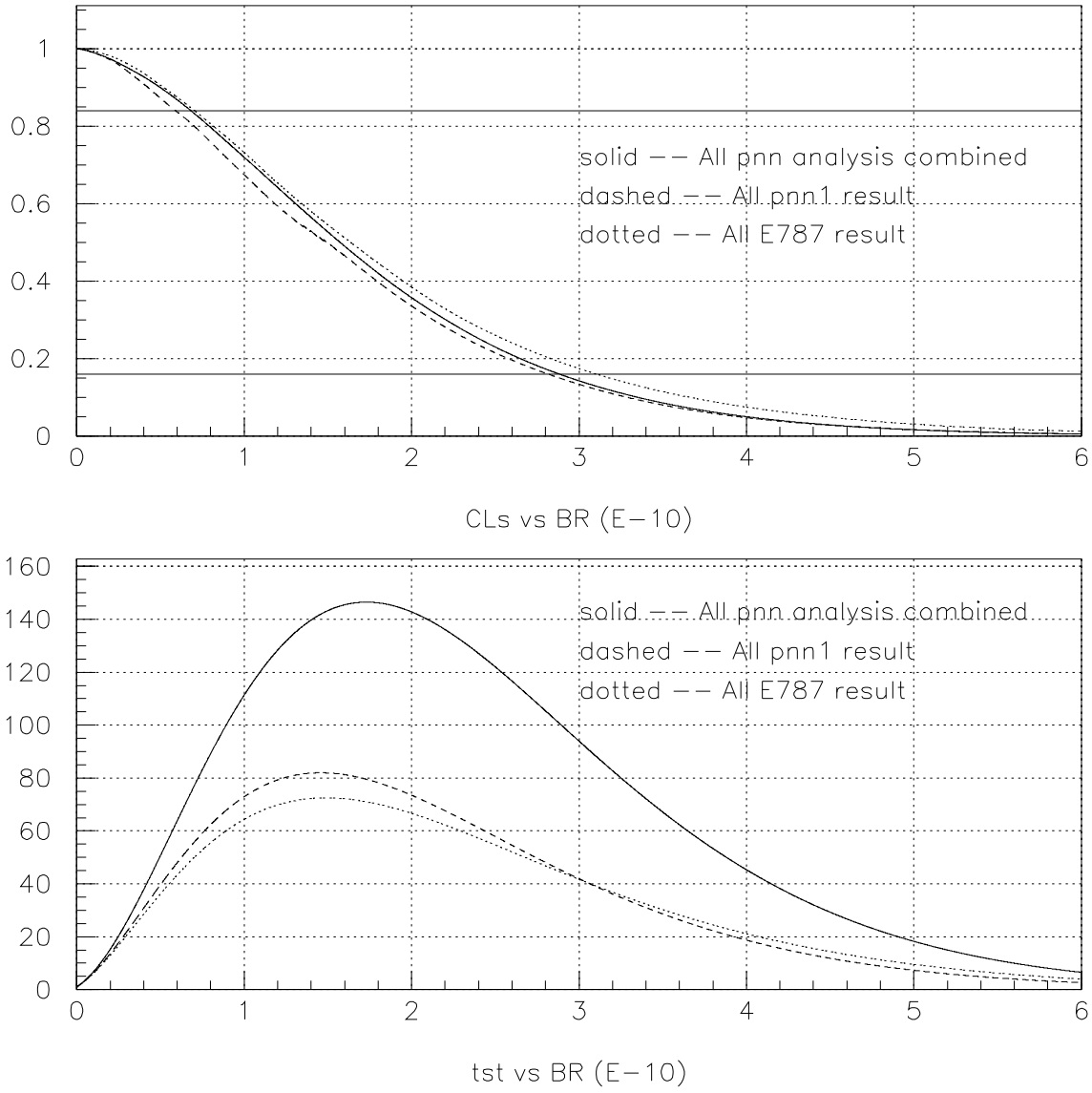

Figure 54: CL_s and test statistic (tst) curves after box opening (group 1). The two horizontal lines in the upper plot indicates the 68% coverage.

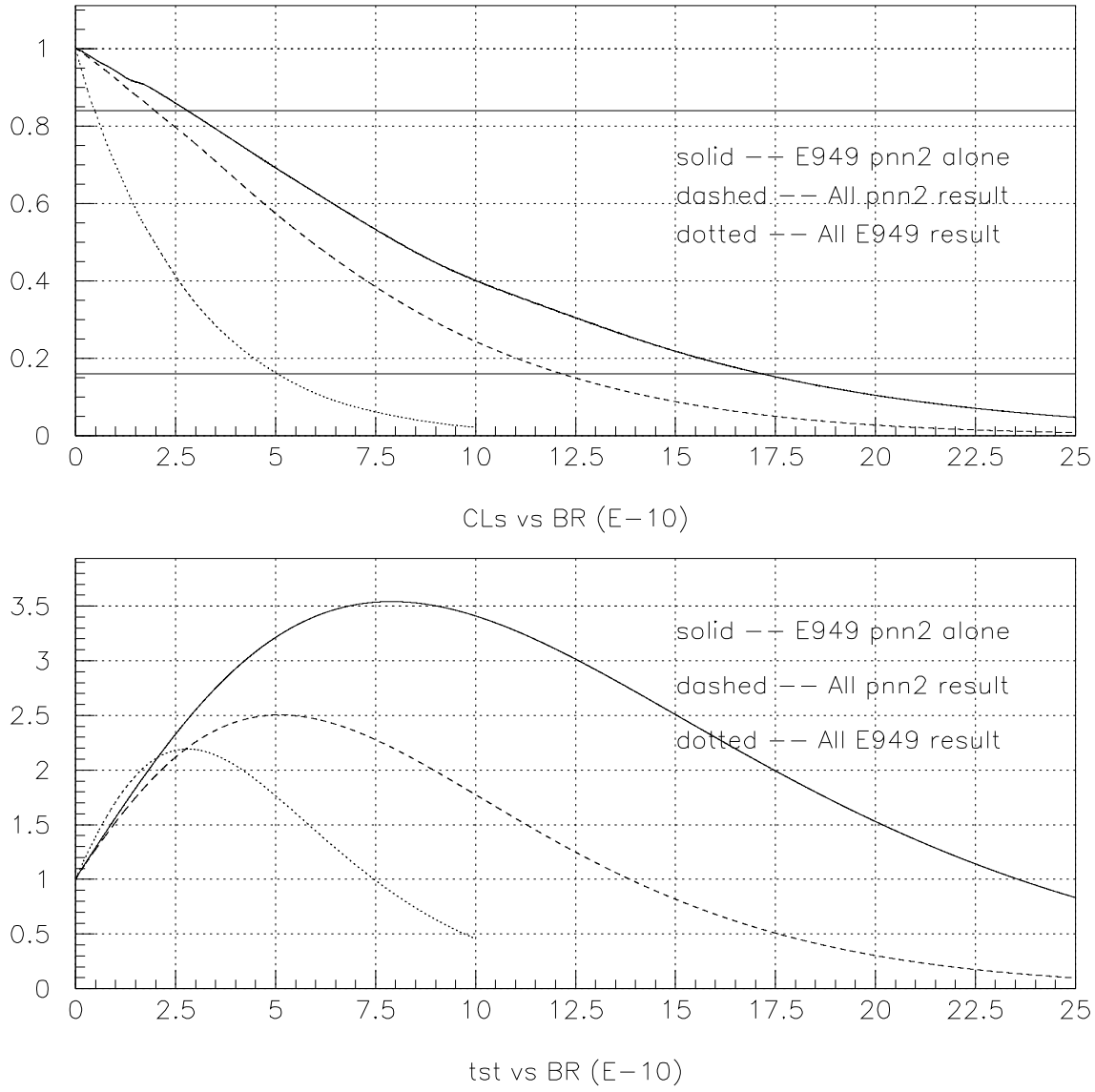

Figure 55: CL_s and test statistic (tst) curves after box opening (group 2). The two horizontal lines in the upper plot indicates the 68% coverage.

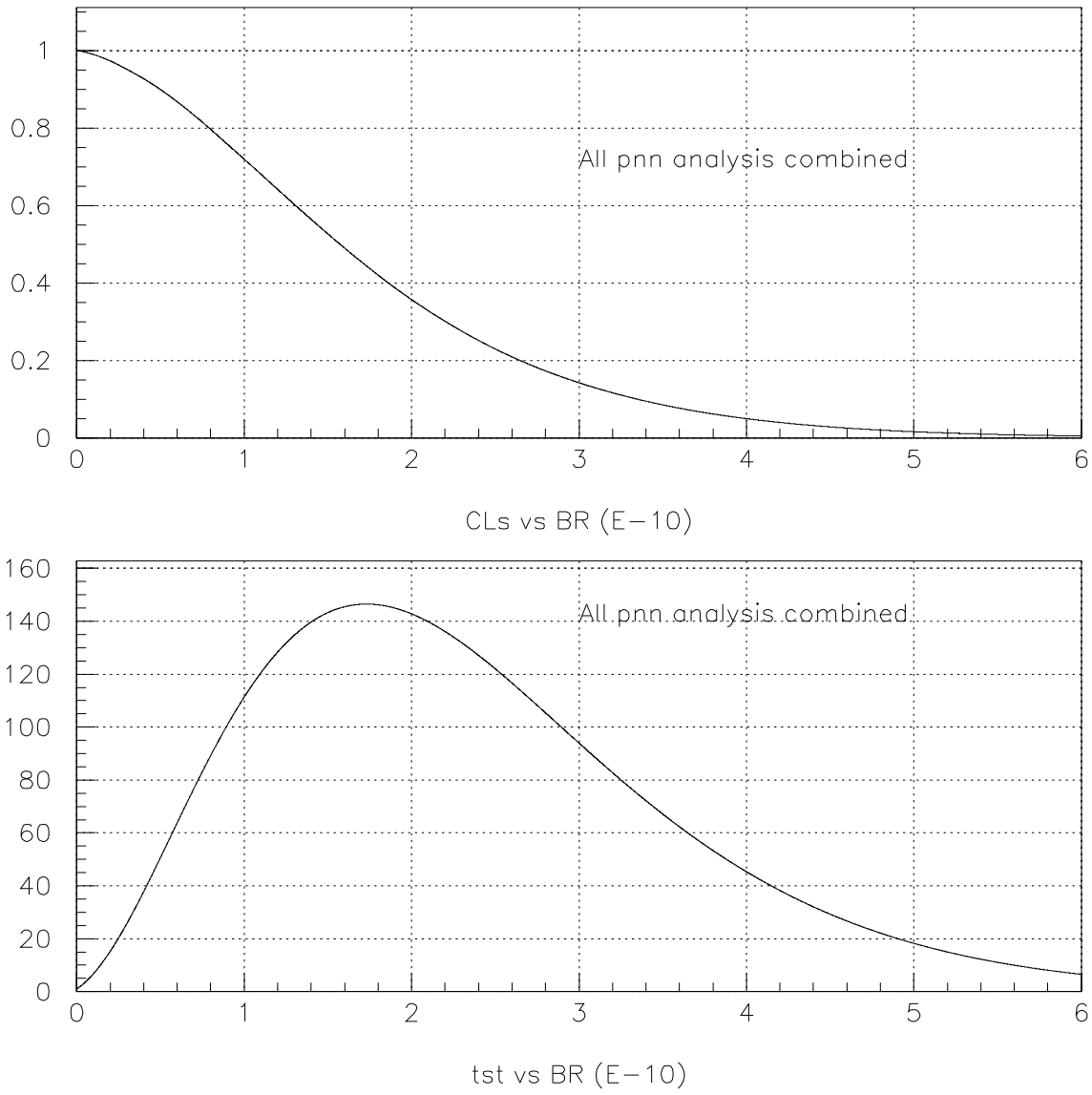

Figure 56: CL_s and test statistic (tst) curves with all pnn analysis combined after box opening.

14.5 Frequentist approach

Some suspicion always exists about Junk method: whether it is a strict statistical approach and whether it gives the right coverage. There is also concern about mistakes in calculation. A frequentist approach using the Monte Carlo has been implemented to check on these concerns.

The method is well established as explained in section 28.6 of PDG96 [21]. Build a confidence belt, determine the upper limit and/or lower limit function, find out the where is the experimental observation and then read off the limit. There is not too much freedom for a person who do this analysis. The only thing can be varied by the analyser is how to calculate the upper (lower) limit function. For instance, to build a 68% confidence interval, a central symmetrical belt can be an option which mean 16% on lower side and another 16% on higher side. Some alternative, like Feldman-Cousin, is also possible, but it won't give a dramatic difference and the choice of an ordering scheme can be tricky. A central symmetrical belt is used in this check to be consistent with the one used in Junk method.

First of all a check is done on poisson processes of a single cell. When observing n events, what are the limits of the true mean μ. A 90% (5% on each side) and 80% (10% on each side) confidence belt is built as shown in Fig. 57 and Fig. 58.

There are two labels on x-axis where the first one is an integer, like 2, 5, 6, that gives the possible outcome of the poisson process, the second one is a real number that is the best estimation of the true mean with that outcome. With respect to the poisson process of a single cell the best estimation of μ is the same as the outcome. The y-axis is the true mean value μ.

The shading of these figures gives the probability of the outcome given the true mean μ. So the sum of each row in the plot is 1 since it is sum of all possible outcomes.

The two polylines demonstrate the upper function and lower function. So the numbers in these two plot can be checked with Table 28.3 of PDG96 [21].

The second test is done on the 9597A data, see Fig. 59. There are two cells, so the best estimation of truth is chosen as the BR which maximize test statistic (X_α, likelihood ratio). The description on the x-axis tells the outcome in each cell, for instance, 10, one in the first and zero in the second, that is the observation of 9597A. With this method, the measured BR is $1.47^{+3.33}_{-0.87}$ (range $0.6-4.8$, coverage is 68%) which is comparable with previous PRL9597 publication [22] $1.5^{+3.4}_{-1.2}$ (range $0.3-4.9$). Note that the factor of 10^{-10} is suppressed in the figures and in citing the results. (The input of these two results is slightly different, since some errors were found for 9597 analysis in 2002.)

The third test is for E949 pnn2 analysis. In total there are nine cells. The first 9 digits number of the x-axis label is the observation in each cell. The first digit is the number of event in the ninth cell and the second is for the eighth cell, the third for the seventh cell, and so on. So 101010000 is our result in entire box. The result is $7.721^{+9.079}_{-5.221}$ (range $2.50-16.80$, coverage is 68%), while the result from Junk method is $7.89^{+9.26}_{-5.10}$ (range $2.79-17.15$). They reach a pretty good agreement. The little discrepancy in central value is because a fit is used in this method, some uncertainty exist with the minimization result. Note that a separate evaluation of the branching ratio using independently written code has confirmed the result of the Junk method.

Note no systematic uncertainties are considered when building these confidence belt and we have established that taking systematic uncertainties into account changes the result by less than 1%.

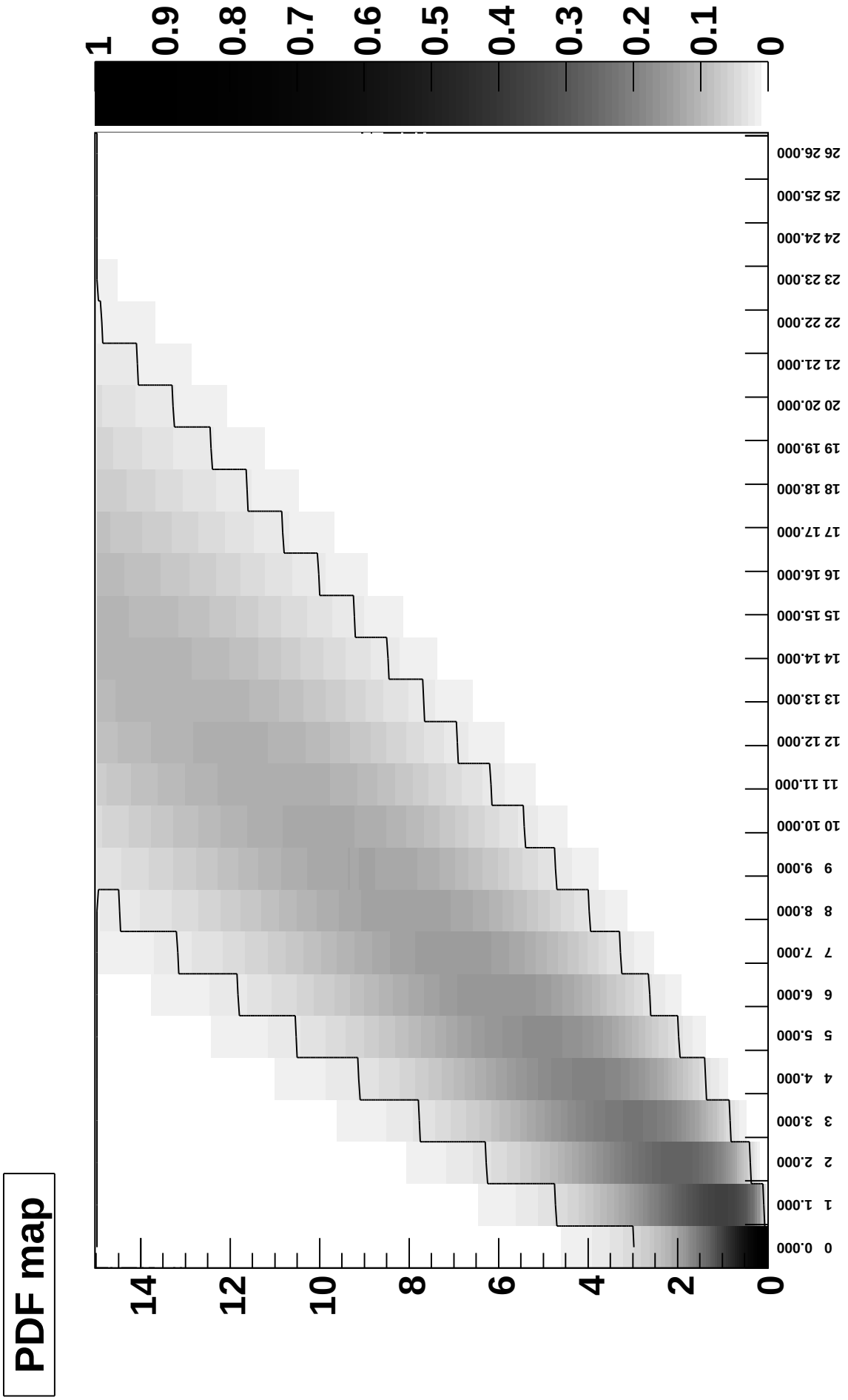

Figure 57: Poisson process of a single cell, 90% confidence belt (5% on each side).

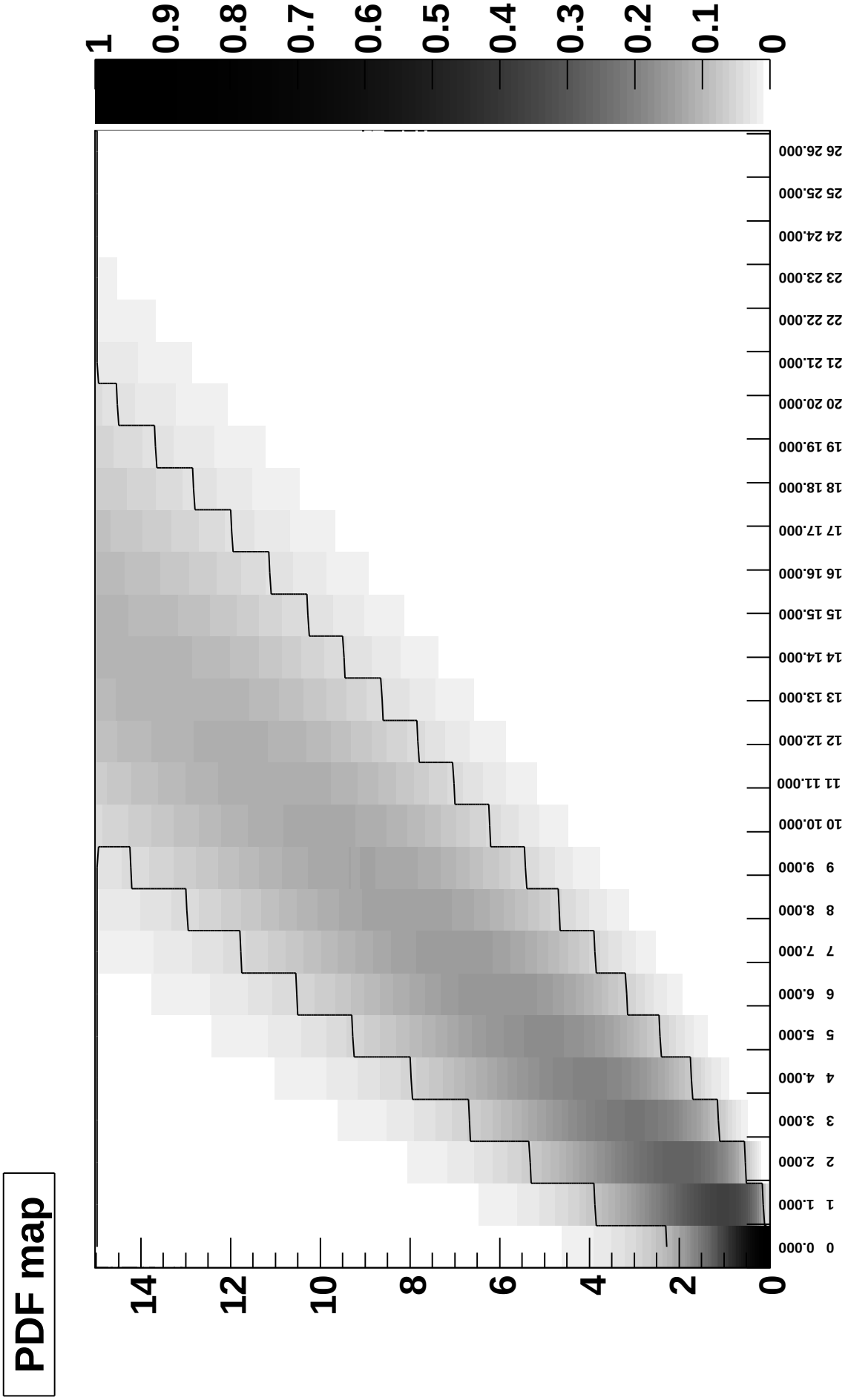

Figure 58: Poisson process of a single cell, 80% confidence belt (10% on each side).

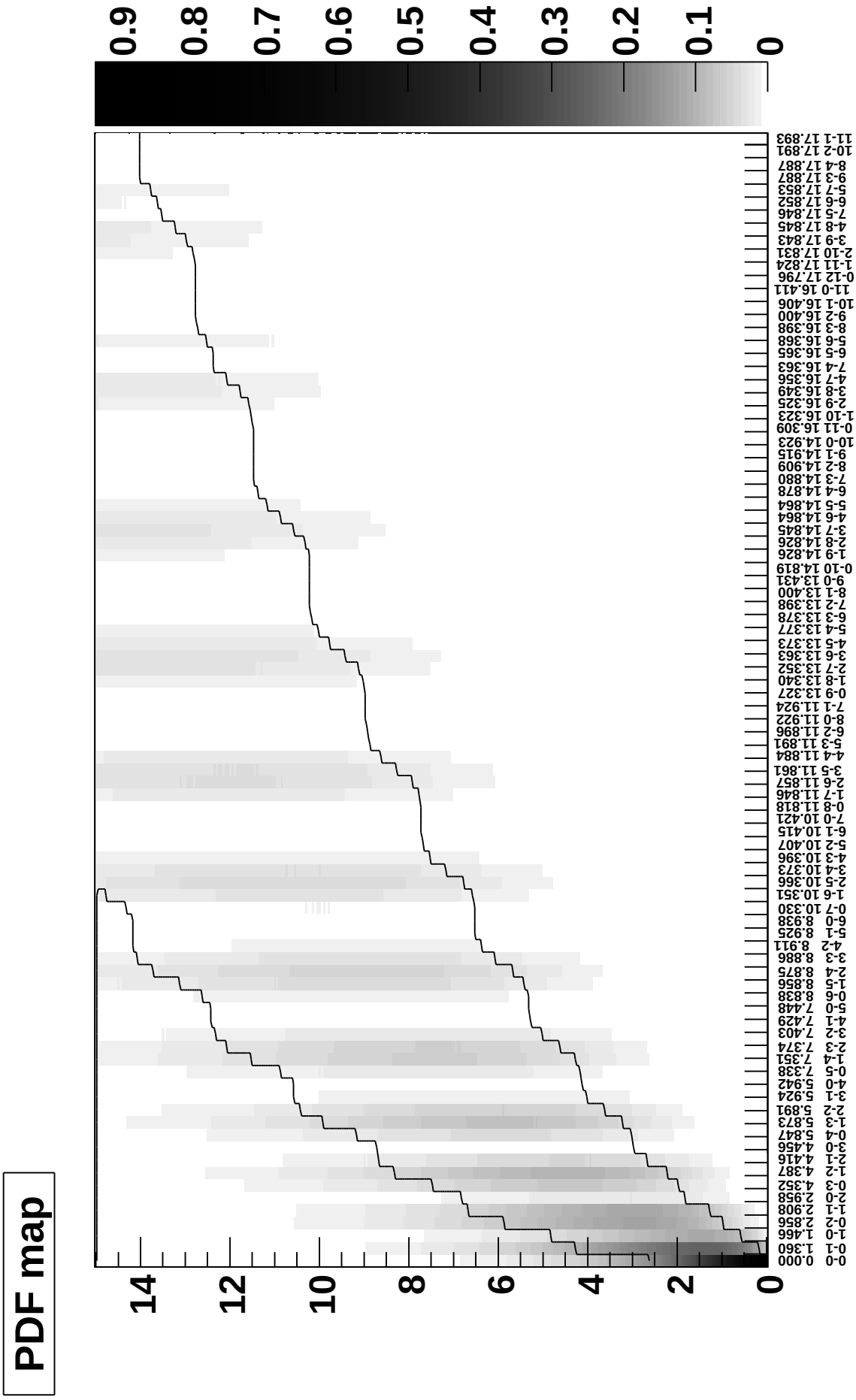

Figure 59: 68% confidence belt of 9597 data.

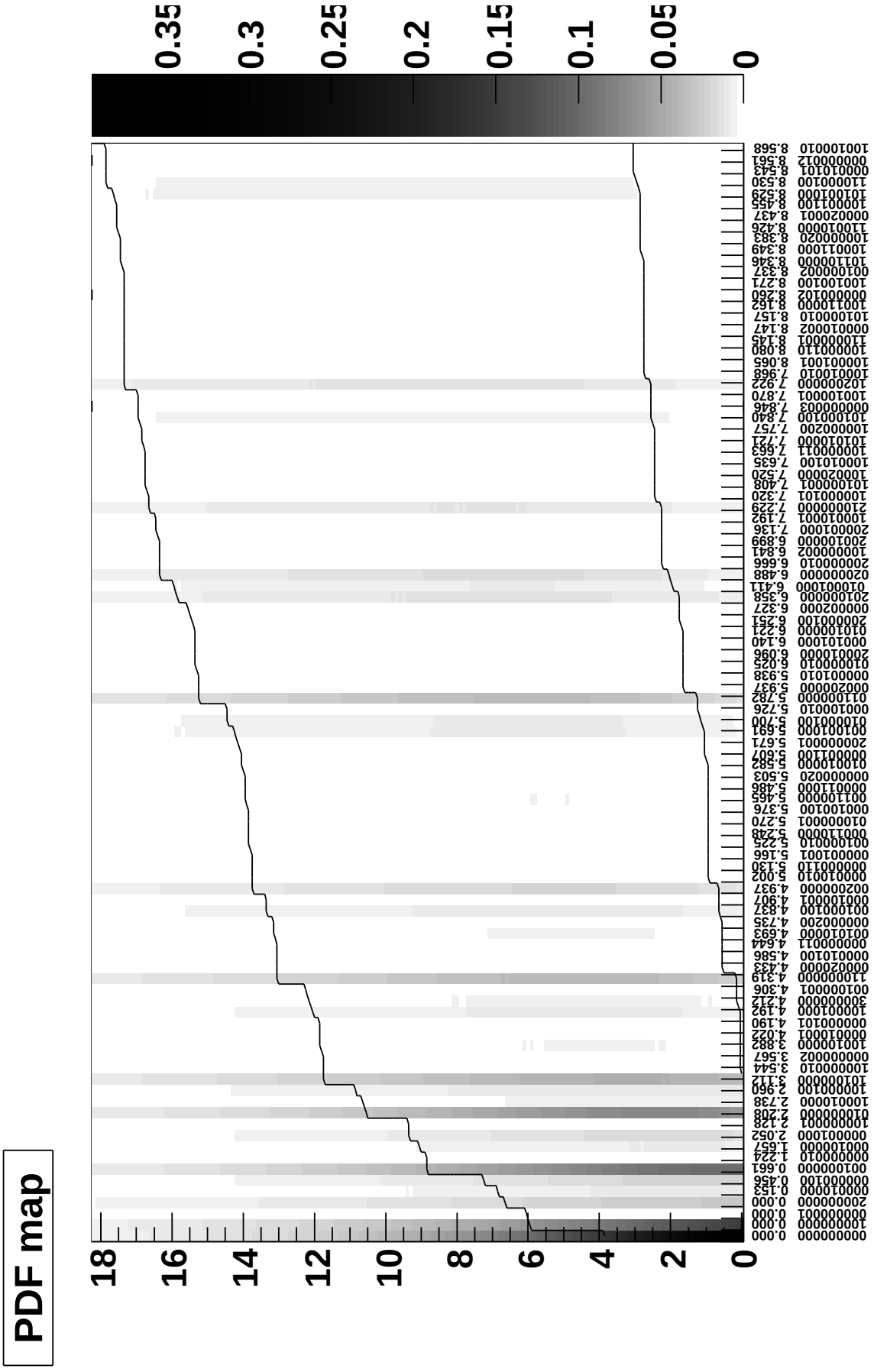

Figure 60: 68% confidence belt of E949 pnn2 data.

15 Signal Candidates

15.1 Candidate summary

There were 3 signal candidates in the PNN2 signal box. The basic information is shown in Table 90.

The decay positron is identified by `EV5_TDC` using TDC information. $N(e^+)$ is the total number of counters within ± 2 sectors of the stopping counter in time with the e^+ candidate. (min,max) layers is the minimum and maximum layer numbers within ± 2 sectors of the stopping counter with e^+ activity.

Additional information is given in Table 91.

15.2 P/E/R reconstruction

Kp2 events' momentum, kinetic energy and range of the run with candidates observed are plotted and fitted in Fig. 61. For run 47876, pnn1, pnn2 and kp21 are used to enhance statistic. For the other two runs only pnn1 and pnn2 triggered events are used. Comparing the result here with Tab. 1 of TN055 (part of it is posted at Tab 92) where the P/E/R resolution is studied for whole E949 sample, nothing suspicious is found. The result of these three runs agrees well with other runs and, along with the information in Table 91, shows that the magnet was on and producing the nominal field.

15.3 Run Dependence

Fig. 62 shows the number of single and double-cut failures along with the plot normalized to KB_{Live}. Figures 63-65 show a ± 60 run range around each candidate. The figures indicate no problems in the signal-candidate runs nor the adjacent runs about the signal-candidate runs. Specifically, run 47876 (Event A) has zero 1-cut failures and 20 2-cut failures with 4.99×10^8 KB_{Live}, run 49352 (Event B) has two 1-cut failures and 221 2-cut failures with 2.29×10^9 KB_{Live}, and run 49787 (Event C) has two 1-cut failures and 173 2-cut failures with 1.98×10^9 KB_{Live}. The runs with signal candidates are very close to the average rate (892 1-cut events; 156252 2-cut events with 1.7×1012 total KB_{Live}) for both the 1-cut and 2-cut run dependences.

	A	B	C
Run #	47876	49352	49787
Event #	76855	217702	87944
Tape #	30230.3.1	30321.3.2	30360.3.2
Spill #	266	927	329
Event # in spill			
Timing in the spill	0.94s	1.51s	0.471s
Collection Date	15 Mar 2002	7 May 2002	21/22 May 2002
Day of Week	Friday	Tuesday	Tuesday
Time of Run start	07:36:00	09:13:55	22:46:36
Time of Run end	08:11:25	10:45:03	00:02:26
Events in Run	100724	238749	203888
Shift takers	Tetsuro	Tetsuro Kentaro	Steve Tamaki
In what Sample	2/3	2/3	2/3
Trigger	pnn2	pnn2	pnn1 &pnn2
Cell info: passes tight cuts	TD,PV	TD,DELCO,BOX	TD, BOX
fails tight PV	-	EC 2^{nd} pulse	EC 2^{nd} pulse
cell number†	9	2	4
Acceptance of cell†	0.188	0.287	0.028
Background in cell†	0.379	0.243	0.027
S/B ($\mathcal{B} = 1.73 \times 10^{-10}$)†	0.20	0.47	0.42
π^+ RS $T \cdot 2$ sector	19	12	16
π^+ RS stopping sector	19	11	15
π^+ RS stopping layer	8	8	11
Kaon time in TG (*tk*)	-0.147	-0.147	0.557
π^+ time in TG (*tpi*)	3.55	15.59	5.70
π^+ time in IC *ictime*	4.09	15.81	5.81
π^+ time in RS (*trs*)	4.83	16.95	6.49
π^+ lifetime	22.4	16.7	10.2
μ^+ energy	3.43	3.37	2.90
μ^+ lifetime	5959.4	2270.6	9507.8
$N(e^+)$ (min,max) layers	5 (5,8)	3 (8,10)	4 (9,11)
Total π^+ momentum (*ptot*)	161.46	188.40	191.30
Total π^+ range (*rtot*)	17.29	24.16	26.10
Total π^+ kinetic energy (*etot*)	76.07	95.57	97.94
Kaon energy in TG (*ek*)	132.48	101.94	89.87
π^+ energy in TG (*etg*)	4.11	14.27	6.45
π^+ range in TG (*rtg*)	2.05	4.87	2.76
cos3d of π^+ track	0.1887	-0.2219	-0.1339
phi0 of π^+ track	-0.8713	-2.8515	-2.0387
Kaon Decay Vertex (x,y,z)	(-1., -4.73)	(2.21,-4.51)	(0.53,-3.88)
Kaon Decay Vertex z	9.36	3.46	2.91
Range-momentum	0.32275	-0.22109	0.80481

Table 90: Signal event summary. Times are in *ns*, distances are in *cm*, and energy is in *MeV* unless otherwise denoted. † = see Table 87 for details. See text for further details.

	A	B	C
Run #	47876	49352	49787
Event #	76855	217702	87944
Tape #	30230.3.1	30321.3.2	30360.3.2
Spill #	266	927	329
D03 current(Dibbuk)	3544	3543	3544
QOD Bfield	9.875kG	none	none
Xe Bfield	1968.99 ± 0.26	1966.03 ± 0.22	1967.95 ± 0.31
Trigger	smx_v12u	smx_v15	smx_v15
ssp namelist	all_v5.cfg	all_v7.cfg	all_v7.cfg
andor file	33300333	33300333	33300333
dwf file	.dwf.020301	.dwf.020419	.dwf.020419
pnn1 RR files	v7_prompt.tt.rr1	v7_prompt.tt.rr1	v7_prompt.tt.rr1
pnn2 RR files	notgt15.tt.rr2	notgt15.tt.rr2	notgt15.tt.rr2
online HEX files	v1.tt.hex	v1.tt.hex	v1.tt.hex

Table 91: Additional information concerning the signal candidates. QOD and Xe_mon both read the Bfield from the same scanning ADC that we use for offline analysis. Both of these programs integrate for a run or longer. (It is not clear why there were no QOD files to read for the last two events. For the first run QOD was read from the file for Run 47862). The Dibbuk reading of the shunt current is in "counts". The Xe Bfield units are scanning ADC counts. In "andor" the 3 indicates that L1.1 and L1.2 were enabled for triggers 1-3 and 6-8. The dwf file contains delays and widths for ADC gates, TDC starts, etc. The files downloaded for the pnn1 refined range, the pnn2 refined range and the online HEX cut are also listed.

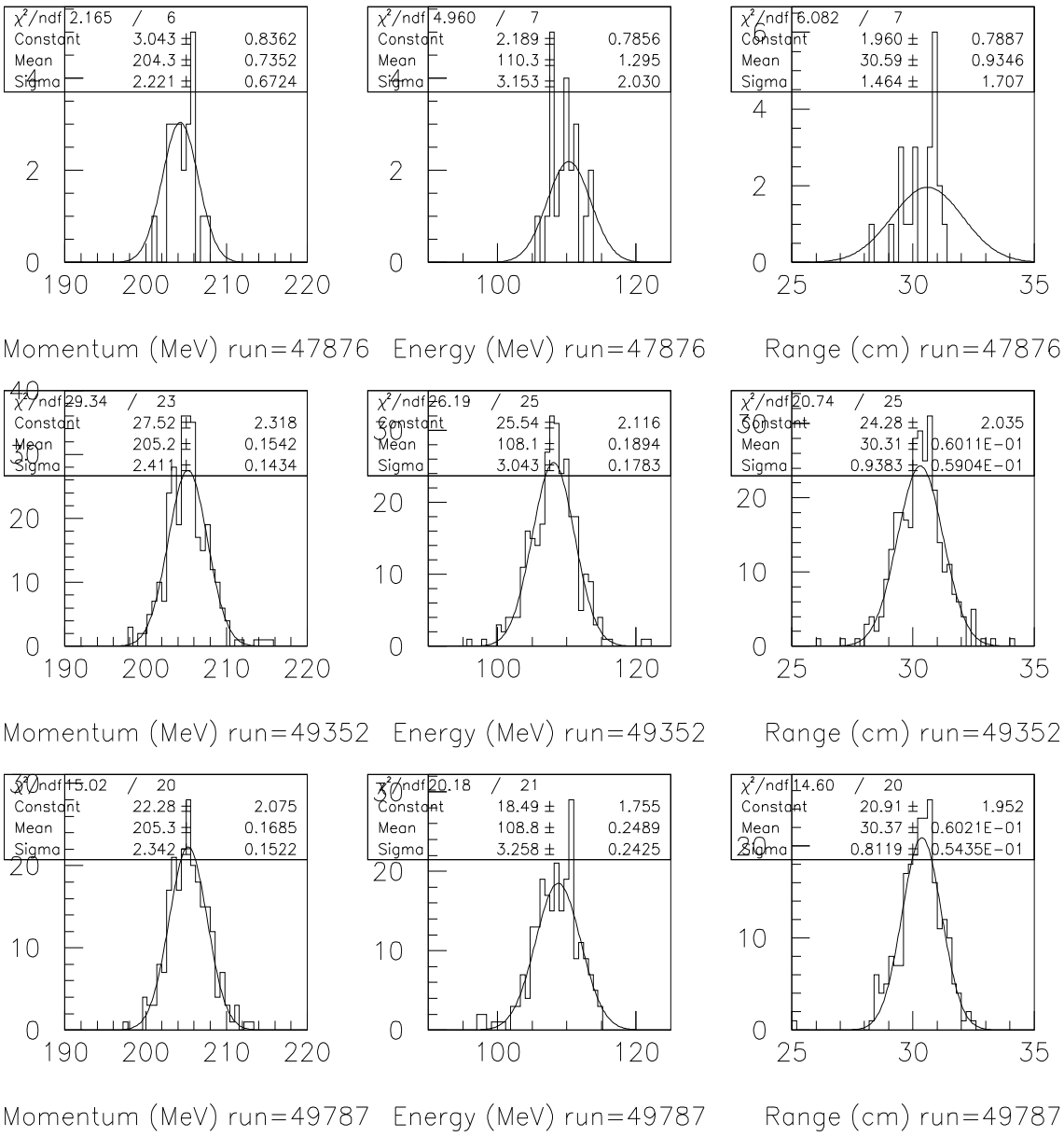

Figure 61: Momentum, kinetic energy and range distributions for kp2 events in the candidate runs.

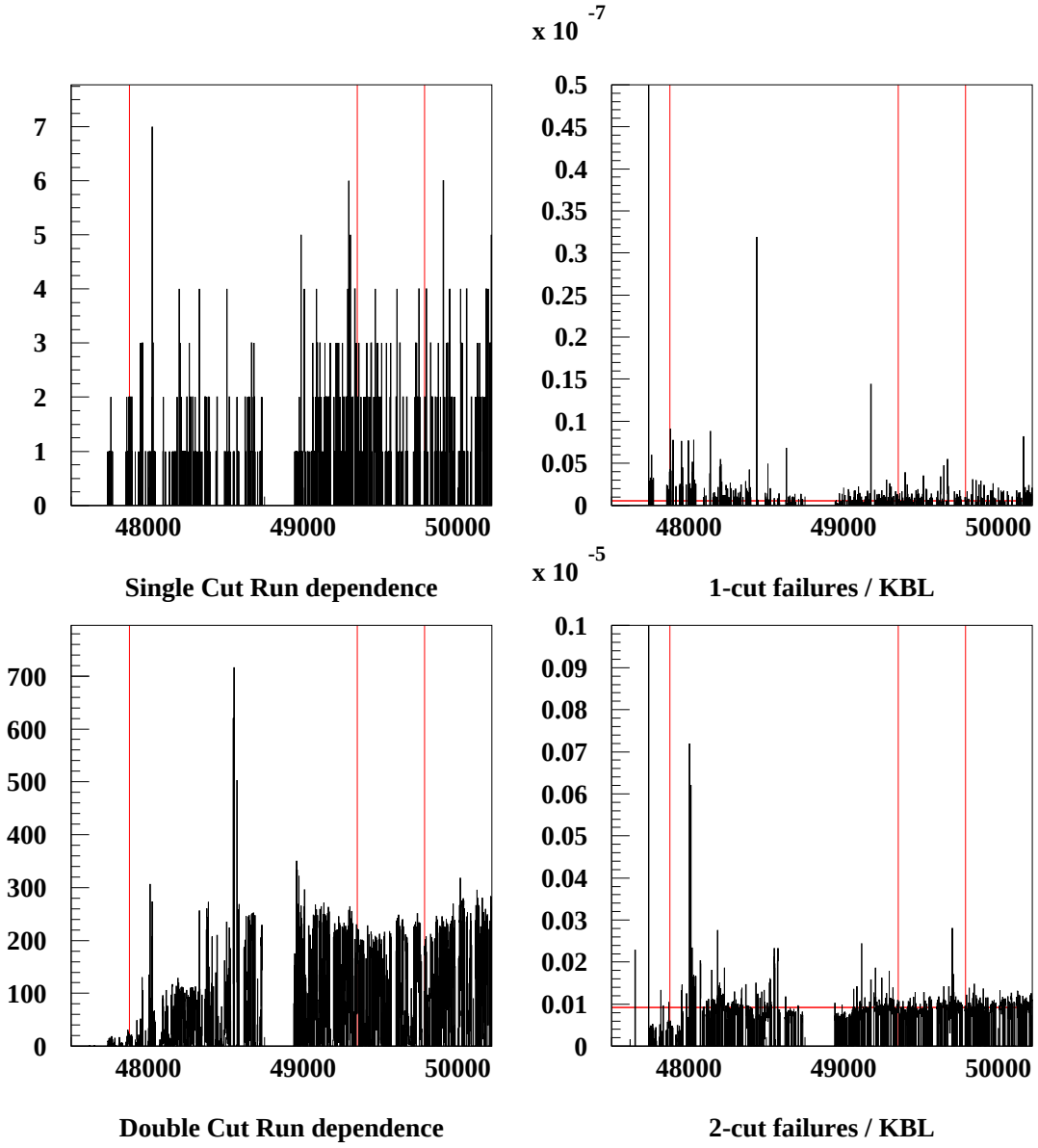

Figure 62: **Run Dependence** of single and double-cut failures (left column) and 1 and 2-cut failures / KB_{Live} (right). Bin size is one run; the vertical red line indicates a run with a signal candidate, and the horizontal red line is the global average.

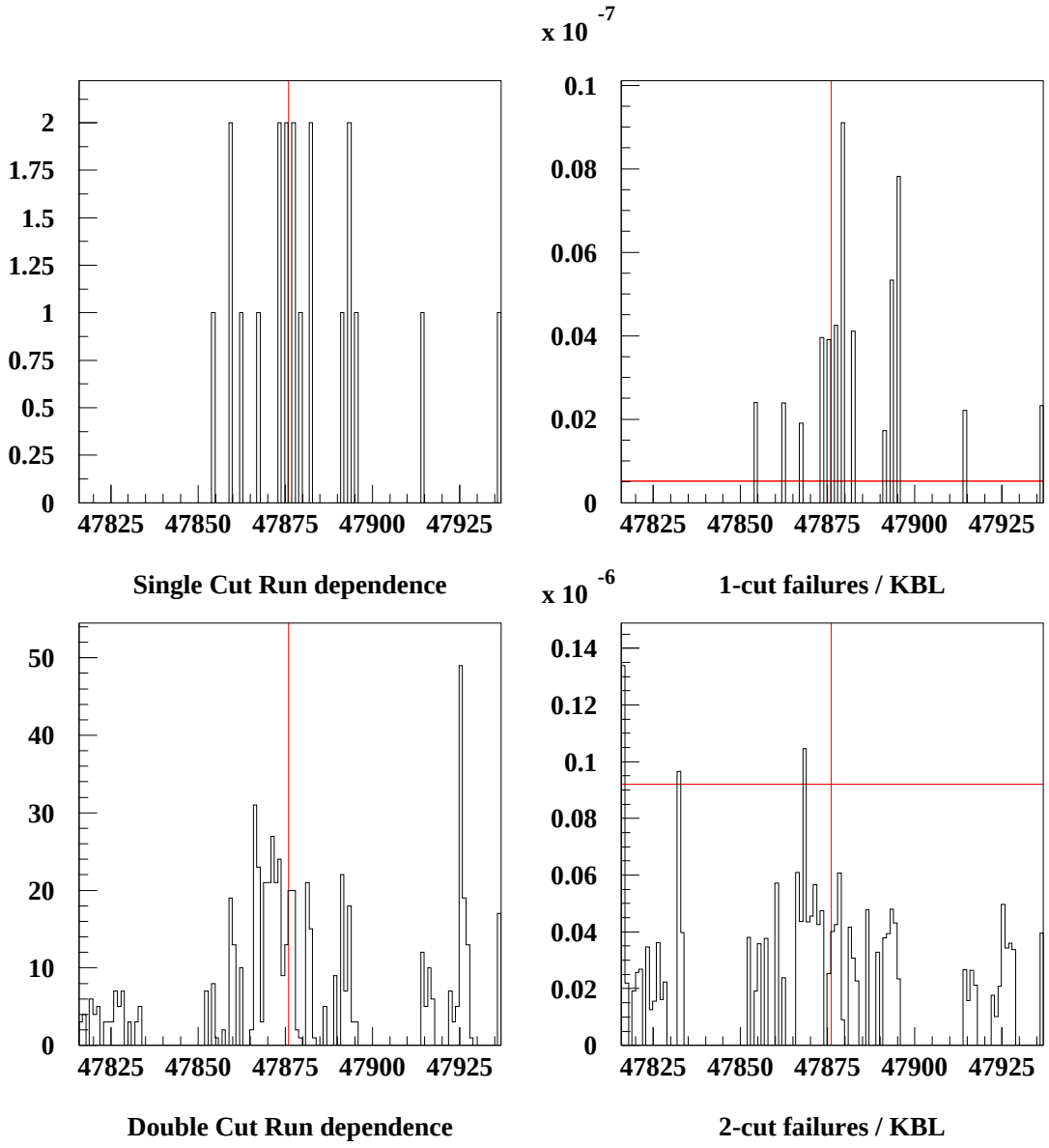

Figure 63: **Run Dependence**, around event A, of single and double-cut failures (left column) and 1 and 2-cut failures / KB_{Live} (right). Bin size is one run; the vertical red line indicates a run with a signal candidate, and the horizontal red line is the global average.

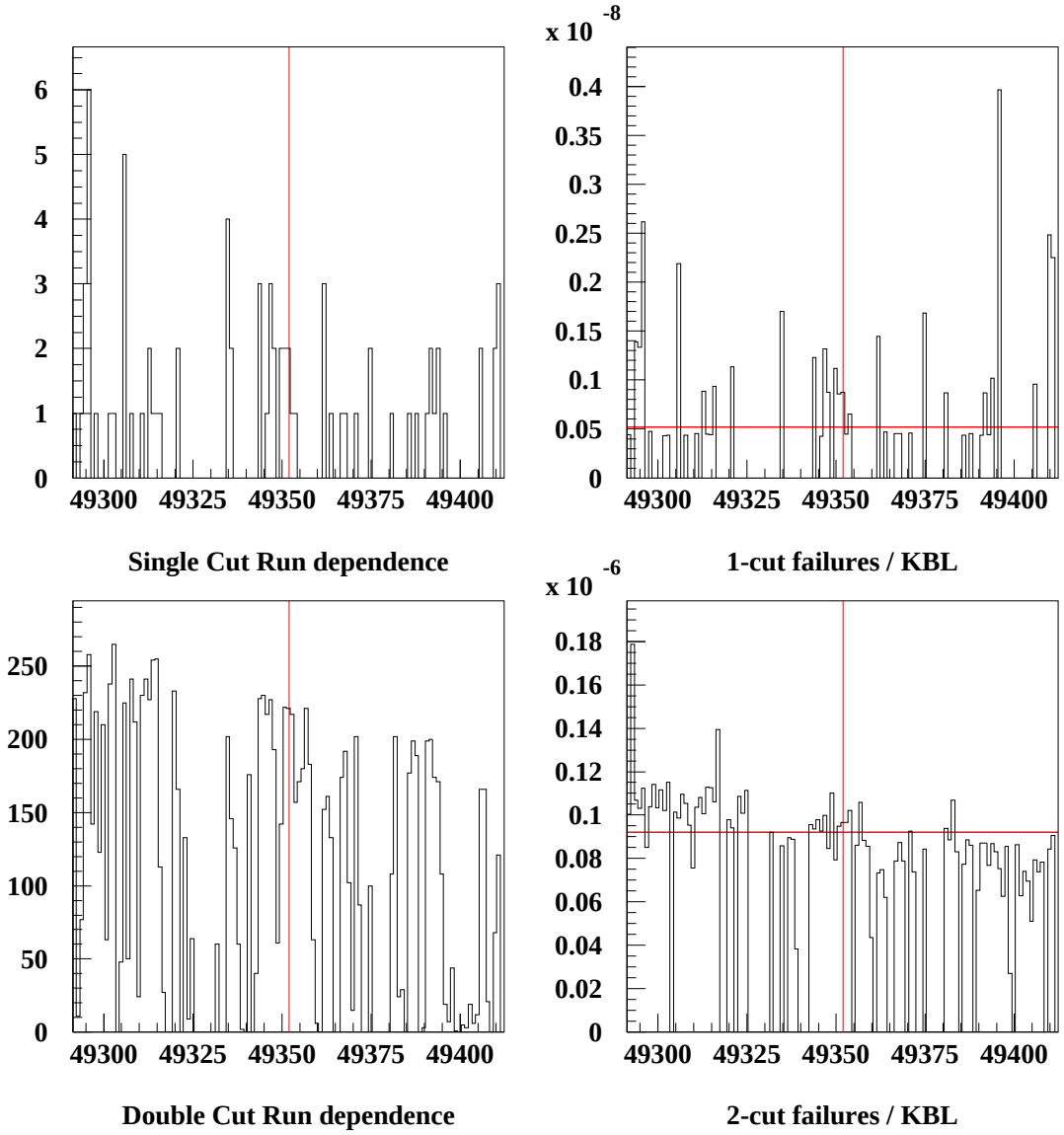

Figure 64: **Run Dependence**, around event B, of single and double-cut failures (left column) and 1 and 2-cut failures / KB_{Live} (right). Bin size is one run; the vertical red line indicates a run with a signal candidate, and the horizontal red line is the global average.

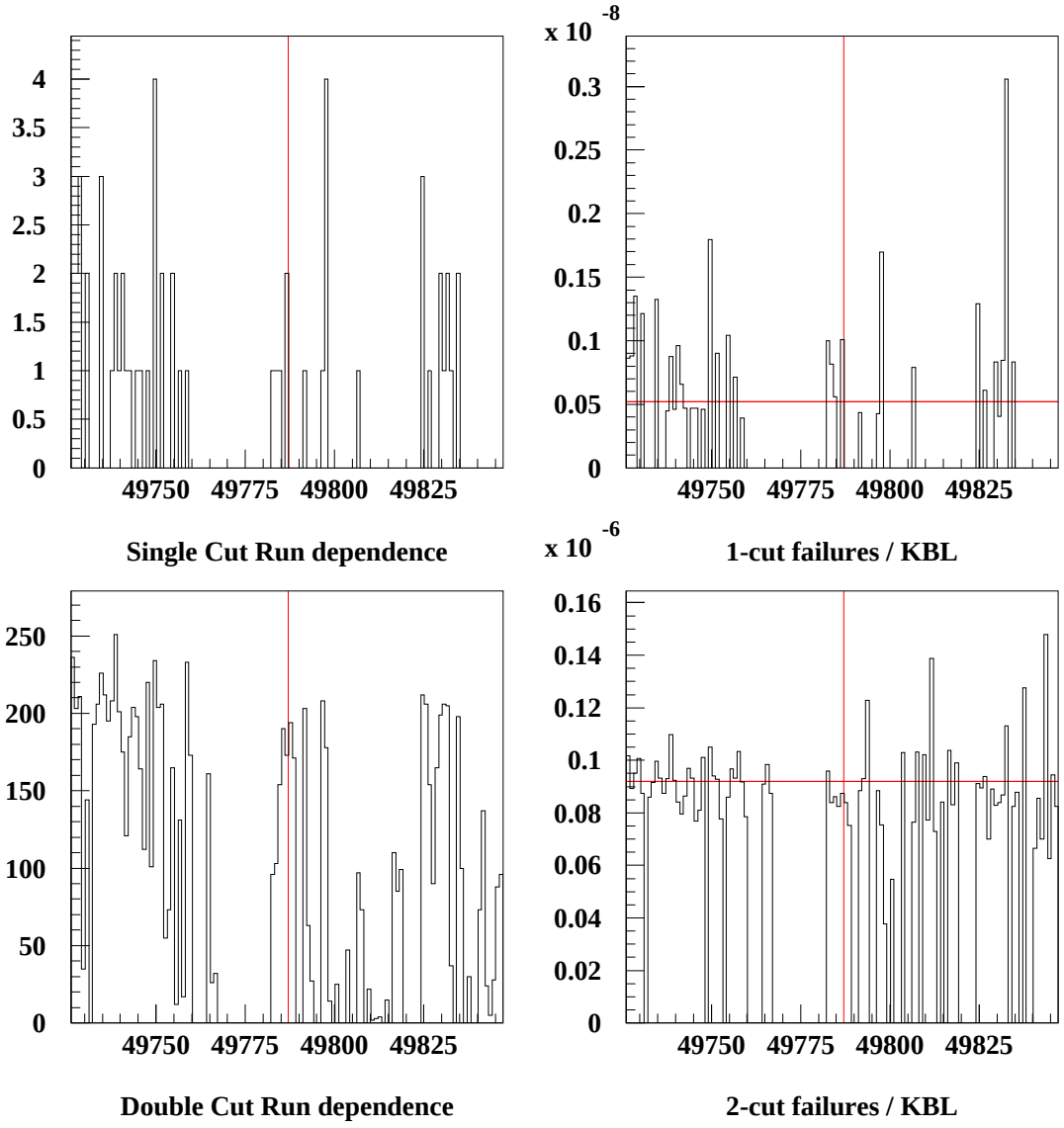

Figure 65: **Run Dependence**, around event C, of single and double-cut failures (left column) and 1 and 2-cut failures / KB_{Live} (right). Bin size is one run; the vertical red line indicates a run with a signal candidate, and the horizontal red line is the global average.

ptot (MeV)	$204.94 \pm 0.02 \pm 0.02$
σ_{ptot}	$2.29 \pm 0.01^{0.0}_{0.04}$
etot (MeV)	$108.77 \pm 0.01 \pm 0.01$
σ_{etot}	$3.03 \pm 0.02 \pm 0.02$
rtot (cm)	$30.254 \pm 0.004 \pm 0.010$
σ_{rtot}	$0.901 \pm 0.005 \pm 0.002$

Table 92: P/E/R measurement for all E949 sample from Tab. 1 of TN055

Candidate	Position (o'clock)	Time wrt `trs` (ns)
A	10	-80 ± 20
B	3	0 ± 100
B	4	-120 ± 20
B	7	0 ± 80
B	11	$+50 \pm 20$
C	4	$+80 \pm 20$

Table 93: The estimate track times of the tracks visible in the upper right displays of Figures 66, 72 and 77. This analysis was provided by Toshio.

15.4 Candidate A

15.4.1 Electric Logs

- Fri Mar 15 07:36:00 2002

  "Starting run 47876 trig=smx_v12u ssp=all_v5.cfg to 3 tapes 30230"

- Fri Mar 15 08:06:57 2002 : Shift Summary

  "between 6:55 - 7:05 DAQ problem" otherwise everything was good.

- Fri Mar 15 08:11:25 2002

  "Stopping run 47876 with 100724 events; DUI: exceeded event limit"

15.4.2 Event displays

The paw photo event displays for Candidate A are shown in Figures 66-70. A description of how to interpret the paw photo event displays is given in Section 13.3.

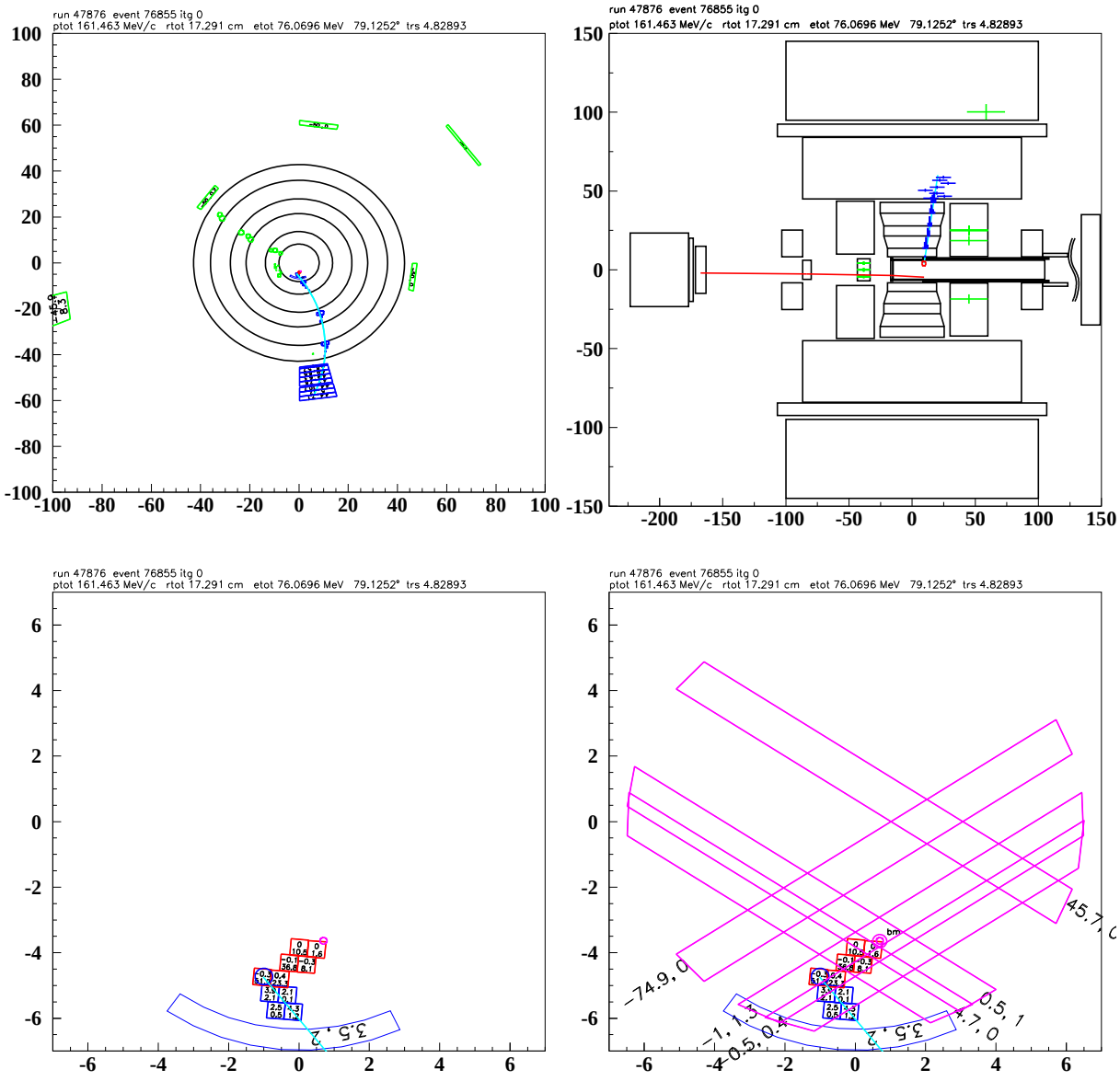

Figure 66: Clockwise from upper left: XY-view, Z-view, target XY-view with B4 information superimposed, target XY-view. Results of Toshio's analysis of the timing of tracks visible in the UTC XY-view are given in Table 93. This is for candidate A.

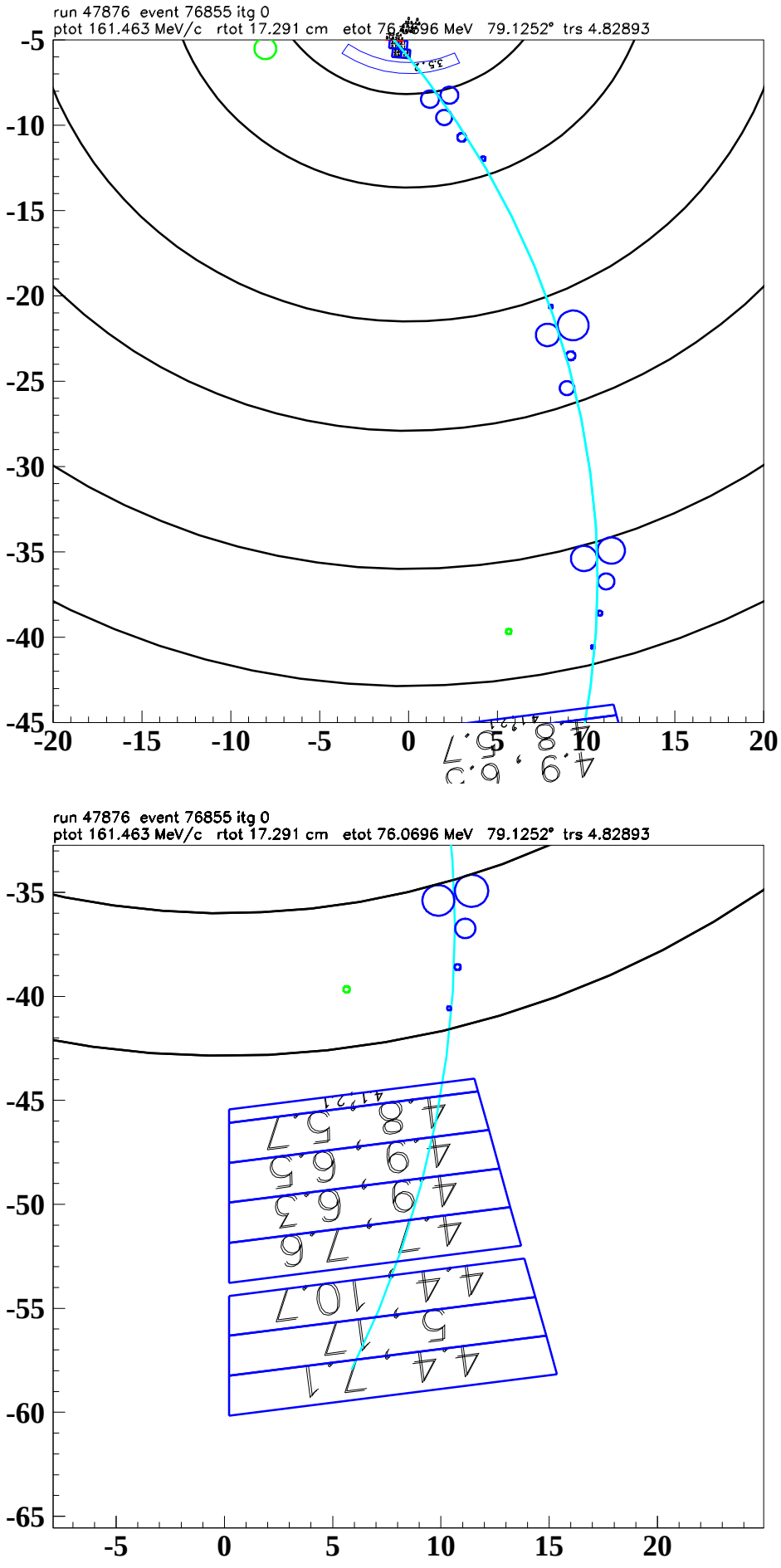

Figure 67: **Candidate A**. UTC and RS views.

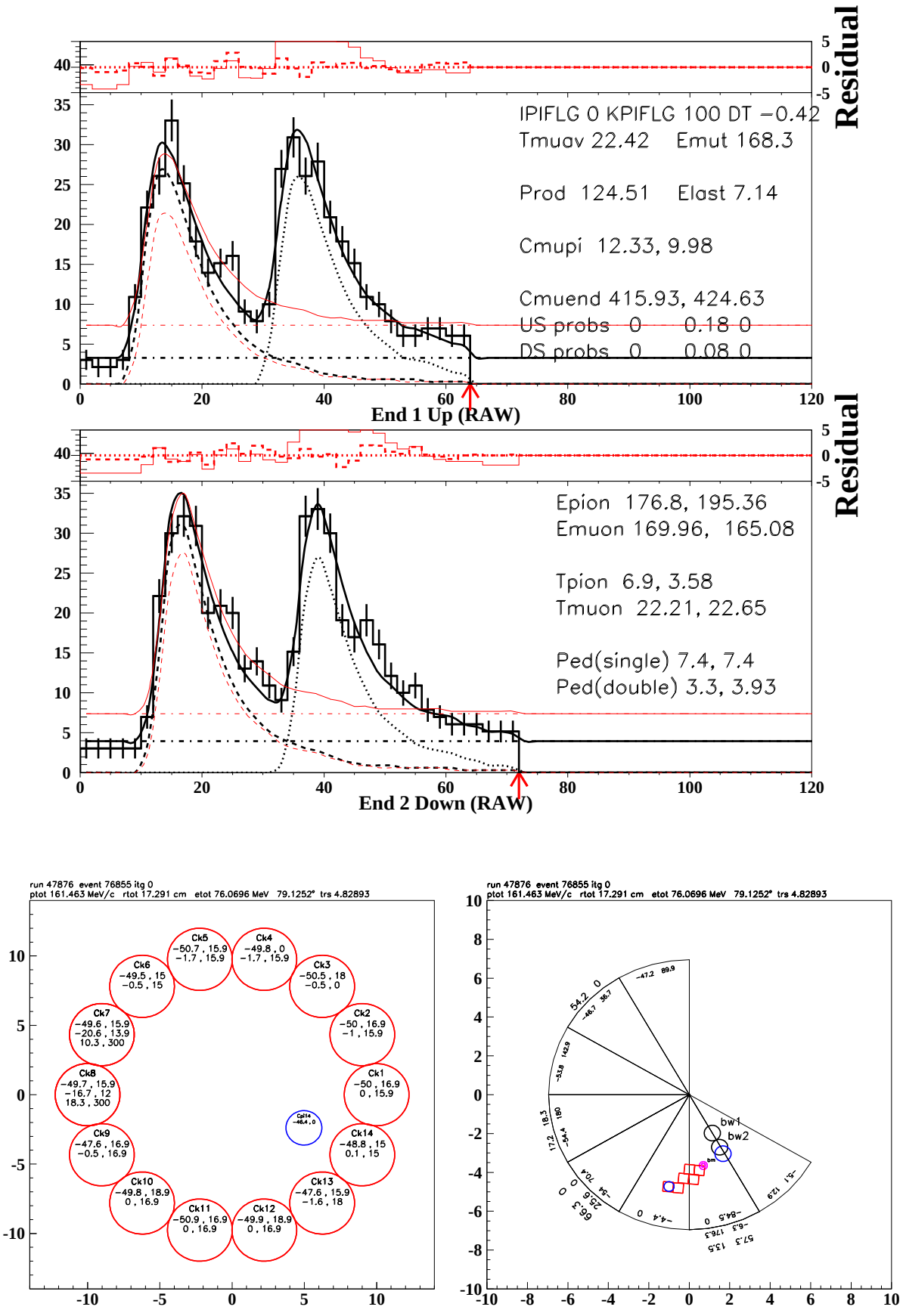

Figure 68: Top: TD display. Lower left: Cerenkov. Lower right: AD display with kaon target fibers and wire chamber positions. This is for Candidate A.

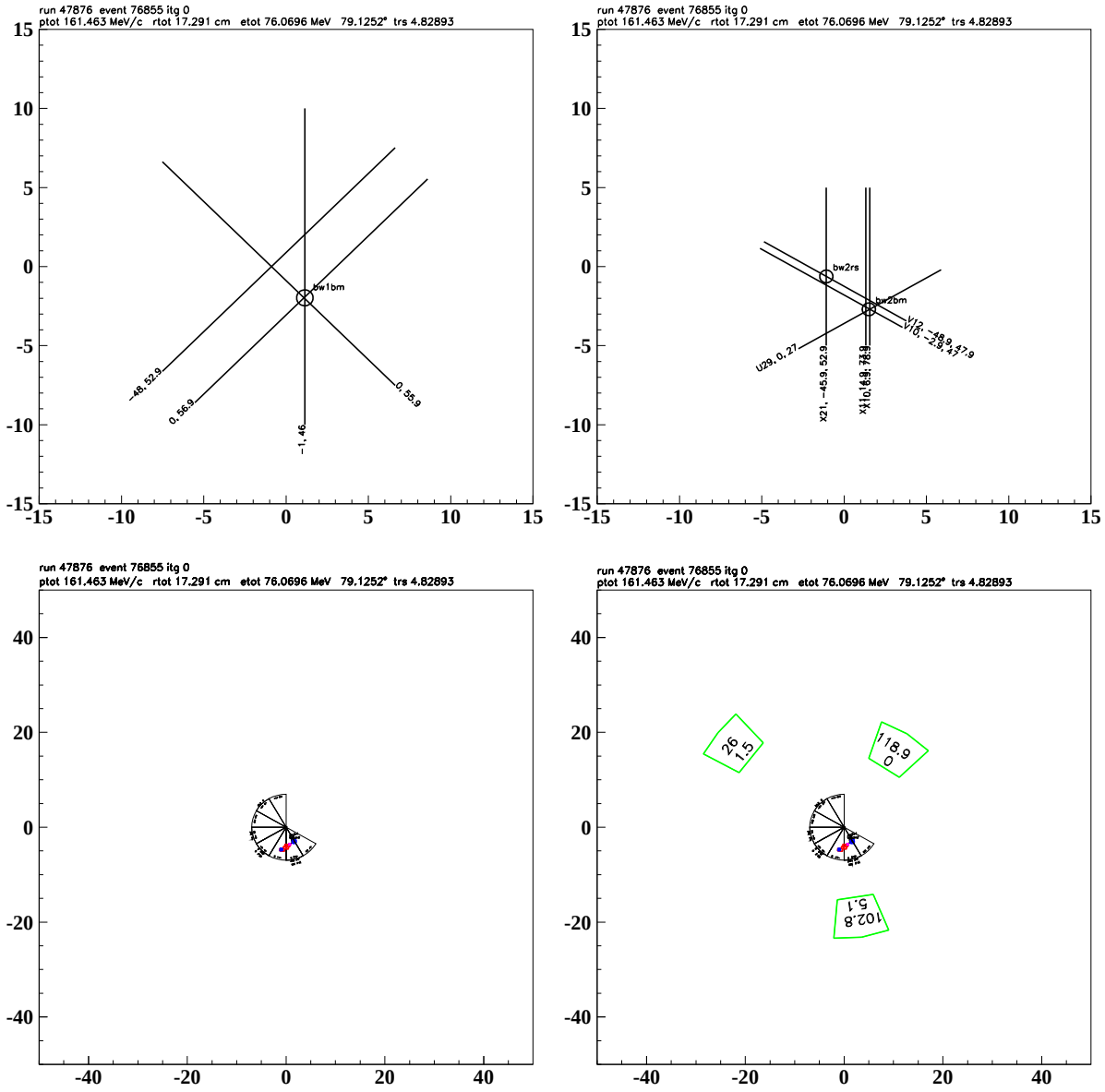

Figure 69: Top left: BW1. Top right: BW2. Lower left: Upstream EC with AD display. Lower right: Downstream EC with AD display. This is for Candidate A.

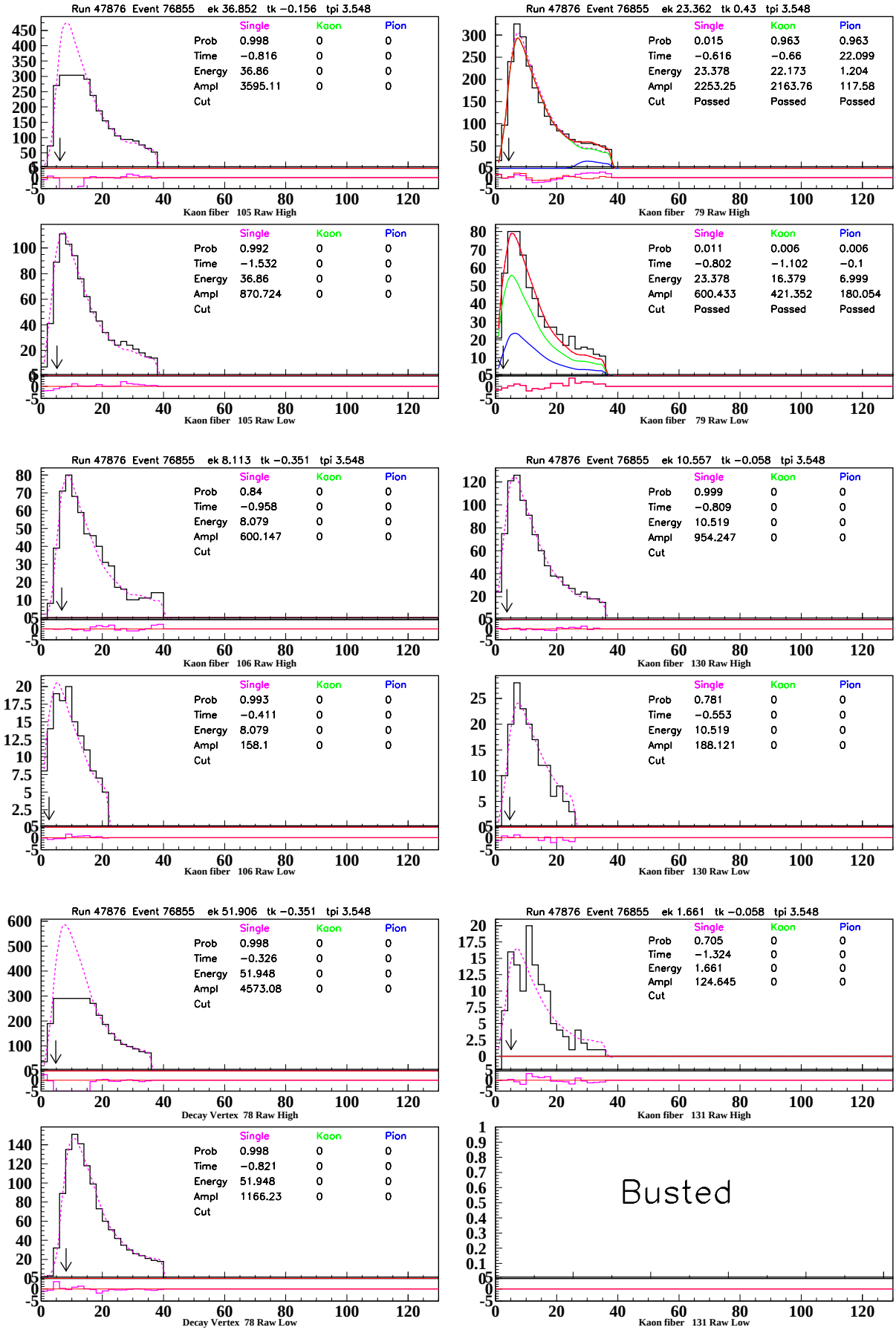

Figure 70: CCD plots for all kaon fibers. This is for Candidate A.

15.5 Candidate B

15.5.1 Electric Logs

- Tue May 7 09:13:55 2002

  "Starting run 49352 trig=smx_v15 ssp=all_v7.cfg to 3 tapes 30321"

- Tue May 7 09:37:57 2002

  Monitor backup

- Tue May 7 10:45:03 2002

  "Stopping run 49352 with 238749 events; DUI: exceeded disk file limit"

- Tue May 7 12:20:57 2002 : Shift Summary

  We had a momentary glitch in writing the tape on drive 2 (Tue May 7 11:34:41 2002); Dick recycled the power on drive 0 to test it, maybe it cause this failure.)

  Tue May 7 11:53:46 2002: "RSSC #5 tripped"

15.5.2 Event displays

The paw photo event displays for Candidate B are shown in Figures 72-76. A description of how to interpret the paw photo event displays is given in Section 13.3.

One issue under investigation is the evidence for an early kaon at ~ -12 ns in the Cerenkov display (Figure 74) and the 3-wire intersection in BW1 labelled "bw1trs" in Figure 75. There is also a hit in the UPV at -11.9 ns. As there is no other evidence in the detector of this early kaon, it is possible that the kaon was scattered in the UPV and entered the magnet.

We are examining the raw Cerenkov CCD information to confirm the entrance of a second kaon that gave rise to the BW1, BW2, B4 and target hits near t=0 that apparently decayed at $t_{\rm RS} = 16.95$ ns.

It is extremely unlikely that the early kaon underwent a charge exchange interaction and gave rise to the pion track in the target because of the large delay of $\sim$29 ns between the early kaon and the pion track (Figure 72, the excellent agreement of the pion track and the kaon decay fiber and the agreement of the B4 and target energy and `tgz` with that expected for a decaying, stopped kaon as shown in Figure 71.

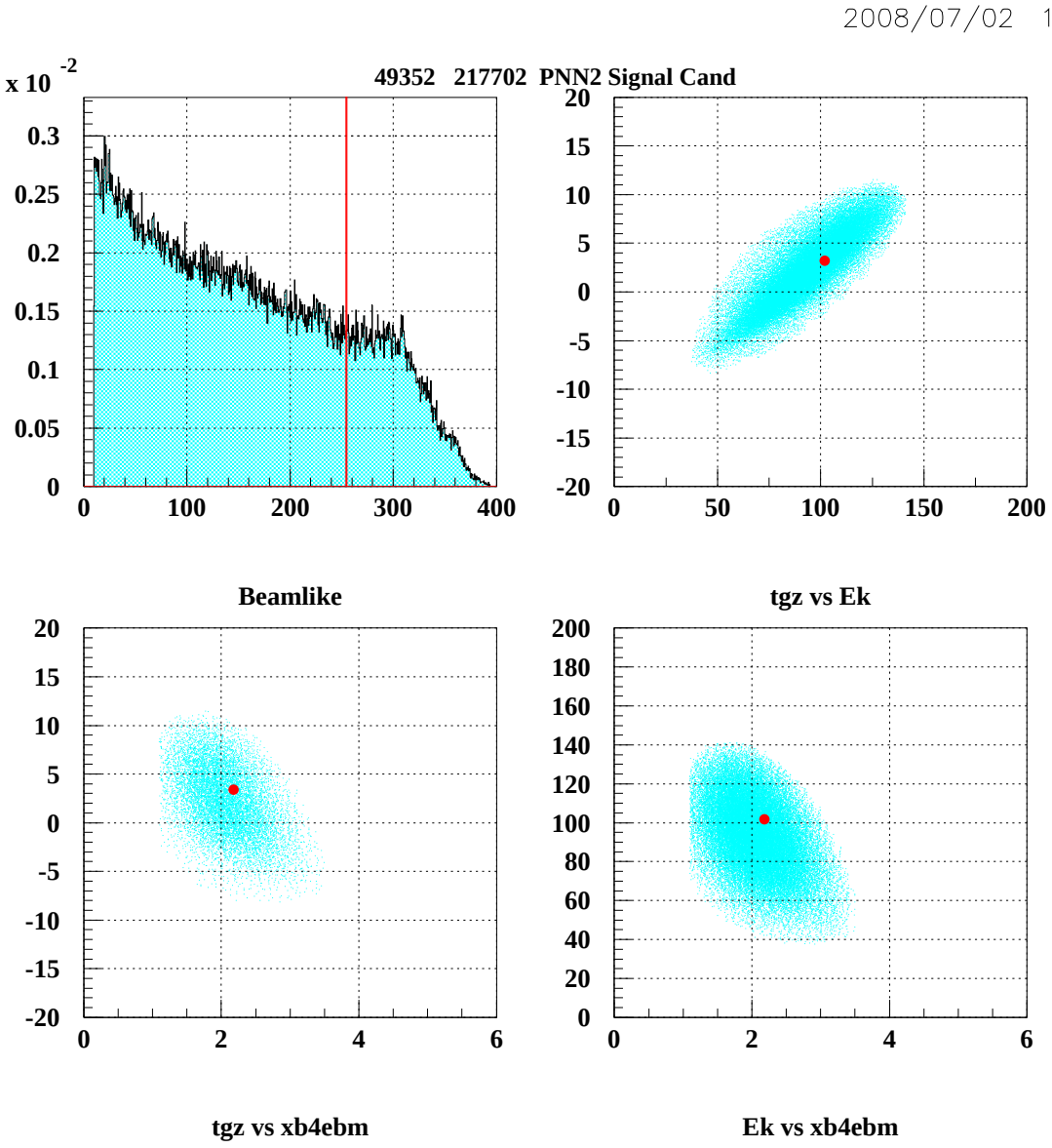

Figure 71: The beam likelihood, `tgz` and energy in B4 and the target for the candidate B (red line or point) and the reference distributions.

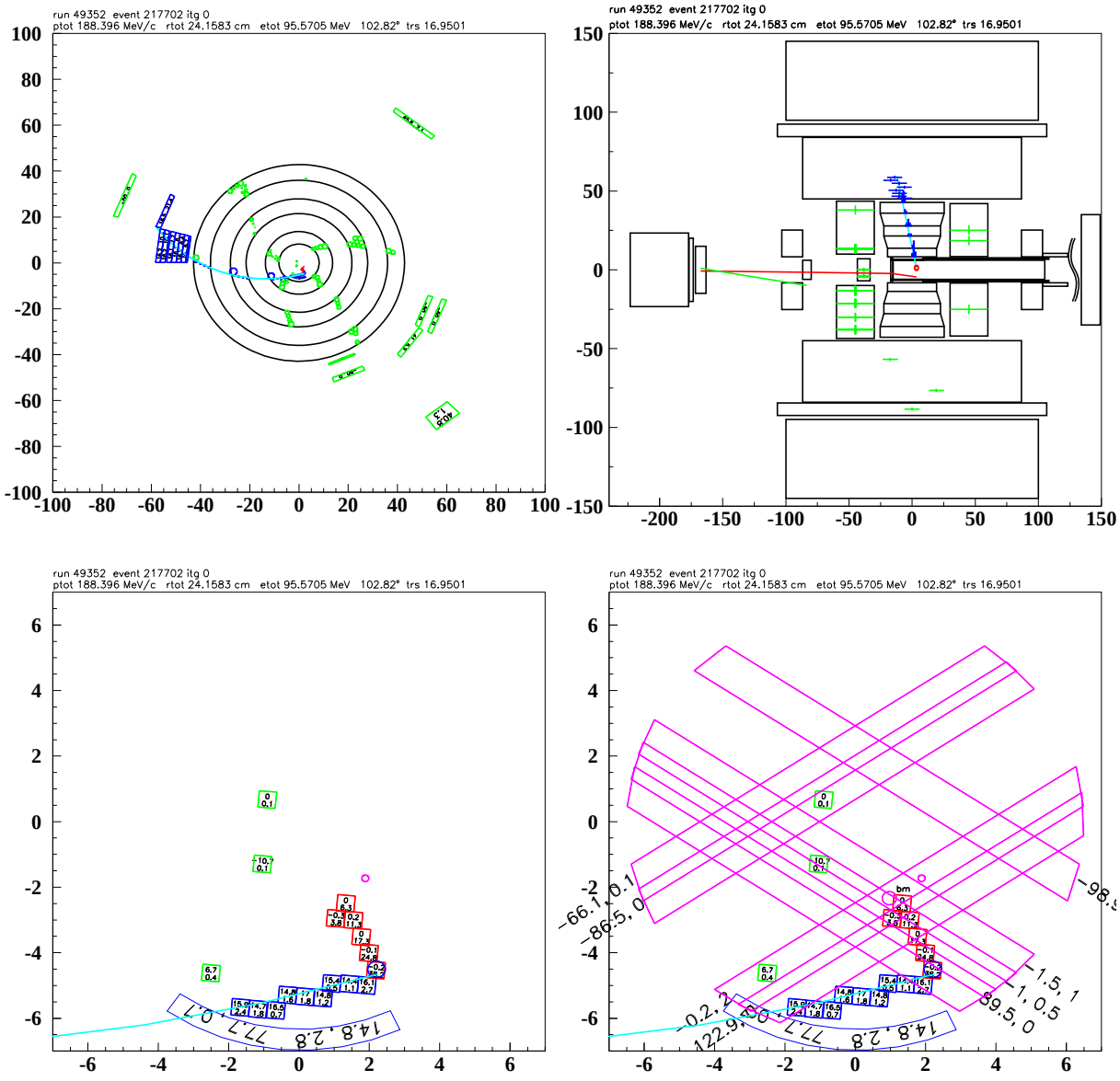

Figure 72: Clockwise from upper left: XY-view, Z-view, target XY-view with B4 information superimposed, target XY-view. Results of Toshio's analysis of the timing of tracks visible in the UTC XY-view are given in Table 93. This is for candidate B.

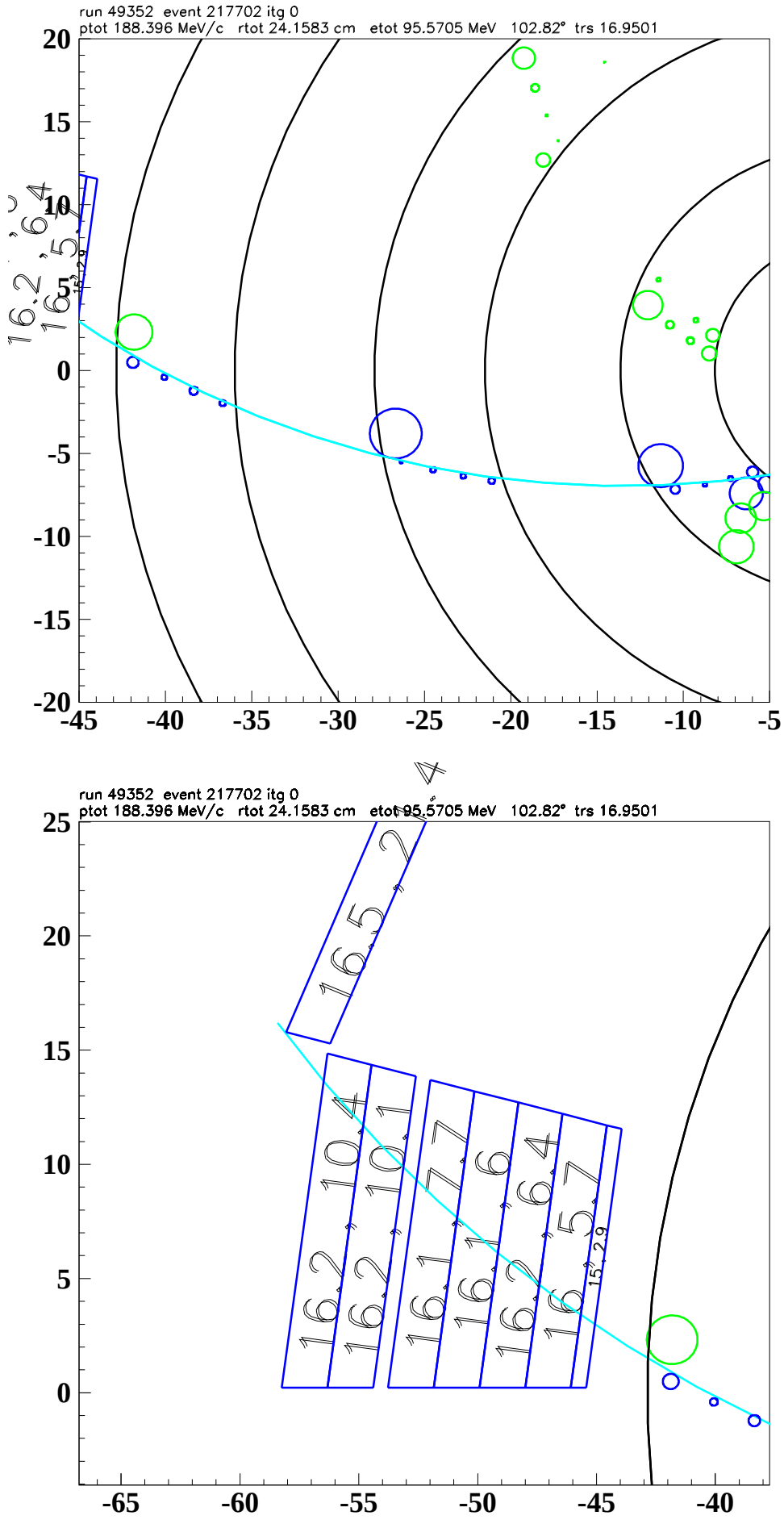

Figure 73: **Candidate B**. UTC and RS views.

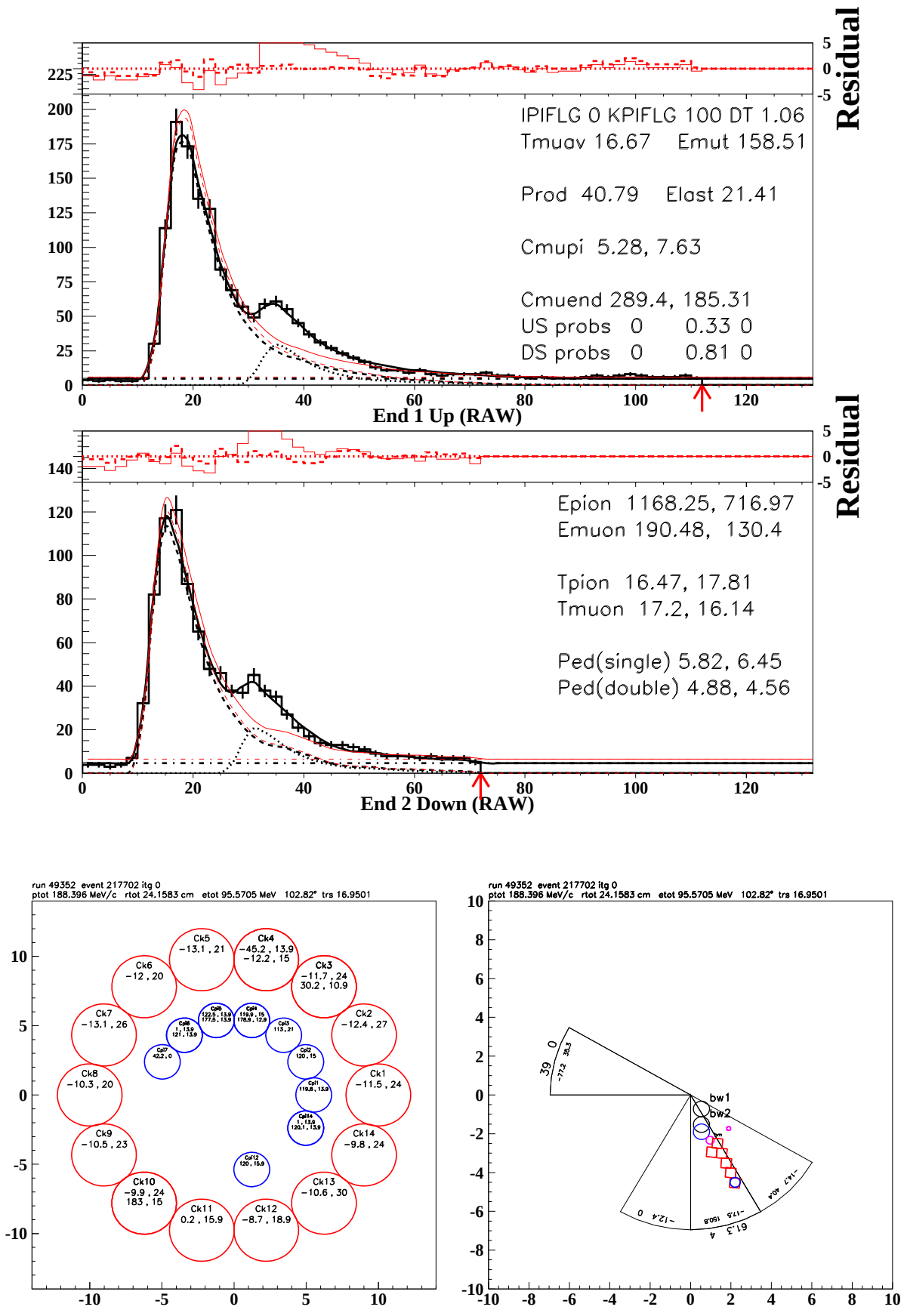

Figure 74: Top: TD display. Lower left: Cerenkov. Lower right: AD display with kaon target fibers and wire chamber positions. This is for Candidate B.

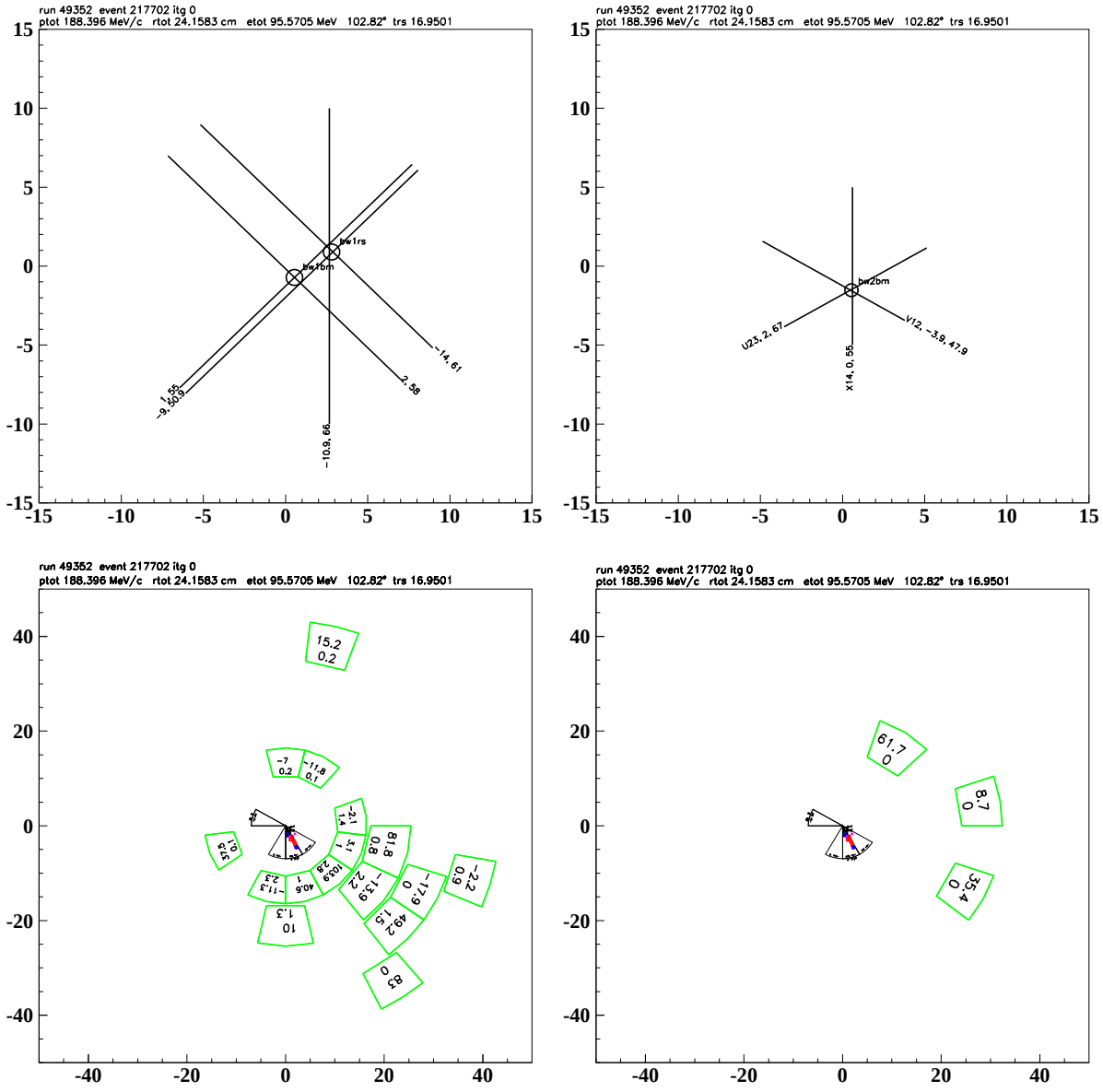

Figure 75: Top left: BW1. Top right: BW2. Lower left: Upstream EC with AD display. Lower right: Downstream EC with AD display. This is for Candidate B.

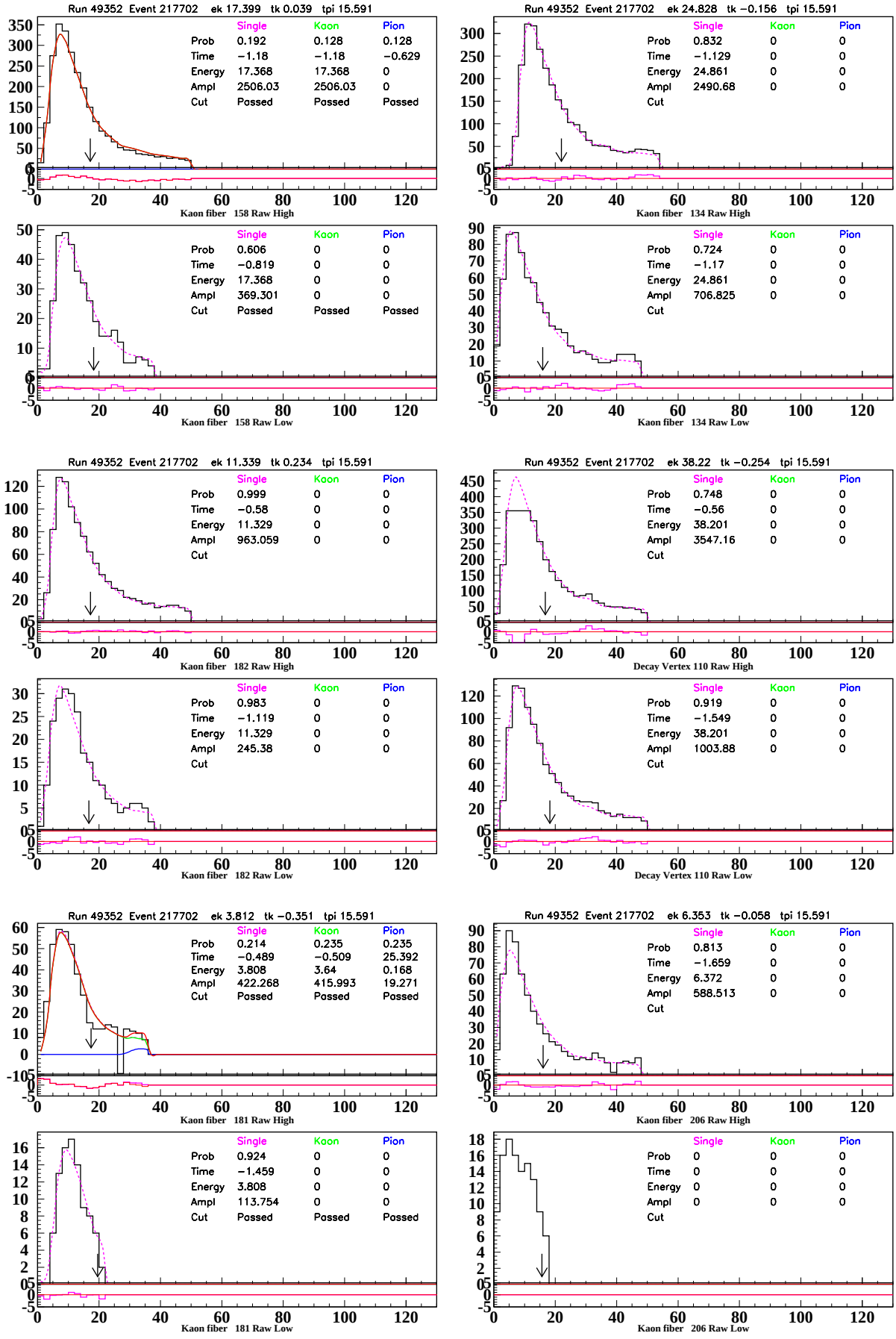

Figure 76: CCD plots for all kaon fibers. This is for Candidate B.

15.6 Candidate C

Candidate C is in run 49787 and event 87944.

15.6.1 Electronic Logs

There was an incident with the Separator during the run.

- Tue May 21 22:46:36 2002

  "Starting run 49787 trig=smx_v15 ssp=all_v7.cfg to 3 tapes 30360"

- Tue May 21 22:51:36 2002 by Steve Kettell

  "Sep #2 both plate tripped to zero. Paused the run."

- Tue May 21 23:22:06 2002 a Beam/DAQ Status report was issued

  "... Sep#1 (+150 kV -100 kV) Sep#2 (+259 kV -261 kV)."

  "Ck = 13.4M, Cpi =5.6M ... K/pi = 2.5"

- Wed May 22 00:02:26 2002

- "Stopping run 49787 with 203888 events; DUI: di has halted data taking unexpectedly"

15.6.2 Event displays

The paw photo event displays for Candidate C are shown in Figures 77-81. A description of how to interpret the paw photo event displays is given in Section 13.3.

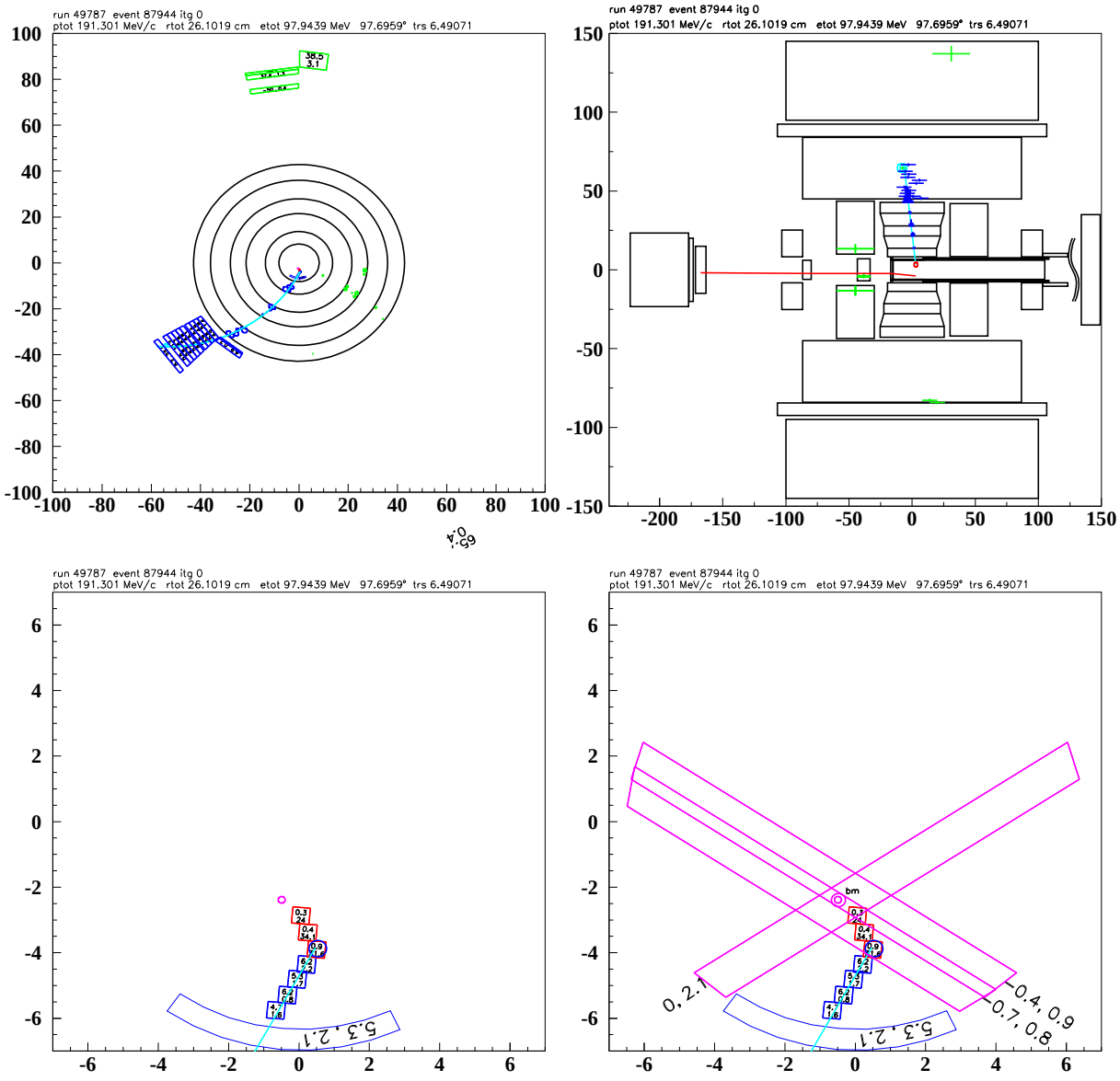

Figure 77: Clockwise from upper left: XY-view, Z-view, target XY-view with B4 information superimposed, target XY-view. Results of Toshio's analysis of the timing of tracks visible in the UTC XY-view are given in Table 93. This is for candidate C.

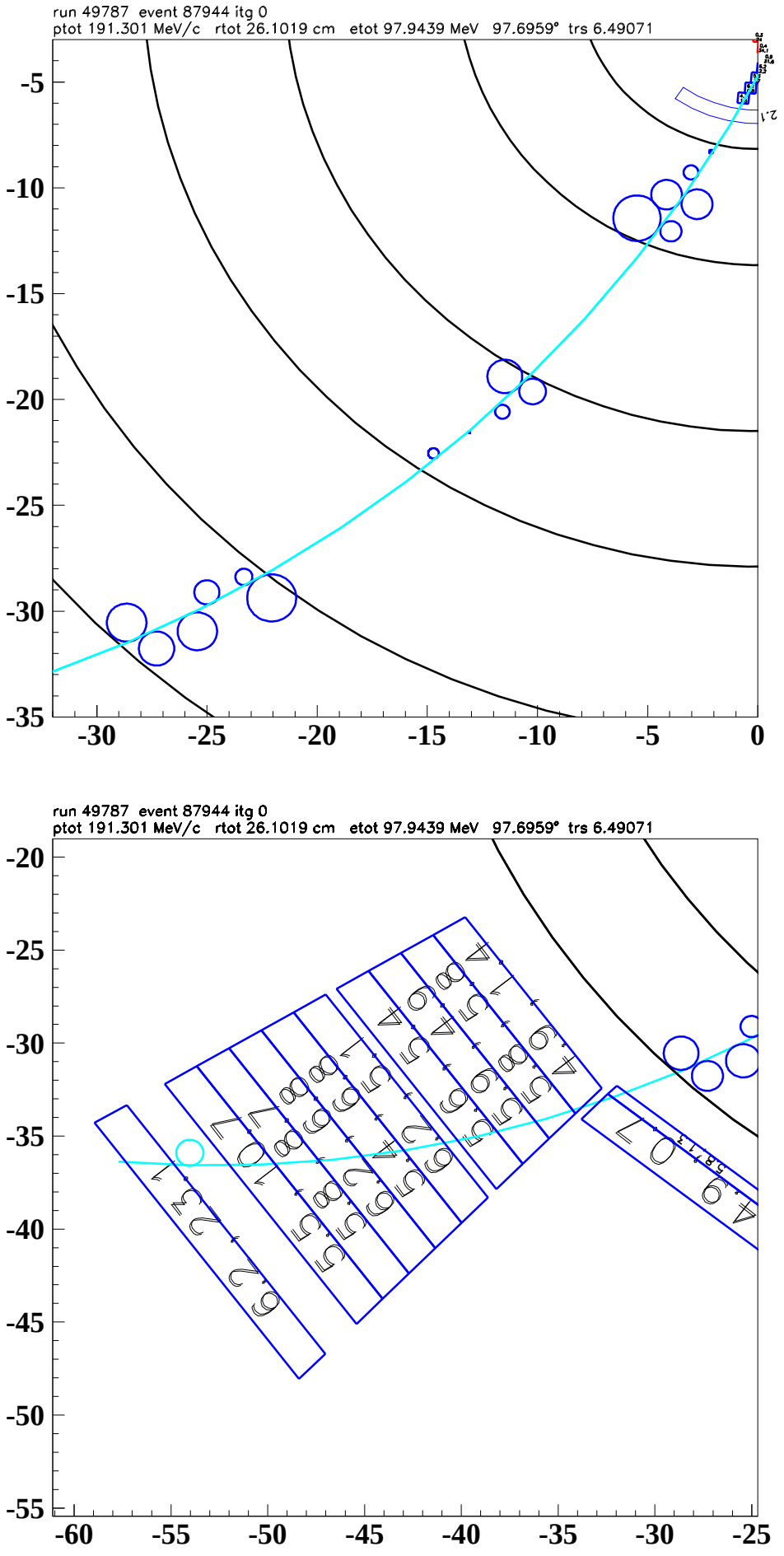

Figure 78: **Candidate C**. UTC and RS views.

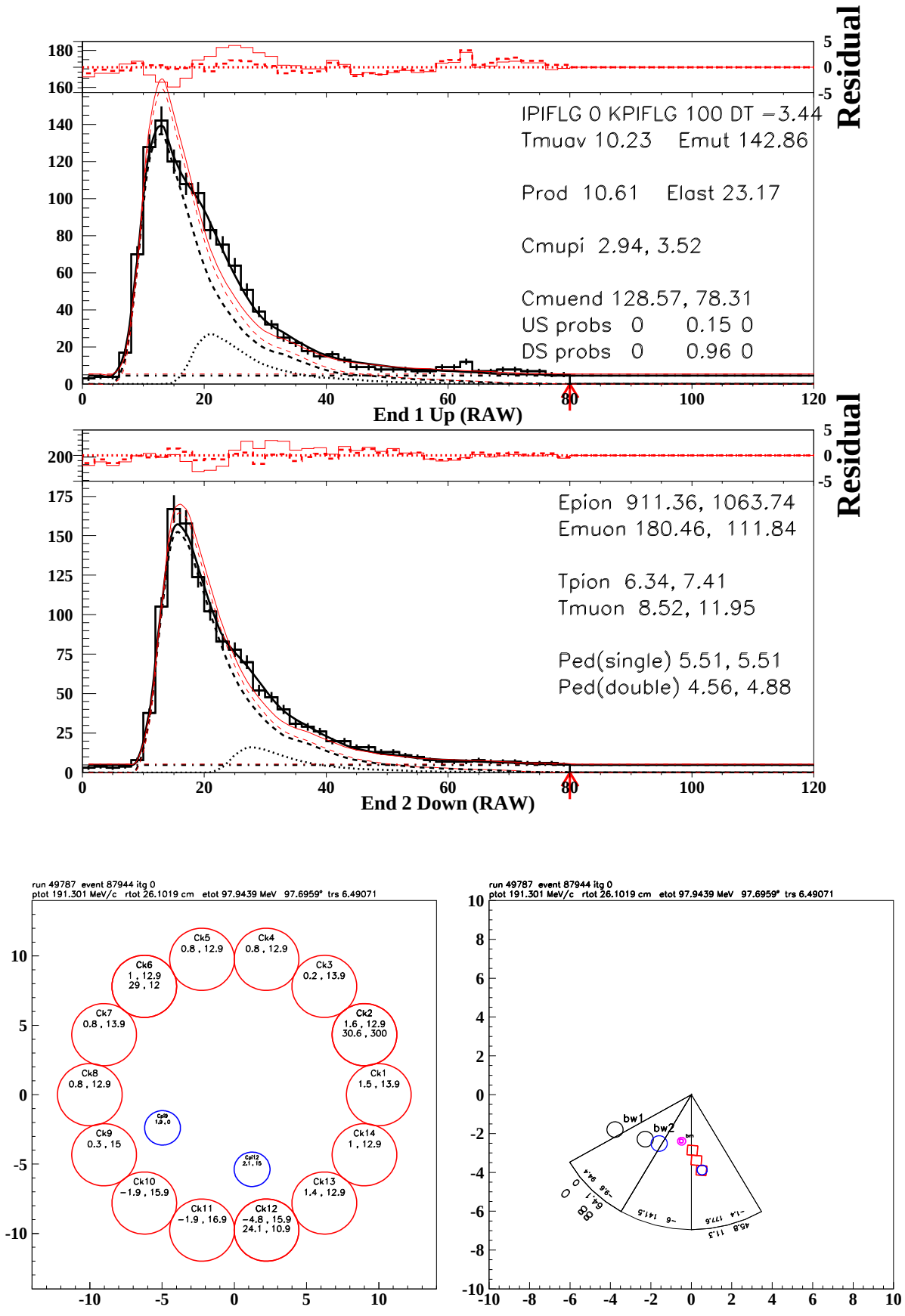

Figure 79: Top: TD display. Lower left: Cerenkov. Lower right: AD display with kaon target fibers and wire chamber positions. This is for Candidate C.

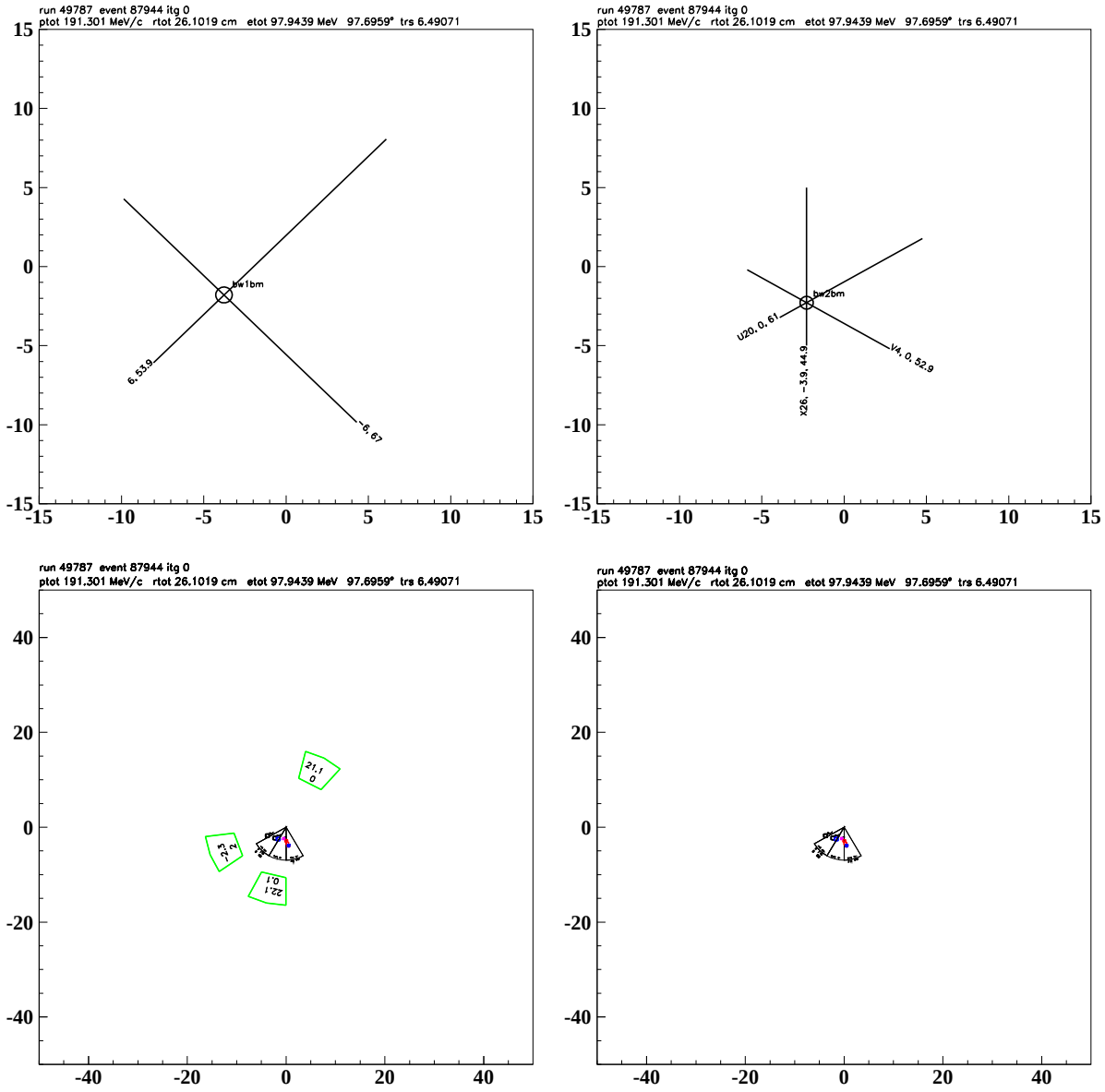

Figure 80: Top left: BW1. Top right: BW2. Lower left: Upstream EC with AD display. Lower right: Downstream EC with AD display. This is for Candidate C.

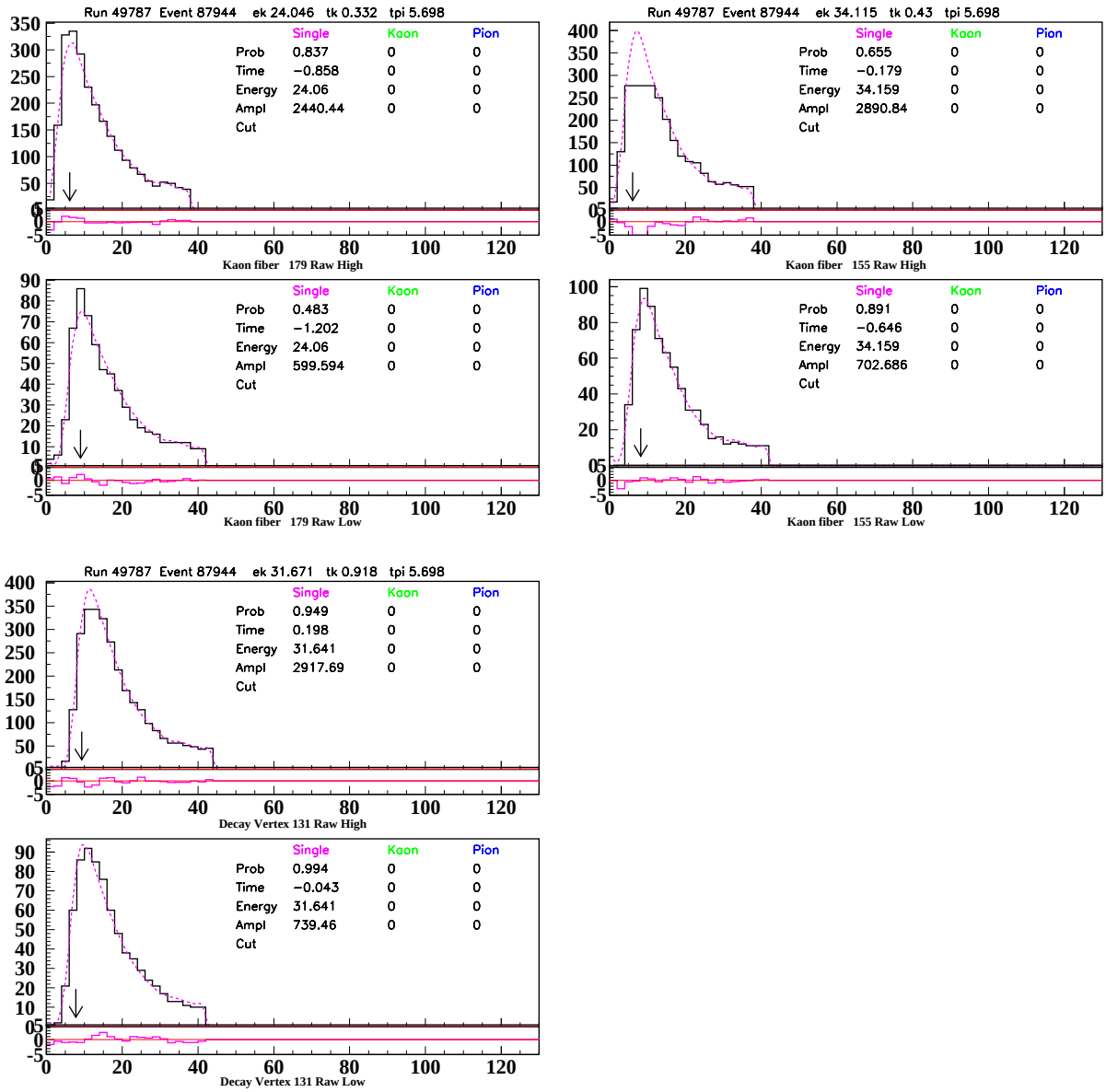

Figure 81: CCD plots for all kaon fibers. This is for Candidate C.

CCD counts	E(MeV)	$t_{\rm AD} - t_\pi$ (ns)	$t_{\rm AD} - t_{\rm RS}$(ns)	$t_{\rm AD} - t_K$(ns)
94.4	11.3	-9.6	-10.4	-4.5
141.5	16.9	-6.0	-6.8	-0.9
177.6	21.2	-1.4	-2.2	3.7

Table 94: Properties of AD hits for candidate C. See text for discussion of energy calibration.

15.6.3 AD hits

There are 3 AD hits near kaon or pion time for candidate C listed in Table 94.

The energy calibration of the AD is derived from the expected mean energy deposit for a kaon of 23.9 MeV from simulation [18][19] and from the peak at 200 CCD counts in the upper left plot in Figure 82. This gives 0.1195 MeV/CCD count.

The total CCD counts within 5 ns of t_K is 235.9 which corresponds to 28.2 MeV and occurs in adjacent AD elements. From the upper left plot in Figure 82, there are ≥ 236 CCD counts per kaon about 15% of the time, so these two energy deposits are consistent with a kaon.

The remaining AD element near in time to the candidate has 177.6 counts which would correspond to 21.2 MeV visible energy. The PV requirements for an AD element in `adpv.function` are $-2 < t_{\rm AD} - t_{\rm RS} < 8$ ns and $t_{\rm AD} - t_K > 5$ ns. This element fails both these requirements. These requirements are motivated by the distributions show in Figure 83. The remnant of the kaon necessitates the cuts at early $t_{\rm AD} - t_{\rm RS}$ (lower figures) and on $t_{\rm AD} - t_K$ (upper figures).

It appears unlikely that the 177.6 CCD counts are due to the kaon, although the energy deposit occurs in the AD element adjacent to the element with 141.5 CCD counts. From the right column in Figure 82, the probability to observe ≥ 178 CCD counts in a $K_{\pi 2}$ peak (kink) event is a few (~ 20) %, if we interpret the CCD count distribution for $K_{\mu 2}$ events (upper right) as being background. Thus the apparent energy of the event appears consistent with a photon from $K_{\pi 2}$, but the timing is not.

In retrospect, we could have mitigated some of the veto blindness of the AD caused by the kaon by eliminating events with $t_{\rm AD} - t_K < 5$ ns and a total CCD count in excess of that expected for a single kaon (i.e.,$>$ 400 CCD counts).

Further evidence that the excess AD energy is due to a photon is seen in the display of the upstream EC in Figure 80. The EC counter at (-10,-5)cm has 2 MeV of energy at -2.3 ns with respect to $t_{\rm RS}$ that is consistent with 177.6 count hit in Table 94. Such an EC-AD correlation had been demonstrated during AD PV studies [3].

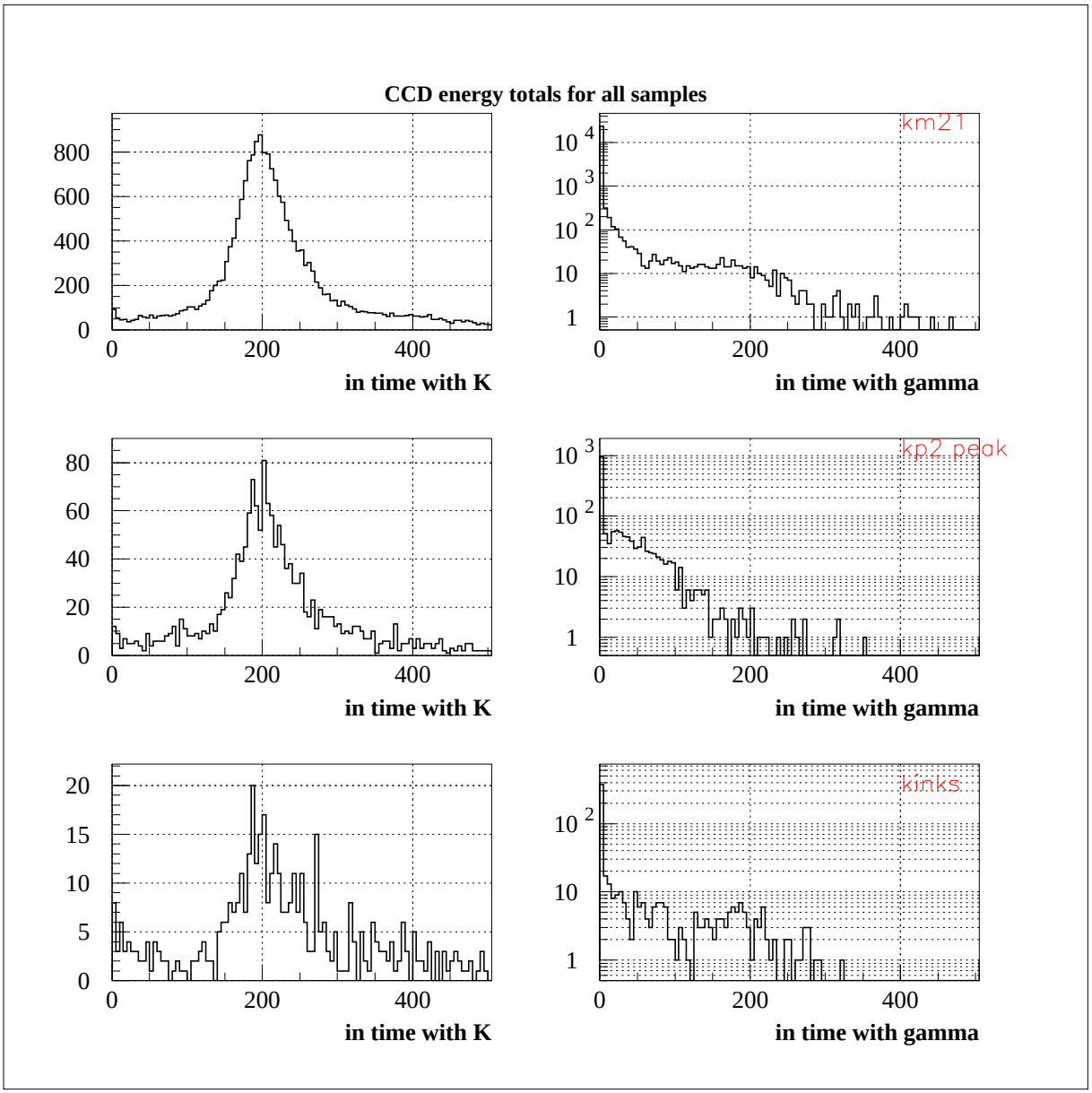

Figure 82: CCD counts in the AD for various samples. Top: $K_{\mu 2}$, Middle: $K_{\pi 2}$ peak, Bottom: kinks. Left side: $|t_{\rm AD} - t_K| < 5$ ns, Right side:$0 < t_{\rm AD} - t_\pi < 8$ns. AD time information taken from the CCDs. This is Figure 8.17 of [3].

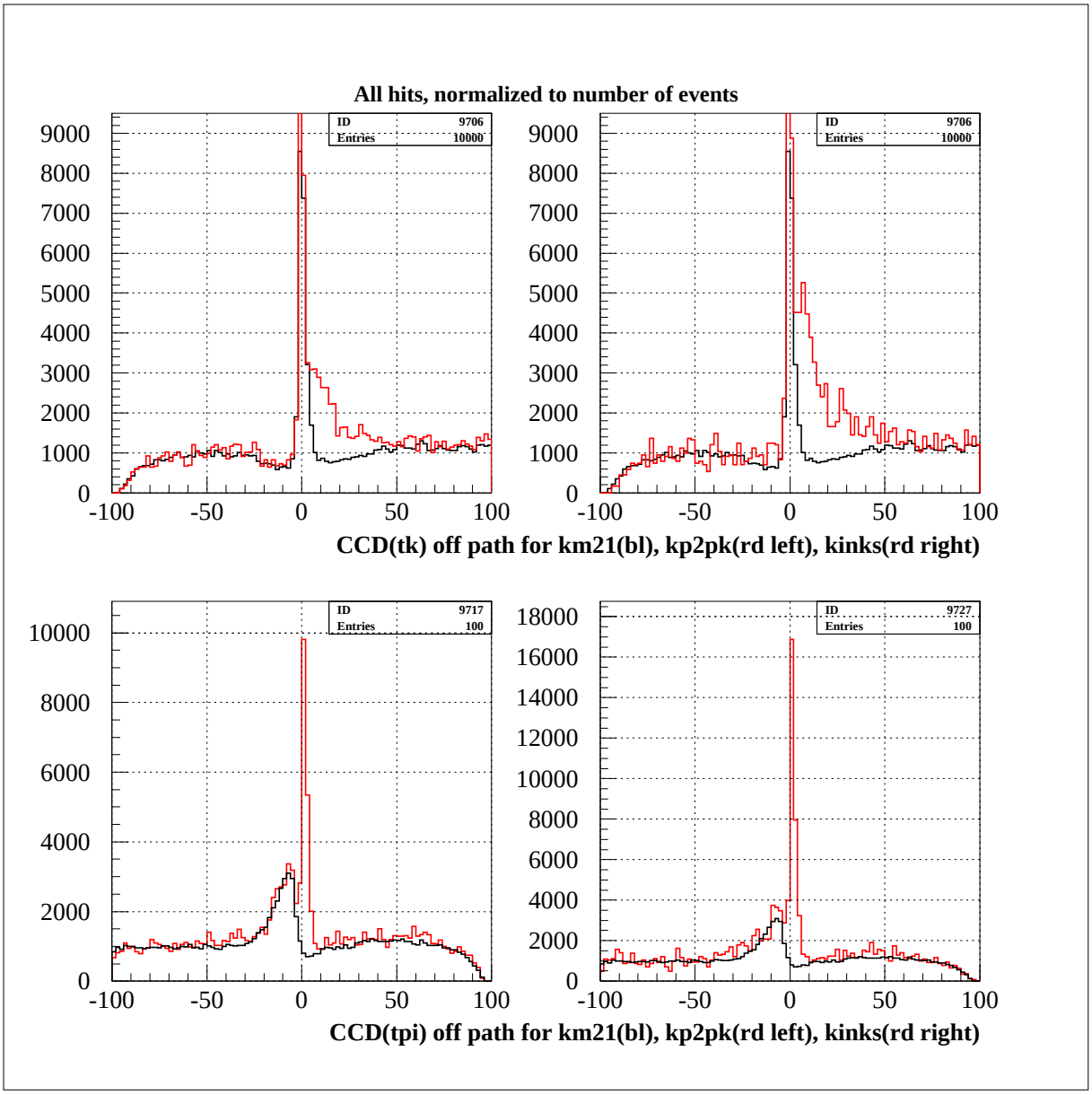

Figure 83: CCD time distributions in the AD for various samples. The bin width is 2 ns. Black: $K_{\mu 2}$, Red,left: $K_{\pi 2}$ peak, Red, right: kinks. Top: $t_{\rm AD} - t_K$(ns), Bottom: $t_{\rm AD} - t_\pi$. The histograms are normalized to the number of entering kaons. This is Figure 8.12 of [3].

15.7 Bad runs close to signal candidate runs

A search for bad runs near each of the signal candidate runs was performed. The function `bad_run_01.function` contains only bad run information on runs before 46100. Information from `bad_run.02002` is included within about 50 runs on either side to show no observed hardware problems.
Candidate A - Run 47876

- `bad_run_02.function`
  - 47963 - Has bad target ccd data as found during TIMKF tuning.
  - 47656 to 47659 - Have bad cktbm data as found during TIMKF tuning.
- `bad_run.02002`
  - 47837:47850 # not smx eckmu2_mix Mar:14,2002- Mar:14,2002
  - 47856:47856 # .lt.500 events smx_v12u 0- 0
  - 47858:47858 # .lt.500 events smx_v12u 0- 0
  - 47861:47861 # all events killed by L1.1 (gr, K-033)
  - 47863:47864 # .lt.500 events smx_v12u 0- 0
  - 47880:47880 # .lt.500 events smx_v12u 0- 0
  - 47884:47885 # not smx km21_mix.ps800.veto 03/15/02- Mar:15,2002

Candidate B - Run 49352

- `bad_run_02.function`
  - 49380 - reason not given
- `bad_run.02002`
  - 49340:49340 # not smx unknown_trig unknown- unknown
  - 49342:49342 # .lt.500 events smx_v15 0- 0
  - 49361:49361 # .lt.500 events smx_v15 0- 0
  - 49365:49365 # .lt.500 events smx_v15 0- 0
  - 49373:49374 # .lt.500 events smx_v15 0- 0
  - 49376:49379 # not smx pulser.1hz May:8,2002- 05/08/02
  - 49385:49385 # .lt.500 events smx_v15 0- 0
  - 49389:49389 # pnn data lost

Candidate C - Run 49787

- `bad_run_02.function`
  - No nearby runs
- `bad_run.02002`
  - 49762:49763 # no events written to tape (sk, K-033)
  - 49764:49764 # .lt.500 events smx_v15 0- 0
  - 49768:49781 # not smx cosmic_rsmon_Xe.predet May:21,05:21- May:21,18:44

- 49782:49782 # .lt.500 events smx_v15 0- 0
- 49790:49791 # .lt.500 events smx_v15 0- 0
- 49795:49796 # .lt.500 events smx_v15 28- 0
- 49800:49800 # not smx unknown_trig unknown- unknown
- 49802:49803 # .lt.500 events smx_v15 0- 0
- 49820:49820 # .lt.500 events smx_v15 0- 0
- 49824:49824 # .lt.500 events smx_v15 0- 0
- 49840:49840 # .lt.500 events smx_v15 0- 0
- 49848:49848 # no events written to tape (sk, K-033)

15.8 Probability of signal

To verify each of the candidates are signal, quantities classified into four categories are checked: reconstruction quality, kaon identification quality, pion identification quality and single beam particle quality.

15.8.1 Reconstruction quality

To make sure the candidates are of good reconstruction quality the quantities checked fall into the categories of timing consistency (Figure 84), target reconstruction (Figure 85), and UTC reconstruction (Figure 89).

15.8.2 Kaon identification quality

To make sure the beam particle in candidate events is a kaon The quantities checked involve the B4 counters, Cerenkov hits at beam time and some target quantities (Figure 84).

15.8.3 Pion identification quality

To make sure the charged track in candidate events was due to a pion the quantities checked fall into the categories of energy deposited in IC counters (Figure 87), Range Stack kinematics (Figure 90), Range Stack TD variables (Figure 91), and kinematics from UMC $\pi^+\nu\bar{\nu}$ events (Figure 92).

15.8.4 Single beam particle quality

To make sure there was only a single beam particle in the candidate events the quantities checked were related to beam detectors at *trs* (Figures 87 and 88).

15.8.5 Probability of signal

Based on the reference distributions, the probability of being signal is computed for each candidate for each of the quantities as summarized in Figure 93. These probabilities are determined using a cumulative integral for each of the reference distributions and are formed such that low probability corresponds to more background-like and high probability corresponds to more signal-like quantities.

For distributions where one side is signal-like and the other side background-like the probability distribution is built going from low probability on the background-like side to high probability on the signal-like side. For quantities where extreme values are

background-like and median values are signal-like the probability distribution was constructed to be very low for extreme values and high for median values. For quantities where extreme values are signal-like and median values are background-like the probability distribution was constructed to be very high for extreme values and low for median values.

Candidate A (red) does not fail PRRF1 despite a prrf value of 0 due to only reaching Range Stack layer 8 where PRRF1 can only fail events reaching the RSSC between layers 10 and 11.

Candidates A (red) and B(green) both have prutcxy (probability of utc fit in xy) values very near zero for the cut UTCFIT07 which is part of UTC_QUAL. Events with low prutcxy (or prutcz) are rejected only if they also have a low number of xy hits. Both of these candidates have a large number of these hits.

Candidate C (blue) is the most muon like based on TDVARNN quantities, but the tdvarnn value of 0.82 passes both the loose and tight version of this cut.

Candidate B (green) has large values of approximately 1 for the quantities used in the TGDB4 cuts, but these cuts reject events only if these values are 1.8 or higher.

Candidate B (green) is very close to the minimum value of 0.05 in VERRNG with a value of 0.08.

The energy deposited in the B4 for Candidate A (red) was only 1.4 MeV where the threshold energy is 1.1 MeV. This candidate also has a very low beam likelihood value of 20.1 for B4EKZ where the threshold for this cut is 10.0 since *tpi* was not determined from the IC.

Laur asked why the UMC PTOT distribution in Figure 92 does not look more like the form factor expected for V-A. There are three reasons. Low values of PTOT are rejected by the trigger requirement of layer 6 or higher. This gives a rising distribution with a threshold at $\sim$140 MeV/c and gives the impression of the form factor at low PTOT. The increased loss of pions due to nuclear interactions at high PTOT flattens the distributions as the effect of PTOT resolution.

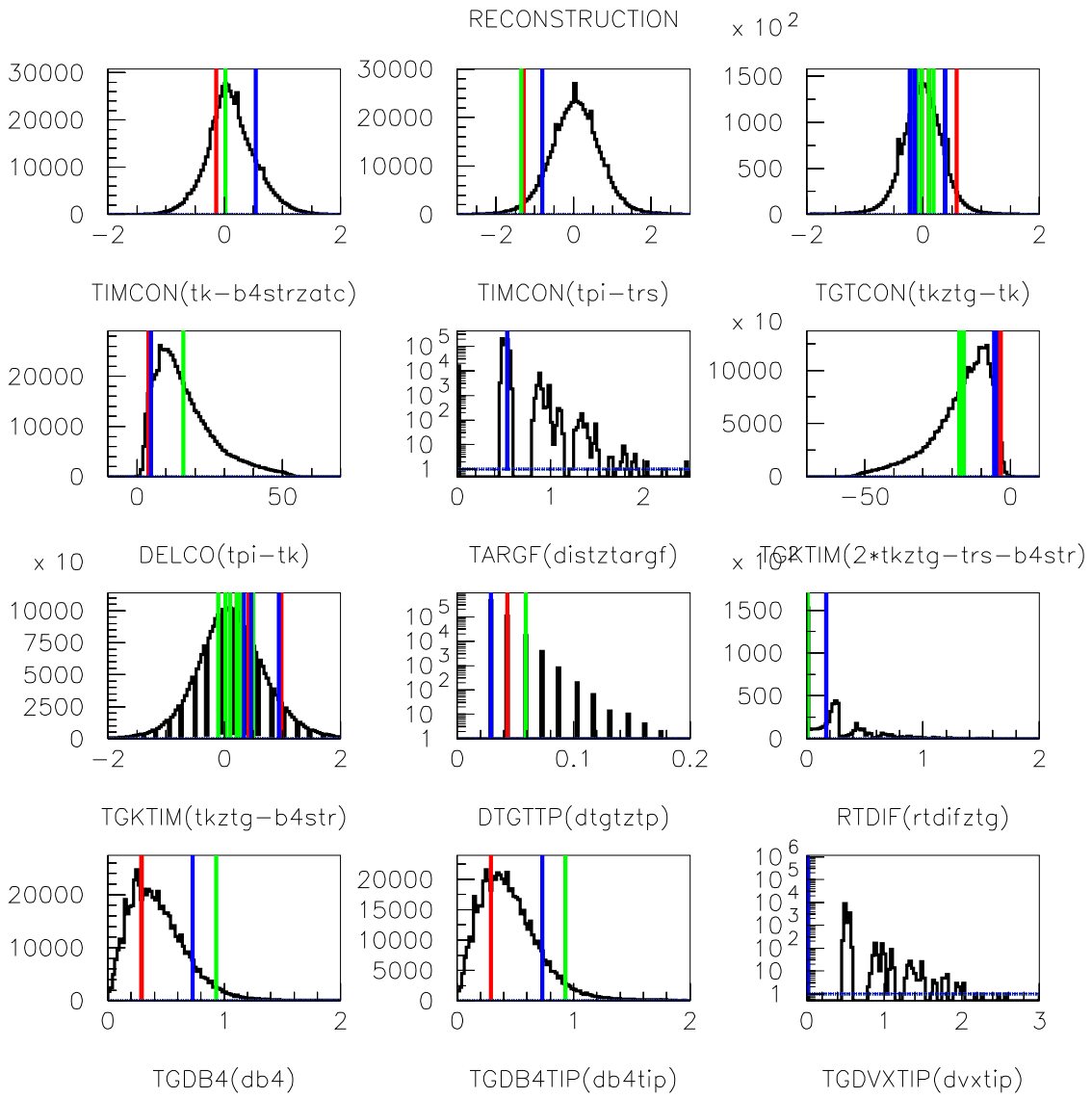

Figure 84: Quantities related to timing consistency in reconstruction cuts. Sample is from $K_{\mu 2}$ monitors. Candidates are color coded: candidate **A in red**, candidate **B in green** and candidate **C in blue**. Note that the quantities for some candidates fall in the same histogram bin such that only one candidate is displayed. The abscissa label contains the cut name in UPPERCASE and the actual variables plotted in lowercase in parentheses.

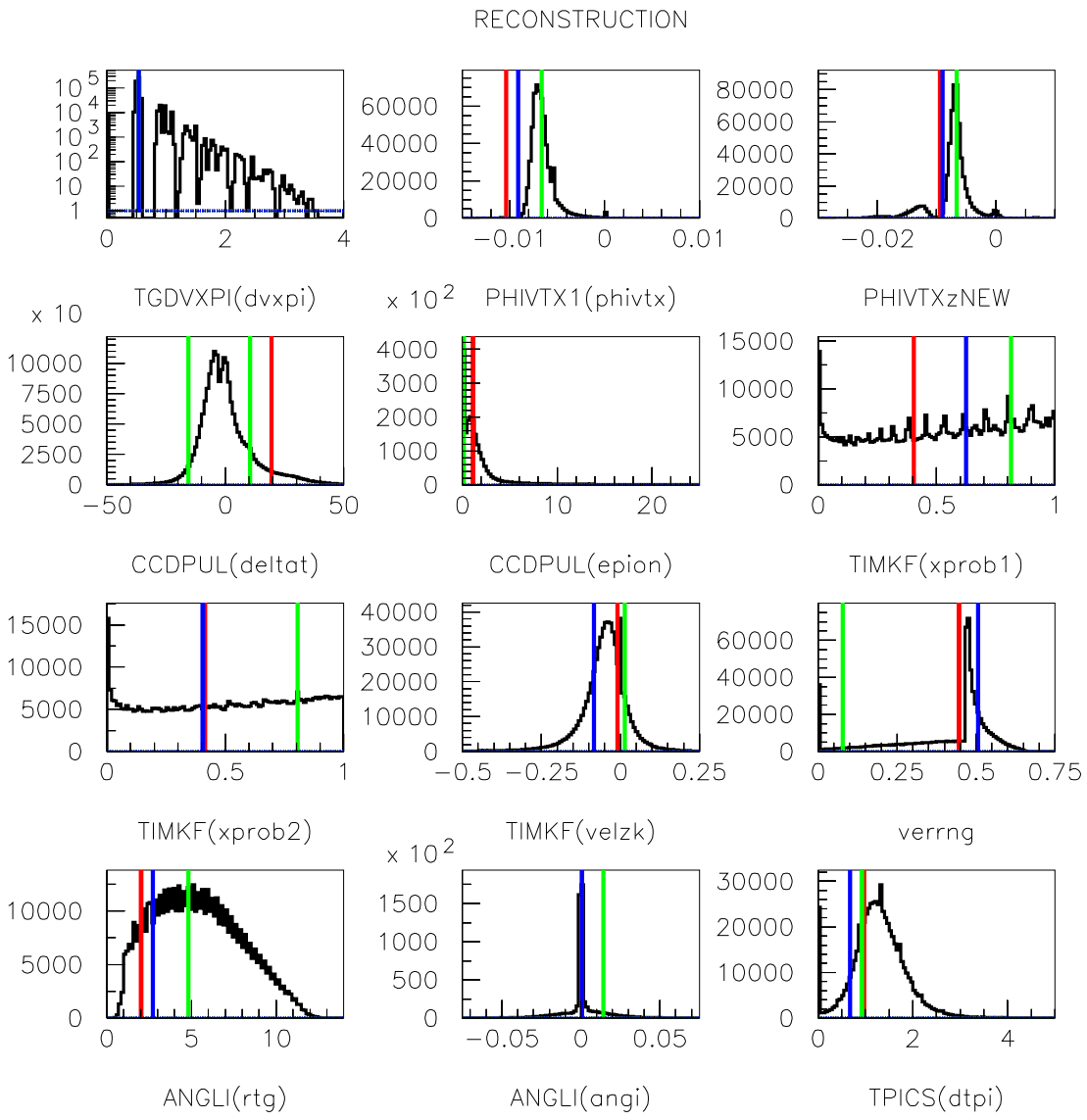

Figure 85: Quantities related to reconstruction cuts in the target. Sample is from $K_{\mu 2}$ monitors. Candidates are color coded: candidate **A in red**, candidate **B in green** and candidate **C in blue**. Note that the quantities for some candidates fall in the same histogram bin such that only one candidate is displayed. The abscissa label contains the cut name in UPPERCASE and the actual variables plotted in lowercase in parentheses.

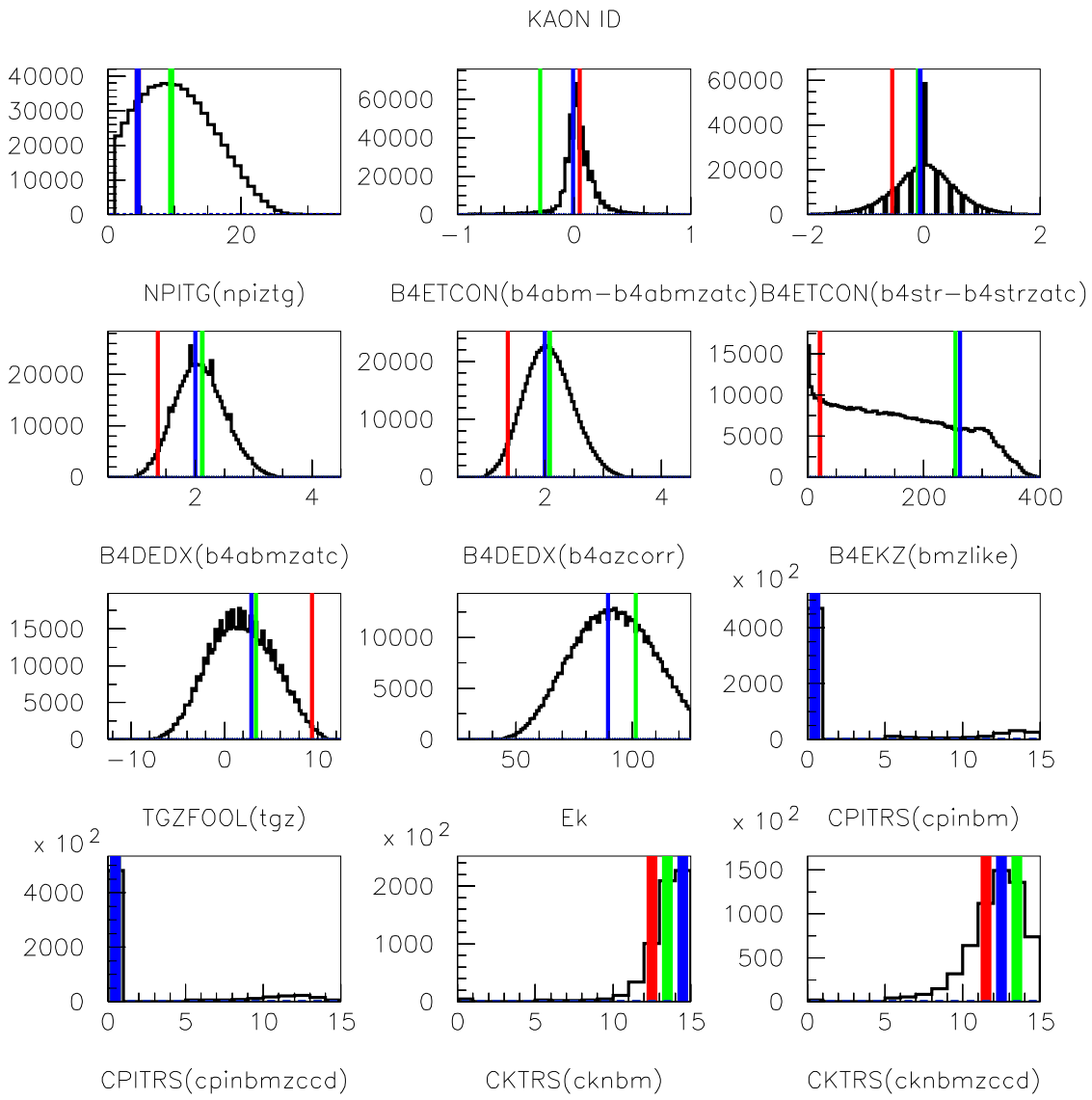

Figure 86: Quantities related to target kaon reconstruction. Sample is from $K_{\mu 2}$ monitors. Candidates are color coded: candidate **A in red**, candidate **B in green** and candidate **C in blue**. Note that the quantities for some candidates fall in the same histogram bin such that only one candidate is displayed. The abscissa label contains the cut name in UPPERCASE and the actual variables plotted in lowercase in parentheses.

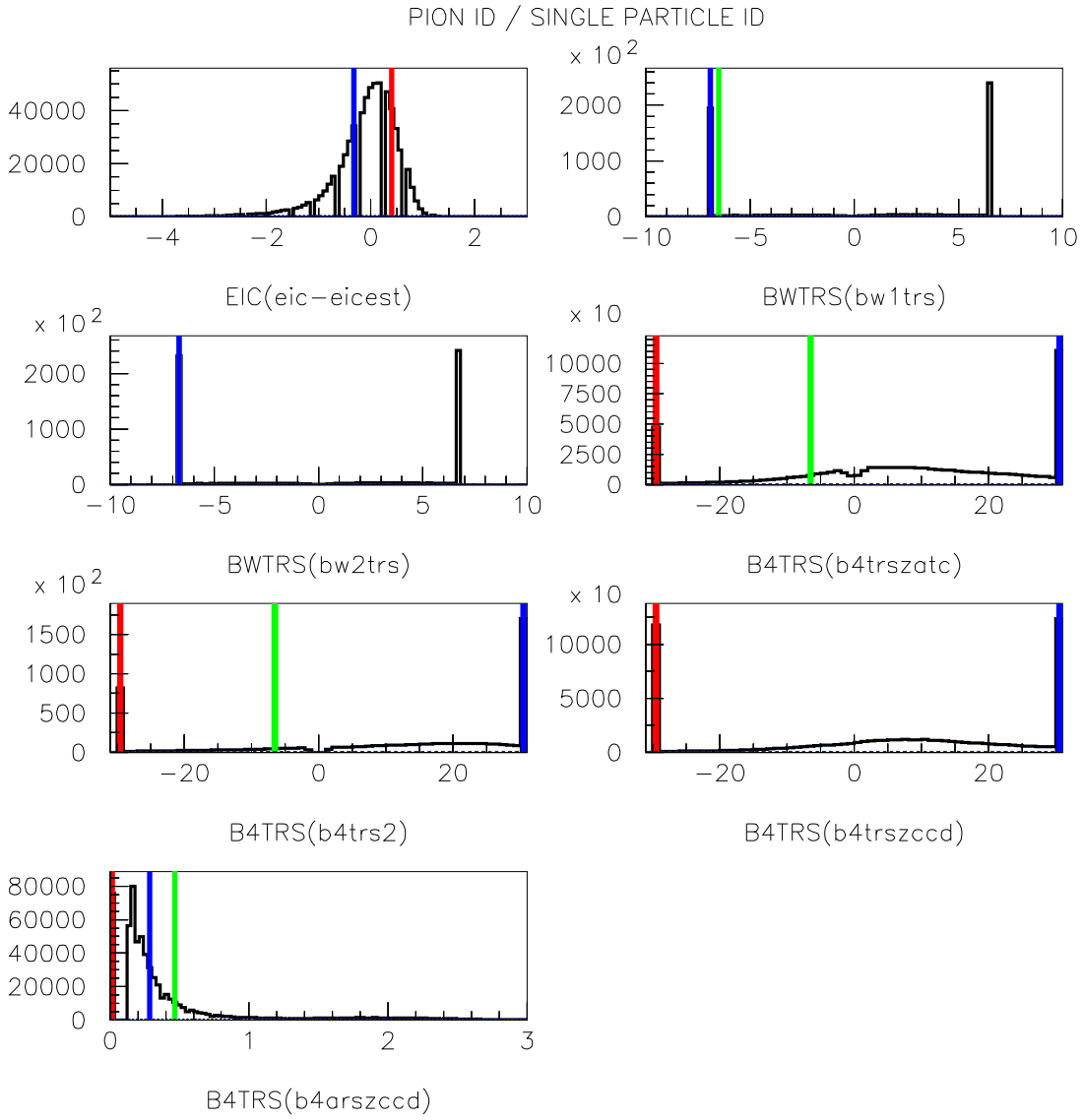

Figure 87: Quantities related to pion identification, single beam detection and photon veto. The top-left plot is related to pion identification and the rest of the plots to single beam detection and photon veto. Sample is from $K_{\mu 2}$ monitors. Candidates are color coded: candidate **A in red**, candidate **B in green** and candidate **C in blue**. Note that the quantities for some candidates fall in the same histogram bin such that only one candidate is displayed. The abscissa label contains the cut name in UPPERCASE and the actual variables plotted in lowercase in parentheses.

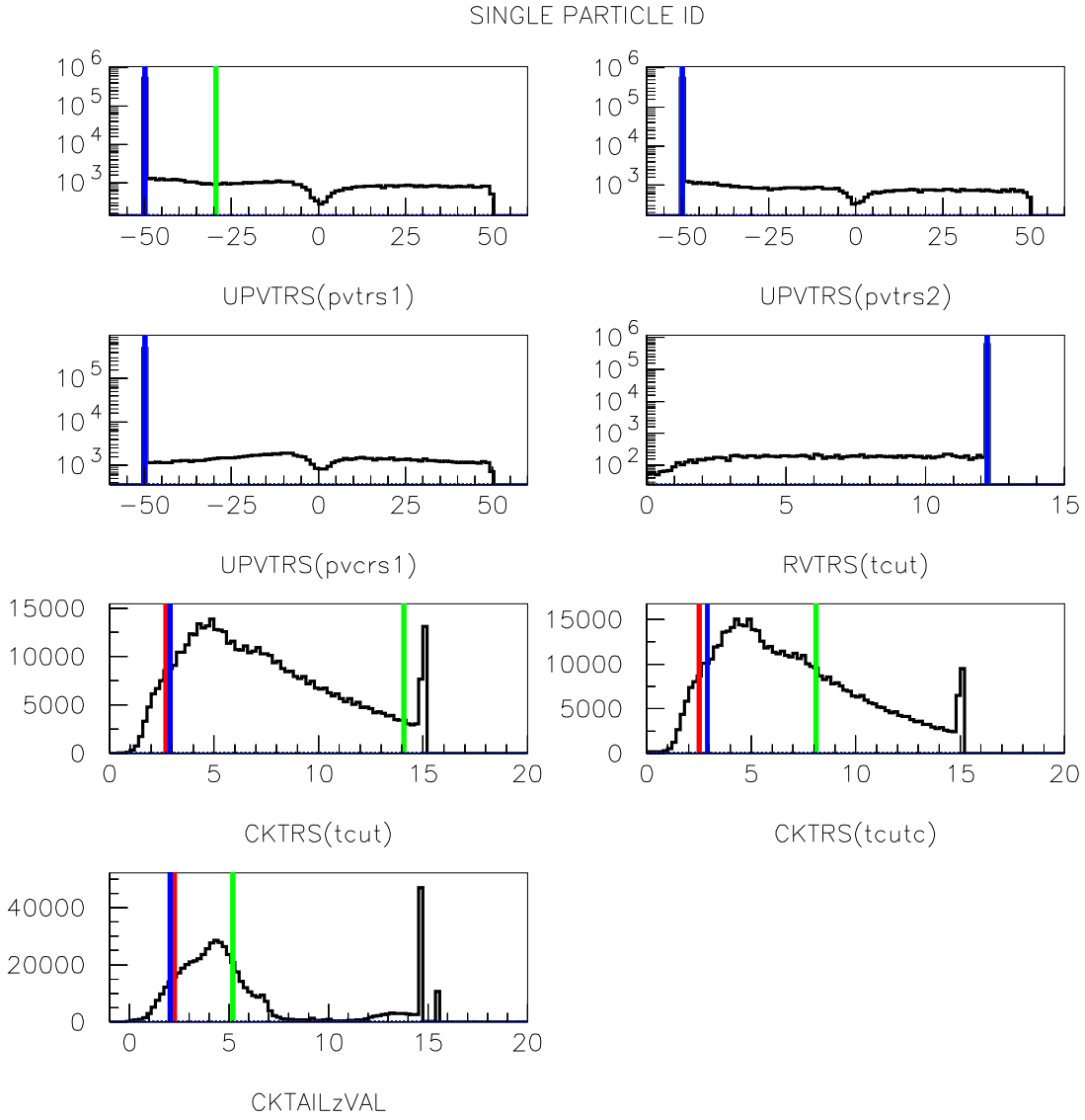

Figure 88: More quantities related to single beam detection and photon veto. Sample is from $K_{\mu 2}$ monitors. Candidates are color coded: candidate **A in red**, candidate **B in green** and candidate **C in blue**. Note that the quantities for some candidates fall in the same histogram bin such that only one candidate is displayed. The abscissa label contains the cut name in UPPERCASE and the actual variables plotted in lowercase in parentheses.

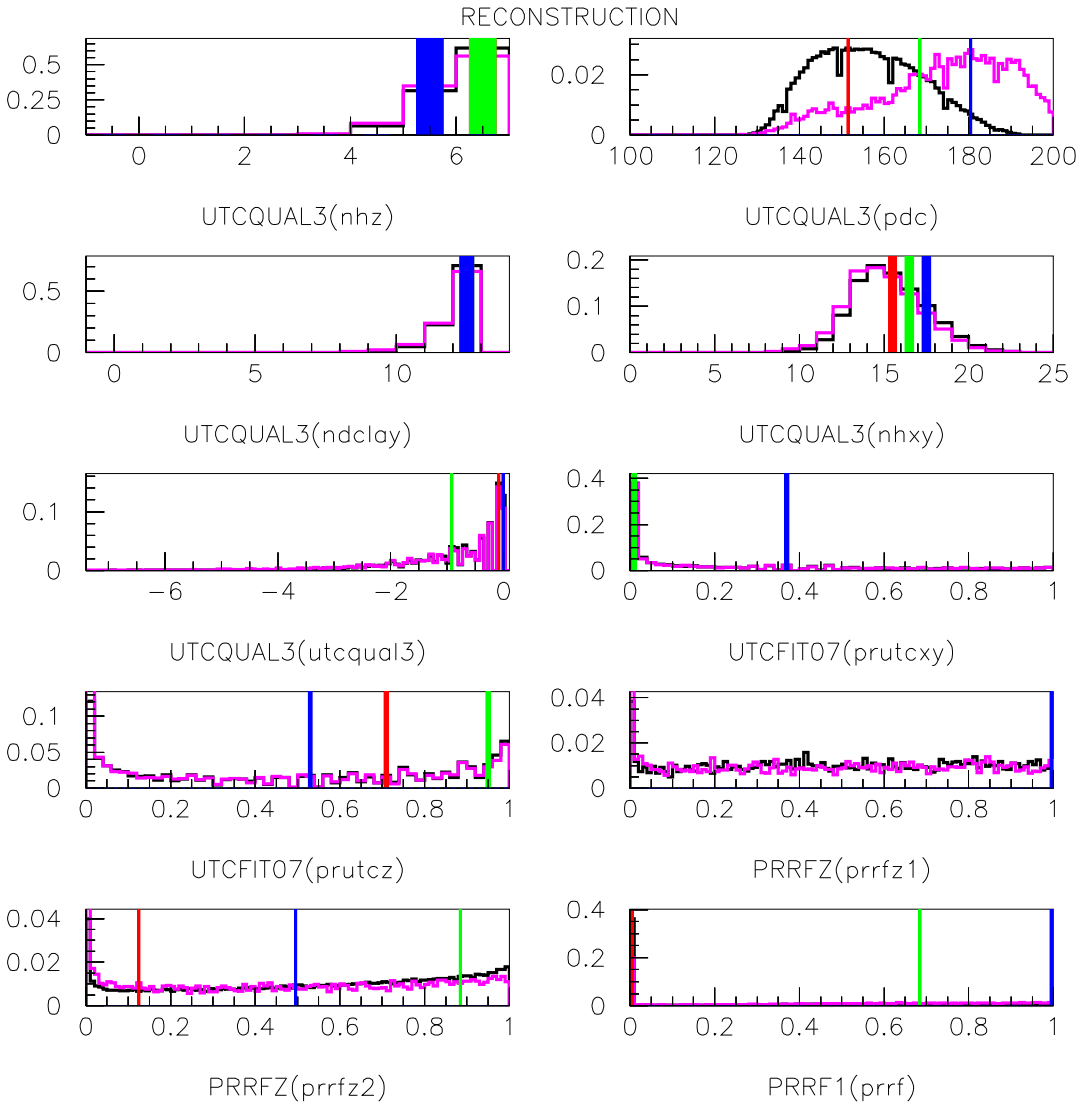

Figure 89: Quantities related to UTC and Range Stack reconstruction. Sample is from $\pi_{scatter}$ monitors in PNN2BOX. The purple histograms show $K_{\pi 2}$ monitors in KP2BOX. Candidates are color coded: candidate **A in red**, candidate **B in green** and candidate **C in blue**. Note that the quantities for some candidates fall in the same histogram bin such that only one candidate is displayed. The abscissa label contains the cut name in UPPERCASE and the actual variables plotted in lowercase in parentheses.

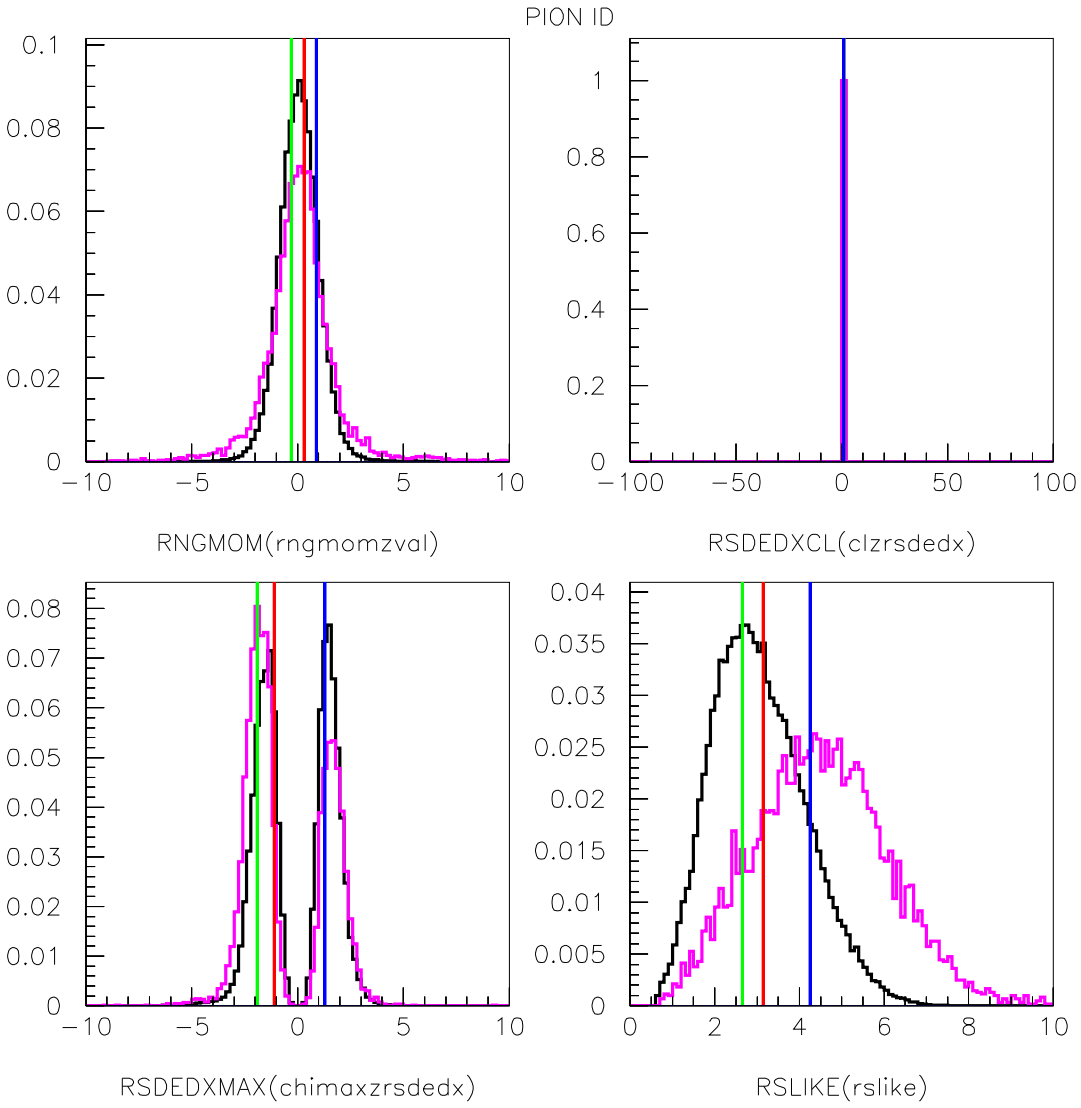

Figure 90: Quantities related to pion identification by Range Stack kinematics. Sample is from $\pi_{scatter}$ monitors in PNN2BOX. The purple histograms show $K_{\pi 2}$ monitors in KP2BOX. Candidates are color coded: candidate **A in red**, candidate **B in green** and candidate **C in blue**. Note that the quantities for some candidates fall in the same histogram bin such that only one candidate is displayed. The abscissa label contains the cut name in UPPERCASE and the actual variables plotted in lowercase in parentheses.

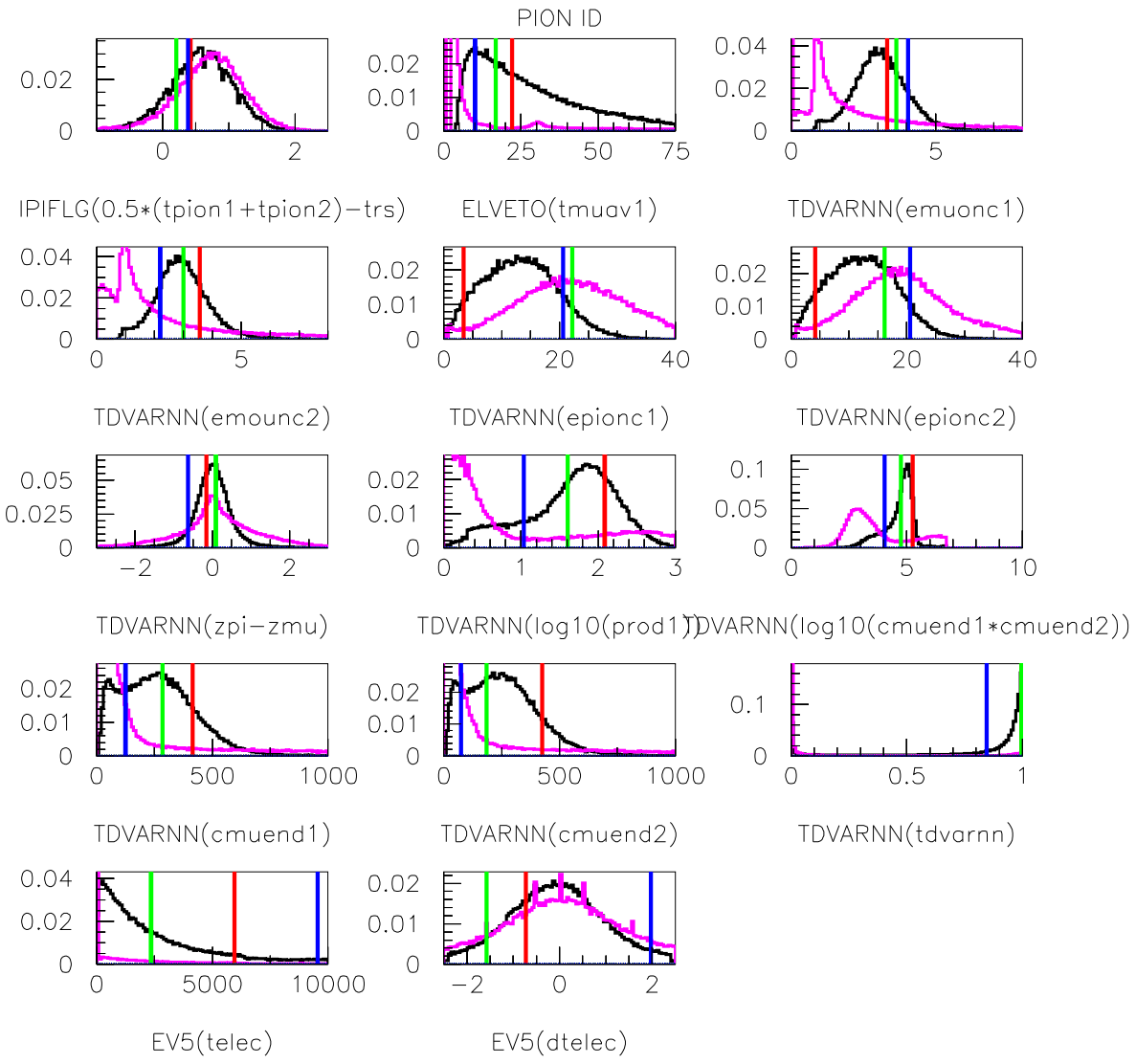

Figure 91: Quantities related to pion particle identification from TD variables. Signal sample (black) is from $\pi_{scatter}$ monitors and background sample (purple) is from $K_{\mu 2}$ monitors. Candidates are color coded: candidate **A in red**, candidate **B in green** and candidate **C in blue**. Note that the quantities for some candidates fall in the same histogram bin such that only one candidate is displayed. The abscissa label contains the cut name in UPPERCASE and the actual variables plotted in lowercase in parentheses.

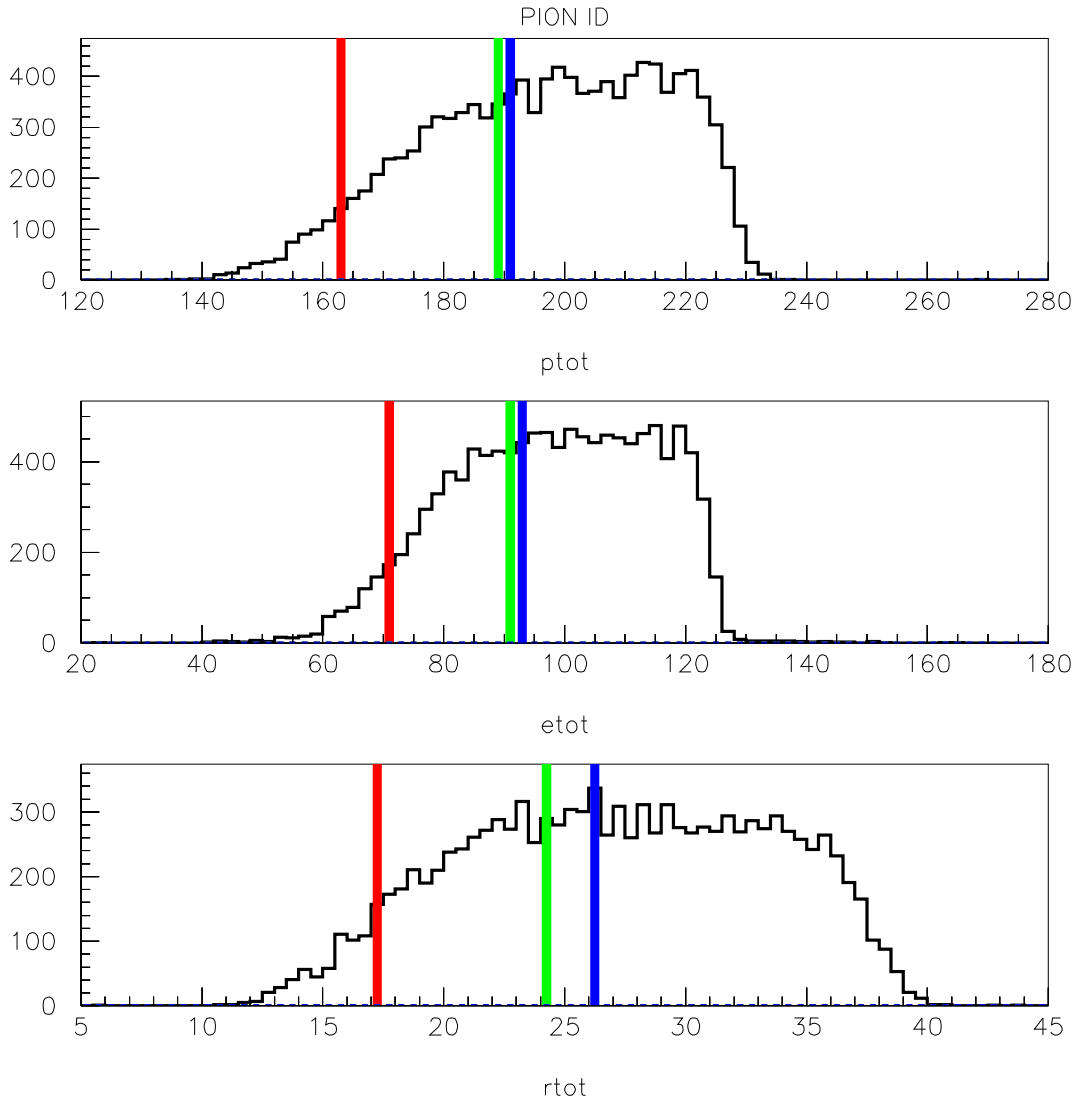

Figure 92: Quantities related to pion particle identification from kinematic variables. Sample is UMC $K^+ \to \pi^+\nu\bar{\nu}$ events passing $\pi\nu\bar{\nu}(1)$ or $\pi\nu\bar{\nu}(2)$ triggers. For the sample, each kinematic variable is plotted without cutting on the other two. Candidates are color coded: candidate **A in red**, candidate **B in green** and candidate **C in blue**. Note that the quantities for some candidates fall in the same histogram bin such that only one candidate is displayed.

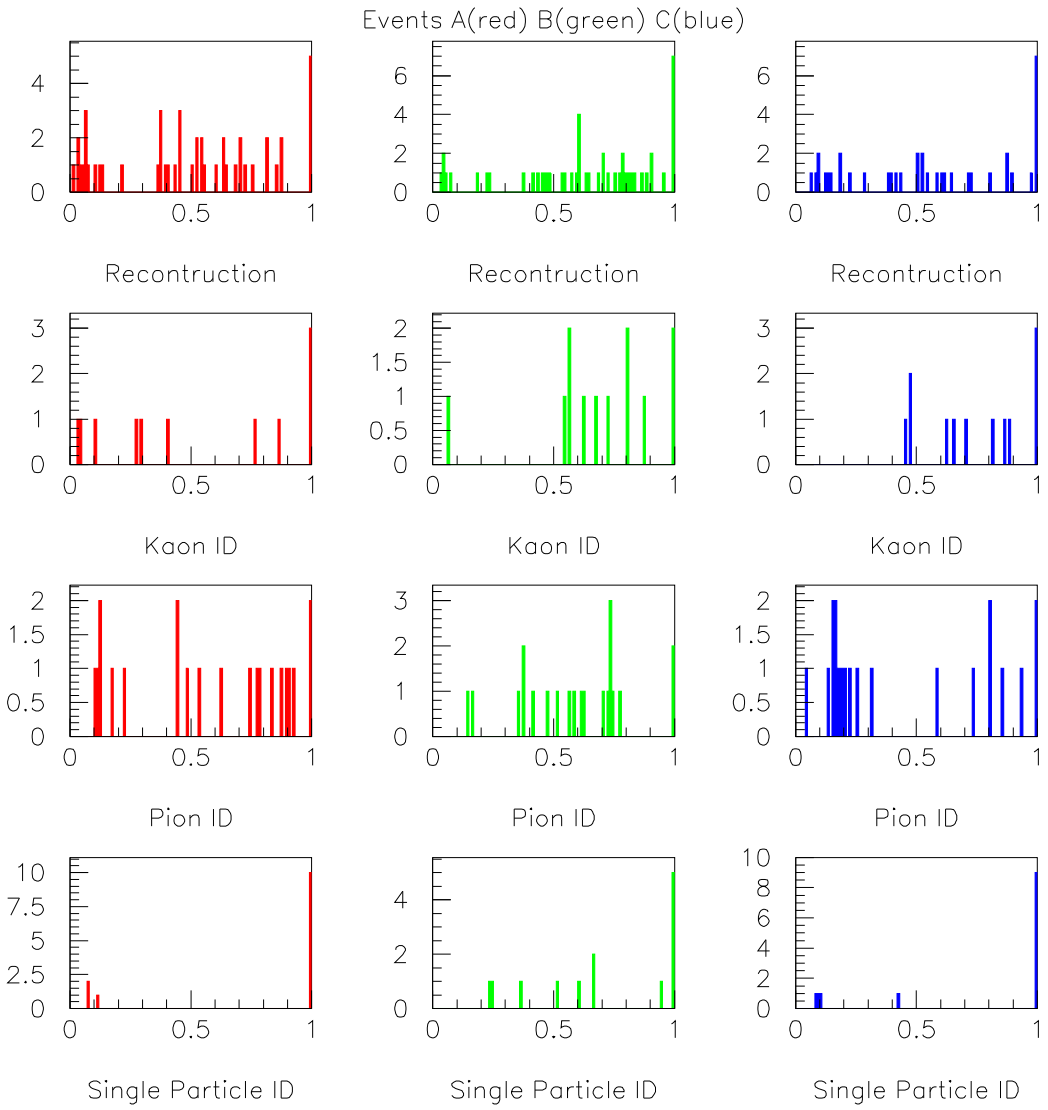

Figure 93: Probability of signal for the three candidate events. Candidates are color coded: candidate **A in red**, candidate **B in green** and candidate **C in blue**.

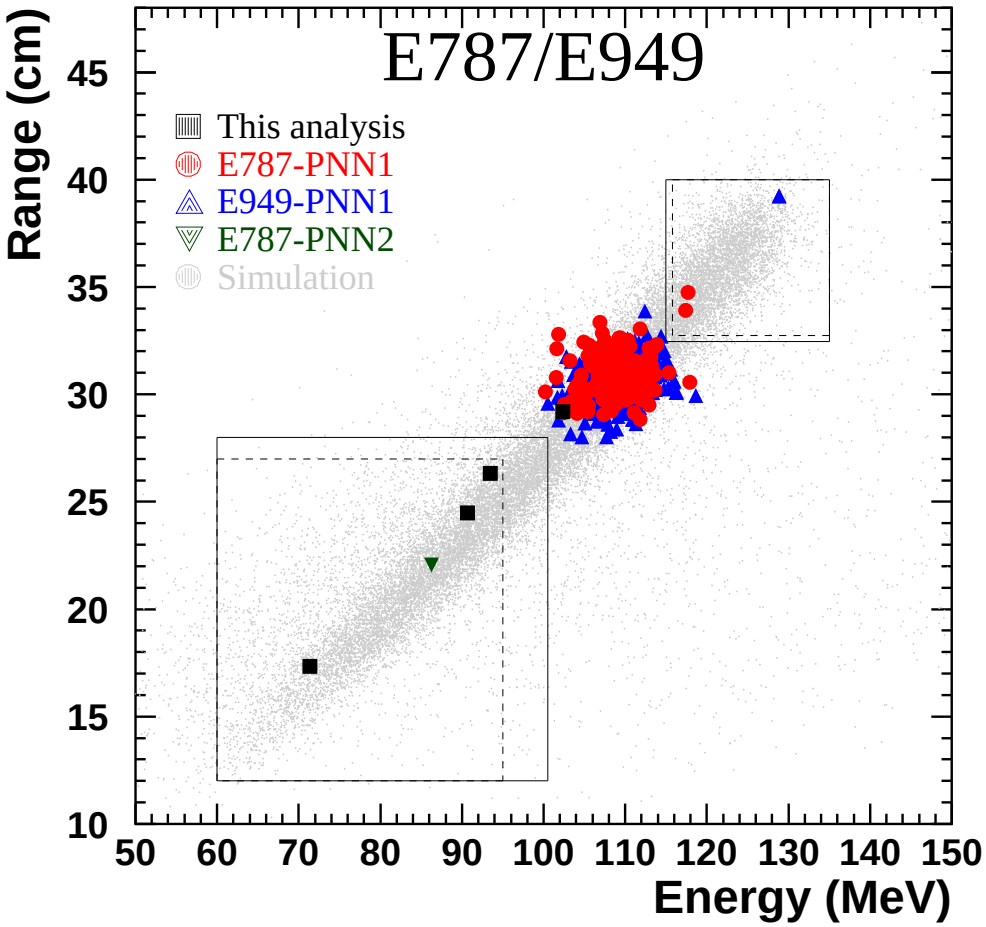

Figure 94: Proposed figure for PRL publication. The range *vs.* energy of all pnn1 and pnn2 candidates in E787 and E949 after all other cuts is shown.

16 Publication Issues

Toshio pointed out that relative normalization and sensitvity of the pnn1 and pnn2 regions in the proposed R *vs.* E figure for the PRL (Fig. 94) need to be carefully explained. There are several issues:

1. Relative sensitivity
2. Relative $K_{\pi 2}$ peak rates
3. Relevant cuts that shape the acceptance such as the trigger or layer cuts.
4. Acceptance gain due to looser TD cuts

16.1 Relative sensitivity of the pnn1 and pnn2 analyses

The sensitivity of the pnn1 analyses relative to the pnn2 analyses shown in Fig. 94 is 4.17. The details are in Table 95.

Analysis	$N_K(\times 10^{12})$	Acceptance $(\times 10^{-3})$	$N_K \times$ Acc $(\times 10^9)$
E787 pnn1	5.9	2.0 ± 0.2	11.8
E949 pnn1	1.8	2.2 ± 0.2	3.96
pnn1 all	7.7	—	15.76
E787 pnn2 96	1.12	0.765	0.857
E787 pnn2 97	0.61	0.97	0.592
E949 pnn2	1.7	1.37	2.329
pnn2 all	3.43	—	3.78
pnn1/pnn1	2.24		4.17

Table 95: Comparison of pnn1 and pnn2 sensitivity. N_K is the number of stopped kaons. Acceptance (Acc) is the total acceptance.

16.2 Relative $K_{\pi 2}$ peak rates

To estimate the relative rates of $K_{\pi 2}$ peak events in the pnn1 and pnn2 samples, we need an estimate of the relative photon veto rejection in addition to the information in the previous section. For this analysis, the rejection of the PV60 cuts on the $K_{\pi 2}$ peak is 1156 ± 112 (Class 1, 2/3 sample in Table 9). The rejection of the pnn1 PV cut on the $K_{\pi 2}$ peak is 80 ± 2 (Class 1 in Table 12). As a check, the $K_{\pi 2}$ peak PV rejection for the E949 pnn1 analysis was measured to be 84.3 ± 1.2 (Table 6 of [6]). The 5% difference between these two measurements is probably due to some dependence of the PV rejection on setup cuts and can be used as an estimate of the systematic uncertainty.

The E949 pnn1 analysis(p.33 of [6]) estimated that the total (online and offline) E949 pnn1 PV rejection was twice the nominal E787 pnn1 PV rejection. However, for the extended signal region used in the E949 pnn1 analysis, the PV to be loosened such that the nominal rejection was reduced by a factor of 4.00 (Sec 4.9 of K-034 [6]).

For the E787 and E949 pnn2 analyses, the ratio of the total PV rejection can be obtained from a comparison of the $K_{\pi 2}$ peak samples used to estimate the $K_{\pi 2\gamma}$ background. For the E787 pnn2 1996 analysis, there were 117 $K_{\pi 2}$ peak events in the 2/3 sample (p.83 of TN-386 [2]). For the E949 pnn2 analysis, there were 106 $K_{\pi 2}$ peak events in the 2/3 sample (Table 29). The ratio of these two event rates, corrected by the kaon exposure, provides the total pnn2 PV rejection of E949 relative to E787:

$$\frac{117/1.12 \times 10^{12}}{106/1.7 \times 10^{12}} = 1.68 \pm 0.23 \quad . \tag{111}$$

The relative rate of $K_{\pi 2}$ events is proportional to the acceptance times the kaon exposure divided by the rejection. This assumes that the signal acceptance is proportional to the $K_{\pi 2}$ acceptance. Including all factors

$$\begin{aligned} r(K_{\pi 2}) &= \frac{\frac{5.9\times 10^{12}}{(80\pm 2)/2} + \frac{1.8\times 10^{12}}{(80\pm 2)/4}}{\frac{1.72\times 10^{12}}{(1156\pm 112)/(1.68\pm 0.23)} + \frac{1.7\times 10^{12}}{(1156\pm 112)}} \times 4.17 & (112)\\ &= \frac{1156 \pm 112}{80 \pm 2} \times \frac{2 \times 5.9 + 4 \times 1.8}{1.72 \times (1.68 \pm 0.23) + 1.7} \times 4.17 & (113)\\ &= (14.5 \pm 1.4) \times (4.14 \pm 0.36) \times 4.17 & (114)\\ &= 250 \pm 33 & (115) \end{aligned}$$

Including the 5% systematic uncertainty mentioned earlier means that we expect $r(K_{\pi 2}) = 250 \pm 35$ more $K_{\pi 2}$ peak events from the pnn1 analyses compared to the pnn2

analyses based on acceptance and PV rejection only. Since the pnn1 analysis, at least in E949, employs a cut on $Pdev$ from the $K_{\pi 2}$ peak, there is probably a small factor due to kinematics that would increase $r(K_{\pi 2})$. The number of non-signal events in Fig. 94 is 269 and 1 for the pnn1 and pnn2 analyses, respectively, in good agreement with the estimate.

As a partial check, the expected ratio of $K_{\pi 2}$ peak events for the E787 and E949 pnn1 analyses should be the relative E787 and E949 kaon exposures divided by the relative E787 and E949 PV rejection or $2 \times 5.9/(4 \times 1.8) = 1.63$. The number of non-signal events in the E787 and E949 pnn1 analyses is 141 and 269, respectively, so the ratio is 1.91 ± 0.20, also in reasonable agreement with expectation.

16.3 Other relevant cuts

The pnn1 analysis uses only pnn1 trigger events. The pnn1 trigger requires a charge track hit in layer 6 or 7. The offline requirement is that the stopping layer is from layer 11 to layer 18 inclusive. As shown in Figure 95, the layer 11 requirement corresponds roughly to 180.2 MeV/c, 86.2 MeV, and 22 cm cuts on $PTOT$, $ETOT$ and $RTOT$, respectively.

The pnn2 analysis uses the logical OR of the pnn1 and pnn2 triggers which effectively requires a charged track in layers 3 through 6 inclusive. The offline requirement is that the stopping layer is from layer 6 to layer 18 inclusive.

16.4 Acceptance gain from loosened TD cuts

This subsection contains justification for the statement in the PRL that we increased the TD acceptance by 10% in the E949 pnn2 analysis with respect to the E787 pnn2 analysis.

FITPI3 was the TD-fitting algorithm used in E787. FITPI4 was used in E949. In Table 5 of K-029 [24], the acceptance of FITPI3 on E787 piscat 1998 data was $73.6 \pm 0.05\%$ and on the E949 2002 piscat data was $73.1 \pm 0.9\%$. The FITPI4 acceptance on E949 2002 piscat data was $80.2 \pm 0.8\%$ as measured by Shaomin. In Section 3.1 of K-034 [6], the acceptance of FITPI3 is stated to be 73.1% and the acceptance of FITPI4 is stated to be 80.3%.

According to Table 31 of TN-386 [2], the E787 1996 pnn2 analysis applied the additional TD-related cuts in the sequence `RSHEX`, `L1.1`, `ELVETO`, `PROBTD` and `TDFOOLERY`. The sequential acceptance of `PROBTD` was 93.6%. According to Table 50 of TN-391, the E787 1997 pnn2 analysis applied the additional TD-related cuts in the sequence `RSHEX2`, `L1.N`, `ELVETO`, `PROBTD`, `TDFOOL` and `TAIL_F`. The sequential acceptance of `PROBTD` was 93.31% and of `TAIL_F` was 98.73%.

According to Table 53 of K-073.v1 [1], the sequential acceptance of "loose" `TDVARNN` was 94.28%. Under the assumption that the replacement of `PROBTD` by `TDVARNN` is the only significant difference between the E787 and E949 TD cuts and neglecting any rate-dependent effects, the relative acceptance is

$$\frac{A(2002 \text{ pnn2})}{A(1996-7 \text{ pnn2})} = \frac{0.80}{0.73} \times \frac{0.943}{0.93} = 1.11 \quad . \tag{116}$$

This neglects the 1.3% lower acceptance in 1997 pnn2 due to the application of `TAIL_F`.

The rate dependence can be somewhat taken into account by comparing the `L1.N` acceptance between 1997 and 2002. From Table 50 of TN391, the `L1.N` acceptance was 76.9%. From Table 53 of K-073.v1, the `L1.N` acceptance in the "tight box" was 75.11%. Note, in Table 53, that the `L1.2` acceptance was 85.34% for the "loose box" and 91.15% for the "tight box". This difference was found to be due to the correlation with the PV cuts. With this in mind, the relative acceptance is

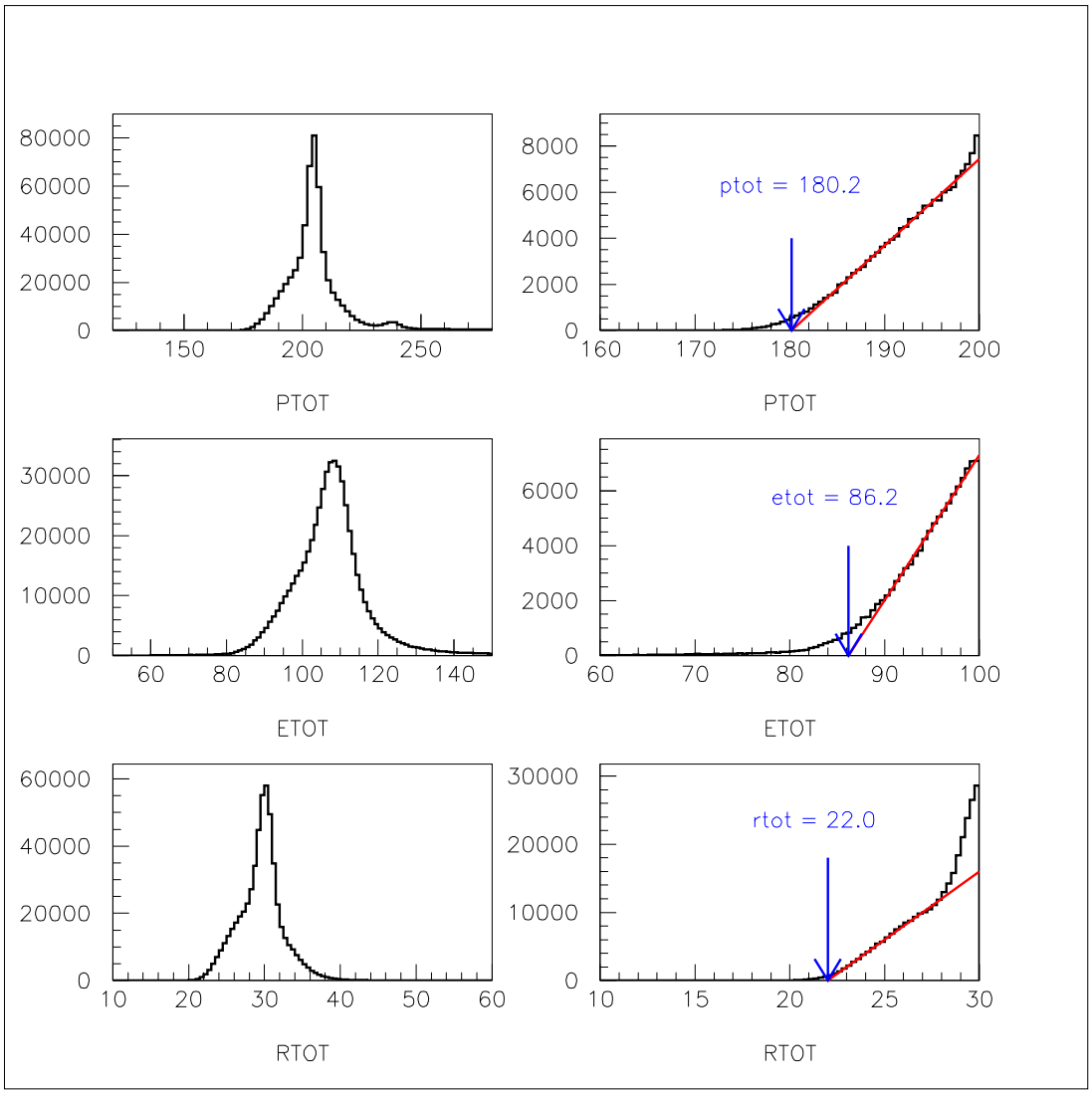

Figure 95: Cutoff in ptot, etot and rtot due to Layer 11 condition. Plots on the right are zoomed into the cutoff region relative to the plots on the left. Sample is $\pi\nu\bar{\nu}(1)$ or $\pi\nu\bar{\nu}(2)$ trigger with COS3D, RNGMOM and PASS1 setup cuts.

$$\frac{A(2002\text{ pnn2})}{A(1996-7\text{ pnn2})} = \frac{0.80}{0.73} \times \frac{0.943}{0.93} \times \frac{0.751}{0.769} = 1.085 \quad . \tag{117}$$

It should be clear from the preceding discussion that it is difficult to make a precise comparison between the E949 and E787 TD-related acceptance due to changes in cuts and analyses and differing accidental rates. In this light, an estimated gain in acceptance of 10% seems to be a reasonable estimate.

As a final note, the E787 analyses did not use `EV5` at all. In retrospect, we could have probably discarded it also and increased the acceptance of the regions using the "tight" TD cut by $1/0.837 = 1.19$ (see Table 71) with only a minimal increase in muon background.

17 Scaler information for signal candidates

This information provided by Steve Kettell:

It seems to me that these runs are very much like the rest of the runs in 2002, or at least much like their neighboring runs.

We can see that the first event came soon after the AGS increased the spill length and before our beam line was very well tuned up. Our online PV was using the analog sums instead of the meantimers. We had fewer monitor triggers (high prescale factors) during this period. The IC rate was relatively higher (per Ck+Cpi) than later in the run for reasons that I have not uncovered. During this period we had reduced efficiency of reconstructing UTC ADC hits in the inner layer due to an AC coupling problem that was fixed later (a software fix mitigated the problem somewhat during these early runs). The online L0_zfrf and Cpi veto were not enabled for this first event. The L1.n rejection was low for the first event because the L1.2 return code was not working and L1.2 was not applied online. We had longer TD and CCDA readout windows, but shorter RSTDC window (6us instead of 10us)

The run 49787 comes soon after the IC CFD widths were increased back to 30ns from 10ns and a subsequent increase in L0 rejection (49751).

The run 49352 occurs during a period when the BVL rate was higher than at other times for reasons that I have not understood.

In Figures 96 through 142, the runs containing the scaler information are indicated by black histograms or black dots. The black dots are missing from some plots, either due to the range of ordinate or a PAW plotting 'feature' to omit the point when it is too close to an axis.

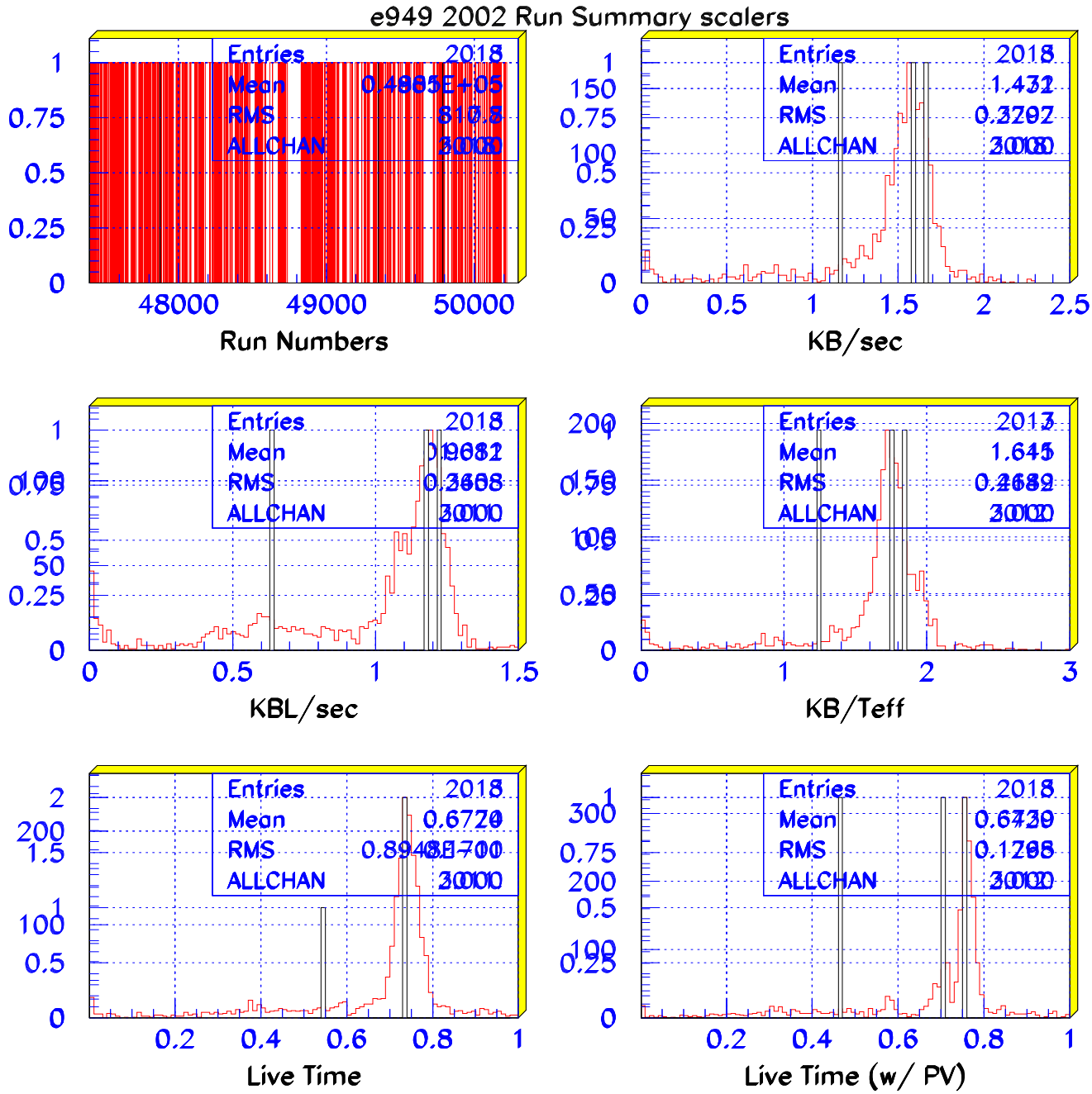
e949 2002 Run Summary scalers
Entries
Mean
RMS
ALLCHAN
Run Numbers
KB/sec
KBL/sec
KB/Teff
Live Time
Live Time (w/ PV)

Figure 96:

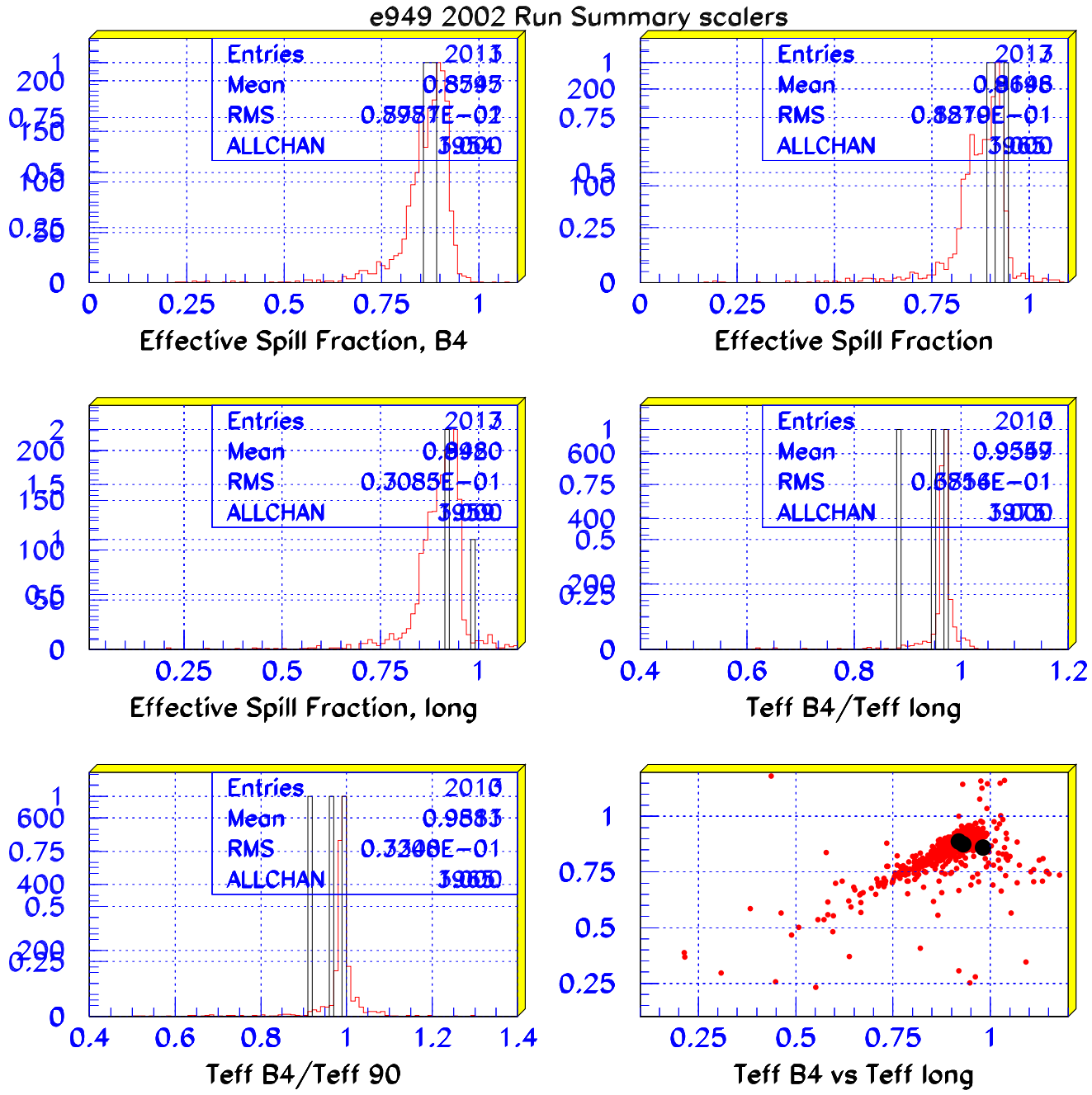
e949 2002 Run Summary scalers
Entries
Mean
RMS
ALLCHAN
Effective Spill Fraction, B4
Effective Spill Fraction
Effective Spill Fraction, long
Teff B4/Teff long
Teff B4/Teff 90
Teff B4 vs Teff long

Figure 97:

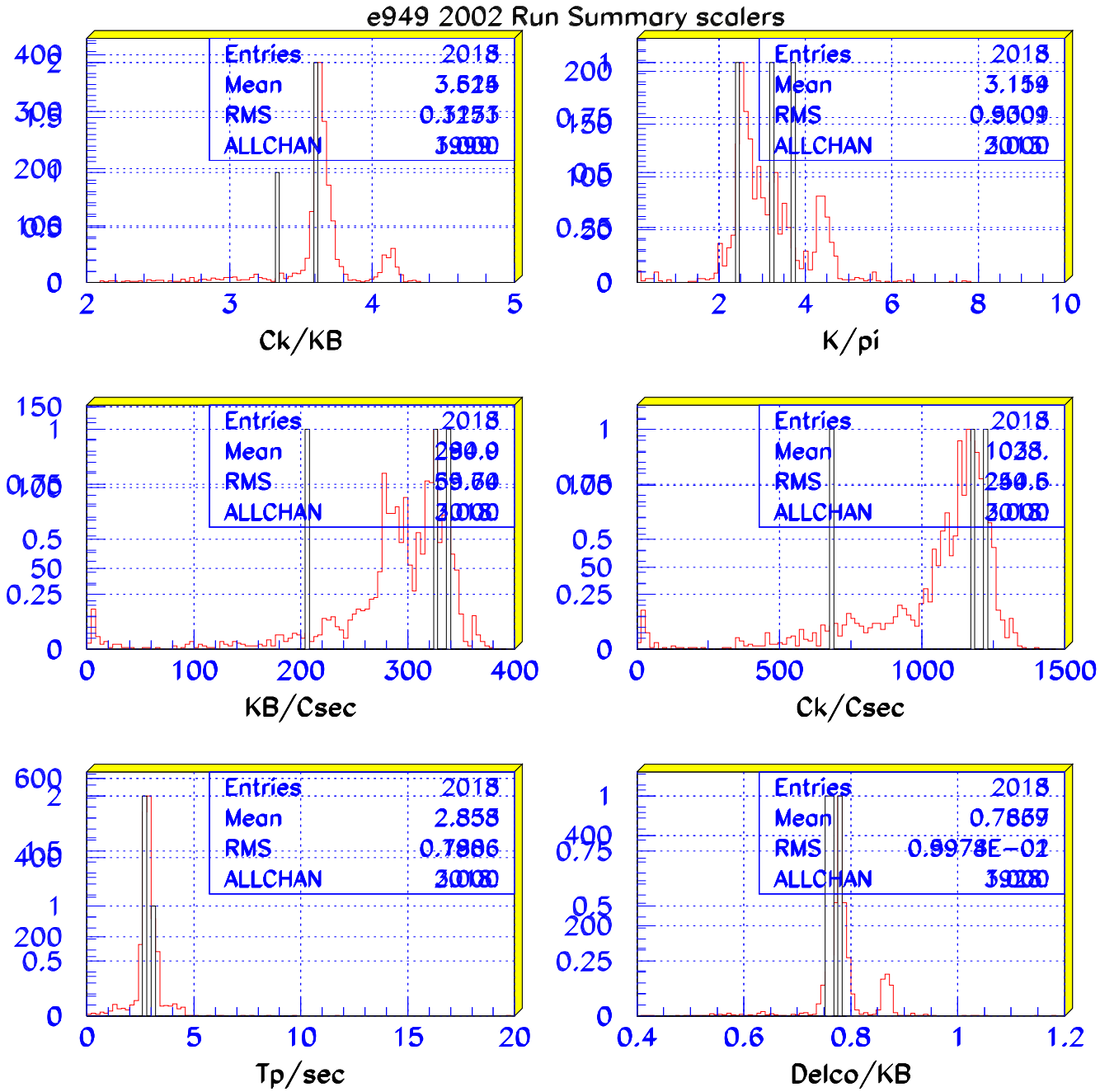
e949 2002 Run Summary scalers
Entries
Mean
RMS
ALLCHAN
Ck/KB
K/pi
KB/Csec
Ck/Csec
Tp/sec
Delco/KB

Figure 98:

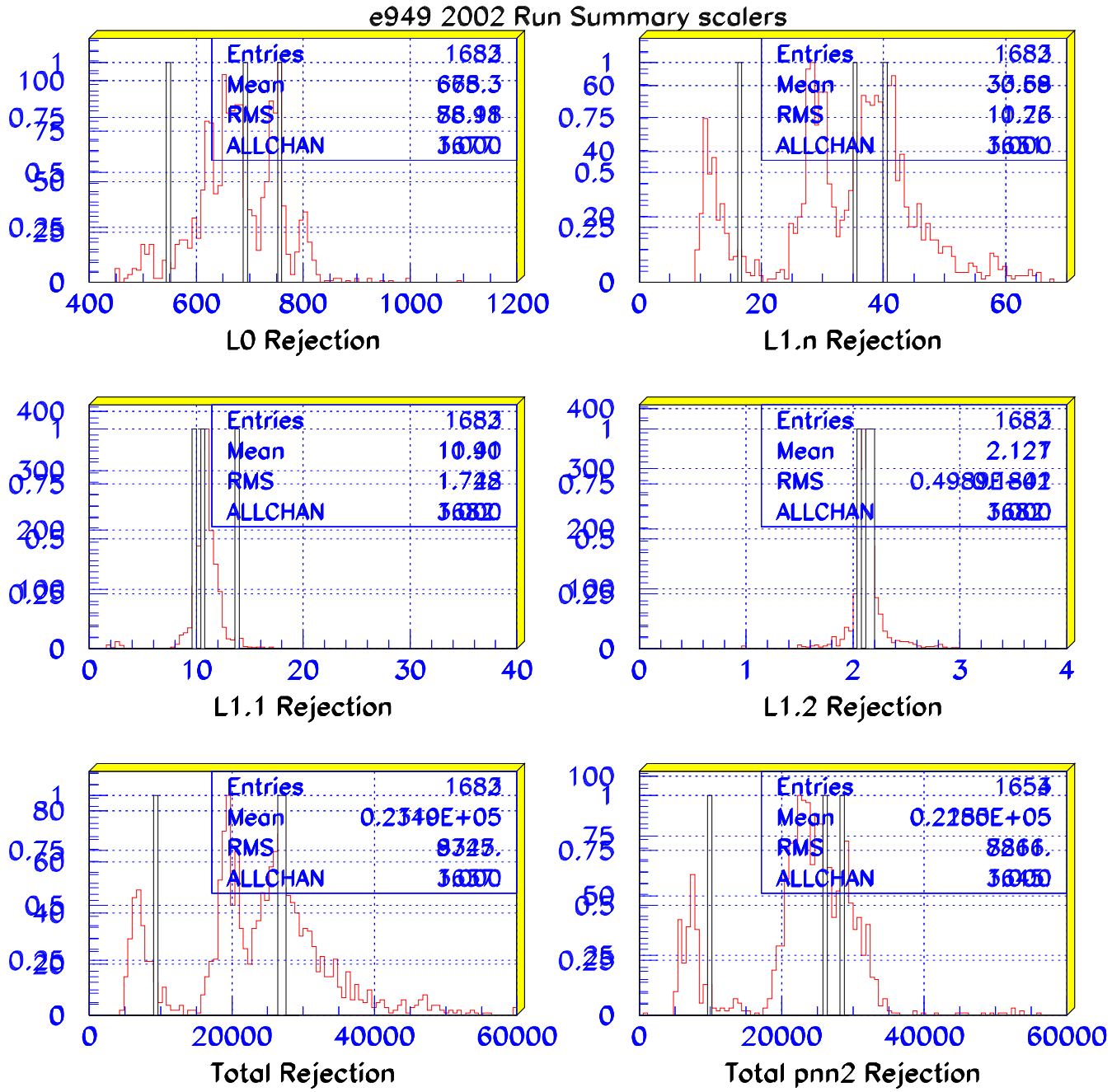
e949 2002 Run Summary scalers
Entries
Mean
RMS
ALLCHAN
L0 Rejection
L1.n Rejection
L1.1 Rejection
L1.2 Rejection
Total Rejection
Total pnn2 Rejection

Figure 99:

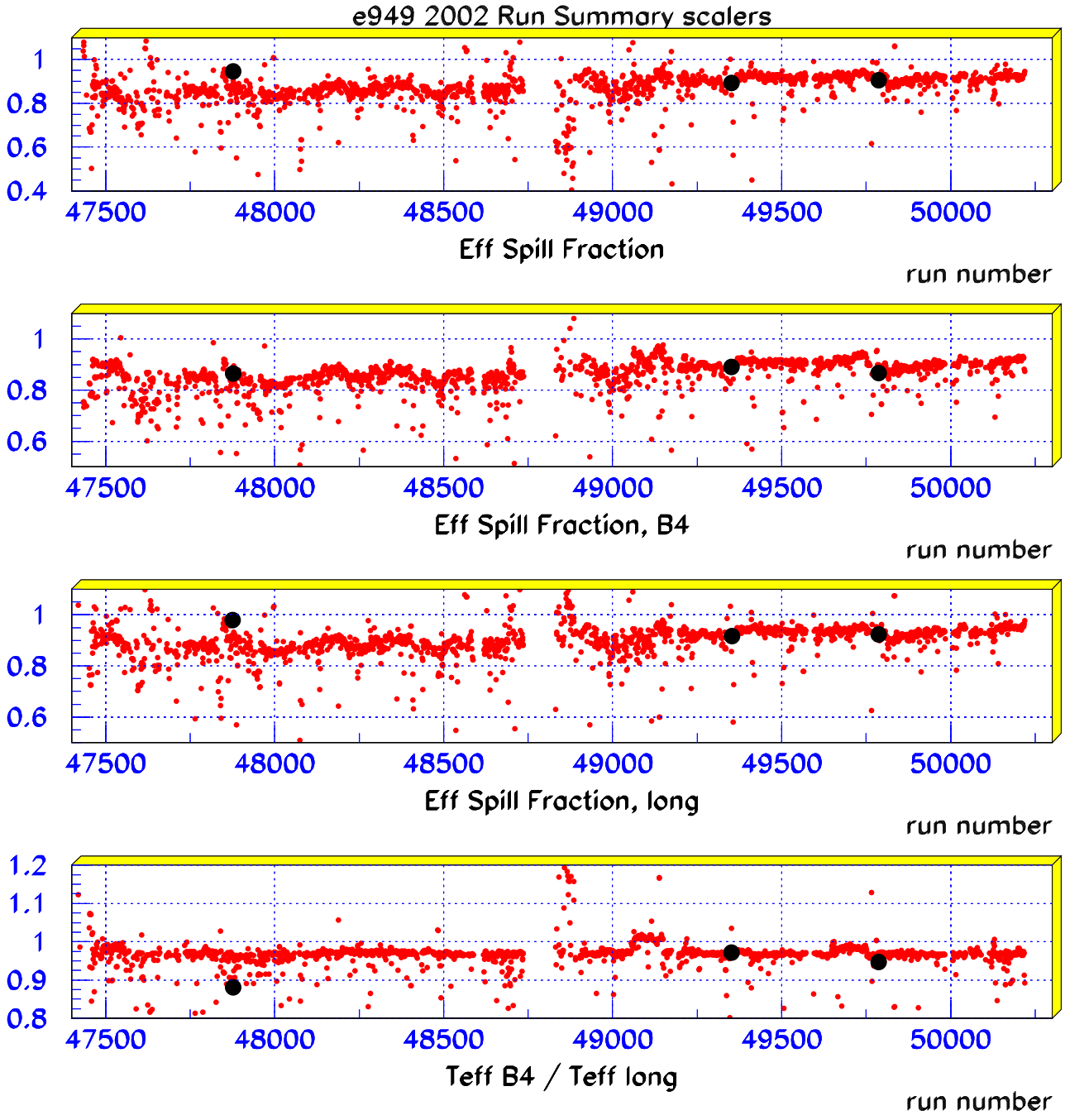
e949 2002 Run Summary scalers
1
0.8
0.6
0.4
47500
48000
48500
49000
49500
50000
Eff Spill Fraction
run number
1
0.8
0.6
47500
48000
48500
49000
49500
50000
Eff Spill Fraction, B4
run number
1
0.8
0.6
47500
48000
48500
49000
49500
50000
Eff Spill Fraction, long
run number
1.2
1.1
1
0.9
0.8
47500
48000
48500
49000
49500
50000
Teff B4 / Teff long
run number

Figure 100:

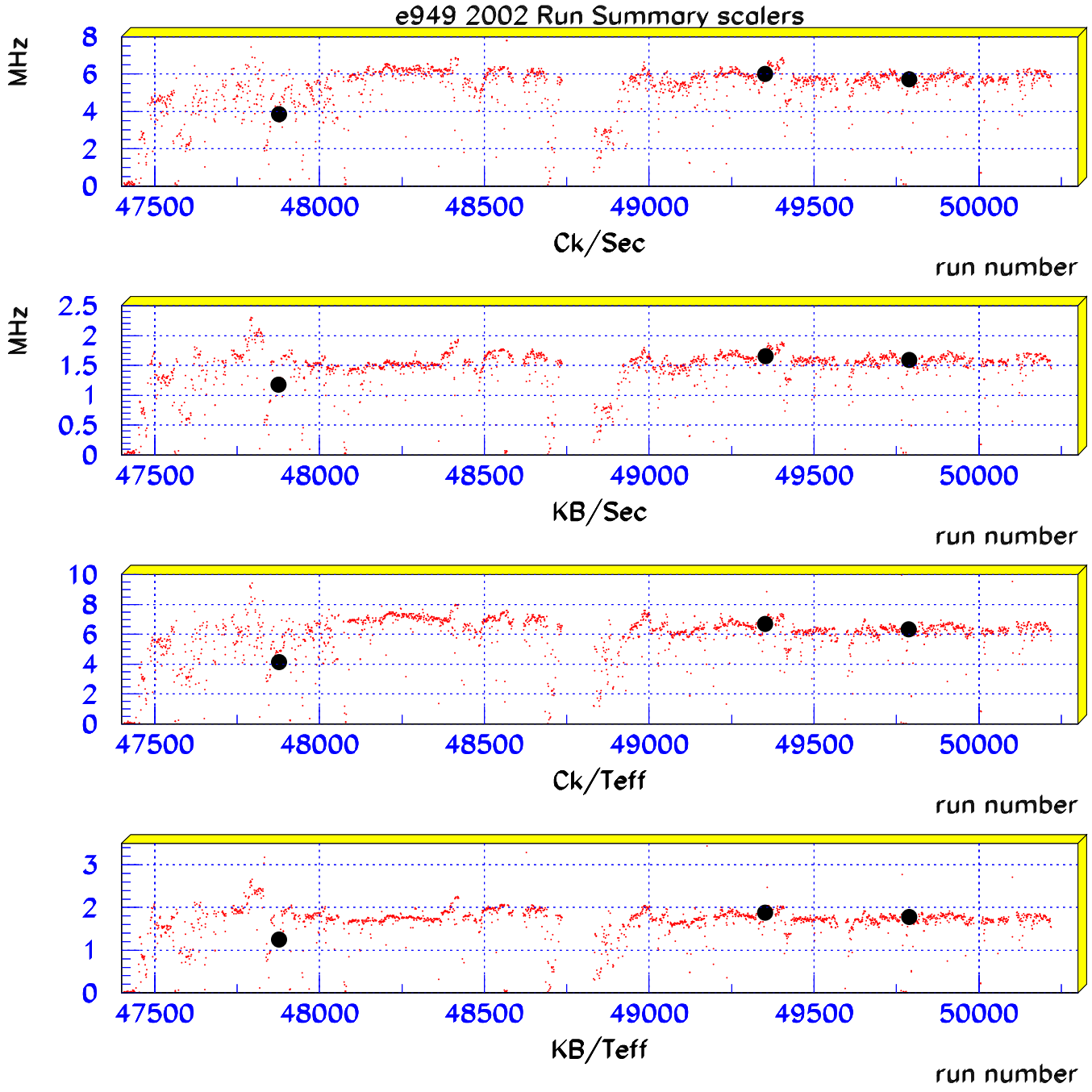
e949 2002 Run Summary scalers
MHz
8
6
4
2
0
47500
48000
48500
49000
49500
50000
Ck/Sec
run number
MHz
2.5
2
1.5
1
0.5
0
47500
48000
48500
49000
49500
50000
KB/Sec
run number
10
8
6
4
2
0
47500
48000
48500
49000
49500
50000
Ck/Teff
run number
3
2
1
0
47500
48000
48500
49000
49500
50000
KB/Teff
run number

Figure 101:

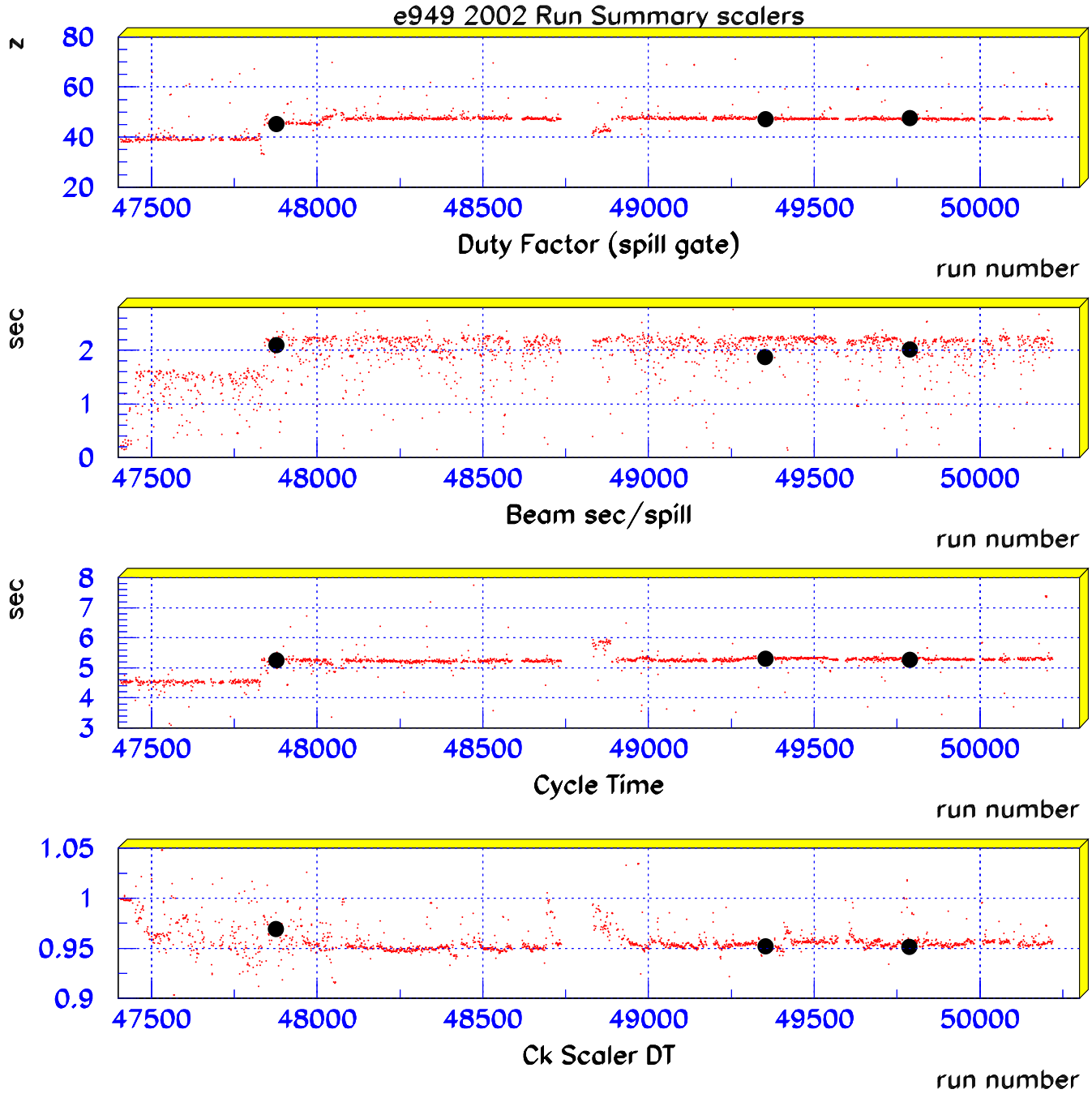
e949 2002 Run Summary scalers
z
80
60
40
20
47500
48000
48500
49000
49500
50000
Duty Factor (spill gate)
run number
sec
2
1
0
Beam sec/spill
run number
sec
8
7
6
5
4
3
Cycle Time
run number
1.05
1
0.95
0.9
Ck Scaler DT
run number

Figure 102:

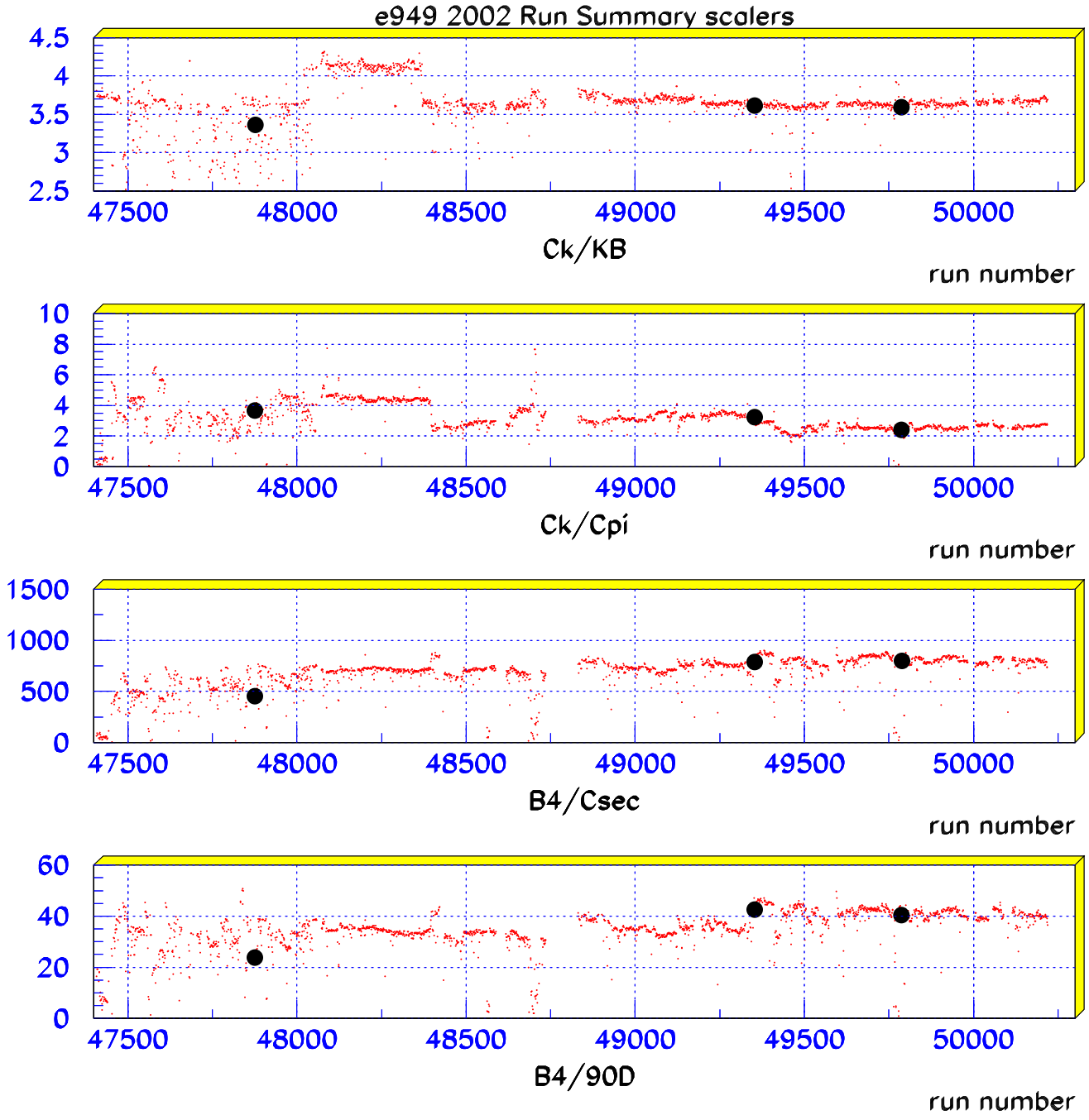
e949 2002 Run Summary scalers
4.5
4
3.5
3
2.5
47500
48000
48500
49000
49500
50000
Ck/KB
run number
10
8
6
4
2
0
47500
48000
48500
49000
49500
50000
Ck/Cpi
run number
1500
1000
500
0
47500
48000
48500
49000
49500
50000
B4/Csec
run number
60
40
20
0
47500
48000
48500
49000
49500
50000
B4/90D
run number

Figure 103:

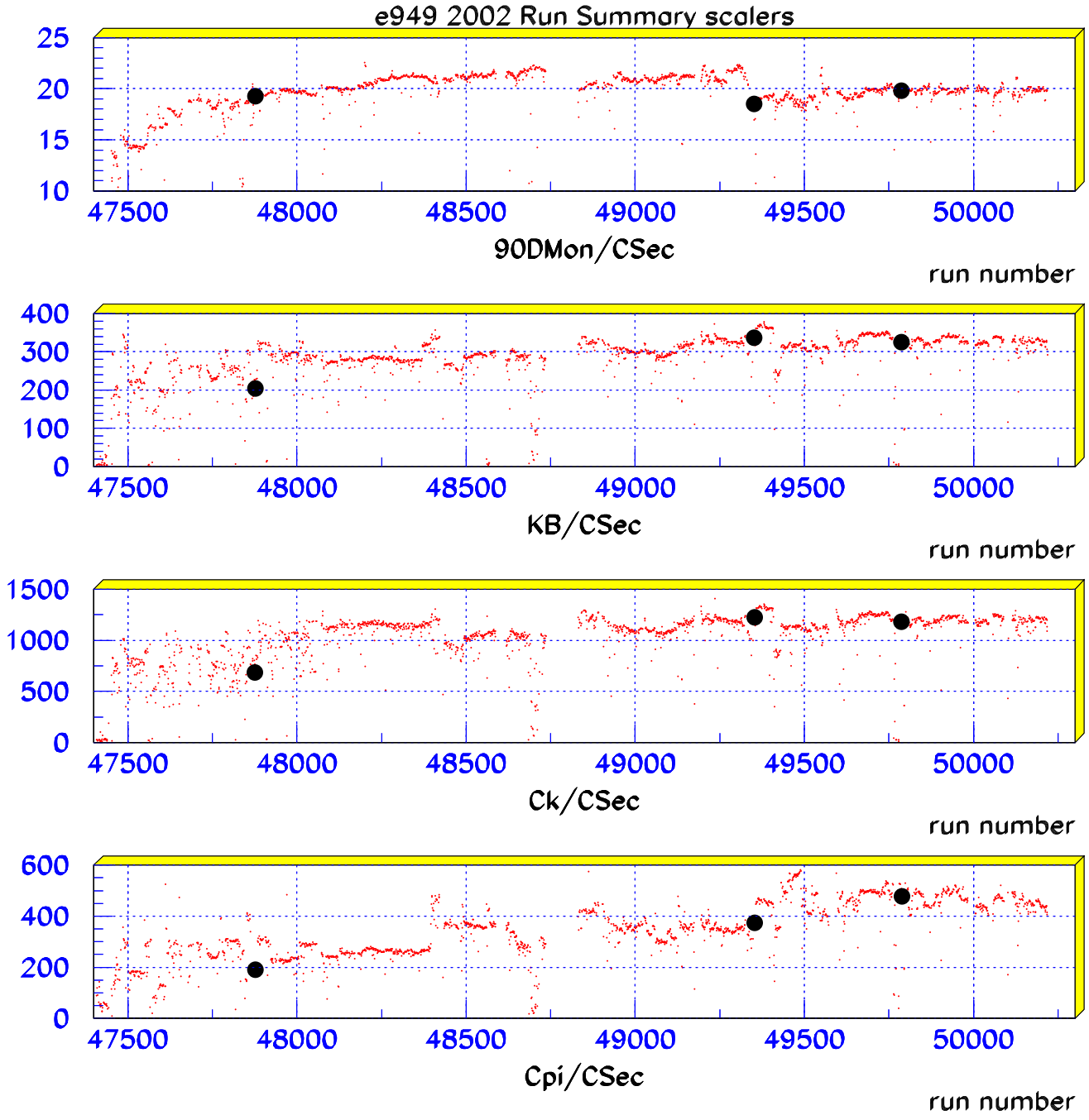
e949 2002 Run Summary scalers
25
20
15
10
47500
48000
48500
49000
49500
50000
90DMon/CSec
run number
400
300
200
100
0
47500
48000
48500
49000
49500
50000
KB/CSec
run number
1500
1000
500
0
47500
48000
48500
49000
49500
50000
Ck/CSec
run number
600
400
200
0
47500
48000
48500
49000
49500
50000
Cpi/CSec
run number

Figure 104:

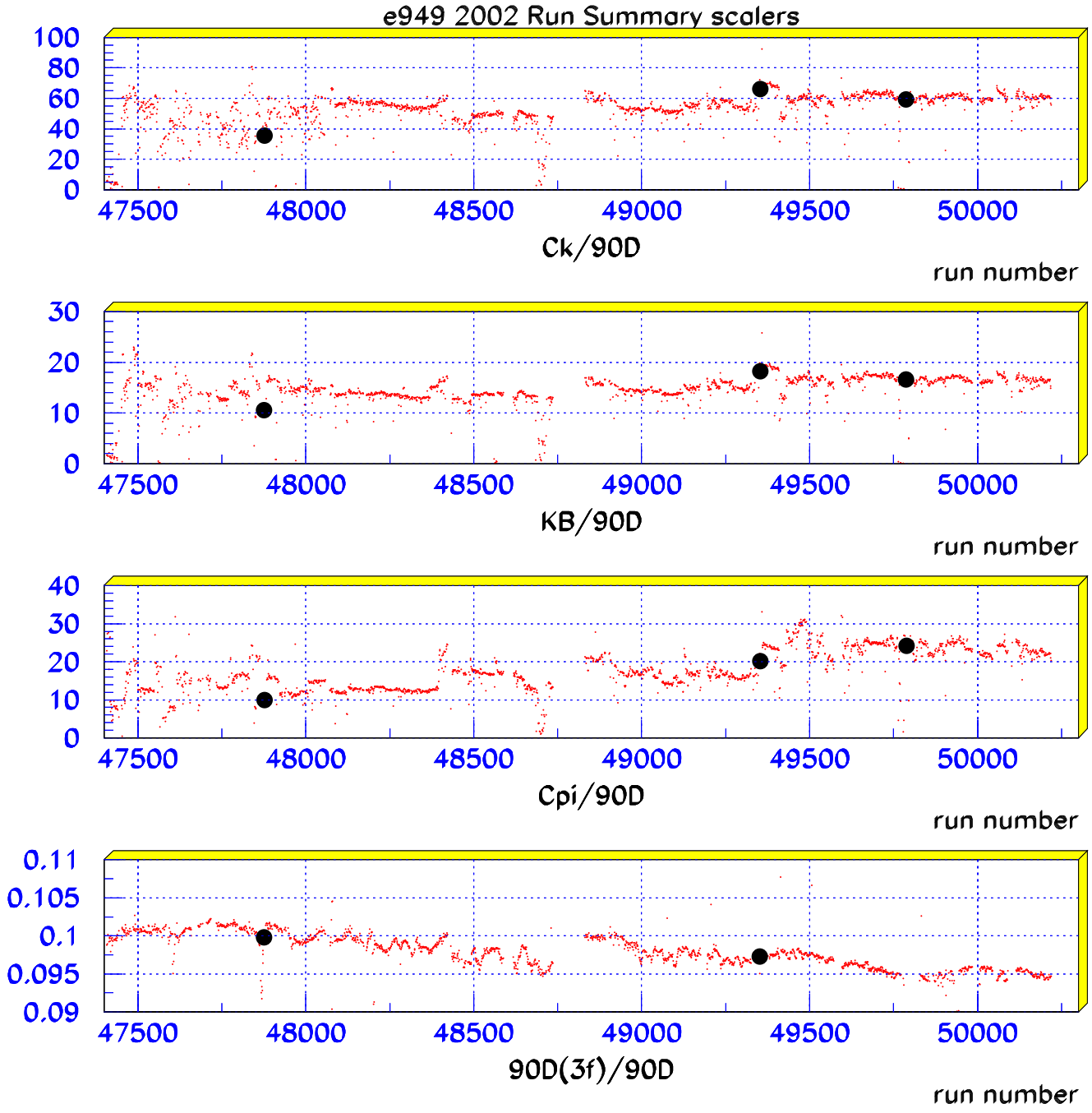
e949 2002 Run Summary scalers
100
80
60
40
20
0
47500
48000
48500
49000
49500
50000
Ck/90D
run number
30
20
10
0
47500
48000
48500
49000
49500
50000
KB/90D
run number
40
30
20
10
0
47500
48000
48500
49000
49500
50000
Cpi/90D
run number
0.11
0.105
0.1
0.095
0.09
47500
48000
48500
49000
49500
50000
90D(3f)/90D
run number

Figure 105:

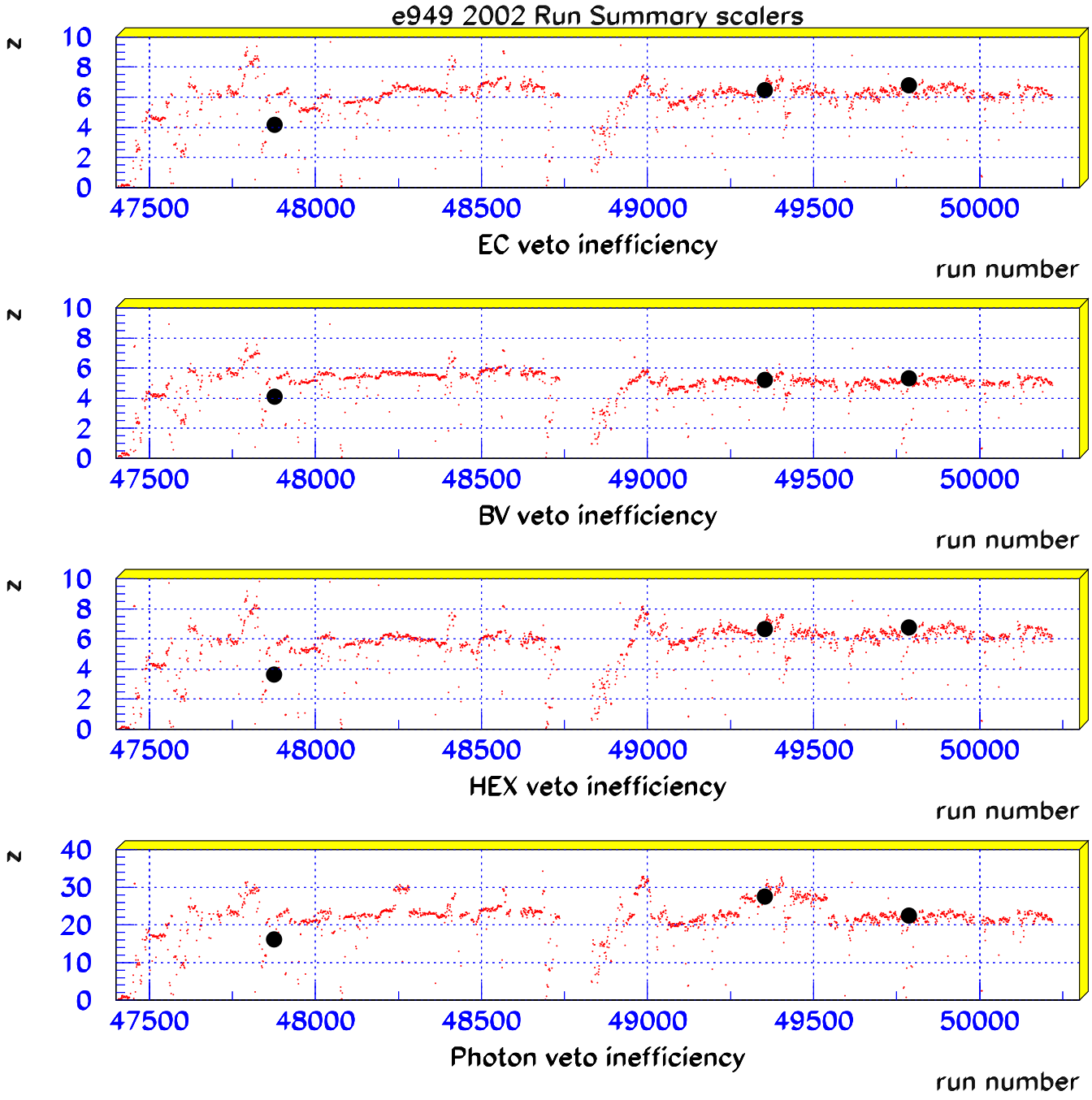
e949 2002 Run Summary scalers
N
10
8
6
4
2
0
47500
48000
48500
49000
49500
50000
EC veto inefficiency
run number
BV veto inefficiency
run number
HEX veto inefficiency
run number
40
30
20
10
Photon veto inefficiency
run number

Figure 106:

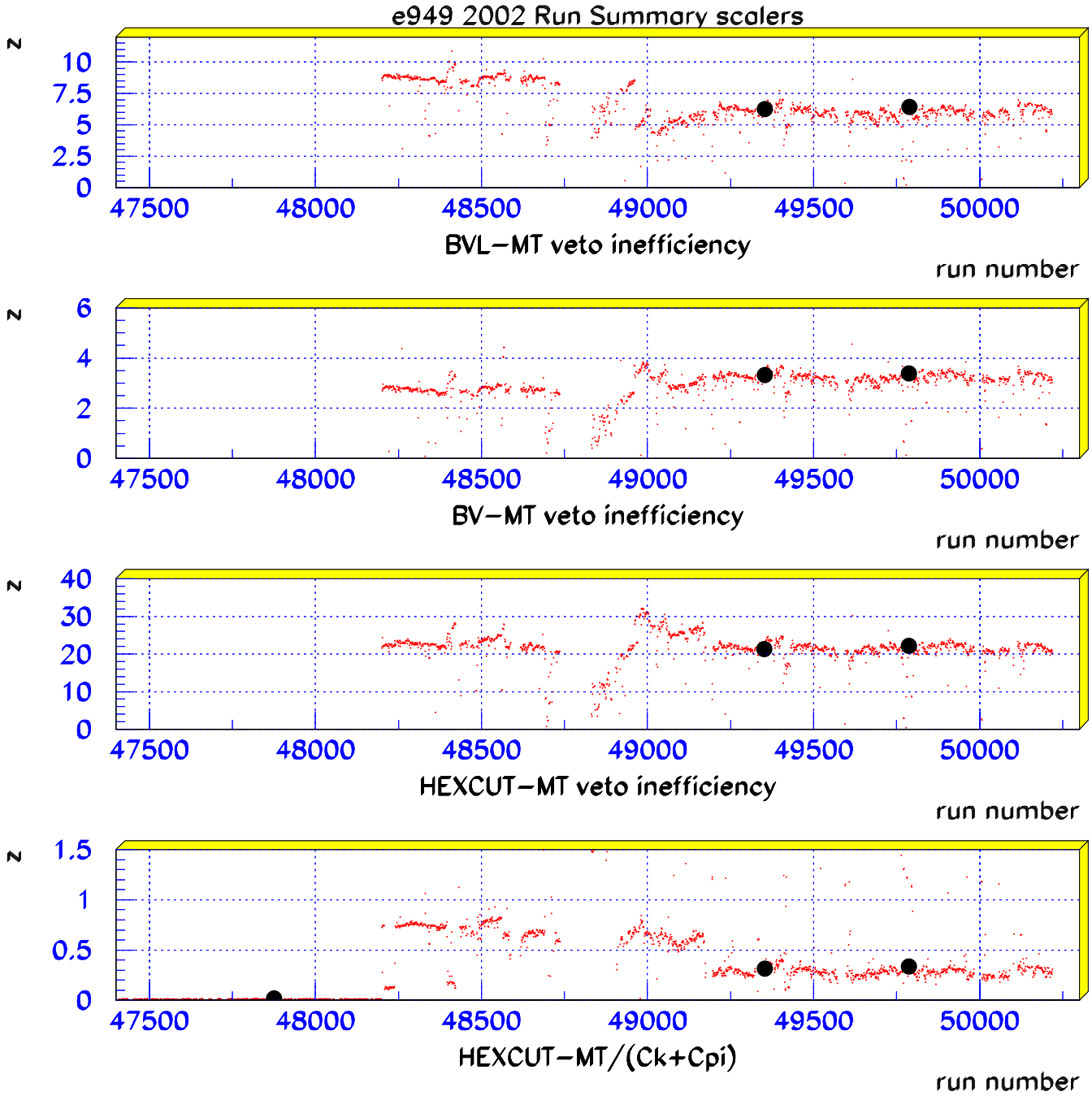
e949 2002 Run Summary scalers
z
10
7.5
5
2.5
0
47500
48000
48500
49000
49500
50000
BVL−MT veto inefficiency
run number
z
6
4
2
0
47500
48000
48500
49000
49500
50000
BV−MT veto inefficiency
run number
z
40
30
20
10
0
47500
48000
48500
49000
49500
50000
HEXCUT−MT veto inefficiency
run number
z
1.5
1
0.5
0
47500
48000
48500
49000
49500
50000
HEXCUT−MT/(Ck+Cpi)
run number

Figure 107:

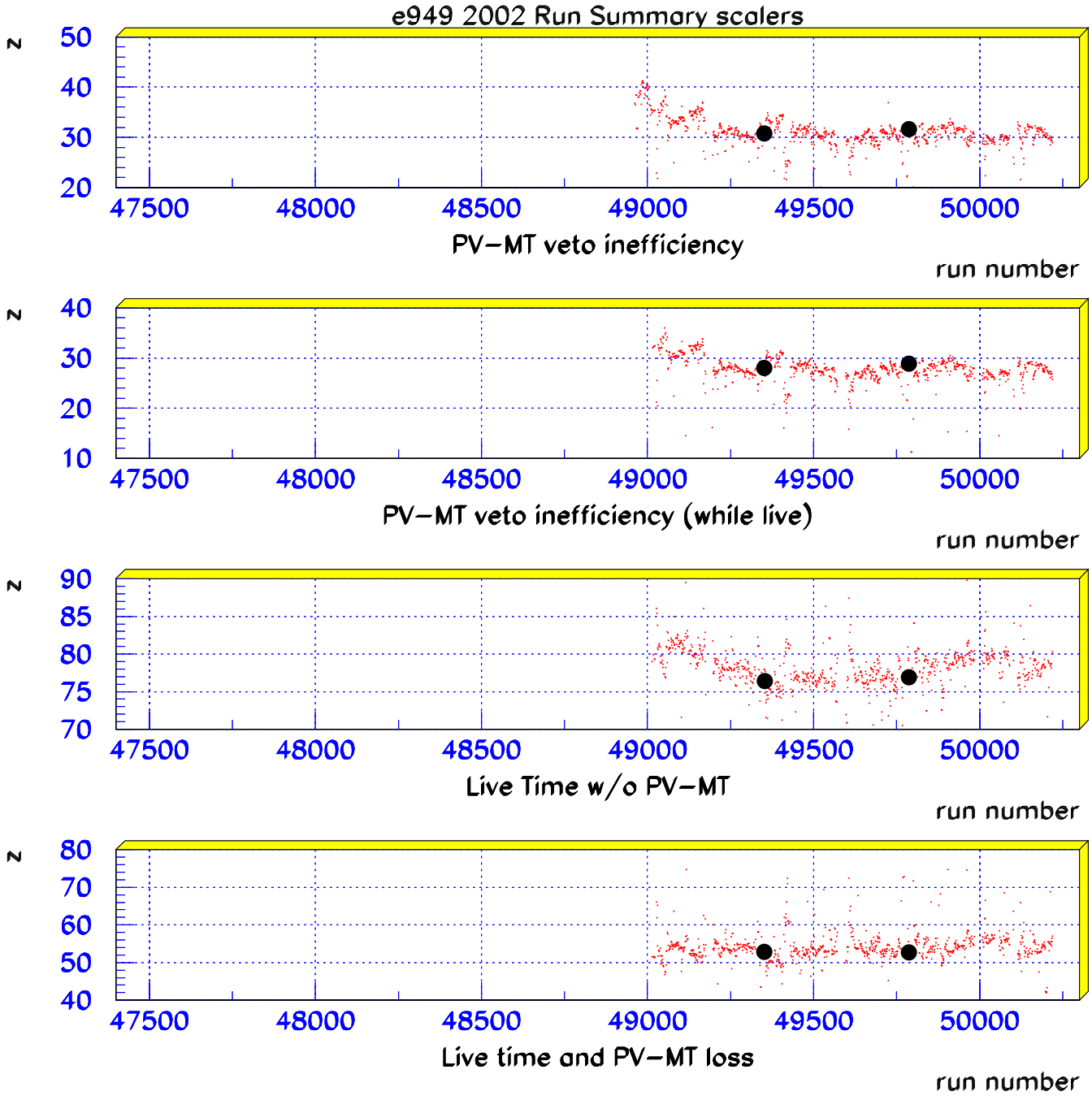
e949 2002 Run Summary scalers
z
50
40
30
20
47500
48000
48500
49000
49500
50000
PV−MT veto inefficiency
run number
z
40
30
20
10
47500
48000
48500
49000
49500
50000
PV−MT veto inefficiency (while live)
run number
z
90
85
80
75
70
47500
48000
48500
49000
49500
50000
Live Time w/o PV−MT
run number
z
80
70
60
50
40
47500
48000
48500
49000
49500
50000
Live time and PV−MT loss
run number

Figure 108:

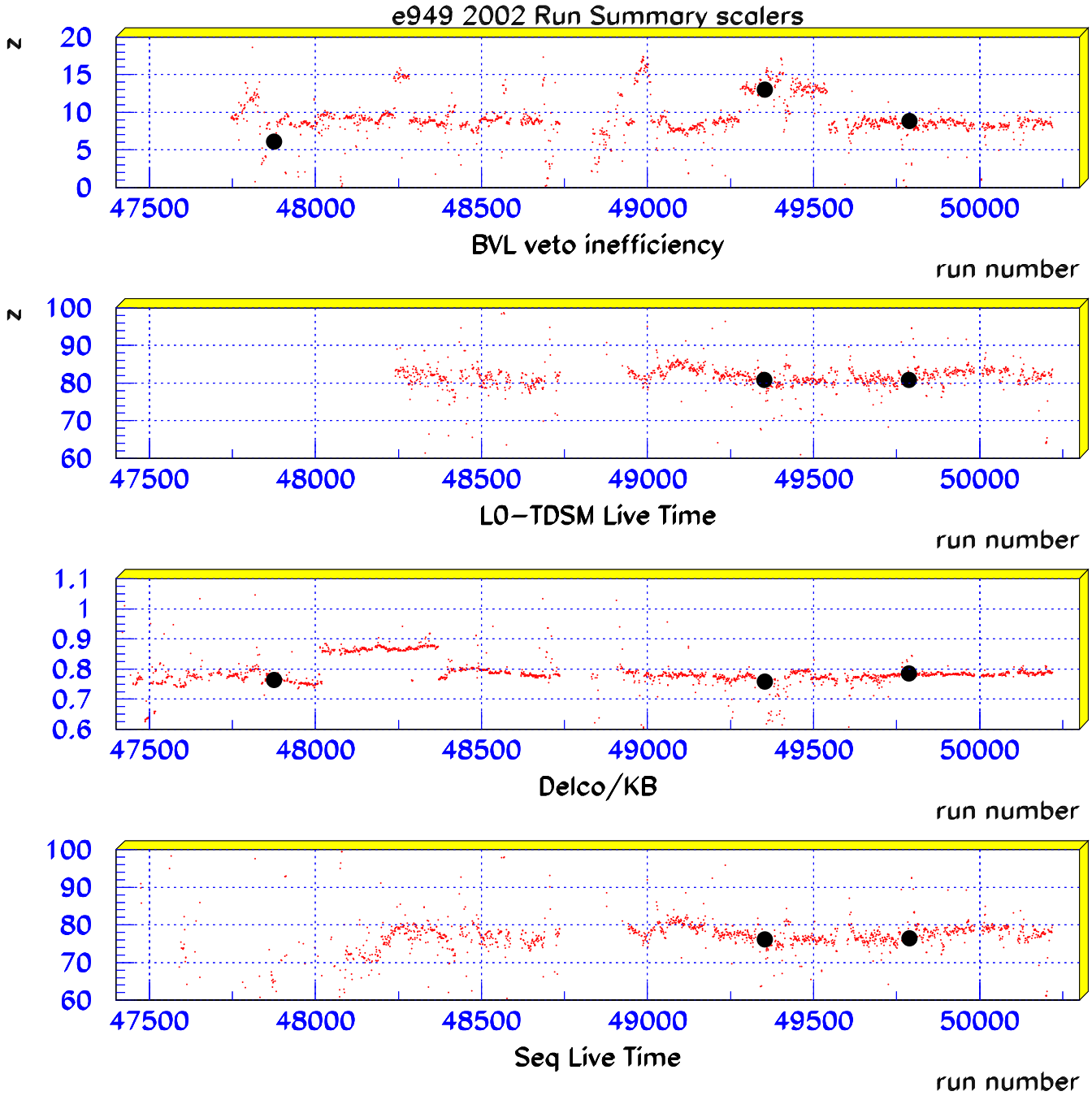
e949 2002 Run Summary scalers
z
20
15
10
5
0
47500
48000
48500
49000
49500
50000
BVL veto inefficiency
run number
z
100
90
80
70
60
47500
48000
48500
49000
49500
50000
L0−TDSM Live Time
run number
1.1
1
0.9
0.8
0.7
0.6
47500
48000
48500
49000
49500
50000
Delco/KB
run number
100
90
80
70
60
47500
48000
48500
49000
49500
50000
Seq Live Time
run number

Figure 109:

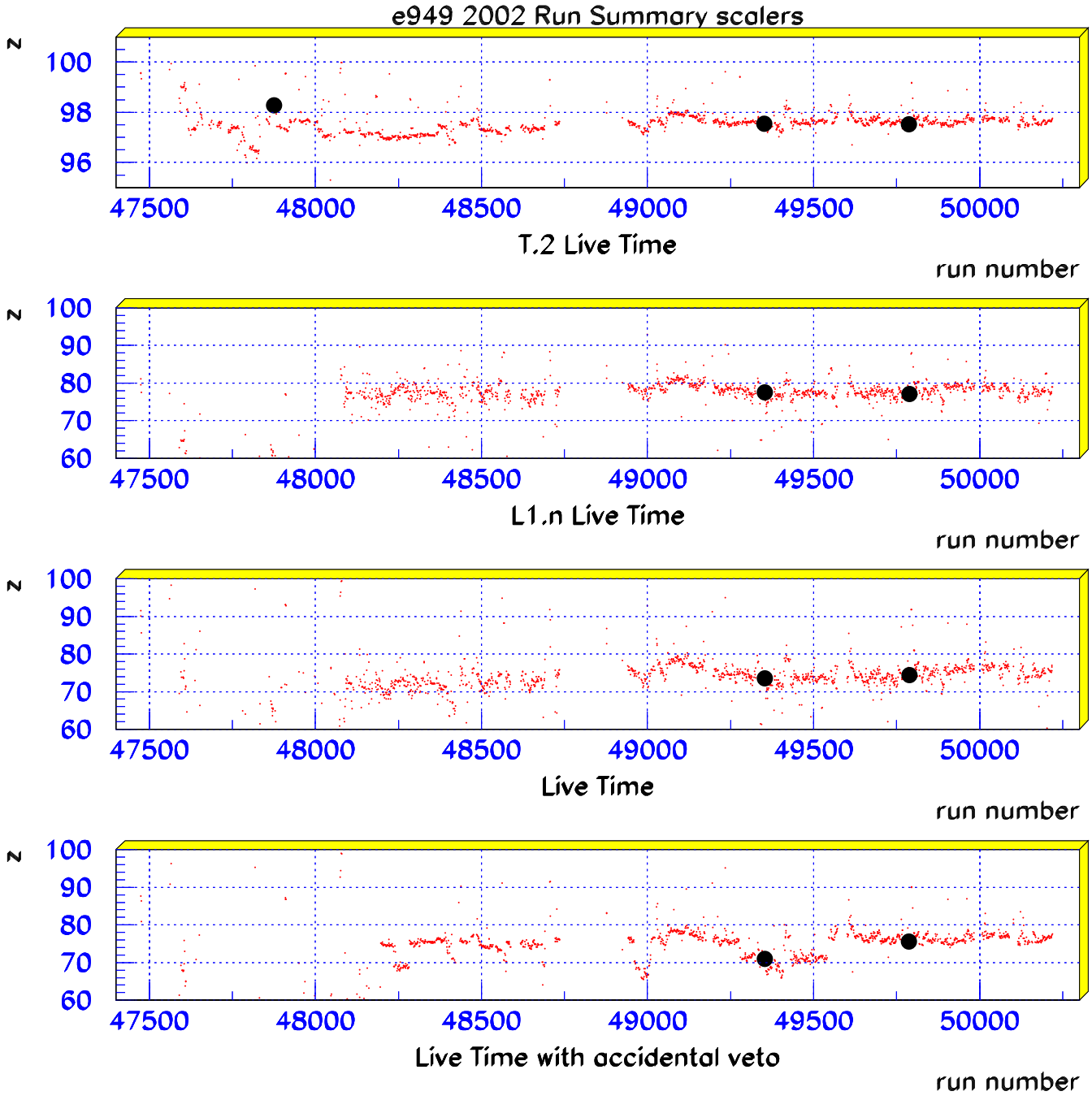
e949 2002 Run Summary scalers
z
100
98
96
47500
48000
48500
49000
49500
50000
T.2 Live Time
run number
z
100
90
80
70
60
47500
48000
48500
49000
49500
50000
L1.n Live Time
run number
z
100
90
80
70
60
47500
48000
48500
49000
49500
50000
Live Time
run number
z
100
90
80
70
60
47500
48000
48500
49000
49500
50000
Live Time with accidental veto
run number

Figure 110:

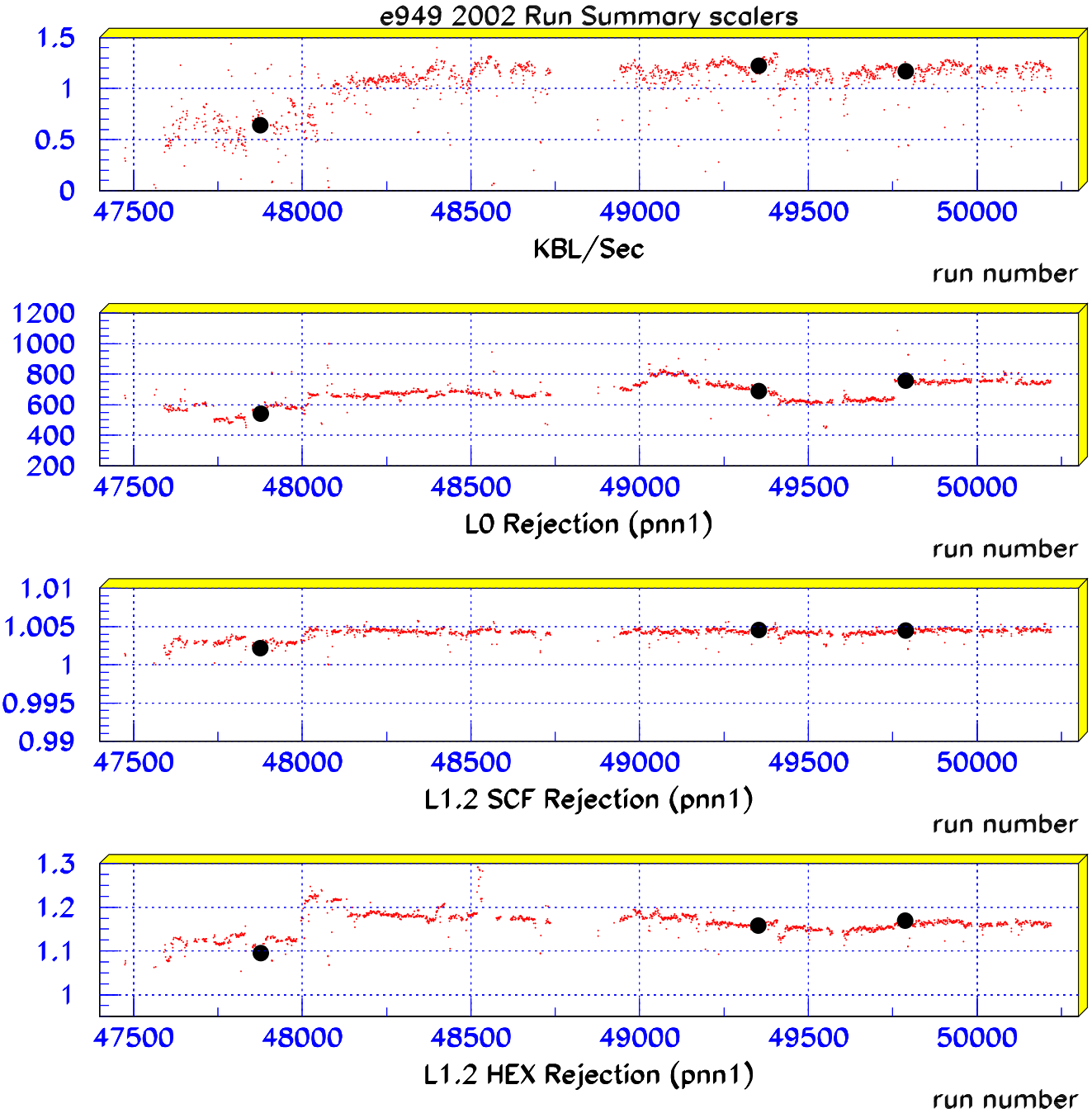
e949 2002 Run Summary scalers
1.5
1
0.5
0
47500
48000
48500
49000
49500
50000
KBL/Sec
run number
1200
1000
800
600
400
200
47500
48000
48500
49000
49500
50000
L0 Rejection (pnn1)
run number
1.01
1.005
1
0.995
0.99
47500
48000
48500
49000
49500
50000
L1.2 SCF Rejection (pnn1)
run number
1.3
1.2
1.1
1
47500
48000
48500
49000
49500
50000
L1.2 HEX Rejection (pnn1)
run number

Figure 111:

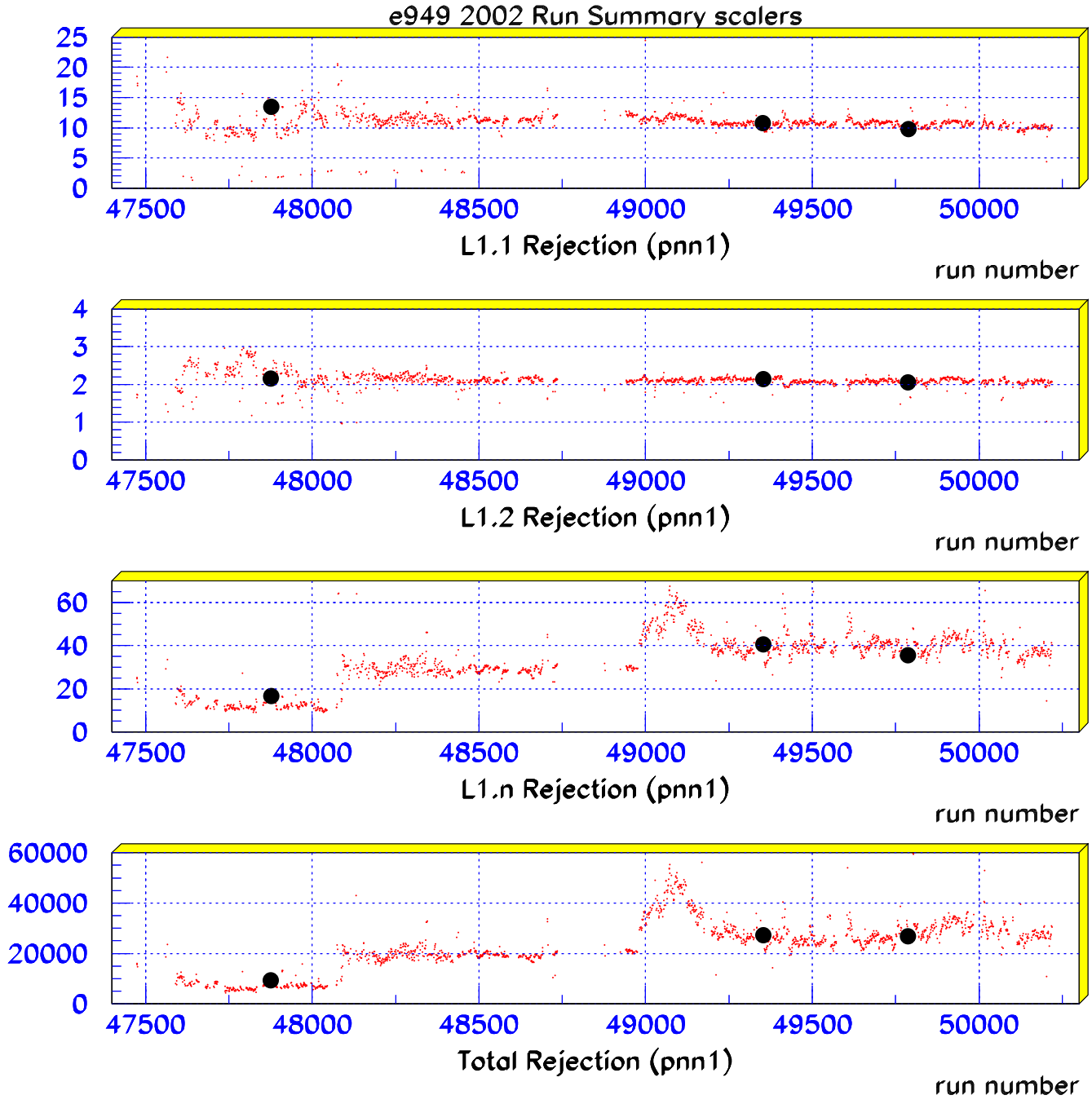
e949 2002 Run Summary scalers
25
20
15
10
5
0
47500
48000
48500
49000
49500
50000
L1.1 Rejection (pnn1)
run number
4
3
2
1
0
47500
48000
48500
49000
49500
50000
L1.2 Rejection (pnn1)
run number
60
40
20
0
47500
48000
48500
49000
49500
50000
L1.n Rejection (pnn1)
run number
60000
40000
20000
0
47500
48000
48500
49000
49500
50000
Total Rejection (pnn1)
run number

Figure 112:

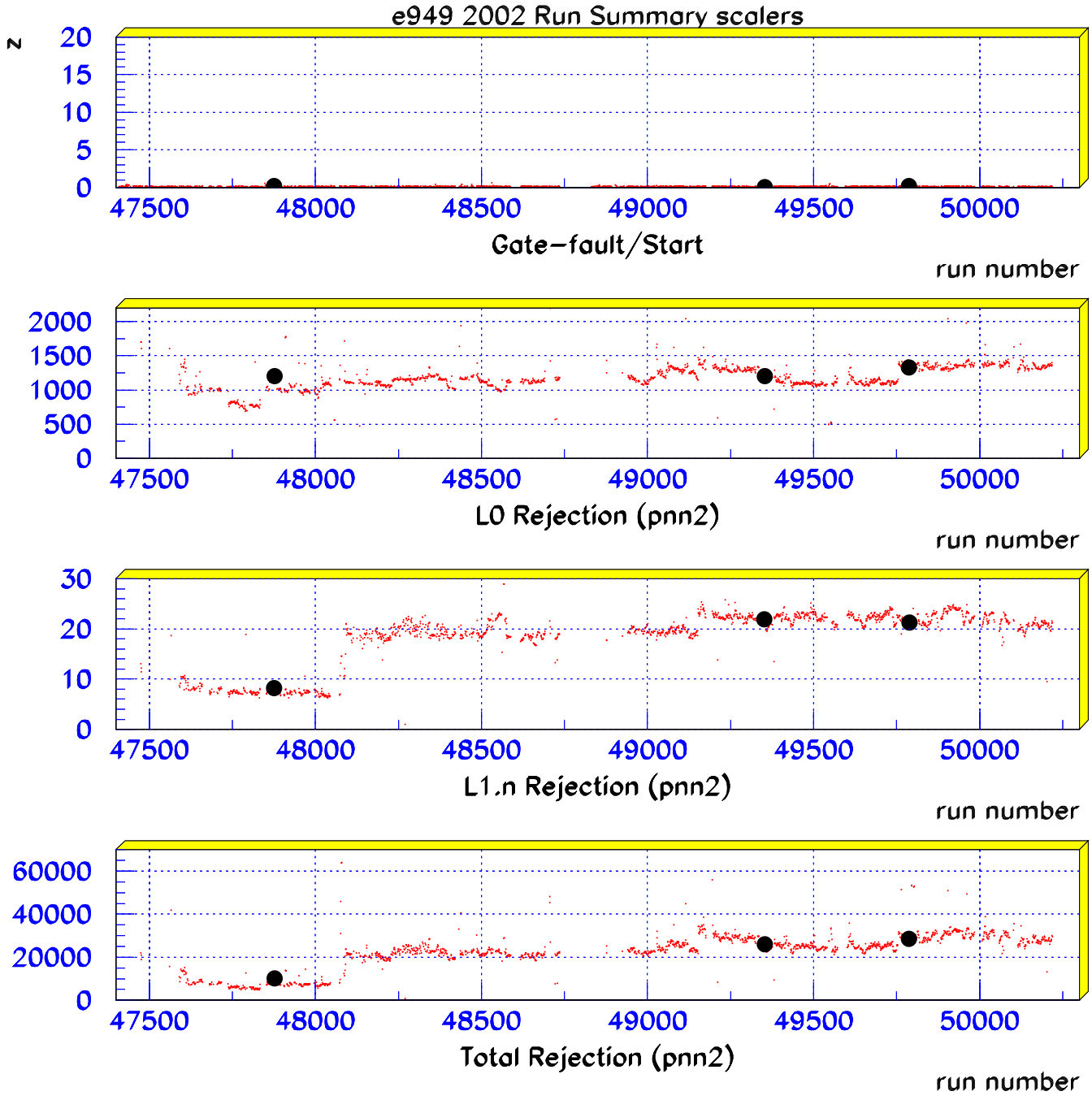
e949 2002 Run Summary scalers
z
20
15
10
5
0
47500
48000
48500
49000
49500
50000
Gate−fault/Start
run number
2000
1500
1000
500
0
47500
48000
48500
49000
49500
50000
L0 Rejection (pnn2)
run number
30
20
10
0
47500
48000
48500
49000
49500
50000
L1.n Rejection (pnn2)
run number
60000
40000
20000
0
47500
48000
48500
49000
49500
50000
Total Rejection (pnn2)
run number

Figure 113:

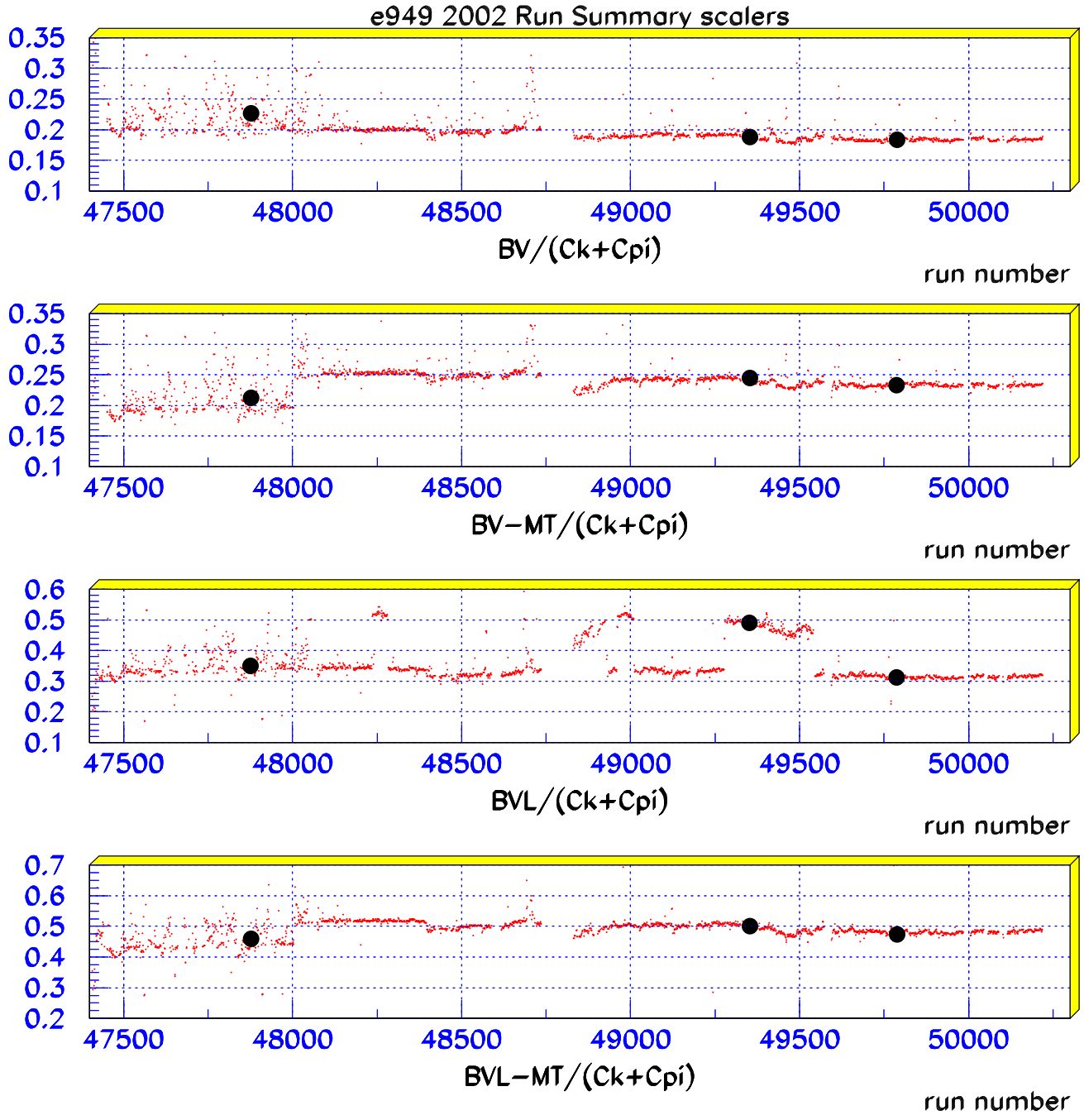
e949 2002 Run Summary scalers
0.35
0.3
0.25
0.2
0.15
0.1
47500
48000
48500
49000
49500
50000
BV/(Ck+Cpi)
run number
BV−MT/(Ck+Cpi)
run number
0.6
0.5
0.4
0.3
0.2
0.1
BVL/(Ck+Cpi)
run number
0.7
0.6
0.5
0.4
0.3
0.2
BVL−MT/(Ck+Cpi)
run number

Figure 114:

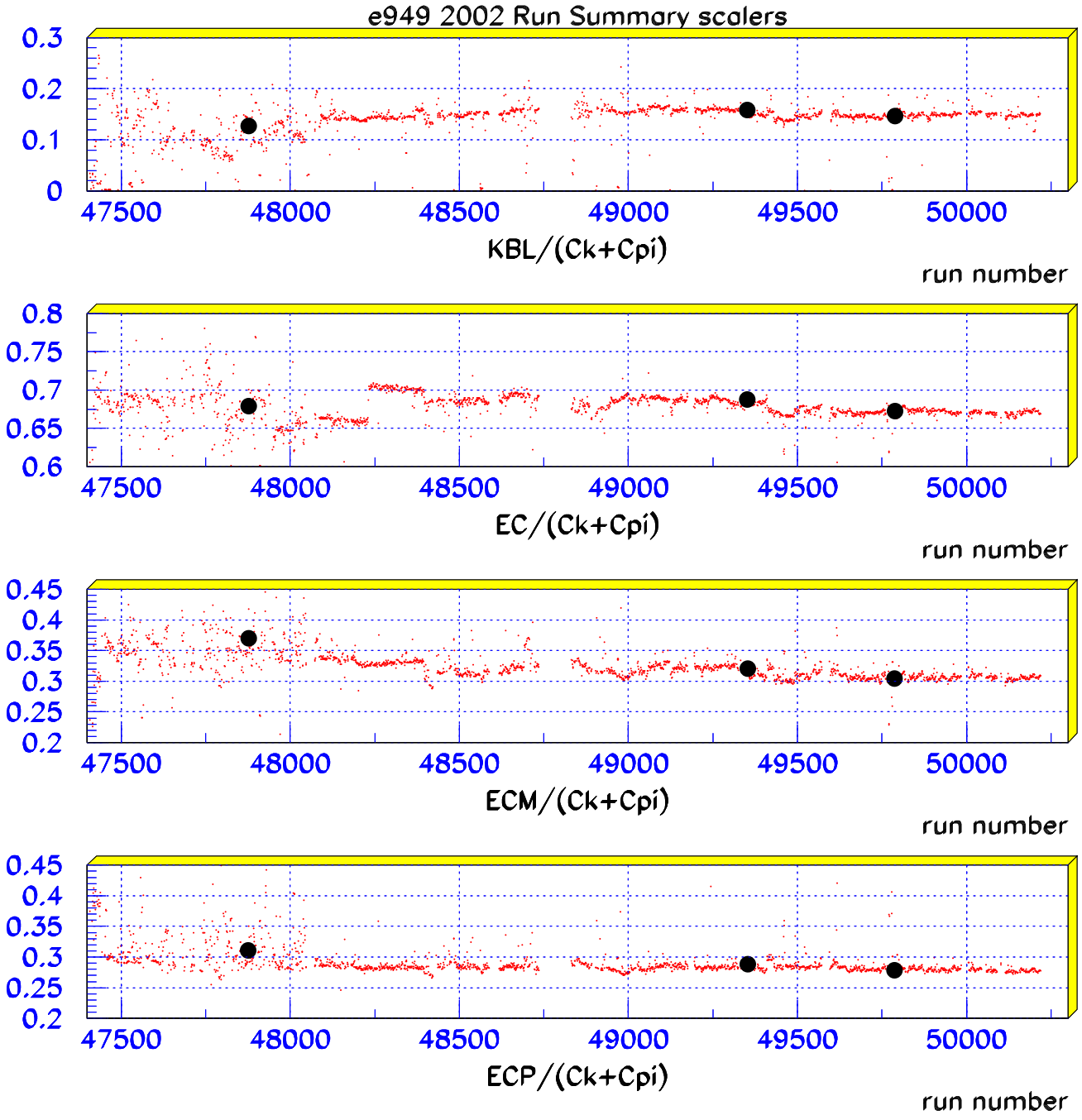
e949 2002 Run Summary scalers
0.3
0.2
0.1
0
47500
48000
48500
49000
49500
50000
KBL/(Ck+Cpi)
run number
0.8
0.75
0.7
0.65
0.6
47500
48000
48500
49000
49500
50000
EC/(Ck+Cpi)
run number
0.45
0.4
0.35
0.3
0.25
0.2
47500
48000
48500
49000
49500
50000
ECM/(Ck+Cpi)
run number
0.45
0.4
0.35
0.3
0.25
0.2
47500
48000
48500
49000
49500
50000
ECP/(Ck+Cpi)
run number

Figure 115:

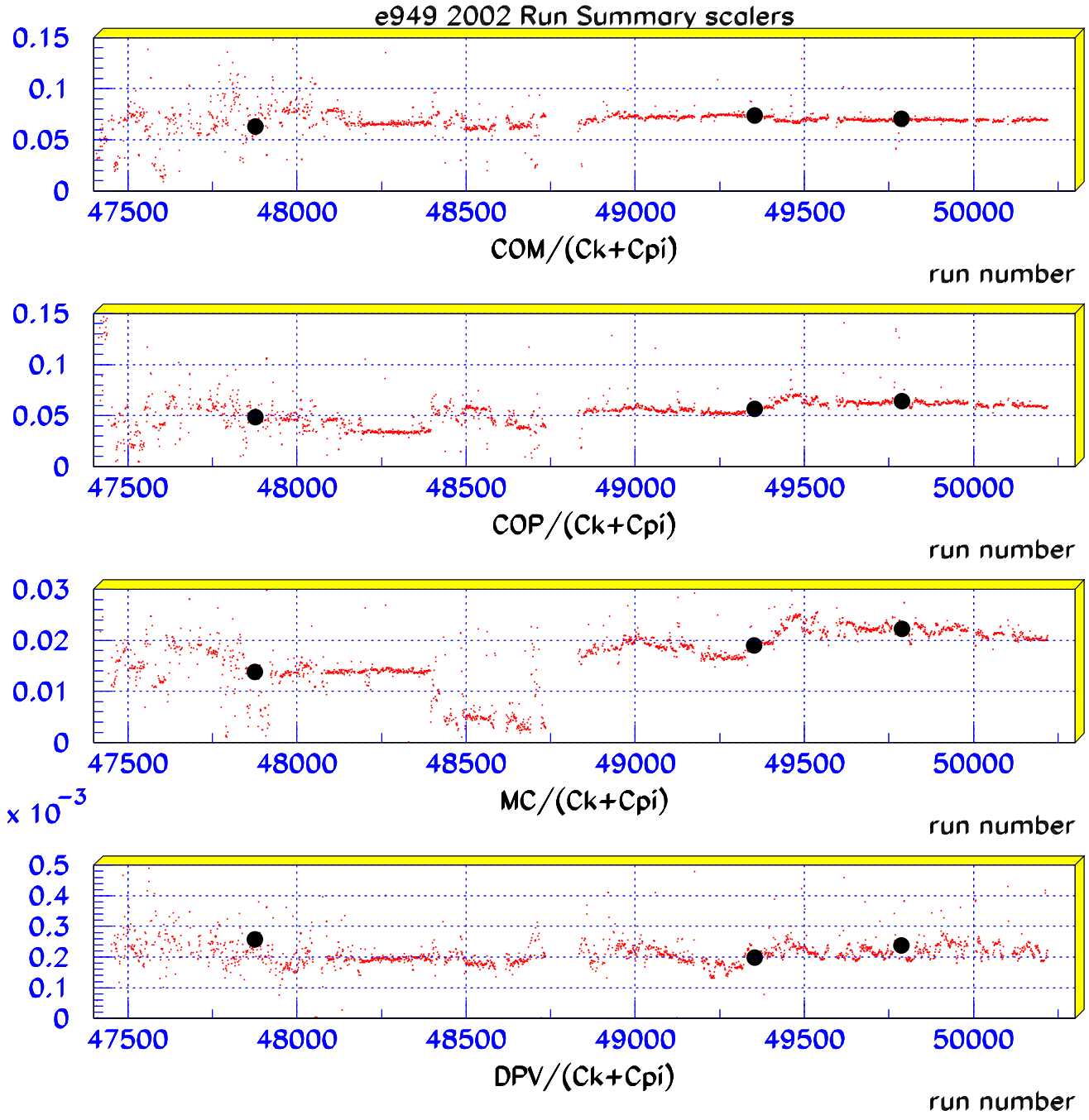
e949 2002 Run Summary scalers
0.15
0.1
0.05
0
47500
48000
48500
49000
49500
50000
COM/(Ck+Cpi)
run number
0.15
0.1
0.05
0
47500
48000
48500
49000
49500
50000
COP/(Ck+Cpi)
run number
0.03
0.02
0.01
0
47500
48000
48500
49000
49500
50000
x 10^-3
MC/(Ck+Cpi)
run number
0.5
0.4
0.3
0.2
0.1
0
47500
48000
48500
49000
49500
50000
DPV/(Ck+Cpi)
run number

Figure 116:

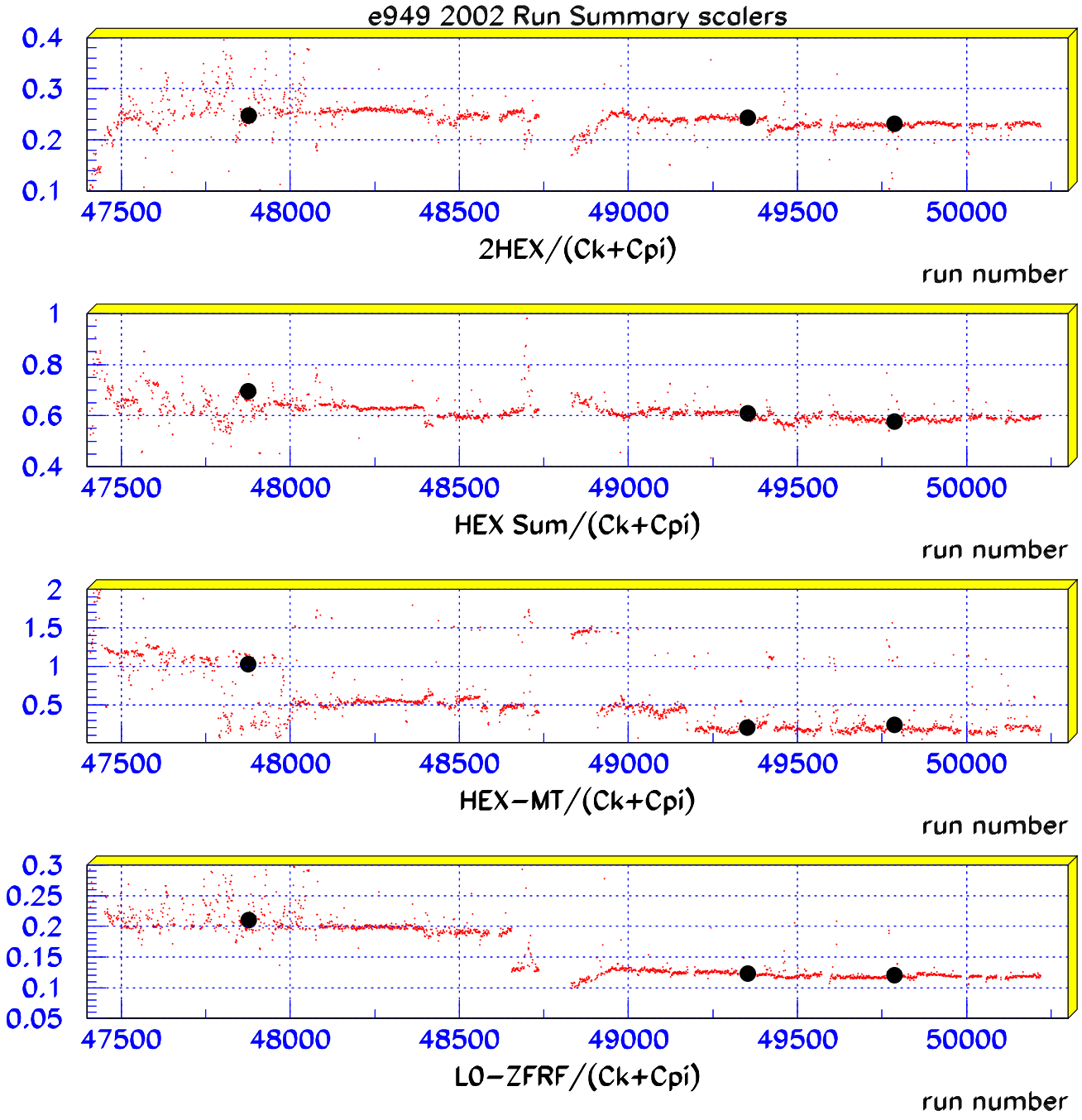
e949 2002 Run Summary scalers
0.4
0.3
0.2
0.1
47500
48000
48500
49000
49500
50000
2HEX/(Ck+Cpi)
run number
1
0.8
0.6
0.4
HEX Sum/(Ck+Cpi)
2
1.5
1
0.5
HEX−MT/(Ck+Cpi)
0.3
0.25
0.2
0.15
0.1
0.05
LO−ZFRF/(Ck+Cpi)

Figure 117:

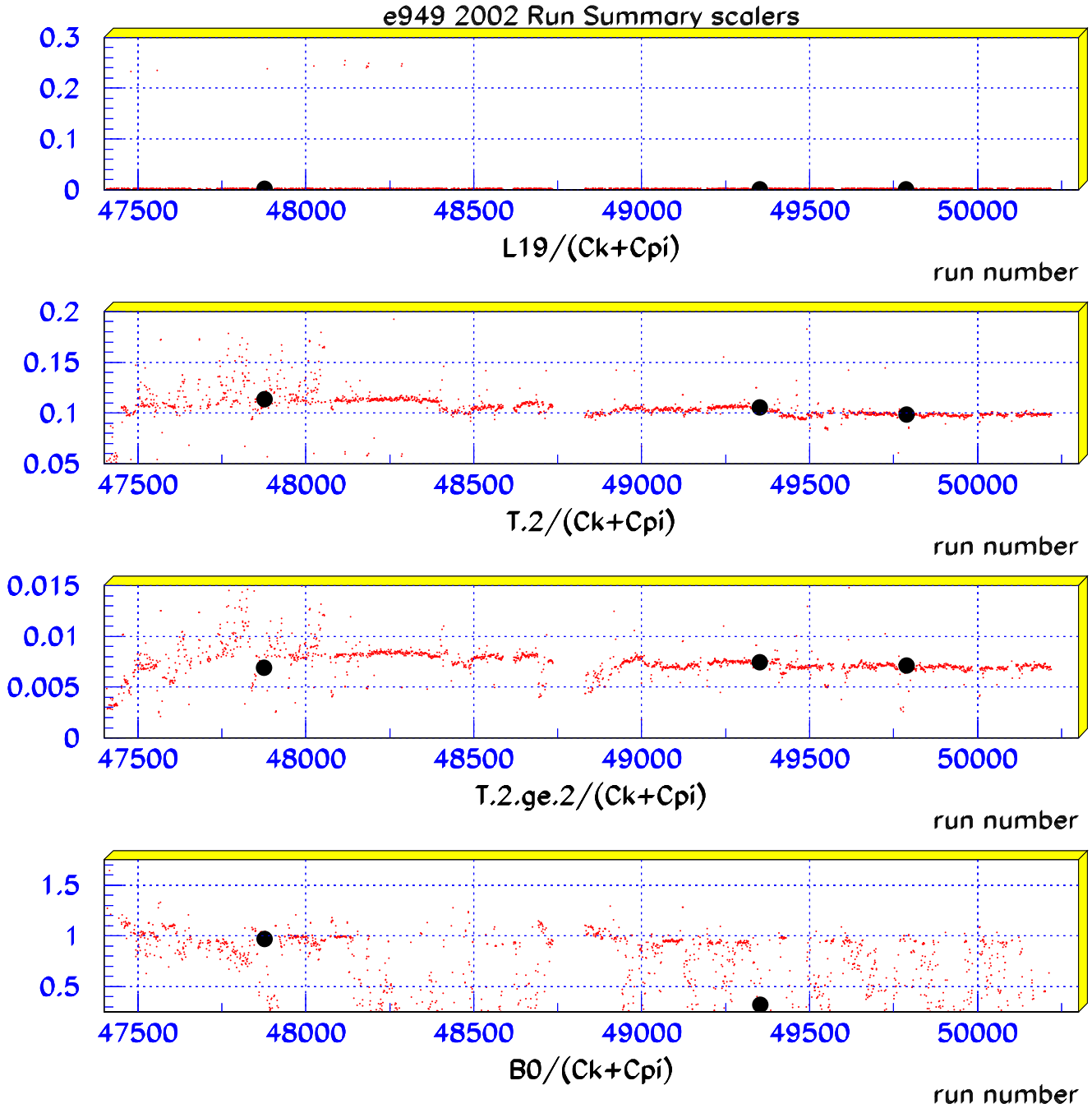
e949 2002 Run Summary scalers
0.3
0.2
0.1
0
47500
48000
48500
49000
49500
50000
L19/(Ck+Cpi)
run number
0.2
0.15
0.1
0.05
47500
48000
48500
49000
49500
50000
T.2/(Ck+Cpi)
run number
0.015
0.01
0.005
0
47500
48000
48500
49000
49500
50000
T.2.ge.2/(Ck+Cpi)
run number
1.5
1
0.5
47500
48000
48500
49000
49500
50000
B0/(Ck+Cpi)
run number

Figure 118:

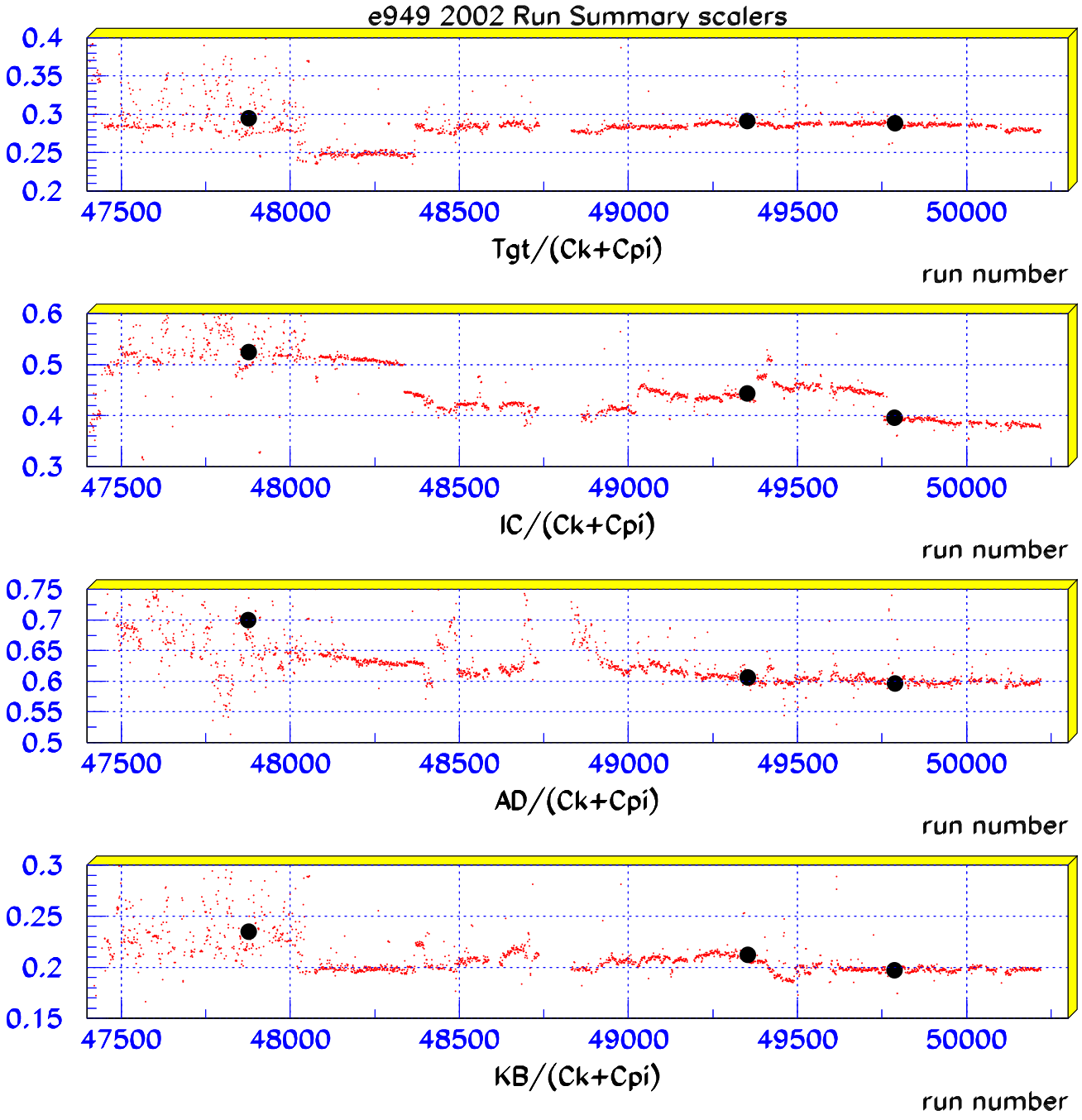
e949 2002 Run Summary scalers
0.4
0.35
0.3
0.25
0.2
47500
48000
48500
49000
49500
50000
Tgt/(Ck+Cpi)
run number
0.6
0.5
0.4
0.3
47500
48000
48500
49000
49500
50000
IC/(Ck+Cpi)
run number
0.75
0.7
0.65
0.6
0.55
0.5
47500
48000
48500
49000
49500
50000
AD/(Ck+Cpi)
run number
0.3
0.25
0.2
0.15
47500
48000
48500
49000
49500
50000
KB/(Ck+Cpi)
run number

Figure 119:

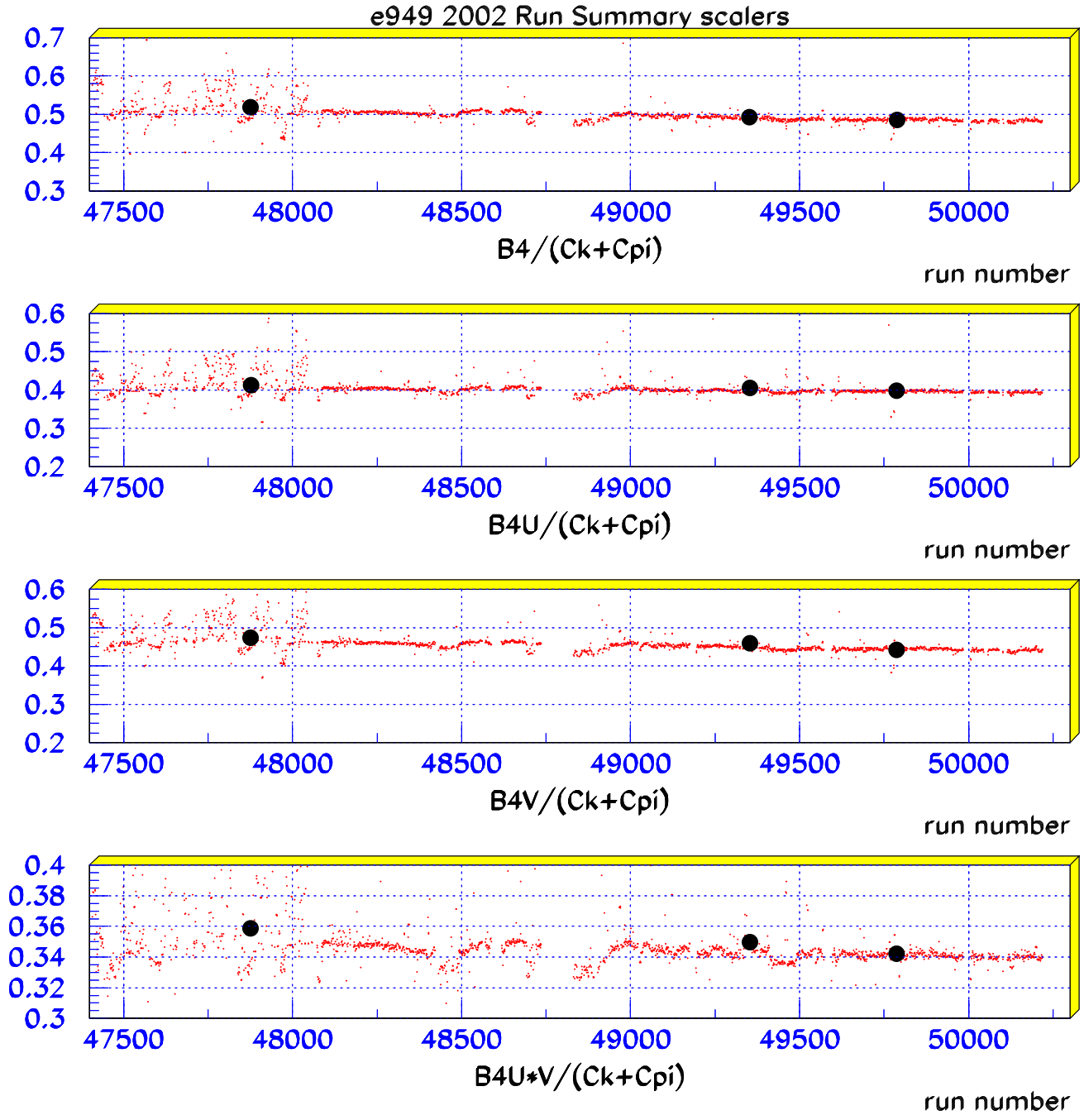
e949 2002 Run Summary scalers
0.7
0.6
0.5
0.4
0.3
47500
48000
48500
49000
49500
50000
B4/(Ck+Cpi)
run number
0.6
0.5
0.4
0.3
0.2
47500
48000
48500
49000
49500
50000
B4U/(Ck+Cpi)
run number
0.6
0.5
0.4
0.3
0.2
47500
48000
48500
49000
49500
50000
B4V/(Ck+Cpi)
run number
0.4
0.38
0.36
0.34
0.32
0.3
47500
48000
48500
49000
49500
50000
B4U*V/(Ck+Cpi)
run number

Figure 120:

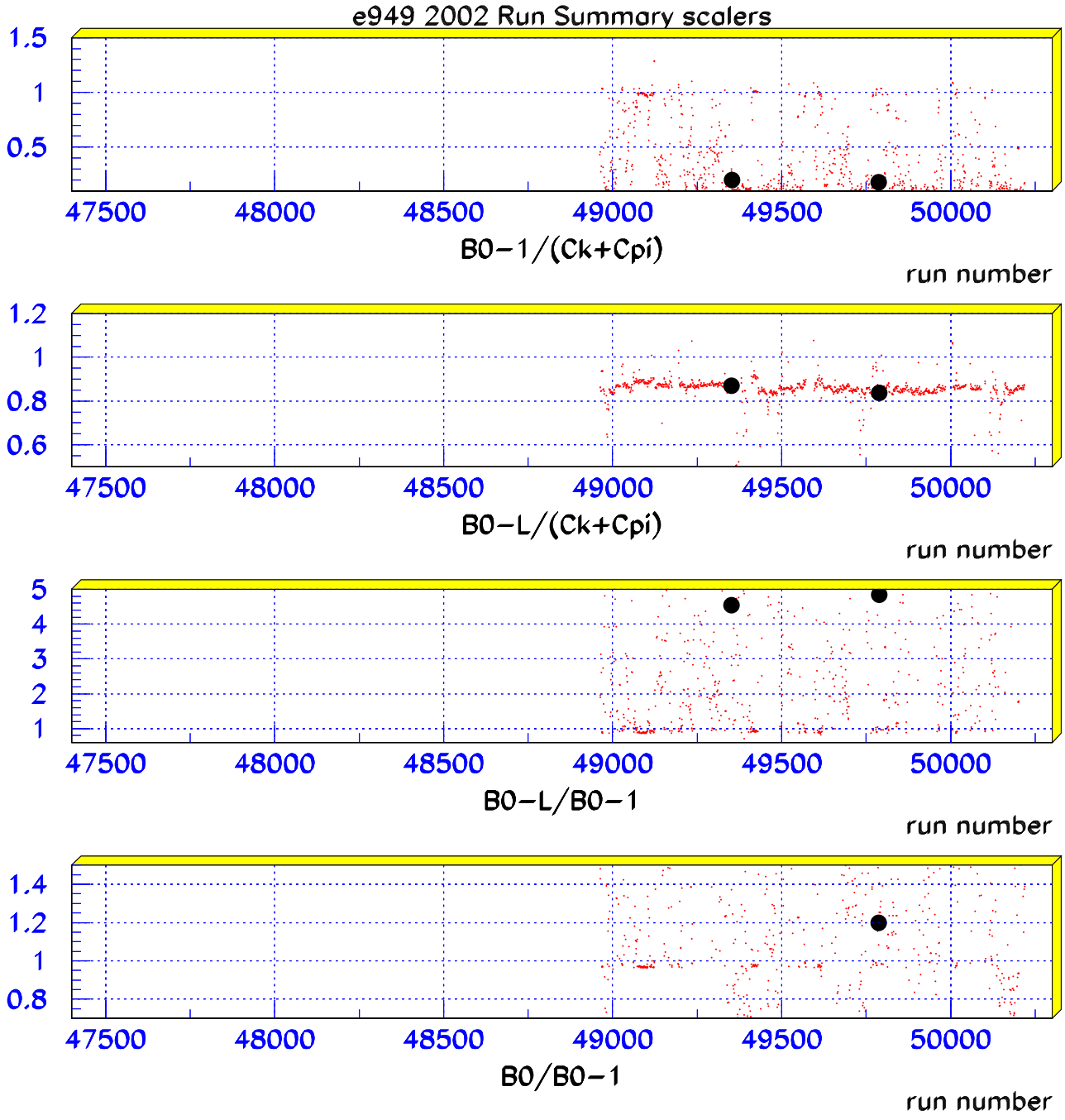
e949 2002 Run Summary scalers
1.5
1
0.5
47500
48000
48500
49000
49500
50000
B0−1/(Ck+Cpi)
run number
1.2
1
0.8
0.6
47500
48000
48500
49000
49500
50000
B0−L/(Ck+Cpi)
run number
5
4
3
2
1
47500
48000
48500
49000
49500
50000
B0−L/B0−1
run number
1.4
1.2
1
0.8
47500
48000
48500
49000
49500
50000
B0/B0−1
run number

Figure 121:

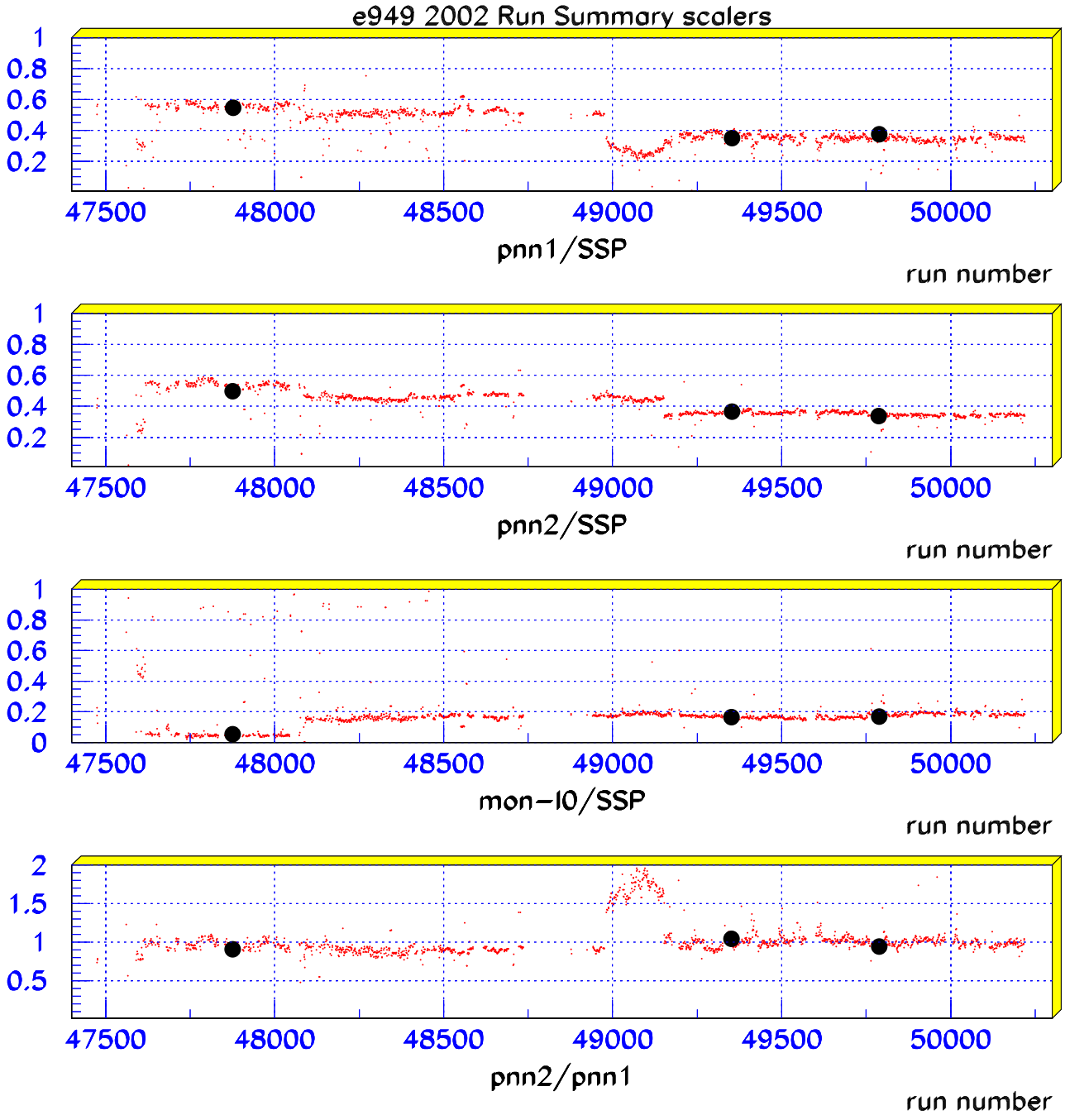
e949 2002 Run Summary scalers
1
0.8
0.6
0.4
0.2
47500
48000
48500
49000
49500
50000
pnn1/SSP
run number
1
0.8
0.6
0.4
0.2
47500
48000
48500
49000
49500
50000
pnn2/SSP
run number
1
0.8
0.6
0.4
0.2
0
47500
48000
48500
49000
49500
50000
mon-10/SSP
run number
2
1.5
1
0.5
47500
48000
48500
49000
49500
50000
pnn2/pnn1
run number

Figure 122:

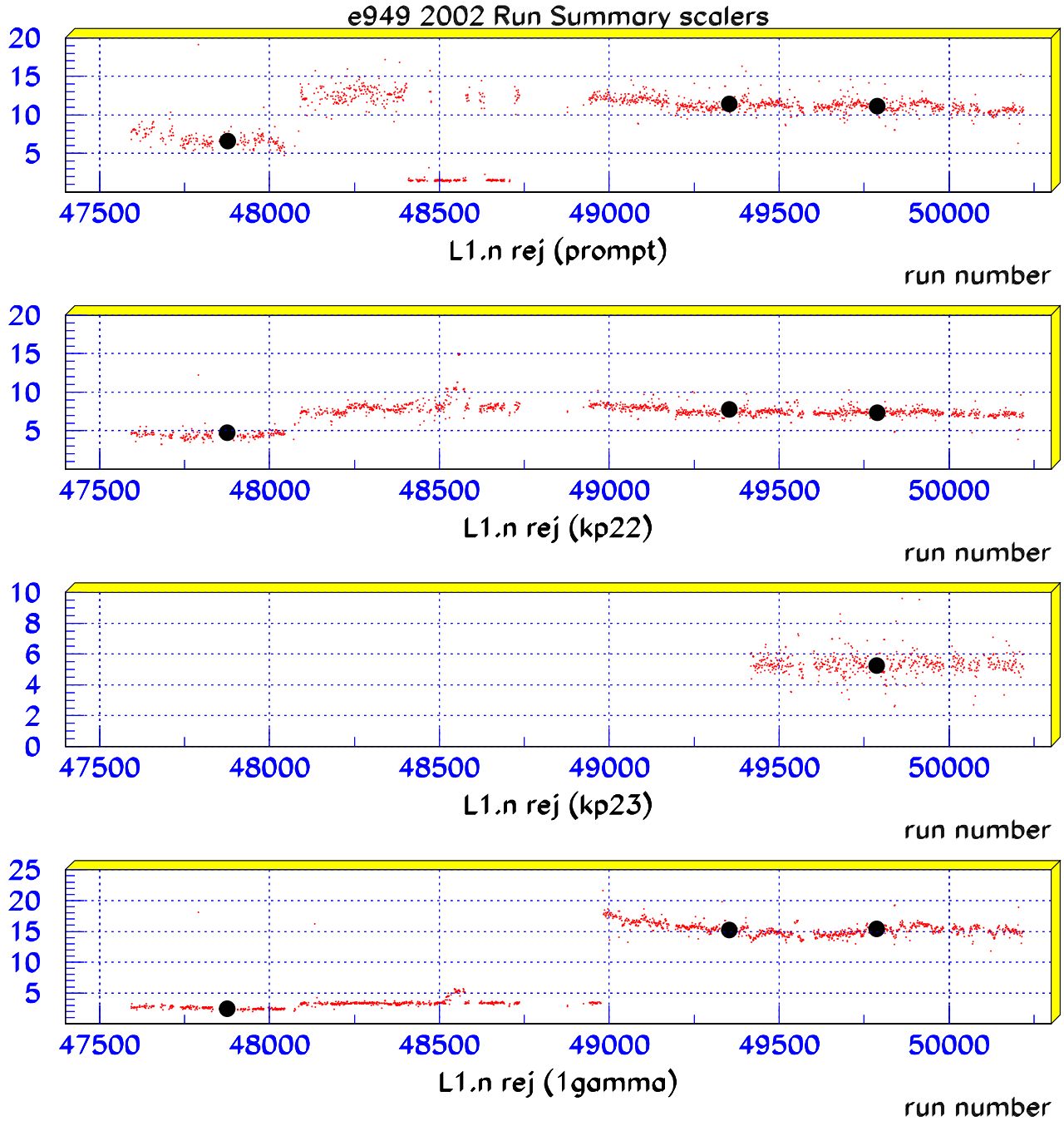
e949 2002 Run Summary scalers
20
15
10
5
47500
48000
48500
49000
49500
50000
L1.n rej (prompt)
run number
20
15
10
5
47500
48000
48500
49000
49500
50000
L1.n rej (kp22)
run number
10
8
6
4
2
0
47500
48000
48500
49000
49500
50000
L1.n rej (kp23)
run number
25
20
15
10
5
47500
48000
48500
49000
49500
50000
L1.n rej (1gamma)
run number

Figure 123:

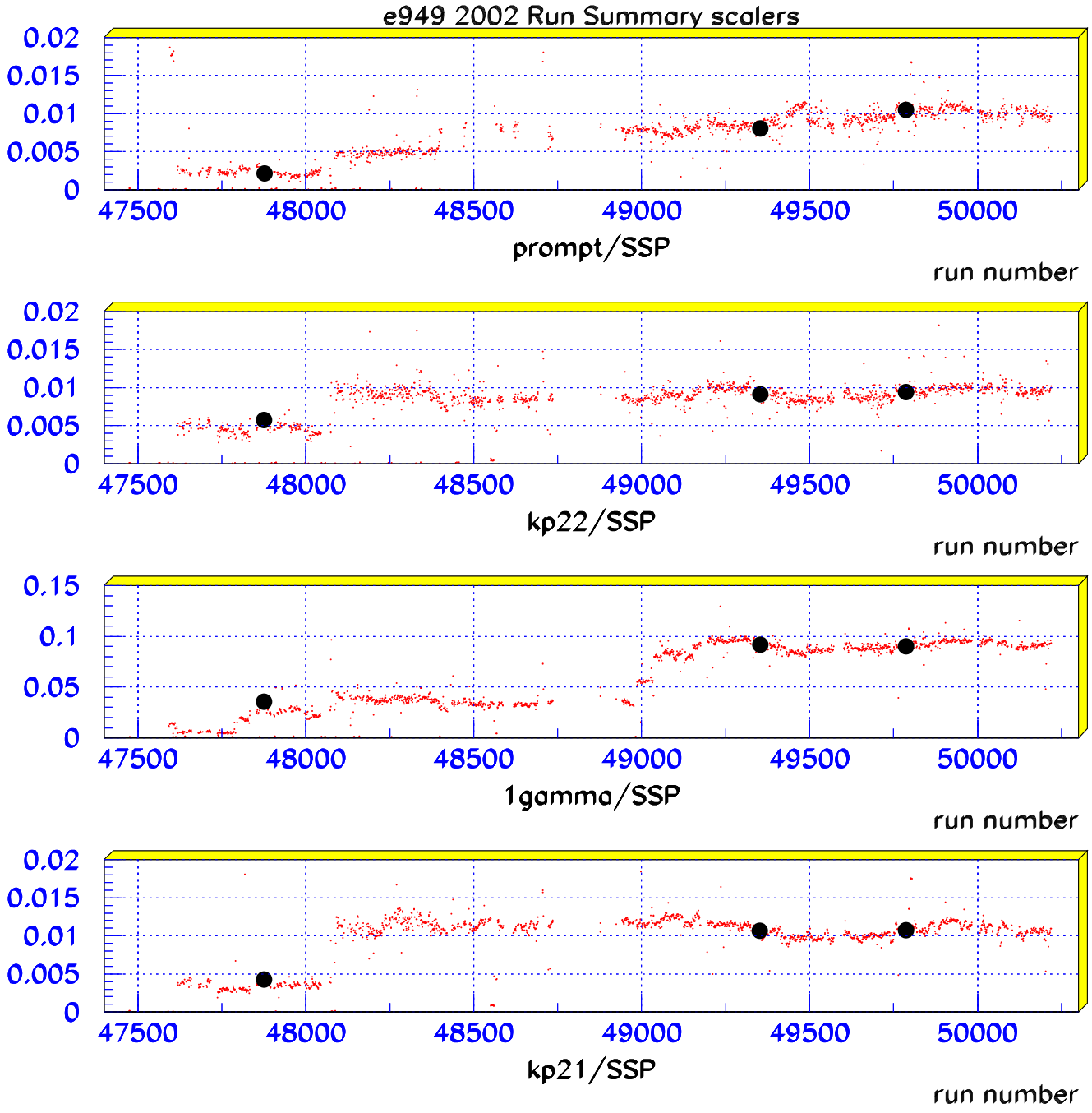
e949 2002 Run Summary scalers
0.02
0.015
0.01
0.005
0
47500
48000
48500
49000
49500
50000
prompt/SSP
run number
kp22/SSP
run number
0.15
0.1
0.05
1gamma/SSP
run number
kp21/SSP
run number

Figure 124:

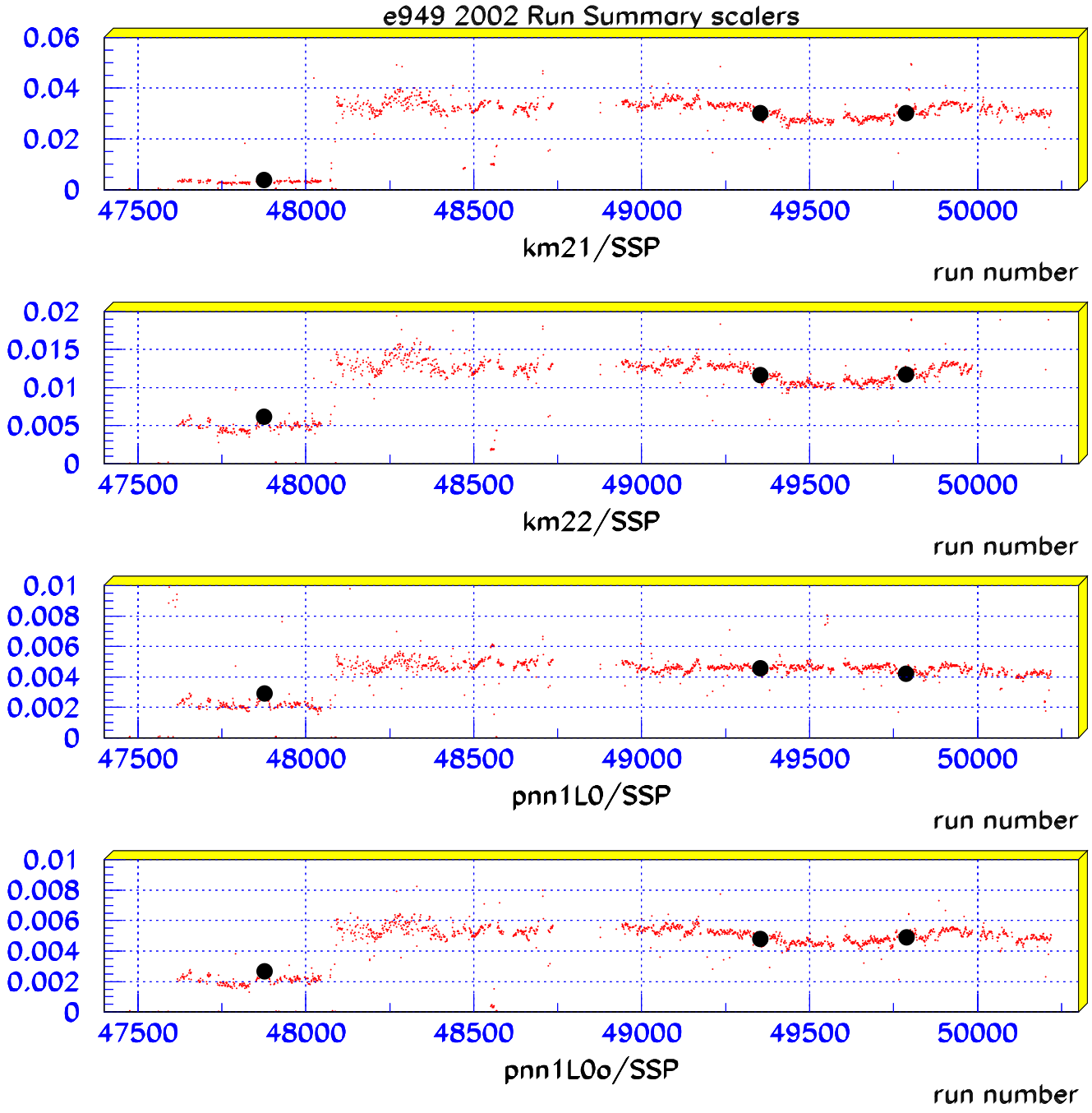
e949 2002 Run Summary scalers
0.06
0.04
0.02
0
47500
48000
48500
49000
49500
50000
km21/SSP
run number
0.02
0.015
0.01
0.005
0
47500
48000
48500
49000
49500
50000
km22/SSP
run number
0.01
0.008
0.006
0.004
0.002
0
47500
48000
48500
49000
49500
50000
pnn1L0/SSP
run number
0.01
0.008
0.006
0.004
0.002
0
47500
48000
48500
49000
49500
50000
pnn1L0o/SSP
run number

Figure 125:

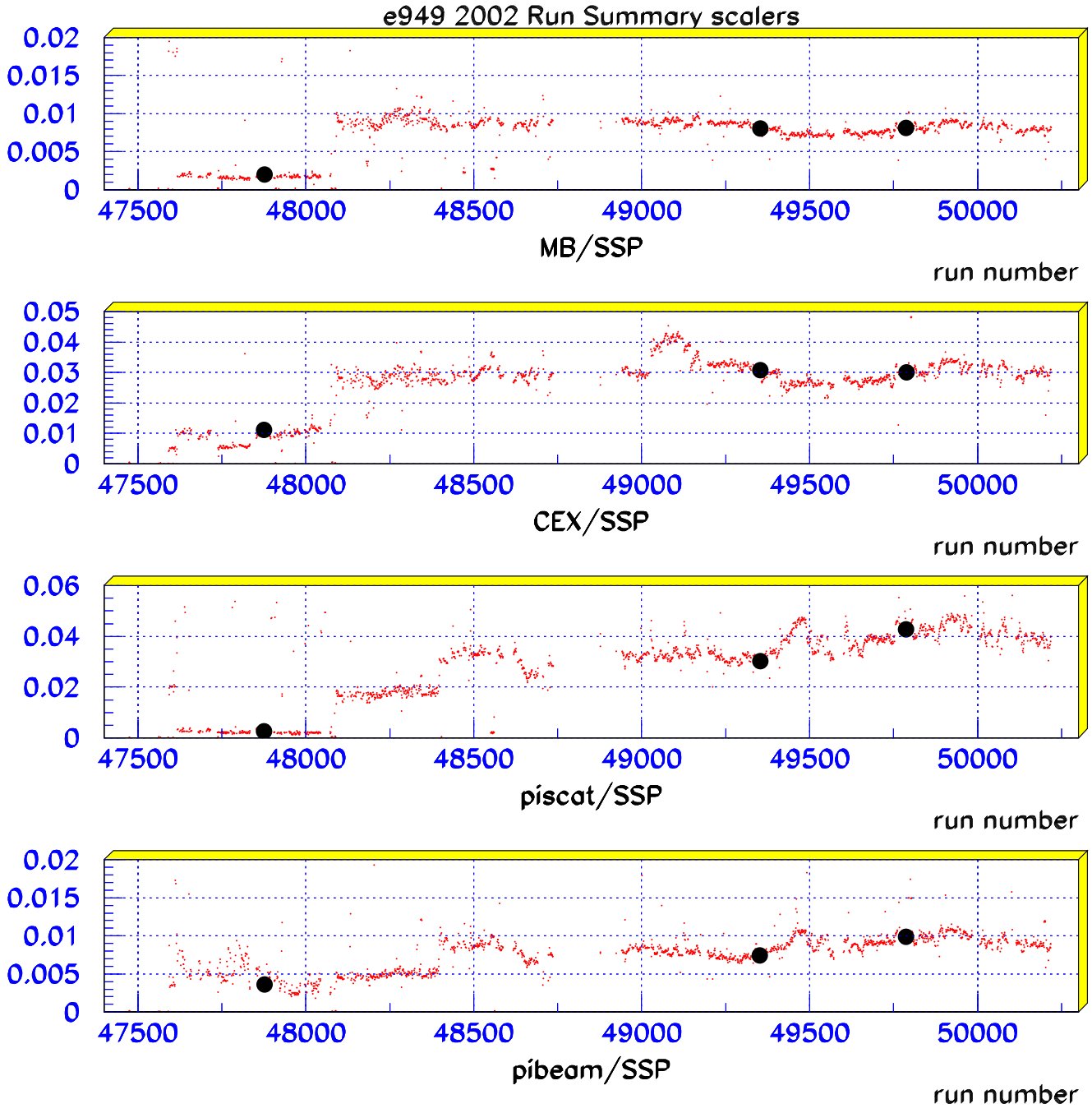
e949 2002 Run Summary scalers
0.02
0.015
0.01
0.005
0
47500
48000
48500
49000
49500
50000
MB/SSP
run number
0.05
0.04
0.03
0.02
0.01
0
47500
48000
48500
49000
49500
50000
CEX/SSP
run number
0.06
0.04
0.02
0
47500
48000
48500
49000
49500
50000
piscat/SSP
run number
0.02
0.015
0.01
0.005
0
47500
48000
48500
49000
49500
50000
pibeam/SSP
run number

Figure 126:

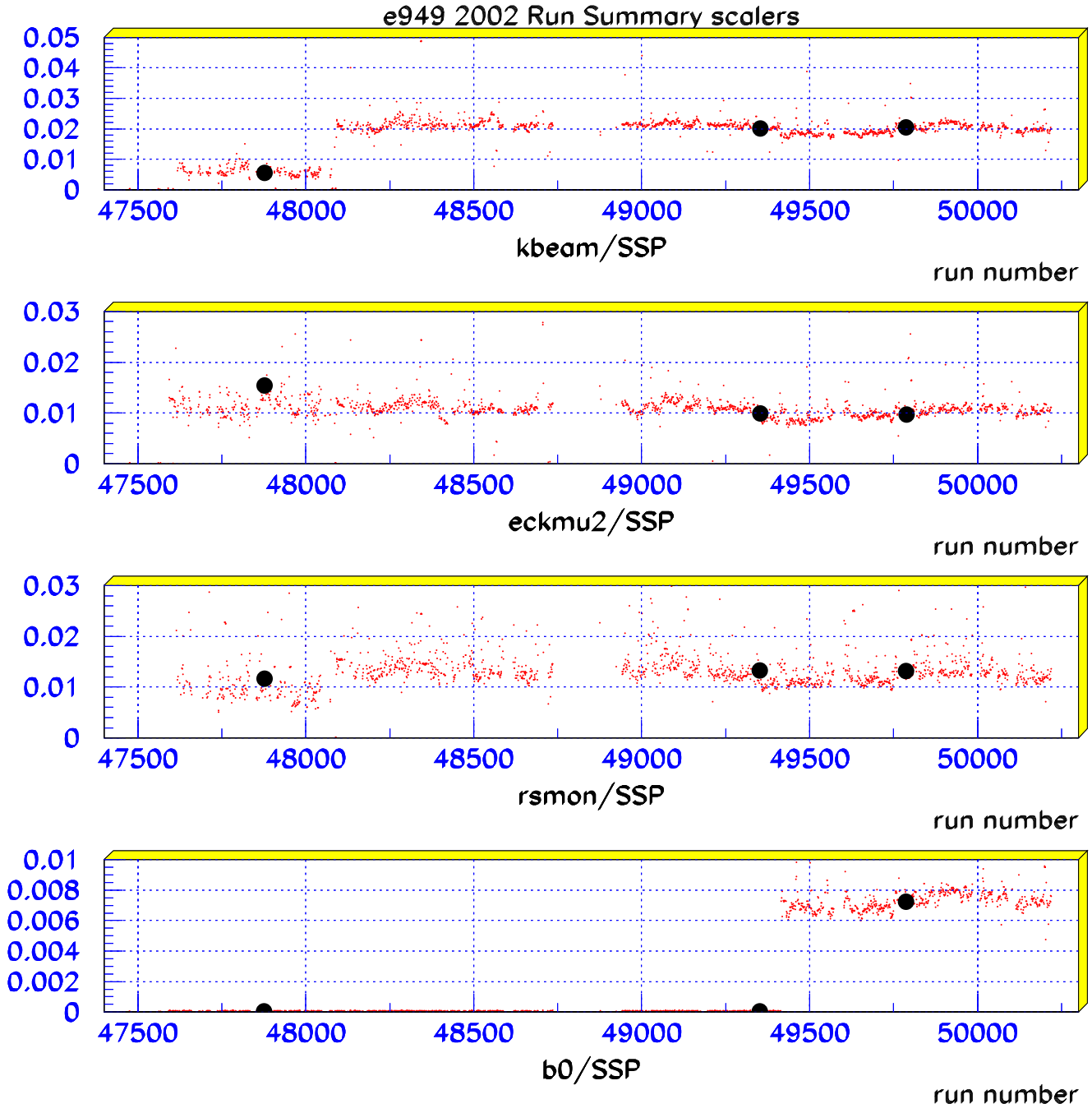
e949 2002 Run Summary scalers
0.05
0.04
0.03
0.02
0.01
0
47500
48000
48500
49000
49500
50000
kbeam/SSP
run number
0.03
0.02
0.01
0
47500
48000
48500
49000
49500
50000
eckmu2/SSP
run number
0.03
0.02
0.01
0
47500
48000
48500
49000
49500
50000
rsmon/SSP
run number
0.01
0.008
0.006
0.004
0.002
0
47500
48000
48500
49000
49500
50000
b0/SSP
run number

Figure 127:

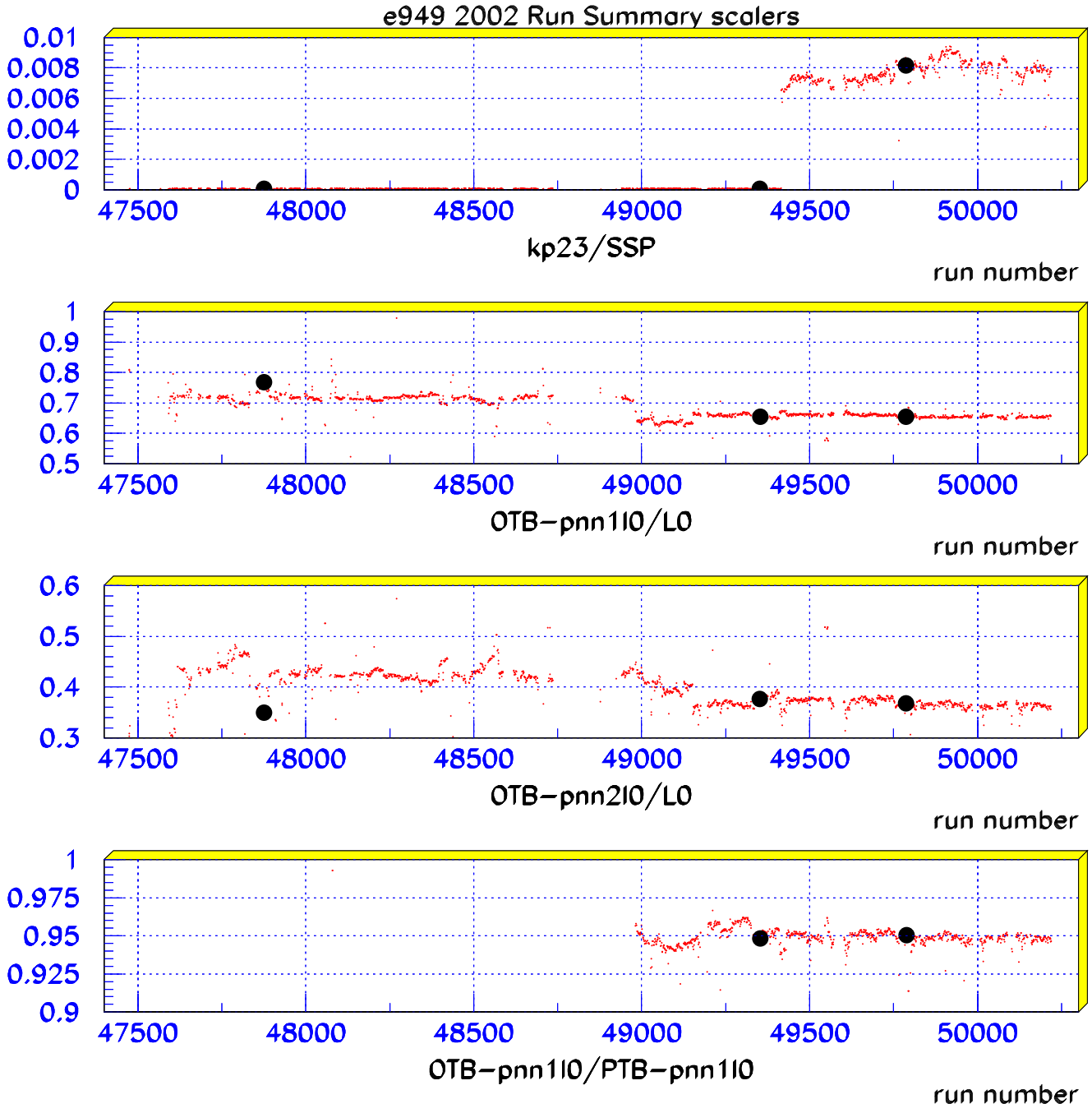
e949 2002 Run Summary scalers
0.01
0.008
0.006
0.004
0.002
0
47500
48000
48500
49000
49500
50000
kp23/SSP
run number
1
0.9
0.8
0.7
0.6
0.5
47500
48000
48500
49000
49500
50000
OTB−pnn110/L0
run number
0.6
0.5
0.4
0.3
47500
48000
48500
49000
49500
50000
OTB−pnn210/L0
run number
1
0.975
0.95
0.925
0.9
47500
48000
48500
49000
49500
50000
OTB−pnn110/PTB−pnn110
run number

Figure 128:

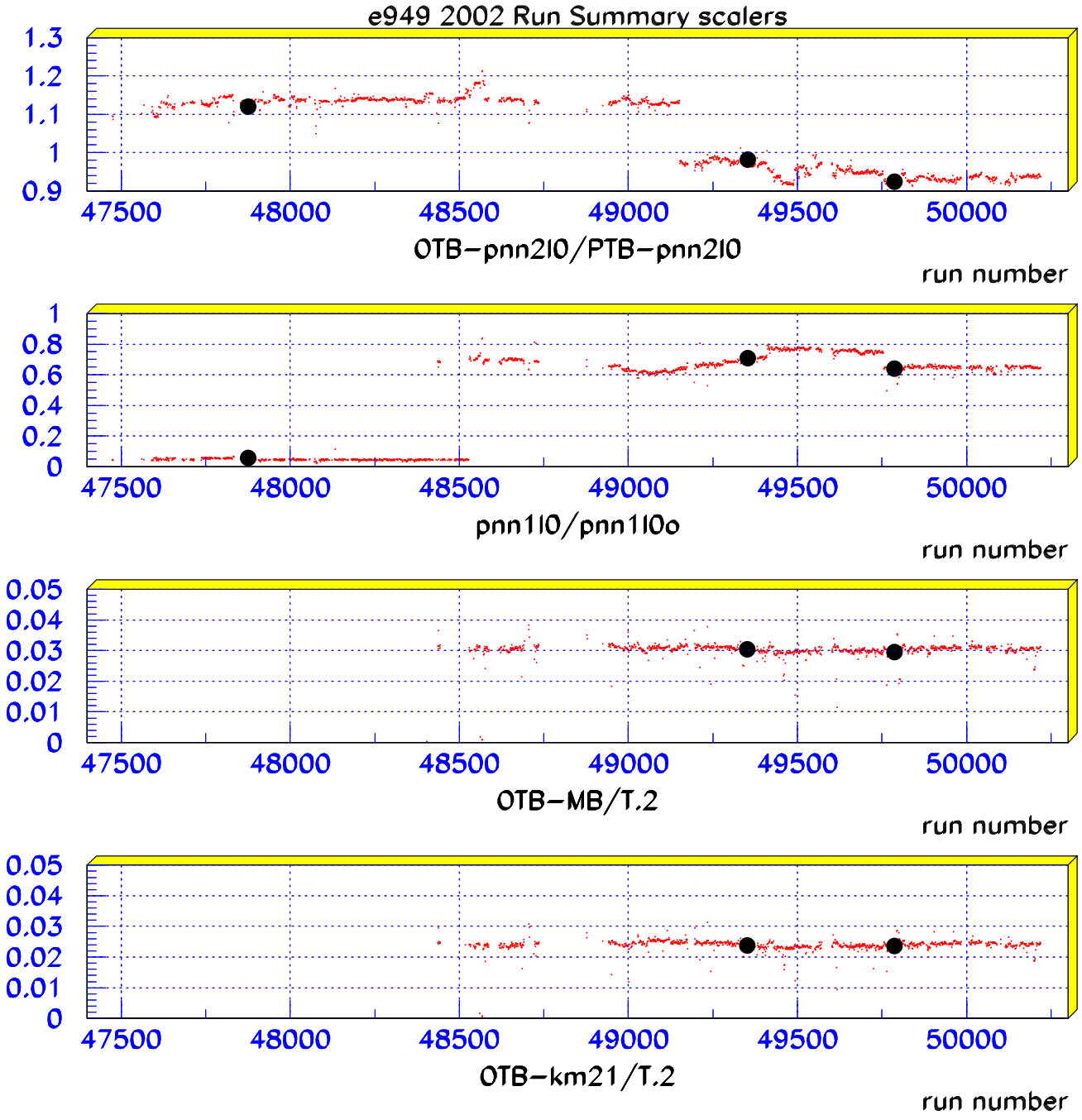
e949 2002 Run Summary scalers
1.3
1.2
1.1
1
0.9
47500
48000
48500
49000
49500
50000
OTB−pnn210/PTB−pnn210
run number
1
0.8
0.6
0.4
0.2
0
pnn110/pnn110o
run number
0.05
0.04
0.03
0.02
0.01
0
OTB−MB/T.2
run number
OTB−km21/T.2
run number

Figure 129:

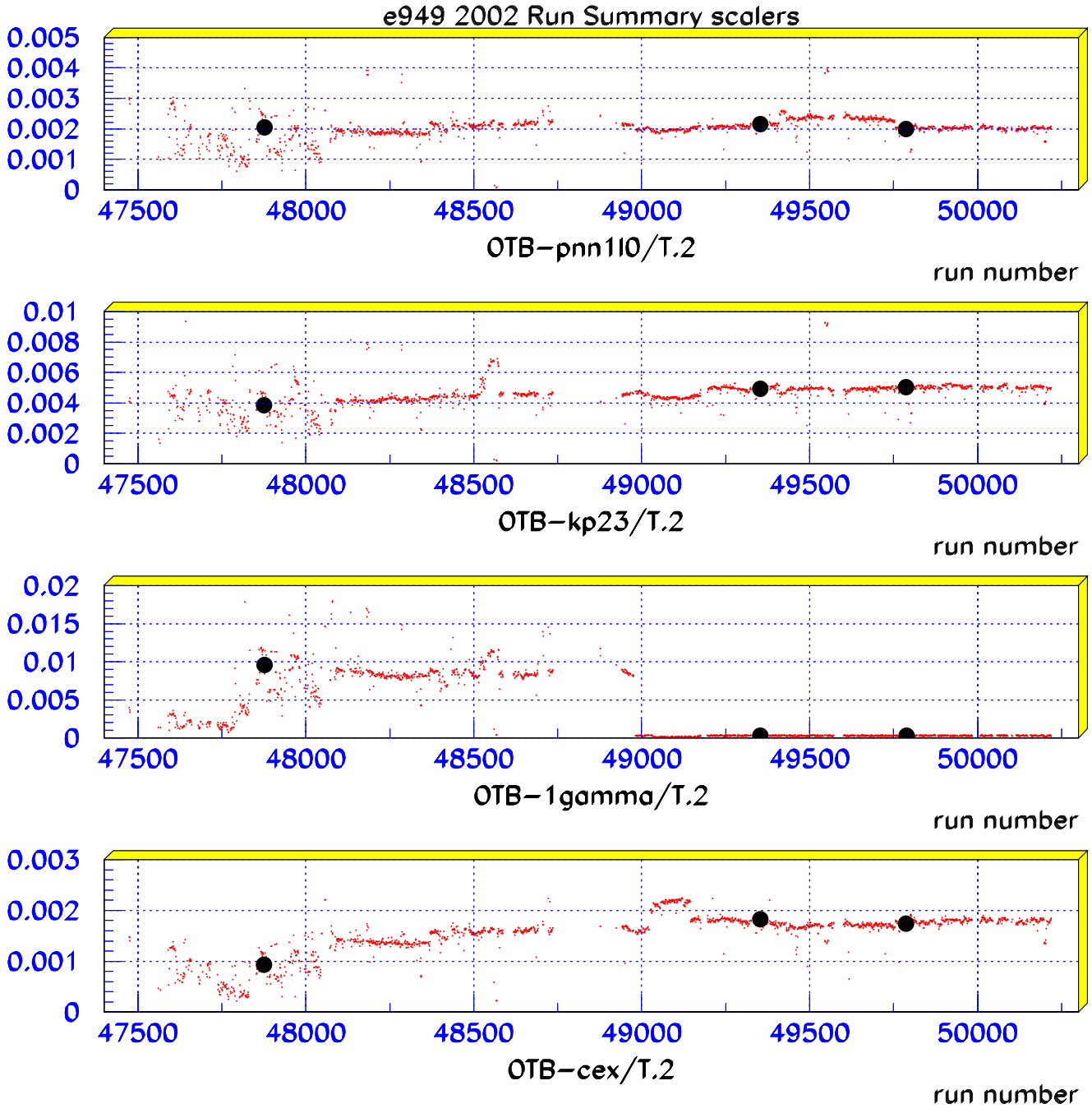
e949 2002 Run Summary scalers
0.005
0.004
0.003
0.002
0.001
0
47500
48000
48500
49000
49500
50000
OTB−pnn110/T.2
run number
0.01
0.008
0.006
0.004
0.002
0
47500
48000
48500
49000
49500
50000
OTB−kp23/T.2
run number
0.02
0.015
0.01
0.005
0
47500
48000
48500
49000
49500
50000
OTB−1gamma/T.2
run number
0.003
0.002
0.001
0
47500
48000
48500
49000
49500
50000
OTB−cex/T.2
run number

Figure 130:

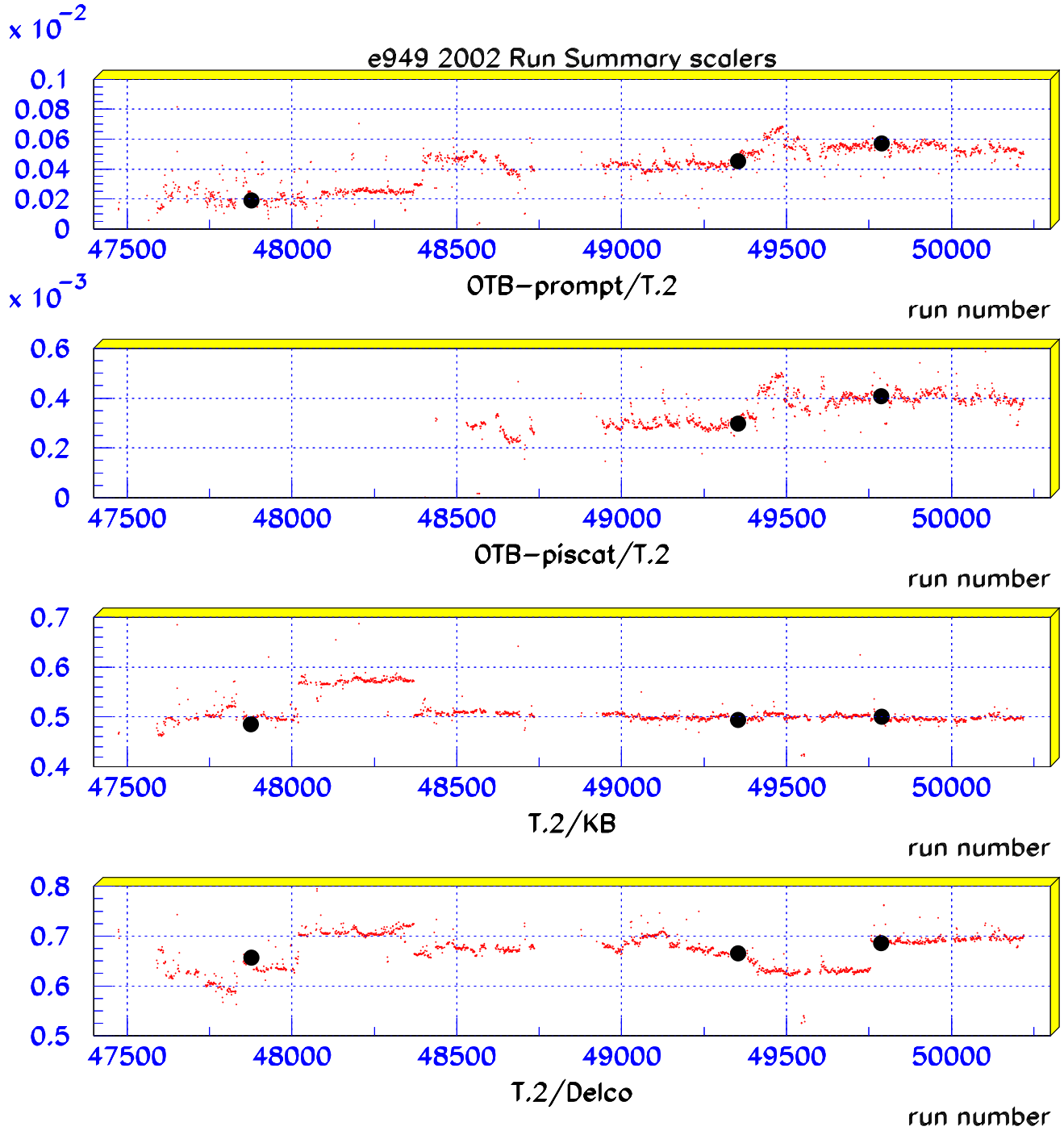
e949 2002 Run Summary scalers
x 10^-2
0.1
0.08
0.06
0.04
0.02
0
47500
48000
48500
49000
49500
50000
OTB−prompt/T.2
run number
x 10^-3
0.6
0.4
0.2
0
OTB−piscat/T.2
run number
0.7
0.6
0.5
0.4
T.2/KB
run number
0.8
0.7
0.6
0.5
T.2/Delco
run number

Figure 131:

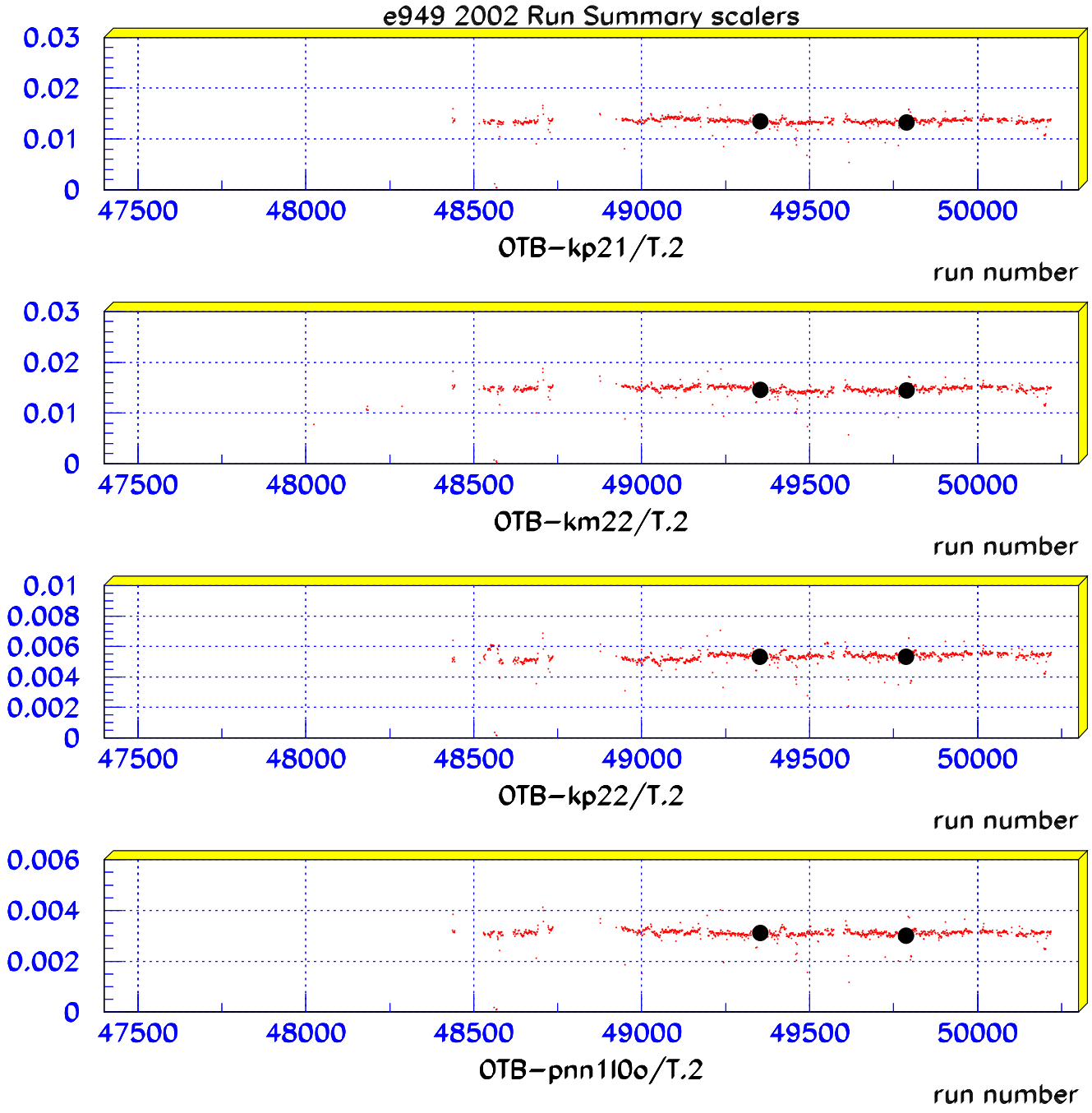
e949 2002 Run Summary scalers
0.03
0.02
0.01
0
47500
48000
48500
49000
49500
50000
OTB−kp21/T.2
run number
0.03
0.02
0.01
0
47500
48000
48500
49000
49500
50000
OTB−km22/T.2
run number
0.01
0.008
0.006
0.004
0.002
0
47500
48000
48500
49000
49500
50000
OTB−kp22/T.2
run number
0.006
0.004
0.002
0
47500
48000
48500
49000
49500
50000
OTB−pnn110o/T.2
run number

Figure 132:

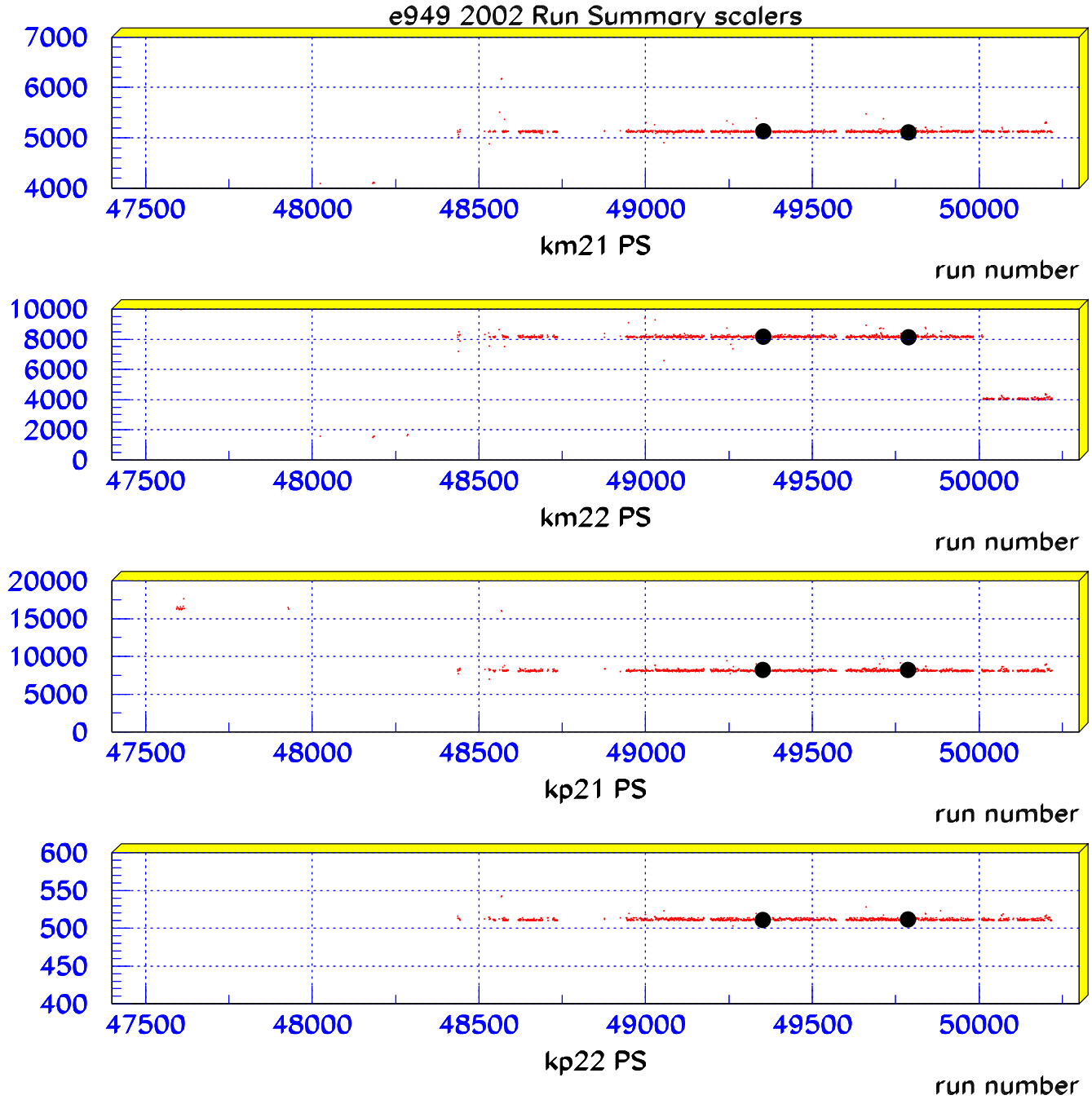
e949 2002 Run Summary scalers
7000
6000
5000
4000
47500
48000
48500
49000
49500
50000
km21 PS
run number
10000
8000
6000
4000
2000
0
47500
48000
48500
49000
49500
50000
km22 PS
run number
20000
15000
10000
5000
0
47500
48000
48500
49000
49500
50000
kp21 PS
run number
600
550
500
450
400
47500
48000
48500
49000
49500
50000
kp22 PS
run number

Figure 133:

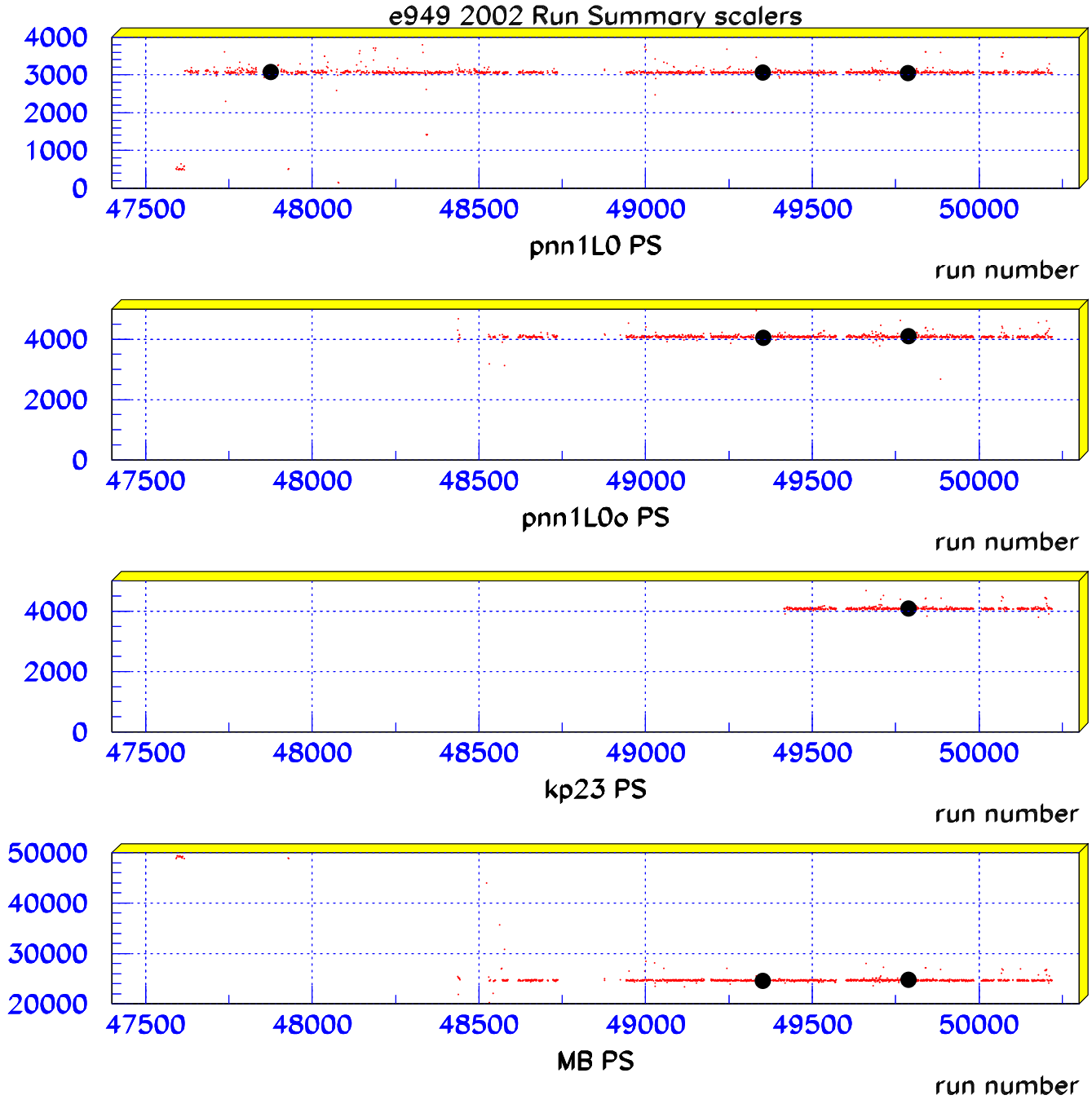
e949 2002 Run Summary scalers
4000
3000
2000
1000
0
47500
48000
48500
49000
49500
50000
pnn1L0 PS
run number
4000
2000
0
47500
48000
48500
49000
49500
50000
pnn1L0o PS
run number
4000
2000
0
47500
48000
48500
49000
49500
50000
kp23 PS
run number
50000
40000
30000
20000
47500
48000
48500
49000
49500
50000
MB PS
run number

Figure 134:

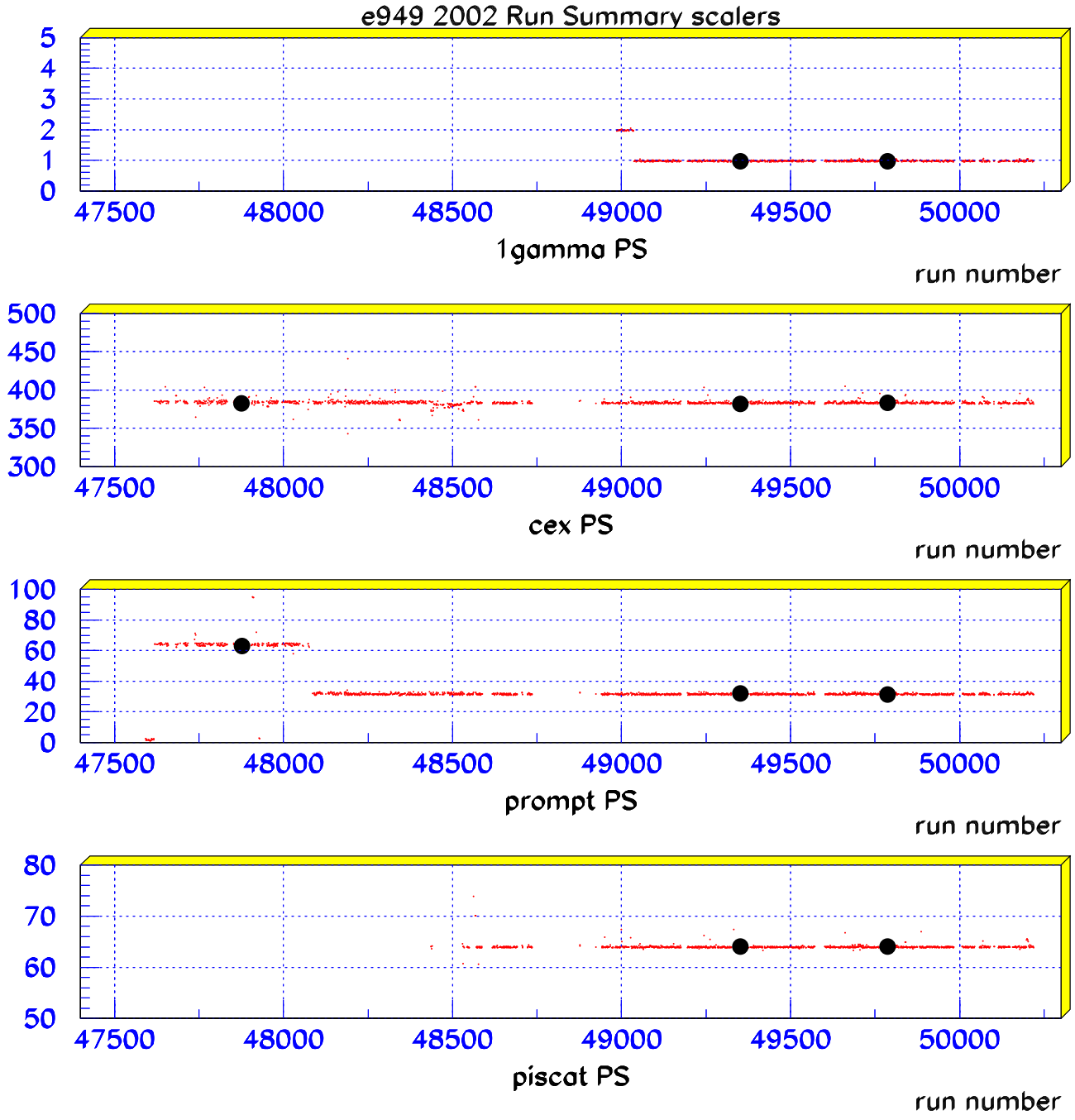
e949 2002 Run Summary scalers
5
4
3
2
1
0
47500
48000
48500
49000
49500
50000
1gamma PS
run number
500
450
400
350
300
47500
48000
48500
49000
49500
50000
cex PS
run number
100
80
60
40
20
0
47500
48000
48500
49000
49500
50000
prompt PS
run number
80
70
60
50
47500
48000
48500
49000
49500
50000
piscat PS
run number

Figure 135:

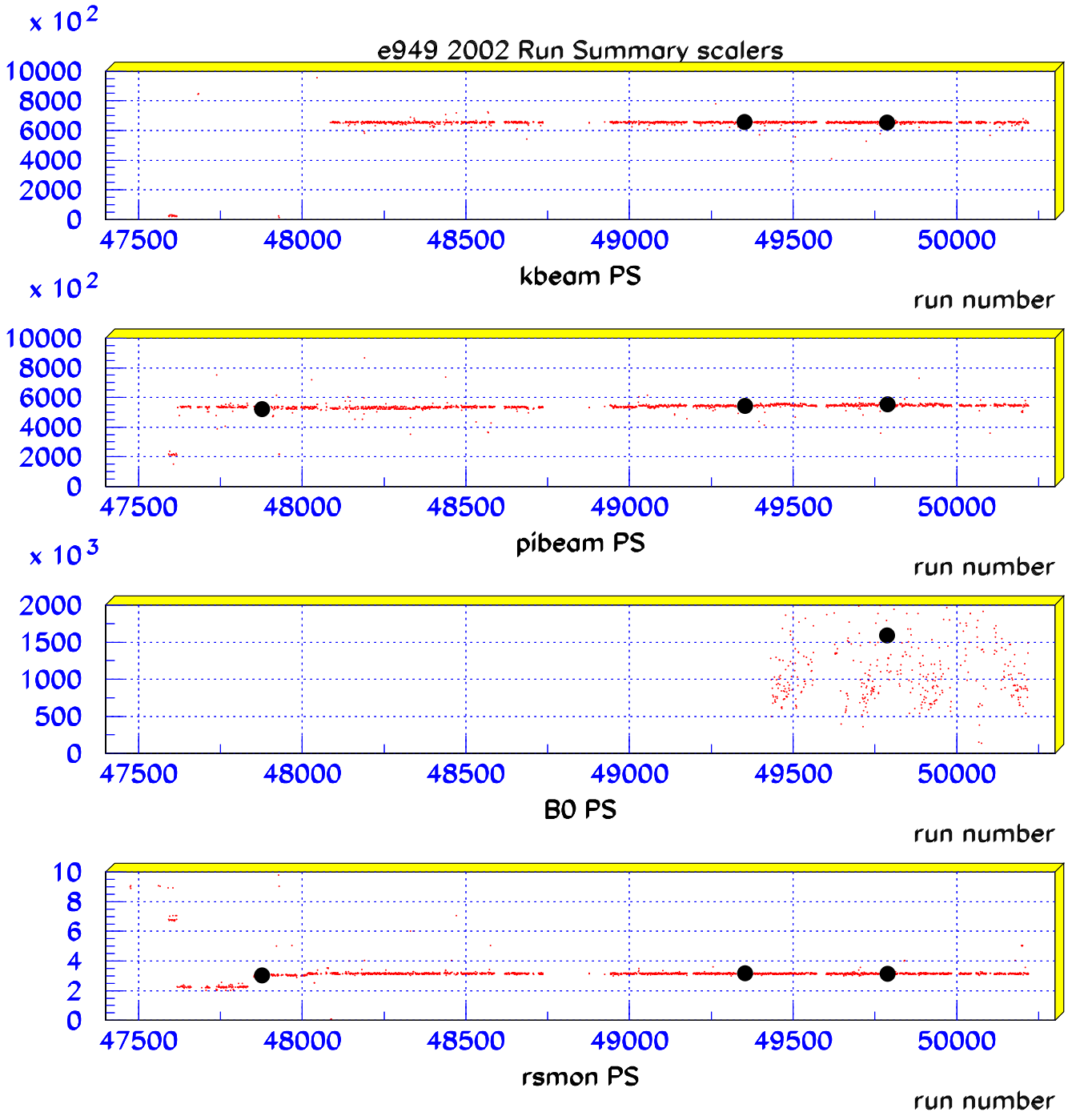
e949 2002 Run Summary scalers
x 10^2
10000
8000
6000
4000
2000
0
47500
48000
48500
49000
49500
50000
kbeam PS
run number
x 10^2
pibeam PS
run number
x 10^3
2000
1500
1000
500
B0 PS
run number
10
8
6
4
2
rsmon PS
run number

Figure 136:

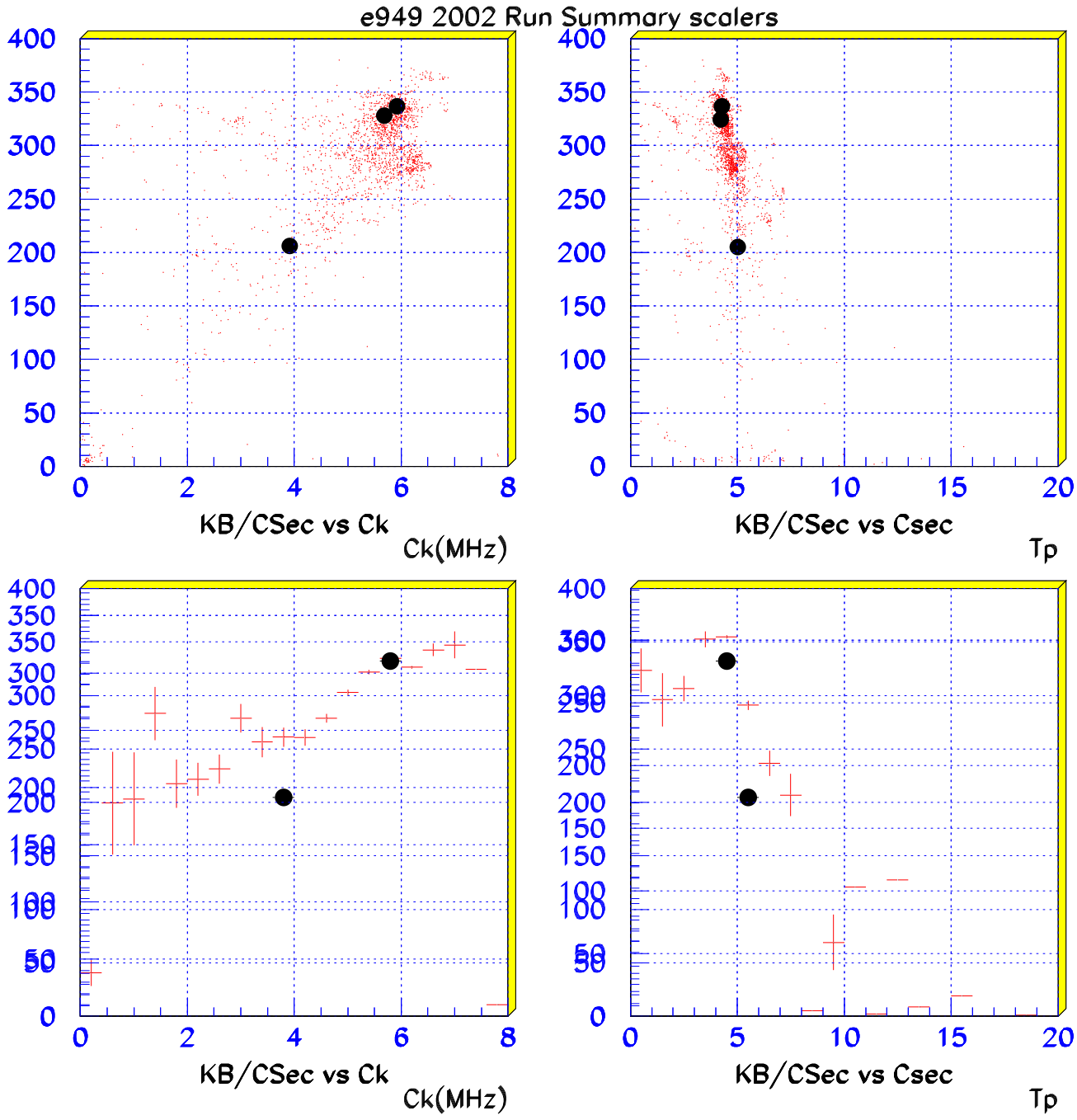
e949 2002 Run Summary scalers
KB/CSec vs Ck
Ck(MHz)
KB/CSec vs Csec
Tp
KB/CSec vs Ck
Ck(MHz)
KB/CSec vs Csec
Tp

Figure 137:

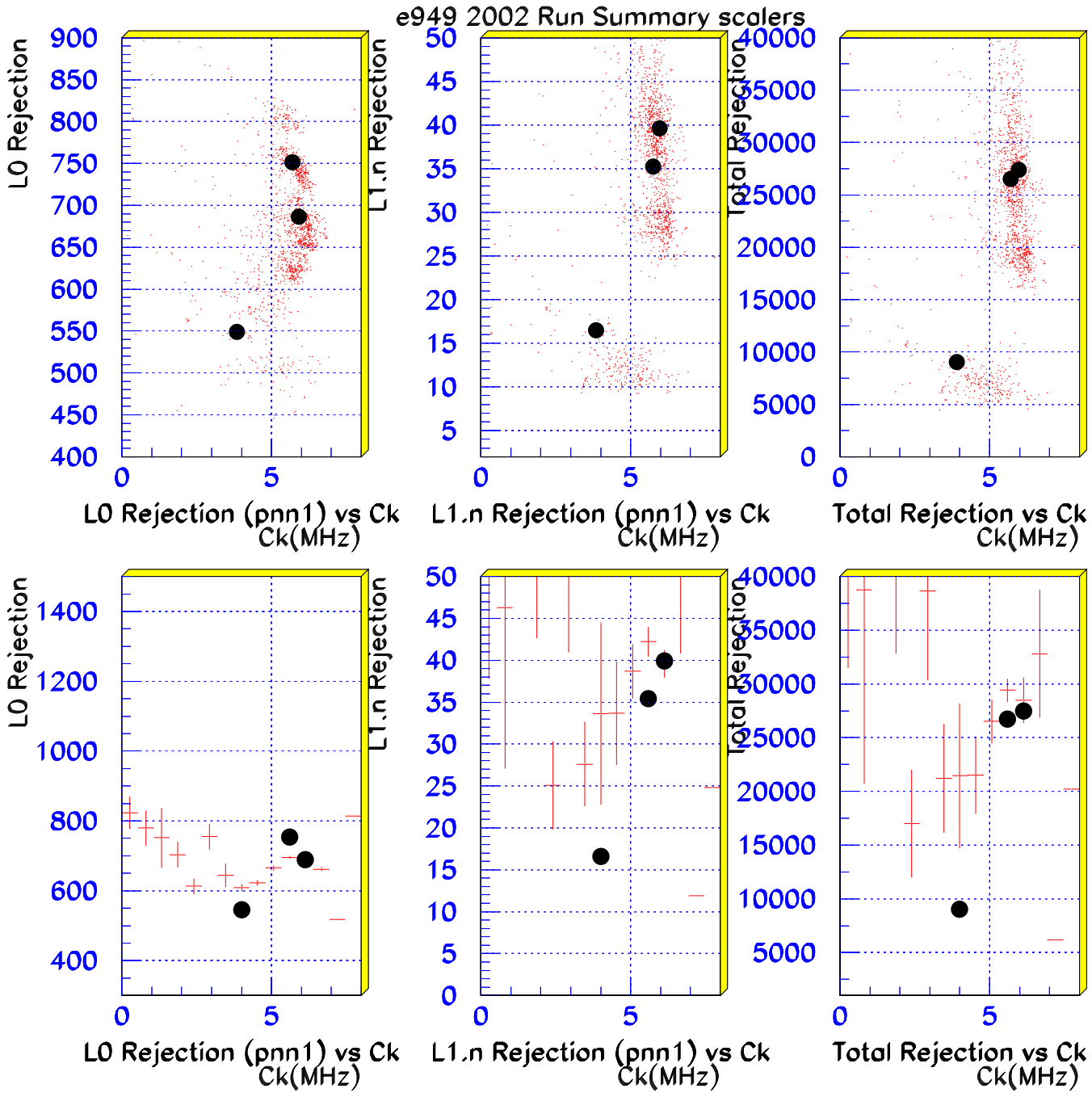
e949 2002 Run Summary scalers
L0 Rejection
L1.n Rejection
Total Rejection
L0 Rejection (pnn1) vs Ck
L1.n Rejection (pnn1) vs Ck
Total Rejection vs Ck
Ck(MHz)

Figure 138:

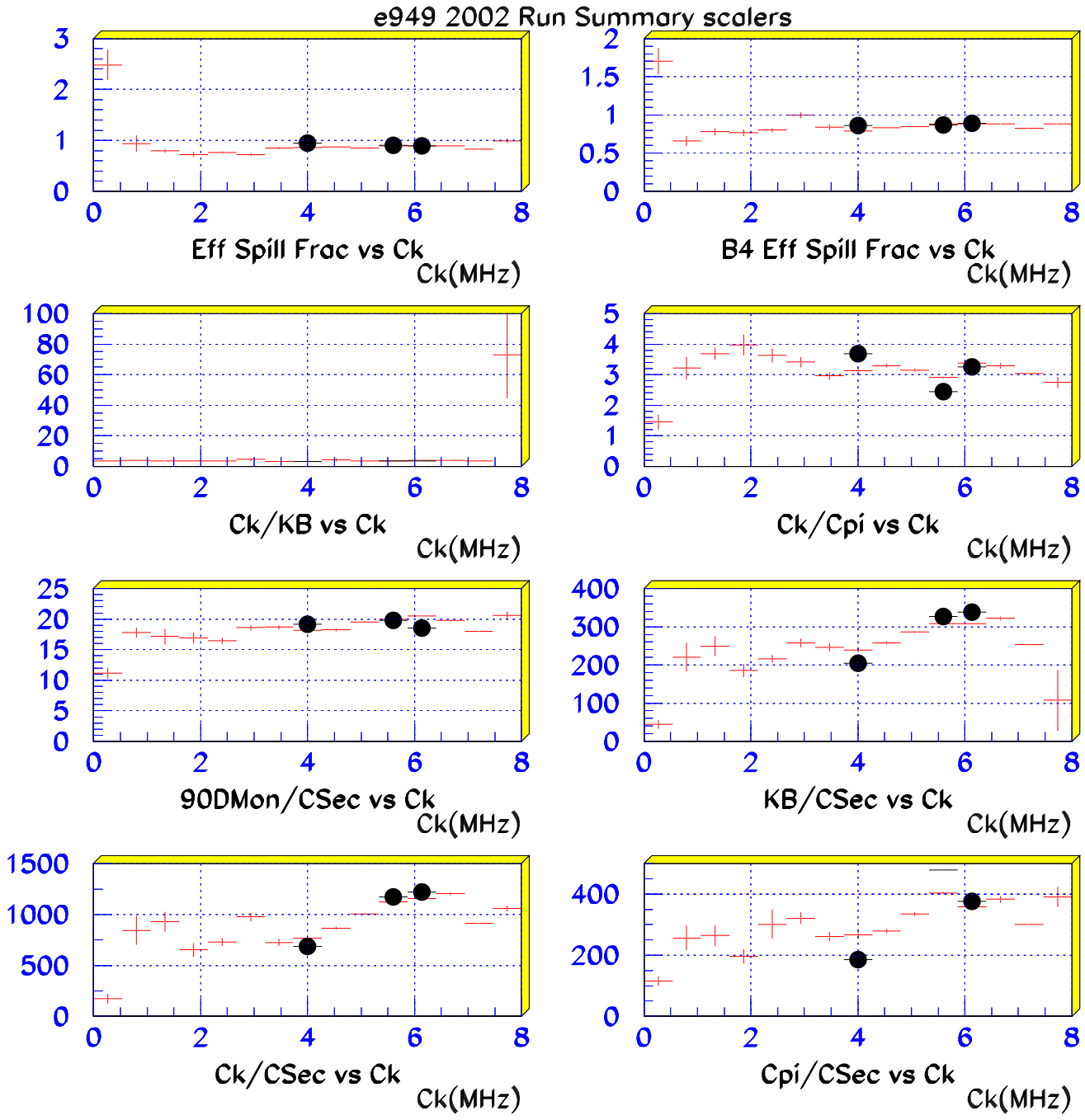
e949 2002 Run Summary scalers
Eff Spill Frac vs Ck
Ck(MHz)
B4 Eff Spill Frac vs Ck
Ck(MHz)
Ck/KB vs Ck
Ck(MHz)
Ck/Cpi vs Ck
Ck(MHz)
90DMon/CSec vs Ck
Ck(MHz)
KB/CSec vs Ck
Ck(MHz)
Ck/CSec vs Ck
Ck(MHz)
Cpi/CSec vs Ck
Ck(MHz)

Figure 139:

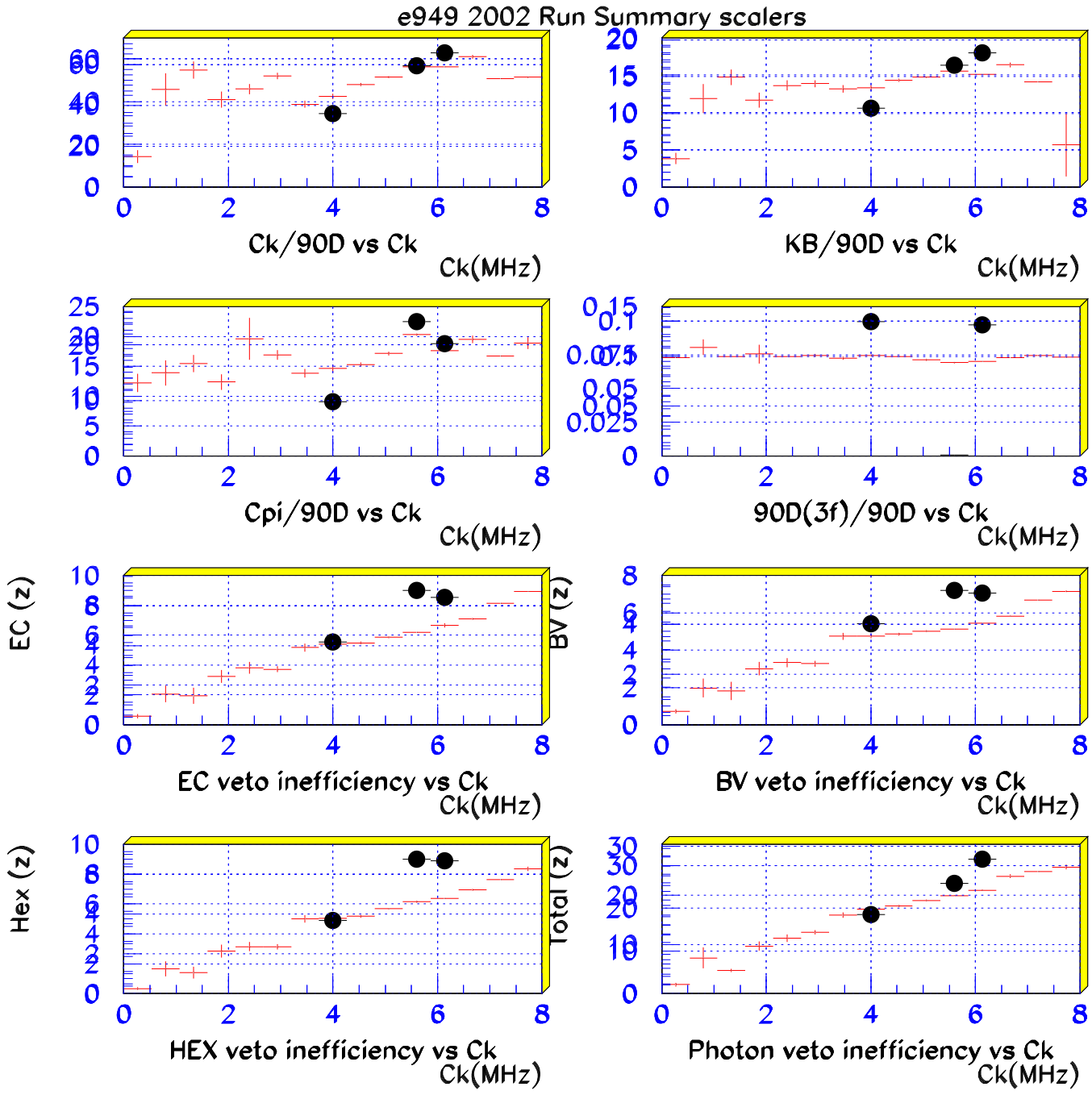
e949 2002 Run Summary scalers
Ck/90D vs Ck
Ck(MHz)
KB/90D vs Ck
Ck(MHz)
Cpi/90D vs Ck
Ck(MHz)
90D(3f)/90D vs Ck
Ck(MHz)
EC (z)
BV (z)
EC veto inefficiency vs Ck
Ck(MHz)
BV veto inefficiency vs Ck
Ck(MHz)
Hex (z)
Total (z)
HEX veto inefficiency vs Ck
Ck(MHz)
Photon veto inefficiency vs Ck
Ck(MHz)

Figure 140:

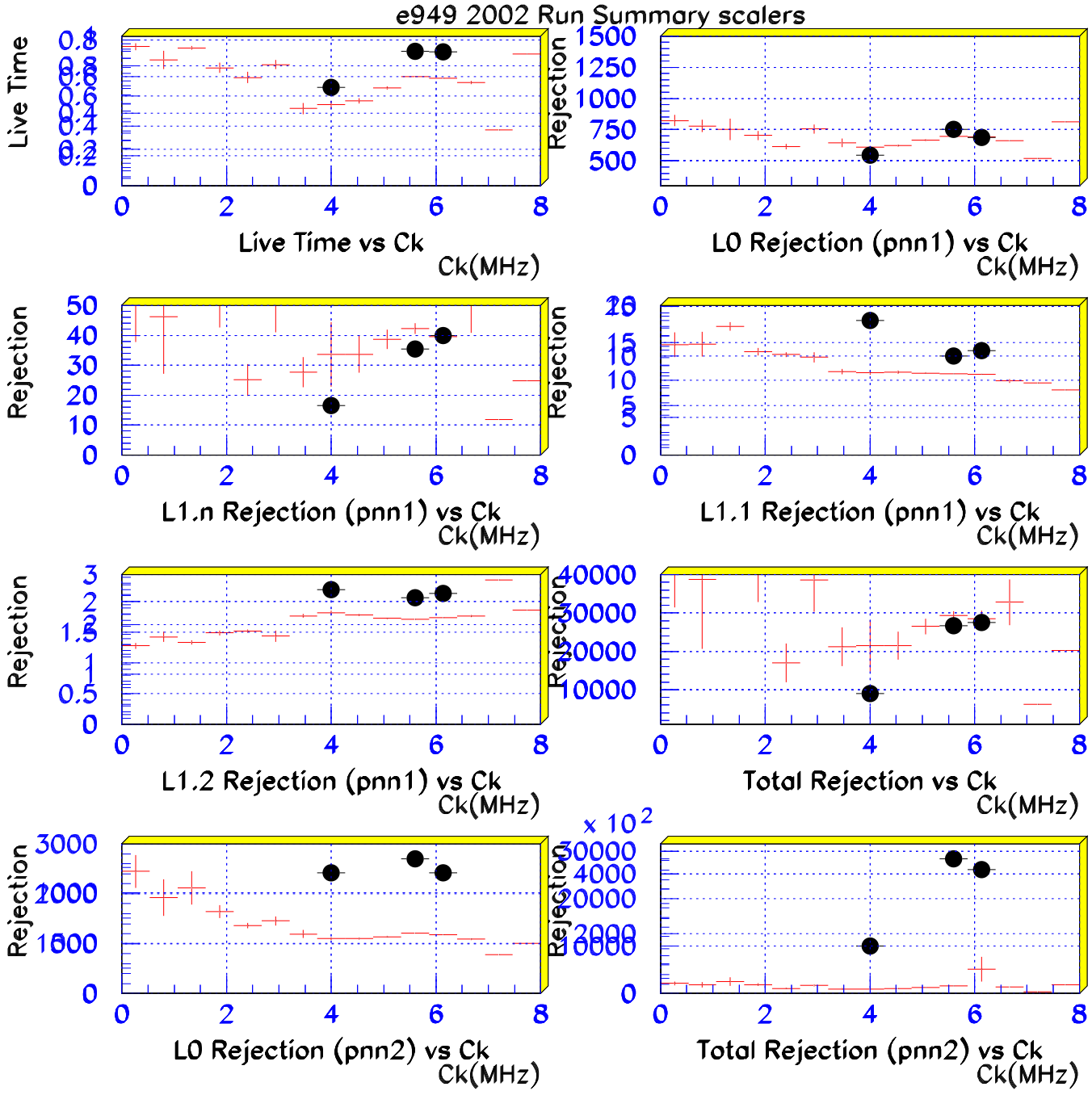
e949 2002 Run Summary scalers
Live Time
Rejection
Live Time vs Ck
Ck(MHz)
L0 Rejection (pnn1) vs Ck
L1.n Rejection (pnn1) vs Ck
L1.1 Rejection (pnn1) vs Ck
L1.2 Rejection (pnn1) vs Ck
Total Rejection vs Ck
L0 Rejection (pnn2) vs Ck
Total Rejection (pnn2) vs Ck
x 10 2

Figure 141:

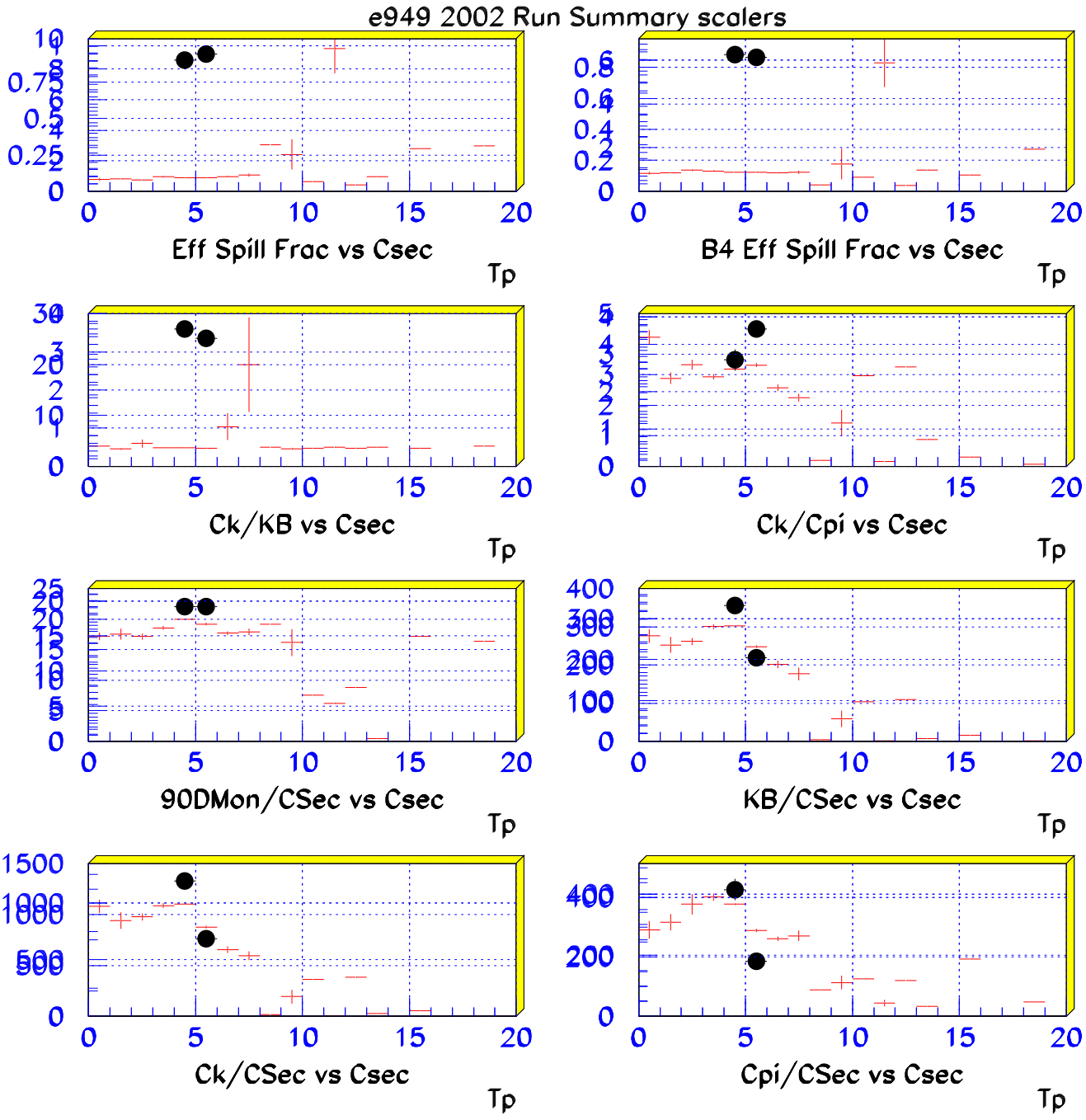
e949 2002 Run Summary scalers
Eff Spill Frac vs Csec
Tp
B4 Eff Spill Frac vs Csec
Tp
Ck/KB vs Csec
Tp
Ck/Cpi vs Csec
Tp
90DMon/CSec vs Csec
Tp
KB/CSec vs Csec
Tp
Ck/CSec vs Csec
Tp
Cpi/CSec vs Csec
Tp

Figure 142:

References

[1] J.Ives et. al.,"Analysis of the 1/3 E949 pnn2 data", E949 Technical Note **K-073.v1**.

[2] M. Diwan, et. al. "PNN2 1/3 Analysis", "PNN2 2/3 Analysis", E787 Technical Notes **tn385**, **tn386**, 2001.

[3] I. Christidi, "Search for the rare decay $K^+ \to \pi^+\nu\bar{\nu}$ with $p_{\pi^+} < 199$ MeV/c", Ph.D. thesis, 2006

[4] Vivek Jain, "Simulation of elastic scatters of pi+ in the target from Kp2 decays" E787 Technical note 375, 3 November 1999.

[5] B. Lewis, "PNN2 1/3 Beam Background", E949 Technical Note **K-061**, 2006. Unpublished.

[6] S. Chen *et al.*, "2002 pnn1 Data Analysis", E949, note K-034 (2003).

[7] Bipul Bhuyan, Ph. D thesis (2003).

[8] B. Lewis, "Addition to Bad Runs List", E949 Technical Note **K-060**, 2006. Unpublished.

[9] D. Perkins, Introduction to high eneryg physics, 4th edition, page 229.

[10] H. Davis et al., Nuovo Cimento, 53A, 313 (1968)

[11] W. Slater et al., PRL 7, 378 (1961)

[12] T. Yamazaki et al., PL 144B, 177 (1984)

[13] A.D. Martin, Nuclear Physics B179, 33 (1981)

[14] G.A. Sayer et al., Physical Review 169, 1045 (1968)

[15] Thomas Junk, "Confidence level computation for combining searches with small statistics", NIM, A434 (1999) 435-443.

[16] S. Chen *et al.*, "Further 2002 pnn1 Data Analysis", E949, note K-038 (2004).

[17] W.T. Eadie, D. Drijard, F.E. James, M. Roos and B. Sadoulet, "Statistical Methods in Experimental Physics", North-Holland, 1971, pp.282-283.

[18] G.H.Coombes, P.Kitching, J.A.Macdonald, T.Numao, "Proposed New Beam Instrumentation II", E949 note K-020, 15 June 2001.

[19] D.E.Jaffe, "Estimate of number of photoelectrons in the active degrader", E949 note K-057, 12 may 2006.

[20] V.V.Anisimovsky *et al.*, Phys. Rev. Lett. **93**, 031801 (2004).

[21] R.M. Barnett *et al.*, Physical Review D**54** 1, (1996)

[22] S. Adler *et al.*, PRL84, 3768 (2000)

[23] S. Adler *et al.*, Phys. Rev. D**77**, 052003 (2008).

[24] D.E. Jaffe, "FITPI: Triple-pulse fitting and other modifications", E949 note K-029, 31 Oct 2002.